

Regd. No. C-3911

# INDIAN JOURNAL OF PHYSICS

VOL. 39

AND

PROCEEDINGS

OF THE

Indian Association for the Cultivation of Science, Vol. 48

*(Edited in Collaboration with the Indian Physical Society)*

( With Six Plates ).

Published by the Registrar, Indian Association for the Cultivation of Science,  
Jadavpur, Calcutta 32 and printed by Kalipada Mukherjee, Eka  
Press, 204/1, B. T. Road, Calcutta

**1965**

## BOARD OF EDITORS

K. BANERJEE	S. R. KHASTGIR
G. N. BHATTACHARYA	D. S. KOTHARI
D. M. BOSE	B. D. NAG CHOUDHURI
S. N. BOSE	K. R. RAO
S. D. CHATTERJEE	D. B. SINHA
P. S. GILL	S. C. SIRKAR
B. N. SRIVASTAVA	A. BOSE ( <i>Secretary</i> )

## EDITORIAL COLLABORATORS

PROF. R. K. ASUNDI, Ph.D., F.N.I.  
PROF. D. BASU, Ph.D.  
PROF. J. N. BHAR, D.Sc., M.I.E.R.E., F.N.I.  
PROF. V. G. BHIDE, Ph.D.(Nag.), Ph.D.(Lond)  
PROF. H. N. BOSE  
PROF. S. K. CHAKRABORTY, D.Sc., F.N.I.  
DR. J. S. CHATTERJEE,  
DR. K. DAS GUPTA, Ph.D.,  
PROF. N. N. DAS GUPTA, Ph.D., F.N.I.  
DR. J. DHAR, D.Phil. (Sc)  
PROF. A. K. DUTTA, D.Sc., F.N.I.,  
DR. S. DUTTA MAZUMDAR, D.Sc.,  
PROF. C. S. GHOSH, M.Sc., S.M., F.N.I. M.I.E.E.,  
PROF. S. GHOSH, D.Sc., F.N.I.  
PROF. S. N. GHOSH, D.Sc.,  
PROF. S. GUPTA, M.Sc., F.N.I.  
PROF. D. N. KUNDU, Ph.D., F.N.I.  
PROF. R. C. MAZUMDAR, Ph.D., F.N.I.  
PROF. A. MOOKHERJI, D.Sc.,  
PRINCIPAL Y. G. NAIK, Ph.D.,  
PROF. S. R. PALIT, D.Sc., F.R.I.C., F.N.I.  
PROF. H. RAKSHIT, D.Sc., F.N.P., F.I.T.E., F.N.I.  
PROF. A. SAHA, D.Sc., F.N.I.  
PROF. VIKRAM A. SARABHAI, M.A., Ph.D., F.N.I.  
PROF. A. K. SENGUPTA, D.Sc.  
PROF. NAND LAL SINGH, D.Sc.,  
PROF. M. S. SINHA, D.Sc., F.N.I.  
DR. N. R. TAWDE, Ph.D., F. Inst. P. M.I. Nuc. E.F.A.So. F.N.I.  
DR. P. VENKATESWARLU.



# INDIAN JOURNAL OF PHYSICS VOL. 39, 1965

## CONTENTS

### No. 1. January

	PAGE
1. Determination of the Elastic Constants of Monoclinic Crystals from the Study of Diffuse X-Ray Reflections—S. K. Talapatra and R. K. Sen .. .. .	1
2. Ligand field Theory of Magnetic Susceptibility and Anisotropy in $\text{CoSiF}_6 \cdot 6\text{H}_2\text{O}$ —A. Bose, L. C. Jackson and R. Rai .. .. .	7
3. On the Derivation of the Coupled Wave Equations in the Magneto-Ionic Theory—S. K. Banerjee .. .. .	17
4. Variational Principles for Compressible Viscous Fluid in Magnetohydro-dynamics—N. K. Sharma and S. R. Sharma .. .. .	25
5. An Automatic Recording B-H Meter—A. K. Mukherjee and (Late) N. G. Sutradhar. .. .. .	33
6. The Significance of the Minimum Doppler Displacement in Canal Rays—B. V. Sitakumari .. .. .	41

#### LETTERS TO THE EDITOR—

1. On the Non-Coherent Formation of Absorption Lines in Stellar Atmospheres—Santi Ranjan Das Gupta .. .. .	46
2. Crystal Structure of Thiodiglycolic Acid—Sukla Roy .. .. .	49
3. The Energy Density of Solar Wind and its Correlation with Cosmic Ray Intensity—CH. V. Sastry .. .. .	51

### No. 2. February

7. Magnetoresistance in Single Crystals of Graphite—R. Bhattacharya	53
8. The Visible Emission Spectrum of $\text{BiCl}$ Molecule—V. Satyanarayana Rao and P. Tiruvenganna Rao .. .. .	65
A Hybrid Potential for Inert Gas Atoms—Anil Saran .. .. .	72
10. Measurement of Dielectric Properties of Metal Halides—M. N. Sharma, M. P. Madan and B. P. Pradhan .. .. .	78
11. Electron Velocity Distribution in Slightly Ionized Argon with Crossed Electric and Magnetic Fields—D. C. Jain, B. D. Nag Chaudhuri, B. Das Gupta, D. K. Bose and S. N. Sen Gupta .. .. .	88

#### LETTERS TO THE EDITOR—

4. Goniometric Study of Terbium Sulphate Octahydrate—Rupendra Kumar Kashyap .. .. .	97
5. The Magic Direction—T. C. Roy .. .. .	99

**No. 3. March**

- |  |     |
|--|-----|
| 12. Properties of Artificial Dielectrics at Radio Frequency—S. S. Gupta and M. N. Sharma .. .. .                           | 101 |
| 13. An Analysis of the J-Phenomenon in Scattered X-Rays Part II—Hirendra Kumar Pal .. .. .                                 | 108 |
| 14. Light Absorption in NO <sub>3</sub> Ion in State of Solution Part II 203mμ Band—A. Mookherjee and S. P. Tandon .. .. . | 137 |

**LETTERS TO THE EDITOR—**

- |  |     |
|--|-----|
| 6. Crystallographic Data for Ammonium Nitrate-Sulphate—S. K. Ghosh, V. K. Srinivasa and B. K. Banerjee .. .. . | 143 |
| 7. A Simple Method for Calculating Thermal Expansion of Ionic Crystals—C. M. Kachhava and S. C. Saxena .. .. . | 145 |

**No. 4. April**

- |   |     |
|---|-----|
| 15. Relaxation Times, Mutual and Averaged Mutual Viscosities of some Di-Substituted Benzenes in Solutions of Cyclohexane—S. I. Ahmad and M. N. Sharma .. .. . | 149 |
| 16. Hall Mobility of Tellurium Films Deposited on BaTiO <sub>3</sub> Crystal—A. K. Choudhuri and S. K. Dutta Roy .. .. .                                      | 156 |
| 17. Hall Effect in Single Crystals of Graphite—R. Bhattacharya .. .. .  | 163 |
| 18. Crystallographic Data for Nickel and Cobalt Biuret Complex—S. K. Ghosh, R. M. Sanyal and B. K. Banerjee .. .. .   | 170 |
| 19. Ligand Field Theory of Susceptibility and Anisotropy in Trigonal Distorted Fe <sup>3+</sup> Complex—A. Bose and R. Rai .. .. .                            | 176 |
| 20. Determination of the Relative Distribution of Layers in Density Packed Colloidal Systems—Wool—T. Ratho and B. C. Panda .. .. .                            | 187 |
| 21. A Modified Procedure of Scanning Nuclear Emulsions for Obtaining Absolute Neutron Yields of Reactions—J. P. Sah .. .. .                                   | 193 |
| 22. Incoherent Scattering of 280 KEV Gamma Rays—P. V. Ramana Rao, J. Rama Rao and V. Lakshminarayana .. .. .  | 195 |

**LETTERS TO THE EDITOR—**

- |  |     |
|--|-----|
| 8. Dimorphism of DL-Aspartic Acid—G. S. R. Krishna Murti, R. Natarajan and A. R. Deb .. .. . | 199 |
|--|-----|

**No. 5. May**

- |  |     |
|--|-----|
| 23. Thermal Conductivity and Composition Profile of a Chemically Reacting Gas Mixture Placed in a Hot-Wire Cell—T. K. Dastidar and A. K. Barua .. .. . | 203 |
| 24. Estimation of Air-Fraction, Specific Surface and other Parameters of Micelle systems—Wool—low Angle X-Ray Methods—T. Ratho and B. C. Panda .. .. . | 207 |

25. Gamma-Gamma Angular Correlation in Sn —A. K. Nigam and R. Bhattacharyya .. .. .	215
26. Ionization Cross-Sections of Atoms and Molecules by Electron Impact—A. K. Batabyal, A. K. Barua and B. N. Srivastava ..	219
27. On the Representation of the Distortions in Is Orbitals in the Bonding Molecular Orbital of a Homonuclear Diatomic Molecule—S. Chatterjee and A. K. Barua .. .. .	227
28. Dehydroxylation Reaction Kinetics of some Indian Kaolinitic Clays—J. Prasad and B. M. Bishui .. .. .	231
29. Elastic Scattering and Polarization of Electrons by Atom in Second Born Approximation—G. Chatterjee and N. C. Sil .. .. .	239

LETTERS TO THE EDITOR—

9. On Measurement of Electron Density of Plasma—A. K. Ghosal and S. K. Sen and J. Basu .. .. .	248
10. Copper-Molybdenite Thermo-Couple—A. K. Dutta and R. Bhattacharya .. .. .	251

**No. 6. June**

30. An Observation on a New Type of Distortion in Nuclear Emulsions —Prem K. Aditya .. .. .	253
31. Fourth-Order Elastic Coefficients for some Crystal Classes—P. B. Ghate .. .. .	257
32. Non-Radiative Transitions During the Decay of a Phosphor—Y. L. Arora .. .. .	265
33. Decay of Oscillations of a Sphere and Cylinder in a Liquid—A New Method of Determining Viscosity—J. C. Kameswar Rao and J. Ramakrishna .. .. .	271
34. Viscosity of Polar-Nonpolar Gas Mixtures Empirical Method—S. Mathur and S. C. Saxena .. .. .	278
35. An Analysis of the J-Discontinuity in Scattered X-Rays—Part III —Hirendra Kumar Pal .. .. .	283

LETTERS TO THE EDITOR—

11. Effect of Resonance on Neutron Scattering by Carbon—Paresh Kumar Biswas .. .. .	297
12. Quantitative Estimation Misalignment of the Layers in Natural Crystals of Graphite—S. Roy and R. Bhattacharya .. .. .	300
13. Role of Relaxation in an Adiabatic Change—M. P. Saksena and S. C. Saxena .. .. .	302
14. A Note on Broken Su(3) Symmetry—P. Ghose and S. Sen .. .. .	305
15. Su(3) Symmetry in a Bootstrap Model—T. Roy and P. Ghose .. .. .	306

## No. 7. July

	PAGE
36. X-Ray Study of a Second Dehydrated Phase of Copper Ammonium Sulphate Hexahydrate—Gouri Ray .. .. .	307
37. Singlet Triplet Absorption in Meta- and Parachlorotoluene—D. K. Mukherjee, P. K. Bishui and S. C. Sirkar .. .. .	313
38. Molecular Orbital Theory of the Ligand Field in $[\text{NiHal}_4]$ Complexes—A. Bose, R. Rai and S. Mitra .. .. .	318
39. Absorption of 7.7 mm Microwaves by Solutions of some Substituted Nitrobenzenes in Different Non-Polar Solvents—(Miss) B. Sinha, S. B. Roy and G. S. Kastha .. .. .	328
40. Principal Susceptibilities of $\text{Eu}^{+++}$ on in the Crystal of $\text{Eu}_2(\text{SO}_4) \cdot 8\text{H}_2\text{O}$ at Low Temperatures—D. Neogy and A. Mookherje .. .. .	342
41. Scattering of Electromagnetic Waves by Plasma—R. M. Khan and T. P. Khan .. .. .	347

## LETTERS TO THE EDITOR—

16. Variation of the Relaxation time and the Molar Free Energy of Activation with the C-Axis Spacing ( $d_{001}$ ) of some Complexes of Bentonite—Sabita Ghosh .. .. .	352
--	-----

## BOOK REVIEW

355

## No. 8. August

42. Magnetic Studies of Single Crystals Containing Tetrahedrally Co-ordinated $\text{Cu}^{2+}$ , $\text{Ni}^{2+}$ and $\text{Co}^{2+}$ Ions between 300°K and 90°K—A. Bose, S. Mitra and R. Rai .. .. .	357
43. Infrared and Raman Study of Parachloronitrobenzene—K. C. Medhi .. .. .	390
44. Light Absorption in $\text{NO}_2$ Ion in State of Solution (Part III—Effect of Cation) A. Mookherji and S. P. Tandon .. .. .	396

## LETTERS TO THE EDITOR—

17. Matrix Relations between Direction Cosines and Millerian Indices J. K. Ghosh .. .. .	400
18. The Intrinsic Dielectric Constant of salicylic Acid and Benzoic Acid Tathagata Sen .. .. .	402
BOOK REVIEW .. .. .	404

## No. 9. September

45. Mean Amplitudes of Variation, Bastiansenmorino Shrinkage Effect and Molecular Polarizabilities for the Dihalides of some Group IIA Elements—G. Nagarajan .. .. .	405
46. An X-Ray Study of Coir Fibre—P. K. Ray and S. B. Bandyopadhyay .. .. .	421

## Contents

	PAGE
47. Finite Spherical Inhomogeneities in Concentric Shells—B. D. Bhargava and D. Pande .. .. .	428
48. On a New Transformation Scheme Related to a 4-Dimensional Lorentz Transformation—N. N. Ghosh .. .. .	434

### LETTERS TO THE EDITOR—

19. Investigation on Raman and Infrared Spectra of two Isomeric Aromatic Nitriles in Different States—D. K. Mukherjee and K. K. Deb .. .. .	443
20. Effect of Electric Field on the Natural Convective Heat-Transfer to Insulating Liquids—S. P. Basu and D. B. Sinha .. .. .	447
21. Coupling Constant Sum Rules for the Decay of the $J \pm 2$ Nonet in Broken $SU(3)$ —V. P. Gautam and P. Ghose .. .. .	451
22. Change in the Shape of the $NO_3$ Ion during the Formation of a Hydrate in Aqueous Solutions—N. Rajeswara Rao, K. V. Ramanaiah and S. Mohana Rao .. .. .	453
BOOK REVIEW .. .. .	454

### No. 10. October

49. Variational Method and the Elastic Scattering of slow Electrons by Hydrogen Atom—Satyanarayan Banerjee, Rameshwar Jah and N. C. Sil .. .. .	455
50. $\pi^* \leftarrow \pi$ System in the Electronic Spectra of Para-Bromophenol—Kailash Chandra .. .. .	464
51. Vibration of a Clamped—Clamped Bar under Tension—Sunil Kumar Banerjee .. .. .	476
52. Responses in a Piezo-Electrical Plate-Transducer—S. K. Ghosh and Sunil Kumar Banerjee .. .. .	486

### LETTERS TO THE EDITOR—

23. The Crystal Structure of $\alpha$ -Lead Azide, $\alpha$ - $Pb(N_3)_2$ —Prasenjit Saha	494
24. Integrated Field Intensity of Atmospherics in Relation to Monsoon Thunder-clouds—M. K. Das Gupta and A. K. Sen .. .. .	498
25. Space Group and Unit Cell Dimensions of Copper Propionate Monohydrate—(Mrs.) Aloka Poddar and S. N. Giri .. .. .	502
BOOK REVIEW .. .. .	504

### No. 11. November

53. Study of some Alpha Groups from Americium—241—M. Rama Rao	505
54. Dispersion Relations for Electron Plasma in an External Magnetic Field—Saroj K. Majumdar .. .. .	511

	PAGE
55. Directional Correlation Study of Gamma Cascades in the Decay of $\text{Sb}^{124}$ —R. V. Rama Mohan, K. Venkata Reddy, B. B. Venkata-pathi Raju and Swami Janananda .. .. .	521
56. Crystal Field Theory of $\text{Cu}^{++}$ Ion in the Magnetically Diluted Crystal of $2\text{K}_2(\text{Zn,Cu})(\text{SO}_4)_2 \cdot 6\text{H}_2\text{O}$ —S. Banerjee and A. Mookherji ..	530
57. On the Infrared Spectra of p-Fluoro- and o-, m-, and p-Chloro Toluene in the Vapour State—D. K. Mukherjee, P. K. Bishui and S. C. Sirkar .. .. .	537
LETTERS TO THE EDITOR—	
25. Low Energy Scattering of Electron by Helium Atom by the Variational Method—Satya Narayan Banerjee, Rameshwar Jha and N. C. Sil .. .. .	552
BOOK REVIEW .. .. .	554

### No. 12. December

58. Effect of Anharmonicity on the Thermo-Dynamic Behaviour of a Solid—D. N. Singh .. .. .	555
59. Density-Wake of a Charged Particle Moving Through a Plasma—Saroj K. Majumdar .. .. .	562
60. Light Absorption in $\text{NO}_3$ ion in State of Solution Part IV—Effect of Dilution—A. Mookherji and S. P. Tandon .. .. .	569
61. The Visible Emission Spectrum of $\text{BiF}$ —K. Madhusudhana Rao and P. Tiruvenganna Rao .. .. .	572
62. Dynamics of the Vibration of an Elastic-Plastic String under Transverse Impact—S. K. Ghosh and Sunil Kumar Banerjee ..	580
63. Performance of Unstable Pendant Drops in Surface Tension Measurements—K. G. Parvatikar .. .. .	588
64. Elastic Misfitting Sheets—R. D. Bhargava and D. Pande ..	592

### LETTERS TO THE EDITOR—

26. A Possible Example of a $\Lambda \text{B}^{12}$ Hyperfragment—K. M. Pathak ..	600
Book Review .. .. .	602

# AUTHOR INDEX

AUTHOR	SUBJECT	PAGE
Aditya, Prem K.	An observation on a new type of distortion in nuclear emulsions	253
Ahmad, S. I. and Sharma, M. N.	Relaxation times, natural and averaged mutual viscosities of some di-substituted benzenes in solution of cyclohexane	149
Arora, Y. L.	Non-radiative transitions during the decay of phosphor	265
Bandyopadhyay, S. B.	See Ray, P. K.	
Banerjee, B. K.	See Ghosh, S. K.	
Banerjee, S. and Mookherji, A.	Crystal field theory of $Cu^{++}$ ion in the magnetically diluted crystal of $2K_2 (Zn, Cu) (SO_4)_2 6H_2O$	530
Banerjee, S. K.	On the derivation of the coupled waved equations in the magneto-ionic theory	17
Banerjee, S. K.	See Ghosh, S. K.	
	Vibration of a clamped-clamped bar under tension	476
Banerjee, S. N., Jah, R. and Sil, N. C.	Variational method and the elastic scattering of slow electrons by hydrogen atom	455
"      "      "	Low energy scattering of electrons by helium atom by the variational method (L)	552
Barua, A. K.	See Batabyal, A. K.	
"	See Chatterjee, S.	
"	See Rai Dastidar, T. K.	
Basu, J.	See Ghoshal, A. K.	
Basu, S. P. and Sinha, D. B.	Effect of electric field on the natural convective heat-transfer to insulating liquids (L)	447
Batabyal, A. K., Barua, A. K. and Srivastava, B. N.	Ionization cross-section of atoms and molecules by electron impact	219
Bhargava, B. D. and Pande, D.	Finite spherical inhomogeneities in concentric shells	428
Bhattacharya, R.	Hall effect in single crystals of graphite	156

AUTHOR	SUBJECT	PAGE
Bhattacharya, R.	See Dutta, A. K.	
"	See Nigam, A. K.	
"	See Ray, S.	
Bishui, B. M.	See Prasad, J.	
Bishui, P. K.	See Mukherjee, D. K.	
Biswas, P. K.	Effect of resonance on neutron scattering by carbon(L)	297
Bose, A, Jackson, L. C. and Rai, R.	Ligand field theory of magnetic susceptibility and anisotropy in $\text{CoSiF}_6 \cdot 6\text{H}_2\text{O}$	7
Bose, A. and Rai, R.	Ligand field theory of susceptibility and anisotropy in trigonally distorted $\text{Fe}^{2+}$ complex	176
Bose, A., Rai, R. and Mistra. S.	Molecular orbital theory of the ligand field in $[\text{NiHaI}_4]^2$ complexes	318
Bose, A., Mitra, S. and Rai, R.	Magnetic studies of single crystals containing tetrahedrally co-ordinated $\text{Cu}^{2+}$ , $\text{Ni}^{2+}$ $\text{Co}^{2+}$ ions between $300^\circ\text{K}$ and $90^\circ\text{K}$	357
Bose, D K	See Jain, D	
Chandra, Kailash	$\pi^* \leftarrow \pi$ systems in the electronic spectra of para-bromo-phenol	464
Chatterjee, G. and Sil, N. C.	Elastic scattering and polarization of electrons by atom in second born approximation	239
Chatterjee, S. and Barua, A. K.	On the representation of the distortions in 1s orbitals in the bonding molecular orbital of a homonuclear diatomic molecule	227
Choudhuri, A. K. and Dutta Roy, S. K.	Hall mobility of tellurium films deposited in $\text{BaTiO}_3$ crystal	156
Das Gupta, B.	See Jain, D. C.	
Das Gupta, M. K. and Sen, A. K.	Integrated field intensity of atmospheric in relation to monsoon thunderclouds (L)	498
Das Gupta, S. R.	On the non-coherent formation of absorption lines in stellar atmospheres (L)	46
Deb, A. R.	See Krishna Murti, G. S. R.	
Deb, K. K.	See Mukherjee, D. K.	
Dutta, A. K. and Bhattacharya, R.	Copper-molybdenite thermo-couple (L)	252



AUTHOR	SUBJECT	PAGE
Dutta Roy, S. K.	See Choudhuri, A. K.	
Gautam, V. P. and Ghose, P.	Coupling constant sum rules for the decay of $J^P = 2^+$ Nonet in Broken SU(3) (L)	451
Ghate, P. B.	Fourth-order elastic coefficients for some crystals classes	257
Giri, S. N.	See Podder, Aloka (Mrs)	
Ghosh, J. K.	Matrix relations between direction cosines and Millerian indices (L)	400
Ghosh, N. N.	On a new transformation scheme related to a 4-dimensional Lorentz transformation	434
Ghose, P. and Sen, S.	A note on broken Su(3) symmetry (L)	305
Ghose, P.	See Gautam, V. P.	
" "	See Roy, T.	
Ghosh, S.	Variation of the relaxation time and the molar free energy of activation with the C-axis spacing( $d_{001}$ ) of some complexes of bentonite(L)	352
Ghosh, S. K., Srinivasa, V. K. and Banerjee, B. K.	Crystallographic data for ammonium nitrate-sulphate (L)	143
Ghosh, S. K., Sanyal, R. M. and Banerjee, B. K.	Crystallographic data for nickel and cobalt biuret complex	170
Ghosh, S. K. and Banerjee, S. K.	Responses in a piezo-electrical plate-transducer	486
Ghoshal, A. K., Sen, S. K., and Basu, J.	On measurement of electron density of plasma (L)	248
Gupta, S. S. and Sharma, M. N.	Properties of artificial dielectrics at radio frequency	101
Jackson, L. C.	See Bose, A.	
Jain, D. C. Nag Chaudhuri, B. D., Das Gupta, B., Bose, D. K. and Sen Gupta, S. N.	Electron velocity distribution in slightly ionized argon with crossed electric and magnetic fields	88
Jha, R.	See Banerjee, S. N.	
Kachhava, C. M. and Saxena, S. C.	A simple method for calculating thermal expansion of ionic crystals (L)	145
Kashyap, R. K.	Goinometric study of terbium sulphate octahydrates (L)	97

AUTHOR	SUBJECT	PAGE
Kastha, G. C.	See Sinha, B(Miss.)	
Khan, R. M. and Khan, T. P.	Scattering electromagnetic waves by plasma	347
Khan, T. P.	See Khan, R. M.	
Krishna Murti, G. S. R., Natarajan, R. and Deb, A. R.	Dimorphism of DL-aspartic acid (L)	199
Lakshminarayana, V.	See Rao, V. P. V.	
Madan, M. P.	See Sharma, M. N.	
Majumdar, S. K.	Dispersion relations for electrons plasma in an external magnetic field	511
Mathur, S. and Saxena, S. C.	Viscosity of polar-nonpolar gas mixtures empirical method	278
Medhi, K. C.	Infrared and Raman study of parachloronitrobenzene	390
Mitra, S.	See Bose, A.	
Mookherji, A.	See Banerjee, S.	
„	See Neogy, D.	
Mookherjee, A. and Tandon, S. P.	Light absorption in NO <sub>3</sub> ion in state of solution Part II 203mμ band	137
Mookherji, A. and Tandon, S. P.	Light absorption in NO <sub>3</sub> ion in state of solution (Part III-effect of Cation)	396
Mukherjee, A. K. and Sutradhar, N. G. (Late)	An automatic recording B-H meter	33
Mukherjee, D. K. and Deb, K. K.	Investigation on Raman and infrared spectra of two isomeric aromatic nitriles in different states (L)	443
Mukherjee, D. K., Bishui, P. K. and and Sirkar, S. C.	Singlet-triplet absorption in meta and parachlorotoluene	313
	On the infrared spectra of p-fluoro- and o-, m-, and p-chloro toluene in the vapour state	537
Nagarajan, G.	Mean amplitudes of variation, Bastiansenmorino Shrinkage effect and molecular polarizabilities for the dihalides of some group IIA elements	405

AUTHOR	SUBJECT	PAGE
Nag Chaudhuri, B. D.	See Jain, D. C.	
Natarajan, R.	See Krishna Murti, G. S. R.	
Neogy, D. and Mookherji, A.	Principal susceptibilities of $\text{Eu}^{+++}$ ion in the crystal of $\text{Eu}_2(\text{SO}_4)_3 \cdot 8\text{H}_2\text{O}$ at low temperatures	342
Nigam, A. K. and Bhattacharyya, R.	Gamma-gamma angular correlation in $\text{Sn}^{125}$	215
Pal, H. K.	An analysis of the J-phenomenon in scattered X-rays Part II	108
	An analysis of the J-discontinuity in scattered X-rays Part III	283
Panda, B. C.	See Ratho, T.	
Pande, D.	See Bhargava, B. D.	
Podder, Aloka (Mrs.) and Giri, S. N.	Space group and unit cell dimensions of copper propionate monohydrate (L)	502
Pradhan, B. P.	See Sharma, M. N.	
Prasad, J. and Bishui, B. M.	Dehydroxylation reaction kinetics of some Indian kaolinitic clays	231
Rai Dastidar, T. K. and Barua, A. K.	Thermal conductivity and composition profile of a Chemically reacting gas mixture placed in a hot-wire cell	203
Rai, R.	See Bose, A.	
Ramakrishna, J.	See Rao, Kamesvar, J. C.	
Rama Mohan, R. V., Reddy, Venkata, K., Raju, B. B., Venkatapathi, and Jnanananda, Swami	Directional correlation study of gama cascades in the decay of $\text{Sb}^{124}$	521
Ramanaiah, K. V.	See Rao, Rajeswara N.	
Rao, J. Rama	See Rao, P. V.	
Rao, Kamesvar, J. C. and Ramakrishna, J.	Decay of oscillation of a sphere and cylinder in a liquid—a new method of determining viscosity	271
Rao, Mohana S.	See Rao, Rajeswara N.	
Rao, P. Tiruvenganna	See Rao, V. Satyanarayana	
Rao, P. V. Ramana ; Rao, J. Rama and Lakshminarayana, V.	Incoherent scattering of 280 KEV gamma rays	195
Rao, Rajeswara N., Ramanaiah, K. V. and Rao, Mohana S.	Change in the shape of the $\text{NO}_2$ ion during the formation of a hydrate in aqueous solutions (L)	453

AUTHOR	SUBJECT	PAGE
Rao, Rama M.	Study of some alpha groups from americium	505
Tiruvenganaa Rao, P. and Satyanarayana Rao, V.	The Visible emission Spectrum of BiCl molecule	65
Ratho, T. and Panda, B. C.	Estimation of air-fraction, specific surface and other parameters of Micelle systems-wool-low angle X-ray methods	207
Ratho, T. and Banda, B. C.	Determination of the relative distribution of layers in densely packed colloidal systems-wool	187
Ray, Gouri	X-ray study of a second dehydrated phase of copper ammonium sulphate dexamhydrate	307
Ray, P. K. and Bandyopadhyay, S. B.	An X-ray study of coir fibre	421
Ray, S. and Bhattacharya, R.	Quantitative estimation misalignment of the layers in natural crystals of graphite (L)	300
Reddy, Venkata K.	See Rama Mohan, R. V.	
Roy, S.	Crystal structure of thiodiglycolic acid (L)	49
Roy, S. B.	See Sinha, B. (Miss)	
Roy, T. and Ghose, P.	Su(3) symmetry in a Bootstrap model (L)	306
Roy, T. C.	The magic direction (L)	
Sah, J. P.	A modified procedure of scanning nuclear emulsions for obtaining absolute neutron yields of reactions	193
Saha, P.	The crystal structure of a $\alpha$ -lead azide, $\alpha$ -Pb(N <sub>3</sub> ) <sub>2</sub> (L)	494
Saksena, M. P. and Saxena, S. C.	Role of relaxation in an adiabatic change (L)	302
Sanyal, R. M.	See Ghosh, S. K.	
Saran, A.	A hybrid potential for inert gas atoms	72
Sastry, Ch. V.	The energy density of solar wind and its correlation with cosmic ray intensity (L)	51
Saxena, S. C.	See Kachhava, C. M.	
"	See Mathur, S.	
"	See Saksena, M. P.	
Sen, A. K.	See Das Gupta, M. K.	

# Author Index

xiii

AUTHOR	SUBJECT	PAGE
Sen, R. K.	See Talapatra, S. K.	
Sen, S.	See Ghose, P.	
Sen, S. K.	See Ghoshal, A. K.	
Sen, T.	The intrinsic dielectric constant of salicylic acid and benzoic acid (L)	402
Sen Gupta, S. N.	See Jain, D. C.	
Sharma, M. N.	See Ahmed, S. I.	
„	See Gupta, S. S.	
Sharma, M. N., Madan, M. P. and Pradhan, B. P.	Measurement of dielectric properties of metal halides	78
Sharma, N. K. and Sharma, S. R.	Variational principles for com- pressible viscous fluid in magnetohydrodynamics	25
Sharma, S. R.	See Sharma, N. K.	
Sil, N. C.	See Banerjee, S. N.	
„	See Chatterjee, G.	
Sinha, B. (Miss), Roy, S. B. Kastha, G. S.	Absorption of 7.7 mm microw- aves by solutions of some substituted nitrobenzenes in different non-polar solvent	328
Sinha, D. B.	See Basu, S. P.	
Sirkar, S. C.	See Mukherjee, D. K.	
Sitakumari, B. V.	The significance of the minimum Doppler displacement in Canal rays	41
Srivastava, B. N.	See Batabyal, A. K.	
Srinivasa, V. K.	See Ghosh, S. K.	
Sutradhar, N. G. (Late)	See Mukherjee, A. K.	
Swami, Jnanananda	See Rama Mohan, R. V.	
Talapatra, S. K. and Sen, R. K.	Determination of the elastic cons- tants of monoclinic crystals from the study of diffuse X-ray reflections	1
Tandon, S. P.	See Mookherji, A.	
Venkatapathi, B. B.	See Rama Mohan, R. V.	

# SUBJECT INDEX

SUBJECT	AUTHOR	PAGE
Absorption of 7.7 mm microwaves by solutions of some substituted nitrobenzenes in different non-polar solvents	(Miss) B. Sinha, S. B. Roy and G. S. Kastha	328
Air-fraction, specific surface and other parameters of Micelle systems.—Wool-low angle X-ray methods.—Estimation of	T. Ratho and B. C. Panda	207
Alpha groups from Americium-241.—Study of some	M. Rama Rao	505
Anharmonicity on the thermo-dynamic behaviour of a solid.—Effect of	D. N. Singh	555
Artificial dielectric at radio frequency.—Properties of	S. S. Gupta and M. N. Sharma	101
Automatic recording B-H meter.—An	A. K. Mukherjee and (Late) N. G. Sutradhar	33
Broken Su(3) symmetry.—A note on (L)	P. Ghose and S. Sen	305
Change in the shape of the NO <sub>3</sub> ion during the formation of hydrate in aqueous solutions (L)	N. Rajeswara Rao, K. V. Ramanaiah and S. Mohana Rao	453
Copper-molybdenite thermo-couple (L)	A. K. Dutta and R. Bhattacharya	251
Coupled wave equations in the magneto-ionic theory.—On the derivation of the	S. K. Banerjee	17
Coupling constant sum rules for the decay of the J <sup>2</sup> =2 nonet in Broken SU(3). (L)	V. P. Gautam and P. Ghose	451
Crystal field theory of Cu <sup>++</sup> ion in the magnetically diluted crystal of 2K <sub>2</sub> (Sn, Cu)(SO <sub>4</sub> ) <sub>2</sub> ·6H <sub>2</sub> O	S. Banerjee and A. Mookherji	530
Crystal structure of thiodiglycollic acid(L)	Sukla Roy	49
Crystal structure of -lead azide, α-Pb(N <sub>3</sub> ) <sub>2</sub> .—The (L)	Prasenjit Saha	494
Crystallographic data for ammonium nitrate-sulphate (L)	S. K. Ghosh, V. K. Srinivasa and B. K. Banerjee	143

SUBJECT	AUTHOR	PAGE
Crystallographic data for nickel and cobalt biuret complex	S. K. Ghosh, R. M. Sanyal and B. K. Banerjee	170
Decay of oscillations of a sphere and cylinder in a liquid of determining viscosity	J. C. Kamesvar Rao and J. Ramakrishna	271
Dehydrozylation reaction kinetic of some Indian kaolinitic clays	J. Prasad and B. M. Bishui	231
Density-wave of a charged particle moving through a plasma	Saroj K. Majumdar	562
Dielectric properties of metal halides. —Measurement of	M. N. Sharma, M. P. Madan and B. P. Pradhan	78
Dimorphism of Dl-aspartic acid (L)	C. S. R. Krishna Murty, R. Natarajan and A. R. Deb	199
Directional correlation study of Gamma cascades in the decay of Sb <sup>124</sup>	R. V. Rama Mohan, K. Venkata Reddy, B. B. Venkatapathi Rau and Swami Jannananda	521
Dispersion relations for Electron plasma in an external magnetic field	Saroj K. Majumdar	511
Distortions in Is orbitals in the bonding molecular orbital of a homonuclear diatomic molecule.—On the representation of the	S. Chatterjee and A. K. Barua	227
Dynamics of the vibration of an elastic-plastic string under transverse impact	S. K. Ghosh and Sunil Kumar Banerjee	580
Elastic constants of monoclinic crystals from the study of diffuse X-ray reflections.—Determination of the	S. K. Talapatra and R. K. Sen	1
Elastic misfitting shells	R. D. Bhargava and D. Pande	592
Elastic scattering and polarization of electrons by atom in second born approximation	G. Chatterjee and N. C. Sil	239
Electric field on the natural convective heat-transfer to insulating liquids. —Effect of (L)	S. P. Basu and D. B. Sinha	447
Electron density of plasma.—On measurement of (L)	A. K. Ghoshal; S. K. Sen and J. Basu	248

SUBJECT	AUTHOR	PAGE
Electronic spectra of para-bromophenol — $\pi^* \leftarrow \pi$ system in the	Kailash Chandra	464
Electron velocity distribution in slightly ionized argon with crossed electric and magnetic fields	D. C. Jain, B. D. Næg Chaudhuri, B. Das Gupta, D. K. Bose, and S. N. Sen Gupta	88
Energy density of solar wind and its correlation with cosmic ray intensity. —The (L)	CH. V. Sastry	51
Finite spherical inhomogeneities in con- centric shells	B. D. Bhargava and D. Pande	428
Fourth-order elastic coefficients for some crystal classes	P. B. Ghate	257
Gamma-gamma angular correlation in $\text{Sn}^{125}$	A. K. Nigam and R. Bhattacharyya	215
Goniometric study of terbium sulphate octahydrate (L)	Rupendra Kumar Kashyap	97
Hall effect in single crystals of graphite	R. Bhattacharya	163
Hall mobility of tellurium films deposi- ted on $\text{BaTiO}_3$ crystal	A. K. Chondhuri and S. K. Dutta Roy	156
Hybrid potential for inert gas atoms.—A Incoherent scattering of 280KEV gama rays	Anil Saran P. V. Ramana Rao; J. Rama Rao and V. Lakshminarayana	72 195
Infrared and Raman study of parach- loronitrobenzene	K. C. Medhi	390
Infrared spectra of p-fluoro- and o-, m-, and p-chloro toluene in the vapour state—On the	D. K. Mukherjee, P. K. Bishui and S. C. Sirkar	537
Integrated field intensity of atmospherics in relation to monsoon thunderclouds (L)	M. K. Das Gupta and A. K. Sen	498
Intrinsic dielectric constant of salicylic acid and benzoic acid (L)	Tathagata Sen	402
Ionization cross-sections of atoms and molecules by electron impact	A. K. Batabyal, A. K. Barua and B. N. Srivastava	219



SUBJECT	AUTHOR	PAGE
J-discontinuity in scattered X-rays- part III.—An analysis of the	Hirendra Kumar Pal	283
J-phenomenon in scattered X-rays part II.—An analysis of the	Hirendra Kumar Pal	108
Ligand field theory of magnetic suscep- tibility and anisotropy in $\text{CoSiF}_6 \cdot 6\text{H}_2\text{O}$ .	A. Bose, L. C. Jackson and R. Rai	7
Ligand field theory of susceptibility and anisotropy in trigonally distorted $\text{Fe}^{2+}$ complex	A. Bose and R. Rai	176
Light absorption in $\text{NO}_3$ ion in state of solution part II 203 $m\mu$ band	A. Mookerji and S. P. Tandon	137
Light absorption in $\text{NO}_3$ ion in state of solution (Part III-effect of cation)	A. Mookherji and S. P. Tandon	396
Light absorption in $\text{NO}_3$ ion in state of solution part IV-effect of dilution	A. Mookherji and S. P. Tandon	569
Low energy Scattering of electron by Helium atom by the variational method (L)	S. N. Banerjee, R. Jha and N. C. Sil	552
Magic direction.—The (L)	T. C. Roy	99
Magnetic studies of single crystals con- taining tetrahedrally co-ordinated $\text{Cu}^{2+}$ , $\text{Ni}^{2+}$ , and $\text{Co}^{2+}$ ions between 300°K and 90°K	A. Bose, S. Mitra and R. Rai	357
Magnetoresistance in single crystals of graphite	R. Bhattacharya	53
Matrix relations between direction cos- ines and Millerian indices (L)	J. K. Ghosh	400
Maen amplitudes of variation, bastian- senmorino shrinkage effect and mole- cular polarizabilities for the dihalides of some group IIA elements	G. Nagarajan	405
Minimum Doppler displacement in canal rays.—The significance of the	B. V. Sitakumari	41
Molecular orbital theory of the ligand field in $(\text{NiH}_2\text{I}_4)^{2-}$ complexes	A. Bose, R. Rai and S. Mitra	318
Neutron scattering by carbon.—Effect of resonance on (L)	Paresh Kumar Biswas	297
New type of distortion in nuclear emul- sions.—An observation on a	Prem K. Aditya	253
Non-coherent formation of absorption lines in stellar atmospheres.—On the (L)	Santi Ranjan Das Gupta	46

SUBJECT	AUTHOR	PAGE
Non-radiative transitions during the decay of a phosphor	Y. L. Arora	265
Performance of unstable pendant drops in surface tension measurements	K. G. Parvatikar	588
Possible example of a $A B^{12}$ hyperfragment. —A(L)	K. M. Pathak	600
Principal susceptibilities of $Eu^{+++}$ ion in the crystal of $Eu_2(SO_4) \cdot 8H_2O$ at low temperatures	D. Neogy and A. Mookherji	342
Quantitative estimation misalignment of the layers in natural crystals of graphite(L)	S. Ray and R. Bhattacharya	300
Raman and infrared spectra of two isomeric aromatic nitriles in different states.—Investigation on (L)	D. K. Mukherjee and K. K. Deb	443
Relative distribution of layers in densely packed colloidal systems-wool.—Determination of the	T. Ratho and B. C. Panda	187
Relaxation in an adiabatic change. Role of (L)	M. P. Saksena and S. C. Saxena	302
Relaxation time and the molar free energy of activation with the C-axis spacing ( $d_{100}$ ) of some complexes of bentonite.—Variation of the (L)	Sabita Ghosh	352
Relaxation times, mutual and averaged mutual viscosities of some di-substituted benzenes in solutions of cyclohexane	S. I. Ahmad and M. N. Sharma	149
Responses in a Piezo-Electrical Plate Transducer	S. K. Ghosh and S. K. Banerjee	486
Scanning nuclear emulsions for obtaining absolute neutron yields of reactions.—A modified procedure of	J. P. Sah	193
Scattering of electromagnetic waves by plasma	R. M. Khan and T. P. Khan	347
Singlet-triplet absorption in meta- and parachlorotoluene	D. K. Mukherjee, P. K. Bishui and S. C. Sirkar	313
Space group and unit cell dimensions of copper propionate monohydrate. (L)	(Mrs.) A. Podder and S. N. Giri	502
Su(3) symmetry in a Bootstrap model(L)	T. Roy and P. Ghose	306

# *Subject Index*

*xix*

SUBJECT	AUTHOR	PAGE
Thermal conductivity and composition profile of a chemically reacting gas mixture placed in a hot-wire cell	T. K. Rai Dastidar and A. K. Barua	203
Thermal expansion of ionic crystals.—A simple method for calculating (L)	C. M. Kachhava and S. C. Saxena	145
Transformation scheme related to a 4-dimensional Lorentz transformation.—On a new	N. N. Ghosh	434
Variational method and the elastic scattering of slow electrons by hydrogen atom.	S. B. Rameshwar Jah and N. C. Sil	455
Variational principles for compressible viscous field in magnetohydrodynamics	N. K. Sharma and S. R. Sharma	25
Vibration of a clamped-clamped bar under tension	S. K. Banerjee	476
Visible emission spectrum of BiCl molecule.—The	V. Satyanarayana Rao and P. Tiruvenganna Rao	65
Visible emission spectrum of BiF.—The	K. Madhusudhana Rao and P. Tiruvenganna Rao	572
Viscosity of polar-nonpolar gas mixture —empirical method	S. Mathur and S. C. Saxena	278
X-ray study of a second dehydrated phase of copper ammonium sulphate hexahydrate	Gouri Ray	307
X-ray study of Coir fibre.—An	P. K. Ray and S. B. Bandyopadhyay	421
BOOK REVIEWS		355, 404, 454 504, 554, 602



VOL. 39 **INDIAN JOURNAL OF PHYSICS** No. 1

AND

VOL. 48 **PROCEEDINGS** No. 1

OF THE

**INDIAN ASSOCIATION FOR THE  
CULTIVATION OF SCIENCE**

*(Edited in collaboration with the Indian Physical Society)*

**JANUARY 1965**

PUBLISHED BY THE  
**INDIAN ASSOCIATION FOR THE CULTIVATION OF SCIENCE**  
*JADAVPUR, CALCUTTA-32*



# DETERMINATION OF THE ELASTIC CONSTANTS OF MONOCLINIC CRYSTALS FROM THE STUDY OF DIFFUSE X-RAY REFLECTIONS

S. K. TALAPATRA AND R. K. SEN

INDIAN ASSOCIATION FOR THE CULTIVATION OF SCIENCE, CALCUTTA-32

(Received September 21, 1964)

**ABSTRACT** Theoretical relationships connecting diffusely scattered X-ray intensities from monoclinic class of crystals with its elastic constants have been derived by a proper choice of reflecting planes and lattice wave normals. Methods of evaluation of all the thirteen elastic constants from quantitative measurements of thermal diffuse scattering of X-rays have been described.

## INTRODUCTION

The elastic constants of the monoclinic class of crystals have not been determined up to the present by the quantitative study of thermal diffuse scattering of X-rays. Since a large number of crystals, specially the organic ones, belong to the monoclinic class, it is of interest to see how best the X-ray method could be applied in this case. Crystals of higher symmetry have got fewer number of elastic constants and they were determined quite satisfactorily from the study of diffuse X-ray reflection by Wooster *et al* (Wooster, 1962) Chakraborty and Sen (1958) and others (Srivastava and Chakraborty, 1962; Joshi and Kashyap, 1964). In the case of monoclinic crystals which involve 13 elastic constants, a given measurement of diffuse intensity depends in general on a number of elastic constants and hence reduces considerably the accuracy of evaluation of any individual constant. However the reciprocal lattice nodes and wave vectors have been carefully chosen only for those  $K$ -values which are associated with minimum number of elastic constants and they are given in Table I and II.

## THEORY

According to the classical theory of elasticity (Voigt, 1910) the elastic constants,  $C_{11}$ ,  $C_{12}$  etc. in the monoclinic system of crystals are given by the matrix

$$\begin{pmatrix}
 C_{11} & C_{12} & C_{13} & 0 & 0 & C_{16} \\
 & C_{22} & C_{23} & 0 & 0 & C_{26} \\
 & & C_{33} & 0 & 0 & C_{36} \\
 & & & C_{44} & C_{45} & 0 \\
 & & & & C_{55} & 0 \\
 & & & & & C_{66}
 \end{pmatrix}$$

where the frame of reference is the three orthogonal elastic axes in the crystal. The  $X$  and  $Z$  elastic axes coincide respectively with the  $c$  and  $b$  crystallographic axes, and the  $Y$  elastic axis completes the righthanded orthogonal axial system, thus making an acute angle with the axis of the monoclinic lattice.

The intensity of the first order thermal diffuse reflection in a direction from an element of reciprocal space has been found to be proportional to

$$K|f_1 f_2 f_3|_{hkl} = g_1^2 (A^{-1})_{11} + g_2^2 (A^{-1})_{22} + g_3^2 (A^{-1})_{33} + 2g_1 g_2 (A^{-1})_{12} \\ + 2g_2 g_3 (A^{-1})_{23} + 2g_3 g_1 (A^{-1})_{31}$$

where  $f_1, f_2, f_3$  are the direction cosines of the thermal wave vector and  $g_1, g_2, g_3$  are the direction cosines of the reciprocal lattice vector corresponding to the point  $hkl$  with respect to the elastic axes of the crystal, and  $(A^{-1})_{11}$  etc. are the elements of matrix inverse to the matrix  $A$  which is given by

$$\begin{pmatrix} A_{11} \\ A_{22} \\ A_{33} \\ A_{12} \\ A_{13} \\ A_{23} \end{pmatrix} = \begin{pmatrix} C_{11} & C_{66} & C_{55} & 0 & 0 & 2C_{16} \\ C_{66} & C_{22} & C_{44} & 0 & 0 & 2C_{26} \\ C_{55} & C_{44} & C_{33} & 0 & 0 & 2C_{35} \\ C_{16} & C_{26} & C_{45} & 0 & 0 & (C_{12} + C_{66}) \\ 0 & 0 & 0 & (C_{36} + C_{45}) & (C_{13} + C_{55}) & 0 \\ 0 & 0 & 0 & (C_{23} + C_{44}) & (C_{36} + C_{45}) & 0 \end{pmatrix} \begin{pmatrix} f_1^2 \\ f_2^2 \\ f_3^2 \\ f_2 f_3 \\ f_3 f_1 \\ f_1 f_2 \end{pmatrix}$$

It is evident from Table I that the elastic constants  $C_{55}$ ,  $C_{44}$  and  $C_{33}$  can be determined independently from the observed values of  $K[100]_{oko}$ ,  $K[010]_{oko}$  and  $K[001]_{oko}$ . By substituting the values of  $C_{55}$  and  $C_{44}$  in the expression for  $K[001]_{hoo}$ ,  $K[001]_{ool}$  and  $K[001]_{hol}$ ,  $C_{45}$  can be evaluated. The constants,  $C_{44}$ ,  $C_{45}$  and  $C_{55}$ , when substituted in  $K[001]_{hko}$ , would also give  $C_{33}$ . From  $K[100]_{hoo}$ ,  $K[100]_{ho1}$  and  $K[100]_{ool}$  three first degree equations in terms of  $C_{11}$ ,  $C_{16}$  and  $C_{66}$  can be obtained, and by solving them the constants can be found as follows :

$$C_{11} = K[100]_{hoo} \begin{vmatrix} g_1^2 & -2g_1 g_2 \\ \sin^2 \beta & 2 \sin \beta \cos \beta \end{vmatrix} / \Delta$$

$$C_{66} = \begin{vmatrix} g_1^2 & -2g_1 g_2 \\ \sin^2 \beta & 2 \sin \beta \cos \beta \end{vmatrix} \begin{vmatrix} -2g_1 g_2 & g_2^2 - K[100]_{ho1} \\ 2 \sin \beta \cos \beta & \cos^2 \beta - K[100]_{ool} \end{vmatrix} / \Delta$$

$$C_{16} = \begin{vmatrix} g_1^2 & -2g_1 g_2 \\ \sin^2 \beta & 2 \sin \beta \cos \beta \end{vmatrix} \begin{vmatrix} g_2^2 - K[100]_{ho1} & g_1^2 \\ \cos^2 \beta - K[100]_{ool} & \sin^2 \beta \end{vmatrix} / \Delta$$





where the frame of reference is the three orthogonal elastic axes in the crystal. The  $X$  and  $Z$  elastic axes coincide respectively with the  $c$  and  $b$  crystallographic axes, and the  $Y$  elastic axis completes the righthanded orthogonal axial system, thus making an acute angle with the axis of the monoclinic lattice.

The intensity of the first order thermal diffuse reflection in a direction from an element of reciprocal space has been found to be proportional to

$$K[f_1 f_2 f_3]_{hkl} = g_1^2 (A^{-1})_{11} + g_2^2 (A^{-1})_{22} + g_3^2 (A^{-1})_{33} + 2g_1 g_2 (A^{-1})_{12} + 2g_2 g_3 (A^{-1})_{23} + 2g_3 g_1 (A^{-1})_{31}$$

where  $f_1, f_2, f_3$  are the direction cosines of the thermal wave vector and  $g_1, g_2, g_3$  are the direction cosines of the reciprocal lattice vector corresponding to the point  $hkl$  with respect to the elastic axes of the crystal, and  $(A^{-1})_{11}$  etc. are the elements of matrix inverse to the matrix  $A$  which is given by

$$A = \begin{pmatrix} A_{11} & A_{12} & A_{13} \\ A_{22} & A_{23} & A_{24} \\ A_{33} & A_{34} & A_{35} \end{pmatrix} = \begin{pmatrix} C_{11} & C_{16} & 0 \\ C_{16} & C_{26} & 0 \\ C_{55} & C_{45} & 0 \\ C_{66} & C_{46} & 0 \\ 0 & 0 & 0 \\ 0 & 0 & 0 \end{pmatrix} \begin{pmatrix} f_1^2 \\ f_2^2 \\ f_3^2 \\ f_2 f_3 \\ f_3 f_1 \\ f_1 f_2 \end{pmatrix}$$

It is evident from Table I that the elastic constants  $C_{55}$ ,  $C_{44}$  and  $C_{33}$  can be determined independently from the observed values of  $K[100]_{oko}$ ,  $K[010]_{oko}$  and  $K[001]_{oko}$ . By substituting the values of  $C_{55}$  and  $C_{44}$  in the expression for  $K[001]_{hoo}$ ,  $K[001]_{ool}$  and  $K[001]_{hko}$ ,  $C_{45}$  can be evaluated. The constants,  $C_{44}$ ,  $C_{45}$  and  $C_{55}$ , when substituted in  $K[001]_{hko}$ , would also give  $C_{33}$ . From  $K[100]_{hoo}$ ,  $K[100]_{hoi}$  and  $K[100]_{ool}$  three first degree equations in terms of  $C_{11}$ ,  $C_{16}$  and  $C_{66}$  can be obtained, and by solving them the constants can be found as follows :

$$C_{11} = K[100]_{hoo} \begin{vmatrix} g_1^2 & -2g_1 g_2 \\ \sin^2 \beta & 2 \sin \beta \cos \beta \end{vmatrix} / \Delta$$

$$C_{66} = \begin{vmatrix} g_1^2 & -2g_1 g_2 \\ \sin^2 \beta & 2 \sin \beta \cos \beta \end{vmatrix} \begin{vmatrix} -2g_1 g_2 & g_2^2 - K[100]_{hoi} \\ 2 \sin \beta \cos \beta & \cos^2 \beta - K[100]_{ool} \end{vmatrix} / \Delta$$

$$C_{16} = \begin{vmatrix} g_1^2 & -2g_1 g_2 \\ \sin^2 \beta & 2 \sin \beta \cos \beta \end{vmatrix} \begin{vmatrix} g_2^2 - K[100]_{hoi} & g_1^2 \\ \cos^2 \beta - K[100]_{ool} & \sin^2 \beta \end{vmatrix} / \Delta$$

TABLE I  
K-values in the monoclinic system;  $\beta$  = monoclinic angle.

Direction Cosines of Wave Vectors	Indices of the planes using $b$ axis as the unique axis, and direction cosines of the reciprocal lattice vector				
	$hkl \rightarrow$	$hoo$	$oko$	$ool$	$hko$
$[f_1 f_2 f_3]$	$g_1, g_2, g_3 \rightarrow$	$[010]$	$[001]$	$[\sin \beta, -\cos \beta, 0]$	$[0, g_2, g_3]$
$[100]$		$\frac{C_{11}}{C_{11}C_{66}-C_{16}^2}$	$\frac{1}{C_{55}}$	$\frac{C_{66}\sin^2\beta + C_{11}\cos^2\beta + 2C_{16}\sin\beta\cos\beta}{C_{11}C_{66}-C_{16}^2}$	$\frac{g_1^2C_{11}-2g_1g_2C_{16}}{C_{11}C_{66}-C_{16}^2}$
$[010]$		$\frac{C_{66}}{C_{66}C_{22}-C_{26}^2}$	$\frac{1}{C_{14}}$	$\frac{C_{22}\sin^2\beta + C_{66}\cos^2\beta + 2C_{16}\sin\beta\cos\beta}{C_{66}C_{22}-C_{26}^2}$	$\frac{g_1^2C_{22}+g_2^2C_{66}-2g_1g_2C_{26}}{C_{66}C_{22}-C_{26}^2}$
$[001]$		$\frac{C_{55}}{C_{55}C_{44}-C_{45}^2}$	$\frac{1}{C_{33}}$	$\frac{C_{44}\sin^2\beta + C_{55}\cos^2\beta + 2C_{45}\sin\beta\cos\beta}{C_{55}C_{44}-C_{45}^2}$	$\frac{g_1^2C_{44}+g_2^2C_{55}-2g_1g_2C_{45}}{C_{55}C_{44}-C_{45}^2}$

TABLE II  
K-values in the monoclinic system

Direction Cosines of Wave Vectors	Indices of the planes using $b$ axis as the unique axis, and direction cosines of the reciprocal lattice vector			
	$hkl \rightarrow$	$hoo$	$oko$	$hol$
	$q_1 g_2 g_3 \rightarrow$	$[010]$	$[001]$	$[g_1, g_2, 0]$
$\begin{bmatrix} 1 & 1 & 1 \\ \sqrt{2} & \sqrt{2} & 0 \end{bmatrix}$	$2(C_{11} + C_{66} + 2C_{16})$	$\Delta_1$	$2$	$2\{g_1^2(C_{66} + C_{33} + 2C_{36}) + g^2(C_{11} + C_{66} + 2C_{16}) - 2g_1 g_2(C_{16} + C_{36} + C_{12} + C_{66})\}$
		$(C_{55} + C_{44} + 2C_{45})$		$\Delta_1$
$\begin{bmatrix} 1 & 1 & 1 \\ 0 & \sqrt{2} & \sqrt{2} \end{bmatrix}$	$2\{(C_{66} + C_{55})(C_{44} + C_{33}) - (C_{36} + C_{45})^2\}$	$\Delta_2$	$2\{(C_{66} + C_{55})(C_{22} + C_{44}) - (C_{36} + C_{45})^2\}$	$2\{g_1^2(C_{22} + C_{44})(C_{11} + C_{33}) - (C_{23} + C_{44})^2 - g^2(C_{66} + C_{55})(C_{11} + C_{33}) - (C_{36} + C_{45})^2 - g_1 g_2(C_{36} + C_{45})(C_{23} + C_{44}) - (C_{36} + C_{45})(C_{23} + C_{44})\}$
		$\Delta_2$		$\Delta_2$
$\begin{bmatrix} 1 & 0 & 1 \\ \sqrt{2} & \sqrt{2} & \sqrt{2} \end{bmatrix}$	$2\{(C_{11} + C_{55})(C_{33} + C_{44}) - (C_{13} + C_{55})^2\}$	$\Delta_3$	$2\{(C_{11} + C_{55})(C_{33} + C_{44}) - (C_{16} + C_{45})^2\}$	$2\{g_1^2\{(C_{66} + C_{44})(C_{55} + C_{33}) - (C_{36} + C_{45})^2\} - g^2\{(C_{11} + C_{55})(C_{33} + C_{44}) - (C_{13} + C_{55})^2\} - 2g_1 g_2\{(C_{13} + C_{55})(C_{36} + C_{45}) - (C_{16} + C_{45})(C_{55} + C_{33})\}$
		$\Delta_3$		$\Delta_3$

$$\Delta_1 = \{(C_{11} + C_{66} + 2C_{16})(C_{66} + C_{22} + 2C_{26}) - (C_{16} + C_{26} + C_{12} + C_{66})^2\}$$

$$\Delta_2 = \{(C_{66} + C_{55})(C_{44} + C_{33}) - (C_{66} + C_{55})(C_{22} + C_{44}) - (C_{36} + C_{45})^2 - (C_{26} + C_{33})^2 - 2(C_{26} + C_{45})(C_{36} + C_{45})(C_{22} + C_{44}) - (C_{36} + C_{45})^2 - (C_{22} + C_{44})\}$$

$$\Delta_3 = \{(C_{11} + C_{55})(C_{66} + C_{44})(C_{55} + C_{33}) - (C_{11} + C_{55})(C_{16} + C_{45})^2 - (C_{11} + C_{55})(C_{13} + C_{45}) - (C_{13} + C_{45})^2 - (C_{66} + C_{44})\}$$

where

$$\Delta = K[100]_{h00} \begin{vmatrix} 2g_1g_2 & g_2^2 - K[100]_{hol} & g_1^2 - 2g_1g_2 \\ 2 \sin \beta \cos \beta & \cos^2 \beta - K[100]_{ool} & \sin^2 \beta - 2 \sin \beta \cos \beta \\ g_2^2 - K[100]_{hol} & g_1^2 & \cos^2 \beta - K[100]_{ool} \\ & & \sin^2 \beta \end{vmatrix}$$

Having obtained the value of  $C_{66}$ , the constants  $C_{22}$  and  $C_{26}$  can be easily evaluated with the help of  $K[010]_{hol}$ ,  $K[010]_{ool}$  and  $K[010]_{hoo}$  as follows :

$$C_{22} = \frac{C_{66}(g_1g_2 K[010]_{hoo} + \sin \beta \cos \beta K[010]_{hol})}{g_1 \sin \beta K[010]_{hoo}(g_1 \cos \beta + g_2 \sin \beta)} - \frac{C_{66} g_2 \cos \beta}{g_1 \sin \beta}$$

$$C_{26} = \frac{C_{66}(g_1^2 K[010]_{ool} - \sin^2 \beta K[010]_{hol})}{2 \sin \beta g_1 K[010]_{hoo}(g_2 \sin \beta + g_1 \cos \beta)} - \frac{C_{66}(g_1 \cos \beta - g_2 \sin \beta)}{2g_1 \sin \beta}$$

These two constants can also be determined from the two equations derived by associating  $K[010]_{ool}$  with  $K[010]_{hko}$  and  $K[010]_{hol}$  with  $K[010]_{hko}$ . The value of  $C_{12}$  is derivable from the relation,

$$\frac{K \left[ \frac{1}{\sqrt{2}} \quad \frac{1}{\sqrt{2}} \quad 0 \right]_{hol}}{K \left[ \frac{1}{\sqrt{2}} \quad \frac{1}{\sqrt{2}} \quad 0 \right]_{hoo}} = \frac{\{g_1^2(C_{66} + C_{22} + 2C_{26}) + g_2^2(C_{11} + C_{66} + 2C_{16}) - 2g_1g_2(C_{16} + C_{26} + C_{12} + C_{66})\}}{(C_{11} + C_{66} + 2C_{16})}$$

if all the other constants in it are known earlier.

This can also be obtained by linking  $K \left[ \frac{1}{\sqrt{2}} \quad \frac{1}{\sqrt{2}} \quad 0 \right]_{hoo}$  with

$K \left[ \frac{1}{\sqrt{2}} \quad \frac{1}{\sqrt{2}} \quad 0 \right]_{oko}$  or  $K \left[ \frac{1}{\sqrt{2}} \quad \frac{1}{\sqrt{2}} \quad 0 \right]_{okv}$  with  $K \left[ \frac{1}{\sqrt{2}} \quad \frac{1}{\sqrt{2}} \quad 0 \right]_{ool}$ . From the

ratio of  $K \left[ 0 \quad \frac{1}{\sqrt{2}} \quad \frac{1}{\sqrt{2}} \right]_{hoo}$  and  $K \left[ 0 \quad \frac{1}{\sqrt{2}} \quad \frac{1}{\sqrt{2}} \right]_{oko}$  we obtain the relation,

$$\frac{K \left[ 0 \quad \frac{1}{\sqrt{2}} \quad \frac{1}{\sqrt{2}} \right]_{hoo}}{K \left[ 0 \quad \frac{1}{\sqrt{2}} \quad \frac{1}{\sqrt{2}} \right]_{oko}} = \frac{(C_{66} + C_{55})(C_{44} + C_{33}) - (C_{36} + C_{45})^2}{(C_{66} + C_{55})(C_{22} + C_{44}) - (C_{26} + C_{45})^2}$$

and when the known values of  $C_{66}$ ,  $C_{44}$ ,  $C_{45}$ ,  $C_{26}$  and  $C_{55}$  are substituted, a second degree equation giving two values of  $C_{36}$  is obtained. Similarly, dividing

$K \begin{bmatrix} 1 & 1 \\ \sqrt{2} & \sqrt{2} \end{bmatrix}_{hol}$  by  $K \begin{bmatrix} 0 & -1 \\ \sqrt{2} & \sqrt{2} \end{bmatrix}_{oko}$  two values of  $C_{23}$  are available.

Therefore, the above two constants can be determined uniquely by comparing the value of  $\Delta_2$ , as obtained from  $K \begin{bmatrix} 0 & -1 \\ \sqrt{2} & \sqrt{2} \end{bmatrix}_{oko}$  with that calculated from its general expression using different combinations of the possible values of  $C_{36}$  and  $C_{23}$ . The only constant that is left now is  $C_{13}$  and this can be ascertained from the common value of the two pairs of values obtained by solving the two independent second degree equation in  $C_{13}$  derived from the ratios

$$\begin{aligned} & K \begin{bmatrix} 1 & 0 & 1 \\ \sqrt{2} & \sqrt{2} \end{bmatrix}_{hol} \quad \text{and} \quad K \begin{bmatrix} 1 & 0 & 1 \\ \sqrt{2} & \sqrt{2} \end{bmatrix}_{hoo} \\ & K \begin{bmatrix} 1 & 0 & 1 \\ \sqrt{2} & \sqrt{2} \end{bmatrix}_{oko} \quad K \begin{bmatrix} 1 & 0 & 1 \\ \sqrt{2} & \sqrt{2} \end{bmatrix}_{oko} \end{aligned}$$

the expressions for which can be obtained from Table II.

The accurate determination of the elastic constants from the study of diffuse X-ray reflections, specially when the photographic technique is applied, is limited by the errors involved in the measurements of intensities. In the present case maximum accuracy is attainable only in the evaluation of  $C_{44}$  and  $C_{55}$ . The measurement of  $K(001)_{oko}$ , which involves same direction cosines for the wave vector as well as the reciprocal lattice vector, is not likely to provide an accurate value of  $C_{33}$ . Inaccuracy in the estimation of each of the other constants depends on the number of predetermined elastic constants required for its computation. The method of evaluation of all the 13 elastic constants discussed above is being utilised for finding the constants of a few crystals.

#### ACKNOWLEDGEMENT

The authors wish to express their gratitude to Prof. K. Banerjee, D.Sc., F.N.I., for his keen interest and encouragement during the progress of the work. They have great pleasure to thank Sri B. Mukherjee for help in calculation and discussions.

#### REFERENCES

- Chakraborty, S. C., and Sen, R. K., 1958, Proceeding of the Symposium of Crystal Physics, *Nat. Inst. Sci. Ind. Bulletin* No. 14, 20-35.  
 Joshi, S. K. and Kashyap, B. M. S., 1964, *Acta Cryst.*, **17**, 629.  
 Srivastava R. C., and Chakraborty S. C., 1962, *J. Phys. Soc. of Japan*, **17**, 1760.  
 Wooster, W. A., 1962, *Diffuse X-ray Reflection from Crystals*, Oxford University Press, London.

# LIGAND FIELD THEORY OF MAGNETIC SUSCEPTIBILITY AND ANISOTROPY IN $\text{CoSiF}_6 \cdot 6\text{H}_2\text{O}$

A. BOSE, L. C. JACKSON\* AND R. RAI

DEPARTMENT OF MAGNETISM,

INDIAN ASSOCIATION FOR THE CULTIVATION OF SCIENCE,

JADAVPUR, CALCUTTA 32

(Received November 27, 1964)

**ABSTRACT.** We have derived an expression for the principal ionic magnetic susceptibilities  $K_z$  ( $\parallel$  or  $\perp$ ) along and perpendicular to the trigonal axis of  $\text{CoSiF}_6 \cdot 6\text{H}_2\text{O}$  crystal, on the basis of molecular orbital theory of Stevens (1953), Bose *et al* (1960) and compared this with the experimental results by one of us (L.C.J.) The anisotropic reduction in spin-orbit coupling coefficient is due to the overlap of  $\text{Co}^{2+}$   $d$ -charge clouds with  $s$ - and  $p$ -ligand charge clouds. The increase in trigonal field coefficient  $\Delta$  below  $90^\circ\text{K}$  is due to thermal expansion or relaxation effects but the large decrease in the region of  $250^\circ\text{K}$  appears to be due to some kind of phase transition reversible in character, evidence for which is available from some of the recent measurements between  $90^\circ\text{K}$  to  $300^\circ\text{K}$  in our laboratory.

## INTRODUCTION

An octahedral field of the type  $O_h$  splits up the ground state  $3d^7\ ^4F$  of free  $\text{Co}^{2+}$  into two triplets  $^4T_1$ ,  $^4T_2$  and a singlet  $^4A_2$  of successively increasing energies, the overall separation being  $\sim 21000\text{ cm}^{-1}$  (Abragam and Pryce, 1951). There is another term  $^4T_1(^4P)$  coming out of the same configuration  $3d^7$  of the free ion which lies above  $^4T_1(F)$  at about  $19,800\text{ cm}^{-1}$  in the crystal (Abragam and Pryce, 1951). Abragam and Pryce (1951) have given a theory of the  $\text{Co}^{2+}$  ion in a cubic field with a small tetragonal or trigonal component to explain the paramagnetic resonance data on  $\text{Co}^{2+}$  Tutton salts and  $\text{CoSiF}_6 \cdot 6\text{H}_2\text{O}$  (Bleaney and Ingram, 1951). The effect of admixture of excited  $^4T_1(P)$ ,  $^4A_2$ ,  $^4T_2$  levels upon the lowest  $^4T_1(F)$  level in this theory, has been included through the orbital Landé  $g$  factors  $\alpha$ ,  $\alpha'$  ( $\parallel$  or  $\perp$  respectively, to the trigonal or tetragonal symmetry axis as the case may be of the  $\text{Co}^{2+}$  ion), which are appreciably different from the free ion value  $3/2$  for  $F$  state, Bose *et al* (1961) have used this theory to explain the magnetic susceptibilities of  $\text{Co}^{2+}$  Tutton salts, without introducing the effect of the overlap between the  $3d$ -orbitals of  $\text{Co}^{2+}$  and the  $s$ - and  $p$ -orbitals of the ligand atoms. In the present paper while deriving the expressions for magnetic susceptibility and

\*Address:—L. C. Jackson, Royal Military College, Kingston, Ontario, Canada.

anisotropy of the trigonally distorted  $\text{Co}^{2+}$ ,  $6\text{H}_2\text{O}$  complex the more general molecular orbital approach is followed. The susceptibility measurements of one of us (L.C.J.) on  $\text{CoSiF}_6 \cdot 6\text{H}_2\text{O}$  in the range 300 K to 1.67°K, have been used to evaluate the theoretical parameters. The salt is isomorphous to the hydrated  $\text{Fe}^{2+}$ ,  $\text{Ni}^{2+}$  and  $\text{Cu}^{2+}$  fluosilicates and is of trigonal symmetry (space gr.  $\text{C}_{3i}^2$ , Pauling 1930), with a single trigonally distorted  $[\text{Co}^{2+}, 6\text{H}_2\text{O}]$  octahedral complex in the unit cell, so that the principal ionic susceptibilities  $K_i$  ( $i = \parallel$  or  $\perp$  to the trigonal axis of the ion) are identical with the measured values  $\chi_i$  (principal gm. molecular susceptibilities) of the crystal, corrected for diamagnetism.

#### MOLECULAR ORBITAL THEORY OF TRIGONALLY DISTORTED ( $\text{Co}^{2+}$ , $6\text{H}_2\text{O}$ ) COMPLEXES

##### (a) The cubic field orbitals of ( $\text{Co}^{2+}$ , $6\text{H}_2\text{O}$ )

$\text{Co}^{2+}$  ion can be considered as a system consisting of three  $d$ -holes in the  $3d$  subshell and the several states  ${}^4T_1(F)$ ,  ${}^1T_2(F)$ ,  ${}^1A_2(F)$  and  ${}^3T_1(P)$  arise out of  $\{[(t_{2g})^1(e_g)^2]$ ,  $[(t_{2g})^2(e_g)^1]$ ,  $[(t_{2g})^3]$  and  $[(e_g)^1(t_{2g})^2]$  configurations respectively. The determinantal wave functions for the lowest triplet  ${}^1T_1(F)$  (considering only the orbital part) can be written as

$$\left. \begin{aligned} \psi_1 &= |e_a e_b t_a| \\ \psi_2 &= |e_a e_b t_b| \\ \psi_3 &= |e_a e_b t_c| \end{aligned} \right\} \quad \dots (1)$$

which are inclusive of the overlap of surrounding ligand  $s$ - and  $p$ -orbitals with central metal  $d$ -orbitals as given by

$$\left. \begin{aligned} t_a &= N \left[ d_{xy} + \frac{\lambda}{2} (\pi x_1 + \pi y_2 + \pi x_5 + \pi y_4) \right] \\ t_b &= N \left[ d_{yz} + \frac{\lambda}{2} (\pi x_2 + \pi y_3 + \pi x_6 + \pi y_5) \right] \\ t_c &= N \left[ d_{xz} + \frac{\lambda}{2} (\pi x_3 + \pi y_1 + \pi x_4 + \pi y_6) \right] \\ e_a &= N' \left[ dx^2 - y^2 + \frac{\lambda'}{2} (\sigma_1 + \sigma_3 - \sigma_2 - \sigma_5) \right] \\ e_b &= N' \left[ d3z^2 - r^2 + \frac{\lambda'}{2\sqrt{3}} (2\sigma_3 + 2\sigma_6 - \sigma_1 - \sigma_4 - \sigma_2 - \sigma_5) \right] \end{aligned} \right\} \quad \dots (2)$$



where  $N$ 's are normalizing constants  $\lambda$ 's are the amounts of admixtures of the  $s$ - and  $p$ -orbitals with the  $d$ -orbitals. Here all  $\sigma$ -bonds are described by using  $z$ -coordinates of the ligands and  $\pi$ -bonds by using  $x$  and  $y$  coordinates, all  $z$ -coordinates of the ligands pointing towards the metal atom (Van Vleck, 1935).

### (b) Trigonal orbitals

The appropriate trigonal orbital states for the lowest triplet of  $\text{Co}^{2+}$  complex on quantization along the trigonal axis, are

$$\left. \begin{aligned} |+\rangle &= \frac{1}{\sqrt{3}} [\omega |\psi_2\rangle + \omega^2 |\psi_3\rangle + |\psi_1\rangle] \\ |0\rangle &= \frac{1}{\sqrt{3}} [|\psi_2\rangle + |\psi_3\rangle + |\psi_1\rangle] \\ |-\rangle &= \frac{1}{\sqrt{3}} [\omega^2 |\psi_2\rangle + \omega |\psi_3\rangle + |\psi_1\rangle] \end{aligned} \right\} \quad (3)$$

where  $\omega = \exp\left(\frac{2\pi i}{3}\right)$  and  $\psi_1$  etc., are given by (1). The overlap of the surrounding ligand  $s$ - and  $p$ -orbitals with the central  $d$ -orbitals introduces two orbital reduction factors. (Griffiths, 1961) (i)  $\kappa$  within a manifold of  $t_{2g}$  orbitals (ii)  $\kappa'$  between a  $t_{2g}$  and  $e_g$  manifold. On actual calculation it is seen that so long as we are confined only to  ${}^4T_1(F)$  state of  $\text{Co}^{2+}$ , only the factor  $\kappa$  is of importance. Also in consequence of this the anisotropic reduction in  $\zeta_i$  ( $i = \parallel$  or  $\perp$  to the trigonal axis of the ion) the spin-orbit coupling parameter, from its free ion value, is mainly due to the overlap of  $p$ -orbitals with the  $d$ -orbitals.

### FINE STRUCTURE

The three states  $|+\rangle, |0\rangle, |-\rangle$  behave as the three orbital components of atomic  ${}^4P$  state with  $l_s' = 1, 0, -1$  respectively. The appropriate Hamiltonian for the lowest triplet state is (Bose *et al*, 1960, 1964)

$$H = V_{trig} - \alpha U_{\xi} S_{\xi} - \alpha' (U_{\xi} S_{\xi} + U_{\eta} S_{\eta}) \quad (4)$$

where  $\xi$  is a coordinate (not to be confused with  $\zeta_i$  spin-orbit coupling) along the trigonal axis of the crystal and  $\xi, \eta, \zeta$  form a mutually orthogonal right handed set of coordinates.

Operating with the above Hamiltonian upon the effective  ${}^4P$ -term and solving we get the eigen-values as follows :

$$\left. \begin{aligned} E_1 &= \alpha \zeta_{||} \cdot x_1 \\ E_2 &= \alpha \zeta_{||} \cdot x_2 \\ E_3 &= \frac{1}{2} [(\Delta - \frac{1}{2} \alpha \zeta_{||}) - \{(\Delta + \frac{1}{2} \alpha \zeta_{||})^2 + 6\alpha'^2 \zeta_{\perp}^2\}^{\frac{1}{2}}] \\ E_4 &= -\frac{3}{2} \alpha \zeta_{||} \\ E_5 &= \frac{1}{2} [(\Delta + \frac{1}{2} \alpha \zeta_{||}) + \{(\Delta + \frac{1}{2} \alpha \zeta_{||})^2 + 6\alpha'^2 \zeta_{\perp}^2\}^{\frac{1}{2}}] \\ E_6 &= \alpha \zeta_{||} \cdot x_6 \end{aligned} \right\} \quad (5)$$

where  $x_1, x_2$  and  $x_6$  are the roots of the cubic eqn.

$$x^3 - x^2(2+\delta) + \left(2\delta + \frac{3}{4} - \frac{7}{2} \rho^2\right) x - \frac{3}{4} \delta + \frac{15}{4} \rho^2 = 0$$

where

$$\delta = \frac{\Delta}{\alpha \zeta_{||}} \quad , \quad \rho = \frac{\alpha' \zeta_{\perp}}{\alpha \zeta_{||}}$$

$\Delta$  is the trigonal field separation between the split components (a doublet and a singlet) of the ground triplet  ${}^4T_1$ . The corresponding eigenstates are :

$$\left. \begin{aligned} \phi_1 &= a_1 | -1, \frac{3}{2} \rangle + b_1 | 0, \frac{1}{2} \rangle + c_1 | 1, -\frac{1}{2} \rangle \\ \phi_{1-} &= a_1 | 1, -\frac{3}{2} \rangle + b_1 | 0, -\frac{1}{2} \rangle + c_1 | -1, \frac{1}{2} \rangle \\ \phi_2 &= a_2 | -1, \frac{3}{2} \rangle + b_2 | 0, \frac{1}{2} \rangle + c_2 | 1, -\frac{1}{2} \rangle \\ \phi_{2-} &= a_2 | 1, -\frac{3}{2} \rangle + b_2 | 0, -\frac{1}{2} \rangle + c_2 | -1, \frac{1}{2} \rangle \\ \phi_3 &= a_3 | 0, \frac{3}{2} \rangle + b_3 | 1, \frac{1}{2} \rangle \\ \phi_{3-} &= a_3 | 0, -\frac{3}{2} \rangle + b_3 | -1, -\frac{1}{2} \rangle \\ \phi_4 &= | 1, \frac{3}{2} \rangle \\ \phi_{4-} &= | -1, -\frac{3}{2} \rangle \\ \phi_5 &= a_5 | 0, \frac{3}{2} \rangle + b_5 | 1, \frac{1}{2} \rangle \\ \phi_{5-} &= a_5 | 0, -\frac{3}{2} \rangle + b_5 | -1, -\frac{1}{2} \rangle \\ \phi_6 &= a_6 | -1, \frac{3}{2} \rangle + b_6 | 0, \frac{1}{2} \rangle + c_6 | 1, -\frac{1}{2} \rangle \\ \phi_{6-} &= a_6 | 1, \frac{3}{2} \rangle + b_6 | 0, -\frac{1}{2} \rangle + c_6 | -1, \frac{1}{2} \rangle \end{aligned} \right\} \quad \dots \quad (6)$$

where

$$\begin{aligned}
 a_i &= \frac{\sqrt{\frac{3}{2}} \alpha' \zeta_{\perp}}{\frac{3}{2} \alpha \zeta_{\parallel} - E_i} \cdot b_i \\
 c_i &= \frac{\sqrt{2} \alpha' \zeta_{\perp}}{\frac{3}{2} \alpha \zeta_{\parallel} - E_i} \cdot b_i \\
 a_i^2 + b_i^2 + c_i^2 &= 1, \quad i = 1, 2, 6. \\
 a_j &= \frac{\sqrt{\frac{3}{2}} \alpha' \zeta_{\perp}}{\Delta - E_j} b_j \\
 a_j^2 + b_j^2 &= 1, \quad j = 3, 5.
 \end{aligned} \tag{7}$$

The energy values are formally the same as in our earlier paper (Bose *et al.*, 1961) except that in the present the spin-orbit coupling coefficient in crystal is necessarily anisotropic and the effect of covalency overlap is automatically introduced in the wavefunctions operated upon by the Hamiltonian (eqn. 4).

#### EXPRESSION FOR SUSCEPTIBILITY

Calculating the effect of the magnetic perturbations  $\beta H(L+2S)$ , upto the second order, we get the expressions for principal magnetic susceptibility  $K_i$  ( $i = \parallel$  or  $\perp$  to the trigonal axis of the crystal).

In the present case these are :

$$\begin{aligned}
 K_{\parallel} &= \frac{N\beta^2}{kW} \left[ \frac{1}{T} \left\{ \sum_{i=1,2,6} G_{1z}^i \exp \left( -\frac{E_i - E_1}{kT} \right) + \sum_{j=3,5} G_{1z}^j \exp \left( -\frac{E_j - E_1}{kT} \right) \right. \right. \\
 &+ 2(3 - \alpha \kappa_{\parallel}) \exp \left( -\frac{E_4 - E_1}{kT} \right) \left. \right\} + 2k \left\{ \sum_{i=1,2,6} \sum_{i', i \neq i'} \frac{S_{ii'}}{E_{i'} - E_i} \exp \left( -\frac{E_i - E_1}{kT} \right) \right. \\
 &+ 2(3a_3a_5 - \alpha k_{\parallel} b_3b_5 + b_3b_5) \left( \exp \left( -\frac{E_3 - E_1}{kT} \right) - \exp \left( -\frac{E_5 - E_1}{kT} \right) \right) \left. \right\} \right] \\
 K_{\perp} &= \frac{N\beta^2}{kW} \left[ \frac{1}{T} \left\{ \sum_{i=1,2,6} G_{1x}^i \exp \left( -\frac{E_i - E_1}{kT} \right) \right\} \right. + 2k \left\{ G_{2x}^1 + G_{2x}^2 \exp \left( -\frac{E_2 - E_1}{kT} \right) \right. \\
 &+ G_{2x}^3 \exp \left( -\frac{E_3 - E_1}{kT} \right) + G_{2x}^4 \exp \left( -\frac{E_4 - E_1}{kT} \right) \\
 &+ G_{2x}^5 \exp \left( -\frac{E_5 - E_1}{kT} \right) + G_{2x}^6 \exp \left( -\frac{E_6 - E_1}{kT} \right) \left. \right\} \left. \right] \tag{8}
 \end{aligned}$$

where

$$W = 2 \sum_{i=1} \exp \left( -\frac{E_i - E_1}{kT} \right)$$

$$\left. \begin{aligned} G_{1z}^1 &= \frac{1}{2} [ \{ 2(a_i^2 - c_i^2) \alpha \kappa_{11} + 6a_i^2 + 2b_i^2 - 2c_i^2 \} + \{ (3a_i^2 - c_i^2) v_1 + b_i^2 v_2 \\ &\quad + (\sqrt{6} a_i b_i - \sqrt{8} b_i c_i) v_3 \}^2 ] \\ G_{1z}^2 &= 2 [ -b_i^2 \alpha \kappa_{11} + 3a_j^2 + b_j^2 ]^2 \\ G_{1z}^3 &= \frac{1}{2} \left[ \left\{ -\frac{4\alpha' \kappa_{11}}{\sqrt{2}} b_i c_i + 4\sqrt{3} a_i c_i + 4b_i^3 \right\} \right. \\ &\quad \left. + \left\{ b_i^2 v_4 + c_i^2 v_5 + \sqrt{3} a_i c_i v_6 + \sqrt{2} b_i c_i v_7 \right\} \right]^2 \\ G_{2z}^1 &= \sum_{i=2,6} \frac{t_{11}}{E_i - E_1} + \sum_{j=3,5} \frac{u_{1j}}{E_j - E_1} \\ G_{2z}^2 &= \sum_{i=1,6} \frac{t_{21}}{E_i - E_2} + \sum_{j=3,5} \frac{u_{2j}}{E_j - E_2} \\ G_{2z}^3 &= \sum_{i=1,2,6} \frac{u_{i3}}{E_i - E_3} + \frac{v_3}{E_4 - E_3} \\ G_{2z}^4 &= \sum_{i=3,5} \frac{v_j}{E_j - E_4} \\ G_{2z}^5 &= \sum_{i=1,2,6} \frac{u_{i5}}{E_i - E_5} + \frac{v_5}{E_4 - E_5} \\ G_{2z}^6 &= \sum_{i=1,2} \frac{t_{i6}}{E_i - E_6} + \sum_{j=3,5} \frac{u_{6j}}{E_j - E_6} \end{aligned} \right\} \dots (9)$$

$$\left. \begin{aligned} S_{ii} &= 2 [ \alpha \kappa_{11} (a_i a_i - c_i c_i) + (3a_i a_i + b_i b_i - c_i c_i) ]^2 \\ t_{ii} &= 2 \left[ -\frac{\alpha' \kappa_{11}}{\sqrt{2}} (b_i c_i + b_i c_i) + (\sqrt{3} a_i c_i + 2b_i b_i + \sqrt{3} a_i c_i) \right]^2 \\ u_{ij} &= 2 \left[ -\frac{\alpha' \kappa_{11}}{\sqrt{2}} (a_i a_j + b_i b_j) + (\sqrt{3} a_j b_i + 2b_j c_i) \right]^2 \\ v_j &= 2 \left[ -\frac{\alpha' \kappa_{11}}{\sqrt{2}} a_j + \sqrt{3} b_j \right]^2 \end{aligned} \right\} \dots (10)$$

's' are as given by Abragam and Pryce (1951, page—182 eqn. 4.7)

## DISCUSSION OF EXPERIMENTAL RESULTS

 (a) *g-values*

It is not possible in the present instance to decide *a priori* from the *g*-values the sign of  $\Delta$ , without exhaustive trial and error fitting of susceptibility and anisotropy data, since for both positive or negative signs the ground energy level  $\phi_{1\pm}$  remains unaltered. With  $\Delta$  positive the next higher energy levels of sufficient importance are  $\phi_{2\pm}$ ,  $\phi_{3\pm}$ ,  $\phi_{4\pm}$ ,  $\phi_{5\pm}$  and  $\phi_{6\pm}$  in ascending order of energy, whereas, with  $\Delta$  negative these are  $\phi_{3\pm}$ ,  $\phi_{2\pm}$ ,  $\phi_{6\pm}$ ,  $\phi_{5\pm}$  and  $\phi_{4\pm}$ . For  $\text{CoSiF}_6 \cdot 6\text{H}_2\text{O}$  absorption bands have been observed at  $21000\text{ cm}^{-1}$  and  $18800\text{ cm}^{-1}$  which have been assigned to the transitions  ${}^4\text{T}_1(\text{F}) \rightarrow {}^4\text{A}_2$  and  ${}^4\text{T}_1(\text{F}) \rightarrow {}^4\text{T}_1(\text{P})$  (Abragam and Pryce 1951). It has been found that in order to fit both the experimental susceptibility and anisotropy values for the salts, with a reasonable set of parameters (see Table I) in the given range of temperatures, consistent with the above spectroscopic data,  $\Delta$  must be positive. For this, the energy level scheme is as given in equation (5) in correct order of increasing magnitude. The *g*-values are given by :

$$\left. \begin{aligned} g_{\parallel} &= 2\{2ak_{\parallel}(a^2 - c^2) + 3a^2 + b^2 + c^2\} \\ g_{\perp} &= 2\{-\sqrt{2bca'}k_{\perp} + 2\sqrt{3ac + 2b^2}\} \end{aligned} \right\} \dots (11)$$

Bleaney and Ingram's (1951) experiment at  $20.4^\circ\text{K}$  on  $\text{CoSiF}_6 \cdot 6\text{H}_2\text{O}$  diluted with  $\text{ZnSiF}_6 \cdot 6\text{H}_2\text{O}$  yields four sets of  $g_{\parallel}$  and  $g_{\perp}$  values

	$g_{\parallel}$	$g_{\perp}$
Main transition	5.80	3.44
Subsidiary transitions	6.60	2.62
	6.60	2.82
	3.58	4.09

Since the intensity of the lines of subsidiary groups remain unchanged due to further lowering of temperature, Abragam and Pryce (1951) interpret the extra lines to be due to the ground states of inequivalent cobalt ions situated at different lattice points, where crystal field was different in magnitude. The *g*-values at room temperature cannot be measured owing to very small spin lattice relaxation time. It is very interesting to note in this connection, that the undiluted salt  $\text{CoSiF}_6 \cdot 6\text{H}_2\text{O}$  shows a sharp break in the magnetic anisotropy and susceptibility curves in the liquid oxygen range at  $255^\circ\text{K}$  (Mazumdar and Datta, 1964). The crystals which are uniaxial above the transition temperature, start showing orthorhombic symmetry below that temperature. The transition is reversible with temperature except for a small thermal hysteresis loop formed in the region of  $250^\circ\text{K}$ — $260^\circ\text{K}$ . Repeated rapid cooling and heating in this region produces shattering and opacity of the crystal. The absorption spectra of this salt observed here (Mazumdar *et al* 1964) shows the incidence of two new peaks at  $20600$

$\text{cm}^{-1}$  and  $22200 \text{ cm}^{-1}$  below transition temperature in addition to the normal peaks at  $21000 \text{ cm}^{-1}$  and  $19800 \text{ cm}^{-1}$ . X-ray findings by one of our colleagues (Ray, 1964) are very interesting and show the simultaneous existence of a new pseudo-trigonal phase below  $250^\circ\text{K}$ , along with the original trigonal phase, retaining the original trigonal axis as common axis of both these phases. All these appear to indicate a change in phase of the crystal accompanied by possible change of symmetry of the crystal field. These detailed results are being published separately elsewhere. It will be found that  $g$ -values calculated from susceptibility at  $300^\circ\text{K}$  of the undiluted salt is close to those of the main phase of the diluted at  $20^\circ\text{K}$ , whereas at  $20^\circ\text{K}$  the values for the undiluted salt is close to those of the first two subsidiary phases of the diluted salt. Of course, the calculation for the undiluted salt from susceptibility can give only the average value of coexisting phases if any. More investigations on these salts are necessary to clarify the apparent similarity in transition behaviours in them.

(b) *Mean susceptibility and anisotropy values :*

Since a change in phase of the undiluted crystal occurs below  $255^\circ\text{K}$  and we lack as yet detailed structural data for the new coexisting phase apparently having orthorhombic magnetic symmetry, it would be difficult to give exact theoretical calculation of the field parameters to fit exactly the experimental observations. However, since the development of orthorhombicity is only about 5% of the original anisotropy and the original trigonal axis is still the main anisotropy axis of both the phases (Ray—1964), we may limit our discussions to an approximation which considers the mixed phase as a single crystal with trigonal symmetry. In other words, we may neglect the small orthorhombicity normal to the original trigonal axis developed below  $255^\circ\text{K}$ . The break in the susceptibility curve would then correspond to a large sudden change in the trigonal field separation  $\Delta$ , with the reservation inherent in the present approximation. However, in treating one of the coauthor's (Jackson) value of susceptibilities (measured at Bristol) taken at wide gaps of temperatures we cannot pay attention even to this break in the curve and for the present have to average out the variation through the temperature of transition. Fitting the theoretical parameters  $\Delta$ ,  $\alpha\zeta_{||}$ ,  $\alpha'\zeta_{||}$  and  $\alpha k_{||}$ ,  $\alpha'k_{||}$  by exhaustive trial and error with the mean susceptibility and anisotropy as usual, consistently with the optical absorption levels (Mazumdar *et al.*, 1964) we had to increase the trigonal field coefficient  $\Delta$  from a value of  $830 \text{ cm}^{-1}$  at  $1.67^\circ\text{K}$  to  $952 \text{ cm}^{-1}$  at  $90^\circ\text{K}$  and then decrease it to  $560 \text{ cm}^{-1}$  at  $290^\circ\text{K}$ ; the values for the other parameters which are considered as temperature independent to a first approximation are as given in the Table I.  $\alpha$ 's,  $\zeta$ 's and  $\kappa$ 's cannot be independently calculated owing to the product forms in which they appear in the equations.

In spite of the approximations involved the major fact about the anisotropic reduction of spin-orbit coupling due to  $3d$ -charge overlap with  $s$ - and  $p$ -ligand

charge clouds, and the general variation in  $\Delta$  with temperature due to lattice expansion and relaxation effects are prominently brought out in  $\text{Co}^{2+}$  fluosilicate. Without more structural data it is not possible to say whether the tendency for a maximum value of  $\Delta$  in the region of  $90^\circ\text{K}$  for the salt, is connected entirely with the phase transition or not, though this is very likely as indicated by the detailed anisotropy data in the liquid oxygen range taken by some of our co-workers to be published elsewhere.

TABLE I

Temperature variation of effective mean moment ( $\mu_{\text{eff}}$ ) and anisotropy ( $p_{\parallel}^2 - p_{\perp}^2$ ) of  $\text{CoSiF}_6 \cdot 6\text{H}_2\text{O}$

Temp $^\circ\text{C}$	$\Delta\text{cm}^{-1}$	$p_{\parallel}^2 - p_{\perp}^2$	$\mu_{\text{eff}}^2$	$g$ -values
290.4	525	10.06 (10.05)	25.06 (25.10)	$\left\{ \begin{array}{l} g_{\parallel} = 5.98 \\ \quad (5.80) \\ g_{\perp} = 3.37 \\ \quad (3.44) \end{array} \right.$
90.1	950	31.38 (31.34)	22.16 (22.19)	$\left\{ \begin{array}{l} g_{\parallel} = 6.90 \\ \quad (5.80) \\ \quad (6.6) \\ g_{\perp} = 2.42 \\ \quad (3.44) \\ \quad (2.62) \end{array} \right.$
20.4	880	33.81 (33.92)	17.62 (17.53)	
4.2	840	30.19 (30.25)	15.06 (15.06)	
1.67	830	29.60 (29.67)	14.60 (14.54)	

$$P_{\parallel} = \alpha' \zeta_{\parallel} = -170\text{cm}^{-1}$$

$$Q_{\parallel} = \alpha \kappa_{\parallel} = 1.21$$

$$P_{\perp} = \alpha' \zeta_{\perp} = -194\text{cm}^{-1}$$

$$Q_{\perp} = \alpha' \kappa_{\perp} = 1.39$$

Values in parentheses are the experimental values. Those for  $g$ 's within parantheses are for the diluted salt (Bleaney *et al*, 1951).

#### ACKNOWLEDGEMENT

Many valuable suggestions and discussions by our colleagues Dr. R. Chatterjee and U. S. Ghosh are gratefully acknowledged.

#### REFERENCES

- Abragam, A. and Pryce M. H. L., 1951, *Proc. Roy. Soc. A* **206**, 175.  
Bleaney, B. and Ingram D. J. E., 1951, *Proc. Roy. Soc. A* **206**, 143.

- Bose, A. Chakraborty, A. S. and Chatterjee R., 1960, *Proc. Roy. Soc.* **A255**, 145.  
-do- 1961, *Proc. Roy. Soc.* **A261**, 43.
- Bose, A Chatterjee, R. and Rai R., 1964, *Proc. Phys. Soc.* **83**, 959.
- Griffiths, J. S., 1961, *The Theory of Transition Metal Ions* Cambridge University Press  
page 284.
- Mazumdar, M. and Datta, S. K., 1964, *J. Chem. Phys.* (In course of publication)
- Pauling, L. C., 1930, *Zeits. f. Krist.* **72A**, 482.
- Ray, S., 1964, *Indian J. Phys.* **38**, 176.
- Stevens, K. W. H., 1953, *Proc. Roy. Soc.* **A219**, 542.
- Van Vleck, J. H., 1935, *J. Chem. Phys.* **3**, 807.



# ON THE DERIVATION OF THE COUPLED WAVE EQUATIONS IN THE MAGNETO-IONIC THEORY

S. K. BANERJEE

UNIVERSITY COLLEGE OF SCIENCE, CALCUTTA.

(Received November 4, 1964)

**ABSTRACT.** It has been shown that there exists ambiguity of sign in the coupled wave equations as deduced by Saha, Banerjee and Guha (1951). It has also been shown that the same ambiguity of sign appears when the coupled wave equations as given by Budden (1952) are expressed in the form given by Saha *et al.*

## INTRODUCTION

It has been shown in our previous paper (1964) that the coupled wave equations are given by :

$$\ddot{V}_1 + (q_x^2 - \phi_1^2) V_1 = 2\phi_1 \dot{W}_1 + \ddot{\phi}_1 \dot{W}_1 \text{ (for the X-mode)} \quad \dots (1)$$

$$\ddot{W}_1 + (q_0^2 - \phi_1^2) W_1 = -2\phi_1 \dot{V}_1 - \ddot{\phi}_1 V_1 \text{ (for the 0-mode)} \quad \dots (2)$$

$$\ddot{W}_2 + (q_x^2 - \phi_2^2) W_2 = -2\phi_2 \dot{V}_2 - \ddot{\phi}_2 V_2 \text{ (for the X-mode)} \quad \dots (1.1)$$

$$\ddot{V}_2 + (q_0^2 - \phi_2^2) V_2 = 2\phi_2 \dot{W}_2 + \ddot{\phi}_2 W_2 \text{ (for the 0-mode)} \quad \dots (2.1)$$

where,

$$V_1 = E_x \cos \phi_1 + jE_y \sin \phi_1 = \frac{E_x + j\rho_1 E_y}{\sqrt{1 + \rho_1^2}} \text{ (for the X-mode)} \quad \dots (3)$$

$$W_1 = -E_x \sin \phi_1 + jE_y \cos \phi_1 = \frac{-\rho_1 E_x + jE_y}{\sqrt{1 + \rho_1^2}} \text{ (for the 0-mode)} \quad \dots (4)$$

$$V_2 = E_x \cos \phi_2 + jE_y \sin \phi_2 = \frac{E_x + j\rho_2 E_y}{\sqrt{1 + \rho_2^2}} \text{ (for the 0-mode)} \quad \dots (4.1)$$

$$W_2 = -E_x \sin \phi_2 + jE_y \cos \phi_2 = \frac{-\rho_2 E_x + jE_y}{\sqrt{1 + \rho_2^2}} \text{ (for the X-mode)} \quad \dots (3.1)$$

$$\begin{aligned}
 q_1^2 &= 1 - \frac{r}{\beta' + \rho_1 \omega_z} = K_1 \cos^2 \phi_1 + K_2 \sin^2 \phi_1 - 2L \sin \phi_1 \cos \phi_1 \\
 q_0^2 &= 1 - \frac{r}{\beta' + \rho_2 \omega_z} = K_1 \cos^2 \phi_2 + K_2 \sin^2 \phi_2 - 2L \sin \phi_2 \cos \phi_2 \\
 q_0^2 &= 1 - \frac{r}{\beta' + \rho_2 \omega_z} = K_1 \sin^2 \phi_1 + K_2 \cos^2 \phi_1 + 2L \sin \phi_1 \cos \phi_1 \\
 q_2^2 &= 1 - \frac{r}{\beta' + \rho_1 \omega_z} = K_1 \sin^2 \phi_2 + K_2 \cos^2 \phi_2 + 2L \sin \phi_2 \cos \phi_2
 \end{aligned} \quad \dots (5)$$

$$\begin{aligned}
 \rho_1 &= \tan \phi_1 = G - \sqrt{1 + G^2} \\
 \rho_2 &= \tan \phi_2 = G + \sqrt{1 + G^2}
 \end{aligned} \quad \dots (6)$$

$$\dot{\phi}_1 = \frac{\partial \rho_1 / \partial u}{1 + \rho_1^2}, \quad \dot{\phi}_2 = \frac{\partial \rho_2 / \partial u}{1 + \rho_2^2}, \quad u = \frac{2\pi}{\lambda} z \quad \dots (7)$$

$$G = \frac{K_1 - K_2}{2L} = \frac{\omega_z^2}{2\omega_z(r - \beta')}$$

$$K_1 = 1 - \frac{\beta'^2 - r\beta' - \omega_z^2}{C'} r, \quad K_2 = 1 - \frac{r(\beta'^2 - r\beta')}{C'}$$

$$L = \frac{r(r - \beta')\omega_z}{C'}, \quad C' = \beta'(\beta'^2 - \omega_z^2) - r(\beta'^2 - \omega_z^2)$$

$$\omega_s = \omega \sin \theta, \quad \omega_z = \omega \cos \theta, \quad \omega = p_H / p, \quad p_H = eH / mc$$

$$\beta' = 1 - j \frac{v}{p}, \quad r = \frac{p_0^2}{p^2} = \frac{4\pi N e^2}{m p^2}$$

$$\dot{V} = \frac{dV}{du}, \quad \dot{W} = \frac{dW}{du}$$

#### AMBIGUITY OF SIGN IN THE COUPLED WAVE EQUATIONS OF SAHA *et al.*

Using (6), (4), (4.1), and (6), (3), (3.1) we have :

$$\begin{aligned}
 V_1 &= \pm W_2 \\
 W_1 &= \pm V_2
 \end{aligned} \quad \dots (8)$$

From eqn. (8) we can make the following combinations :

$$\begin{pmatrix} V_1 = W_2 \\ W_1 = V_2 \end{pmatrix} \quad \dots \quad (8.1)$$

$$\begin{pmatrix} V_1 = -W_2 \\ W_1 = -V_2 \end{pmatrix} \quad \dots \quad (8.2)$$

$$\begin{pmatrix} V_1 = W_2 \\ W_1 = -V_2 \end{pmatrix} \quad \dots \quad (8.3)$$

$$\begin{pmatrix} V_1 = -W_2 \\ W_1 = V_2 \end{pmatrix} \quad \dots \quad (8.4)$$

It can be easily shown from (6) that

$$\phi_2 - \phi_1 = n \frac{\pi}{2} \quad \dots \quad (9)$$

where

$$n = 0, \pm 1, \pm 2, \pm 3 \dots$$

For

$$n = 0$$

$$\phi_2 = \phi_1 \quad \dots \quad (9.1)$$

Using (9.1) and (5) it can be shown that the electron number density  $N$  must be zero. Similarly for  $n = \pm 2, \pm 4, \pm 6 \dots$  using (5) and (9) we get  $N = 0$ . We can therefore exclude the cases  $n = 0, \pm 2, \pm 4 \dots$ . However for  $n = \pm 1, \pm 3 \dots$  eqns (5) are satisfied by (9). It can be shown using (3), (3.1), (4), (4.1) and (9) that we can take the combination (8.1) only when the following two equations hold good *simultaneously* :

$$\phi_2 - \phi_1 = n \frac{\pi}{2} \quad \text{where } n = 1, 5, 9, \dots, -3, -7, -11, \dots$$

$$\phi_2 - \phi_1 = n \frac{\pi}{2} \quad \text{where } n = -1, -5, -9, \dots, 3, 7, 11, \dots$$

which is absurd. Hence we reject combination (8.1). Similarly combination (8.2) must be rejected. For  $n = -1, -5, -9 \dots +3, +7, +11 \dots$  using (3), (3.1), (4), (4.1) and (9) we get the combination (8.3). Similarly for  $n = -3, -7, -11 \dots, +1, +5, +9 \dots$  we get the combination (8.4). Hence using (8.3) eqns. (1), (1.1), (2) and (2.1) can be combined into :

$$\ddot{V}_1 + (q_x^2 - \phi^2) V_1 = -2\ddot{\phi} \dot{V}_2 - \ddot{\phi} V_2 \quad (\text{for the X-mode}) \quad \dots \quad (1.2)$$

$$\ddot{V}_2 + (q_0^2 - \phi^2) V_2 = 2\ddot{\phi} \dot{V}_1 + \ddot{\phi} V_1 \quad (\text{for the 0-mode}) \quad \dots \quad (2.2)$$

and using (8.4), eqns. (1), (1.1), (2) and (2.1) can be combined into :

$$\ddot{V}_1 + (q_x^2 - \dot{\phi}^2) V_1 = 2\dot{\phi} \dot{V}_2 + \ddot{\phi} V_2 \text{ (for the } X\text{-mode)} \quad \dots (1.3)$$

$$\ddot{V}_2 + (q_0^2 - \dot{\phi}^2) V_2 = -2\dot{\phi} \dot{V}_1 - \ddot{\phi} V_1 \text{ (for the 0-mode)} \quad \dots (2.3)$$

Comparing (1.2) and (2.2) with (1.3) and (2.3), we find that there is an ambiguity of signs in these coupled wave-equations.

#### STATEMENT OF THE COUPLED WAVE-EQUATIONS AS GIVEN BY BUDDEN

In Budden's treatment (1952)  $E_1$ ,  $E_2$  and  $E_3$  were the components of the electric vector  $E$  of the wave, where  $E_1$  was horizontal and perpendicular to the earth's magnetic field,  $E_2$  was parallel to the horizontal component of the earth's magnetic field and  $E_3$  was directed vertically upwards and the following notations were used :

$$\left. \begin{aligned} \pi_0 &= E_{10} \sqrt{1 - R_0^2} \\ \pi_{x_i} &= E_{1x} \sqrt{1 - R_x^2} \\ \psi &= \frac{j}{R_0^2 - 1} \frac{dR_0}{dh} \end{aligned} \right\} \quad \dots (10)$$

$$\left. \begin{aligned} \frac{R_0}{R_x} &= - \frac{jY_T^2}{2Y_L(1-X-jZ)} \pm j \sqrt{1 + \frac{Y_T^4}{4Y_L^2(1-X-jZ)^2}} \\ M^2 &= 1 - \frac{X}{1-jZ-jY_L/R} \end{aligned} \right\} \quad \dots (11)$$

$$R = \frac{E_3}{E_1} \quad \dots (12)$$

$$\left. \begin{aligned} X &= \frac{4\pi Ne^2}{\epsilon_0 m p^2} \\ Y &= p_H/p \\ Z &= v/p \\ p_H &= \frac{\mu_0 e H}{m} \end{aligned} \right\} \quad \dots (13)$$

$Y_L$  = Vertical component of  $Y$ .

$Y_T$  = horizontal component of  $Y$ .

$N$  = electron number density.

$\nu$  = electronic collisional frequency.

$e, m$  = charge and mass of an electron

$H$  = strength of the earth's magnetic field.

$\epsilon_0, \mu_0$  = electric and magnetic permittivities of free space. With these notations, it was shown by Budden that the coupled wave-equations would be given by :

$$\frac{d^2\pi_0}{dh^2} + (K^2 M_0^2 - \psi^2) \pi_0 = -\pi_X \frac{d\psi}{dh} - 2\psi \frac{d\pi_X}{dh} \quad \dots \quad (14)$$

$$\frac{d^2\pi_X}{dh^2} + (K^2 M_X^2 - \psi^2) \pi_X = \pi_0 \frac{d\psi}{dh} + 2\psi \frac{d\pi_0}{dh} \quad (15)$$

#### INCORRECT ASSOCIATION OF THE EXPRESSIONS FOR $R$ AND $M^2$ WITH THE O- AND X-MODES

We shall consider the following equations of motion of an electron of charge  $e$  as given by Budden :

$$\frac{e_0 X}{4\pi} E_1 = \left[ \frac{Y_T^2}{1 - X - jZ} - (1 - jZ) \right] P_1 - jY_L P_2 \quad (16)$$

$$\frac{e_0 X}{4\pi} E_2 = -(1 - jZ) P_2 + jY_L P_1$$

As the axes of the co-ordinate system in Budden's treatment are not clearly defined we shall compare eqn. (16) with the following equations which are derived with reference to the co-ordinate system as shown in Fig. 1.

$$\frac{e_0 X}{4\pi} E_y = -(1 - jZ) P_y + jY_L P_x \quad (17)$$

$$\frac{e_0 X}{4\pi} E_x = \left[ \frac{Y_T^2}{(1 - X - jZ)} - (1 - jZ) \right] P_x - jY_L P_y$$

The comparison shows that  $E_1$  is along  $ox$ , and  $E_2$  is along  $Oy$  of Fig. 1. Hence eqn. (12) can be written as :

$$R = \frac{E_y}{E_x} \quad (12.1)$$

Using eqns. (12.1) and (11) we get for the 0-mode :

$$\left( \frac{E_x}{E_y} \right)_0 = -\frac{j}{Y_L} \left[ \frac{\frac{1}{2} Y_T^2}{(1 - X - jZ)} + \sqrt{Y_L^2 + \frac{1/4 Y_T^4}{(1 - X - jZ)^2}} \right]$$

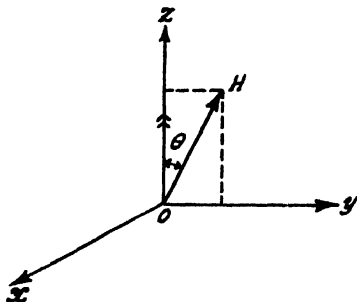


Fig. 1. Coordinate System (present paper)  
 OZ → direction of wave propagation  
 OH → direction of the Earth's magnetic field in the plane yz

This equation shows that the expression for the wave-polarization which Budden associated with the 0-mode is actually that for the X-mode in the ray treatment (Ratcliffe, 1962). Again using (11) we get for the 0-mode :

$$M_0^2 = 1 - \frac{X}{1 - jZ - \frac{Y_T^2}{2(1 - X - jZ)} - \sqrt{Y_L^2 + \frac{Y_T^4}{4(1 - X - jZ)^2}}}$$

This equation shows that the expression for the square of the complex refractive index which Budden associated with the 0-mode agrees with that for the X-mode in the ray treatment (Ratcliffe, 1962). Thus we find that what Budden (1952) called the 0-mode in his wave-treatment is actually the x-mode in the same treatment and is identified with that for the X-mode in the ray-treatment. Hence eqn. (11) should be written as follows :

$$\left[ \frac{R_x}{R_0} \right] = - \frac{jY_T^2}{2Y_L(1 - X - jZ)} \pm j \sqrt{1 + \frac{Y_T^4}{4Y_L^2(1 - X - jZ)^2}} \quad \dots (11.1)$$

$$M^2 = 1 - \frac{X}{1 - jZ - jY_L/R}$$

The question now naturally arises about the correct labelling of the coupled wave-equations (14) and (15). We have given below the reasons that eqns. (14) and (15) were *correctly* labelled.

Budden (1952) deduced the coupled wave-equations from the following :

$$\frac{d^2 E_1}{dh^2} + \frac{K^2}{\epsilon_0} D_1 = 0, \quad \frac{d^2 E_2}{dh^2} + \frac{K^2}{\epsilon_0} D_2 = 0$$

where

$$E_1 = E_{10} + E_{1X}, \quad E_2 = E_{20} + E_{2X}$$

$$R_0 = \frac{E_{20}}{E_{10}}, \quad R_X = \frac{E_{2X}}{E_{1X}}$$

$$D_1 = \epsilon_0 [M_0^2 E_{10} + M_X^2 E_{1X}]$$

$$D_2 = \epsilon_0 [M_0^2 E_{20} + M_X^2 E_{2X}]$$

It is to be noted that the expressions on the right hand side of Eqn. (11) did not enter in the method of derivation of the coupled wave equations given in (14) and (15) by Budden (1952). Hence these equations (14) and (15) were correctly labelled. However whenever the values of  $R_0$ ,  $R_X$ ,  $M_0^2$  and  $M_X^2$  are to be substituted in eqns. (14) and (15) or in solutions of these equations, the equations (11.1) must be used.

#### BUDDEN'S COUPLED WAVE-EQUATIONS EXPRESSED IN THE FORM GIVEN BY SAHA *et al*

We start from the equation given in our previous paper (1964) :

$$D_y = q^2 E_y = K_2 E_y + j L E_x \quad \dots (18)$$

Using (18) and (5), it can be easily shown that for the 0-mode :

$$\left( \frac{E_x}{E_y} \right)_0 = -j\rho_1 \quad \dots (19)$$

Similarly it can be shown for the X-mode.

$$\left( \frac{E_x}{E_y} \right)_X = -j\rho_2 \quad \dots (19.1)$$

Equations (19) and (19.1) are referred to the co-ordinate system of Fig. 2.

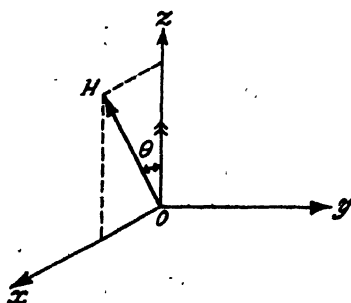


Fig. 2. Co-ordinate System (Saha *et al*)

OZ  $\rightarrow$  direction of wave propagation

OH  $\rightarrow$  direction of the Earth's magnetic field in the plane xz

Comparing the co-ordinate systems of Figs. 1 and 2 and using the equations (3), (4.1), (6), (7), (10), (11.1), (12), (12.1), (19) and (19.1) we have

$$\left. \begin{aligned} \pi_X &= \pm jV_1, \quad \pi_0 = \pm jV_2 \\ \psi/K &= \dot{\phi}_1 = \dot{\phi}_2 = \dot{\phi} \end{aligned} \right\} \quad \dots (20)$$

From eqn. (20) we can make the following combinations :

$$\left( \begin{array}{l} \pi_X = jV_1 \\ \pi_0 = jV_2 \end{array} \right) \quad \dots (20.1)$$

$$\left( \begin{array}{l} \pi_X = -jV_1 \\ \pi_0 = -jV_2 \end{array} \right) \quad \dots (20.2)$$

$$\left( \begin{array}{l} \pi_X = jV_1 \\ \pi_0 = -jV_2 \end{array} \right) \quad \dots (20.3)$$

$$\left( \begin{array}{l} \pi_X = -jV_1 \\ \pi_0 = jV_2 \end{array} \right) \quad \dots (20.4)$$

It can be easily shown using either (20.1) or (20.2) and  $\psi/K = \dot{\phi}$ ,  $q^2 = M^2$  that the equations (14) and (15) can be transformed into (2.3) and (1.3) respectively. Similarly using either (20.3) or (20.4), the equations (14) and (15) can be transformed into (2.2) and (1.2) respectively.

We have shown elsewhere (1964) that the wave-equations of Saha *et al.* were incorrectly labelled i.e., the wave-equation which they associated with the 0-mode should actually be that for the X-mode and *vice-versa*. Moreover we have shown in the present paper that the wave-equations were correctly labelled by Budden (1952). But according to Kelso (1953) the coupled wave-equations, as deduced by Saha *et al.* (1951) are identical with those given by Budden (1952). The discrepancy is due to the fact that Kelso (1953) incorrectly associated the wave function  $\pi_0$  used by Budden for the 0-mode with the wave function  $V$  which Saha *et al.* used for the 0-mode where  $V$  (which is the same as  $V_1$  in the present paper) is *actually* the wave function for the X-mode.

#### ACKNOWLEDGEMENT

The author is deeply indebted to Prof. S. R. Khastgir, D.Sc., F.N.I., for his keen interest and constant guidance.

#### REFERENCE

- Banerjee, S. K. and Khastgir, S. R., 1964, *Ind. Jour. Phys.* **38**, 347.  
 Budden, K. G., 1952, *Proc. Roy. Soc. Series A*, **215**, 215.  
 Kelso, J. M. 1953, *J. Geophys. Res.*, **58**, 431.  
 Ratcliffe, J. A. 1962, *The Magneto-Ionic Theory and its Applications to the Ionosphere* (Cambridge University Press), p. 19.  
 Saha, M. N., Banerjee, B. K. and Guha, U. C., 1951, *Proc. Nat. Inst. Sci. (India)* **17**, 205.



# VARIATIONAL PRINCIPLES FOR COMPRESSIBLE VISCOUS FLUID IN MAGNETOHYDRODYNAMICS

N. K. SHARMA\* AND S. R. SHARMA

DEPARTMENT OF PHYSICS, UNIVERSITY OF RAJASTHAN, JAIPUR

(Received December 2, 1963; Resubmitted August 25, 1964)

**ABSTRACT.** Variational principles with proper Lagrangian densities for the case of a magnetohydrodynamic viscous compressible fluid have been used to derive momentum equations and the equations governing the magnetic field. As an illustration the case of a perfectly conducting plasma continuum has been treated.

## INTRODUCTION

Recently several papers (Herivel 1954, Katz 1961, Su 1961) have treated the variational principles for non-dissipative plasmas. Rosen (1958) has used a variational method for such a dissipative system using Onsager's (1931) dissipation function  $\phi$ . In this communication we have used a very straight forward and simple variational approach for deriving the momentum equations and the equations governing the magnetic field for a dissipative magnetohydrodynamic compressible fluid.

The actual formulation has been divided into two parts. In the first part we derive the momentum equations for the motion of the fluid, and the equations governing the magnetic field have been taken as admissibility conditions. In the second part the later have been derived treating the former as admissibility conditions. The method used in this formulation is due to Bateman (1931).

As an illustration we have considered the case of a perfectly conducting plasma continuum, our formulation gives exactly the equations for this continuum, which is really very straight forward and simple as compared to the recent derivation given by Lundgren (1963).

## VARIATIONAL PRINCIPLE — I

The appropriate equations for the problem under consideration are (Chandrasekhar 1961)

$$\rho D u_i = X_i - \frac{\partial \bar{w}}{\partial x_i} + \frac{\partial}{\partial x_j} \left\{ \mu \left( \frac{\partial u_i}{\partial x_j} + \frac{\partial u_j}{\partial x_i} \right) \right\} - \frac{2}{3} \frac{\partial}{\partial x_i} \left( \mu \frac{\partial u_b}{\partial x_b} \right) + H_j \frac{\partial H_i}{\partial x_j} \quad (1)$$

---

\*Present address :—Tata Institute of Fundamental Research, Bombay 5, India.

with 
$$\bar{\omega} = p + \frac{|\vec{H}|^2}{8\pi} \quad \dots (2)$$

The equation of motion governing the magnetic field is

$$\frac{\partial H_i}{\partial t} + \frac{\partial}{\partial x_j} (u_j H_i - u_i H_j) = \eta \nabla^2 H_i \quad \dots (3)$$

The equation of continuity is

$$\frac{\partial \rho}{\partial t} + \frac{\partial}{\partial x_i} (\rho u_i) = 0. \quad \dots (4)$$

and the magnetic field satisfies the divergence condition,

$$\frac{\partial H_i}{\partial x_i} = 0 \quad \dots (5)$$

The symbols in the above equations have the following meanings :

$\rho$ , denotes the density of the fluid and is a function of space coordinates  
i.e.  $\rho = \rho(x, y, z)$

$U_i$ , denotes the  $i$ -th component of the velocity vector.

$X_i$ , denotes the  $i$ -th component of the external forces of non-magnetic origin.  
 $\mu$ , is the viscosity of the fluid assumed to be a function of space coordinates  
i.e.  $\mu = \mu(x, y, z)$ .

$p$ , denotes the fluid pressure.

$H_i$  is the  $i$ -th component of magnetic intensity.

$\eta$ , denotes the resistivity, assumed constant.

$\bar{\omega}$ , is a function involving  $p$  and  $\vec{H}$  as defined in eq (2) and  $D$  is the total derivative.

It may be pointed out that throughout the formulations the method of Cartesian tensors has been used. In this section the appropriate Euler-Lagrangian density yield equations (1) and equation (3) has been taken as admissibility condition. The boundary conditions are the usual ones, namely, the fluid under consideration is supposed to occupy a finite region of space whose boundary is formed partly of the surfaces with motions and partly of free surfaces. The time interval of the motion of the fluid is considered from  $t = t_0$  to  $t = t_1$ , and the region occupied by the fluid at these instants is  $R_0$  and  $R_1$  respectively with the corresponding boundaries as  $S_0$  and  $S_1$  respectively.  $x_i$ ,  $Dx_i$  are continuous and  $\delta x_i$  is zero at  $t = t_0$  and  $t = t_1$ .

For simplicity we define the following symbols :

$$a_{ij} = \frac{1}{2} \left( \frac{\partial u_i}{\partial x_j} + \frac{\partial u_j}{\partial x_i} \right) \quad \dots \quad (6)$$

$$b_{ij} = \frac{1}{2} \left( \frac{\partial H_i}{\partial x_j} + \frac{\partial H_j}{\partial x_i} \right) \quad \dots \quad (7)$$

$$C_{ij} = \frac{1}{2} \left( \frac{\partial U_i}{\partial x_j} + \frac{\partial U_j}{\partial x_i} \right) \quad \dots \quad (8)$$

and 
$$u_i = Dx_i \quad \dots \quad (9)$$

We have taken  $U_i = \delta x_i$ , therefore  $DU_i = D\delta x_i = \delta Dx_i = \delta u_i \quad \dots \quad (10)$

We define the Ligrangian density  $L$  as follows :

$$\delta \int_{t_0}^{t_1} L dt = \delta \int_{t_0}^{t_1} (A+B+C)dt = 0. \quad \dots \quad (11)$$

Where  $A$ ,  $B$  and  $C$  have been defined as the volume integrals as follows.

$$\begin{aligned} \delta A &= \int_R U_i D\rho \delta x_i d\tau + \int_R \rho U_i \delta U_i d\tau \\ &= \int_R U_i D\rho \delta x_i d\tau + \int_R \rho U_i D\delta x_i d\tau \\ &= \int_R U_i D(\rho \delta x_i) d\tau \quad \dots \quad (12) \end{aligned}$$

Here  $d\tau$  denotes the volume element  $dx dy dz$  of the fluid under consideration.

Therefore,

$$\begin{aligned} \int_{t_0}^{t_1} \delta A dt &= \int_{t_0}^{t_1} dt \int_R U_i D(\rho \delta x_i) d\tau \\ &= \int_R d\tau [U_i \rho \delta x_i]_{t_0}^{t_1} - \int_{t_0}^{t_1} dt \int_R DU_i \rho \delta x_i d\tau \\ &= - \int_{t_0}^{t_1} dt \int_R \rho DU_i \delta x_i d\tau \quad \dots \quad (13) \end{aligned}$$

Next,

$$\delta B = - 2 \int_R \mu C_{ij} a_{ij} d\tau - \int_R H_i H_j \frac{\partial U_i}{\partial x_j} d\tau + \frac{2}{3} \int_R \mu a_{kk} \frac{\partial U_i}{\partial x_i} d\tau$$

$$\begin{aligned}
&= - \int_R [\mu a_{ij}(\delta x_i)_{,j} + (\mu a_{ij})(\delta x_j)_{,i}] - \int_R H_i H_j (\delta x_i)_{,j} d\tau + \frac{2}{3} \int_R \mu a_{kk} (\delta x_i)_{,i} d\tau \\
\delta B &= - \int_R [(\mu a_{ij} \delta x_i)_{,j} - (\mu a_{ij})_{,j} \delta x_i] d\tau \\
&\quad - \int_R [(\mu a_{ij} \delta x_j)_{,i} - (\mu a_{ij})_{,i} \delta x_j] d\tau \\
&\quad - \int_R [(H_i H_j \delta x_i)_{,j} - (H_i H_j)_{,j} \delta x_i] d\tau \\
&\quad + \frac{2}{3} \int_R [(\mu a_{kk} \delta x_i)_{,i} - (\mu a_{kk})_{,i} \delta x_i] d\tau \quad \dots \quad (14)
\end{aligned}$$

The application of Gauss' theorem and a little simplification yields

$$\begin{aligned}
\delta B &= -2 \int_S \mu a_{ij} l_j \delta x_i ds + 2 \int_R \frac{\partial}{\partial x_j} (\mu a_{ij}) \delta x_i d\tau \\
&\quad - \int_S H_i H_j l_j \delta x_i ds + \int_R \frac{\partial}{\partial x_j} (H_i H_j) \delta x_i d\tau \\
&\quad + \frac{2}{3} \int_S \mu a_{kk} l_i \delta x_i ds - \frac{2}{3} \int_R \frac{\partial}{\partial x_i} (\mu a_{kk}) \delta x_i d\tau \quad \dots \quad (15)
\end{aligned}$$

Lastly we define

$$\delta c = \int_R \left( X_i - \frac{\partial \bar{w}}{\partial x_i} \right) \delta x_i d\tau + \int_S X_{oi} \delta x_i ds \quad \dots \quad (16)$$

Where  $X_{oi}$  are the components of surface traction. Therefore, the variational principle is

$$\begin{aligned}
\delta \int_{t_0}^{t_1} (A+B+C) dt &= \int_{t_0}^{t_1} dt \int_R d\tau \left[ X_i - \frac{\partial \bar{w}}{\partial x_i} - \rho D u_i \right. \\
&\quad \left. + 2 \frac{\partial}{\partial x_j} (\mu a_{ij}) + \frac{\partial}{\partial x_j} (H_i H_j) - \frac{2}{3} \frac{\partial}{\partial x_i} (\mu a_{kk}) \right] \delta x_i \\
&\quad + \int_{t_0}^{t_1} dt \int_S ds \left[ X_{oi} - H_i H_j l_j - 2 \mu a_{ij} l_j + \frac{2}{3} \mu a_{kk} l_i \right] = 0. \quad \dots \quad (17)
\end{aligned}$$

This on further simplification gives

$$\begin{aligned} \int_{t_0}^{t_1} dt \int_R \delta x_i \left\{ X_i - \frac{\partial \bar{\omega}}{\partial x_i} - \rho Du_i + \frac{\partial}{\partial x_j} \left[ \mu \left( \frac{\partial u_i}{\partial x_j} + \frac{\partial u_j}{\partial x_i} \right) \right] \right. \\ \left. - \frac{2}{3} \frac{\partial}{\partial x_j} \left( \mu \frac{\partial u_k}{\partial x_k} \right) + H_j \frac{\partial H_i}{\partial x_j} \right\} d\tau \\ + \int_{t_0}^{t_1} dt \int_S \left[ X_{oi} - H_i H_j l_j - 2\mu a_{ij} l_j + \frac{2}{3} \mu a_{kk} l_i \right] ds = 0 \quad \dots (18) \end{aligned}$$

Since the variations  $\delta x_i$  are arbitrary on  $S$  and also at each point interior to  $R$ , the above relations can be satisfied if

$$\begin{aligned} \rho Du_i = X_i - \frac{\partial \bar{\omega}}{\partial x_i} + \frac{\partial}{\partial x_j} \left\{ \mu \left( \frac{\partial u_i}{\partial x_j} + \frac{\partial u_j}{\partial x_i} \right) \right\} \\ - \frac{2}{3} \frac{\partial}{\partial x_i} \left( \mu \frac{\partial u_k}{\partial x_k} \right) + H_j \frac{\partial H_i}{\partial x_j} \quad \dots (19) \end{aligned}$$

under the natural boundary conditions

$$X_{oi} - H_i H_j l_j - 2\mu a_{ij} l_j + \frac{2}{3} \mu a_{kk} l_i = 0 \quad \dots (20)$$

Equation (16) are the hydromagnetic equations of motion (eq. 1) for the viscous, compressible fluid under natural boundary conditions specified by eq. (17).

## VARIATIONAL PRINCIPLE—II

In this section we have taken equations of motion of the fluid as the admissibility conditions and the equation governing the motion of the magnetic field has been derived.

The appropriate Lagrangian for this problem is

$$\delta \int_{t_0}^{t_1} L dt = \delta \int_{t_0}^{t_1} (G + M + N) dt = 0 \quad \dots (21)$$

Where the quantities  $G$ ,  $M$  and  $N$  are defined as follows :

The variation in  $G$  is given by

$$\delta G = \int_R H_i \delta u_i d\tau = \int_R H_i D(\delta x_i) d\tau \quad \dots (22)$$

Therefore,

$$\begin{aligned}
 \int_{t_0}^{t_i} \delta G dt &= \int_{t_0}^{t_1} dt \int_R H_i D(\delta x_i) d\tau \\
 &= \int_R [H_i \delta x_i]_{t_0}^{t_1} d\tau - \int_{t_0}^{t_1} dt \int_R DH_i \delta x_i d\tau \\
 &= - \int_{t_0}^{t_1} dt \int_R DH_i \delta x_i d\tau \quad \dots \quad (23)
 \end{aligned}$$

Next the variation in  $M$  is defined by

$$\delta M = \int_S X_{oi} \delta x_i ds + \int_R u_j \frac{\partial H_i}{\partial x_j} \delta x_i d\tau$$

and therefore

$$\int_{t_0}^{t_1} \delta M dt = \int_{t_0}^{t_1} dt \int_S X_{oi} \delta x_i ds + \int_{t_0}^{t_1} dt \int_R u_j \frac{\partial H_i}{\partial x_j} \delta x_i d\tau \quad \dots \quad (24)$$

Lastly we define

$$\delta N = -2 \int_R \eta C_{ij} b_{ij} d\tau - \int_R (u_i H_j - u_j H_i) \frac{\partial U_i}{\partial x_j} d\tau \quad \dots \quad (25)$$

Proceeding as for eq. (14) and simplifying we have

$$\begin{aligned}
 \delta N &= -\eta \int_R b_{ij} [(\delta x_i)_{,j} + (\delta x_j)_{,i}] d\tau - \int_R (u_i H_j - u_j H_i) (\delta x_i)_{,j} d\tau \\
 &= -2\eta \int_R b_{ij} (\delta x_i)_{,j} d\tau - \int_R (u_i H_j - u_j H_i) (\delta x_i)_{,j} d\tau \\
 &= - \int_R (2\eta b_{ij} l_j + u_i H_j l_j - u_j H_i l_j) \delta x_i ds \\
 &\quad + 2\eta \int_R \frac{\partial}{\partial x_j} (b_{ij}) \delta x_i d\tau + \int_R \frac{\partial}{\partial x_j} (u_i H_j - u_j H_i) \delta x_i d\tau \quad \dots \quad (26)
 \end{aligned}$$

Combining equations (26), (24) and (23) we have

$$\begin{aligned}
 \int_{t_0}^{t_1} dt \int_R \left\{ \eta \frac{\partial}{\partial x_j} \left( \frac{\partial H_i}{\partial x_j} + \frac{\partial H_j}{\partial x_i} \right) + \frac{\partial}{\partial x_j} (u_i H_j - u_j H_i) + u_j \frac{\partial H_i}{\partial x_j} - DH_i \right\} \delta x_i d\tau \\
 - \int_{t_0}^{t_1} dt \int_S \{ 2b_{ij} l_j \eta + u_i H_j l_j - u_j H_i l_j - X_{oi} \} \delta x_i = 0 \quad \dots \quad (27)
 \end{aligned}$$

But since the variations  $\delta x_i$  are arbitrary on  $S$  and also at each point interior to  $R$ , equation (27) can be satisfied if

$$\frac{\partial H_i}{\partial t} + \frac{\partial}{\partial x_j} (u_j H_i - u_i H_j) = \eta \nabla^2 H_i \quad \dots \quad (28)$$

and

$$2\eta b_{ij} l_j + u_i H_j l_j - u_j H_i l_j - X_{\sigma i} = 0 \quad \dots \quad (29)$$

Equation (28) is the equation (3) governing motion of the magnetic field under the natural boundary-conditions specified by equation (29).

#### CASE OF A PERFECTLY CONDUCTING PLASMA CONTINUUM

As an illustration we consider the case of a perfectly conducting inviscid plasma continuum with density  $\rho$  and pressure  $p$  obviously in this case  $\mu = 0$ ,  $\eta = 0$  and  $X_i = 0$ .

Using equation (11) we have

$$\delta \int_{t_0}^{t_1} L dt = \delta \int_{t_0}^{t_1} (A + B + C) dt = 0. \quad \dots \quad (30)$$

where equation (13) gives

$$\delta A = - \int \rho D u_i \delta x_i d\tau \quad \dots \quad (31)$$

Equation (15) gives

$$\delta B = - \int_S H_i H_j l_j \delta x_i ds + \int_R \frac{\partial}{\partial x_j} (H_i H_j) \delta x_i d\tau \quad \dots \quad (32)$$

and equation (16) gives

$$\delta C = \int_S X_{\sigma i} \delta x_i ds - \int_R \left( \frac{\partial \bar{w}}{\partial x_i} \right) \delta x_i d\tau \quad \dots \quad (33)$$

where  $X_{\sigma i}$  are the components of surface traction. On substituting in (30) we have

$$\begin{aligned} \delta \int_{t_0}^{t_1} L dt &= \delta \int_{t_0}^{t_1} (A + B + C) dt \\ &= \int_{t_0}^{t_1} dt \int d\tau \left[ \frac{\partial}{\partial x_j} (H_i H_j) - \rho D u_i - \frac{\partial \bar{w}}{\partial x_i} \right] \delta x_i \\ &\quad + \int_S (X_{\sigma i} - H_i H_j l_j) \delta x_i ds = 0 \quad \dots \quad (34) \end{aligned}$$

Since the variations  $\delta x_i$  on  $S$  and also at each point interior to  $R$  are arbitrary, therefore equation (34) can be satisfied if

$$\rho Du_i + \frac{\partial \omega}{\partial x_i} - \frac{\partial}{\partial x_j} (H_i H_j) = 0 \quad \dots (35)$$

under the boundary conditions

$$X_{oi} - H_i H_j l_j = 0. \quad \dots (36)$$

Equation (35) on further simplification gives

$$\rho \frac{du}{dt} = -\nabla p + J \times H \quad \dots (37)$$

Where  $J = \frac{1}{4\pi} \nabla \times H$  Equation (37) is the desired equation for the Perfectly Conducting Plasma Continuum.

#### ACKNOWLEDGMENT

We are thankful to Professor M. F. Soonawala for providing research facilities and other necessary help.

#### REFERENCES

- Bateman H. 1931, *Phy. Rev.* **38**, 815.  
 Chandra Sekhar, *Hydrodynamic and Hydromagnetic Stability*, Oxford Clarendon Press 1961, pp. 148-149.  
 Herivel J. W. 1954, *Proc. Cambridge. Phil. Soc.* **54**, 344.  
 Katz S. 1961, *Phy. Fluids.* **4**, 345.  
 Lundgren 1963, *Phy. Fluids* **6**, 898.  
 Onsagar 1931, *Phy., Rev.* **37**, 405.  
 Rosen P. 1958, *Phy. Fluids*, **3**, 251.  
 SU C. H., 1961, *Phy. Fluids* **4**, 1376.



# AN AUTOMATIC RECORDING B-H METER

A. K. MUKERJEE AND (Late) N. G. SUTRADHAR\*

DEPARTMENT OF MAGNETISM  
INDIAN ASSOCIATION FOR THE CULTIVATION  
OF SCIENCE, CALCUTTA-32.

(Received November 11, 1964)

**ABSTRACT.** An automatic recording B—H meter operating on 220 V, 50 c.p.s. has been constructed. The hysteresis loop is observed on the screen of a C.R.O. from which informations regarding its magnetic properties e.g. coercive force, magnetic induction etc. can be obtained.

The present paper describes the construction and working of the B—H meter, also some test measurements on carbon steel, high speed steel and magnetite are given.

## INTRODUCTION

In connection with the choice of proper indigenous materials for the construction of cores of electromagnets and development of various magnetic instruments and apparatus in this country, a detailed knowledge of the usual ferromagnetic properties of these materials is essential. Hence a programme for the development of techniques for quick and quantitative measurement of B—H curves at different temperatures was undertaken by the authors. Various methods for the purpose have been adopted by Crittenden *et al* (1951), Howling (1956) and others. But the balancing and calibrating systems of their methods are very complicated and the results obtained are not always free from uncertainties.

We have therefore constructed an automatic hysteresis loop tracer where-in the balancing and calibrating systems have been made much simpler and with which we could obtain quick and accurate information regarding saturation magnetisation, coercive field, hysteresis loss, residual induction and saturating field at different temperatures of any ferromagnetic material in convenient size and shape.

Demand for the construction of such an instrument also came from the workers of this laboratory studying ferromagnetism of naturally occurring single crystals to enable them to obtain preliminary informations on curie temperature, saturation induction etc. The present paper describes such a B—H meter working at 50 c.p.s. with provisions for observations at different temperatures in the range of 90°K to 1000°K.

---

\*Co-author N. G. Sutradhar died after the work for the paper was completed.

## WORKING PRINCIPLE OF THE INSTRUMENT

If an a.c. voltage is applied to the primary of  $n$  turns of a mutual inductance system with a magnetic core in which magnetisation  $I$  is produced, then a voltage  $v$  is produced in the secondary of  $N$  turns, given by

$$v = NA \left( \omega H_0 \cos \omega t + 4\pi \frac{dI}{dt} \right) \times 10^{-8} \text{ volts} \quad \dots (1)$$

where  $A$  is area of the core and  $H_0$  is the peak field produced inside the primary and the rest of the symbols have their usual significances.

If the voltage in the secondary before the introduction of the core, given by the first term in (1), is eliminated by balancing, say, by putting another secondary connected in opposition then the additional voltage  $NA 4\pi \frac{dI}{dt} \times 10^{-8}$  develops in the secondary on introduction of the core. This voltage after proper integration will evidently furnish us with a value directly proportional to the magnetisation of the material of the core. If this voltage after integration and a voltage proportional to the magnetising field are simultaneously fed with proper phase-relationship to the  $y$ - and  $x$ -plates respectively of a C.R.O., a trace of hysteresis loop will be obtained.

## DESCRIPTIONS OF THE INSTRUMENT

The instrument essentially consists of :

- a) Two primary magnetising coils (m.c.)
- b) Two secondary coils (s.c. and b.c.)
- c) Amplifying and integrating units
- d) The cathode ray oscilloscope.

a) *Primary magnetising coils*

The alternating magnetic field is produced by the two primary magnetising coils (m.c.), wound on brass spools, each having about 1150 turns of 22 S.W.G. super enamelled copper wire. Average diameter of each coil is 8.2 cms. and length is about 3.2 cms. The two coils are placed coaxially at a distance of 3.5 cms. from each other. The two coils are connected in series and fed by current from 220 volts, 50 c.p.s. power mains. A drop of voltage across a resistance ( $R$ ) placed in this circuit is fed to the horizontal plates of the C.R.O.

b) *Secondary coils*

Each of the secondary coils consists of 1700 turns of 36 S.W.G. super enamelled copper wire wound on brass spools of 2.5 cms. in length and an average diameter

of about 6.5 cms. One of these (s.c.) is placed coaxially with the primaries and in the gap between the two primary coils and the other (b.c.) similarly at one end

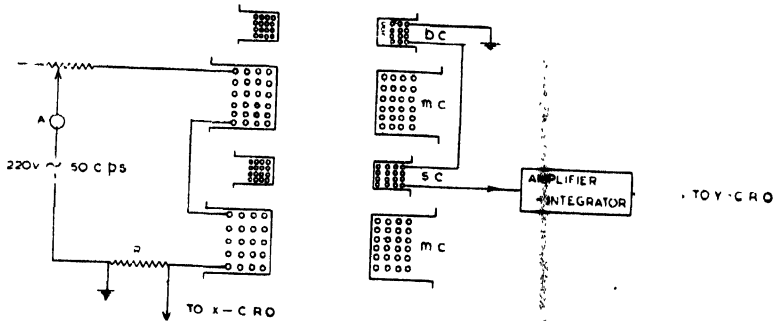


Fig. 1. A schematic diagram of the hysteresis loop tracer.

of the magnetising coils. These two secondary coils are connected in opposition so that when there is no ferromagnetic sample inside the coil (s.c.) the output voltage is zero. The output side of the two secondaries in opposition being connected, through an amplifier and an integrator, to the  $y$ -plates of the C.R.O., there should only be a horizontal trace on C.R.O. even with the full gain of the amplifier so long as the voltage of the two secondary coils are completely balanced.

When the sample is introduced inside the secondary coil (s.c.) in between the two primaries, the vertical deflection that is now observed in the C.R.O is only due to the sample and is obviously proportional to its magnetisation  $I$ . The two, the vertical and the horizontal deflections, combine to trace the hysteresis loop.

An auxiliary coil (a.c.) of 50 turns is wound over the secondary coil (s.c.) for calibration of the  $y$ -axis. The method of calibration etc. are described in a subsequent section.

### c) The Amplifier and the Integrator

The output voltage of the secondary being usually very small and after time integration only a small part of this being available it becomes necessary to amplify it suitably. Required amplification is obtained by using a high gain tube. It is so selected as to have a high plate resistance ( $r_p$ ). For integration, the plate load is shunted by a capacitance, so that at the working frequency (50 c.p.s.) the plate load is almost capacitative the time constant being almost one second.

In our case a single stage amplifier using a 6 SJ 7 vacuum tube operating at 90 volts from battery has been utilised. However successive stages may be added whenever, higher gains are desired.

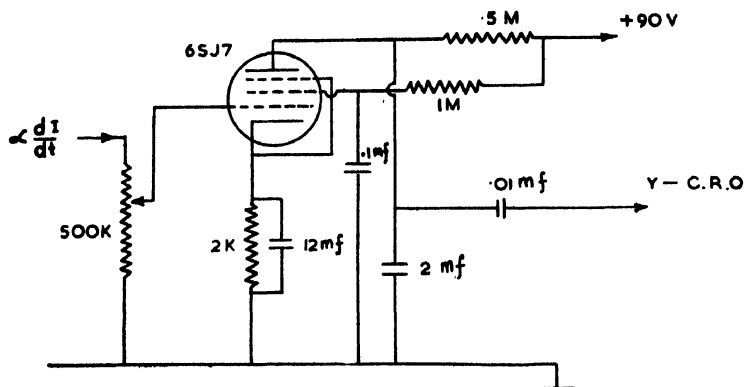


Fig. 2. The amplifier and the integrating circuit.

The disposition of the different parts of the apparatus, can be best followed from the block diagrams 1 and 2.

#### CALIBRATION

In order to obtain quantitative information regarding the various ferro-magnetic constants from the trace of the loop on C.R.O., calibration of its  $y$  and  $x$  axes which as already indicated are proportional to  $I$  and  $H$ , is essential.

##### *Magnetic field Calibration (x-Calibration).*

If  $i'$  amps. r.m.s. current flows through the two magnetising coils, and the magnetic field produced in the gap between the two coils is  $H'$ , then

$$H' = H'_0 \sin \omega t$$

$H'_0$  being the peak value of the a.c. magnetic field. The corresponding voltage  $V$  induced in the secondary coil (s.c.) of area of cross section  $A$  sq. cm. will be

$$\begin{aligned} V &= NA \frac{dH'}{dt} \times 10^{-8} \text{ volts} \\ &= NA \omega H'_0 \cos \omega t \times 10^{-8} \text{ volts} \end{aligned}$$

and the average value of  $V$  is given by

$$\bar{V} = NA \omega \left| \frac{H'_0}{\sqrt{2}} \right| \times 10^{-8} \text{ volts} \quad \dots (2)$$

Knowing this voltage  $\bar{V}$ ,  $H'_0$  can be determined and  $(H'_0/i')$  peak field per ampere r.m.s is also correspondingly known.

Thus for any current  $i$  amperes r.m.s the peak value of the magnetic field  $H_0$  is given by

$$H_0 = i \left( \frac{H'_0}{i'} \right) \quad (3)$$

The resistive voltage drop due to various currents across a fixed resistance  $R$ , placed in the magnetising circuit, when fed to the ~~plates~~ of C.R.O. produces proportional horizontal traces. The magnetic field correspondingly produced will therefore be proportional to these  $x$  deflections.

Therefore magnetic field  $H_0$  corresponding to deflection  $x$  will be  $H_0 = kx$  where  $k$  is the constant of proportionality, which can be obtained from a separate experiment as suggested by the relations (2) and (3). From an actual experiment we have found  $k = 50$  oersted/cm.

#### Calibration for Magnetisation ( $y$ -Calibration)

A sample of cross section  $\alpha$  sq. cm. when placed in the magnetic field in between the two magnetising coils will, as stated earlier, induce a voltage  $v$  in the secondary, given by

$$v = 4\pi\alpha N \frac{dI}{dt} \times 10^{-8} \text{ volts}$$

Let this voltage give a vertical deflection  $y$  on C.R.O. after necessary amplification and integration so that

$$4\pi\alpha NI \times 10^{-8} \times C = y \quad \dots (4)$$

where  $C$  is a constant.

Now a small voltage due to induction in the auxiliary coil (a.c.), having a small number of turns  $n$ , due to the same magnetising a.c. field  $H'_0$  is fed to the amplifier and the integrator and from there to the  $y$  plates of C.R.O. and a trace  $y'$  is obtained (without any sample inside) on C.R.O. then,

$$n a H'_0 \times 10^{-8} \times C = y' \quad \dots (5)$$

where  $a$  is the area of cross section of the auxiliary coil. Then from (4) and (5) we have

$$I = y \left( \frac{n a H'_0}{y' 4\pi\alpha N} \right).$$

For a field of 254 oersted, which has generally been used for calibration and the corresponding deflection 1.5 cm., the above expression reduces to

$$I = 4.65 \frac{y}{\alpha},$$

It may be mentioned in this connection that in order to study the temperature variation of the ferromagnetic properties of different materials, the lower portion of a narrow tailed dewar incorporating a low temperature cryostat or

a tubular electric heater with a water jacket around it can easily be introduced inside the primary of the system.

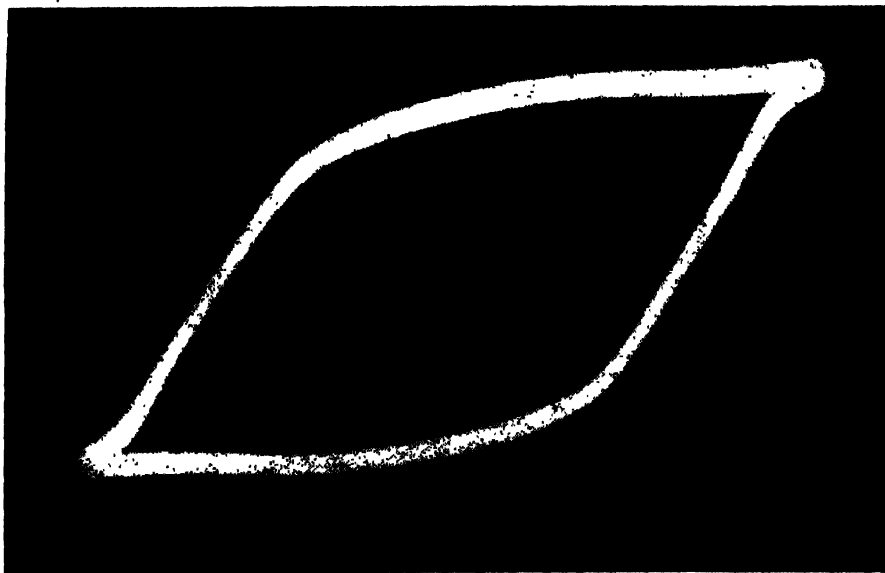


Fig. 3. Hysteresis loop of carbon steel,



Fig. 4. Hysteresis loop of high speed steel.



Fig. 5. Hysteresis loop of magnetite.

## SOME TEST OBSERVATIONS

Some observations have been recorded for test purposes with carbon steel and high speed steel, both of which were supplied from our workshop. Observation have also been recorded with single crystals of magnetite. The C.R.O. traces are shown in figure 3, 4 and 5 and the values in the adjoining tables(I and II). It is to be noted here that the maximum field available (400 gauss) in the present instrument though sufficient to saturate the various grades of ferrous materials is not enough to do so in case of ferromagnetic minerals as in case of magnetite. However, in case of magnetite the value of magnetisation for any particular field as obtained from the C.R.O. trace is the same as obtained from measurements with a sensitive magnetic balance for the corresponding field. We are now engaged in modifying the instrument so that higher fields may be obtained sufficient to saturate almost all ferromagnetic crystals.

TABLE I

	Carbon Steel		High speed Steel	
	Present observer	Reported (Bozorth, 1951)	Present observer	Reported (Bozorth, 1951)
Saturation Magnetisation (in c.g.s units)	800	not available	600	not available
Residual Magnetism (gauss)	650	830	480	860
Coercive force (in gauss)	110	50	90	70
Hysteresis loss, ergs/cycle	45,000	not available	30,000	not available

Though the observations agree in order yet they differ from absolute values. This is due to small variation in composition and difference in history.

TABLE II

## Magnetite

Field	Magnetisation from C.R.O. trace	Magnetisation from measurements with magnetic balance done in this laboratory
400 oersted	150 c.g.s.	145 c.g.s.

## ACKNOWLEDGMENT

The authors wish to express their best thanks to Prof. A. Bose who suggested the necessity of constructing such an instrument and to Shri A. K. Dutta for help and guidance throughout the course of the work.

## REFERENCES

- Bozorth, R. M. 1951, *Ferromagnetism* D. Van Nostrand Company Inc. New York p. 872.  
 Crittenden, E. C., Jr., Hudimac, A. A., and Strough. R. I. 1951, *Rev. Sci. Instr.* **22**, 872.  
 Howling, D. H., 1956, *Rev. Sci. Instr.* **27**, 952.



# THE SIGNIFICANCE OF THE MINIMUM DOPPLER DISPLACEMENT IN CANAL RAYS

B. V. SITAKUMARI

PATNA WOMEN'S COLLEGE, PATNA

(Received October 21, 1963)

**ABSTRACT.** Measurements of the gap of zero intensity which exists between the undisplaced line of  $H_\alpha$ ,  $H_\beta$  and  $H_\gamma$  and the Doppler band in pure hydrogen are presented when the current in discharge tube is kept constant. The gap width rises as the accelerating voltage is increased. The width shows two small maxima at 3 kV and 6 kV which are interpreted as due to relatively large numbers of  $H_4^+$  and  $H_5^+$  ions respectively. These findings are in accord with earlier measurements of the intensity maxima observed in the Doppler band. The gap width maxima for  $H_\alpha$ ,  $H_\beta$  and  $H_\gamma$  do not lie at the same accelerating voltage because an increase in the voltage is thought to be associated with a decrease in the width of the ion energy distribution. Thus with increasing voltage, the gap width should increase more than linearly as has in fact been observed.

## INTRODUCTION

When a potential difference  $\geq 1kV$  is applied between the two electrodes of a canal ray tube, and the discharge tube, is filled with hydrogen at pressures of  $10^{-2}$  to  $10^{-3}$  mm of Hg with a cathode having a hole at its centre, a beam of positively charged and of neutral particles pass through the hole and finally enters a gas filled and field free space behind the cathode. The maximum kinetic energy of the positive ions in the canal rays is in general somewhat smaller than the equivalent voltage applied to the discharge tube. When the light emitted from canal rays is analysed by means of a spectrograph, the Doppler band, i.e. light at lower wavelength than the undisplaced Balmer lines of wavelength  $\lambda$ , is observed. The maximum wavelength of this band is given by  $\frac{d\lambda}{\lambda} = v/c \cos \theta$  where  $\theta$  is the angle of observation with respect to the axis of the canal rays.

The width of the Doppler band can be up to  $50\text{\AA}$  or more, depending upon the applied voltage. Fig. 1 shows schematically the light intensity as a function of wavelength, the undisplaced line and the Doppler band are separated by a region of nearly zero intensity—a gap of width  $d\lambda_{min}$ . Since these observations make use of a photographic plate, 'zero intensity' can be due to lack of measurable blackening or lack of numbers of the light emitting centres. The variation of the  $\Delta\lambda_{max}$  with the applied voltage has been extensively studied. However the nature of the variation of the  $d\lambda_{min}$  with  $V$  and the particles radiating in the

region of lowest wavelength of the band have been investigated only in a few cases. In particular Sakuntala has studied the variation of the  $d\lambda_{min}$  up to 8kV and found that  $d\lambda_{min}$  increases with  $V$  and then approaches a constant

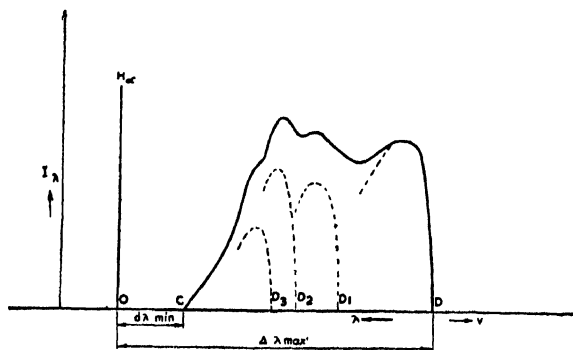


Fig. 1. Schematic diagram of a typical microphotometric trace of the Doppler band.  $I_\lambda$ , light intensity;  $H_\alpha$  undisplaced line (6563Å);  $\Delta\lambda$  total width of the band;  $d\lambda_{min}$  minimum wave length shift from the centre of the undisplaced line;  $\Delta\lambda_{max}$  maximum wavelength shift;  $v$  beam velocity of excited atoms;  $D_1, D_2, D_3$ ...maximum speeds of  $H_\alpha$  emitting atoms produced by  $H^+$ ,  $H_2^+$  etc. respectively.

value. The rise in gap width with voltage was thought to be due to the disappearance of  $H_4^+$  ions. In this paper the variation of  $d\lambda_{min}$  with  $V$  has been studied up to 16 kV in hydrogen for  $H_\alpha$ ,  $H_\beta$  and  $H_\gamma$  lines.

### EXPERIMENTAL

A Steinheil three prism glass spectrograph of light gathering power  $f/3$  and a tele-objective of focal length  $f = 250$  cm, attached to the Camera, were used. The dispersion was  $11.92 \text{ Å per mm}$  for  $H_\alpha$  and  $4.3 \text{ Å per mm}$  for  $H_\beta$ . With a Camera lens of  $f = 640$  mm a dispersion of  $16.5 \text{ Å per mm}$  and  $9.8 \text{ Å per mm}$  was obtained for  $H_\beta$  and  $H_\gamma$  respectively. High purity of hydrogen was maintained by Wiens' method of capillary streaming and continuous pumping. The speed of flow of hydrogen was such that no appreciable pressure differences developed between the canal ray tube and the field free space behind the cathode. In this arrangement  $p$ , the gas pressure, could not be varied independently of  $V$ , thus  $V$  and  $p$  plotted on the same abscissa.

### RESULTS

The results are shown in Fig. 2. It is seen that all the curves  $d\lambda_{min} = f(V)$  have a similar trend. However the maximum at 3 kV does not appear as prominently as in Sakuntala's work (1953). Here  $d\lambda_{min}$  rises with  $V$  and shows two small maxima at about 3kV and 6kV. It is interesting to note that Kreffit (1924) observed for  $H_\beta$  that  $d\lambda_{min}$  first increased with  $V$  but became constant between 3kV and 5 kV.

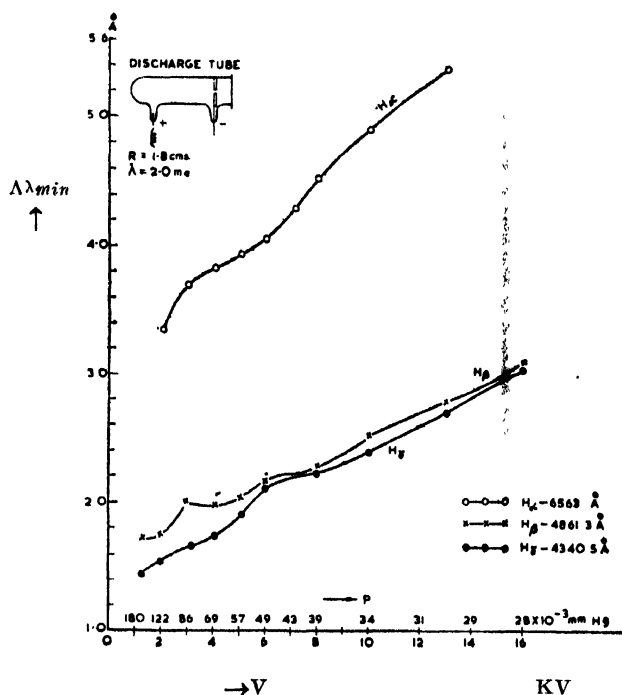


Fig. 2. Minimum wavelength shift  $\Delta\lambda_{min}$  as a function of the discharge potential  $V$ ;  $i = 2 \text{ ma}$ ; for each line  $t = 1 \text{ hour}$  (exposure),  $H_{\alpha}$  alone being taken with teleobjective.

The relative maxima for  $H_{\alpha}$ ,  $H_{\beta}$  and  $H_{\gamma}$  are found here to be at the different values of  $V$ . This may be due to the decrease in the width of the ion energy distribution at higher values of  $V$  as a result of which the light that originates from a particular type of ion may decrease more rapidly at larger  $\lambda$  the larger  $V$ .

#### DISCUSSION

Before discussing the processes which are responsible for the appearance and changes in the width of the gap, it is necessary to recall the findings concerning the origin of the light emission in Canal rays. W. Wien (1927) and his school made an extensive study of the emission processes and discovered charge transfer collisions early in 1900. It was concluded that the Doppler band arises from encounters between ions and gas molecules. They also found that the Canal ray light cannot be the result of an elastic collision and that it cannot be caused by electron ion recombination in stages. In spite of the fundamental importance this question has not been discussed for a long time.

Recently Sakuntala and von Engel (1960) suggested that the light in canal rays is the result of an inelastic collision. The fast ion in the canal ray hits a gas molecule or atom and forms a lived compound molecule which decays into several particles one of which is an electronically excited neutral particle which emits the light. Thus the collision results in a charge transfer associated with

dissociation and excitation. From spectrographic data they were able to estimate the order of the cross section which they found to be between  $10^{-19}$  and  $10^{-20}$   $\text{cm}^2$ .

As to the origin of the gap it is clear that its width corresponds to the smallest observable velocity of the radiating atoms. Since the radiating atoms acquire their velocity from the fast ions, it is to be expected that as the ion speed is increased the gap width should rise. Since  $d\lambda_{min}$  should increase with  $V$  the centre of the ion distribution would move to higher speeds and therefore the slowest ions too would have larger speeds. This should be more so since the ion distribution becomes narrow at larger ion energy. The same argument should hold in the case when ions of different mass are present in the beam. Complications may arise, if ions of a certain type are more likely to be produced in the discharge than others.

The new mechanism indicated above explains earlier observations of the disappearance of the gap between the undisplaced line and the end of the Doppler band. For in the presence of impurities, such as organic molecules (oil), the fast ion can dissociate a hydrogenic substance and the kinetic energy of the ion would be shared by a large number of excited hydrogen atoms of low average speed. Owing to the distribution in energy and the angular scattering, light emitting centres down to zero kinetic energy are now present and the gap disappears.

The variation of the gap width with the voltage (Fig. 2) is therefore thought to be due to the charge transfer emission process, the change in the energy distribution of the ions present and changes in their relative abundance. We note first that  $d\lambda_{min}$  rises with  $V$  in  $H_\alpha$ ,  $H_\beta$  and  $H_\gamma$ . This is in accordance with expectation as has been stated above. However two points require amplification. Firstly the gap  $d\lambda_{min}$  was found to be finite and not zero as  $V$  approaches zero; this value seems to be higher for  $H_\alpha$  than for  $H_\beta$  and  $H_\gamma$ . As the  $H_\alpha$  line was studied with the teleobjective attachment the intensity in its case was much less than that of  $H_\beta$  or  $H_\gamma$ . It is suggested that this is caused also by the inertia of the photographic emulsion. The spectral sensitivity together with the threshold of the emulsion causes an apparently larger gap width for red line than for the blue line, a suggestion which would also explain the small difference between  $H_\beta$  and  $H_\gamma$ . For the photographic plate used (Kodak P1200) the relative photographic sensitivity for  $H_\alpha$ ,  $H_\beta$  and  $H_\gamma$  (the product of sensitivity of the emulsion the relative intensity of the black body radiation) is in the ratio 8 to 45 to 56 which supports the suggestion made. If the width of the ion energy distribution curves and the relative abundances would remain constant,  $d\lambda_{min}$  would be expected to rise linearly with  $V$ , provided de-excitation processes are independent of  $V$  and  $p$ . In fact quenching can be ruled out because the deviation from the linearity in Fig. 2 occurs at larger  $V$  and hence smaller  $p$ .

The relative maxima observed in the three curves of Fig. 2, can be explained in the following way : when  $V$  is increased (and  $p$  reduced) the peaks of two successive ion energy distribution curves will increase and the width of the curves

decrease. Hence  $d\lambda_{min}$  will rise faster than linearly. If however, the relative abundance of ions of lower mass number increases faster than those of higher mass, the net result can be a slowing down of the increase in  $d\lambda_{min}$  which means that a maximum in  $d\lambda_{min}$  arises. It is seen that the maxima in  $H_\alpha$  do not appear precisely at the same  $V$  as those of  $H_\beta$  and  $H_\gamma$ . Whether this is due to low photographic sensitivity in red or not is not certain.

The maxima in light emission in the Doppler band have been connected with  $H^+$ ,  $H_2^+$  etc. and so have their relative maxima in  $d\lambda_{min}$ . In particular the existence of a moderate number of  $H_4^+$  ions has been suggested from the earlier measurements. However Dopel (1925) thought to have observed such species by mass spectroscopy. Recently new evidence has been supplied by measurements of ion species produced in glow discharge in  $H_2$  and analysed with mass spectrometer. Dawson and Tickner found ions of mass 4 and 5. The mass 4 ion was interpreted as  $H_2D^+$  but I think that not sufficient convincing data have been supplied not to interpret this species as a  $H_4^+$  ion. The author suggests that the ion of mass 5 is  $H_5^+$ . Since a small relative maximum has been observed on the low wavelength side of the Doppler band when  $V$  is above 2kV, it is suggested that the first maximum in  $d\lambda_{min}$  is associated with disappearance of  $H_4^+$  ions whose existence still requires more evidence. The second maximum in  $d\lambda_{min}$  is probably associated with  $H_3^+$  which is found to exist even up to 16kV but decreases in abundance having a peak value at 6KV<sup>3</sup>.

#### ACKNOWLEDGMENT

I am indebted to Dr. B. Dasannacharya, Retired Head of the department of Physics, Banaras Hindu University under whose guidance the above work was done by me for the Ph.D. Dissertation during the years 1953-1955. I am very thankful to Dr. M. Sakuntala, Physics Department, Banaras Hindu University, now in the Atomic Energy Research Establishment, Harwell, U. K. for the discussion and help she gave in the presentation of the matter. I have great pleasure in offering to Professor A. Von Engel of Oxford University my sincere thanks for his kind criticism and helpful suggestions.

#### REFERENCES

- Dassanacharya, B. and Dakshinamurti, C., 1944 *Nature*; **154**, 22.  
 Dassanacharya, B. and Das, G. K., 1948, *Phil. Mag.* **39**, 966.  
 Dassanacharya, B. *Current Sci.*, Canal Rays special number pp. 10-19 Sept. 1937.  
 Dopel, R. 1925, *Ann. Phys.* L p. 376, 1.  
 Dawson, P. H. and Tickner, A. W. 1962, *J. Chem. Phys.* **37**, 672.  
 Krefft, H. 1924, *Ann. d. Phys.*, **75**, 75.  
 Kodak Handbook on Photographic plates.  
 Strasser, B. 1920, *Ann. D. Phys.* **31**, 895.  
 Sitakumari, B. V. Doctorate Dissertation BHU, 1956.  
 Sakuntala, M. and Dassanacharya, B. 1953, *Curr. Sci.* **22**, 167.  
 Sakuntala, M. and von Engel, A. 1960, *Journal of Electronics and Control* **9**, 1, 31.  
 Wien, W., 1927, Handbook Exp. Phys. L p. 2 14.

# Letters to the Editor

The Board of Editors does not hold itself responsible for opinions expressed in the letters published in this section. The notes containing short reports of original investigations communicated to this section should not contain many figures and should not exceed 500 words in length. The contributions reaching the Secretary by the 15th of any month may be expected to appear in the issue for the next month. No proof will be sent to the author.

## 1

### ON THE NON-COHERENT FORMATION OF ABSORPTION LINES IN STELLAR ATMOSPHERES

SANTI RANJAN DAS GUPTA

DEPARTMENT OF MATHEMATICS, UNIVERSITY OF NORTH BENGAL, RAJA RAMMOHUNPUR

(Received January 13, 1964)

The equation of transfer for partly coherent and partly non-coherent formation of absorption lines in stellar atmospheres can be written as

$$\mu \frac{dI_\nu(t, \mu)}{dt} = (1 + \eta_\nu)I_\nu(t, \mu) + (1 - \epsilon) \cdot a \cdot \eta_\nu J_\nu(t) + (1 + \epsilon \eta_\nu)B_\nu(t) + (1 - \epsilon)b \cdot \eta_\nu J(t), \dots \quad (1)$$

where  $I_\nu(t, \mu)$  is the specific intensity of radiation of frequency  $\nu$  in the direction  $\theta = \cos^{-1}\mu$  and at the optical depth  $t$  measured in the continuous absorption coefficient  $k_\nu$ ,  $k_\nu$  being constant over the width of the line considered.  $t = 0$  corresponds to the outer surface of the atmosphere supposed to be stratified in plane parallel layers.  $J_\nu(t)$  is the average intensity.

$\epsilon$  = fraction of atoms excited by radiation of frequency  $\nu$  and prevented from contributing to the coherent re-emission by superelastic collisions.  
 $\epsilon$  is however much less than 1.

$$\eta_\nu = \frac{l_\nu}{k_\nu} = \frac{\text{line absorption co-efficient}}{\text{continuous absorption co-efficient}} \quad (2)$$

is assumed to be independent of the optical depth.

$$a + b = 1, \quad a \text{ and } b \text{ are both positive.} \quad \dots \quad (3)$$

The second term on the right hand side of (1) gives the coherent part of emission while the last term in the equation (1) accounts for the non-coherent part of emission.  $J(t)$  will be called pseudo average intensity and will be regarded to be insensitive to the variation of frequency over the absorption line considered. The boundary conditions are \*

$$I_\nu(0, -\mu') = 0, \quad 0 < \mu' \leq 1. \quad \dots \quad (4)$$

$$I_\nu(t, \mu) \exp(-t/\mu\lambda) \rightarrow 0 \text{ as } t \rightarrow \infty, \quad \lambda = 1/(1+\eta_\nu), \quad \dots \quad (5)$$

$$J(t) \rightarrow B_\nu(t) \text{ as } t \rightarrow \infty. \quad \dots \quad (6)$$

where  $B_\nu(t)$  is the Planck's function assumed to be constant over the line. We now put

$$\lambda = 1/(1+\eta_\nu), \quad \gamma = 1+c\eta_\nu, \quad \sigma = (1-\epsilon)\eta_\nu, \quad \dots \quad (7)$$

$$C(\mu) = \left\{ \frac{\partial I_\nu(0, \mu)}{\partial \sigma} \right\}_{\sigma \rightarrow 0}, \quad E_n(t) = \int_1^\infty \exp(-xt) dx/x^n, \quad (8)$$

$$D_{r+1}(t) = \frac{t^r}{1 \cdot r!} - \frac{t^{r-1}}{2 \cdot (r-1)!} + \dots \frac{(-1)^r}{(r+1)!}, \quad (9)$$

$$\phi_{r+1}(t) = D_{r+1}(t) + (-1)^{r+1} E_{r+2}(t), \quad (10)$$

$$\omega' = \sigma \lambda, \quad \omega = \alpha \omega', \quad \text{both } \omega, \omega' \text{ lie between } 0 \text{ and } 1.$$

$$T(z) = 1 - \omega \frac{1}{2} z \ln \frac{z+1}{z-1}, \quad L_1(z) = 1 - \omega' \lambda z \ln \frac{z+1/\lambda}{z}. \quad (12)$$

$H(z)$  is the unique solution of the integral equation

$$T(z) H(z) = \omega \frac{1}{2} \int_0^1 \frac{x H(x) dx}{x-z} + \sqrt{(1-\omega)}, \quad (13)$$

and

$$H(-z) \rightarrow 1 + (\omega - R_0) z \ln z + O(z) \text{ as } z \rightarrow 0, \quad (14)$$

We further put

$$\omega_0 = \omega'(1+\lambda) - R_0, \quad (15)$$

$$L_2(z) = 1 - \omega_0 z \ln \frac{z+1}{z}, \quad (16)$$

$$U(z) = H(-z)L_1(z) - L_2(z) = u_0 + U_-(z) - U_+(z), \quad (17)$$

where  $u_0 = \lim_{z \rightarrow \infty} U(z)$  and  $U_-(z)$  is a function regular outside a loop enclosing the branch cut  $(0, -1/\lambda)$  on the left of the imaginary axis, while  $U_+(z)$  is a function regular outside a loop enclosing the cut  $(0, 1)$  and the pole  $K$  (real) which is the positive real root of  $T(z)$  outside the cut  $(0, 1)$ .

$$B_\nu(t) = \sum_0^N b_r t^r, \quad g^0(z) = -\frac{1}{2} \sum_0^N b_r r! \lambda^r z^r, \quad \dots \quad (18)$$

$$Q^0(z) = \sum_0^N Q_r^0 z^r, \quad Q_r^0 = \frac{1}{2} \sum_{s=0}^N \frac{b_{r+s} (r+s)!}{s+1} \quad \dots \quad (19)$$

$$R(z) = \sum_0^N \frac{r+1-\epsilon}{1-\epsilon} b_r r! z^r, \quad \dots \quad (20)$$

$$f^0(z) = \sum_0^N \{b \omega' (Q_r^0 + C_r^0) + \lambda \gamma b_r r!\} \lambda^r z^r, \quad \dots \quad (21)$$

where  $C^0(z) = \sum c_r^0 z^r$ ,  $c_r^0$ 's are determined from the boundary condition (6), (22)

$\delta_0$  = wing-damping constant of a broadened line, (23)

$\delta$  = damping constant of the profile of the absorption co-efficient, (24)

$r_0(\mu)$  = central residual intensity of the line, (25)

$I_v^c(0, \mu) = \sum b_r r! \mu^r$  = intensity in the continuum, (26)

$$\beta = \frac{\delta_0^2}{(1-\epsilon)\delta^2\eta_v}, \quad G(z) = \frac{1}{2}\omega' \int_0^1 \frac{x I_v(0, x) dx}{x-z} \quad (27)$$

The solution of the integro-differential equation (1) is obtained with the help of Laplace transformation in combination with the principle of analytic continuation. In obtaining our solution it has been possible to avoid the normal practice of assuming an approximate form of  $J(t)$ . We have been able to find an explicit, closed expression for  $J(t)$  by a new approach based on the expansion of  $I_v(0, \mu)$  in powers of  $\sigma$  (justification for this expansion has been advanced).

If  $C(z)$  in (8) is assumed to be a polynomial in  $z$  (an assumption analytically unjustifiable) we can find an expression depending on the coefficients  $b_r$ 's and  $a_r$ 's provided  $r_0(z)$  can be determined by  $r_0(z) = \sum_0^N a_r z^r / I_v''(0, z)$ . The solution of (1) is then obtained on this basis.

However an analytically correct expression for  $C(z)$  has been found and is given by

$$C(z) = Q^0(z) + \left\{ \sum_0^N b_r r! z^r \right\} \frac{1}{2} z \ln \frac{z+1}{z} - R(z) + b C^0(z), \quad \dots (28)$$

and then the pseudo average intensity  $J(t)$  is obtained as

$$J(t) = \sum_0^N Q_r^0 t^r / r! + \sum_0^N C_r^0 t^r / r! + \frac{1}{2} \sum_0^N b_r r! \phi_{r+1}(t). \quad \dots (29)$$

After getting an expression for  $J(t)$  as given by (29) it is possible to solve the equation (1) and the emergent intensity is then obtained and given by

$$I_v(0, z) = H(z) A^0(z) + b H(z) g^0(z) \{U_-(z) + L_2(z)\}, \quad \dots (30)$$

where

$$A^0(z) = \text{Lt.}_{z \rightarrow \infty} \{b g^0(z) [u_0 - U_+(z)] + H(-z) [a G(z) + f^0(z) - b g^0(z)]\} \quad \dots (31)$$

From the solution (30) we can get the emergent intensity for coherent scattering simply by putting  $b = 0$  in it (as we should). The solution based on the polynomial representation of  $C(z)$  is defective in this respect. The solution for completely non-coherent scattering is deduced by putting  $a = 0$  in (30). The expression (29) giving  $J(t)$  is interesting.

#### REFERENCE

W. Busbridge, M. N., 1953, **113**, 52.



## CRYSTAL STRUCTURE OF THIODIGLYCOLLIC ACID

SUKLA ROY

INDIAN ASSOCIATION FOR THE CULTIVATION OF SCIENCE,  
CALCUTTA-32.

(Received November 12, 1964)

The unit cell and space group of thiodiglycollic acid has already been determined (Roy, 1962). The lattice is orthorhombic and there are 4 molecules per unit cell. The systematic absences observed are consistent with the space group Pnam or Pna2<sub>1</sub> with

$$a = 5.03 \pm .03 \text{ \AA}$$

$$b = 6.66 \pm .03 \text{ \AA}$$

$$c = 17.76 \pm .03 \text{ \AA}$$

All the intensity data were obtained from Weissenberg photograph about *a* and *b* axis using multiple film technique (Robertson, 1943). Intensities were estimated visually by comparison with a standard intensity strip. After correction for Lorentz and polarisation factors  $F_o^2(okl)_e$  were put on an absolute scale by Wilson's method. No correction for absorption was made at this stage.

The  $N(Z)$  statistical test (Howells *et al.*) was applied to 100 zone reflections for which the projection is centric for Pnam and acentric for Pna2<sub>1</sub>. It was found that the experimental values of  $N(Z)$  agreed very well with the theoretical curve for the centrosymmetric case, thereby implying the space group Pnam.

There are 8 general positions for the space group Pnam. Since each unit cell of the crystal contains 4 molecules the sulphur atoms must occupy the following special position,

$$x, y, \frac{1}{2}; \quad \bar{x}, \bar{y}, 3/4; \quad \frac{1}{2}-x, \frac{1}{2}+y, 3/4; \quad \frac{1}{2}+x, \frac{1}{2}-y, 1/4;$$

Using the *okl* data a two-dimensional Patterson was computed to facilitate the determination of approximate *y, z* parameters of the sulphur atoms.

Approximate coordinates of the sulphur atoms thus obtained were used to calculate the structure factors of the *okl* reflections.

Signs of some of the structure factors thus obtained were then used to compute the (100) electron density projection (Fig. 1) from which an approximate trial structure could be postulated. At this stage the reliability index was 0.42. The overall temperature factor was taken throughout to be 1.34.

Three cycles of Fourier refinement reduced the  $R$  value to .34. But no further change was observed. Two cycles of difference fourier were then carried

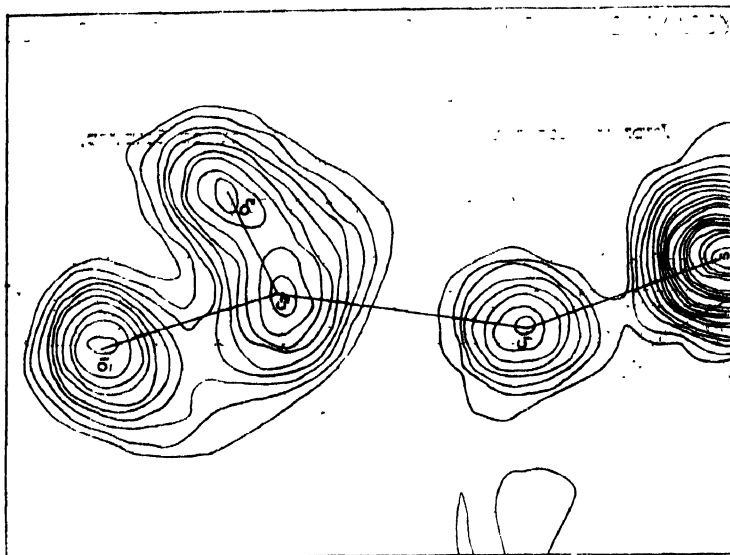


Fig. 1

out and these reduced the  $R$  value to 0.26. It was apparent from the difference Fourier that some atoms had a temperature factor higher than 1.34 and the sulphur atom had an anisotropic temperature factor.

Another Patterson projection was computed to determine the third co-ordinate from the 'b' axis 0-layer data. The  $R$  value for this zone is now 0.30.

Further refinement is proceeding using difference synthesis and least squares method.

Throughout the analysis of the crystal the scattering factor value of Berghus *et al.* were used for carbon and oxygen while scattering factors of sulphur were based on values given by C. H. Stam.

#### ACKNOWLEDGMENT

The author is thankful to Prof. B. N. Srivastava, D.Sc., F.N.I., for his keen interest in the problem and to Dr. Sankar Kumar Datta for suggesting the problem and guidance throughout the piece of work.

#### REFERENCES

- Berghus, J., Haanappel, Y. M., Patters, M., Loopstra, B. O., Mac Gillary, C. H., Veenendaal, A. L., 1956, *Acta Cryst.*, **3**, 478.  
 Howels, E. R., Phillips, D. C. and Rogers, D., 1950, *Acta Cryst.*, **3**, 21.  
 Roy, S., 1962, *Ind. J. Phys.*, **38**, 493.  
 Robertson, J. M., 1943, *J. Sci. Inst.*, **20**, 175.  
 Tomlin, Y. H., and Stam, C. H., 1958, *Acta Cryst.*, **11**, 126.  
 Wilson, A. J. C., 1942, *Nature*, **150**, 162.

# THE ENERGY DENSITY OF SOLAR WIND AND ITS CORRELATION WITH COSMIC RAY INTENSITY

CH. V. SASTRY

YALE UNIVERSITY OBSERVATORY, U.S.A.

(Received November 11, 1964)

In a recent investigation Snyder *et al.* (1963) found a strong correlation between the daily average velocity of solar wind measured with the space probe Mariner 2 at a distance of 0.7 to 1.0 AU and the geomagnetic planetary index  $K_p$  for the period Aug. 20 thru Dec. 17, 1962. They compared the average plasma velocity with data on daily mean cosmic ray intensity and also the diurnal variations of cosmic ray intensity but found no significant correlations. Snyder (1964) calculated the number density, temperature and energy density Kev/cm<sup>3</sup> of the interplanetary plasma with certain simplifying assumptions (e.g. Maxwell-Boltzmann velocity distribution etc.) In the present study a power spectrum analysis (Blackman and Tukey 1958) is made on the daily mean energy density (actually daily average of three hour averages) and the daily mean cosmic ray intensity recorded at Climax for the period Aug. 29 thru. Dec. 17, 1962. Fig. 1 shows the

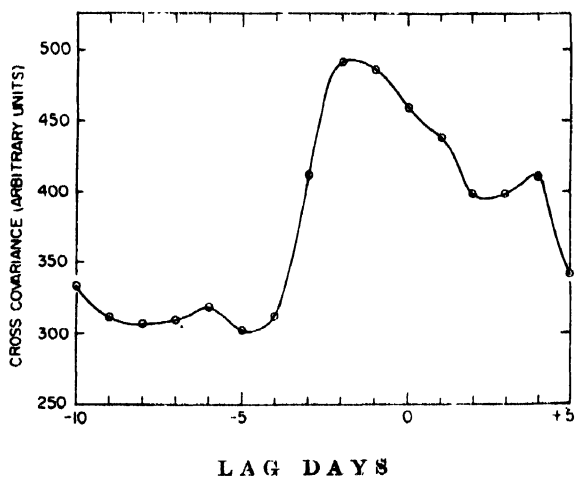


Fig. 1

cross covariance function from  $-10$  to  $+5$  days. It can be seen from Fig. 1 that the cross covariance reaches a maximum value around  $-2$  to  $-1$  days. The linear cross correlation coefficient corresponding to the peak in Fig. 1 is  $+0.56 \pm 0.06$ . The power spectrum of each of the time series shows that they have approximately same periodicities of the order of 25 days and the cross spec-

trum indicates that the maximum contribution to the cross covariance comes from periods of the same order.

In view of the present day accepted theories of cosmic ray intensity variations, interplanetary plasma variations and geomagnetic disturbances the lack of dependence of  $K_p$  variations on kinetic pressure of interplanetary plasma (Snyder *et al.* 1963) and the present correlation of cosmic ray intensity changes with the energy density, particularly the phase lag, are interesting. The computations will be extended to the plasma data collected in 1963 for well over six months (Snyder 1964) and if the present results are confirmed many important conclusions can be arrived regarding interplanetary gas dynamics and solar modulation of galactic cosmic rays.

The author wishes to thank Prof. Conway W. Snyder of the Jet Propulsion Laboratory for providing the plasma data and for helpful discussions. The cosmic ray data are taken from CRPL F series.

#### REFERENCES

- Blackman R. B. and Tukey J. W.—The measurement of power spectra. Dover publications Inc. 1958.
- Snyder C. W., Neugebauer M. and Rao, U. R. 1963, *Journ. Geophys. Res.* **68**, 6361.

# MAGNETORESISTANCE IN SINGLE CRYSTALS OF GRAPHITE

R. BHATTACHARYA

DEPARTMENT OF MAGNETISM, INDIAN ASSOCIATION FOR THE CULTIVATION OF SCIENCE,  
CALCUTTA-32

(Received January 19, 1965)

**ABSTRACT.** Transverse and longitudinal magnetoresistance in single crystals of graphite have been studied at room temperature for currents both along and perpendicular to the basal plane. The effect of orientation of the magnetic field with respect to the direction of current as well as of the crystallo-graphic axis have also been studied. It has been observed that for both transverse and longitudinal cases with currents along or perpendicular to the basal plane, maximum magnetoresistance is obtained only when the magnetic field is parallel to the hexagonal axis. Magnetoresistance has been found to deviate from a  $H^2$  ( $H$  being the magnetic field strength) law of magnetic field variation down to the minimum field available for this investigation, namely about 350 Oersteds.

## INTRODUCTION

Magnetoresistance effects in crystals of graphite studied so far (Kinchin, 1953; Berlincourt and Steele, 1955; Soule 1958) have been only for currents along the basal plane and magnetic field mostly normal to the direction of the current (i.e. the transverse magneto-resistance effect only). But it has been shown by Krishnan and Ganguli (1939), Dutta (1953) Ubbelohde (1960), Primak and Fuchs (1954) and others that there is an appreciable amount of contribution to the electrical properties, from electrons or holes, (probably thermally excited) along the direction perpendicular to the basal plane. Further, it has been pointed out (Wilson 1954; Pearson and Suhl, 1951; Allgaier, 1958) that in cases of anisotropic semiconducting crystals longitudinal magnetoresistance i.e. change of resistance with magnetic field along the direction of the current, in specific directions of the crystal may be very large, even larger than the transverse effect. It therefore appears necessary to study the transverse as well as longitudinal magnetoresistance effects in graphite crystals for currents along the  $c$ -axis as also the longitudinal effects for currents along the basal plane.

The present communication describes the results of measurements of magnetoresistance in these cases as also for different necessary and possible orientations of directions of electric current and magnetic field with respect to crystallographic axes. It is to be mentioned here that our observations are all for low magnetic fields and at room temperatures so that quantum effects are unobservable.

## EXPERIMENTAL

When a material of electrical resistance  $R$  is placed in a magnetic field its magnetoresistance is given by  $\Delta R/R$  where  $\Delta R$  is the change of resistance caused by the magnetic field and can be observed in the following cases :

- (i) When the magnetic field is parallel to the direction of electric current and its effect is measured in the direction of current.
- (ii) When the magnetic field is perpendicular to the direction of current and the effect is measured in the direction of the current.
- (iii) When the magnetic field is perpendicular to the direction of electric current and the effect is measured perpendicular to both current and magnetic field.

The case (i) above is the longitudinal magneto-resistance effect referred to in the previous section. Of the two remaining cases, the last one is nothing but the Hall effect. It will be noticed that a small misalignment of the Hall electrodes, in the measurement of the Hall effect, from exact normal direction to  $H$  and  $E$  will cause an appreciable superimposed effect from transverse magneto-resistance effect. From the remaining case i.e. case (ii) one can obtain transverse magneto-resistance effect directly. In our case we have usually measured the transverse magnetoresistance effect, adopting the arrangement of case (ii) though some measurements by the arrangement (iii) were also taken.

The specimens used were flakes of well developed single crystals of graphite obtained from Ceylon and carefully cut into suitable forms. In order to be sure that no appreciable crystalline defects are produced by these cutting treatments the specimens were examined by X-rays before and after such operations. The specimens are mounted in specially designed holders so that crystals of different sizes can be accommodated in them, maintaining at the same time the appropriate length to breadth ratio. Resistances were measured by the usual potentiometric method using a "Pye" precision vernier potentiometer reading down to one micro-volt. Any thermal effects superposed on the effects studied were eliminated in the usual way.

The following sets of observations were taken in course of this investigation.

A. For currents in the basal plane of the crystal :

- (1) direction of current vertical and magnetic field horizontal; rotation axis vertical (basal plane of crystal necessarily vertical)
- (2) directions of current and magnetic field both horizontal; rotation axis vertical; basal plane vertical.

B. For current along the  $c$ -axis (perpendicular to the basal plane) :

- (1) direction of current and magnetic field both horizontal; rotation axis vertical (basal plane necessarily vertical)

In all cases observations were taken for different angles between the  $c$ -axis and the magnetic field. It is to be noted that other dispositions of the crystal specimen in the magnetic field are possible, but a little consideration will show that these will lead to no new information.

# RESULTS

Results of different observations are represented in Tables II to IV and in figures 1 to 4. In Table I, are represented for the sake of comparison, values of magnetoresistance obtained from direct observations also from Hall effect measurements. The values obtained by the two methods are more or less the same. So at room temperature we found no difference in the two methods of observation as was found by Berlincourt and Steele (1955) at low temperature.

TABLE I

Values of transverse  $\Delta R/R$  obtained directly and from Hall effect measurements

Magnetic field strength in Oersteds	Transverse $\Delta R/R$ from direct observation; current in the basal plane	Transverse $\Delta R/R$ from Hall effect measurements; current in the basal plane
4000	.0630	.0685
3000	.0400	.0420
2000	.0190	.0195
1000	.0053	.0055
500	.0015	.0017

For currents along  $c$ -axis observed Hall e.m.f.s. being very small, magnetoresistance obtained after necessary corrections will not be accurate and hence has not been included in the Table I.

For currents along the basal plane maximum magnetoresistance is always observed when the angle between the magnetic field and the  $c$ -axis is zero, disposition of current and magnetic field being transverse to each other. But when current is perpendicular to the basal plane, though magnetoresistance is maximum when the above angle is zero yet the relative disposition of current and field instead of being transverse is parallel and the magnetoresistance we observed is a longitudinal one.

TABLE II

Variation of  $\Delta R/R$  with the magnetic field and with orientation in the magnetic field. Current along basal plane and vertical;  $\theta$  is the angle between  $c$ -axis and magnetic field

Magnetic field in Oersteds	$\Delta R/R$			
	$\theta = 0^\circ$	$\theta = 30^\circ$	$\theta = 70^\circ$	$\theta = 90^\circ$
7500	.1792	.1330	.0462	.0059
7175	.1657	.1242	—	—
6750	.1518	.1131	.0388	.0051
6350	.1356	—	—	—
5800	.1198	.0882	.0300	.0040
5100	.0938	—	—	—
4275	.0729	.0534	.0178	.0024
3400	.0473	.0344	.0116	.0014
2875	.0353	—	—	—
2300	.0243	.0173	.0059	.0008
1750	.0160	.0109	.0035	.0004
1175	.0069	.0057	.0018	.0002
600	.0019	.0014	.0003	—
350	.0007	.0005	.0002	—

TABLE III

Variation of  $\Delta R/R$  with magnetic field and with orientation in magnetic field. Current along basal plane and horizontal,  $\theta$  is the angle between  $c$ -axis and magnetic field

Magnetic field in Oersteds	$\Delta R/R$			
	$\theta = 0^\circ$	$\theta = 30^\circ$	$\theta = 60^\circ$	$\theta = 90^\circ$
7500	.1762	.1370	.0572	.0038
6750	.1485	.1163	.0470	.0033
5800	.1151	.0899	.0402	.0026
4275	.0692	.0543	.0219	.0017
2300	.0232	.0179	.0078	.0006
1175	.0068	.0054	.0023	.0001
350	.0005	.0005	.0002	—



TABLE IV

Variation of  $\Delta R/R$  with magnetic field and with orientation in magnetic field. Current perpendicular to basal plane and horizontal.  $\theta$  is the angle between current and magnetic field i.e. between  $c$ -axis and the field.

Magnetic field in Oersteds	$\Delta R/R$			
	$\theta = 0^\circ$	$\theta = 30^\circ$	$\theta = 60^\circ$	$\theta = 90^\circ$
7500	.0421	.0327	.0135	.0008
6750	.0364	.0279	.0118	.0005
5800	.0281	.0214	.0090	The values became too low to be reliably measured with our potentiometer.
4275	.0180	.0136	.0056	
3400	.0118	.0089	.0039	
2300	.0062	.0059	.0022	
1175	.0025	.0018	.0006	
350	—	—	—	

In order to test the observations of magnetoresistance for current along the basal plane and flowing in a vertical direction with the magnetic field horizontal, observations have also been recorded with a thin flake of graphite crystal having a minimum width as well as with a plate of extruded sample of graphite, the disposition of current and magnetic field being same as before. The importance of these observations will be discussed in the next section.

It may be pointed out here that for currents along the basal plane the magnetoresistance effects observed for the cases when the current is vertical and when it is horizontal are slightly different and is obviously a consequence of crystal anisotropy.

#### DISCUSSION

Before proceeding to discuss the various results of observations on the magnetoresistance effects in graphite, it should be borne in mind that graphite is a natural crystal and a considerable amount of mosaicity in structure is present in it in addition to foreign impurities. Any attempt to remove the foreign impurities increases the mosaicity further (Ray, 1959) which again considerably affects the different bulk properties of the crystal (Bhattacharya, 1959). Therefore all discussions on the observed properties of graphite will be under this limitation, that is, there is present an appreciable amount of mosaicity of structure in all crystals of graphite obtained from natural sources whether purified or not.

- (i) *Current along the basal plane flowing in a vertical direction, magnetic field being horizontal and the rotation axis vertical*

Under this arrangement, for all orientations of the crystal with respect to the magnetic field, the latter is always transverse to the current. But the magnetoresistance observed changes (figures 1 and 4) as the angle between the

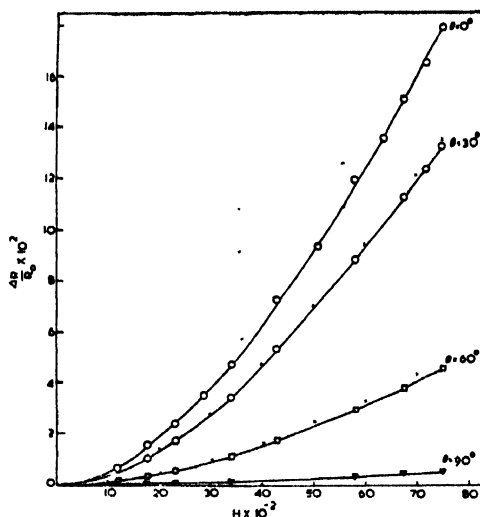


Fig. 1.—Variation of transverse  $\Delta R/R$  with magnetic field  $H$  for different values of the angle between magnetic field and  $c$ -axis of the Crystal; current along the basal plane and vertical,  $\Delta$  field being horizontal.  $\times \times \times$  Calculated points.

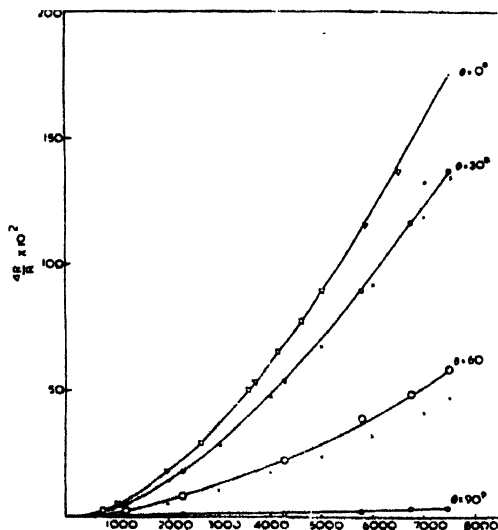


Fig. 2.—Variation of  $\Delta R/R$  with  $H$ , the magnetic field for different values of  $\theta$ ; current along basal plane and horizontal; field horizontal.  $\times \times \times$  Calculated points.

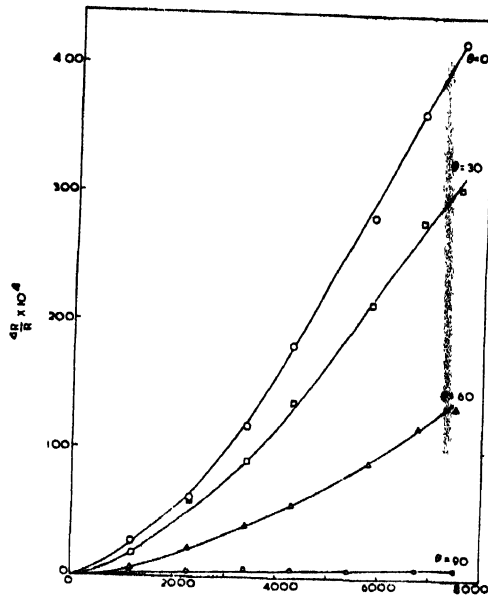


Fig. 3.— Variation of  $\Delta R/R$  with  $H$ , the magnetic field for different values of current  $I$  to the basal plane and horizontal, field also horizontal.

$c$ -axis and the magnetic field changes, being maximum when this angle is zero and minimum when it is  $90^\circ$ . That this observation is a consequence of crystal anisotropy and not a size effect is verified by repeating the experiment with a crystal having a minimum width, when similar results were obtained; but when it was repeated with an extruded sample of graphite which is practically polycrystalline and whose dimensions are similar to those utilised for this investigation, magnetoresistance was found to remain practically constant for all orientations of the crystal with respect to the magnetic field. The observations may therefore be explained on the basis of high anisotropy of graphite due to which effective mass of the carriers for motion in the basal plane is, as is well known, (Shoenberg, 1952-53; Krishnan and Ganguli, 1941; Dutta, 1958) very small in comparison with that in directions parallel to the  $c$ -axis. Magnetoresistance which is inversely related to the effective masses of the electrons (or holes) will evidently be much larger in the basal plane than in a perpendicular direction. At any intermediate orientation the effect observed will be a resultant in that particular direction of the components of the two extreme values, the effective part of the Lorentz force producing the effect being different for each orientation. In addition to these there will be a contribution from the magnetoresistance effects due to differently misoriented crystallites in the specimen. Our observed values are the statistical averages of all these.

In view of what has been stated above, magnetoresistance  $\Delta R/R$  at any

angle between the field and the  $c$ -axis will evidently be given by the relation of the type

$$\Delta R/R = A \cos^2\theta + B \sin^2\theta$$

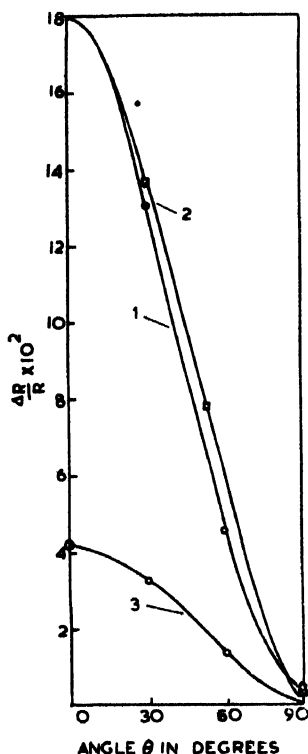


Fig. 4.— Variation of  $\Delta R/R$  with  $\theta$  for different directions of current.

H = 7500 Oersteds.

Curve (1) Current parallel to basal plane and vertical, H horizontal, rotation axis vertical; arrangement always transverse.

Curve (2) Current parallel to the basal plane and horizontal, H horizontal, rotation axis vertical; arrangement transverse when  $\theta = 0^\circ$  and longitudinal when  $\theta = 90^\circ$ .

Curve (3) Current perpendicular to the basal plane and horizontal, H horizontal, rotation axis vertical; arrangement transverse when  $\theta = 90^\circ$  and longitudinal when  $\theta = 0^\circ$ .

where  $A$  and  $B$  are respectively the maximum and minimum values of magnetoresistance. The calculated values according to this relation are plotted in figures 1 and 2 alongside the curves showing the variation of observed  $\Delta R/R$  with angle of orientation and with magnetic field. The slight deviations observed are due presumably to experimental missettings and misoriented crystallites present in the basal plane and whose contributions to magnetoresistance are not related in any simple way with the variations of  $\theta$  and magnetic field, since in considering the contributions towards the principal magnetoresistance of the crystal both the

transverse as well as longitudinal components from the different misoriented crystallites will have to be taken into account. This can however be done provided we know the number of misoriented blocks at any particular angle of misorientation. We have recently developed a method of doing this and the results obtained after employing the method are going to be published soon.

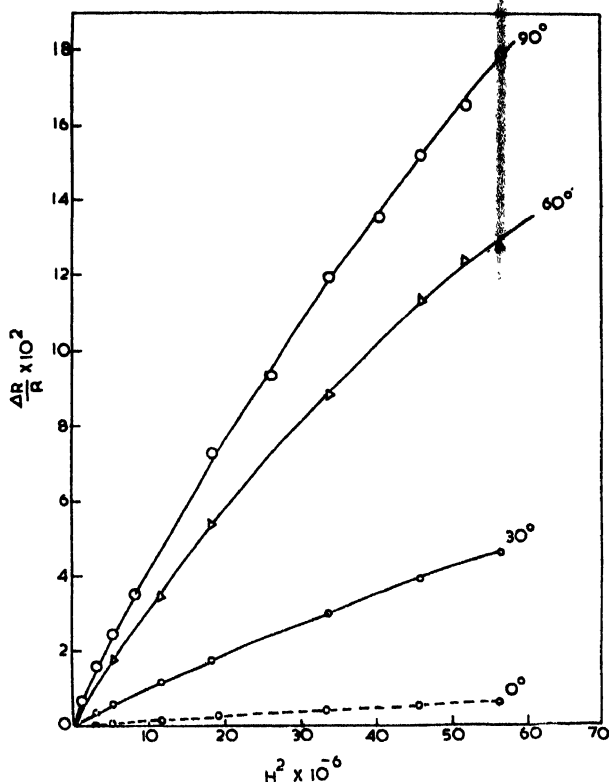


Fig. 5.—Variation of transverse  $\Delta R/R$  with  $H^2$  for currents along the basal plane and  $\theta = 0^\circ$

Before concluding this section it may be remarked that the very low value of  $\Delta R/R$  observed when the angle between the  $c$ -axis and the field is  $90^\circ$  may be considered to be due not only to transverse magnetoresistance considerably diminished as a consequence of the bending of electron paths taking place in directions parallel to the  $c$ -axis of the crystal but also to contributions from mis-settings and misorientations of crystallites which are also very small.

- (ii) *Current along the basal plane flowing in a horizontal direction, magnetic field being horizontal and rotation axis vertical*

The observations recorded (figures 2 and 4) in this arrangement are more or less of the same type as in (i) above with the exception that when the field and the current are parallel i.e. when the angle between the field and the basal plane is

zero (angle between the  $c$ -axis and field is  $90^\circ$ ) the feeble magnetoresistance (much feebler than in the similar disposition with the transverse case discussed above) observed, is due to contributions from misalignment of crystallites in the basal plane, as well as longitudinal magnetoresistance in the basal plane.

(iii) *Current along  $c$ -axis flowing in a horizontal direction, magnetic field being horizontal and rotation axis vertical*

Magnetoresistance in graphite with this arrangement has not been studied earlier. The nature of variation of  $\Delta R/R$  with the angle between field direction and current direction though more or less of the same type as discussed above yet differ in one important aspect. In all the earlier cases the transverse magnetoresistance was always much larger than the longitudinal one (see figure 4) but in this arrangement the reverse is the case (figure 3). Similar behaviour, namely longitudinal  $\Delta R/R$  value greater than transverse one has been observed in semiconductors like  $n$ -type germanium (Pearson and Soule, 1951) and  $p$ - and  $n$ -type PbTe (Allgaier, 1958) for currents in some specified directions. Incidentally, it may be mentioned here that graphite behaves as a semiconductor for currents along directions parallel to the  $c$ -axis (Dutta 1953), currents being most probably mainly carried by holes (Ubbelohde *et al.* 1960).

In this connection it is interesting to note that whether the arrangement is transverse or longitudinal, magnetoresistance is maximum when the magnetic field is perpendicular to the basal plane for both directions of current.

(iv) *Variation of  $\Delta R/R$  with Magnetic field.*

In order to test the usual  $H^2$  law of variation of  $\Delta R/R$  we plotted for current along the basal plane transverse  $\Delta R/R$  against  $H^2$  where  $H$  is the field strength in figure 5. It is observed that deviations are quite appreciable. These deviations may be either genuine or due to crystal defects present in the samples or both. However, from the logarithmic plot (figure 6) made for the purpose we obtained a  $H^{1.69}$  variation for currents along the basal plane flowing in a vertical direction for higher fields 2000 to 7500 Oersteds and a  $H^{1.88}$  variation for lower values of fields (350 to 2000 Oersteds). Similar is the case for currents along the basal plane flowing in a horizontal direction. When current is along directions parallel to the  $c$ -axis we could utilise the values of the longitudinal case, only, the transverse values being too small to be relied upon for any discussion. In the range of fields within which the observed values can be taken to be reliable the variation follows a  $H^{1.62}$  law. Other workers (Kinchin, 1953; Berlincourt and Steele, 1955; Soule 1958), who also studied the field variation of  $\Delta R/R$  obtained deviations from  $H^2$  law. Their values can be summarised in the following table (Table V), our values also being included for comparison. Soule (*loc cit.*), who has made somewhat exhaustive study of the field variation of  $\Delta R/R$  at room temperatures and low fields, suggests that deviation from  $H^2$  law which takes

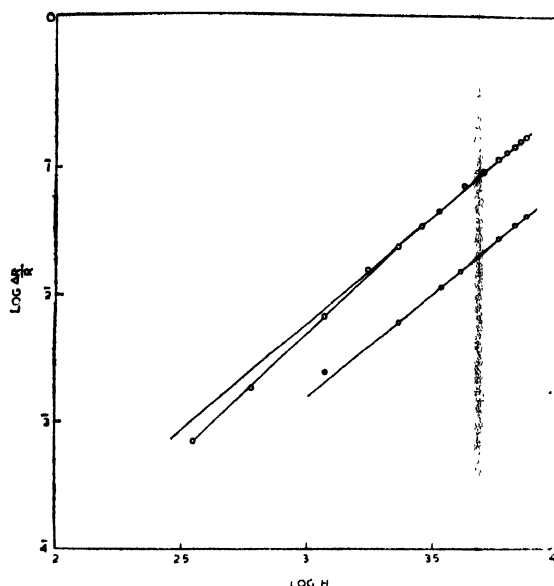


Fig. 6. Variation of  $\log \Delta R/R$  with  $\log H$ .  
 Curve (1) Current along basal plane,  $\theta = 0^\circ$  (transverse)  
 Curve (2) Current  $\perp$  to basal plane,  $\theta = 0$  (longitudinal)

TABLE V

Values of  $p$  in the relation  $\Delta R/R = BH^p$  obtained by different authors

Sample studied	Relative orientations of current and magnetic field	$H^p$				
		Author				
		Berlincourt Steele (loc.cit)	Soula (loc.cit)	Kinchin (loc.cit)	McClelland (1955)	Present Author
Poly crystalline graphite	transverse	—	—	H1.74 temp. 77°K to 290°K field not mentioned.	H1.77 temp. 300°K Field 5-15 K.O.	—
Single crystal	transverse Current along basal plane, $H \perp$ to current	H.80 at liq. He temp. field 25 K.O.	H1.78±03 above 77°K H.82 at liq. He temp. Field in both cases 25 K.O.	H1.74 temp. 290°K Field upto 6 K.O. and at 4.2°K $H < 1.74$	—	H1.69 at 2 K.O. to 7.5 K.O. & H1.88 at .35 K.O. to 2 K.O. and all at room temp.
Single Crystal	Current parallel to c-axis and $H$ parallel to Current.	—	—	—	—	H1.62 with fields from 1 K.O. to 7.5 K.O. and at room temperatures.

place above a critical field  $H_c$  is a consequence of the purity of the crystal,  $\Delta R/RH^2$  increasing and  $H_c$  decreasing with purity. In view of this we may remark that our specimens were sufficiently pure since we did not observe any  $H_c$  even down to 350 Oersteds (Fig. 6). It therefore appears that deviation from  $H^2$  law is a genuine one at least at room temperatures. But before accepting such a view proper consideration of the crystal defects which are naturally present and are further developed in course of chemical purification (crystals used by Soule were also purified in the usual way) should be taken into account.

#### CONCLUDING REMARKS

The results of the observations reported here have not obviously been discussed in the light of any theory partly because no proper theory for magnetoresistance in anisotropic crystals for transverse and longitudinal cases has yet been developed and partly because observations have not been extended down to low temperatures. Investigations are in progress in these lines and will be published soon.

#### ACKNOWLEDGMENTS

The author expresses his best thanks to Shri A. K. Dutta for suggesting the problem and for his guidance throughout the course of the work and to Prof. A. Bose for his keen interest in the work. Thanks are also due to Mr. L. J. D. Fernando, Director, Geological Survey Department, Government of Ceylon, for kindly presenting us with some crystals of graphite with which measurements reported in this paper have been made. The author is also indebted to Professor E. W. J. Mitchel of the University of Reading for the extruded samples of graphite and to the Workshop of the Association for the cooperation received from them whenever it was called for.

#### REFERENCES

- Allgaier, R. S. 1958, *Phys. Rev.*, **112**, 828.  
 Berlincourt, T. G. and Steele, M. C., 1955, *Phys. Rev.*, **98**, 956.  
 Bhattacharya, R., 1959, *Ind. Jour. Phys.*, **33**, 407.  
 Dutta, A. K., 1953, *Phys. Rev.*, **90**, 187.  
 Dutta, A. K., 1958, *Physics*, **34**, 343.  
 Kinchin, F. H., 1953, *Proc. Roy. Soc.*, **A217**, 9.  
 Krishnan, K. S. and Ganguli, N., 1939, *Nature*, **144**, 667.  
 Krishnan, K. S. and Ganguli, N., 1941, *Proc. Roy. Soc.*, **A177**, 168.  
 McClelland, J. D., 1955, *Phys. Rev.*, **100**, 1807.  
 Pearson, G. L. and Suhl, H., 1951, *Phys. Rev.*, **83**, 768.  
 Primak, W. and Fuchs, L. H., 1954, *Phys. Rev.*, **95**, 22.  
 Ray, S., 1959, *Ind. Jour. Phys.*, **33**, 282.  
 Shoenberg, D., 1952-53, *Phil. trans.*, **A245**, 1.  
 Soule, D. E., 1958, *Phys. Rev.*, **112**, 698.  
 Ubbelohde, A. R., Blackman, L. C. F. and Dundas, P. H., 1960, *Proc. Roy. Soc.*, **255**, 293.  
 Wilson, A. H., 1954. The theory of metals, Second Edition. Cambridge, At the University Press, Page 241,



# THE VISIBLE EMISSION SPECTRUM OF BiCl MOLECULE

V. SATYANARAYANA RAO AND P. TIRUVI NGANNA RAO

SPECTROSCOPIC LABORATORIES, DEPARTMENT OF PHYSICS, ANJARA UNIVERSITY, WALTAIR.

(Received August 17, 1964; Resubmitted November 1964)

## PLATE I

**ABSTRACT.** The spectrum of BiCl was reinvestigated in a high frequency discharge both under low and high dispersion. A new system of 12 bands degraded to red designated an  $A'-X$  system has been observed and analysed in the region  $\lambda$  4220–4000 Å. The approximate vibrational constants were determined for the upper state of this system. The rotational analysis of (2,0), (3,0) and (4,0) bands of the  $A'-X$  system of BiCl has led to the determination of the rotational constants. The bands appears to arise from a case (c)  $0^+ - 0^+$  as was assumed previously by Khanna (1961).

## INTRODUCTION

Two discrete band systems, one in the region  $\lambda$  5400– $\lambda$  4220 Å and the other lying in the region  $\lambda$  4000– $\lambda$  3600 Å were analysed and attributed to BiCl molecule. A summary of the early work on this molecule can be found in a paper recently published by Venkateswarlu and Khanna (1960). The vibrational analysis of the visible system was considerably extended to include many new bands in the region  $\lambda$  6170– $\lambda$  4220 Å. From a rotational analysis of five bands (0, 2), (0, 3), (0, 4), (1, 2) and (1, 1) of this system, they have suggested that the system arises from a case (C)  $0^+ - 0^+$  transition. The visible emission spectrum of BiCl has been investigated by the authors both under low and high dispersion. A new system of bands in the region  $\lambda$  4220– $\lambda$  4000 has been observed and analysed. The rotational structure of (2, 0), (3, 0) and (4, 0) has been examined in the second order of a 21 ft. concave grating spectrograph having dispersion (1.25 Å/mm), with the object of gaining new information of the rotational constants of the  $v' = 2, 3, 4$  levels of the upper state and  $v'' = 0$  level of the lower state of the visible system. The results of the rotational analysis of those three bands and the vibrational analysis of the system ( $A'-X$ ) of bands in the region  $\lambda$  4220– $\lambda$  4000 Å are presented in this paper.

## EXPERIMENTAL

The spectrum was excited in a high frequency discharge through the vapour of anhydrous BiCl<sub>3</sub> under low pressure conditions. Photographs of the spectra in the visible region were taken on a Hilger 3 prism glass Littrow spectrograph

and in the second order of 21 ft. concave grating spectrograph using Agfa Super Special plates. Exposure of one hour's duration was found sufficient for developing the rotational structure of the visible system. The bands (2, 0), (3, 0) and (4, 0) which were found to be free from overlapping of neighbouring bands, were selected for measurement of the rotational lines. Further these bands are not previously analysed by Khanna (*loc. cit.*). A new group of bands in the region  $\lambda 4220 - \lambda 4000 \text{ \AA}$  degraded towards the red were measured from the plates taken on the glass littrow instrument. The accuracy of the measurements of the band heads is  $2 \text{ cm}^{-1}$  while that of the rotational lines is  $0.07 \text{ cm}^{-1}$ .

#### VIBRATIONAL ANALYSIS

Photographs of the spectra reveal the wellknown visible system of BiCl in the region  $\lambda 6170 - \lambda 4220 \text{ \AA}$ . In the region  $\lambda 4220 - \lambda 4000$  a new group of bands degraded towards the longer wavelengths. These do not appear to be related in any way to the bands of the *B-X* system ( $\lambda 4000 - \lambda 3600$ ). The bands of the *B-X* system were not observed in the source of excitation employed in the present work. The new bands in the region  $\lambda 4220 - \lambda 4000 \text{ \AA}$  could not also be fitted into the vibrational scheme of the *A-X* system analysed by Venkateswarlu and Khanna (*loc. cit.*). The bands appear therefore to constitute a new system of BiCl and can be seen in Fig. 1. The analysis of this system was greatly facilitated by the identification of a long  $v'$  progression with  $v'' = 0$  and short  $v'$  progression with  $v'' = 1$ . The  $\Delta G_1$  interval of the levels  $v'' = 0$  and  $v'' = 1$  agrees very closely with the corresponding interval of the ground state 'X' of BiCl. Thus the analysis confirms that the emitter of this system is diatomic BiCl. The two  $v'$  progressions of this new system designated as *A'-X* are shown in Fig. 1. The bands of this system are too weak for a study of the rotational structure on the 21 ft. concave grating spectrograph. Table I gives the vibrational assignments and wave

TABLE I

Vibrational assignments and wave number data of *A'-X* system of BiCl

$v', v''$	Wave number in $\text{Cm}^{-1}$
0,1	23321.0
1,1	23513.0
0,0	23628.0
2,1	23700.0
1,0	23817.0
2,0	24006.0
3,0	24188.0
4,0	24369.0
5,0	24538.0
6,0	24703.0
7,0	24860.0
8,0	25006.0

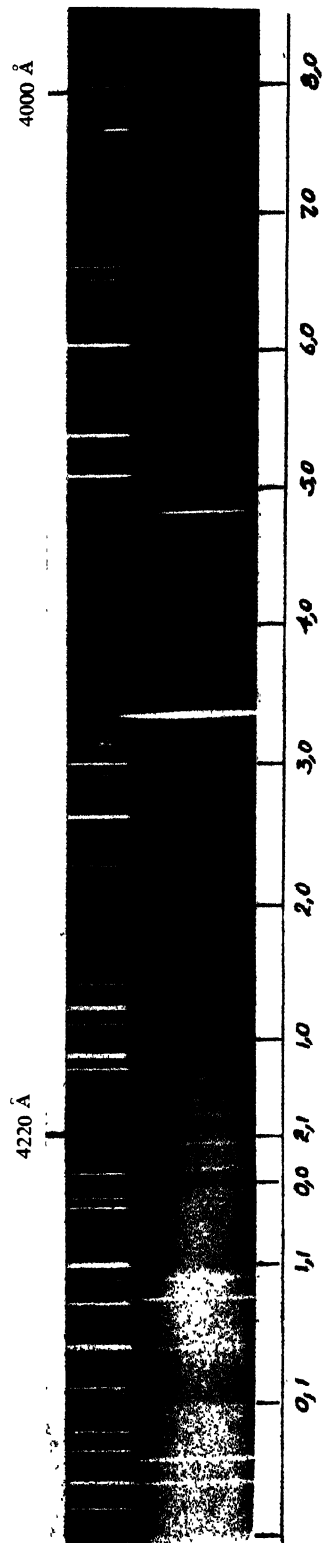


Fig. 1.—Emission Spectrum of  $A^1-X$  System of  $\text{BiCl}$ .

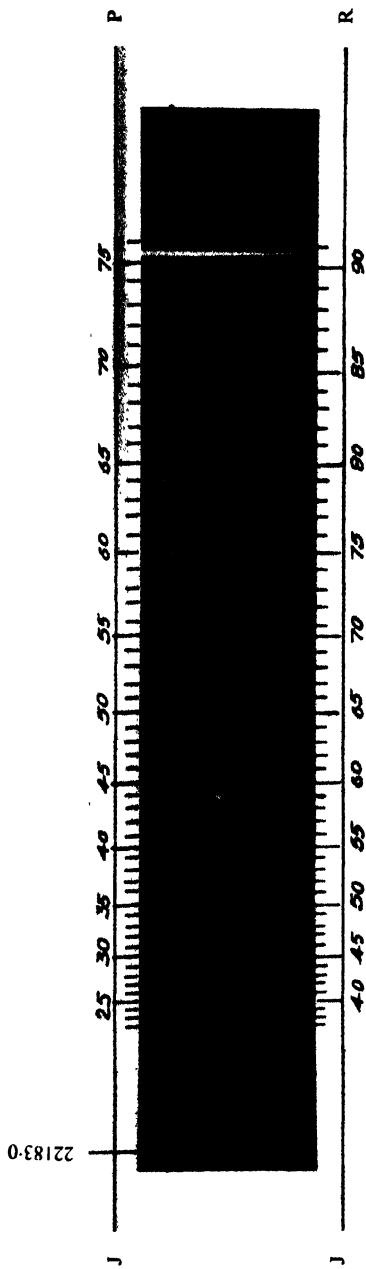


Fig. 2.—Rotational Structure of 2.0 band of  $A^1-X$  system of  $\text{BiCl}$ .



number and Table II gives the vibrational scheme of  $R$  heads of the  $A' - X$  system. Approximate vibrational constants were determined from the vibrational analysis of the  $A' - X$  system of BiCl. They are  $\nu_e = 193.67 \text{ cm}^{-1}$  and  $x'_e \nu_e = 3.17 \text{ cm}^{-1}$ . From the magnitude of the vibrational constants of  $A$  and  $A'$  levels it may be concluded that they arise from the same electron configuration.

TABLE II  
Vibrational analysis of  $A' - X$  system of BiCl

$v'$	$v''$	0	1
0		23628.0	23321.0
		189	192
1		23817.0	23513.0
		189	187
2		24006.0	23700.0
		182	
3		24188.0	
		181	
4		24369.0	
		169	
5		24538.0	
		165	
6		24703.0	
		157	
7		24860.0	
		147	
8		25006.0	

#### ROTATIONAL ANALYSIS

Khanna (1961) reported the rotational analysis and rotational constants of the upper and lower state of (0, 2), (0, 3), (0, 4) (1, 2) and (1, 1) bands. From considerations of electronic configurations for the ground and first excited states of BiCl, the observed simplicity of the bands consisting of only  $P$  and  $R$  branches was attributed to a case (c)  $0^+ \rightarrow 0^+$  transition. Since the information about the rotational constants of the  $v'' = 0$  and  $v' = 2, 3, 4$  is still incomplete, the rotational analysis of the (2, 0), (3, 0) and (4, 0) bands have been carried by the authors. Each of these bands is found to consist of only two branches  $P$  and  $R$ , the branch that forms the head and which becomes weaker at high  $J$  values, is easily identified as  $R$  branch. It is observed that the  $P$  and  $R$  branches are resolved only at high  $J$  values as in the case of each of the five bands analysed by Khanna. As the lines of  $P$  and  $R$  branches do not show any sign of doubling even at high  $J$  values, it is assumed that the bands arise from a case (c)  $0^+ \rightarrow 0^+$  transition.<sup>1</sup>

The procedure for the determination of  $J$  numbering of the rotational lines of five incompletely resolved bands of BiCl has been discussed in detail by

Khanna in his paper. The  $J$  numbering of the rotational lines of (2, 0), (3, 0) and (4, 0) bands has been fixed in the usual way by comparison of the lower state combination differences. The rotational lines of the  $P$  and  $R$  branches of (2, 0) band are shown in Fig. 2. The vacuum wave numbers and rotational assignment of (2, 0) (3, 0) and (4, 0) bands are given in Table III.

TABLE III

Vacuum wave-numbers and rotational assignments for (2, 0), (3, 0) and (4, 0) bands of  $A-X$  system of  $\text{BiCl}$

$J$	(2,0)		(3,0)		(4,0)	
	$R(J)$	$P(J)$	$R(J)$	$P(J)$	$R(J)$	$P(J)$
20						
21						
22		22169.46				
23		168.55				
24		167.72				
25		166.84				
26		165.90				
27		165.01				
28		164.10				22570.28
29		163.16				569.24
30		162.07				568.22
31		160.99				567.24
32		159.91				566.17
33		158.78				565.08
34		157.69				563.91
35		156.42				562.80
36		155.30				561.65
37	22169.46	154.16				560.49
38	168.55	152.85				559.41
39	167.72	151.50				558.06
40	166.84	150.35				556.85
41	165.90	149.06				555.52
42	165.01	147.69				553.99
43	164.10	146.33			22570.28	552.74
44	22163.16	22144.88			22569.24	22551.39
45	162.07	143.43				
46	160.99	142.04	22343.91	568.22	549.94	
47	159.91	140.52	342.48	567.24	548.66	
48	158.78	139.09	341.00	566.17	547.10	
49	157.69	137.57	339.58	565.08	545.58	
			337.86	563.91	544.30	
50	156.42	136.05				
51	155.30	134.47	336.02	562.80	542.76	
52	154.16	132.91	334.39	561.65	541.00	
53	152.85	131.20	332.66	560.49	539.50	
54	151.50	129.50	331.02	559.41	537.65	
			329.36	558.06	535.92	
55	150.35	127.94				
56	149.06	126.36	327.60	556.85	534.42	
57	147.69	124.43	325.79	555.52	532.80	
58	146.33	122.58	323.57	553.99	530.80	
59	144.88	120.78	321.65	552.74	529.04	
			22343.91	551.39	527.22	
			319.80			

TABLE III (Contd.)

<i>J</i>	(2,0)		(3,0)		(4,0)	
	<i>R(J)</i>	<i>P(J)</i>	<i>R(J)</i>	<i>P(J)</i>	<i>R(J)</i>	<i>P(J)</i>
60	143.43	119.00	342.48	317.88	549.94	525.41
61	142.04	117.03	341.00	315.91	548.66	523.58
62	140.52	115.10	339.58	313.96	547.10	521.61
63	139.09	113.22	337.86	311.96	545.58	519.65
64	137.57	111.24	336.02	309.90	544.30	517.78
65	136.05	109.49	334.39	307.90	542.76	515.93
66	134.47	107.47	332.66	305.74	541.00	513.79
67	132.91	105.57	331.02	303.60	539.50	511.87
68	131.20	103.11	329.36	301.50	537.65	509.75
69	129.53	101.11	327.60	299.27	535.92	507.63
70	22127.94	22099.01	22325.79	22297.00	22534.42	22505.56
71	126.36	096.82	323.97	294.86	532.80	503.39
72	124.43	094.72	322.16	292.63	530.80	501.30
73	122.58	092.54	320.30	290.24	529.04	499.09
74	120.78	090.23	318.35	287.93	527.68	496.82
75	119.00		316.36	285.61	526.03	494.36
76	117.03		314.40	283.24	524.11	492.26
77	115.10		312.36	280.84	522.25	490.05
78	113.22		310.44	278.34	520.32	487.74
79	111.24		308.38	275.96	518.40	485.21
80	109.49		306.35	273.52	516.44	482.79
81	107.47		304.25	270.87	514.52	480.42
82	105.57		302.16	268.37	512.55	
83	103.55		300.00	265.74	510.51	
84	101.59		297.81	263.16	508.47	
85	099.43		295.67		506.37	
86	097.36		293.39		504.39	
87	095.18		291.09		502.29	
88	092.98		288.83		500.02	
89	090.79		286.61		497.80	
90	088.63		284.29		495.52	
91	086.43		281.82		493.27	
92			279.46			
93			22276.96			
94			274.56			
95			271.96			
96			269.52			
97			267.08			
98			264.41			
99			261.69			

100

The rotational constants of upper and lower states were determined from the relationship

$$\Delta_2 F(J) = 4B_v(J+1/2)$$

neglecting the effect of *D* correction term. The average value of  $\Delta_2 F''(J)$  for (2, 0), (3, 0) and (4, 0) bands was used for determining the rotational constants

$B_0''$ . Table IV summarises the rotational constants of various levels of the upper and lower states, including also the values obtained by Khanna (1961). The band origins obtained by plotting

$$R(J-1)+P(J) = 2\nu_0 + 2(B'-B'')J^2$$

against  $J^2$  are also included in Table IV.

TABLE IV

Rotational constants of various levels of  $A-X$  system of BiCl

Band Assign- ment	Band Head in $\text{cm}^{-1}$	$B_{P'}$ in $\text{cm}^{-1}$	$B_{P''}$ in $\text{cm}^{-1}$	Band Origin in $\text{cm}^{-1}$
2,0	22183.0	0.101 <sub>7</sub>	0.115 <sub>4</sub>	22181.2
3,0	22388.7	0.101 <sub>3</sub>	0.115 <sub>4</sub>	22386.8
4,0	22588.0	0.101 <sub>0</sub>	0.115 <sub>4</sub>	22586.3
*1,1	21666.0	0.102 <sub>1</sub>	0.114 <sub>6</sub>	21664.5
*1,2	21362.0	0.101 <sub>6</sub>	0.113 <sub>8</sub>	21360.3
*0,2	21147.0	0.102 <sub>5</sub>	0.114 <sub>4</sub>	21144.8
*0,3	20844.0	0.102 <sub>0</sub>	0.113 <sub>6</sub>	20842.0
*0,4	20543.0	0.101 <sub>3</sub>	0.112 <sub>6</sub>	20541.5

\* Constants obtained by Khanna.

TABLE V

Rotational Constants of upper and lower states of  $A-X$  system of BiCl

State	$B_e$ $\text{cm}^{-1}$	$\alpha_e$ $\text{cm}^{-1}$	$D_e$ $\text{cm}^{-1}$	$\beta_e$ $\text{cm}^{-1}$	$r_e$ $\text{\AA}$	$I_e$ $10^{-40}$ $\text{g cm}^2$
Upper	.102 <sub>0</sub>	—	—	—	2.349	274.3
Lower	.115 <sub>4</sub>	—	—	—	2.208	242.5

The  $r_e$  and  $I_e$  values for the upper and lower states are determined from the wellknown relations (Herzberg, 1950). The rotational constants of the upper and lower states are summarised in Table V. The  $D$  terms are not included in the table as they are too small to be determined with the accuracy of the present measurements.

The electronic transition of the  $A-X$  system of BiCl has been fully discussed by Khanna and attributed to a case (c)  $0^+ - 0^+$  transition.



ACKNOWLEDGMENT

The authors wish to express their thanks to Prof. K. R. Rao for his interest and encouragement throughout the progress of this work. One of the authors (V. S. N. Rao) is grateful to the C.S.I.R. for the award of Junior Research Assistantship.

REFERENCES

- Herzberg, G., 1950, *Spectra of Diatomic Molecules* (D. Van Nostrand Co., Inc. New York), p. 180.
- Morgan, F., 1936. *Phys. Rev.*, **49**, 41.
- Khanna, B. N., 1961, *Jour. Mol. Spectroscopy*, **6**, 319-332.
- Prasada Rao, T. A. and Rao, P. T., 1962, *Can. J. Phys.*, **40**, 1077-1084.
- Vonkateswarlu P. and Khanna, B. N., 1960, *Proc. Indian Acad. Sci.*, **51**, 14.

# A HYBRID POTENTIAL FOR INERT GAS ATOMS

ANIL SARAN

INDIAN ASSOCIATION FOR THE CULTIVATION OF SCIENCE, CALCUTTA-32.

(Received December 21, 1964)

**ABSTRACT.** A potential model for inert gas atoms comprising the Morse potential function in the region of potential minimum, molecular beam scattering data in the repulsive region and the experimental  $B(T)$  data for large values of intermolecular separation has been suggested. This hybrid potential has been determined for neon, argon and krypton with fairly satisfactory results.

## INTRODUCTION

The most commonly used forms of the intermolecular potential are the Lennard-Jones (12:6) and the modified Buckingham exp-6 models which involve two and three unknown parameters respectively. Generally these parameters are determined from a set of experimental data and the same parameters are used to calculate other properties. However, it has been found that even for spherically symmetric molecules it is not possible to represent quite satisfactorily the equilibrium and non-equilibrium properties, in terms of a single set of parameters. This has led several workers to suggest that the intermolecular potential can not be adequately represented over the whole range of intermolecular distances by only two or three parameters.

Guggenheim and McGlashan (1960a) were first to suggest a six-parameter potential to obtain the potential energy curve for interaction between two argon atoms. They have utilized different equations to represent the intermolecular potential at different ranges of intermolecular distances. The potential energy curve thus obtained is much deeper and wider than those on the Lennard-Jones (12 : 6) and the exp-6 models. This result is in agreement with the suggestion of Kihara (1953, 1955) that at least for inert gases the intermolecular potential should be wider than those on the Lennard-Jones (12,6) potential. Barua and Chakraborti (1961) and Chakraborti (1963) have extended the treatment of Guggenheim and McGlashan (1960a) with some modification to the case of Kr and Xe respectively. The results obtained were similar to that of Guggenheim and McGlashan.

Recently Konowalow and Hirschfelder (1961) have used the Morse potential function to interpret the various transport and equilibrium properties of substances. The parameter  $c$  of the Morse potential function, which is related to the curvature of the potential at its minimum, makes this potential more flexible than the Lennard-Jones (12:6) potential. Konowalow and Hirschfelder have pointed

out that this potential will be better representation near the potential minimum although at small and large separations it may be lead to erroneous results. They have utilized mainly the crystal properties data to determine the force constants for several nonpolar molecules. Saran (1963) has used transport properties data to obtain the parameters on the Morse potential. The two sets of parameters are, however, found to differ considerably from each other and probably this points to the failure of the Morse potential far from the regions of potential minimum which is stressed by crystal properties data. It is seen from Table I that the depth (also the width which can be seen by actual drawing of the potentials) on the Morse potential as obtained from crystal properties data is very close to the values obtained on the six-parameter potential. This has led Saran and Barua (1964) to suggest the use of the Morse potential (as obtained from the crystal properties data) near the potential minimum. The amount of data required and the calculations involved will be much less than the six-parameter potential. Consequently, they have proposed the use of following hybrid potential which should be nearly as good as the six-parameter and have successfully applied to the case of xenon.

In the region of the potential minimum, a Morse potential function, for  $r < \sigma$ , the repulsive energy function as obtained from the scattering experiments and for large value of  $r$ , the following expression

$$\phi(r)/k = -\frac{\lambda}{k} \left( \frac{r_m}{r} \right)^6 \quad (\text{for } r \geq 1.4r_m) \quad \dots (1)$$

TABLE I

Force constants of Ne, Ar, Kr and Xe on Morse, six-parameter and Lennard-Jones (12:6) Models

Potential parameters on											
Substance	Morse potential model			Six-parameter model						L-J(12 : 6) model	
<i>c</i>	<i>r<sub>m</sub></i> Å	<i>ε</i> /k °K	<i>r<sub>m</sub></i> Å	<i>ε</i> /k °K	<i>K</i> /k × 10 <sup>-2</sup> °K	<i>α</i> /k × 10 <sup>-3</sup> °K	<i>β</i> /k × 10 <sup>-4</sup> °K	<i>λ</i> /k °K	<i>r<sub>m</sub></i> Å	<i>ε</i> /k °K	
Ne	5.1	3.152	43.99 <sup>a</sup>	3.130	40.6	13.26	5.78	0.578	44.3 <sup>b</sup>	3.086	35.60 <sup>f</sup>
Ar	5.0	3.855	144.8 <sup>a</sup>	3.812	137.5	44.9	19.6	1.96	150 <sup>c</sup>	3.826	119.49 <sup>g</sup>
Kr	4.5	4.038	182.7 <sup>a</sup>	4.074	192.8	65.95	30.74	0	185 <sup>d</sup>	4.130	166.67 <sup>g</sup>
Xe	4.9	4.420	274.7 <sup>a</sup>	4.418	277.7	87.9	38.58	0	255 <sup>e</sup>	4.568	225.30 <sup>g</sup>

<sup>a</sup>Konowalow and Hirschfelder (1961) :

<sup>b</sup>Guggenheim and McGlashan (1960b) :

<sup>c</sup>Guggenheim and McGlashan (1960a) :

<sup>d</sup>Barua and Chakraborti (1961) ;

<sup>e</sup>Chakraborti (1963) ;

<sup>f</sup>Hirschfelder, Curtiss and Bird (1954) ;

<sup>g</sup>Whalley and Schneider (1955).

is to be used.  $\sigma$  is the value of intermolecular separation  $r$  at which  $\phi(r) = 0$ .  $\lambda/k$  is a constant to be determined by fitting the experimental second virial data  $B(T)$ .  $r_m$  is the value of  $r$  at which the attractive energy is maximum. In this paper, the treatment of Saran and Barua (1964) has been extended to the cases of neon, argon and krypton.

## CALCULATIONS AND RESULTS

### (i) Determination of Potential Energy Curve

In the neighbourhood of the potential minimum, the interaction energy on the Morse potential is expressed as

$$\phi(r) = \epsilon \{ \exp[-2c(r^* - r_m^*)] - 2 \exp[-c(r^* - r_m^*)] \} \quad \dots (2)$$

where  $\phi(r)$  is the potential energy of two atoms separated by a distance  $r$ ,  $\epsilon$  is the depth of the potential at its minimum where  $r = r_m$ ,  $r^* = r/\sigma$ ,  $r_m^* = r_m/\sigma$ ;  $\sigma$  being the value of  $r$  for which  $\phi(r) = 0$ . The parameter  $c$  is related to the curvature at the potential minimum. The force constants recorded in Table I were used to get the potential energy curves at the potential minimum region for the above mentioned gases.

When the intermolecular separation is large, the interaction energy is given by eqn. (1). The values of  $\lambda/k$  for the above mentioned gases as obtained by fitting the experimental second virial coefficient data are given in Table II.

Following Chakraborti (1963) in the region  $r < \sigma$ , we have utilized the potential energy function as determined by Amdur and Mason (1954, 1955a, 1955b) from scattering experiments. Their results may be expressed as

$$\phi(r) = A/r^n \quad \text{erg (for } r < sA^0) \quad \dots (3)$$

The values of  $A$ ,  $n$  and  $s$  are given in Table II for gases considered here.

TABLE II

Values of the constants  $A$ ,  $n$ ,  $s$  and  $\lambda/k$ .

Substance	$A \times 10^{10}$		$s, \text{\AA}$	$\lambda/k, ^\circ\text{K}$
Ne	6.07	10.41	2.13	71.0
Ar	13.60	8.33	2.69	180.0
Kr	2.55	5.42	3.14	333.0

The potential energy curves were obtained by joining the points in the different regions of  $r$  by smooth lines. The potential energy curves thus obtained on the hybrid potential are shown in Figs. 1-3 for the gases neon, argon and krypton respectively. For the sake of comparison the potential energy curves on the Lennard-Jones (12:6) as well as on six-parameter potentials are also

shown. The potential energy curve for neon on six-parameter potential has not been shown in Fig. 1.

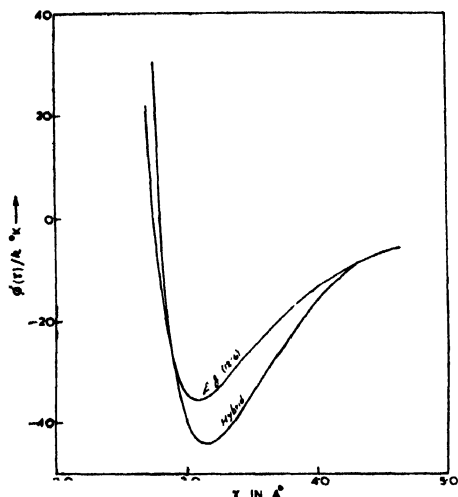


Fig. 1.—The potential energy curve of Neon plotted against the internuclear distance on the hybrid and Lennard-Jones (12:6) potentials.

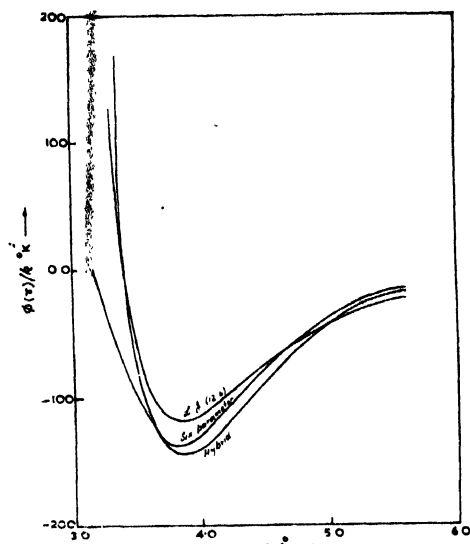


Fig. 2.—The potential energy curve of Argon plotted against the internuclear distance on the hybrid, Lennard-Jones (12:6) and six-parameter potentials.

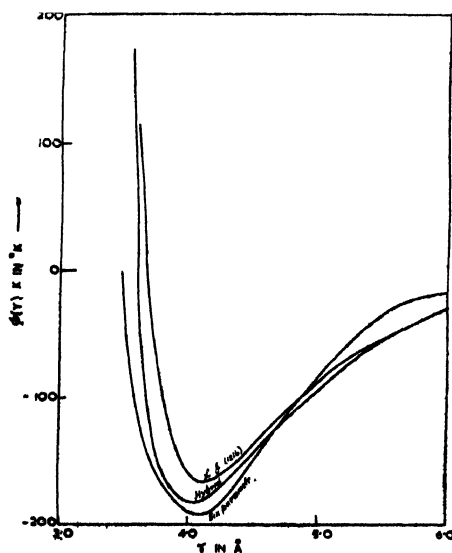


Fig. 3.—The potential energy curve of Krypton plotted against the internuclear distance on the hybrid, Lennard-Jones (12:6) and six-parameter potentials.

(ii) *Calculation of Second Virial Coefficient.*

The second virial coefficient  $B(T)$  of a gas is expressed as

$$B(T) = 2\pi N \int_0^{\infty} \{1 - \exp[-\phi(r)/kT]\} r^2 dr, \quad (4)$$

where  $N$  is Avogadro's number.

The integral is split up as

$$\int_0^{\infty} = \int_0^s + \int_s^{\sigma} + \int_{\sigma}^{r_1} + \int_{r_1}^{\infty} \quad (5)$$

where  $r_1 = 1.4r_m$ .

In the region  $r = 0$  to  $r = s$ ,  $\phi(r)$  is very large so that  $\exp[-\phi(r)/kT] = 0$ .  $\sigma$  is the value of  $r$  at which  $\phi(r) = 0$  and its value is obtained from potential energy curve. Eqn. (5) now becomes

$$B(T) = \frac{2\pi N}{3} \left[ s^3 + \int_s^{\sigma} \{1 - \exp[-\phi(r)/kT]\} d(r^3) + \int_{\sigma}^{r_1} \{1 - \exp[-\phi(r)/kT]\} d(r^3) + \frac{\lambda}{kT} \frac{r_m^6}{r_1^3} \right] \quad (6)$$

The experimental  $B(T)$  values of Ne (Michels, Wassenaar and Louwerse, 1960 ; Holborn and Otto, 1925), Ar (Holborn and Otto, 1925 ; Whalley, Lupien and Schneider, 1953) and Kr (Whalley and Schneider, 1954; Beattie, Brierley and Barriault, 1952) are graphically shown in Figs. (4)–(6) respectively along with the calculated values obtained on the hybrid potential. The agreement between the experimental and the calculated values is quite satisfactory.

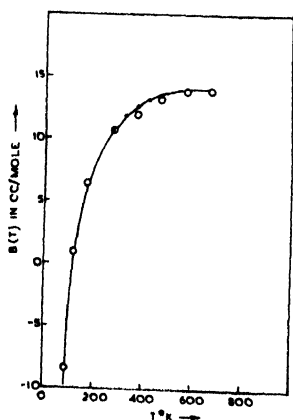


Fig. 4.—The second virial coefficient  $B(T)$  of Neon plotted as a function of temperature. ● Michels, Wassenaar and Louwerse, 1960; ○ Holborn and Otto, 1925.

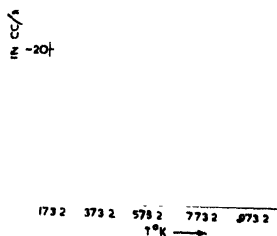


Fig. 5.—The second virial coefficient  $B(T)$  of Argon plotted as a function of temperature. ● Holborn and Otto, 1925; ○ Whalley, Lupien and Schneider, 1953.

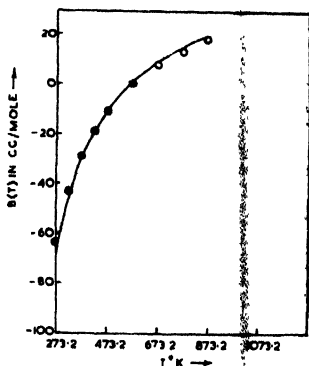


Fig. 6.—The second virial coefficient  $B(T)$  of Krypton plotted as a function of temperature.  
 ● Beattie, Brierley and Barriault, 1952; ○ Whalley and Schneider, 1954.

### CONCLUSIONS

In order to have a more realistic representation of the intermolecular potential, the combination of the Morse potential, molecular beam scattering data and the use of second virial data is found to give fairly satisfactory results. It will be interesting to calculate other properties with this hybrid potential.

### ACKNOWLEDGMENT

The author wishes to express his thanks to Prof. B. N. Srivastava, D.Sc., F.N.I., for his valuable guidance. He is also extremely thankful to Dr. A. K. Barua for suggesting the problem and making available some of his valuable suggestions.

### REFERENCES

- Amdur, I. and Mason, E. A. 1954, *J. Chem. Phys.*, **22**, 670.
- Amdur, I. and Mason, E. A. 1955a, *J. Chem. Phys.*, **23**, 415.
- Amdur, I. and Mason, E. A. 1955b, *J. Chem. Phys.*, **23**, 2268.
- Barua, A. K. and Chakraborti, P. K. 1961, *Physica*, **27**, 753.
- Beattie, J. A., Brierley, J. S. and Barriault, R. J., 1952, *J. Chem. Phys.*, **20**, 1615.
- Chakraborti, P. K., 1963, *Physica*, **29**, 227.
- Guggenheim, E. A., and McGlashan, M. L. 1960a, *Proc. Roy. Soc.*, **A255**, 456.
- Guggenheim, E. A. and McGlashan, M. L. 1960b, *Mol. Phys.*, **3**, 563.
- Hirschfelder, Curtiss and Bird. *Molecular Theory of Gases and Liquids*. (John Wiley & Sons, Inc., N.Y., 1954).
- Holborn, L. and Otto, J. 1925, *Z. Physik*, **83**, 1.
- Kihara, T. 1953, *Rev. Mod. Phys.*, **25**, 831; 1955, *ibid.*, **27**, 412.
- Konowalow, D. D. and Hirschfelder, J. O. 1961, *Phys. Fluids*, **4**, 629.
- Michels, A., Wassenaar, T. and Louwerse, P. 1960, *Physica*, **26**, 539.
- Saran, A. 1963, *Ind. J. Phys.*, **37**, 491.
- Saran, A. and Barua, A. K. 1964, *Canad. J. Phys.*, **42**, 2026.
- Whalley, E., Lupien, Y. and Schneider, W. G. 1953, *Canad. J. Chem.*, **31**, 772.
- Whalley, E. and Schneider, W. G. 1954, *Trans. Am. Soc. Mining Met., Engrs*, **76**, 1001.
- Whalley, E. and Schneider, W. G. 1955, *J. Chem. Phys.*, **23**, 1644.

# MEASUREMENT OF DIELECTRIC PROPERTIES OF METAL HALIDES

M. N. SHARMA, M. P. MADAN AND B. P. PRADHAN

DEPARTMENT OF PHYSICS, UNIVERSITY OF LUCKNOW, INDIA

(Received January 22, 1963)

**ABSTRACT.** The values of the dielectric constants have been determined experimentally by a method described in an earlier paper. The values of the force constant  $K$  have been evaluated and compared with other determinations and have been further utilized to compute cohesive energies, compressibilities and reststrahlen frequencies. For cohesive energies both exponential and inverse power models have been assumed. The agreement with experimental values and also with other determinations is reasonable and the analysis presents a simple and adequate approach.

## INTRODUCTION

The study of dielectric properties of any material gives the information about the atomic and molecular structure and also about various properties such as compressibilities, reststrahlen frequencies. Therefore, dielectric constants have been measured as functions of densities and of temperatures in substances of various types : pure substances in gas, liquid or solid form; solutions; mixtures of solid particles with other solid particle and so on. The variation with frequency has also been studied over the whole spectrum from static fields through the radio and infra red frequencies to the optical region.

In the present paper we have measured the dielectric constants of alkali halide crystals at radio frequency (15.6MC/S) using the method of mixtures. Experimental technique was based on the method of Hartshorn and Ward (1936) used earlier for vegetable oils by Sharma (1960).

Wiener (1910) has developed a formula taking into account the geometrical shape of the particles and their influence on the distribution of electric field, because the dielectric constant of crystalline powder depends also on the size and shape of the particles. Fricke (1924) has modified Wiener's formula and this modified formula has been used by us.

Since compressibility and reststrahlen frequency of a crystal are related to the dielectric constant and therefore they can be evaluated theoretically. Further, the force constant can also be evaluated with its help and if the law of interaction is known, the interaction energies can also be computed. Dielectric constant data obtained experimentally has been treated for these properties.



# THEORY

Wiener (1910) derived an equation for calculating the dielectric constant of mixtures by introducing a constant which depends on the geometrical shape of the particles. He realized that in a continuous medium the geometrical shape of the dispersed particles might influence the distribution of the electric field and consequently the dielectric constant of the mixture. He derived the following formula for calculating the dielectric constant of a mixture :

$$\frac{\epsilon_m - 1}{\epsilon_m + u} = v_1 \frac{\epsilon_1 - 1}{\epsilon_1 + u} + v_2 \frac{\epsilon_2 - 1}{\epsilon_2 + u} \quad \dots (1)$$

where  $\epsilon_m$ ,  $\epsilon_1$  and  $\epsilon_2$  are the dielectric constants of the mixture and the two components respectively,  $v_1$ ,  $v_2$  are the volume ratios of the two components to that of the whole mixture ( $v_1 + v_2 = 1$ ), and  $u$  is a constant depending on the shape of the particles. But it was found that equation (1) will hold only for spheres isotropically arranged in a uniform field.

Fricke (1924) has derived a formula for the case of a mixture when one component is dispersed in the other, the latter medium being continuous and homogeneous. Fricke formula is given by the relation

$$\epsilon_m - \epsilon_2 / \epsilon_m + u\epsilon_2 = v_1(\epsilon_1 - \epsilon_2) / (\epsilon_1 + u\epsilon_2) \quad \dots (2)$$

where  $u$  is a factor depending on  $\epsilon_1$ ,  $\epsilon_2$  and the shape of the particles. At radio frequencies  $\epsilon_1$  and  $\epsilon_2$  are complex quantities and  $u$  is also complex. Since  $u$  is unknown for crystalline particles, it is difficult to solve equation (2) for  $\epsilon_1$ .

To avoid such complications, we have used in the present study crystal powders and binding medium of negligible loss. Liquid paraffin has been used as the binding medium.

## DETERMINATION OF THE VALUE OF $\epsilon_1$

Fricke's equation for  $\epsilon_1$  has been solved for  $\epsilon_1$  by the method of Burton and Turnbull (1937) as modified by Pradhan and Gupta (1960). The method consists of plotting  $(\epsilon_m - \epsilon_2) / (\epsilon_m + u\epsilon_2)$  against  $v$  (volume fraction of crystal powder in mixture) on a log log graph paper for several assumed values of  $u$  (near about 2). The tangents of each line were evaluated, and by plotting  $u$  against the tangents obtained, a smooth curve was obtained. The value of  $u$  corresponding to a line giving the value of the tangent equal to unity was obtained. Now using this value of  $u$ , a straight line graph between  $(\epsilon_m - \epsilon_2) / (\epsilon_m + u\epsilon_2)$  and  $v$  was drawn on a log log graph paper (Fig. 1) and the straight line was interpolated to  $v_1 = 0.1$ . This value of  $(\epsilon_m - \epsilon_2) / (\epsilon_m + u\epsilon_2)$  from the graph for  $v_1 = 0.1$  gives the value for  $v_1 = 1$  on multiplying by 10.

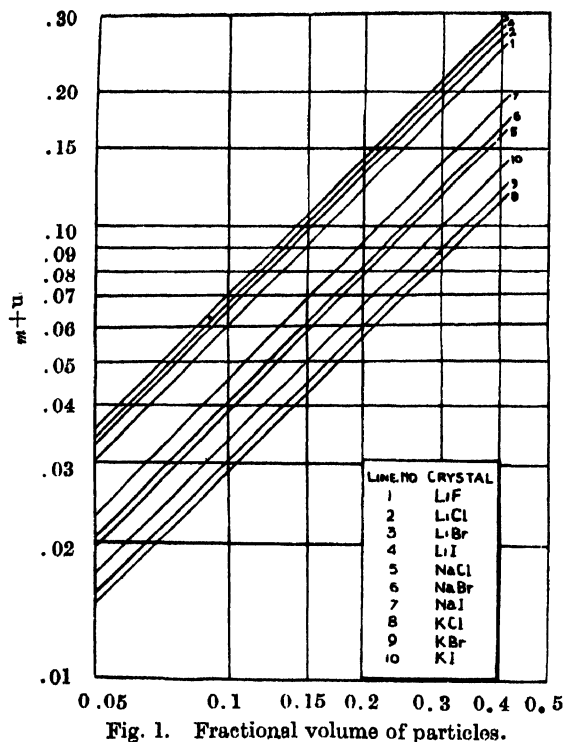


Fig. 1. Fractional volume of particles.

Now at  $v_1 = 1$ ,  $\epsilon_m$  becomes  $\epsilon_1$  and we have

$$- - - \frac{1+ux}{1-x} \quad \dots (3)$$

where

$$x = \frac{\epsilon_m - \epsilon_2}{\epsilon_m + u\epsilon_2} \times 10 \quad (\text{for } v_1 = 0.1).$$

#### MEASUREMENTS AND RESULTS

Hartshorn's method for the measurement of permittivity and power factor of dielectrics at radio frequencies from 10 KC/S to 100 MC/S was employed. The method involves capacitance variation in a tuned circuit, a thermionic voltmeter being employed as a detector of resonance. The basic information for measuring the above parameters has been discussed in detail by Sharma (1960). Since the size and shape of the samples are of utmost importance for obtaining accurate results, mixtures were carefully prepared. The crystal powders were grounded in a mortar and were filtered through a mesh (1000 B.S.). The filtered particles were supposed to be of the same size. These crystal particles were mixed with liquid paraffin in known percentages. The mixtures were stirred well and samples of required size were made. Dielectric constants of mixtures thus measured at

different concentrations are given in Table I. From this the dielectric constants of alkali halides were evaluated by the method described in the preceding section. They are given in Table III. The constant used for obtaining these dielectric constants are given in Table II.

TABLE I  
Dielectric constant of mixtures at radio frequency (15.6MC/S)

Crystal	Concentration of Salt				
	5	10	20	30	40
LiF	2.346	2.500	2.833	3.225	3.677
LiCl	2.355	2.520	2.869	3.316	3.819
LiBr	2.348	2.509	2.864	3.286	3.792
LiI	2.350	2.508	2.861	3.274	3.762
NaCl	2.317	2.435	2.687	2.963	3.260
NaBr	2.318	2.440	2.699	2.984	3.294
NaI	2.326	2.458	2.737	3.049	3.395
KCl	2.294	2.389	2.586	2.797	3.019
KBr	2.295	2.392	2.595	2.812	3.043
KI	2.299	2.398	2.611	2.839	3.085

TABLE II  
Values of  $u$  and  $x$  for alkali halide crystals

Cry- stal	LiF	LiCl	LiBr	LiI	NaCl	NaBr	NaI	KCl	KBr	KI
$u$	1.12	1.04	0.83	0.91	1.66	1.55	1.41	1.91	1.76	1.60
$x$	0.60	0.66	0.71	0.68	0.38	0.41	0.46	0.28	0.30	0.33

TABLE III  
Dielectric constants of alkali halide crystals at 15.6 MC/S

Crystal	Present work	Pradhan and Gupta (1960)	Born and Huang (1954)	von Hippel (1954)	International Critical Tables (1929)
LiF	9.20	....	9.27	....	....
LiCl	11.00	....	....	....	....
LiBr	11.92	....	....	....	....
LiI	11.02	....	....	....	....
NaCl	5.84	5.86	5.62	5.90	5.90
NaBr	6.04	6.10	5.99	....	....
NaI	6.70	6.72	6.60	....	....
KCl	4.73	4.77	4.68	....	5.03
KBr	4.86	4.88	4.78	4.90	5.10
KI	5.07	5.09	4.94	....	5.40

CORRELATION OF DIELECTRIC CONSTANT WITH  
OTHER PROPERTIES

The dielectric properties of ionic crystals are intimately connected with the compressibilities, reststrahlen frequencies and cohesive energies. The ions in the crystal may be regarded as held in their respective positions by (1) the electrostatic forces between the charges carried by them and (2) by forces such as the forces of repulsion, the van der Waals forces and also the homopolar interaction forces if any. In view of the spherical symmetry of the ions, both (1) and (2) types of forces are regarded to be central.

The potential energy  $E(r)$  of the crystal per pair of ions can be written as

$$E(r) = -\frac{\alpha e^2}{r} + \phi(r) \quad \dots (4)$$

where  $\alpha$  is the Madelung constant.  $\phi(r)$  contains all the rest of the energy which is not contained in the electrostatic term  $-\frac{\alpha e^2}{r}$ .

There are various expressions for  $\phi(r)$ . Born assumes the form

$$\phi(r) = B e^{-r/\rho} \quad \dots (5)$$

considering only the repulsion interaction between any two neighbouring ions separated by a distance  $r$ , whereas the form

$$\phi(r) = Br^{-n} \quad \dots (6)$$

has also been proposed. Equations (5) and (6) do not take into account the van der Waals forces or forces of homopolar character. Usually, the latter forces are not strong enough and can be neglected, but the former, that is the van der Waals forces may be quite important and should be taken into account, as is indicated by an analysis of the available data on dielectric and other properties of crystals by Hardy (1961), Cubicciotti (1959) and Huggins (1937).

Hence the equations (5) and (6) take the form

$$\phi(r) = Be^{-r/\rho} - \frac{C}{r^6} \quad \dots (7)$$

and

$$\phi(r) = Br^{-n} - \frac{C}{r^6}.$$

Equation (8) is known as Lennard-Jones interaction form with empirical values for the index  $n$ . Fowler (1955) using  $n = 9$ , attempts to explain the various properties of crystals, whereas  $n = 12$  has been more popular and successful in explaining the data on liquids and gases and in a few cases of solids. For ionic crystals it is found that  $n < 12$  is more suitable for lighter salts whereas  $n = 12$  is more appropriate for heavier ones as shown by Sharma and Madan (1964). Nevertheless, as has been assumed for liquids and gases, for a unified approach,

one can reasonably assume  $n = 12$  for the data analysis of a number of properties of crystals also. In the present discussion we have considered equation (7) and equation (8) in which  $n = 12$ .

If the lattice formed by one type of ions is displaced with reference to the lattice of other type of ions by a smaller distance  $r$ , then the potential energy of the deformed crystal per pair of ions can be expressed as a power series in  $r$ , in which terms involving odd powers of  $r$  will be absent as shown by Krishnan and Roy (1951).

The coefficient of  $r^2$  which we denote by ' $a$ ' will determine the reststrahlen frequency of the crystal.

Relation between the force constants used by Born and Huang (1954) and Krishnan and Roy (1951) is given by

$$K = 2 a_1$$

where

$$K = \frac{1}{3} \left[ \phi''(r) + \frac{2}{r} \phi'(r) \right]. \quad (9)$$

There is no contribution of the electrostatic interaction to the  $r^2$  term and  $\phi(r)$  as given by either equation (7) or (8), as the case may be.

If we consider a uniformly polarized sphere in the absence of an external electric field, the only forces acting are due to the  $\phi(r)$  term as shown by Szigeti (1951), the Lorentz effective field  $F$  being equal to zero, and we can write a relation connecting  $K$  and  $\beta$  the compressibility as

$$K = \frac{3u}{\beta r^2} \quad \dots \quad (10)$$

where  $u$  is the volume occupied by an ion pair. Equation (10) for NaCl structure becomes

$$K = \frac{6r}{\beta}. \quad (11)$$

The force constant  $K$ , when  $F = 0$ , is connected with the reststrahlen frequency  $\omega_0$  as

$$K = \frac{\epsilon + 2}{\epsilon_0 + 2} m \omega_0^2 \quad (12)$$

where  $\epsilon$  and  $\epsilon_\infty$  are the static and high frequency dielectric constants and  $m$  is the reduced mass. Krishnan and Roy (1951) treated this problem in a slightly different way. As a result of lattice displacement, there is a development of a homogeneous electric polarization in the crystal and the value of force coefficient,  $K$ , instead of being only due to  $\phi(r)$  term will be less by an amount proportional to the force due to the polarization field.

From the polarization, the contribution to the force coefficient will be

$$2 a_2 = -\frac{4}{3}\pi N e^2. \quad \dots (13)$$

The total force coefficient will then be

$$2 a = 2 a_1 + 2 a_2 = m \omega_0^2. \quad \dots (14)$$

Therefore,

$$K = 2 a_1 = m \omega_0^2 - 2 a_2. \quad \dots (15)$$

Utilizing the experimentally determined values of the dielectric constant  $\epsilon$ , we can evaluate the force coefficient  $K$ , provided we know the reststrahlen frequency  $\omega_0$ . This in turn will enable a determination of the interaction energy of the undeformed crystal as well as its compressibility. The expressions for the interaction energy will depend on whether we are using equation (8) or (7). They are obtained by using relation (9) and are respectively,

$$U_0 = \frac{r_0^2}{44} \left( K - 44 \frac{\alpha e^2}{r_0^3} - 34 \frac{C}{r_0^8} \right), \quad \dots (16)$$

and

$$U_0 = \left( \frac{r_0 \rho^2}{r_0 - 2\rho} \right) \left( 3K + 30 \frac{C}{r_0^8} \right) - \left( \frac{\alpha e^2}{r_0} + \frac{C}{r_0^6} \right) \quad \dots (17)$$

The values of  $\beta$  and  $K$  (from equations 15 and 12) thus computed are given in Table IV(A) and V respectively, where they have been compared with other determinations as well. The values of  $U_0$  (from equations 16 and 17) are given in Table VI.

TABLE IV(A)

Calculated and experimental values of compressibilities from various Determinations

Crystal	Compressibilities in $10^{-12}$ Cm <sup>2</sup> /dyne.			
	Experimental Cubicciotti (1959)	From equation (11)	Using Equation (15) and $\omega_0$ Experimental	Using Equations (18) and (15)
LiF	1.43	1.53	1.49	1.33
NaCl	3.97	4.16	3.88	4.09
NaBr	4.75	5.48	4.86	4.98
NaI	6.21	7.02	6.50	7.19
KCl	5.50	5.27	5.04	5.08
KBr	6.45	5.39	5.96	6.06
KI	8.07	9.25	7.60	7.85

TABLE IV(B)

Calculated and observed values of reststrahlen frequencies and dielectric constant

Crystal	Reststrahlen Frequency $\times 10^{-13}/\text{Sec.}$					Dielectric Constant	
	Born and Huang (1954)	Krishnan and Roy (1959)	Using $\beta$ Experimental and Equ. (12)	Using $\beta$ Experimental and Equ. (15)	Using Equ. (18) and $\epsilon$ Experimental	Born and Huang (1954)	Using Equations (11) and (12)
LiF	5.78	5.28	5.92	5.48	6.11	9.20	9.76
NaCl	3.09	2.95	3.16	3.02	2.92	5.84	6.19
NaBr	2.52	2.58	2.71	2.58	2.46	6.04	7.29
NaI	2.20	2.45	2.34	2.30	2.17	6.70	7.84
KCl	2.67	2.51	2.61	2.47	2.65	4.73	4.44
KBr	2.13	2.07	2.11	1.97	2.10	4.86	4.74
KI	1.85	1.89	1.88	1.76	1.80	5.07	5.28

TABLE V

Calculated values of force constants using different crystal properties

Crystal	Force Constant $\times 10^{-4}$				
	From Equ. (12)	From Equ. (15)	From Equ. (11) and Using $\beta$ Experimental	From Equ. (18)	Krishnan and Roy (1951)
LiF	7.90	8.10	8.45	9.07	8.26
NaCl	4.07	4.36	4.26	4.13	4.22
NaBr	3.27	3.69	3.78	3.60	3.80
NaI	2.77	2.99	3.13	2.95	3.38
KCl	3.58	3.75	3.43	3.72	3.48
KBr	3.74	3.32	3.07	3.27	3.20
KI	2.29	2.79	2.63	2.70	2.90

TABLE VI

Comparison of observed and calculated values of cohesive energies in  
K Cal/mole.

Crystal	Experimental Born and Huang (1954)	From Equation (17)			From Equation (16)		
		Using K from Equ.(12)	Using K from Equ.(11)	Using K from Equ.(18)	Using K from Equ.(12)	Using K from Equ.(11)	Using K from Equ.(18)
LiF	....	239.4	236.0	232.2	280.7	280.0	279.1
NaCl	184.7	185.5	184.4	185.6	199.2	198.6	199.0
NaBr	175.9	177.9	175.1	183.1	188.8	187.4	187.8
NaI	166.3	166.4	164.3	165.5	174.4	173.2	173.8
KCl	167.8	169.3	170.2	168.6	177.8	178.3	177.4
KBr	161.2	159.0	162.9	161.7	167.8	170.2	169.5
KI	152.8	155.2	153.2	152.9	160.1	158.7	158.4

Recently, data have been compiled by Cubicciotti (1959) for the compressibility and hence one could also take these experimental values of  $\beta$  and use them to evaluate  $K$ . This can then give the reststrahlen frequency using either equation (12) or (15). The values of  $\omega_0$  thus computed are given in Table IV(B). Using experimental  $\omega_0$  and experimental  $\beta$ , theoretical values of dielectric constant can also be calculated. These values of dielectric constants are given in Table IV(B), where they have been compared with experimental values.

Assuming that there are also local distortions present, Szigeti (1951) obtained an equation relating the reststrahlen frequency and the dielectric constant, which is slightly different from equation (12)

$$(\epsilon - \epsilon_\infty)/(\epsilon_\infty + 2)^2 = 4\pi N(Se)^2/9m\omega_0^2 \quad \dots (18)$$

where  $S$  is unity for Lorentz approximation. Equation (12) is obeyed better than equation (18) particularly for the lighter salts as shown by Hardy (1961), who has given a detailed discussion of the importance of relations (12) and (18). The effect of equation (18) can be seen if one uses this relation and the experimental  $\epsilon$  to calculate the energy and the compressibility which can then be compared with the values given in Tables (VI) and IV(A) based on equation (12).

Comparison of various values in Tables IV(A), IV(B), V and VI shows that there is a reasonable agreement between various values among themselves and also with the experimentally determined values.

Cohesive energies calculated on the basis of exponential model are in good agreement with the experimental energies. Inverse power model using  $n = 12$  gives comparatively a poor agreement. This is to be expected because this is more suitable for heavier elements. Most of the salts considered here are lighter and  $n < 12$  will be more appropriate.



A comparison of various reststrahlen frequencies indicates that the values of  $\omega_0$  calculated by using experimental data of compressibilities is in better agreement with the observed frequencies, thus placing confidence in the new values of compressibilities.

#### ACKNOWLEDGMENT

The authors are grateful to Professor P. N. Sharma for his interest in the investigation.

#### REFERENCES

- Born, M. and Huang, K. 1954, *Dynamical Theory of Crystal Lattices*, Clarendon Press, Oxford.
- Burton, E. F., and Turnbull, L. G., 1937, *Proc. Roy. Soc. Lond.*, **A158**, 182.
- Cubicciotti, D., 1959, *J. Chem. Phys.*, **31**, 1648.
- Fowler, R. H., 1955, *Statistical Mechanics*, Cambridge University Press.
- Fricke, H., 1924, *Phys. Rev.*, **24**, 575.
- Hardy, J. R., 1961, *Phil. Mag.*, **6**, 27.
- Hartshorn, L., and Ward, W. H., 1936, *J. Inst. Eng.*, **79**, 597.
- Huggins, M. L., 1937, *J. Chem. Phys.*, **5**, 143.
- International Critical Tables, 1929, **6**, 77, McGraw-Hill Book Company, Inc., New York and London.
- Krishnan, K. S., and Roy, S. K., 1951, *Proc. Roy. Soc. Lond.*, **A207**, 447.
- Pradhan, B. P., and Gupta, R. C., 1960, *J. sci. industr. Res.*, **19B**, 229.
- Sharma, M. N., 1960, *J. sci. industr. Res.*, **19B**, 5.
- Sharma, M. N., and Madan, M. P., 1964, *Ind. J. Phys.*, **38**, 231.
- Sharma, M. N., and Madan, M. P., 1964, *Ind. J. Phys.*, **38**, 305.
- Szigeti, B., 1951, *Proc. Roy. Soc. Lond.*, **A204**, 51.
- von Hippel, A. R., 1954, *Dielectric Materials and Applications*, John Wiley & Sons, New York.
- Wiener, R., 1910, *Ber. Sachs. Ges (Akad.) Wiss.*, **62**, 256.

# ELECTRON VELOCITY DISTRIBUTION IN SLIGHTLY IONIZED ARGON WITH CROSSED ELECTRIC AND MAGNETIC FIELDS

D. C. JAIN\*, B. D. NAG CHAUDHURI, B. DAS GUPTA,  
D. K. BOSE AND S. N. SEN GUPTA

SAHA INSTITUTE OF NUCLEAR PHYSICS, CALCUTTA-9.

(Received December 23, 1964)

**ABSTRACT.** A method of solving the Boltzmann equation for the distribution function of electrons in slightly ionized argon with crossed electric and magnetic fields is outlined using Golant's analytical approximations of the experimental data on the cross-sections for elastic and inelastic collisions. The distribution function is obtained in the presence of an electric field of arbitrary frequency crossed with a constant magnetic field as well as in the presence of crossed d.c. electric and magnetic fields.

It has been found from the plots of the electron distribution function that (i) for a given  $E/p$ , the distribution with crossed d.c. electric and magnetic fields contains more low energy electrons than that with only d.c. electric field, and (ii) that in a given transverse magnetic field, the electron distribution for a higher  $E/p$  is richer in higher energy electrons than that for a lower value of  $E/p$ .

## INTRODUCTION

The problem of electron velocity distribution in a gaseous discharge has been the subject of investigation for many years. The knowledge of the distribution function is important in the study of transport phenomena in ionized gases. Recently Golant (1957, 1959) has determined the electron distribution in argon under the influence of a high frequency field using an analytical approximation of the experimental data on cross-sections of elastic and inelastic collisions of electrons with argon atoms. By solving the Boltzmann equation numerically Engelhardt and Phelps (1964) have found that the electron distribution obtained by them agrees satisfactorily with that of Golant. Thus the approximations used in the analysis of Golant have produced no appreciable distortion in the resulting electron distribution. In the present communication the method of Golant has been extended to obtain the electron distribution in argon in the presence of an electric field of arbitrary frequency crossed with a constant magnetic field. The case of crossed d.c. electric and magnetic fields has also been treated.

\* Now at New York University, New York.

# THE ELECTRON DISTRIBUTION FUNCTION

The electron velocity distribution function  $f(\vec{v})$  can be obtained by solving the well-known Boltzmann transport equation. In the case where the electrons are acted on simultaneously by electric and magnetic fields and where the electron density gradient is negligible, the Boltzmann equation is given by

$$\frac{\partial f}{\partial t} + (\vec{a} + \vec{\omega}_b \times \vec{v}) \cdot \vec{\nabla}_v f = \left( \frac{\delta f}{\delta t} \right)_{coll} \quad \dots (1)$$

where  $\vec{a} = -\frac{e\vec{E}}{m}$  ( $\vec{E}$  is the electric field experienced by the particles),

$\vec{\omega}_b = \frac{e\vec{B}}{mc}$  the electron cyclotron frequency,

$\vec{\nabla}_v$  the gradient operator in the velocity space,

and  $\left( \frac{\delta f}{\delta t} \right)_{coll}$  the change of the distribution function in time due to collision.

Expanding the distribution function  $f(\vec{v})$  in spherical harmonics as

$$f(\vec{v}) = f_0 + \vec{v} \cdot \vec{f}_1 + \dots \quad \dots (2)$$

and substituting the expansion, retaining only first two terms, into Eq. (1) we obtain the following equations for the components of the distribution function (Allis, 1956)

$$\frac{\partial f_0}{\partial t} - \gamma \frac{\cos \omega t}{3v^2} \cdot \frac{\partial}{\partial v} (v^2 \vec{f}_1) = \left( \frac{\delta f_0}{\delta t} \right)_{coll} \quad \dots (3)$$

$$\frac{\partial \vec{f}_1}{\partial t} - \gamma \cos \omega t \frac{\partial f_0}{\partial v} - \vec{\omega}_b \times \vec{f}_1 = \left( \frac{\delta \vec{f}_1}{\delta t} \right)_{coll} \quad \dots (4)$$

where  $\vec{E} = \vec{E}_0 \cos \omega t$

$$\gamma = \frac{e\vec{E}_0}{m}$$

Writing the collision terms for a slightly ionized gas following Golant (1957), Eqs. (3) and (4) become

$$\frac{\partial f_0}{\partial t} - \gamma \frac{\cos \omega t}{3v^2} \cdot \frac{\partial}{\partial v} (v^2 \vec{f}_1) = \frac{m}{M} \frac{1}{v^2} \frac{\partial}{\partial v} \left( \frac{v^4 f_0}{\lambda_s} \right) - \frac{v f_0}{\lambda_{ns}}, \quad \dots (5)$$

$$\frac{\partial \vec{f}_1}{\partial t} - \gamma \cos \omega t \frac{\partial f_0}{\partial v} - \vec{\omega}_b \times \vec{f}_1 = - \frac{\vec{v} f_0}{\lambda_e} \quad \dots (6)$$

Here  $\lambda_e$  is the diffusion mean freepath for elastic collisions and  $\lambda_{ne}$ , the corresponding quantity for inelastic processes. The last term in Eq. (5) is dropped out below the threshold for inelastic processes. The above form of collision terms have been derived on the assumptions that (i) the thermal energy of the neutral particles is negligible in comparison with the average electron energy, that (ii) an electron loses its energy completely during an inelastic collision and that (iii) the inelastic collisions do not affect the distribution symmetry.

In the case of crossed electric and magnetic fields, with the magnetic field along the  $z$ -axis, Eq. (6) can be written as

$$\frac{\partial f_{1x}}{\partial t} - \gamma_x \cos \omega t \frac{\partial f_0}{\partial v} + \omega_b f_{1y} = - \frac{v}{\lambda_e} f_{1x} \quad \dots (6a)$$

$$\frac{\partial f_{1y}}{\partial t} - \gamma_y \cos \omega t \frac{\partial f_0}{\partial v} - \omega_b f_{1x} = - \frac{v}{\lambda_e} f_{1y} \quad \dots (6b)$$

$$\frac{\partial f_{1z}}{\partial t} = - \frac{v}{\lambda_e} f_{1z} \quad \dots (6c)$$

Multiplying Eq. (6b) by  $i$ , adding it to Eq. (6a), and putting

$$f_{1x} + i f_{1y} = f_1^1, \quad \gamma_x + i \gamma_y = \gamma^1$$

the following equation is obtained :

$$\frac{\partial f_1^1}{\partial t} - \gamma^1 \cos \omega t \frac{\partial f_0}{\partial v} = - \left( \frac{v}{\lambda_e} - i \omega_b \right) f_1^1 \quad \dots (7)$$

Considering  $f_0$  to be independent of time, the steady state solution of Eq. (7) is given by

$$f_1^1 = \gamma^1 \frac{\partial f_0}{\partial v} \left[ \frac{\omega}{\omega^2 + (v/\lambda_e - i \omega_b)^2} \sin \omega t + \frac{v/\lambda_e - i \omega_b}{\omega^2 + (v/\lambda_e - i \omega_b)^2} \cos \omega t \right] \quad \dots (8)$$

the steady state solution of Eq. (6c) yielding  $f_{1z} = 0$ . Substituting for  $\vec{f}_1$  in Eq. (5) and taking the time average,

$$\begin{aligned} & - \frac{\gamma^2}{6v^3} \frac{\partial}{\partial v} \left\{ \frac{v^3}{\lambda_e} \frac{\partial f_0}{\partial v} \frac{[\omega^2 + \omega_b^2 + v^2/\lambda_e^2]}{[(\omega - \omega_b)^2 + v^2/\lambda_e^2][(\omega + \omega_b)^2 + v^2/\lambda_e^2]} \right\} \\ & = \frac{m}{M} \frac{1}{v^2} \frac{\partial}{\partial v} \left( \frac{v^4 f_0}{\lambda_e} \right) - \frac{v f_0}{\lambda_{ne}} \quad \dots (9) \end{aligned}$$

Substituting  $v^2 = xu_0$ , where  $u_0 = 2eU_0/m$ ,  $U_0$  being the threshold for inelastic processes, Eq. (9) becomes

$$-\frac{2}{3} \frac{\gamma^2}{\omega^2} x^{\frac{1}{2}} \frac{\partial}{\partial x} \left\{ \frac{x^2}{\lambda_e} \frac{\partial f_0}{\partial x} \frac{[(1 + (\omega_b/\omega)^2 + xu_0/(\lambda_e^2 \omega^2))]}{[(1 - \omega_b/\omega)^2 + xu_0/(\lambda_e^2 \omega^2)][(1 + \omega_b/\omega)^2 + xu_0/(\lambda_e^2 \omega^2)]} \right\} \\ = \frac{2mu_0 x^{1/2}}{M} \frac{\partial}{\partial x} \left( \frac{x^2 f_0}{\lambda_e} \right) - \frac{u_0 x^{3/2} f_0}{\lambda_{ne}} \quad \dots (10)$$

Upto this point the treatment is quite general and Eq. (10) can be solved for the isotropic part of the distribution function in any gas by using suitable values of collision cross sections. Lax, Allis and Brown (1950) have obtained a similar equation which they have eventually treated by assuming constant collision frequency. Following Golant (1957) we assume that the collision mean freepaths  $\lambda_e$  and  $\lambda_{ne}$  have energy dependences given by

$$\lambda_e = \begin{cases} \lambda_e^0 x^{\frac{1}{2}} & \text{for } x > 1 \\ \lambda_e^0/x & \text{for } 1 > x > 0.1 \\ 10\lambda_e^0 & \text{for } x < 0.1 \end{cases} \quad \dots (11a)$$

$$\text{and} \quad \lambda_{ne} = \frac{\lambda_{ne}^0}{x^{\frac{1}{2}}(x-1)} \quad \text{for } x > 1 \quad \dots (11b)$$

where  $x = \frac{U}{U_0}$ ,  $U$  is the electron energy and  $U_0 = 11.5 \text{ ev}$  is the first ionization potential of argon.

Thus for the region  $x > 1$ , Eq. (10) reduces to

$$x^{\frac{1}{2}} \frac{\partial}{\partial x} \left( x^{3/2} \frac{\partial f_0}{\partial x} \right) + \alpha x^{\frac{1}{2}} \frac{\partial}{\partial x} (x^{3/2} f_0) - \beta x^{\frac{1}{2}} (x-1) f_0 = 0, \quad \dots (12)$$

where

$$\alpha = \frac{3m}{M} \frac{u_0^2}{\gamma^2 \lambda_e^0{}^2} [1 + (1 - \omega_b/\omega)^2 \zeta] \left[ 1 + \frac{2\omega_b}{\omega} \left\{ 1 + \left( \frac{\omega_b}{\omega} \right)^2 + \frac{1}{\zeta} \right\}^{-1} \right],$$

$$\beta = \frac{3}{2} \frac{u_0^2}{\gamma^2 \lambda_e^0 \lambda_{ne}^0} \left[ 1 + \left( 1 - \frac{\omega_b}{\omega} \right)^2 \zeta \right] \left[ 1 + \frac{2\omega_b}{\omega} \left\{ 1 + \left( \frac{\omega_b}{\omega} \right)^2 + \frac{1}{\zeta} \right\}^{-1} \right],$$

$$\zeta = \frac{\omega^2 \lambda_e^0{}^2}{u_0}$$

As  $\alpha \ll \beta$ , the effect of elastic collision is negligible in the region  $x > 1$  and Eq. (12) can be solved for the distribution function  $f_0(x)$  in the region  $x > 1$  (Golant, 1957) :

$$f_0(x) = x^{-3/4}(x-1)^{1/3} K_{1/3} \left[ \frac{2}{3} \beta^{1/2}(x-1)^{3/2} \right] \quad \dots (13)$$

where  $K_{1/3}$  is the MacDonald function. An arbitrary multiplying constant is implied in the above solution which is obtained by normalization.

At  $x = 1$  the distribution function  $f_0(x)$  as given in Eq. (13) and its first derivative become

$$f_0(1) = 1.91\beta^{-1/6}; \quad f'_0(1)/f_0(1) = -[0.75 + 0.73\beta^{1/3}] \quad \dots (14)$$

In the regions  $0.1 < x < 1$  and  $x < 0.1$  it has been shown by Golant (1957) that the term involving  $\frac{m}{M}$  can be neglected. Thus substituting for  $\lambda_e$  in Eq. (10) from Eqs. (11) and integrating we obtain for the region  $0.1 < x < 1$

$$\frac{\partial f_0}{\partial x} = \frac{A[(x^3 + q^3)^2 - k]}{x^3(x^3 + q^3)}$$

and

$$f_0(x) = B + A \left[ x - \left( 1 - \frac{k}{q^6} \right) \frac{q^3}{2x^2} + \frac{k}{6q^6} \left\{ \ln \frac{(x+q)^2}{(x^2 - qx + q^2)} + 2\sqrt{3} \tan^{-1} \frac{2x-q}{q\sqrt{3}} \right\} \right], \quad \dots (15)$$

where

$$q^3 = \xi \left\{ 1 + \left( \frac{\omega_b}{\omega} \right)^2 \right\}$$

$$k = 4\xi^2(\omega_b/\omega)^2$$

The constants of integration  $A$  and  $B$  determined by matching  $\partial f_0/\partial x$  and  $f_0(x)$  at  $x = 1$ , are given by

$$A = \frac{(1+q^3)}{[(1+q^3)^2 - k]} f'_0(1), \quad \dots (16)$$

$$B = f_0(1) - A \left[ 1 - \frac{q^3}{2} \left( 1 - \frac{k}{q^6} \right) + \frac{k}{6q^6} \left\{ \ln \frac{(1+q)^2}{(1-q+q^2)} + 2\sqrt{3} \tan^{-1} \frac{2-q}{q\sqrt{3}} \right\} \right] \quad (17)$$

Similarly for the region  $x < 0.1$

$$\frac{\partial f_0}{\partial x} = \frac{c}{x^2} \frac{[(x+10^2q^3)^2 - 10^4k]}{[x+10^2q^3]}$$

and

$$f_0(x) = D + c \left[ \ln x - \frac{10^2 q^3}{x} \left( 1 - \frac{k}{q^6} \right) - \frac{k}{q^6} \ln \left( 1 + \frac{10^2 q^3}{x} \right) \right] \quad \dots (18)$$

The constants of integration  $C$  and  $D$  determined by matching  $\partial f_0 / \partial x$  and  $f_0(x)$  at  $x = 0.1$ , are given by

$$C = 0.1A \quad \dots (19)$$

$$D = f_0(1) - A \left[ 0.6697 - 50.5q^3 \left( 1 - \frac{k}{q^6} \right) - \frac{k}{10q^6} \ln \left( 1 + 10^3 q^3 \right) + \frac{k}{6q^5} \left\{ \ln \left[ \frac{1 - 10q + 10^2 q^2}{1 - q + q^2} \right] \left( \frac{1 + q}{1 + 10q} \right)^2 + 2\sqrt{3} \tan^{-1} \frac{9\sqrt{3}q}{(20q^2 - 11q + 2)} \right\} \right] \quad (20)$$

The above expression [Eqs. (13), (15) and (18)] give the electron distribution function in slightly ionized argon in the presence of an ac electric field of frequency  $\omega$  crossed with a constant magnetic field.

In the case of a d.c. electric field ( $\omega = 0$ ) crossed with constant magnetic field, the following equation is obtained instead of Eq. (9) :

$$-\frac{\gamma^2}{3v^2} \frac{\partial}{\partial v} \left\{ \frac{v^3}{\lambda_e} \left( \omega_b^2 + v^2 / \lambda_e^2 \right) \frac{\partial f_0}{\partial v} \right\} = \frac{n}{M} \frac{1}{v^2} \frac{\partial}{\partial v} \left( \frac{v^4 f_0}{\lambda_e} \right) - \frac{vf_0}{\lambda_{ne}} \quad \dots (9a)$$

the factor of  $1/2$  in the left hand side of Eq. (9), obtained by taking the time average, being omitted. The solutions of Eq. (9a) in the three energy regions are :

$$f_0(x) = x^{-3/4} (x-1)^{1/4} K_{1/3} \left[ \frac{2}{3} \beta_1 (x-1)^{3/2} \right], \quad x > 1; \quad (21)$$

$$f_0(x) = A_1 x - \frac{1}{2} A_1 \zeta_1 / x^2 + B_1, \quad 0.1 < x < 1; \quad \dots (22)$$

$$f_0(x) = -10^2 C_1 \zeta_1 / x + C_1 \ln x + D_1, \quad x < 0.1; \quad \dots (23)$$

where

$$\beta_1 = \frac{3}{4} \frac{\gamma^2 u_0^2}{\lambda_e^0 \lambda_{ne}^0} [1 + \zeta_1],$$

$$\zeta_1 = \frac{\omega_b^2 \lambda_e^0}{u_0^2},$$

$$A_1 = \frac{1}{1 + \zeta_1} f'_0(1)$$

$$B_1 = f_0(1) - f'_0(1) \frac{1 - 0.5\zeta_1}{1 + \zeta_1}$$

$$C_1 = \frac{0.1}{1+\xi_1} f'_0(1),$$

$$D_1 = f_0(1) - f'_0(1) \frac{0.6697 - 50.5\xi_1}{1+\xi_1}$$

These expressions [Eqs. (21), (22) and (23)] for the distribution function with crossed d.c. electric and magnetic fields become similar to those obtained by Golant (1957) for the case of a.c. electric field if  $\omega_b$  is replaced by  $\omega$ . The applicability of this substitution has been pointed out by Engelhardt and Phelps (1963) as well. Further it is to be noted that Eqs. (21), (22) and (23) can be obtained from Eqs. (13), (15) and (18) respectively, by putting  $\omega = 0$  and  $\beta/2 = \beta_1$ .

From the electron velocity distribution function  $f_0(x)$  one obtains then the electron energy distribution function  $F(x)$  by means of the relationship

$$F(x) = \frac{x^{\frac{1}{2}} f_0(x)}{\int_0^{\infty} x^{\frac{1}{2}} f_0(x) dx} \quad \dots \quad (24)$$

Plots of the electron energy distribution function are shown in Figs. (1) and (2) for several values of magnetic field and  $E/p$  in the case of crossed d.c. electric and magnetic fields. The corresponding curves for only d.c. electric field are also plotted in the same figures for comparison.

#### DISCUSSION

By using the cross-sections for elastic and inelastic collisions as given by Golant, we have determined the electron velocity distribution in argon under the influence of crossed electric and magnetic fields. Eqs. (13), (15) and (18) above give, respectively, the isotropic part of the electron distribution function  $f_0(x)$  in the regions  $x > 1$ ,  $0.1 < x < 1$  and  $x < 0.1$  for an a.c. electric field crossed with a constant magnetic field. For the case of crossed d.c. electric and magnetic fields the distribution function is given by the Eqs. (21), (22) and (23). It is evident from these equations as well as from the curves plotted in Figs. (1) and (2) that the presence of the magnetic field perpendicular to the electric field has altered the distribution considerably. In the low energy region curve 1 in Fig. 1 for zero magnetic field is lying below the other curves (2, 3, 4, 5 and 6) for successive values of the magnetic field, indicating fewer low energy electrons in the distribution when the magnetic field is absent. Thus the application of the crossed d.c. electric and magnetic fields causes an excess of low energy electrons over the number when the electric field alone is present and the effect increases as the magnetic field is increased. Our plots of the distribution function further show (Fig. 2) that with the increase of  $E/p$  the distribution becomes richer in higher energy electrons.



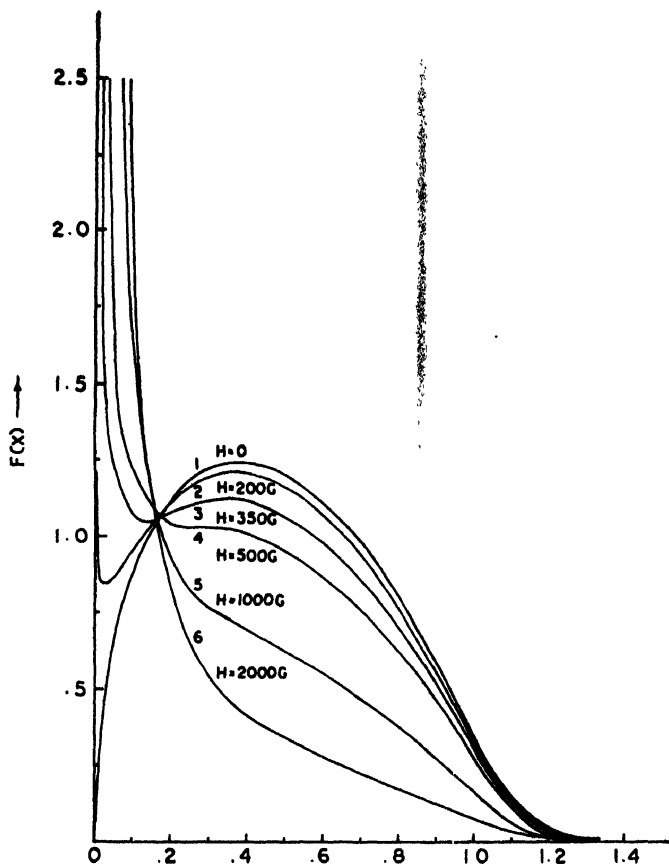


Fig. 1.—Electron energy distribution for d.c. electric field and crossed d.c. electric and magnetic fields with  $E/p = 10$  V/cm. mm. Hg. and different values of the magnetic field. Curve 1 is for zero magnetic field and other curves (2, 3, 4, 5 and 6) for successively increasing value of the magnetic field.

It is interesting to note that the electron distribution obtained by us for crossed d.c. electric and magnetic fields is similar to that found by Golant (1957) for a.c. electric field without magnetic field. The similarity arises due to the fact that in the parameters  $\beta$  and  $\zeta$  determining  $f_0(x)$  the cyclotron frequency  $\omega_c$  and the a.c. frequency  $\omega$  occur in the same place. Perhaps this similarity between the two distributions indicates that the mechanism of energy transfer to the electrons is similar in both the a.c. fields and the crossed d.c. electric and magnetic fields.

Our derivation of the distribution function following the method of Golant has the limitation that the distribution function goes to infinity at  $x = 0$ . This infinity is spurious, since, unless there is a point source of electrons at the origin, the distribution function must be finite. According to Holstein (1946) this spurious infinity is due to break down of basic assumptions in the derivation of

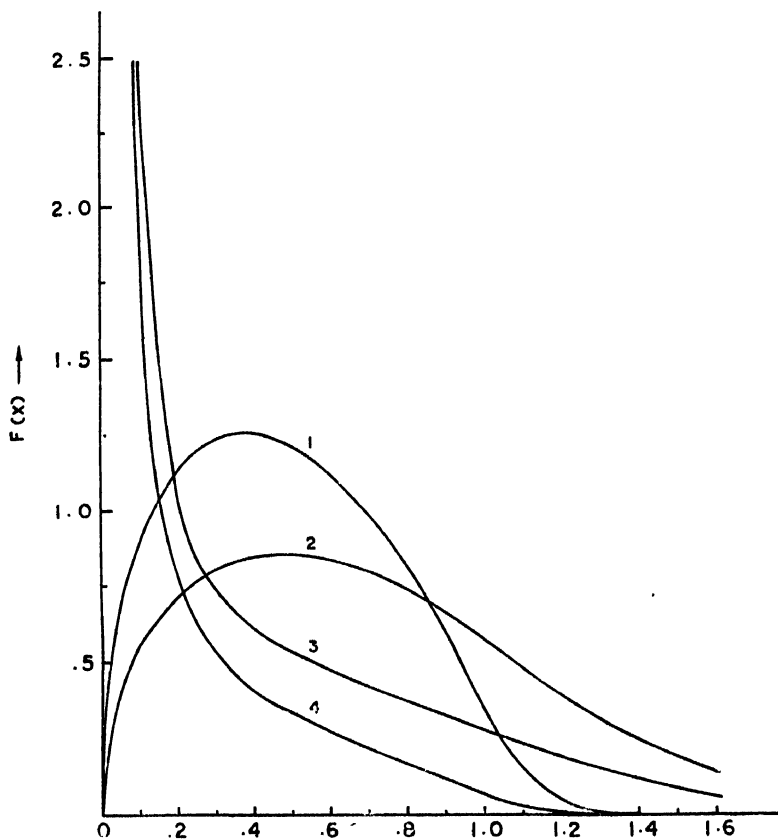


Fig. 2.—Electron energy distribution for different values of  $E/p$  and magnetic field. Curves : (1)  $E/p = 10$  V/cm.mm.Hg,  $H = 0$ ; (2)  $E/p = 100$  V/cm.mm.Hg.,  $H = 0$ ; (3)  $E/p = 100$  V/cm.mm. Hg.  $H = 2000$ G; (4)  $E/p = 10$  V/cm.mm.Hg.,  $H = 2000$ G.

$F(x)$  when  $x \rightarrow 0$ . In particular the representation of the velocity distribution function  $f(v)$  by the first two terms of the expansion in Eq.(2) is incorrect when  $x \ll 1$ . However, this is not a serious defect, since the total number of electrons having energy smaller than any limiting value remains finite and goes to zero as this limit tends to zero. Thus this would not influence derivation of the transport co-efficients by using the distribution function.

#### REFERENCES

- Allis, W. P. 1956, *Handbuch der Physik* (Edited by S. Flugge, Springer-Verlag, Berlin), **21**, 383.  
 Engelhardt, A. G. and Phelps, A. V. 1963, *Phys. Rev.*, **131**, 2115.  
 Engelhardt, A. G. and Phelps, A. V. 1964, *Phys. Rev.*, **133**, A375.  
 Golant, V. E. 1947, *Zh. Tekh. Fiz.*, **27**, 756. (Translation, 1957, *Soviet Physics Tech. Phys.*, **2**, 684).  
 Golant, V. E. 1959, *Zh. Tekh. Fiz.*, **29**, 756. (Translation, 1959, *Soviet Physics-Tech. Phys.*, **4**, 680).  
 Holstein, T. 1946, *Phys. Rev.*, **70**, 367.  
 Lax, B., Allis, W. P. and Brown, S. C. 1950, *J. Appl. Phys.*, **21**, 1297.

# Letters to the Editor

*The Board of Editors does not hold itself responsible for opinions expressed in the letters published in this section. The notes containing short reports of original investigations communicated to this section should not contain many figures and should not exceed 500 words in length. The contributions reaching the Secretary by the 15th of any month may be expected to appear in the issue for the next month. No proof will be sent to the author.*

## 4

### GONIOMETRIC STUDY OF TERBIUM SULPHATE OCTAHYDRATE

RUPENDRA KUMAR KASHYAP

PHYSICAL LABORATORIES, AGRA COLLEGE, AGRA, INDIA

*(Received March 9, 1963)*

Single crystal of  $Tb_2(SO_4)_3 \cdot 8H_2O$  were crystallised from aqueous solution of the rare earth salts in triple distilled water by slow evaporation at room temperature. The salt was prepared from the spectroscopic pure variety of oxide of terbium supplied by Johnson and Mathtie Co. Ltd. (London). Well formed crystals were sorted out and tested under a polarising microscope for checking any probable twining.

A two circle goniometer used for the measurements of the interfacial angles of the crystals was modified to give better and clear reflections even from striated surface of the crystals and thus the labour of selecting crystals with extremely good faces from a large number for goniometric purpose, was avoided. This was achieved by introducing a new form of cross-wire "A CROSSED FILAMENT BULB" in place of non-luminous cross-wire in the collimator. The image of this crossed-filament formed at the telescope after reflection from the crystal surface was bright on a dark background (while the image of non-luminous cross was dark) and so could be seen and located much more precisely and easily.

The forms represented by the crystal are orthopinacoids  $\{100\}$  and basal-pinacoids  $\{001\}$ ,  $\{10\bar{1}\}$  and  $\{11\bar{1}\}$ . The normal crystallographic angles taking symmetry considerations and good reflections are given in Table I. The notations for faces are according to Groth (1908)

The faces  $a(100)$  and  $c(001)$  were chosen following Groth (1908) in case of  $Er_2(SO_4)_3 \cdot 8H_2O$ , and Kashyap (1963) in case of  $Dy_2(SO_4)_3 \cdot 8H_2O$ . A stereogram was drawn to check the symmetry of crystal.

TABLE I

No.	Angles between faces	Measured angles	Calculated angles
1.	a(100):c(001)	61°42'	—
2.	c(001):p(101)	40°34'	—
3.	p(101):w(111)	63°2'	—
4.	a(100):r(101)	—	37°41'
5.	a(100):w(111)	84°36'	84°28'
6.	a(100):q(011)	—	76°31'
7.	c(001):q(011)	—	60°33'

The interfacial angles were calculated by methods as given by Tutton (1922). These are included in Table 1.

From these values we get

$$\text{Axial Angle : } \beta = 180^\circ - a(100) : c(001) = 180^\circ - 6142' = 118^\circ 18'$$

$$\text{Axial Ratios : } \frac{c}{a} = \frac{\sin c(001):r(101)}{\sin a(100):r(101)} = \frac{\sin 24 \ 1'}{\sin 37 \ 41'} = 0.66577$$

$$\frac{c}{b} = \frac{\tan c(001):q(011)}{\sin \beta} = \frac{\tan 60 \ 33'}{\sin 118 \ 18'} = 2.0115$$

$$\frac{a}{b} = \frac{a}{c} \times \frac{c}{b} = \frac{2.0115}{0.66577} = 3.0213$$

$$a : b : c = 3.0213 : 1 : 2.0115$$

It is seen that these ratios of  $a : b : c$  and the value of  $\beta$  agree well with other octahydrated isomorphous sulphate crystals such as of Pr, Nd, Er and Gd (Groth, 1908) and Dy (Kashyap, 1963).

The author is grateful to Prof. A Mookherji, D.Sc. for his kind help and guidance in the work.

#### REFERENCES

- Groth P. (1908), *Chemische Kristallographie*, Leipzig, 2, 454-461.  
 Kashyap R. K. (1963), *Agra University Res. Jour.* 12, part I.  
 Tutton (1922), 'Crystallography and Practical Crystal Measurement'—(London)

# THE MAGIC DIRECTION

T. C. ROY

PHYSICS DEPARTMENT, JADAVPUR UNIVERSITY, CALCUTTA.

(Received October 17, 1964)

Adair (1961) and Shafer *et al* (1963) recently made use of the magic direction for the convenience of analysing the polarization data. It is our purpose to show a few interesting properties of the parity changing term and their effects on this magic direction. The decay matrix element for a half spin particle with momentum  $\vec{p}$  is proportional to  $1$  or  $\vec{\sigma} \cdot \vec{p}$  without or with parity change. If  $\vec{n}$  is any direction, the polarization along  $\vec{n}$  is  $\langle \vec{\psi} | \vec{\sigma} \cdot \vec{n} | \psi \rangle$ . If however  $\vec{\sigma} \cdot \vec{p}$  term is present it changes the  $l$  of the state keeping  $j$  and  $j_z$  unaltered. To prove this we note,

$$[\vec{\sigma} \cdot \vec{p}, L_z + \frac{1}{2}\sigma_z]_- = 0 \quad \{\hbar = 1, \text{etc}\} \quad \dots (1)$$

so that  $j_z$  is not tampered. Also since,

$$\{\vec{\sigma} \cdot \vec{p}, \vec{\sigma} \cdot \vec{L} + 1\}_+ = 0 \quad \dots (2)$$

it follows,

$$[\vec{\sigma} \cdot \vec{p}, (\vec{\sigma} \cdot \vec{L} + 1)^2] = 0 \quad \dots (3)$$

i.e.  $(\vec{\sigma} \cdot \vec{L} + 1)^2 = (\vec{L} + \frac{1}{2}\vec{\sigma})^2 + 1/4$  has the same eigen value  $(j + \frac{1}{2})^2$  for the new state. Further from (3) and (2),

$$(j + \frac{1}{2})^2 \vec{\sigma} \cdot \vec{p} \psi = (L^2 + \sigma \cdot L + 1) \vec{\sigma} \cdot \vec{p} \psi = L^2 \vec{\sigma} \cdot \vec{p} \psi - (\vec{\sigma} \cdot \vec{p})(\vec{\sigma} \cdot \vec{L} + 1) \psi \quad (4)$$

$$\text{But } (j + \frac{1}{2})^2 \psi = L^2 \psi (\vec{\sigma} \cdot \vec{L} + 1) \psi = l(l+1) \psi + (\vec{\sigma} \cdot \vec{L} + 1) \psi \quad \dots (5)$$

Hence (4) becomes,

$$(j + \frac{1}{2})^2 \vec{\sigma} \cdot \vec{p} \psi = L^2 \vec{\sigma} \cdot \vec{p} \psi - \vec{\sigma} \cdot \vec{p} [(j + \frac{1}{2})^2 - l(l+1)] \psi \quad \dots (6)$$

$$\text{or, } L^2 \vec{\sigma} \cdot \vec{p} \psi = [2(j + \frac{1}{2})^2 - l(l+1)] \vec{\sigma} \cdot \vec{p} \psi$$

i.e.  $(\vec{\sigma} \cdot \vec{p} \psi)$  has  $l$  value either  $(l+1)$  or  $(l-1)$  according as  $j = l - \frac{1}{2}$  or  $l + \frac{1}{2}$ . We

thus prove that under  $\vec{\sigma} \cdot \vec{p}$

$$|l, j, j_z\rangle \longleftrightarrow |l \pm 1, j, j_z\rangle$$

or in particular,

$$P_{3/2}^{\pm 3/2} \longleftrightarrow D_{3/2}^{3/2} \quad \text{etc.}$$

Now the magic direction,  $\vec{m}$  is such that  $\vec{p}$  bisects the angle between  $\vec{m}$  and  $\vec{n}$  i.e.

$$\vec{m} = -\vec{n} + 2(\vec{n} \cdot \vec{p})\vec{p}$$

The polarisation along  $\vec{m}$  for  $(\vec{\sigma} \cdot \vec{p})\psi$  is,

$$\begin{aligned} & \langle \vec{\psi} \cdot \vec{p} \cdot \vec{\sigma} \cdot \vec{m} \cdot \vec{\sigma} \cdot \vec{p} \psi \rangle \\ &= \langle \vec{\psi} \cdot \vec{p} \cdot \vec{\sigma} \cdot [-\vec{n} + 2(\vec{n} \cdot \vec{p})\vec{p}] \cdot \vec{\sigma} \cdot \vec{p} \psi \rangle \\ &= \langle \vec{\psi} \cdot \vec{n} \cdot \vec{\sigma} \cdot \vec{p} \psi \rangle \end{aligned}$$

which shows that the percentage of polarization along magic direction  $m$  for  $|l=1, j, j_z\rangle$  when it is 100% polarized along  $n$  is the same as the percentage of polarization along  $n$  for  $|l, j, j_z\rangle$  when it is 100% polarized along  $m$  and vice versa. This result is nicely used by Shafer *et al.*

#### ACKNOWLEDGEMENT

I take this opportunity to thank Prof. J. J. Sakurai of Enrico Fermi Institute of Theoretical Physics whom I met in Bangalore Summer School of Theoretical Physics and Dr. P. Roy of Calcutta University.

#### REFERENCES

- Adair, K. 1961, *Reviews of Modern Physics* **33**, 406.  
 Schafer T, *et al* 1963, *Phys. Rev. Letters* **10**, 206.

# PROPERTIES OF ARTIFICIAL DIELECTRICS AT RADIO FREQUENCY

S. S. GUPTA AND M. N. SHARMA

DEPARTMENT OF PHYSICS, LUCKNOW UNIVERSITY, LUCKNOW

(Received July 5, 1963)

**ABSTRACT.** Dielectric constants and loss tangents of several metal powder artificial dielectrics have been determined in the radio frequency region 126 Kc/s. The results thus obtained have been utilised for the calculation of dielectric conductivities. The results show that amongst the artificial dielectrics studied, the antimony dielectrics have greater dielectric constants while their loss tangents are smallest. These characteristics of antimony dielectrics shall be of special advantage wherever the artificial dielectrics are to be used.

## INTRODUCTION

The development of the artificial dielectrics has been the subject of much theoretical and experimental investigations during the past few years. For obvious reason artificial dielectrics play an important role in the development of modern electronic engineering. Kelly (1953) measured the dielectric properties of metal powders in paraffin wax using microwave technique. Vogan (1952), Negebauer (1952), Peppiatt (1953), Meyer *et al.* (1956) and Mikaelian (1955) have reported on the same type of work. The dielectric properties of such a media are affected by (a) volume fraction of the metal powder (b) size and shape of metal particles (c) binding medium and (d) frequency of operation. Recently Pradhan and Gupta (1961) have shown that the effective dielectric constant also depends on the elemental spacing distribution and size distribution of particles. The effects of binding medium and frequency of operation are not of much importance and the relation between the two can be given as,

$$K_{eff} = KF(\alpha) \quad \dots (1)$$

where  $F(\alpha)$  is an algebraic function of  $\alpha$ , the polarizability of metal particles. It means that the effective dielectric constant of medium ( $K_{eff}$ ) is directly proportional to that of vehicle medium ( $K$ ). The frequency dependence on dielectric constant shall occur if the Debye's (1909) condition

$$a = \frac{\lambda_0}{7.255} \quad (2)$$

is satisfied by the particle size;  $a$  being the semi-major axis of the particles and  $\lambda_0$  is the wavelength in meters. For all practical purposes  $\lambda_0$  corresponds to sub-millimeter region.

The present work was undertaken with a view to observe the effects and suitability of these artificial dielectrics at radio frequencies.

#### EXPERIMENTAL PROCEDURE

Paraffin wax ( $\epsilon = 2.25$  and  $\delta = 0.0002$ ) used as the binding medium, was melted and metal powder was poured into this molten wax and the mixture was stirred until it is solidified. This solid mixture was cooled to a sufficiently low temperature with the help of a freezing mixture, the mass getting quite crisp, it was reduced to fine powder and then dessicated for 36 hours. The fine powder was put into a specially designed brass cast (Fig. 1) which was slowly heated from

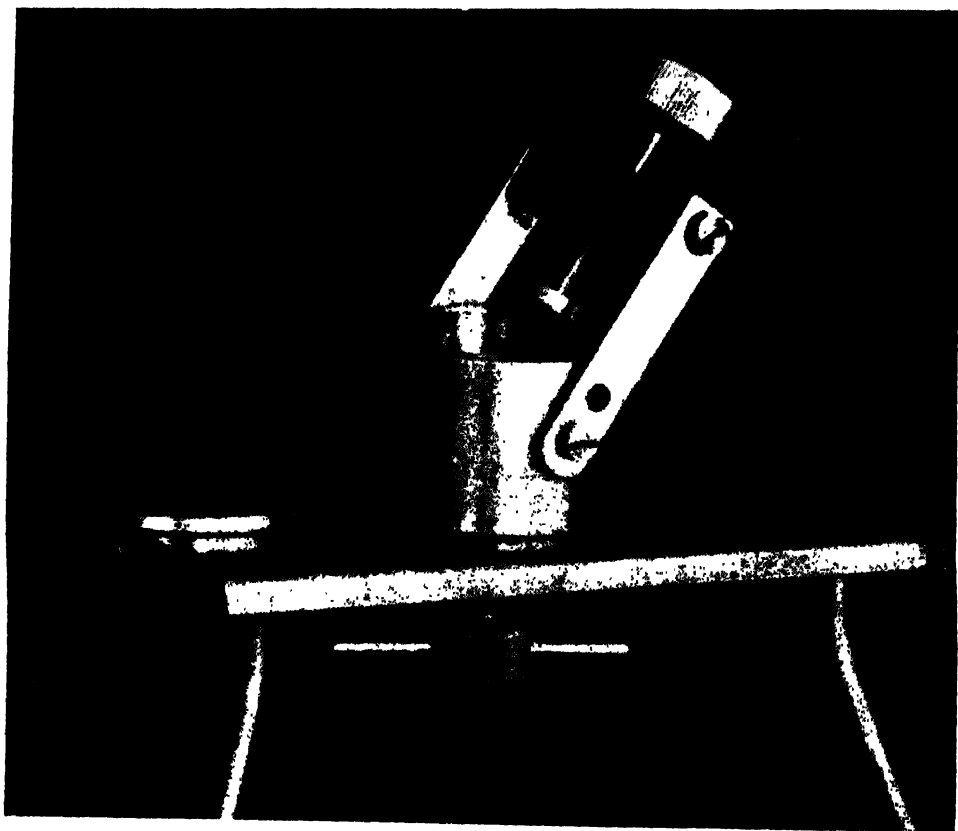


Fig. 1. Cast for moulding the samples.

outside. The specially designed cast is capable of exerting heavy pressure to the mixture, thus providing a sample free of air and giving a definite shape to it. It was then cooled and the sample taken out. Samples thus moulded were cut to desired thickness. The technique provided samples having homogeneous distribution of metal particles.



Exact percentage of metal powders in different samples were determined as follows :

The sample was dissolved in hot liquid paraffin oil and centrifuged, the solid mass was then further dissolved in benzene, filtered and dried. The process was repeated twice, the mass of metal powder was weighed and the percentage calculated.

Hartshorn's (Hartshorn and Ward, 1936) method for the measurement of dielectric constant and loss tangent at radio frequencies was used. The adjustments were made by means of two micrometer condensers, one being a plate condenser in which the sample was inserted and other the cylindrical condenser of linear law and of very small range, which served to measure the sharpness of resonance. Both permittivity and power factor could be obtained as the ratio of the capacitance readings, frequency is not involved in their calculation.

The dielectric constants and loss tangents of different samples were determined at 126 Kc/s as described in detail by Sharma (1960), Pradhan and Sharma (1960) and Sharma and Gupta (1963).

The dielectric constant  $K$  of a solid sample is given by

$$K = \frac{3.6C_s t}{r^2} \quad \dots (3)$$

where  $C_s$  is capacitance of the sample in  $\mu\mu F$ ,  $t$  is the thickness of the sample and  $r$  is the radius of electrodes (2.5 cms.).

The loss tangent is given by

$$\tan \delta = \frac{\Delta C_1 - \Delta C_0}{2C_s} \quad \dots (4)$$

where  $\Delta C_1$  is the capacitance change corresponding to half of the maximum deflection with sample in between the two copper electrodes and  $\Delta C_0$  is the capacitance change corresponding to half of the maximum deflection without the sample.

Dielectric conductivities were calculated by the following formula

$$\sigma = 0.0053024 \left( \frac{\pi K \tan \delta}{\lambda} \right) \quad \dots (5)$$

where wavelength  $\lambda$  is in meters.

## RESULTS AND DISCUSSIONS

Figs. (2) and (3) and Tables I and II show the variation of dielectric constants and loss tangents of copper, antimony, zinc and calcium metal powder artificial dielectrics.

Microscopic examination of these metal particles showed that copper and antimony particles have irregular form ( $20\mu \times 10\mu \times 7\mu$  on average for copper and

$6\mu \times 3\mu \times 2\mu$  for antimony) and zinc and calcium particles have the form of spheres. As the polarizability of sphere is minimum because of the smallest surface area for a given volume, it is expected that copper and antimony dielectric shall have a higher dielectric constant as compared to zinc and calcium dielectrics for the same

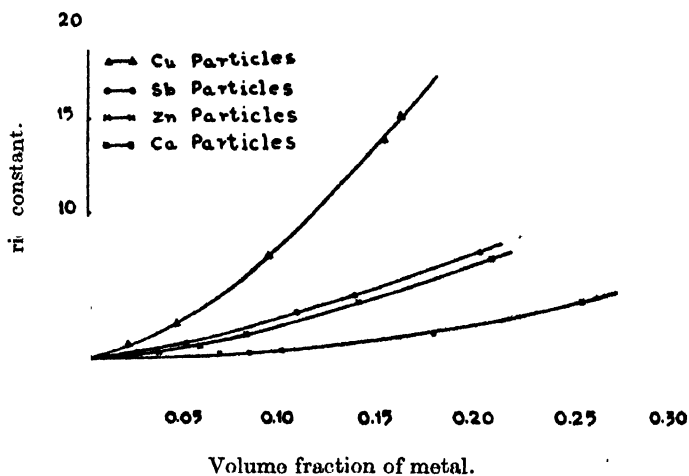


Fig. 2. Variation of dielectric constant of metal powder artificial dielectrics with concentration.

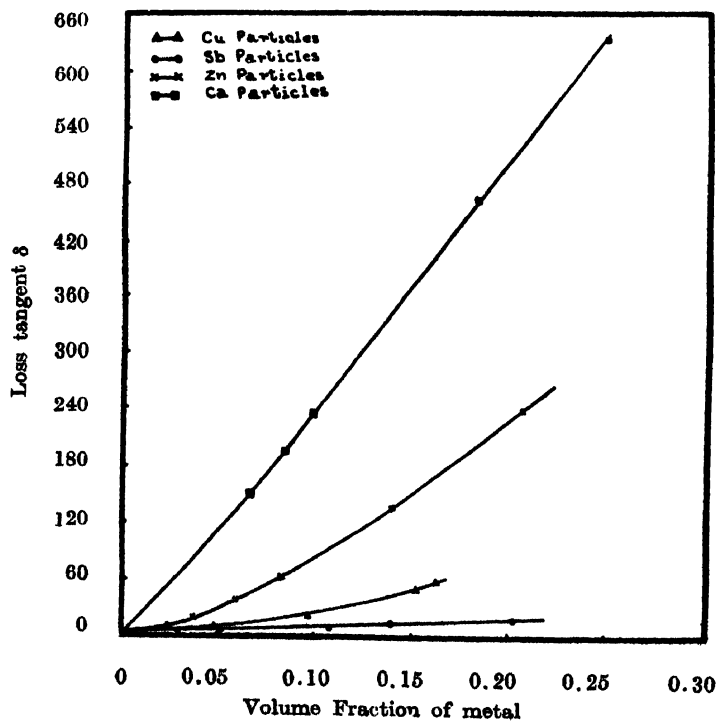


Fig. 3. Variation of loss tangent  $\delta$  of metal powder artificial dielectrics with concentration.

TABLE I

Variation of dielectric constant of Metal powder artificial dielectrics with concentration

Copper		Antimony		Zinc		Calcium	
Fractional Volume	K	Fractional Volume	K	Fractional Volume	K	Fractional Volume	K
0.021	3.066	0.025	2.801	0.038	2.916	0.069	2.772
0.048	4.182	0.052	3.200	0.060	3.300	0.085	2.864
0.096	7.600	0.107	4.620	0.083	3.560	0.101	2.990
0.154	13.570	0.138	5.586	0.140	5.305	0.180	3.715
0.164	14.990	0.204	7.780	0.209	7.496	0.253	5.376

TABLE II

Variation of loss tangent of metal powder artificial dielectrics with concentration

Copper		Antimony		Zinc		Calcium	
Fractional Volume	$\tan \delta \times 10^4$	Fractional Volume	$\tan \delta \times 10^4$	Fractional Volume	$\tan \delta \times 10^4$	Fractional Volume	$\tan \delta \times 10^4$
0.021	3.480	0.025	3.473	0.038	22.400	0.069	152.560
0.048	7.650	0.052	4.100	0.060	39.390	0.085	195.000
0.096	23.850	0.107	8.210	0.083	61.200	0.101	236.320
0.154	53.340	0.138	10.550	0.140	144.800	0.180	452.200
0.164	60.790	0.204	20.040	0.209	234.200	0.253	632.700

TABLE III

Variation of dielectric conductivity of metal powder artificial dielectrics with concentration

Copper		Antimony		Zinc		Calcium	
Fractional Volume	$\sigma \times 10^3$ (mhos/metre)	Fractional Volume	$\sigma \times 10^3$ (mhos/metre)	Fractional Volume	$\sigma \times 10^3$ (mhos/metre)	Fractional Volume	$\sigma \times 10^3$ (mhos/metre)
0.021	7.461	0.025	6.812	0.038	45.671	0.069	295.760
0.048	23.372	0.052	9.203	0.060	90.844	0.085	390.510
0.096	126.770	0.107	26.430	0.083	152340	0.101	494.080
0.154	506.070	0.138	41.263	0.140	537.280	0.180	1174.600
0.164	637.240	0.204	108.990	0.209	1227.500	0.253	2378.600

volume fraction. The investigations verify this. The experimental results on copper, antimony, zinc and calcium show that the antimony dielectrics have minimum loss for a given volume fraction than others and still have got greater values of dielectric constant than for zinc and calcium. From the variation curves for the dielectric constants and the losses it can be suggested that the antimony dielectrics are best suited for any work wherever the artificial dielectrics are to be used.

Let us consider the case of antimony in detail. On calculating  $\left(\frac{\alpha e}{3\epsilon_0}\right)$   $\{ = f/N = \text{constant, the volume fraction for spheres} \}$  from the Clausius-Mossotti relation

$$\frac{K_e - K}{K_e + K} = \frac{N}{3} \left( \frac{\alpha e}{\epsilon_0} \right) \quad \dots (6)$$

and plotting it against the fractional volume (Fig. 4.), it was found that the two have linear relationship, pointing out that the polarizability remains constant

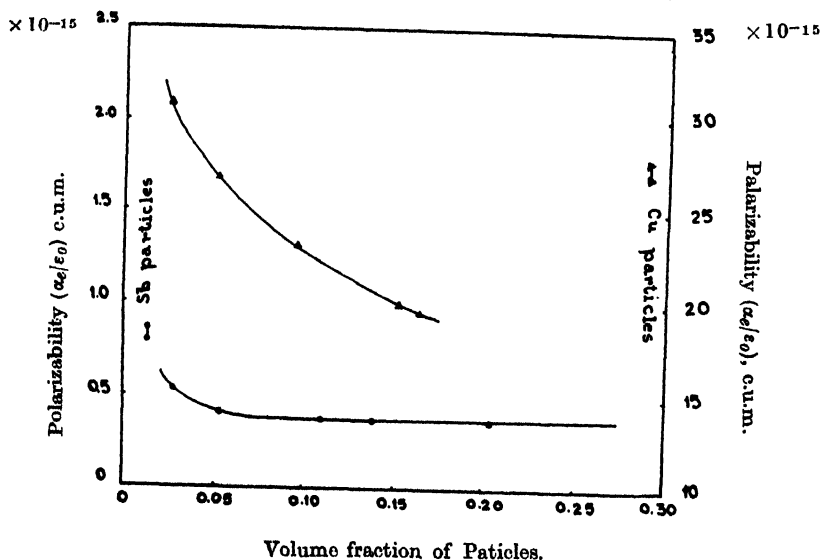


Fig. 4. Polarizability of antimony and copper particles from Clausius-Mossotti relation.

even at higher volumes although it should have increased due to the agglomeration. The investigations point out that there is no agglomeration in this case. At first sight one would think that this result has been obtained just per chance; but this view was obviated by repeated investigations on samples made afresh. Authors have not been able to find out suitable interpretation why the agglomeration does not take place in case of antimony. One can however suggest that the inter particle force between Sb—Sb is possibly smaller than the binding system.

Polarizability, thus found for antimony is five times greater than that of the sphere and remains constant. It implies, therefore that the shape of these particles on the average remains unchanged even at higher volume fractions (35%) and the dielectric constant of antimony dielectric can be calculated theoretically.

#### ACKNOWLEDGMENT

Authors are indebted to Professor P. N. Sharma for his keen interest and encouragement throughout the investigation. They are grateful to Dr. B. P. Pradhan for his guidance and supervision of the work.

#### REFERENCES

- Debye, P., 1909, *Ann. Phys. Lpz.*, **30**, 57.  
Hartshorn, L., and Ward, W. H., 1936, *Proc. Inst. elect. Engrs.*, **78**, 597.  
Kelly, J. M., Stnoien, J. O., and Isbell, D. E., 1953, *J. appl. Phys.* **24**, 258.  
Meyer, E., Schmitt, H. J. and Severin, H., 1956, *Z. angew. Phys.*, **8**, 257.  
Mikaolian, A. L., 1955, *Radiotekhnika*, Moscow, **10**, 1.  
Neugebauer, H. E. J., 1952, Air Force Contract No. AF 19(122)81, Eaton Electronic Research Laboratory Rep. No. 6.  
Poppiatt, H. J., 1953, United States Air Force Contract No. AF 19(122)81, Cambridge Research Centre Rep. No. D6.  
Pradhan, B. P. and Sharma, M. N., 1960, *Proc. Nat. Inst. Sci.*, **26A**, 560.  
Pradhan, B. P. and Gupta, R. C., 1961, *J. Sci. industr. Res.*, **20B**, 581.  
Sharma, M. N., 1960, *J. sci. industr. Res.*, **19B**, 5.  
Sharma, M. N. and Gupta, S. S., 1963, *Ind. J. Phys.*, **37**, 33.  
Vogan, E. L., 1952, United States Air Force Contract No. AF 19(122)81, Eaton Electronic Research Laboratory Rep. No. D3.

# AN ANALYSIS OF THE J-PHENOMENON IN SCATTERED X-RAYS

## Part II

HIRENDRA KUMAR PAL\*

DEPARTMENT OF PURE PHYSICS, CALCUTTA UNIVERSITY, CALCUTTA

(Received November 11, 1964)

**ABSTRACT.** Starting with Barkla's idea of 'radiation-atmosphere', where the different constituents of heterogeneous X-rays are considered as an integrated whole and taking into account the various effects due to (i) Compton scattering, (ii) interference of the scattered radiations (predominantly in the forward direction), (iii) absorption of the various constituents of the beam, (iv) narrowness of the primary beam in contrast with the width of the scattered beam, and (v) ionization produced by the radiations received in the ionization chambers, a theoretical analysis has been given to explain, under suitable conditions, most of the experimental results of Barkla and Khastgir (1925-27), both qualitatively and quantitatively, on the comparative study of the primary and the scattered beams of heterogeneous X-rays, (i) when both the beams were filtered through the same increasing thickness of an absorbing material for a given average wavelength of the primary beam and (ii) when both the beams were (a) unintercepted and (b) intercepted by the same thickness of an absorbing material over a wide range of average wavelengths of the primary beam. The laws of the *J*-phenomenon formulated by Barkla have thus been theoretically justified under certain conditions. Barkla's concept of discrete 'levels' of X-ray activity associated with the *J*-phenomenon has not been considered in the present analysis.

## INTRODUCTION

In a previous paper the writer (Pal, 1964) published an account of his analysis of the *J*-phenomenon in relation to a single beam of X-rays, irrespective of its genesis. Following Barkla's idea of 'radiation-atmosphere', a heterogeneous beam of X-rays was taken as an integrated whole and the average mass-absorption coefficient of the heterogeneous beam was considered more fundamental than the individual wavelengths. On this basis a consistent and comprehensive interpretation of the main features of the phenomenon, as had been observed by Barkla (1925) was given. The present paper attempts an analytical survey of some other aspects of the same phenomenon, which were revealed by a comparative study of two heterogeneous beams of X-rays, chosen out of a primary beam and the same scattered at different angles. In the experimental procedure, this problem was approached from two different directions, as briefly outlined below :

1. Keeping the penetrating power of the incident primary beam constant,

\*Present Address. A-91, H. B. Town, P.O. Sodpur, 24 Parganas, W. B.

- (a) the scattered beam was observed at a particular angle  $\phi$  between the incident and the scattered beams by intercepting both these beams with an equal thickness  $x$  of an absorbing substance (such as Al, Cu, Ag and Sn) and thereafter receiving the transmitted beams into two similar ionization chambers, the ratio of ionizations ( $S'/P'$ ) in the two chambers for the scattered and the primary beams was found and plotted against thickness  $x$ .
- (b) the scattered beam at a certain angle  $\phi$  was similarly compared with the beam scattered at an angle  $\phi'$  or  $90^\circ$  and the ratio of ionizations plotted against the intercepting thickness  $x$ .

2. The penetrating power of the incident primary beam was progressively increased and for each penetrating power the primary beam was compared with the beam, scattered in any direction  $\phi$ , first, when both the beams were unintercepted and later, when both the beams were simultaneously intercepted by sheets of a definite thickness of some particular absorbing substance. The ratios of ionizations,  $S/P$  for the unintercepted and  $S'/P'$  for the intercepted beams were determined as in 1. These ratios or their percentage difference was plotted against the corresponding primary mass-absorption coefficient  $\left(\frac{\mu}{\rho}\right)$  in aluminium. The results furnished by these experiments may be summarised as follows :

- I. The primary and the scattered beams of heterogeneous X-rays or the two beams of heterogeneous X-rays scattered in different directions have either (i) the same absorbability or (ii) a markedly different absorbability, when measured in a particular absorbing substance. This can be expressed as :

$$\left(\frac{\mu}{\rho}\right)_1 - \left(\frac{\mu}{\rho}\right)_2 = 0, \text{ or } a, \text{ or } b, \text{ or } c,$$

where  $a, b, c \dots$  are constants and the subscripts 1 and 2 refer to the primary and the scattered beams or to the scattered beams proceeding in two different directions.

- II. A transition from (i) to (ii) in I is possible, under certain conditions, revealing thereby certain discontinuities.
- III. When a difference appears in the absorbabilities of the primary and the scattered beams, the percentage difference is independent of the angle of scattering and also of the mass-absorption coefficient of the primary beam.
- IV. The position of the discontinuity, when observed appears to depend slightly on the material of the absorbing substance.

These are the laws of the *J*-phenomenon as had been formulated by Barkla.

The experimental results on the comparative study of progressive filtering of primary and the scattered beams of heterogeneous X-rays further revealed certain anomalous features. These are :

(a) When the scattered beam is different from the primary when measured in certain substances, its absorbability may be and frequently is precisely the same as that of the primary beam when measured in certain other substances.

(b) Even after transmission through substances which show the difference between the primary and the scattered beams, there is still no difference between the two, when measured in certain other substances.

In the present paper, an attempt has been made to give an analysis of the experimental results on the comparative study of the above mentioned two heterogeneous beams and to offer a satisfactory explanation of most of the observed features by taking into account the various factors which are known to produce their respective effects on the ultimate observations. We shall refer to the experimental results which had been published by C. G. Barkla and S. R. Khastgir (1925b), 26b, 27)

#### BACKGROUND OF THE ANALYSIS

For a theoretical analysis of the results of experiments in question we have to consider four different types of problems, viz. (i) scattering, (ii) interference, (iii) absorption and (iv) ionization. Each of these effects is known to have a direct bearing on the wavelength of the radiation concerned.

When the X-ray beam experimented upon is heterogeneous, as in the present case, a theoretical approach is beset with many difficulties. For example, a spectrum with a vast multitude of wavelengths has to be confronted. To make things worse, the energy-distribution function over the constituents is not known with certainty and is likely to vary with the tube generating the X-rays. Further, a part of the spectrum, towards the longer wavelength-side, is absorbed while traversing its various air-paths, even before reaching the measuring instruments. This sets an uncertain limit to the longer wavelengths in the spectrum under study and hence any summation-operation carried between limits, one of which is ill-defined, cannot be expected to yield either comparable or reliable results.

It is, therefore, at once obvious that such a heterogeneous complex beam of X-rays should, in a mathematical analysis, be best treated as an integrated whole without any special reference to the individual monochromatic constituents and this should have an 'average' property which, to some extent, is measurable by what is known as the 'mass-absorption coefficient'. This had been frequently stressed by Barkla. On the basis of this, it becomes possible to assign one wavelength—an average one—to the whole beam, as though it were homogeneous.



(i) *Scattering*

According to the classical theory, the intensity scattered by a single 'free' electron at an angle  $\phi$  with the primary beam, is given by the wellknown equation

$$I_s = K_1 I_P (1 + \cos^2 \phi) \quad \dots (1)$$

where  $K_1 = e^4 / 2r^2 m^2 c^4 = \text{constant}$

and  $I_P = \text{Intensity of the primary beam.}$

For the whole atom, the expression is to be multiplied by  $Z^2$  or  $Z$ , (where  $Z$  is the atomic number) according as the packing of the electrons inside the atom is very close or otherwise.

On the quantum theory, the Compton-change of wavelength on scattering, is given by—

$$\partial \lambda_\phi = \frac{h}{mc} \text{ vers } \phi = \delta \lambda_{90^\circ} \text{ vers } \phi \quad \dots (2)$$

and the scattering function, as given by Breit, Dirac (1926) and others can be written as :

$$I_\phi = I_s \left( 1 + \frac{h\nu}{mc^2} \text{ vers } \phi \right)^{-3} = I_s \left( 1 + \frac{\delta \lambda_\phi}{\lambda} \right)^{-3} \quad \dots (3)$$

(The notations used in the above equations have their usual significance.)

Our method of analysis is as follows : The heterogeneous primary beam is regarded as a whole and defined by an average wavelength. The scattered radiation consists of two parts, one of which is 'modified' and the other 'unmodified' after scattering. The modified portion is assumed to follow the scattering function expressed in (3) and the unmodified portion, naturally that given in (1). The effects of interference and absorption on each of the two scattered intensities are then considered separately and finally the ionizations produced by the corresponding transmitted parts. These ionizations when added up give the resultant ionization occurring inside the ionization chamber for the scattered beam. In the case of the ionization in the primary chamber only the effect of absorption on the primary intensity as a whole is considered.

In connection with the scattering of a heterogeneous beam of X-rays the Compton-change of wavelength which should be appropriately ascribed to the modified portion of the scattered rays is, of course, that given by (2). Such a change in a particular direction is always independent of the incident wavelength. Hence an average wavelength  $\lambda$ , when modified, should have an average wavelength  $\lambda + \delta \lambda_\phi$ .

As for the percentage modification (which is defined as :  $100 \times \text{fraction of the incident intensity modified}$ ) occurring in a scattering process, it is learnt from the experiments of Backhurst (1934) with crystal-selected monochromatic X-rays,

that for very hard rays ( $\lambda = 0.25 \text{ \AA}$ ) and light scattering atoms such as beryllium or carbon, the modification, at  $\phi = 150^\circ$ , is approximately 100%. But this figure steadily diminishes either as the wavelength or as the atomic number of the scattering element is increased. The data for  $\phi \lesssim 90^\circ$ , however, are lacking.\* In the case of a heterogeneous complex beam, we are, of course, concerned with an average percentage modification corresponding to an average wavelength.

Let  $C_\phi$  represent the fraction of the incident intensity which is modified on being scattered at an angle  $\phi$ , so that  $(1 - C_\phi)$  represents the corresponding fraction which is unmodified. Therefore, from\*\* (1) and (3), the modified scattered intensity in the direction  $\phi$  is given by

$$I'_\phi = KI_P C_\phi (1 + \cos^2 \phi) \left(1 + \frac{\delta \lambda_\phi}{\lambda}\right)^{-3} \quad \dots (4)$$

and the unmodified scattered intensity in the same direction

$$I''_\phi = KI_P (1 - C_\phi) (1 + \cos^2 \phi) \quad \dots (5)$$

where  $K = \text{constant}$ .

## (ii) Interference

The effect of interference of the scattered radiations from the scattering electrons has been observed to play an important role in determining the nature of results in the absorption experiments with heterogeneous scattered X-rays. Indeed, in course of a previous publication (Pal, 1949), the writer definitely showed that the 'excess scattering' in the forward direction, arising from interference of the scattered radiations, could introduce anomalies into the results even to the extent of concealing or refuting the Compton-effect. So far as the  $J$ -phenomenon is concerned, the effect of interference does not seem to have received due consideration from the workers on the subject. Excess scattering, owing to the preponderance of longer wavelengths in the heterogeneous scattered beam, produces a general softening of this beam increasing its average wavelength. This has to be taken into account, remembering that the effect increases with an increase in the incident wavelength or in the atomic number of the scattering element and with a decrease in the scattering angle  $\phi$  (Pal, 1948).

The effect due to interference is two-fold : There is (i) an enhancement of the scattered intensity and (ii) an increase in the average wavelength of the scattered beam.

\* Although Backhurst's results lack in data for  $\phi \lesssim 90^\circ$ , yet it will not be unreasonable to expect that they are in line with those for  $\phi = 150^\circ$ , in a general way at least.

\*\* Here we neglect the small amount of polarization that may be present in the incident radiation.

Let us represent the enhancement of intensity by a factor  $\{1 + \psi(\phi, \lambda)\}$  for a given scatterer. Let us also put:

$$f(\phi, \lambda) = (1 + \cos^2 \phi) \{1 + \psi(\phi, \lambda)\} \quad \dots \quad (6)$$

Now, when  $\phi \gtrsim 90^\circ$ , the effect of interference is negligible, so that  $\psi = 0$  and we get

$$f = 1 + \cos^2 \phi = 1, \text{ when } \phi = 90^\circ.$$

We also get

$$f' = \frac{df}{d\lambda} = \dots \quad (7)$$

Let the increase in the average wavelength due to interference be represented by  $\Delta_\phi$  and that produced by the Compton-effect by  $\delta\lambda_\phi$ , so that the total increase in the average wavelength for the modified scattered rays is given by

$$\Delta_\phi = \Delta_\phi + \delta\lambda_\phi \quad \dots \quad (8)$$

and that for the unmodified scattered rays by  $\Delta_\phi$  only. Here it is recognised that, strictly speaking, the contributions by interference are different for the modified and unmodified rays. But the difference is regarded as one of second-order smallness and hence neglected.

After interference has taken place, the intensities of the scattered radiation, in the direction  $\phi$ , are obtained from (4), (5) and (6). Thus for the modified part, we get

$$\begin{aligned} I'_\phi &= KI_P C_\phi (1 + \cos^2 \phi) \left(1 + \frac{\delta\lambda_\phi}{\lambda}\right)^{-3} \{1 + \psi(\phi, \lambda + \delta\lambda_\phi)\} \\ &= KI_P C_\phi \left(1 + \frac{\delta\lambda_\phi}{\lambda}\right) f(\phi, \lambda + \delta\lambda_\phi) \end{aligned} \quad (9)$$

and for the unmodified part,

$$\begin{aligned} I''_\phi &= KI_P (1 - C_\phi) (1 + \cos^2 \phi) \{1 + \psi(\phi, \lambda)\} \\ &= KI_P (1 - C_\phi) f(\phi, \lambda) \end{aligned} \quad \dots \quad (10)$$

### (iii) *Absorption*

When a heterogeneous beam of X-rays traverses a thickness  $x$  of an absorbing sheet of matter it is hardened up owing to its softer constituents being more readily absorbed. As  $x$  increases,  $(\mu/\rho)$  for the emergent beam decreases, so also its average wavelength  $\lambda$ . The rate of variation of  $(\mu/\rho)$  or of  $\lambda$ , however, becomes smaller and smaller with an increase in  $x$ , till at a certain stage, this variation is practically indistinguishable for any further increase in  $x$ , so that the course of the  $(\mu/\rho, x)$ -curve is then practically parallel to the  $x$ -axis, signifying that the transmitted rays have become more or less homogeneous.

*Critical absorbing thickness* : If two heterogeneous beams with slightly different penetrating powers (such as a primary and the corresponding scattered beam) be each passed through a thickness  $x$  of an absorbing material, their  $(\mu/\rho)$ -values, on emergence, should generally exhibit a difference. But as the softer of the two beams is absorbed in a somewhat greater proportion, the rate of fall of  $(\mu/\rho)$  with increasing  $x$ , for the softer beam, will be steeper than that for the beam which is less soft. This means that the difference  $\delta(\mu/\rho)$  between them gradually diminishes as  $x$  increases, till for a thickness equal to or greater than a certain value  $x_c$ , this difference is practically indistinguishable. The minimum absorbing thickness  $x$  which, so to say, brings down both the beams to the same level of absorbability, will be hereafter, called *critical absorbing thickness*

Thus an important property of critical thickness is that,

if  $x \geq x_c$

$$\left. \begin{aligned} \left[ \delta \left( \frac{\mu}{\rho} \right) \right]_x &= 0 \\ \text{or } (\delta\lambda)_x &= 0 \end{aligned} \right\} \dots (11)$$

where the subscript  $x$  signifies to transmission of each of the beams concerned through an absorbing substance of thickness  $x$ .

It is easy to see that the critical thickness for an absorber should increase with the hardness of the radiation and for any radiation should decrease with an increase in the atomic number of the absorbing element.

*Mass-absorption coefficient* : This coefficient, in the case of a monochromatic beam of X-rays, follows a linear relation with  $\lambda^3$ . Thus

$$\frac{\mu}{\rho} = A + B\lambda^3 \quad (12)$$

where  $A$  and  $B$  are constants depending upon the material of the absorber.

The first term  $A$  arises from the energy absorbed by recoil electrons and is called the 'scattering absorption coefficient' and the second term  $B$  is due to the energy absorbed by the ejected photo-electrons and is called the 'true absorption coefficient'.

For a *narrow* beam of X-rays, like the primary beam, the energy absorbed by recoil-electrons is practically lost to the beam, whereas for a *wide* beam, a part of the scattered energy will remain lodged inside the beam and add to its intensity. Thus the  $(\mu/\rho)$  for a narrow beam is expected to exceed that for a wide beam. The scattered beam in the experiments under review was always very wide. For such a wide beam  $A$  in (12) would be reduced to a somewhat smaller value  $A'$ . The amount of reduction would depend on the geometry of the measuring instrument. This had actually been verified experimentally by Bachem (1923).

The extrapolated values of  $A$  and  $B$  for a few chemically pure\* elements are given in the following Table I. In the 5th column of this table, are also supplied the corresponding maximum values of absorbing thickness employed in the experiments under review, for quick reference.

TABLE I

Absorbing element	Range of wavelength in A.U.	$A$	$B$	$x(\text{max.})$ in cm.
Al	0.2 — 0.7	13	14.1	0.150
Cu	0.2 — 0.4	25	153	0.009
	0.4 — 0.7	15	140	
Ag	0.3 — 0.4	3.5	551	0.012
	0.5 — 0.6	.5	84.6	
Sn	0.25 — 0.3	2.5	600	0.010
	0.3 — 0.7	?	?	
Au	0.25 — 0.55	?	?	0.008

*Transmitted Intensity:* In the case of a narrow monochromatic beam of X-rays, the transmitted intensity is given by

$$I_x = I_0 \exp\left(-\frac{\mu}{\rho} x\right) = I_0 \exp\{-(A + B\lambda^3)x\} \quad \dots (13)$$

where  $I_0$  is the intensity of the incident beam. For a wide beam  $A$  is replaced by  $A'$ .

To calculate the transmitted intensity in the case of a heterogeneous beam, we have to substitute for  $\lambda$  in (13) the average wavelength ' $L$ ' inside the absorbing sheet, which is the mean of the average incident wavelength  $\lambda$  and the average transmitted wavelength  $\lambda_x$ . Thus the required average is given by

$$\therefore L = \frac{1}{2}(\lambda + \lambda_x), \text{ (since } x \text{ is small)}$$

$$\text{We shall here put : } \lambda_x = \lambda(1 - 2\omega) \quad \text{where } \omega = \omega(x, \lambda, Z). \quad \dots (14)$$

$$\begin{aligned} \therefore L &= \frac{1}{2}\{\lambda + \lambda(1 - 2\omega)\} \\ &= \lambda(1 - \omega) \end{aligned} \quad \dots (15)$$

Substituting this in (13),

$$\begin{aligned} I_x &= I_0 \exp\{-(A + BL^3)x\} \\ &= I_0[\exp(-Ax)] \exp\{-Bx\lambda^3(1 - \omega)^3\} \end{aligned} \quad \dots (16)$$

---

\* Traces of impurities as are usually present in the commercial varieties of the metals are apt to affect the values of  $A$  and  $B$  considerably.

'Disparity' :

For  $\lambda$  we have put :

$$\lambda_x = \lambda(1-2\omega)$$

$\therefore$  for  $\lambda + \delta\lambda$  we write

$$(\lambda + \delta\lambda)_x = (\lambda + \delta\lambda)(1-2\omega')$$

so that when  $x = 0$ ,  $\omega = 0$  and  $\omega' = 0$

and when  $x > x_c$ ,  $\omega \approx \text{const.}$  and  $\omega' \approx \text{const.}$

For small values of  $x$ ,  $\omega$  and  $\omega'$  are supposed to be small compared to unity.

Now,  $(\lambda + \delta\lambda)_x = (\lambda + \delta\lambda) \cdot (1-2\omega')$

$$= \lambda \left\{ 1 + \frac{\delta\lambda}{\lambda} - 2\omega' \right\}, \text{ (neglecting second and higher order smallness)}$$

and

$$\lambda_x = \lambda(1-2\omega)$$

$$\therefore (\lambda + \delta\lambda)_x / \lambda_x = 1 + \frac{\delta\lambda}{\lambda} - 2(\omega' - \omega), \quad \dots (17)$$

(neglecting second and higher order smallness)

$$\text{Thus } \frac{(\lambda + \delta\lambda)_x - \lambda_x}{\lambda_x} = \frac{\delta\lambda}{\lambda} - 2(\omega' - \omega) = q_x \text{ (say)} \quad \dots (18)$$

Here  $q_x$  is called the 'disparity'-term which is defined as the fractional difference between the average transmitted wavelengths of the two beams of slightly different average wavelengths after passing through a certain thickness  $x$  of an absorbing substance.

Also from (18) we can write

$$\frac{\delta\lambda}{\lambda} - (\omega' - \omega) = \frac{1}{2} \left( q_x + \frac{\delta\lambda}{\lambda} \right) \quad \dots (19)$$

*Properties of  $q_x$ :*

(a). When  $x = 0$ ,  $\omega' = 0 = \omega \therefore q_0 = \frac{\delta\lambda}{\lambda}$

(b). When  $x \geq x_c$ ,  $(\delta\lambda)_x = 0$  (vide eqn. 11), so that

$$(\lambda + \delta\lambda)_x / \lambda_x = 1 \text{ and } q_x = 0$$

Also  $2(\omega' - \omega) = \delta\lambda / \lambda$  from (18).

(c) When the two beams compared are equally hard

$$\delta\lambda = 0, \quad \omega = \omega' \therefore \text{from (18), } q_x = 0$$

(d) For homogeneous beams,  $\omega' = 0 = \omega$

$\therefore$  from (18),  $q_x = \frac{\delta\lambda}{\lambda} = \text{constant}$

(e) It will be sometimes necessary to know how the quantity,  $(q_x \cdot x)$ , varies with  $x$ . For this, we note that this quantity is always positive, having a value 0 at  $x = 0$  and at  $x \geq x_e$ . Therefore, somewhere between  $x = 0$  and  $x = x_e$ ,  $(q_x \cdot x)$  has a maximum value :

(f) As  $\lambda$  decreases, the quantity  $2(\omega' - \omega)$  i.e.  $\left(\frac{\delta\lambda}{\lambda} - q_x\right)$  increases. For, when  $\lambda$  is large,  $\omega' \simeq \omega$  and when  $\lambda$  is small,  $\omega' > \omega$ .

(iv) *Ionization in  $SO_2$  inside the ionization chamber*

This has been found to be proportional to the intensity and the cube of the wavelength of the rays concerned. Thus if  $I_x$  represent the ionization produced by the radiation transmitted through a thickness  $x$  of the absorbing material, then

$$\begin{aligned} I_x &= gI_x\lambda_x^3 \\ &= gI_x\lambda^3(1-2\omega)^3 \end{aligned} \quad \dots \quad (20)$$

where  $g = \text{Constant}$ .

## SECTION I.

### COMPARISON OF THE SCATTERED AND THE PRIMARY RADIATIONS AT CONSTANT INCIDENT WAVELENGTH AFTER PROGRESSIVE FILTERING

A. *Evaluation of the ratio  $(S'/P')$  :*

Let  $S'$  represent the ionization produced by the scattered beam in the direction  $\phi$  and  $P'$  that by the primary beam, after they have traversed, each a thickness  $x$  of the absorbing material.

Then

$$S' = S'_1 + S'_2$$

where the subscript 1 denotes the contribution by the modified portion of the rays and the subscript 2 that by the unmodified, so that

$$(S'/P')_\phi = (S'_1/P')_\phi + (S'_2/P')_\phi$$

Now, neglecting the absorption inside the scatterer (supposed to be light and thin), and making use of equations (8), (9), (10), (16), and (20) we may write

$$\begin{aligned} P' &= I_P[\exp(-Ax)][\exp\{-B\lambda^3(1-\omega)^3x\}]g_0\lambda^3(1-2\omega)^3 \\ S'_1 &= KI_PC\varphi \left(1 + \frac{\delta\lambda\varphi}{\lambda}\right)^{-3} f(\phi, \lambda + \delta\lambda\varphi)[\exp(-A'x)] \\ &\quad [\exp\{-B(\lambda + \Delta\varphi)^3(1-\omega'')^3x\}]g(\lambda + \Delta\varphi)^3(1-2\omega')^3 \end{aligned}$$

and

$$\begin{aligned} S'_2 &= KI_P(1-C_\varphi)f(\phi, \lambda)[\exp(-A'x)] \\ &\quad [\exp\{-B(\lambda + \Delta\varphi)^3(1-\omega')^3x\}]g(\lambda + \Delta\varphi)^3(1-2\omega')^3 \end{aligned}$$

where  $g$ , a constant in (20) corresponds to the scattered beam and  $g_0$  to the primary beam and  $\omega$ ,  $\omega'$ ,  $\omega''$  refer to the primary beam, the unmodified scattered beam and the modified scattered beam respectively.

Thus  $(S'_1/P')_\varphi = K(g/g_0) C_\varphi \left(1 + \frac{\delta\lambda_\varphi}{\lambda}\right)^{-3} f(\phi, \lambda + \delta\lambda_\varphi) [\exp\{(A-A')x\}]$ .

$$[\exp - Bx\{(\lambda + \underline{\Delta}_\varphi)^3(1 - \omega'')^3 - \lambda^3(1 - \omega)^3\}(\lambda + \underline{\Delta}_\varphi)^3(1 - 2\omega')^3] \lambda^3(1 - 2\omega')^3$$

$$\text{or} \quad \left(\frac{S'_1}{P'}\right)_\varphi = K' C_\varphi [\exp\{(A-A')x\}] f(\phi, \lambda) \left\{1 + \frac{f' \delta\lambda_\varphi}{f}\right\}.$$

$$\left[\exp - 3Bx \lambda^3 \left\{\frac{\underline{\Delta}_\varphi}{\lambda} - (\omega'' - \omega)\right\}\right] \left[1 - 3\frac{\delta\lambda_\varphi}{\lambda}\right] \left\{1 + \frac{3\underline{\Delta}_\varphi}{\lambda} - 6(\omega'' - \omega)\right\},$$

putting  $K' = K \cdot g/g_0 = \text{Const.}$  and neglecting second and higher order smallness. This can be approximately written as :

$$(S'_1/P')_\varphi = K' C_\varphi [\exp\{(A-A')x\}] f(\phi, \lambda) \left[1 + \frac{f'}{f} \delta\lambda_\varphi - 3Bx \lambda^3 \left\{-\frac{\underline{\Delta}_\varphi}{\lambda} - (\omega'' - \omega)\right\} + 3\left\{\frac{\underline{\Delta}_\varphi}{\lambda} - 2(\omega'' - \omega)\right\}\right]$$

Proceeding similarly we may evaluate

$$(S'_2/P')_\varphi = K'(1 - C_\varphi) [\exp\{(A-A')x\}] f(\phi, \lambda) \left[1 - 3Bx \lambda^3 \left\{\frac{\underline{\Delta}_\varphi}{\lambda} - (\omega' - \omega)\right\} + 3\left\{\frac{\underline{\Delta}_\varphi}{\lambda} - 2(\omega' - \omega)\right\}\right]$$

Now considering the Compton-change of wavelength  $\delta\lambda_\varphi$  and the wavelength change  $\underline{\Delta}_\varphi$  due to interference we can write :

$$q_x = \frac{\underline{\Delta}_\varphi}{\lambda} - 2(\omega'' - \omega), \text{ where } \underline{\Delta}_\varphi = \Delta_\rho + \delta\lambda_\varphi \text{ (vide eqn. 8)}$$

$$\text{or} \quad \frac{\underline{\Delta}_\varphi}{\lambda} - (\omega'' - \omega) = \frac{1}{2} \left(q_x + \frac{\underline{\Delta}_\varphi}{\lambda}\right)$$

$$\text{Now putting} \quad p_x = \frac{\underline{\Delta}_\varphi}{\lambda} - 2(\omega' - \omega)$$

$$\text{we get} \quad \frac{\underline{\Delta}_\varphi}{\lambda} - (\omega' - \omega) = \frac{1}{2} \left(p_x + \frac{\underline{\Delta}_\varphi}{\lambda}\right)$$



Substituting these values in the above expressions we have,

$$(S'_1/P')_\phi = K'C_\phi [\exp\{(A-A')x\}]f(\phi, \lambda) \cdot$$

$$\left[ 1 + \frac{f'}{f} \delta\lambda_\phi - \frac{3}{2} Bx\lambda^3 \left( q_x + \frac{\Delta_\phi + \delta\lambda_\phi}{\lambda} \right) + 3 \left( q_x - \frac{\delta\lambda_\phi}{\lambda} \right) \right]$$

and

$$(S'_2/P')_\phi = K'(1-C_\phi)[\exp\{(A-A')x\}]f(\phi, \lambda) \cdot$$

$$\left[ 1 - \frac{3}{2} Bx\lambda^3 \left( p_x + \frac{\Delta_\phi}{\lambda} \right) + 3p_x \right]$$

Adding up the above two expressions we have finally

$$(S'/P')_\phi = (S'_1/P')_\phi + (S'_2/P')_\phi$$

$$= K'f(\phi, \lambda)[\exp\{(A-A')x\}] \left[ 1 + C_\phi \frac{f'}{f} \delta\lambda_\phi \right.$$

$$- \frac{3}{2} Bx\lambda^3 \left\{ \frac{\Delta_\phi}{\lambda} + p_x + C_\phi \left( (q_x - p_x + \frac{\delta\lambda_\phi}{\lambda}) \right) \right\}$$

$$\left. + 3 \left\{ p_x + C_\phi \left( (q_x - p_x - \frac{\delta\lambda_\phi}{\lambda}) \right) \right\} \right] \quad \dots \quad (21)$$

#### B. *Progressive Absorption, $\phi < 90^\circ$*

From the expression (21) it is noted that the curve  $(S'/P')_\phi$  plotted against small values of  $x$ , should steadily slope down. For,  $p_x$  and  $q_x - p_x$  (which is positive) diminish, while  $p_x \cdot x$  and  $(q_x - p_x) \cdot x$  increase with increasing  $x$ , and the exponential term is nearly equal to unity, at least for aluminium and copper. This result is in agreement with those illustrated for  $\phi = 30^\circ, 60^\circ$  and  $90^\circ$  in Fig 4, p. 652 Barkla and Khastgir (1926b)

#### C. *Progressive Absorption, $\phi = 90^\circ$*

When  $\phi = 90^\circ$ , we have  $f = 1, f' = 0, \Delta_\phi = 0$ . Taking  $\omega' = \omega$ , we get  $p_x = 0$ . Putting now  $q_x = r_x$ , we write  $r_x = \frac{\delta\lambda_{90^\circ}}{\lambda} - 2(\omega'' - \omega)$ .

Therefore, substituting these in (21) we have

$$(S'/P')_{90^\circ} = K' \left[ 1 - 3C_{90^\circ} \left\{ \frac{B}{2} x\lambda^3 \left( r_x + \frac{\delta\lambda_{90^\circ}}{\lambda} \right) + \left( \frac{\delta\lambda_{90^\circ}}{\lambda} - r_x \right) \right\} \right] \exp\{(A-A')x\}$$

$$= K' \left[ 1 - 3C_{90^\circ} \left\{ \frac{B}{2} x\lambda^3 \left( r_x + \frac{\delta\lambda_{90^\circ}}{\lambda} \right) + \left( \frac{\delta\lambda_{90^\circ}}{\lambda} - r_x \right) \right\} + (A-A')x \right] \quad \dots \quad (22)$$

since  $(A-A')x$  is small as compared to unity.

---

\* Usually the terms with coefficient  $Bx\lambda^3$  are very small compared to unity and can be neglected in equation (21). This will greatly simplify all subsequent calculations leading, however, to identical results.

Let us now consider different absorbers. The following cases are considered :

(i) For Al and Cu absorbers the term  $(A-A')x$  is negligibly small, so that the course of the curve  $(S'/P')_{90^\circ}$  plotted against small values of  $x$ , should be descending towards the right, as for  $\phi < 90^\circ$ .

(ii) For Ag and Sn, on the contrary, the term  $(A-A')x$  may not be negligible (*Vide* Table I), so that it will counteract the preceding term in equation (22) and may actually balance the same within limits of experimental error, for a suitable wavelength; in which case the only outstanding term on the right hand side of the equation is  $K' = \text{Const.}$  This means that the  $(S'/P')_{90^\circ} - x$  graph will be a horizontal straight line, as though the scattered radiation were 'unmodified' (*Vide* Eqn 31). These results are illustrated in Fig. 2., p. 646, Barkla and Khastgir (1926b).

Similar and confirmatory graphs for the Ag-absorber, with a small downward trend at the right hand side extremity, were obtained by the present writer also, with radiations,  $\lambda = 0.55 \text{ \AA}$  and  $0.60 \text{ \AA}$ . With harder radiations,  $\lambda = 0.46 \text{ \AA}$  (unfiltered) and  $0.38 \text{ \AA}$  (filtered), neutralisation as above, was only partial and the curve sloped down to the tune of 10 and 15% respectively for  $x = 0.009 \text{ cm}$  exactly as theory would have it.

As  $(A-A') \approx 0$  for Cu, we can hardly expect a horizontal straight line for the curve  $(S'/P')_{90^\circ}$  against  $x$ , except in the region of soft unmodified rays ( $C_{90^\circ} = 0$ ). Al may give such a horizontal line graph but that also with radiations which are not modified for some reason or other.

To explain the dual behaviour simultaneously, on the part part of Sn, in the reference mentioned above, the inference that commends itself is that  $C_{90^\circ}$  had changed in the process of scattering. It might also be that the incident radiation concerned had passed through a state of instability during that particular experiment, causing a fluctuation of the hardness of the rays and therewith of  $C_{90^\circ}$ . Such a possibility, of course, cannot be ruled out, especially for gas tubes working continuously for a long time. A fluctuation of  $C_{90^\circ}$  may also be held responsible for the so-called 'sub-level' in Fig. 4 of the same reference.

The foregoing evidences led Barkla and Khastgir to hold that the same radiation could be a modified radiation when tested with Al or Cu—absorber, but an unmodified one when tested with Ag and also, sometimes modified and sometimes unmodified when tested with Sn. In the light of the present analysis we are, however, inclined to the view that scattering was undoubtedly accompanied by a modification of the Compton-type in every case treated above and that the observed difference was due merely to two mutually opposing tendencies at work later during absorption. These tendencies practically balanced each other, as a matter of chance, in the case of Ag and Sn; whereas, for Al and Cu absorbers, such a balance was impossible, the effect then being practically unilateral. Although a truly unmodified' radiation should mean an almost horizontal straight line

in many cases (*Vide* eqn. 31), yet the converse is not necessarily always true. In other words, a Compton-change of wavelength which has actually taken place at scattering, may not be invariably evident from a concomitant change in the absorbability of a heterogeneous scattered beam tested as above.

The experiments with compound absorbers yielded anomalous results which require explanation [*Vide* Fig. 3, p 649, Barikla and Khastgir (1926b). If a second absorber of thickness 'y' and made of a different material, be placed behind the first, i.e. on the emergent sides of the primary and secondary beams, corresponding additional terms have to be introduced into the expression (22) to account for the extra absorption. Denoting the two successive absorptions by double dashes, we have at  $\phi = 90^\circ$ .

$$(S''/P'')_{x+y} = K' \left[ 1 - 3C_{90^\circ} \left\{ \frac{B_1}{2} x \lambda^3 \left( r_x + \frac{\delta\lambda_{90^\circ}}{\lambda} \right) + \left( \frac{\delta\lambda_{90^\circ}}{\lambda} - r_x \right) \right\} + (A_1 - A'_1)x \right. \\ \left. - 3C'_{90^\circ} \left\{ \frac{B_2}{2} y \lambda^3 \left( \bar{r}_y + \frac{(\delta\lambda_{90^\circ})_x}{\lambda_x} \right) + \left( \frac{(\delta\lambda_{90^\circ})_x}{\lambda_x} - \bar{r}_y \right) + (A_2 - A'_2)y \right\} \right] \quad \dots (23)$$

where subscripts 1 and 2 refer to the first and second absorbers respectively and  $\bar{r}_y$  corresponds to the beams which pass through the second absorber after transmission through the first.

Cor. 1. If  $x < x_c$

$$(S''/P'')_{x+y} < (S'/P')_x,$$

since the quantity within each curled bracket is essentially positive and further  $(A_1 - A'_1)x$  and  $(A_2 - A'_2)y$  are small. Hence  $(S''/P'' - x)$  graph lies below the  $(S'/P' - x)$  graph, both sloping downwards. This is illustrated for paper and paper *plus* aluminium in fig. 3 C of the above reference where  $y_{Al} = 0.048$  cm.

Cor. 2. If  $y$  is very small, i.e.  $y \approx 0$ .

then  $(S''/P'')_{x+y} \approx (S'/P')_x$  since  $\bar{r}_y \approx \bar{r}_0 \approx \frac{(\delta\lambda_{90})_x}{\lambda_x}$ .

This means that the two ratios plotted against  $x$ , give coincident graphs as in Fig. 3A or 3B of the above reference, where  $x$  represents the running thickness of Al and  $y$  the constant thickness (0.002 cm) of Ag or of Sn. In an analogous manner, paper and paper *plus* Ag.(0.002 cm.) also give concurrent graphs as in Fig. 3C.

Thus if 0.002 cm. thickness of Ag or of Sn is regarded as very small for the purpose of absorption, the principal feature of Fig. 3. (A, B and C) can be explained easily.

Cor. 3. If  $x \gg x_c$  and  $y$  is small but not very small then also  $(S''/P'')_{x+y} = (S'/P')_x$  since  $r_x = 0$ ,  $(\delta\lambda 90^\circ)_x = 0$  and  $\bar{r}_y = 0$ .  $(A_1 - A'_1) \cdot x$  and  $(A_2 - A'_2) \cdot y$  are supposed to be very small also.

## SECTION II

### COMPARISON OF THE SCATTERED RADIATIONS AT CONSTANT PRIMARY WAVELENGTH: $\phi = \phi^\circ$ AND $\phi \rightarrow 90^\circ$

A. *Evaluation of the ratio  $S'_\phi / S'90^\circ = R'_\phi$  (say).*

Let  $S'_\phi$  represent the ionization produced by the scattered radiation in the direction  $\phi$ , after it has passed through a thickness ' $x$ ' of an absorbing substance and  $S'90^\circ$  the corresponding quantity, in the direction  $\phi = 90^\circ$ . Then  $R'_\phi = S'_\phi / S'90^\circ = (S'/P')_\phi / (S'/P')_{90^\circ}$ . Substituting the values of the ratios from equations (21) and (22) we have, after neglecting second and higher order smallness

$$\begin{aligned} R'_\phi = f\left(\phi, \lambda\right) & \left[ 1 + C_\phi \int_f' \delta\lambda_\phi \right. \\ & - \frac{3}{2} Bx\lambda^3 \left\{ \frac{\Delta_\phi}{\lambda} + p_x + C_\phi \left( q_x - p_x + \frac{\delta\lambda_\phi}{\lambda} \right) - C_{90^\circ} \left( r_x + \frac{\delta\lambda_{90^\circ}}{\lambda} \right) \right\} \\ & \left. + 3 \left\{ p_x + C_\phi \left( q_x - p_x - \frac{\delta\lambda_\phi}{\lambda} \right) + C_{90^\circ} \left( -\frac{\delta\lambda_{90^\circ}}{\lambda} - r_x \right) \right\} \right] \quad \dots (24) \end{aligned}$$

If  $R_\phi$  represent the ratio for the unintercepted scattered beams its value can be deduced by putting  $x = 0$  in the above eqn.(24).

Thus

$$R_\phi = f(\phi, \lambda) \left[ 1 + C_\phi \int_f' \delta\lambda_\phi + 3 \left\{ p_0 + C_\phi \left( q_0 - p_0 - \frac{\delta\lambda_\phi}{\lambda} \right) + C_{90^\circ} \left( -\frac{\delta\lambda_{90^\circ}}{\lambda} - r_0 \right) \right\} \right]$$

Since  $r_0 = \frac{\delta\lambda_{90^\circ}}{\lambda}$  and  $\Delta_\phi = \Delta_\phi + \delta\lambda_\phi$  (*Vide* eqn. 8).

$$R_\phi = f(\phi, \lambda) \left[ 1 + C_\phi \int_f' \delta\lambda_\phi + 3 \frac{\Delta_\phi}{\lambda} \right] \quad \dots (25)$$

This gives the ratio of ionizations produced by the unintercepted scattered beams one of which is in the forward direction,  $\phi < 90^\circ$ . In the backward direction,  $\phi > 90^\circ$ , we have

$$f(\phi, \lambda) = 1 + \cos^2\phi$$

$f' = 0$  and  $\Delta_\phi = 0$  (*Vide* eqn. 7), so that

$R_\phi = 1 + \cos^2\phi$ . This is same for all wavelengths.

This affords an easy experimental test of the accuracy of the foregoing analysis and was verified by the writer at  $\phi = 150^\circ$ , for which  $R_\phi$  should be equal to 1.75. The experimental data (Pal, 1948 and 1950) in this connection, with light paraffin wax scatterer (for which the treatment is more aptly valid), are presented in the following Table II. In it, the observed ratio of the ionizations in the directions concerned, the ratio corrected for polarization of the incident beam and the ratio further corrected for the obliquity of the scattered pencil are entered in the 4th, 5th, and 6th. columns respectively. The last column gives the divergence of each ratio from the mean of the ratios.

TABLE II

Equiv. $\lambda$ in A.U.	P/U*	(2P/U) $\cos^2\phi$	Uncorrected ratio	Ratio corrected for polarization	Ratio next corrected for obliquity	Divergence % of the ratio from the mean
0.77	0.100	0.150	1.79	1.63	1.65	-2.3
0.49	0.023	0.036	1.745	1.71	1.73	+2.3
0.44	0.016	0.024	1.72	1.69	1.71	+1.2
0.34	0.017	0.026	1.725	1.69	1.71	+1.2
0.275	0.026	0.039	1.705	1.66	1.68	-0.6
0.25	0.032	0.048	1.69	1.63	1.65	-2.3
0.225	0.045	0.068	1.65	1.57	1.59	
0.33	0.042	0.063	1.72	1.65	1.67	-1.2
..	..	..	..	..	Mean 1.69	

\* P = Plane-polarized intensity.    U = unpolarized intensity.

It will be noted from the above table that the corrected ratio is fairly constant, lying within  $\pm 2.3\%$  of the mean value (1.69). The small defect of the mean ratio from the theoretical 1.75, may be attributed to the absorption (neglected) occurring inside the scatterer as also inside the thin aluminium sheet (thickness .01 cm.) covering the window of the ionization chamber. For full details of the corrections reference may be made to the previous papers (Pal, 1948 and 1949) published by the author.

### B. *Progressive Absorption*

(a) In the backward direction,  $\phi > 90^\circ$ , there is no interference and the equation (24) may be written down as :

$$R'_\phi = (1 + \cos^2\phi) \left[ 1 - \frac{3B}{2} x \lambda^3 \left\{ C_\phi \left( q_x + \frac{\delta\lambda_\phi}{\lambda} \right) - C_{90^\circ} \left( r_x + \frac{\delta\lambda_{90^\circ}}{\lambda} \right) \right\} \right. \\ \left. + 3 \left\{ C_\phi \left( q_x - \frac{\delta\lambda_\phi}{\lambda} \right) + C_{90^\circ} \left( \frac{\delta\lambda_{90^\circ}}{\lambda} - r_x \right) \right\} \right]$$

We note in this equation that  $\delta\lambda_\phi > \delta\lambda_{90^\circ}$ ,  $C_\phi > C_{90^\circ}$ ,  $q_x > r_x$ ; further as  $x$  increases from zero,  $(q_x - r_x)$  diminishes and  $(q_x \cdot x - r_x \cdot x)$  initially increases. Therefore  $R'_\phi$  diminishes as  $x$  increases from zero and the curve  $R'_\phi$  plotted against  $x$  begins to slope down towards the right. This was verified experimentally by the writer (Pal, 1949), for  $\phi = 150^\circ$ .

(b) In the forward direction,  $\phi < 90^\circ$ , the graph  $R'_\phi - x$  may be (i) ascending, (ii) descending, or (iii) horizontal, depending on the relative magnitude of the interference effect.

(i) *Ascending graph*: When the effect of interference is small—as for light scatterers and short wavelengths or large angle  $\phi$ —as compared with the Compton short effect, we may put  $f' \approx 0$ ,  $\Delta_\phi \approx 0$  and  $p_x \approx 0$  in equation (24) and obtain

$$R'_\phi = f(\phi, \lambda) \left[ 1 + B \frac{3}{2} \cdot x \lambda^3 \left\{ C_{90^\circ} \left( r_x + \frac{\delta\lambda_{90^\circ}}{\lambda} \right) - C_\phi \left( q_x + \frac{\delta\lambda_\phi}{\lambda} \right) \right\} \right. \\ \left. + 3 \left\{ C_{90^\circ} \left( \frac{\delta\lambda_{90^\circ}}{\lambda} - r_x \right) - C_\phi \left( \frac{\delta\lambda_\phi}{\lambda} - q_x \right) \right\} \right]$$

Here  $\delta\lambda_{90^\circ} > \delta\lambda_\phi$ ,  $C_{90^\circ} > C_\phi$  and  $r_x > q_x$ . Further, as  $x$  increases from zero,  $(r_x - q_x)$  diminishes and  $(r_x \cdot x - q_x \cdot x)$  initially increases. Therefore  $R'_\phi$  initially increases with  $x$ , so that the curve  $R'_\phi - x$  is ascending towards the right.

(ii) *Descending graph*: When, however, the effect of interference is large—as for scatterers of high atomic number, long wavelengths or small angle  $\phi$ —as compared with the Compton effect, the latter may be neglected and equation (24) may be written down as:

$$R'_\phi = f(\phi, \lambda) \left[ 1 - \frac{3B}{2} \cdot x \lambda^3 \left\{ \frac{\Delta_\phi}{\lambda} + p_x \right\} + 3p_x \right]$$

Here as  $x$  increases from zero,  $p_x$  diminishes and  $(p_x \cdot x)$  initially increases. Therefore  $R'_\phi$  initially diminishes as  $x$  increases, so that the curve  $R'_\phi - x$  is descending towards the right.

(iii) *Horizontal graph*: The condition for horizontality requires that  $R'_\phi$  should be equal to  $R_\phi$  for all values of  $x$  concerned. Hence equating equations (24) and (25) it may be deduced that:

$$0 = -\frac{B}{2} x \lambda^3 \left\{ \frac{\Delta_\phi}{\lambda} + p_x + C_\phi \left( q_x - p_x + \frac{\delta\lambda_\phi}{\lambda} \right) - C_{90^\circ} \left( r_x + \frac{\delta\lambda_{90^\circ}}{\lambda} \right) \right\} \\ + \left\{ -\frac{\Delta_\phi}{\lambda} + p_x + C_\phi \left( q_x - p_x - \frac{\delta\lambda_\phi}{\lambda} \right) + C_{90^\circ} \left( \frac{\delta\lambda_{90^\circ}}{\lambda} - r_x \right) \right\},$$

for all values of  $x$ .

Collecting the terms free from and independent of 'x' and equating them to zero, we have

$$\frac{\Delta_{\phi}}{\lambda} + C_{\phi} \frac{\delta \lambda_{\phi}}{\lambda} - C_{90^{\circ}} \frac{\delta \lambda_{90^{\circ}}}{\lambda} = 0 \quad \dots (26a)$$

Substituting this in the rest of the above expression which must also be equal to zero, we have

$$\left(1 - \frac{B}{2} x \lambda^3\right) \{p_x + C_{\phi}(q_x - p_x) - C_{90^{\circ}} r_x\} = 0$$

for all values of x.

$$\therefore p_x + C_{\phi}(q_x - p_x) - C_{90^{\circ}} r_x = 0 \quad \dots (26b)$$

for all values of x concerned.

It is noted that the condition (26b) is identical with the condition (26a) when  $x = 0$ .

Thus if the graph  $R'_{\phi} - x$  is to be horizontal, the general condition which must be satisfied is given by eqn. (26b). This relation must hold for values of x concerned from 0 upwards.

Cor. 1. If  $p_x$  is large, the above condition reduces to

$$p_x \approx C_{90^{\circ}} r_x$$

Cor. 2. If  $p_x = 0$  (as in the backward direction) the condition (26b) can never be satisfied and no horizontal graph can be obtained.

Horizontality implies a constancy of the ratio  $R'_{\phi}$  i.e.  $(S'/P')_{\phi} = \text{Const.} \times (S'/P')_{90^{\circ}}$ . Therefore, by suitably choosing the scale of reference for one set of ratios, the graph  $(S'/P')_{\phi} - x$  may be made to superpose exactly on the graph  $(S'/P')_{90^{\circ}} - x$ . This is illustrated for  $\phi = 30^{\circ}$  and  $60^{\circ}$  in Fig. 4. p. 652. Barkla and Khastgir (1926b).

All the above three varieties of the graph were obtained by the writer (Pal, 1949), for  $\phi = 30^{\circ}$  or  $20^{\circ}$ . Graph of the type (i) was yielded by carbon and paraffin was scatterers, of the type (iii) by filter paper and of the type (ii) by aluminium and sulphur, in complete accord with the theoretical results. What Barkla and Khastgir had recorded in Fig. 4, was but one variety which was equivalent to the third. The horizontal and the descending graphs had also been observed by Barkla and Mackenzie (1925—1926).

The results of the types (ii) and (iii) appear to be in conflict with the Compton effect. But this appearance, clearly enough, is only superficial. For the nature of the overall result is determined essentially not by the Compton effect alone, but by the combination and relative magnitudes of the Compton effect and interference. They operate upon the radiations concerned in opposite manners;

e.g. the scattered rays at  $\phi = 30^\circ$  are rendered harder than those at  $\phi = 90^\circ$ , due to the Compton effect, whereas the reverse is the case due to interference.

### SECTION III

#### COMPARISON OF THE SCATTERED AND THE PRIMARY RADIATIONS FOR DIFFERENT INCIDENT WAVELENGTHS

##### A. Evaluation of the percentage difference between the intercepted and unintercepted ratios

Let the ratio of the ionizations produced by the scattered and the primary radiations—both unintercepted—be denoted by  $(S/P)_\phi$  and the same when both the beams are intercepted by a constant thickness  $x$  of an absorber, by  $(S'/P')_\phi$ .

Now,  $(S/P)_\phi$  can be calculated from eqn. (21) by putting  $x = 0$ , so that

$$\begin{aligned}(S/P)_\phi &= K'f(\phi, \lambda) \left[ 1 + C_\phi \frac{f'}{f} \delta\lambda_\phi + 3 \left\{ p_0 + C_\phi \left( q_0 - p_0 - \frac{\delta\lambda_\phi}{\lambda} \right) \right\} \right] \\ &= K'f(\phi, \lambda) \left[ 1 + C_\phi \frac{f'}{f} \delta\lambda_\phi + 3p_0 \right],\end{aligned}$$

since the quantity inside the small bracket contained within the curled bracket is equal to zero. With the help of this equation and equation (21), the fractional difference between the ratios i.e.

$$\begin{aligned}&\{(S/P)_\phi - (S'/P')_\phi\} / (S/P)_\phi \\ &= \left[ 3p_0 + \frac{3B}{2} x\lambda^3 \left\{ \frac{\Delta_\phi}{\lambda} + p_x + C_\phi \left( q_x - p_x + \frac{\delta\lambda_\phi}{\lambda} \right) - (A - A')x \right. \right. \\ &\quad \left. \left. - 3 \left\{ p_x + C_\phi \left( q_x - p_x - \frac{\delta\lambda_\phi}{\lambda} \right) \right\} \right\} \right] / \left( 1 + 3p_0 + C_\phi \frac{f'}{f} \delta\lambda_\phi \right).\end{aligned}$$

(a) If  $x \leq x_c^*$ , then  $p_x = 0$  and  $q_x = 0$ , so that

$$\begin{aligned}\{(S/P)_\phi - (S'/P')_\phi\} / (S/P)_\phi &= \left[ 3p_0 + \frac{3}{2} Bx\lambda^3 \left\{ \frac{\Delta_\phi}{\lambda} + C_\phi \frac{\delta\lambda_\phi}{\lambda} \right\} \right. \\ &\quad \left. - (A - A')x + 3C_\phi \frac{\delta\lambda_\phi}{\lambda} \right] / \left( 1 + 3p_0 + C_\phi \frac{f'}{f} \delta\lambda_\phi \right) \quad \dots (27)\end{aligned}$$

At  $\phi = 30^\circ$ ,  $3p_0$  is large compared to all other terms except 1. Hence approximately

$$\begin{aligned}\{(S/P)_\phi - (S'/P')_\phi\} / (S/P)_\phi &= 3p_0 / (1 + 3p_0) \\ &= \frac{3 \Delta_\phi}{\lambda} / \left( 1 + \frac{3 \Delta_\phi}{\lambda} \right) \quad \dots (28)\end{aligned}$$

$x_c$  corresponds to  $q_x (> p_x)$



$\Delta_p$  increases as  $\lambda$  increases. Now if we assume that  $\Delta_p \propto \lambda$ , to a rough approximation, for a small range of wavelengths at least, then it is at once evident that the above fractional difference and hence the percentage difference between the intercepted and unintercepted ratios is constant, i.e. independent of the incident wavelength  $\lambda$  within that range.

The percentage difference, when computed from the above, may also come out with the right order of magnitude, as the following tentative example will show.

*Example :* Let  $\lambda = 0.6 \text{ \AA}$  (which is approximately equal to the mean of the wavelengths employed by Barkla and Khastgir) and  $\Delta_p = 0.020 \text{ \AA}$  on a modest estimate. Then the percentage difference between the ratios is given by :

$$100 \cdot \frac{(S/P)_\phi - (S'/P')_\phi}{(S/P)_\phi} = 300 \times \frac{0.020}{0.6} \left( 1 - 3 \times \frac{0.020}{0.6} \right) = 9\%.$$

This agrees exactly with that estimated by Barkla and Khastgir (1962b) (*Vide* Fig. 5. p. 653) showing that the agreement is not only qualitative but may be quantitative as well.

(b) Constancy of the percentage difference between the ratios for  $\phi = 90^\circ$  and  $60^\circ$ .

We have already learnt that when the incident radiation satisfies the conditions expressed in (26 a) and (26b),  $R'_\phi$  is constant and independent of  $x$ .

$\therefore$  Taking the log. differential with respect to  $x$ ,  $\delta\{\log R'_\phi\} = 0$ .

$$\text{or} \quad \delta[\log \{(S'/P')_\phi / (S'/P')_{90^\circ}\}] = 0.$$

$$\text{or} \quad \delta[\log \{(S'/P')_\phi - \log (S'/P')_{90^\circ}\}] = 0.$$

$$\text{or} \quad \delta(S'/P')_\phi / (S'/P')_\phi = \delta(S'/P')_{90^\circ} / (S'/P')_{90^\circ}$$

Now, considering the variation of the ratios between  $x = 0$  and  $x = x$  (small), we may rewrite the above in the form

$$100[(S/P)_\phi - (S'/P')_\phi] / (S/P)_\phi = 100[(S/P)_{90^\circ} - (S'/P')_{90^\circ}] / (S/P)_{90^\circ}$$

Putting  $\phi = 60^\circ$  and  $30^\circ$  successively, we have

$$\frac{100\{(S/P)_{60^\circ} - (S'/P')_{60^\circ}\}}{(S/P)_{60^\circ}} = \frac{100\{(S/P)_{90^\circ} - (S'/P')_{90^\circ}\}}{(S/P)_{90^\circ}}$$

$$\frac{100\{(S/P)_{30^\circ} - (S'/P')_{30^\circ}\}}{(S'/P')_{30^\circ}} \quad (29)$$

Thus the percentage difference between the intercepted and unintercepted ratios for  $\phi = 90^\circ$  and the same for  $\phi = 60^\circ$ , are equal and each equal to the corresponding percentage difference for  $\phi = 30^\circ$  (which has been shown to be a constant-independent of  $\lambda$  through a small range of wavelengths, when  $x \geq x_c$ ). This

quality, of course, is valid so long as the particular wavelength employed satisfies the condition (26a) i.e.

$$\Delta_\phi + C_\phi \delta\lambda_\phi = C_{90^\circ} \delta\lambda_{90^\circ}, \text{ for } \phi = 30^\circ \text{ and } 60^\circ.$$

The other condition (26.b) is automatically satisfied on account of  $x \equiv x_0$ .

The validity mentioned above should persist at least over a small range of wavelengths. For, though with a change in  $\lambda$  the equality expressed in (26a) is apparently disturbed (since with an increase in  $\lambda$ ,  $\Delta_\phi$  increases while  $C_\phi$  and  $C_{90^\circ}$  decrease), yet any small unbalance should be counteracted and set right by a corresponding change in absorption occurring inside the scatterer, over that small range of wavelength—of the order of  $0.1 \text{ \AA}$  (as in Barkla and Khastgir's experiments—*vide* Fig. 5, Barkla and Khastgir (1926b)). Over this range, therefore, the percentage difference between the ratios for  $\phi = 60^\circ$  and  $90^\circ$  will be each equal to that for  $\phi = 30^\circ$ , which is again maintained constant ( $= 9\%$ ) through that range. This result is also in accord with Barkla's experimental observation.

But there is yet another point to consider. Beyond this range in question and on the longer wavelength-side, the equation (26a) which was previously fulfilled may break down owing to  $C_{90^\circ}$  and  $C_\phi$  having rapidly fallen to a zero value at a particular wavelength and the scattered radiation, as a whole, becoming unmodified thereby. In that case our above treatment and deduction fall through. To calculate the corresponding percentage difference of the ratios for  $\phi = 90^\circ$ , it is necessary to go back to equation (27), where we have to put  $p_0 = \Delta_\phi/\lambda = 0$ ,  $C_\phi = 0$  and  $(A - A')x \simeq 0$ . This brings down the required percentage difference to a zero value, which explains the zero-line graph in Fig. 5, case A., p. 653, Barkla and Khastgir (1926b).

An analogous reasoning applies to  $\phi = 60^\circ$ . Putting  $C_{60^\circ} = 0$  and remembering that the interference effect for paraffin wax scatterer at this large angle, is small indeed, we may assess from eqn. (27) a magnitude for the percentage difference between the ratios at hardly above 1 or 2% which falls close to the limits of experimental error, thus yielding the zero-line graph again, as in the case of  $\phi = 90^\circ$  above.

A similar argument when  $\lambda$  is large, however, is not tenable in the case  $\phi = 30^\circ$ ; for, the calculation in (28), was independent of the condition (26a). The zero-line graph appearing above, is therefore, missing in this case.

The fact that the percentage difference between the ratios in (29) is equal to either a constant or zero, is equivalent to the law of the *J*-phenomenon :

$$\left( \frac{\mu}{\rho} \right)_s - \left( \frac{\mu}{\rho} \right)_P = a (\text{const.}) \text{ or } 0.$$

for the direction concerned. [See also equations (30)\* and (30(a))]

Thus may be explained, in a general way, the features of the graphs presented in Fig. 5, p. 653, Barkla and Khastgir (1926b), viz.

(i) The double horizontal lines showing modified and unmodified scattering, separately for  $\phi = 90^\circ$  and  $60^\circ$  and a single horizontal line standing for both modified and unmodified scattering, for  $\phi = 30^\circ$ .

(ii) The degree of modification is independent of the angle of scattering  $\phi$  and of the original incident wavelength  $\lambda$  (within a small range) under suitable circumstances.

(iii) The discontinuity ( $J_1$ ) setting in at about the same wavelength ( $\sim 0.6 \text{ \AA}$ ) for  $\phi = 90^\circ$  and  $\phi = 60^\circ$ .

B. *Scattering at  $\phi = 90^\circ$  and the horizontal graph ( $S/P - \lambda$ ) for the unintercepted ratio*

The intercepted ratio obtained in eqn. (22) reads as :

$$(S'/P')_{90^\circ} = K' \left[ 1 - 3C_{90^\circ} \left\{ \frac{B}{2} x \lambda^3 \left( r_x + \frac{\delta \lambda_{90^\circ}}{\lambda} \right) + \left( \frac{\delta \lambda_{90^\circ}}{\lambda} - r_x \right) \right\} + (A - A')x \right]$$

Putting  $x = 0$  the unintercepted ratio is deduced as :

$$(S/P)_{90^\circ} = K' * \text{(which is a constant independent of } \lambda) \quad (30)$$

since 
$$\frac{\delta \lambda_{90^\circ}}{\lambda}$$

Therefore  $(S/P)_{90^\circ}$  plotted against  $\lambda$  or  $(\mu/\rho)_{AL}$  gives a horizontal line graph agreeing with Barkla and Khastgir's observation (1927).—*vide* Figs. 1 and 2 p. 739.

C. *Absorption :  $\phi = 90^\circ$ .*

(a) Absorbing thickness constant and greater than critical: When  $x > x_c$  (where  $x_c$  corresponds to the smallest wavelength employed) and in addition, the condition (26a) is fulfilled over a small range of wavelengths, we know from (29) that over this range

$$100 \cdot \{(S/P)_{90^\circ} - (S'/P')_{90^\circ}\} / (S/P)_{90^\circ} = G, \text{ say, (const.)}.$$

\* An identical result may be obtained in the case of a monochromatic beam also. For,

we can pass over from the heterogeneous beam to the homogeneous, by putting  $r_x = \frac{\delta \lambda_{90^\circ}}{\lambda}$

This again makes  $(S/P)_{90^\circ} = K' = \text{Const.}$

Regarding the heterogeneous incident spectrum as made up of a multitude of monochromatic constituents, represented by numerical subscripts, we have at  $\phi = 90^\circ$ ,

$$K' = (S_1/P_1) = (S_2/P_2) = (S_3/P_3) \dots$$

$$= (S_1 + S_2 + S_3 + \dots) / (P_1 + P_2 + P_3 + \dots)$$

$$= (S/P)_{90^\circ} \text{ which is the same as (30),}$$

where  $P_n$  and  $S_n$  denote actual amounts of ionization produced by primary and scattered beams respectively corresponding to the  $n$ -th constituent.

Substituting the value of  $(S/P)_{90^\circ} = K'$  from (30), we have

$$(S'/P')_{90^\circ} = K' \cdot [1 - G/100] = 0.91K', \quad \dots [30(a)]$$

assuming  $G = 9\%$  as obtained by Barkla and Khastgir.

Thus the intercepted ratio is also constant over the above range of wavelengths, giving another horizontal line below the first, corresponding to the unintercepted ratio. Here also, the percentage difference between the two ratios should be the same (9% as previously) and was actually found to be so, irrespective of the material\* of the absorber, in accordance with theory.

There is a marked bending down of the two graphs mentioned above towards the left-hand side, where presumably, the incident radiations were those which were hardened more and more by progressive filtration of a certain beam. In this region, the relation (26a) ceases to be valid and the ratio  $(S'/P')_{90^\circ}$  has to be recalculated from equation (22). Remembering that  $r_x = 0$  and  $(A - A')x \simeq 0$ , we have

$$\begin{aligned} (S'/P')_{90^\circ} &= K' \left[ 1 - 3C_{90^\circ} \frac{\delta\lambda_{90^\circ}}{\lambda} \left( 1 + \frac{B}{2} x\lambda^3 \right) \right] \\ &\simeq K' \left[ 1 - 3C_{90^\circ} \frac{\delta\lambda_{90^\circ}}{\lambda} \right], \text{ since } \frac{B}{2} x\lambda^3 \ll 1. \end{aligned}$$

Now, as  $\lambda$  decreases  $C_{90^\circ}$  increases. Therefore  $(S'/P')_{90^\circ}$  decreases as  $\lambda$  decreases, which accounts for the observed bending of the graph for the intercepted ratio.

(b) Absorbing thickness constant, but very small: When  $x$  is very ( $x < x_0$ ),  $r_x \simeq \frac{\delta\lambda_{90^\circ}}{\lambda}$  \*\*, so that equation (22) becomes :

$$\begin{aligned} (S'/P')_{90^\circ} &= K' \left[ 1 - 3C_{90^\circ} \left\{ Bx\lambda^3 \frac{\delta\lambda_{90^\circ}}{\lambda} \right\} + (A - A')x \right] \\ &= K' \left[ 1 - x \left\{ 3C_{90^\circ} B\lambda^3 \frac{\delta\lambda_{90^\circ}}{\lambda} - (A - A') \right\} \right] \end{aligned}$$

Referring to Fig. 5., p. 744, Barkla and Khastgir (1927) and considering the case of Ag-absorber of thickness  $x = 0.006$  cm., we may form from the above, an estimate of the ratio  $(S'/P')_{90^\circ}$  for the same.

\* A small difference—about 1%—consistently shown by the Cu and Al lines (intercepted) in fig. 1, p. 739, Barka and Khastgir (1927) may be due to the fact that  $(A - A')x$  is equal to 0 for Cu and about 0.15 for Al (neglected previously).

\*\* For long wavelengths.

Putting  $x = 0.006$  cm.,  $B = 84.6$ ,  $\delta\lambda_{90^\circ} = 0.024 \text{ \AA}$ ,  $\lambda = 0.5 \text{ \AA}$  (mean value) and tentatively,  $C_{90^\circ} = 0.5$  and also  $(A - A') = 0.3$ , one obtains

$$x \left\{ 3C_{90^\circ} B \lambda^2 \frac{\delta\lambda_{90^\circ}}{\lambda} - (A - A') \right\} = 0.003 \text{ (approx)}$$

i.e. 
$$\left( \frac{S'}{P'} \right)_{90^\circ} = K' \text{ (correct to about 0.3\%)}$$

$$= \left( \frac{S}{P} \right)_{90^\circ}$$

Thus the intercepted graph  $(S'/P')_{90^\circ} - \lambda$  for  $Ag(x = 0.006 \text{ cm})$  superposes itself on the unintercepted horizontal graph  $(S/P)_{90^\circ} - \lambda$ , agreeing with the experimental observation of Barkla and Khastgir. The appearance of the unmodified scattering here (see eqn. 31), is simply superficial and illusory for obvious reasons.

The companion parallel straight line for Al in the same figure being 9% below the unintercepted ratio—line, points to the conclusion that its thickness (0.15 cm) is either equal to or greater than the critical corresponding to the smallest wavelength concerned and that the condition (26a) has been realised over the experimental range of wavelengths. The thickness of  $Ag$  (0.006 cm) is certainly less than its critical value; for otherwise, would its graph superpose on that of Al.

For hard filtered radiations, however, the picture appears to be entirely different. In that case,  $r_x$  is no longer approximately equal to  $\frac{\delta\lambda_{90^\circ}}{\lambda}$  and  $\left( \frac{\delta\lambda_{90^\circ}}{\lambda} - r_x \right)$  is not negligible as in (b).

The equation (22), therefore, reduces to

$$(S'/P')_{90^\circ} = K' \left[ 1 - 3C_{90^\circ} \left( \frac{\delta\lambda_{90^\circ}}{\lambda} - r_x \right) \right],$$

since the missing terms all work up together to a negligible magnitude. As the wavelength  $\lambda$  is decreased,  $C_{90^\circ}$  increases (up to a value 1) and so also  $\left( \frac{\delta\lambda_{90^\circ}}{\lambda} - r_x \right)$  vide (f) of "Properties of  $q_x$ ", with the result that the intercepted

This is the interpretation of the marked decline in the ratio  $(S/P)_{90^\circ}$  towards the ratio falls. harder end of the graph [in figs. 1 and 2, p. 739 (Barkla and Khastgir 1927)]. Because, though it is unintercepted in the ordinary sense, the rays concerned have yet to pass through a very small thickness (0.01 cm) of Al which covers the window of the ionization chambers.

(c) Absorption of unmodified scattered radiation: At large values of  $\lambda$ , the scattered radiation is unmodified and  $C_{90^\circ} = 0$ . Hence from (22)

$$\begin{aligned} (S'/P')_{90^\circ} &= K'[1 + (A - A')x] = K'(\text{const.}) \\ &= (S/P)_{90^\circ}, \text{ since } (A - A')x \ll 1. \end{aligned} \quad \dots (31)$$

This relation thus becomes independent of the material of the absorber to some extent and also of its thickness.

Therefore, the graph for the intercepted ratio plotted against  $\lambda$  lies on the same horizontal straight line as the corresponding graph for the unintercepted ratio, which is in conformity with the classical theory of scattering. The feature in question, is clearly borne out by the plots in the longer wavelength region  $-(\mu/\rho)_{Al} > 3.6$  in Fig. 5., p. 653, Barkla and Khastgir (1926b) and in Figs. 3 and 4, pp. 1121 and 1123, Barkla and Khastgir (1925b).

(d) Non-commutative absorption.

Referring to eqn. (23) in connection with the compound absorbers we have

$$(S''/P'')_{x+y} = K' \left[ 1 - 3C_{90^\circ} \left\{ \frac{B_1}{2} x \lambda^3 \left( r_x + \frac{\delta \lambda_{90^\circ}}{\lambda} \right) + \left( \frac{\delta \lambda_{90^\circ}}{\lambda} - r_x \right) \right\} + (A_1 - A'_1)x \right. \\ \left. - 3C_{90^\circ} \left\{ \frac{B_2}{2} y \lambda^3 \left( \bar{r}_y + \frac{(\delta \lambda_{90^\circ})_x}{\lambda_x} \right) + \left( \frac{(\delta \lambda_{90^\circ})_x}{\lambda_x} - \bar{r}_y \right) \right\} + (A_2 - A'_2)y \right]$$

Interchanging the positions of the two absorbers, we have .

$$(S''/P'')_{y+x} = K' \left[ 1 - 3C_{90^\circ} \left\{ \frac{B_2}{2} y \lambda^3 \left( r_y + \frac{\delta \lambda_{90^\circ}}{\lambda} \right) + \left( \frac{\delta \lambda_{90^\circ}}{\lambda} - r_y \right) \right\} + (A_2 - A'_2)y \right. \\ \left. - 3C_{90^\circ} \left\{ \frac{B_1}{2} x \lambda^3 \left( \bar{r}_x + \frac{(\delta \lambda_{90^\circ})_y}{\lambda_y} \right) + \left( \frac{(\delta \lambda_{90^\circ})_y}{\lambda_y} - \bar{r}_x \right) \right\} + (A_1 - A'_1)x \right]$$

Obviously, the ratio  $(S''/P'')_{x+y}$  is not identical with the ratio  $(S''/P'')_{y+x}$ , except when the rays are homogeneous or when the absorbers are of the same material. This is an interesting result, pointing to the importance of the order or sequence in which the absorbers are placed.

It must be noted here, that although the experimental findings of Barkla and Khastgir have, in this paper, been amply corroborated from the theoretical stand-point, yet these findings are not to be accepted as perfectly general. The features in question owe their origin to a particular set of conditions imposed upon the experiments, which under other conditions, may lead to a different picture altogether and that with equal theoretical justification. Indeed, performances of heterogeneous X-rays, have shown themselves to be extremely sensitive to these conditions and variation thereof, brings about appreciable changes in the consequences. The choice of the absorbing thickness, for instance, is often a vital factor in deciding the issue. Many more examples, to this effect, may be cited—some from the writer's own works (unpublished) also. In one experiment, as previously mentioned, progressive absorption by Ag (maximum thickness = .0095 cm) yielded a curve smoothly sloping down, for  $\lambda = 0.46 \text{ \AA}$ , in striking contrast with the horizontal line obtained by Barkla and Khastgir. In another experiment,

the ratio  $(S/P)_{90}$  plotted against  $(\mu/\rho)_{Al}$  traced out a graph which ran horizontal for a certain length but steadily sloped down towards the softer region of the rays. This was accompanied by the corresponding  $(S'/P')_{90}$ —graph for 0.7 mm Al-absorber, which was definitely a descending curve and clearly distinct from the horizontal type, discussed previously. Even the thickness of the scatterer has been noticed to play its part and affects the ensuing results substantially. Yet none of these deviations have so far run counter with the concepts presented in the foregoing pages. Notwithstanding the fact that some of the experimental results were at variance (due undoubtedly to changed conditions) with those under review, there were still, a host of others in line with them.

It is, however, realised that the type of absorption experiments dealt with in this paper, despite possessing certain advantages from experimental point of view, is hardly the type best suited for a crucial test of the Compton effect or of the concept of independent quanta. The reason is that, the individual constituents of the incident spectrum do not act incoherently. Another thing that should be borne in mind in this context is that, the very structure of the heterogeneous complex radiation continually undergoes metamorphosis by absorption, as it passes from layer to layer of the absorbing substance, which considerably complicates the issue. Nevertheless, the present analysis, founded essentially on the validity of the Compton's quantum theory of X-ray scattering, has been able to explain most of the results experimentally observed and to substantiate many of the features of the *J*-phenomenon.

#### SUMMARY AND DISCUSSION

Starting with Barkla's idea of an 'atmosphere' of radiation, mentioned before and taking into account the various effects due to (i) Compton scattering, (ii) interference of the scattered radiations, (iii) absorption of the various constituents of the heterogeneous beam by an absorbing material and (iv) ionization produced by the radiations received in the ionization chambers, it has been possible to explain qualitatively and also quantitatively in many cases, most of the experimental results of Barkla and Khastgir on the comparative study of the primary and the scattered beams of heterogeneous X-radiations, (i) when both the beams were passed through the same increasing thickness of an absorbing substance for a particular average absorbability of the primary beam and (ii) when both the beams were intercepted by the same thickness of an absorbing substance for a wide range of absorbabilities of the primary beam.

With regard to the Compton scattering, the modified and the unmodified parts have been considered separately. In considering the effects of interference of the scattered radiations, predominantly in the forward direction, enhancement of the scattered intensity and the increase in the wavelength of the scattered beam have been taken into account. A function  $f$  depending on the wavelength

and the angle of scattering has been introduced to represent the enhanced intensity due to interference and the increase in the wavelength due to interference has been considered in addition to the Compton change of wavelength.

In the experiments with which we are concerned, the scattered beam was fairly wide in comparison with the primary beam, so that the primary and the scattered beams could be comparable in their ionizing effects. With a narrow beam, the mass-absorption coefficient is slightly higher than that with a wide beam. This increased mass-absorption coefficient of the narrow primary beam relative to the wide scattered beam has been taken into account in the theoretical analysis. In calculating the ratio  $S'/P'$  for the heterogeneous beam, the concept of a critical absorbing thickness has been very useful. Further, a 'disparity'—term,  $q_x$ , has been introduced to characterise the difference in quality between two beams of slightly different wavelengths after transmission through a certain thickness  $x$  of an absorbing material. The average wavelength inside the absorbing material has been taken as the mean of the average incident wavelength and the average transmitted wavelength, and the 'disparity' between the two beams of slightly different wavelengths after transmission has been defined as the fractional difference in the average transmitted wavelengths. The 'disparity'—term has simplified the problem of relative absorption by two beams of slightly different wavelengths, while dealing with heterogeneous X-rays. Finally the ionization produced by the radiations transmitted through an absorbing material and received in the ionization chambers has been considered.

#### (a) *Progressive Absorption*

Considering all the above factors, a theoretical expression for the ratio of the ionizations due to the scattered and the primary beams after transmission through a gradually increasing thickness of an absorbing material has been worked out for a definite average wavelength of the primary beam. This has enabled to explain the experimental results of Barkla and Khastgir on progressive absorption of the scattered and the primary beams of heterogeneous X-rays. The observations that in the case of Al and Cu, the ratio of the ionizations produced by the scattered and the primary beams decreased with the increasing thickness of the absorbing substance and that in the case of Ag and Sn, the ratio was independent of the thickness of the absorber have been interpreted from theoretical considerations.

The progressive absorption of the two beams of heterogeneous X-rays, scattered at any angle  $\phi$  and scattered at  $90^\circ$  has also been theoretically investigated. It has been shown that in the backward direction ( $\phi > 90^\circ$ ), the ratio of the ionizations due to the two scattered beams should decrease with the increase of thickness of the absorbing substance and that in the forward direction ( $\phi < 90^\circ$ ), the ratio should (i) decrease as in the case of backward direction or (ii) increase or (iii) remain constant with the increasing thickness. All the three types of the



variation were actually observed by the author (Pal, 1949). The results of Barkla and Mackenzie (1925, 1926) corresponded to the types (i) and (iii) and those of Barkala and Khastgir corresponded to the type (i) only.

When a decrease in the ratio of the ionizations due to the scattered and primary beams with increasing thickness of the absorbing substance was observed, Barkla and Khastgir occasionally observed a reduced rate of decrease. This 'sub-level' representing a smaller slope of the curve has been attributed by the author to the instability of the scattered beam in course of the observations. An attempt has also been made to explain the apparently anomalous results which had been obtained by Barkla and Khastgir (1926b) with compound absorbers (i.e. with a gradually increasing thickness of Al backed by a constant thickness of Ag or Sn).

(b) *Ratio of the ionizations due to the scattered and the primary beams, intercepted and unintercepted by a given thickness of the absorbing substance for different mass-absorption coefficients of the incident primary beam.*

The percentage difference between the intercepted and the unintercepted ratios has been theoretically worked out. Assuming that the change in wavelength  $\Delta_\varphi$  due to interference of the scattered radiations is directly proportional to the wavelength  $\lambda$  (which is true to a first approximation) for a small range of wavelengths, it has been shown that the percentage difference, as computed theoretically is constant, i.e. independent of the incident wavelength  $\lambda$  within a certain range, provided the thickness is equal to or greater than what has been called the critical absorbing thickness. This is what had been observed by Barkla and Khastgir after the  $J_1$ -discontinuity had set in as in their Case A or throughout the range as in their Case B. It has also been shown that the computed percentage difference between the 'unintercepted' and the 'intercepted' ratios is of the same order of magnitude as had been observed by Barkla and Khastgir (i.e. 9%, when Al was used to intercept the beams). Further, the significant observation of Barkla and Khastgir that the percentage difference between the 'unintercepted' and the 'intercepted' ratios is of the same order for the angles of scattering  $30^\circ$ ,  $60^\circ$  and  $90^\circ$ , has been explained, under certain conditions, from theoretical considerations.

The constancy of the percentage difference between the two ratios  $S/P$  and  $S'/P'$ , over a range of wavelengths implies that difference between the mass-absorption-coefficients of the primary and the scattered beams is also constant over the same range of wavelengths. This difference is of course zero in Case A of Barkla and Khastgir for longer wavelengths. We thus get some theoretical justification for Barkla's law of the  $J$ -phenomenon :

$$\left(\frac{\mu}{\rho}\right)_1 - \left(\frac{\mu}{\rho}\right)_2 = 0 \text{ or constant.}$$

The theoretical analysis has also shown that the 'unintercepted' and the 'intercepted' ratios of the scattered and the primary beams, under certain

conditions are both constant and independent of wavelength. The well-known horizontal lines of Barkla and Khastgir in their curves showing  $S/P$  and  $S'/P'$  for different mass-absorption coefficients of the primary beam are thus explained. A marked bending down of the lines for very small mass-absorption coefficients has also been interpreted. In the case of compound absorbers, a striking result of the theoretical analysis is the inequality of  $((S''/P'')_{x+y})$  and  $((S''/P'')_{y+x})$  for a heterogeneous beam of X-rays, where  $x$  and  $y$  are the thicknesses of two different absorbing substances, in contact with each other, once when placed one behind the other and subsequently, when placed in the reversed order. This non-commutative absorption needs an experimental verification.

#### ACKNOWLEDGMENT

The writer expresses his indebtedness to late Prof. C. G. Barkla, D.Sc., F.R.S., N.L. for affording him all facilities for experimental work in his laboratory at Edinburgh, U.K. and for giving him helpful guidance during 1935-37. His best thanks are also due to Prof. S. R. Khastgir, D.Sc., F.N.I., Head of the Dept. of Physics, Bose Institute, Calcutta, for valuable discussions and assistance in writing the paper.

#### REFERENCES

- Bachem, A., 1923, *Principles of X-ray and Radium Dosage*, Chicago, p. 152et seq.  
 Backhurst, I., 1934, *Phil. Mag.*, Vol. XVII, 321.  
 Barkla, C. G., 1924, *Nature*, Vol. CXIV, 753.  
 Barkla, C. G., 1925, *Phil. Mag.*, Vol. XLIX, 1033.  
 Barkla, C. G., 1926, *Nature*, Vol. CXVII, 448.  
 Barkla, C. G., 1927, *Nature*, Vol. CXIX, 778.  
 Barkla, C. G., 1928, *Phil. Mag.*, Vol. V, 1164.  
 Barkla, C. G., 1929, *International Critical Tables*, Vol. VI, 1.  
 Barkla, C. G., 1931, *Nature*, Vol. CXXXVII, 877.  
 Barkla, C. G., 1933, *Nature*, Vol. CXXXI, 166.  
 Barkla, C. G. and Khastgir, S. R., 1925a, *Phil. Mag.*, Vol. XLIX, 251.  
 Barkla, C. G. and Khastgir, S. R., 1925b, *Phil. Mag.*, Vol. I, 1115.  
 Barkla, C. G. and Khastgir, S. R., 1926a, *Nature*, Vol. XCVII, 228.  
 Barkla, C. G. and Khastgir, S. R., 1926b, *Phil. Mag.*, Vol. II, 642.  
 Barkla, C. G. and Khastgir, S. R., 1927, *Phil. Mag.*, Vol. IV, 735.  
 Barkla, C. G. and Mackenzie, G., 1925, *Nature*, Vol. CXV, 942.  
 Barkla, C. G. and Mackenzie, G., 1926, *Phil. Mag.*, Vol. I, 542.  
 Barkla, C. G. and Mackenzie, G., 1926, *Phil. Mag.*, Vol. II, 1116.  
 Compton, A. H., 1924, *Nature*, Vol. CXIII, 160.  
 Dirac, P. A. M., 1926, *Proc. Roy. Soc., A*, Vol. III, 406.  
 Khastgir, S. R., 1932, *Phil. Mag.*, Vol. XIV, 99.  
 Pal, H. K., 1948, *Ind. Jour. Phys.*, Vol. 22, Part VII, July, 291.  
 Pal, H. K., 1949, *Ind. Jour. Phys.*, Vol. 23, No. 3, March, 111.  
 Pal, H. K., 1950, *Ind. Jour. Phys.*, Vol. 24, No. 2, Feb., 91.  
 Pal, H. K., 1964, *Ind. Jour. Phys.*, Vol. 38, No. 2, Feb., 61.

# LIGHT ABSORPTION IN $\text{NO}_3$ ION IN STATE OF SOLUTION

## Part II—203m $\mu$ BAND

A. MOOKHERJI AND S. P. TANDON\*

PHYSICAL LABORATORIES, BURDWAN UNIVERSITY, BURDWAN (W.B.), INDIA

(Received October 8, 1963; Resubmitted December, 7, 1964)

**ABSTRACT.** 200m $\mu$  band of nitrate ion has been resolved into five peaks. The observed energy, band-width, molar extinction coefficient and oscillator strength show that the strongest peak is due to the symmetry allowed  $A'_1 \rightarrow E'$ ,  $\pi \rightarrow \pi^*$  electronic transition and the others are due to simultaneous electronic and vibrational transitions.

### INTRODUCTION

In previous part of the paper (Mookherji and Tandon, 1962h), which we shall refer as part I, hereafter, a systematic study of the 300m $\mu$  band of nitrate ion in about ten different salts in state of aqueous solution has been reported.

The 200m $\mu$  band is very intense and has large band width. Previous workers (Part I) failed to study this band in detail due to large band width and non-elimination of solvent and container effect. Krishnan and Guha (1934) in the absence of any knowledge of vibrational or electronic energy values of  $\text{NO}_3^-$  ion attributed both the bands to photodissociation of  $\text{NO}_3^-$  into  $\text{NO}_2^-$  and O. But Smith and Boston (1961) could not detect the presence of  $\text{NO}_2^-$  in nitrate melts and Mookherji and Tandon (1962a) failed to detect the presence of  $\text{NO}_2^-$  in state of solution. Moreover, the observed structure of the 300m $\mu$  band in case of nitrate crystals at 20°K (Schauman, 1932) cannot be explained by postulating photodissociation.

The present communication reports a systematic study of the molar extinction coefficient, oscillator strength, etc., of the 200m $\mu$  band, discussed in the light of the theory of Smith and Boston (1961) and McEwen (1961).

### EXPERIMENTAL

The measurements were carried out by Hilger's UVISPEK spectrophotometer. The same procedure as in Part I was followed. To locate close peaks the scanning of the spectrum was carried out at an interval of 2.5 Å (Tandon, 1961).

Chemicals used were of Merck's analytical reagent quality. Triple distilled water was used for making solutions. The measurements centred round about

---

\* Now in Physics Department, University of Jodhpur, Jodhpur, Rajasthan, India.

25°C. No observable change in the position of the peaks was noticed for small room temperature variations.

### RESULTS

Results of measurements are collected in Table I. Five peaks A, B, C, D and E as shown in Fig. 1 are given in Wavelengths.

TABLE I  
Characteristic of 200m $\mu$  band

Sl. No.	Salt	Peak	Absorption maximum A	Molar extinction coefficient $\epsilon_{max}$ (litres/mol-cm)	Band width [ $\delta(+)+\delta(-)$ ] cm <sup>-1</sup>	Oscillator strength P
(1)	(2)	(3)	(4)	(5)	(6)	(7)
1.	LiNO <sub>3</sub>	A	1980	10330	7500	0.18
		B	1910	8738	1700	0.04
		C	1895	6531	1700	0.03
		D	1875	3814	1600	0.02
		E	1865	2542	1600	0.01
2.	NaNO <sub>3</sub>	A	1990	26950	7800	0.48
		B	1912.5	25970	1750	0.11
		C	1895	23110	1650	0.09
		D	1875	15160	1500	0.05
		E	1856.5	5943	1500	0.02
3.	KNO <sub>3</sub>	A	2000	43590	8000	0.80
		B	1917.5	43000	1850	0.18
		C	1896	41850	1700	0.16
		D	1876	27200	1500	0.09
		E	1857.5	13550	1550	0.04
4.	NH <sub>4</sub> NO <sub>3</sub>	A	2005	23920	7000	0.39
		B	1917.5	18140	1700	0.07
		C	1896	15920	1400	0.05
		D	1876	9139	1350	0.03
		E	1857.5	5036	1400	0.02
5.	AgNO <sub>3</sub>	A	1997	40350	8000	0.73
		B	1915.5	39790	1750	0.16
		C	1897	34900	1600	0.13
		D	1875	23210	1500	0.08
		E	1855	12130	1550	0.04
6.	Ba(NO <sub>3</sub> ) <sub>2</sub>	A	1985	18820	7400	0.32
		B	1919	20560	1900	0.09
		C	1895	20560	1700	0.08
		D	1875	17040	1300	0.05
		E	1857.5	7865	1700	0.03
7.	Sr(NO <sub>3</sub> ) <sub>2</sub>	A	1992.5	20240	6000	0.28
		B	1918.5	8149	1400	0.03
		C	1895	1402	500	0.002
		D	1875	323	250	0.0002
		E	1857.5	215	220	0.0001

TABLE I—Contd.

Sl. No.	Salt	Peak	Absorption maximum $\text{\AA}$	Molar extinction coefficient $\epsilon_{\text{max}}$ (litres/mole-cm)	Band width [ $\delta(+1) + \delta(-1)$ ] cm	Oscillator strength P
(1)	(2)	(3)	(4)	(5)	(6)	(7)
8.	$\text{Ca}(\text{NO}_3)_2$	A	2020	24140	5700	0.32
		B	1918	14300	1800	0.06
		C	1895	5277	500	0.006
		D	1875	544	250	0.0003
			18575	272	200	0.0001
9.	$\text{Mg}(\text{NO}_3)_2$	A	2000	23810	7100	0.39
		B	1917.5	17760	1900	0.08
		C	1895	14860	1500	0.05
		D	1875	9696	1300	0.03
		E	1859	5719	1500	0.02
10.	$\text{Cd}(\text{NO}_3)_2$	A	2035	28260	7500	0.48
		B	1917.5	20880	1900	0.09
		C	1895	17880	1600	0.07
		D	1875	12350	1500	0.04
		E	1855	8465	1400	0.03
11.	$\text{Al}(\text{NO}_3)_3$	A	2047	28490	8000	0.52
		B	1919	28880	4000	0.26
		C	1895	30100	1600	0.11
		D	1875	21690	1300	0.06
		E	1855	8561	1500	0.03

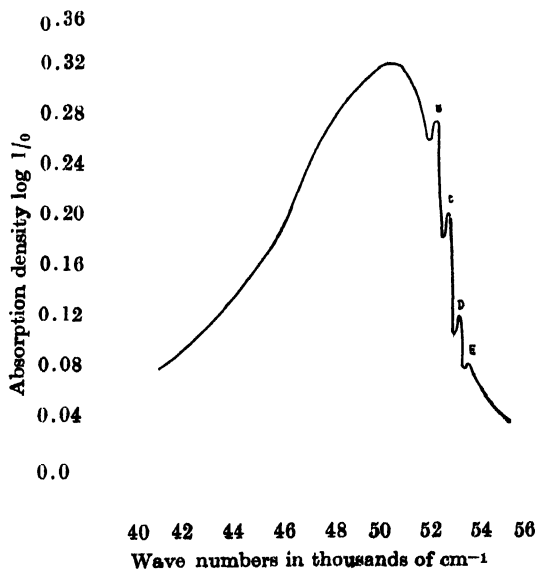


Fig. 1.—Nature of variation of absorption in  $200m\mu$  band of nitrate ion in aqueous solution of  $\text{LiNO}_3$ . The five peaks, which have been resolved, are A, B, C, D and E.

## DISCUSSION

A. *Characteristics of an absorption band*

The essential characteristics which are needed for the assignment of an absorption band are its position, band-width, intensity and structure. We discuss these points one by one.

(a) *Position* : Following Smith and Boston (1961) the position of the band maximum was determined as the limit at the maximum of the mid-points of a sequence of chords drawn across the band parallel to wave-number axis. This could be done with a precision of 5-10 Å. The band maximum could be located at 200m $\mu$ , with a small variation of energy in different nitrates. (Table I).

(b) *Band-width* : The band-width gives a measure of the antibonding character of the orbitals giving rise to the excited state (Jorgensen, 1962). Assuming the shape of the absorption curve to be Gaussian the double half-band-width is given by the expression,

$$2\delta = [\delta(+1) + \delta(-1)] \quad \dots (1)$$

where  $\delta(+1)$  and  $\delta(-1)$  are half band-widths towards larger and smaller wave-numbers respectively.

The band-width of this band  $\sim 10^3 \text{cm}^{-1}$  (Table I), which is of the same order as that of 300m $\mu$  band (Part I), indicates that the orbital giving rise to the excited states for both the bands are antibonding.

(c) *Intensity* : It is customary in spectrophotometry to discuss and to describe the intensities of absorption bands in terms of absorptivities or molar extinction coefficient  $\epsilon_{max}$ . As this is not directly related to any quantity obtainable from theory, we shall discuss in terms of oscillator strength  $P$ , suggested by Mulliken (1939), which is proportional to the intensity, directly deducible from theory and measurable from the area of the absorption curve (Jaffé and Orchin, 1962).

Since the absorption band is of Gaussian shape, following Jørgensen (1954) and Ballhausen (1955), the oscillator strength  $P$  is given by

$$P = 4.60 \times 10^{-9} \epsilon [\delta(+1) + \delta(-1)]/2 \quad \dots (2)$$

where  $\epsilon_{max}$  is the molar extinction coefficient and has a value  $\sim 10^4$  (Table I). This agrees well with the measurements by Meyerstein and Treinin (1961).

The experimental values of  $\epsilon_{max}$  and  $[\delta(+1) + \delta(-1)]$  gave  $P$  values from equation (2) which are collected in Table I. These values of  $\epsilon_{max} \simeq 10^4$  and  $P \simeq 10^{-1}$  suggest that this band is due to an allowed transition. (Part I).

(d) *Fine Structure* : This 200m $\mu$  band could be resolved into five peaks A, B, C, D and E (Table I, Fig. 1.). The observed spacing between peaks 500-600  $\text{cm}^{-1}$  agrees well with that in case of 300m $\mu$  band observed by Schauman

(1932), Rodloff (1934), Sayre (1959) and Strickler (1961). However, the peaks between A and B (Fig. 1) could not be resolved, resulting in wider separation between A and B than other peaks. Following Sayre (1959) and Strickler (1961) these peaks may be interpreted as vibrational structure of the electronic  $\pi \rightarrow \pi^*$  transition.

### B. Assignment of the band

The observed  $\epsilon_{\max}$  values ( $\sim 10^4$  litres/mol.-cm) and oscillator strength  $P$  ( $\sim 10^{-1}$ ) for this band suggest that the band may be due to an allowed transition. Stein and Treinin (1959) and Rhodes and Ubbelohde (1959) have assigned to this band electron transfer or inter-molecular charge transfer transition which is characteristic of halide ions (Strickler and Kasha, 1961; Jortner and Treinin, 1962). This assignment may be ruled out on the grounds that the effects of solvent and foreign ions on  $\text{NO}_3^-$  spectrum in solution though resemble that of halide ions but differ in magnitude markedly (Strickler, 1961).

The 24 electrons in nitrate ion may be divided into  $\pi$ -electrons (bonding and antibonding) and  $\sigma$ -electrons (bonding and antibonding) (Walsh, 1953). McEwen (1961), Strickler (1961) and Smith and Boxton (1961) have calculated by LCAO-MO

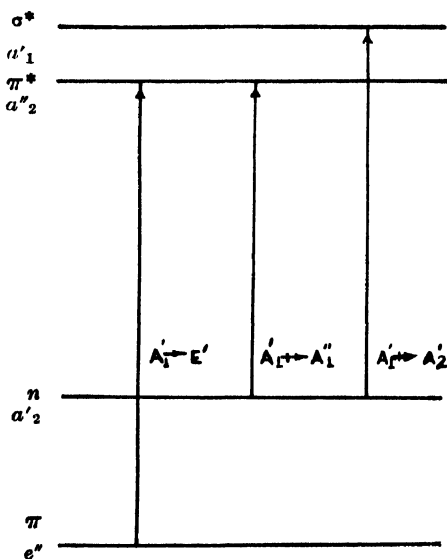


Fig. 2.—Energy level diagram of nitrate ion showing transitions.

method the energy levels of nitrate ion using  $D_3$  symmetry properties of the ion. These energy levels along with transitions are shown in Fig. 2. The observed energy 6.17 to 6.23 eV, of this band of nitrate ion in different salts in state of aqueous solution, agrees well with the calculated value, 6.22 eV of  $\pi \rightarrow \pi^*$  transition of the free ion. The small deviations from the calculated value may be attributed

to the influence of cation (Smith and Boston, 1961) and solvent (Strickler, 1961). The detailed study of solvent effect by Strickler (1961) and Meyerstein and Treinin (1961) coupled with the study with polarised light by Krishnan and Dasgupta (1933) and Friend and Lyons (1959) also confirm its assignment to symmetry allowed  $A_1 \rightarrow E'$ ,  $\pi \rightarrow \pi^*$  transition.

Thus the  $200m\mu$  band may be assigned to the  $D_{3h}$  symmetry allowed  $A_1 \rightarrow E'$ ,  $\pi \rightarrow \pi^*$  transition and its fine structure to the vibrational structure of this electronic transition.

#### REFERENCES

- Ballhausen, C. J., 1955, *Acta. Chem. Scand.*, **9**, 821.  
 Friend, J. A. and Lyons, L. E., 1959, *J. Chem. Soc.*, 1572.  
 Jaffé, H. H. and Orchin, M., 1962, *Theory and Applications of Ultraviolet Spectroscopy* (John Wiley and Sons, Inc., New York), 111.  
 Jørgensen, C. K., 1954, *Acta. Chem. Scand.*, **8**, 1495, 1502.  
 Jørgensen, C. K., 1962, *Absorption spectra and Chemical bonding in Complexes* (Addison-Wesley Publishing Company, Inc., Reading Massachusetts), ed. I., 85.  
 Jortner, J. and Treinin, A., 1962, *Trans. Faraday Soc.*, **58**, 1503.  
 Kutzin, L. I., 1950, *J. Chem. Phys.*, **18**, 789.  
 Krishnan, K. S. and Dasgupta, A. C., 1933, *Indian J. Phys.*, **8**, 49.  
 Krishnan, K. S. and Guha, A. C., 1934, *Proc. Ind. Acad. Sci.*, **1**(4), 242.  
 McEwen, K. L., 1961, *J. Chem. Phys.*, **34**, 547.  
 Meyerstein, D. and Treinin, A., 1961, *Trans. Faraday Soc.*, **57**, 2104.  
 Mookerji, A. and Tandon, S. P., 1962, *Indian J. Phys.*, **36** (a) 211, (b) 344.  
 Mulliken, R. S., 1939, *J. Chem. Phys.*, **7**, 14.  
 Rhodes, E. and Ubbelohde, A. R., 1959, *Proc. Roy. Soc., London*, **A251**, 156.  
 Sayre, E. V., 1959, *J. Chem. Phys.*, **31**, 73.  
 Schauman, 1932, *Z. Physik*, **76**, 106.  
 Smith, G. P. and Boston, C. R., 1961, *J. Chem. Phys.*, **34**, 1396.  
 Stein, G. and Treinin, A., 1959, *Trans. Faraday Soc.*, **55**, 1086.  
 Strickler, S. J., 1961, Ph.D. Dissertations, Florida State University.  
 Strickler, S. J. and Kasha, M., 1961, *J. Chem. Phys.*, **34**, 1077.  
 Tandon, S. P., 1961, *Raj. Univ. Studies*, **7**, 69.  
 Tandon, S. P., 1962, *Proc. Raj Acad. Sci.*, **9**(2), 3.  
 Walsh, A. D., 1953, *J. Chem. Soc.*, 2301.



# Letters to the Editor

The Board of Editors does not hold itself responsible for opinions expressed in the letters published in this section. The notes containing short reports of original investigations communicated to this section should not contain many figures and should not exceed 500 words in length. The contributions reaching the Secretary by the 15th of any month may be expected to appear in the issue for the next month. No proof will be sent to the author.

## CRYSTALLOGRAPHIC DATA FOR AMMONIUM NITRATE-SULPHATE

S. K. GHOSH, V. K. SRINIVASA and B. K. BANERJEE

PLANNING AND DEVELOPMENT DIVISION,  
THE FERTILIZER CORPORATION OF INDIA LTD., SINDHRI, BIHAR.

(Received February 19, 1965)

This laboratory has been investigating the possibilities of the formation of different types of double salts of ammonium nitrate—sulphate under various physical conditions. The possibility of the formation of double salt of 1 : 1 molar ratio of nitrate—sulphate was indicated by Ito (1960) in his studies on the phase-diagram of the system  $(\text{NH}_4)_2\text{SO}_4$ — $\text{NH}_4\text{NO}_3$ — $\text{H}_2\text{O}$ . In our earlier investigation Srinivasa *et al.*, (1964) on this system, we have confirmed its existence as a stable solid phase by preliminary X-ray powder diffraction data. The present investigation was undertaken with a view to obtain more information and clarification of its crystallographic properties.

The sample of the double salt used in this determination has been prepared according to the method already described (Srinivasa *et al.*, 1964). The crystals of double salt of 1 : 1 molar ratio were grown from aq. alcoholic solution. The crystals grown were plate shaped with well formed (010) and (100) faces. The size of a typical crystal was  $2 \times 1 \times 0.2$  mm. Oscillation and Weissenberg photographs were taken around the 'b' axis and 'a' axis with nickel filtered  $\text{CuK}_\alpha$  radiation. From the zero layer Weissenberg photograph the value of  $\beta$  was calculated by the method of Omega separations (Buerger 1942). The values for the unit cell dimensions are :

$$a = 5.91 \text{ \AA} \quad b = 7.95 \text{ \AA} \quad c = 11.05 \text{ \AA} \quad \beta = 112^\circ 54'$$

The crystal belongs to the monoclinic system. After indexing the Weissenberg photograph (around the 'b' and 'a' axes), the following systematic extinctions were observed :

$0k0$  absent when  $k$  is odd.

$h00$  absent when  $h$  is odd.

$h01$  absent when  $h$  is odd.

Accordingly, the space group is determined as  $P2_1/a-C^5_{2h}$ .

There are two molecules per unit cell. Density : calculated  $1.46 \text{ g.cm}^{-3}$ ; observed  $1.48 \text{ g.cm}^{-3}$ .

#### A C K N O W L E D G M E N T

Thanks are due to Dr. K. R. Chakravorty, General Manager, Planning and Development Division, for his constant encouragement and kind permission to publish this paper.

#### R E F E R E N C E S

- Ito, Yukio, (1960) *Kogyo Kagaku Zasshi* **63**, 1913-16.  
Srinivasa, V. K., Ghosh, S. K., Banerjee, B. K., (1964) *Technology* Vol. **I**, No. **3** p. 3.  
Buerger, M. J., 1942 "X-ray crystallography" J. Wiley and Sons, Inc., New York, p.p. 280-3.

# A SIMPLE METHOD FOR CALCULATING THERMAL EXPANSION OF IONIC CRYSTALS

C. M. KACHHAVA AND S. C. SAXENA

PHYSICS DEPARTMENT, RAJASTHAN UNIVERSITY, JAIPUR, INDIA

(Received October 8, 1964)

Simple methods for computing the properties of solids are very useful from a practical standpoint. Smyth (1955) and Kumar (1959, 1960) developed such a simple method for calculating the coefficient of thermal expansion,  $\alpha$ . According to them

$$\alpha = \frac{C_p}{2E} \frac{(n+4)}{n} \sqrt{Z'} \quad \dots (1)$$

Here  $C_p$  and  $E$  are the specific heat at constant pressure and cohesive energy per mole respectively,  $n$  is the repulsive index, and  $Z' = (Z_c N_c + Z_a N_a)(N_c + N_a)^{-1}$ , where  $Z_c$ ,  $N_c$  and  $Z_a$ ,  $N_a$  are the charge and number of the cation and anion respectively. The potential energy function,  $\phi(r)$ , assumed was

$$\phi(r) = -\frac{\alpha Z^2 e^2}{r} + \frac{A}{r^n}, \quad \dots (2)$$

where  $\alpha$  is the Madelung constant,  $e$  the charge of an electron,  $Z$  is the valency,  $r$  the interionic distance and  $A$  and  $n$  are the familiar potential parameters. The other relevant details will not be reproduced here for brevity and further because these are not pertinent for our discussion in this note.

A more general form of Eq. (1) is

$$\alpha = -\frac{C_p}{2r_0} - \frac{\phi'''(r_0)}{[\phi''(r_0)]^2} \sqrt{Z'}, \quad \dots (3)$$

in which  $r_0$  is the interionic equilibrium separation distance,  $\phi'''(r_0)$  and  $\phi''(r_0)$  refer to the values of third and second derivatives of  $\phi(r)$  at  $r = r_0$  respectively. Equation (3) will be convenient to use when more complicated forms for  $\phi(r)$  than given by Eq. (2) are considered. The purpose of this note is to point out that much more reliable values of  $\alpha$  are obtained if one uses an appropriate form for  $\phi(r)$ .

Kachhava and Saxena (1964a) have recently shown that a very appropriate and accurate empirical form for  $\phi(r)$  is

$$\phi(r) = -\frac{\alpha Z^2 e^2}{r} + B \exp(-r/\rho) - \frac{C}{r^8} - \frac{D}{r^8} \quad \dots (4)$$

where  $B$  and  $\rho$  are the potential parameters,  $C$  and  $D$  are the van der Waals' constants. The potential parameters may be obtained by the familiar conditions of Born and Mayer (1964b). As  $\alpha$  is very sensitive (1964b) to the overlap forces it is likely that the use of Eq. (4) instead of Eq. (2) may result in considerable improvement for the  $\alpha$  values. We will examine this for the case of alkali halide crystals where experimental data are also available.

TABLE I  
Thermal expansion of alkali halide crystals,  $\alpha$

Crystal	Cohesive energy KCal/mole	Cp(298°K) Cal/deg. mole	$\alpha \times 10^6$ per deg.				
			Exptl.	Eqs. (3) and (2)	%dev.	Eqs. (3) and (4)	%dev.
LiF	238.9a	10.04c	34.0c	34.85	- 2.5	29.16	-14.2
LiCl	192.1a	12.20c	44.0c	49.53	+ 12.6	44.76	+ 1.7
LiBr	181.9a	12.40c	50.0c	52.01	+ 4.0	44.68	-10.6
LiI	169.5a	13.00c	59.0c	52.31	-11.3	50.08	-15.1
NaF	213.8a	11.00c	36.0c	40.27	+ 11.9	34.29	- 4.7
NaCl	179.2a	11.88c	40.0c	49.50	+23.7	42.90	- 7.2
NaBr	170.5a	12.50c	43.0c	41.66	- 3.1	46.45	+ 8.0
NaI	159.6a	13.00c	48.3c	57.58	+19.2	51.66	+ 7.0
KF	189.2a	11.73c	36.7c	46.27	+26.1	38.62	+ 5.2
KCl	163.2a	12.31c	38.3c	54.23	+41.6	47.29	+23.5
KBr	156.6a	12.82c	40.0c	57.86	+44.7	51.05	+27.6
KI	147.8a	13.16c	45.0c	61.32	+36.3	55.00	+22.2
RbF	180.6a	12.20c	31.67f	49.33	+55.7	41.99	+34.1
RbCl	157.7a	12.30c	36.0c	55.40	+53.7	47.58	+32.2
RbBr	151.3a	12.68c	38.0c	58.56	+54.1	51.61	+35.8
RbI	153.0a	12.50c	43.0c	59.32	+38.0	52.98	+23.2
CsCl	155.1b	12.22d	56.0g	58.79	5.0	49.36	-11.8
			Mean		26.1		16.7

- a. Shorman, J., 1932, *Chem. Rev.* **11**, 93.  
b. Seitz, F., 1940, *The Modern Theory of Solids*, Mc Graw Hill, New York.  
c. U. S. Bur. Standard Circular, 1952, No. 500.  
d. Kelley, K. K., 1934, *Bull. U.S. Bur. Min.*, 371.  
e. Weyl, W. A., 1955, Office of Naval Res. Techn. Reports No. 64-66, Pennsylvania State Univ.  
f. Huggins, M.L., 1937, *J. Chem. Phys.* **5**, 143.  
g. Hummel, F. A., 1950, *J. Amer. Ceram. Soc.* **33**, 102.

Kumar (1959, 1960) used the expression given by Eq. (1) in conjunction with relation (2) and  $n$  values fixed by Pauling (1927). Kumar (1959, 1960) also used the experimental values of cohesive energy but the values of  $E$  obtained from Eq.(2) and Pauling's  $n$  values agree with the experimental  $E$  values very well so that his calculation-procedure becomes consistent with Eq. (3). We will therefore base all our discussion on Eq. (3) only. Values of  $\alpha$  so obtained are given in the Table I along with the experimental values and the percentage deviations. The values of some of the necessary constants are also tabulated.

If we employ potential form given by Eq. (4) in Eq. (3) for evaluating  $\alpha$  we get the values given in Table I, column 7. The constants required in these calculations are those already given by us (1963, 1964b) earlier. The calculated values are now in somewhat better agreement with the experimental values. The average absolute deviation is only 16.7% as compared to the previous value of 26.1%.

A few remarks regarding the experimental  $\alpha$  values listed in the Table I are relevant. The values given in the Table I does not include the results of a few measurements reported in recent years. Pathak and Pandya (1959, 1960a, 1960b) and Pathak, *et al*, (1963) have reported  $\alpha$  values on a few alkali halide crystals as a function of temperature using X-ray diffraction technique. For NaCl the results have been reported by Pathak and Pandya (1959) in a graphical form and therefore we could not include them here for comparison. These authors also represent their data (except for NaCl) by a quadratic equation in temperature and we have calculated the  $\alpha$  values at 25°C in each case. This involves back extrapolation of 5°C which is reasonable. We report these values in Table II. These values on the average differ from the recorded values in Table

TABLE II

Experimental  $\alpha$  ( $\times 10^6$  per deg) values at 25°C

Crystal	$\alpha$
LiF	33.8
NaF	32.0
KBr	38.5
KI	40.3

I by about 6%. It may further be remarked that in certain cases other authors have also reported the  $\alpha$  values. Using the same technique, earlier  $\alpha$  values for LiF, KBr and KI are in good agreement with the values listed in Table II. For NaF Deshpande's (1961) value at 30°C is greater by about 6% than given in Table II and is again obtained by X-ray data. From this analysis it is clear that  $\alpha$  values are correct to within about 6%, if the relative consistency of the data of different workers is any guide. However, this uncertainty does not vitiate in any way the conclusion derived here.

One of the endeavours of this work was to demonstrate the necessity and importance of using the correct potential energy expression in calculating the properties of solids. The success achieved by theory even now is not very satisfactory but this is essentially because of the simple picture of the lattice vibrations we have assumed in developing theory following Einstein.

## REFERENCES

- Deshpande, V. T., 1961, *Acta. Cryst.*, **14**, 794.  
Kachhava, C. M., and Saxena, S. C., 1964a, Being published in *Proc. Natl. Inst. Sci. (India)*.  
Kachhava, C. M., and Saxena, S. C., 1964b, *Ind. Jour. Phys.* **8**, 388.  
Kumar, S., 1959, *Proc. Natl. Inst. Sci. (India)*, **A25**, 364 ;  
— — — 1960, *Central Glass and Ceramic Res. Inst. Bull. (India)*, **7**, 58.  
Pathak, P. D. and Pandya, N. V., 1959, *Curr. Sc.*, **28**, 320.  
— — — 1960a, *Ibid.*, **29**, 14.  
— — — 1960b, *Ind. Jour. Phys.* **34**, 416.  
Pathak, P. D., Pandya, N. V. and Ghadiali, M. P., 1963, *Ind. Jour. Phys.* **37**, 293.  
Pauling, L., 1927, *Proc. Roy. Soc. (Lond.)*, **114**, 181.  
Smyth, H. T., 1955, *J. Amer. Ceram. Soc.* **38**, 140.

# RELAXATION TIMES, MUTUAL AND AVERAGED MUTUAL VISCOSITIES OF SOME DI-SUBSTITUTED BENZENES IN SOLUTIONS OF CYCLOHEXANE

S. I. AHMAD AND M. N. SHARMA

DEPARTMENT OF PHYSICS, UNIVERSITY OF LUCKNOW, INDIA

(Received March 31, 1964; Resubmitted November 16, 1964)

**ABSTRACT.** Relaxation times of o-, m-, and p-nitro toluenes and o-chloro toluene have been determined in the 3 cms micro-wave region using cyclohexane as solvent at a temperature of 24°C. Mutual viscosities of the solute and solvent as proposed by Hill and averaged mutual viscosities as recently introduced by Vaughan and co-workers have also been determined in the solutions of cyclohexane. By differentiating the equations of Hill and Vaughan and coworkers with respect to the solute mole fraction two more equations have been obtained and the values of the mutual and averaged mutual viscosities obtained from these equations have been compared with those obtained directly from the equations of Hill and Vaughan and co-workers. It has been found that for the solutions studied the mutual viscosity coefficient is a better representation of the hindrance to the rotation of the individual solute molecules. The potential barrier heights for dielectric relaxation and viscous flow have also been calculated using Eyring's equations. The potential barrier height for dielectric relaxation is found to be always less than the potential barrier height for the viscous flow of the solvent.

## INTRODUCTION

Hill (1954) suggested that the macroscopic viscosity of the solvent should be treated as the mutual viscosity of the solute and the solvent  $\eta_{12}$ , which is a measure of the solute-solvent interaction, in order to explain the discrepancy between the observed values of relaxation time ( $\tau$ ) and those obtained from Debye's equation. She gave the following expression for the mutual viscosity coefficient

$$\eta_m \sigma_m = x_1^2 \eta_1 \sigma_1 + x_2^2 \eta_2 \sigma_2 + 2x_1 x_2 \eta_{12} \sigma_{12} \quad \dots (1)$$

where  $\eta_m$ ,  $\eta_1$  and  $\eta_2$  are the coefficients of viscosity of the solution, solvent and solute respectively.  $x_1$ ,  $x_2$  are the mole fractions of the solvent and the solute and the quantities  $\sigma$  represent the average inter-molecular distances and are given by

$$\sigma_1 = (M_1/d_1 N)^{1/3}, \quad \sigma_2 = (M_2/d_2 N)^{1/3} \text{ and } \sigma_m = \left( \frac{x_1 M_1 + x_2 M_2}{d_m N} \right)^{1/3}$$

where  $M_1$ ,  $M_2$  are the molecular weights of the solvent and solute respectively and  $d_1$ ,  $d_2$  are the corresponding densities.  $d_m$  is the density of solution.  $\sigma_{12}$  represents the average separation of the solute and solvent molecules, i.e.

$$\sigma_{12} = 1/2(\sigma_1 + \sigma_2)$$

On rearrangement equation (1) yields

$$\left( \frac{\eta_m \sigma_m - x_1^2 \eta_1 \sigma_1}{x_2^2 \sigma_2} \right) = \eta_2 + 2 \frac{x_1}{x_2} \cdot \frac{\sigma_{12}}{\sigma_2} \cdot \eta_{12} \quad \dots (2)$$

This equation represents a straight line. The mutual viscosity  $\eta_{12}$  may be obtained from the slope of this line, drawn taking L.H.S. as ordinate and  $2(x_1/x_2)(\sigma_{12}/\sigma_2)$  as abscissa as all the factors involved can be determined experimentally.

Assuming that  $\sigma_m = \sigma_1$  and differentiating both the sides of equation (1) with respect to  $x_2$  one gets

$$\frac{\sigma_1}{\sigma_2} \cdot \frac{1}{2x_2} \left( \frac{d\eta_m}{dx_2} - 2x_1\eta_1 \right) = \eta_2 + \left( \frac{x_1 - x_2}{x_2} \right) \cdot \frac{\sigma_{12}}{\sigma_2} \cdot \eta_{12} \quad \dots (3)$$

This equation also represents a straight line and can similarly be used to determine  $\eta_{12}$ .

Meakins (1958) determined the mutual viscosity coefficients of large number of solutes in solutions of benzene and decalin and showed that the agreement between the experimental and calculated values of  $\tau$  is much better in the case of Hill's equation of  $\tau$  than that with Debye's equation. Later on Pitts and Smyth (1959) also showed from a similar observation that for the four systems observed by them, the value of  $\tau$  obtained from Hill's equation are three to four times the corresponding experimental values of  $\tau$ .

Recently Vaughan and co-workers (1961) derived on simple considerations an expression very similar to that of Hill, defining another mutual viscosity which they called the "properly averaged mutual viscosity". But they found no advantage of this viscosity over  $\eta_1$ —the solvent viscosity, for the compound studied. Their equation in the present notation is :

$$\eta_m = x_1^2 \eta_1 + x_2^2 \eta_2 + 2x_1 x_2 \eta_{12} \quad \dots (4)$$

which yields on rearrangement

$$\left( \frac{\eta_m - x_1^2 \eta_1}{x_2^2} \right) = \eta_2 + 2 \cdot \frac{x_1}{x_2} \cdot \eta_{12} \quad \dots (5)$$

Differentiating both sides of equation (4) with respect to  $x_2$  one gets

$$\frac{1}{2x_2} \left( \frac{d\eta_m}{dx_2} - 2x_1\eta_1 \right) = \eta_2 + 2 \left( \frac{x_1 - x_2}{x_2} \right) \eta_{12} \quad \dots (6)$$

The equations (2), (3), (5) and (6) are equally good for a system in which the solute is in solid form, in that case  $\eta_2$  represents an unknown factor. The equations (5) and (6) may be used to determine the "averaged mutual viscosities"  $\eta_{12}$ . In the present investigation the relaxation times ( $\tau$ ) of *o*-, *m*- and *p*-nitrotoluenes and *o*-chlorotoluene have been determined in 3 cms micro-wave region by Gopala



Krishna's (1957) fixed frequency method using cyclohexane as solvent. Mutual and averaged mutual viscosities of cyclohexane solutions of *o*-nitrotoluene, *m*-nitrotoluene, *o*-chlorotoluene and *o*-chloroaniline molecules have also been calculated from the slopes of the lines represented by equations (2), (3), (5) and (6) by the least square method.  $\eta_{12}$  for *p*-nitro toluene solutions was calculated from equation (5) by eliminating the factor  $\eta_2$  from the two equations corresponding to two concentrations of the solute.

Potential barrier heights ( $H_7$ ) for dielectric relaxation for the investigated compounds in solutions of cyclohexane and the potential barrier height ( $H_7$ ) for the viscous flow of the solvent i.e. cyclohexane have been calculated using Eyring's (1941) equations.

### EXPERIMENTAL

A 3 cms microwave bench was used for the determination of the dielectric constant,  $\epsilon'$  and the loss factor  $\epsilon''$  of the dilute solutions of increasing concentrations, by the standing wave technique of von Hippel and Roberts (1946). Micro waves were generated by a reflex klystron (CV129). After travelling through a system of wave guides these waves were reflected from a short circuit at the end of a silver cell and standing waves were formed in the waveguide as a result of interference of the incident and reflected waves. The position of any minima of these standing waves, with and without the experimental solution in the cell were determined. This gave the shift of the minimum field position. The width at double the minimum field was also determined for each solution. The shift of the minima and the width at double the minimum field were used to calculate the dielectric constant  $\epsilon'$  and dielectric loss factor  $\epsilon''$  of the solutions. Dakin and Works' (1947) simplified method for the calculations of  $\epsilon'$  and  $\epsilon''$  was used in the case of solutions of *o*-nitrotoluene, *m*-nitrotoluene and *o*-chlorotoluene as the dissipation factor was always found to be less than 0.1. Finally the relaxation times  $\tau$  were calculated using Gopala Krishna's (1957) relation. The viscosities were determined with the help of Hoppler's precision viscometer to an accuracy of  $\pm 2\%$ . This method of determining viscosity is very simple and requires simply the determination of time of fall of a glass or metal ball between two marks in a glass tube filled with the experimental liquid of known density. The viscosities ( $\eta$  cps) of the liquids were calculated from the relation :

$$\eta = F(S_k - S_F) \cdot K$$

where

$F$  = time of fall of the ball in seconds,

$S_k$  = specific gravity of the ball,

$S_F$  = specific gravity of the liquid,

$K$  (ball constant) = 0.009495

It was observed that if an error of 1% is made in any experimental measurement,

the maximum extent to which  $\eta_{12}$  is affected is about 1.6%. The chemicals used were of pure quality and were obtained from Messrs E. Merck, B.D.H. and Light. Cyclohexane used as solvent was of B.D.H. LR grade and was distilled before use.

#### DISCUSSION OF THE RESULTS

The graphs given in the Figs. 1 and 2 represent the values of the factors  $X$   $Y$  calculated from the dielectric constants  $\epsilon'$  and the dielectric loss factors  $\epsilon''$ , for solutions of increasing concentrations of each solute studied. The slopes of these lines, required in the calculations of relaxation times ( $\tau$ ) were determined by the least square method. The values of relaxation time  $\tau$ , the average mutual viscosities  $\eta_{12}$  and the ratios  $\tau/\eta_1$  and  $\tau/\eta_{12}$  together with the corresponding values of molecular weight for each compound are given in Table I. The results show that the relaxation times of the three nitro-toluenes increase from ortho- via meta- to para-compound. The ratios  $\tau/\eta_1$  for these compounds are different from each other and also increase in the same order. This is not in conformity with the Debye's theory (1929). But if  $\eta_1$ —the solvent viscosity is replaced by  $\eta_{12}$ —the averaged mutual viscosity of the solute and solvent as in the last column of Table I, the difference between the ratio ( $\tau/\eta_{12}$ ) for the three nitrotoluenes becomes much

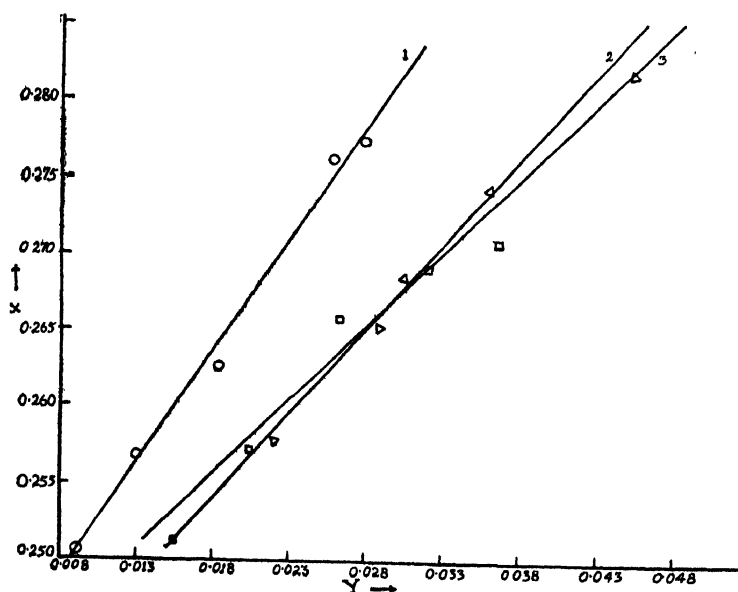


Fig. 1. Plot of X-Y data for :

1. o-nitro-toluene.
2. m-nitro-toluene.
3. p-nitro-toluene.

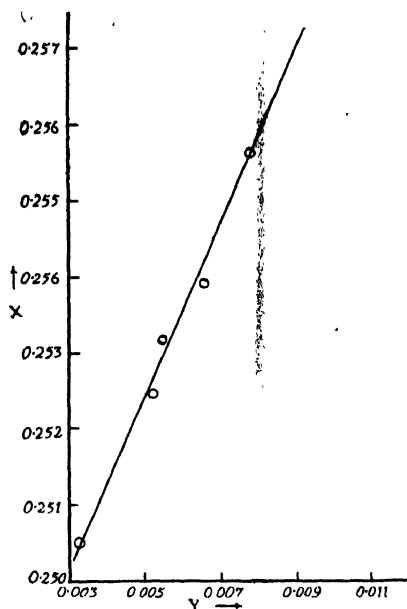


Fig. 2. Plot of X-Y data for *o*-chloro toluene.

less than with  $\eta_1$ . The ratios for *m*- and *p*-nitro toluenes are found to be almost equal. Therefore in these cases  $\eta_{12}$  seems to be a better representation of the resistance to the rotation of individual solute molecules. From the results it is evident that the relaxation times of three nitro-toluenes increase from ortho- via meta- to para-compound because the resistance experienced by a nitro-toluene molecule, also increases in the same order. The results also show that the values of  $\tau$ ,  $(\tau/\eta_1)$  and  $(\tau/\eta_{12})$  for *o*-nitro-toluene which has greater molecular weight are greater than those for *o*-chlorotoluene as expected. But the difference between the  $(\tau/\eta_{12})$  values for these molecules is less than that between the values of  $(\tau/\eta_1)$  for the same molecules. This is due to the fact that the resistance experienced by a *o*-nitro toluene molecule in rotation is greater than that experience by a *o*-chloro-toluene molecule as can be seen from the values of  $\eta_{12}$  for the solutions of these compounds.

The Table II contains the values of the viscosity co-efficients  $\eta_{12}$  as determined from the equations (2), (3), (5) and (6) for four compounds. The values of the averaged mutual viscosity for different solutions as determined from the equation of Vaughan and co-workers (1961) i.e. equation (5) are almost equal to those of the corresponding mutual viscosities determined from the equation (2) of Hill (1954) except in the case of *o*-chloro toluene where the difference is slightly more than that in the case of other compounds. This is in agreement with the results obtained earlier by Vaughan and co-workers (1961) in the case of some other polar molecules. In the 4th and 5th columns of the Table II, are given

respectively the values of  $\eta_{12}$  as obtained from equation (3) of Hill and equation (6) of Vaughan and co-workers. It is found that the corresponding values of  $\eta_{12}$  in the two columns are approximately equal, but they are slightly different respectively from the values of  $\eta_{12}$  obtained from the corresponding equations (2) and (5) and given respectively in the 2nd and 3rd columns, the difference being comparatively larger in the case of *o*-chloro aniline.

In the Table III are listed the values of the potential barrier heights for dielectric relaxation ( $H_\tau$ ) for the polar disubstituted benzenes studied and the potential barrier height ( $H_\eta$ ) for viscous flow of the solvent calculated from the Eyring's equations, together with the corresponding values of relaxation time. In these calculations the Eyring's value of the constant  $A$  i.e.  $(k/h) = 4.8 \times 10^{-11}$  and that of the constant  $B = (hN/V)$  (where  $h$  = Planck's constant,  $K$  = Boltzmann constant,  $N$  = Avogadro's number and  $V$  = molar volume), were used. A study of the Table III shows that the potential barrier heights  $H_\tau$  are slightly different for different molecules. The values of  $H_\tau$  for the three nitro toluenes which have the same size, are found to be slightly different, probably because a constant value of  $A$  has been used in all the cases while it has been shown by Sobhanadri (1959)

TABLE I

Values of relaxation times ( $\tau$ ), averaged mutual viscosity ( $\eta_{12}$ ) and the ratios ( $\tau/\eta_1$ ), ( $\tau/\eta_{12}$ ) for the investigated compounds  
( $f = 9567$  MC/Sec. Viscosity of cyclohexane at  $24^\circ\text{C} = 0.9754$  cps)

Substance	Molecular Weight	$\tau \times 10$ sec.	$\tau/\eta_1 \times 10$	$\eta_{12}$ cps.	$\tau/\eta_{12} \times 10$
<i>o</i> -nitro toluene	137.13	10.9	11.18	1.142	9.54
<i>m</i> -nitro toluene	137.13	15.1	15.48	1.350	11.19
<i>p</i> -nitro toluene	137.13	18.8	19.27	1.668	11.27
<i>o</i> -chloro toluene	126.58	10.0	10.25	1.080	9.26

TABLE II

Values of mutual viscosities ( $\eta_{12}$ ) as determined from different equations

Substance	$\eta_{12}$ cps from			
	Eqn.(2)	Eqn.(5)	Eqn.(3)	Eqn.(6)
<i>o</i> -nitro toluene	1.165	1.142	1.049	1.064
<i>m</i> -nitro toluene	1.365	1.350	1.089	1.103
<i>o</i> -chloro toluene	1.041	1.080	1.009	1.021
<i>o</i> -chloro aniline	0.943	0.954	1.427	1.427

TABLE III

Values of relaxation time ( $\tau$ ) and the potential barrier heights for dielectric relaxation and viscous flow

Substance	$\tau \times 10^{12}$ Sec	$H_\tau$ (K cal/mole)	$H_\eta$ (K cal/mole)	$H_\eta/H_\tau$
o-nitro toluene	10.9	2.49	3.30	1.33
m-nitro toluene	15.1	2.68	3.30	1.23
p-nitro toluene	18.8	2.81	3.30	1.17
o-chloro toluene	10.0	2.44	3.30	1.35

and Bhanumati (1963), that 'A' has different values for different solutes. The barrier heights  $H_\tau$  are definitely less than  $H_\eta$ , the ratio of  $H_\eta$  and  $H_\tau$  being as 1.35. This result is in conformity with the view of Franklin *et al* (1950). They determined the activation energies  $H_\tau$  of *n*-octyl bromide in heptane, cyclohexane and hexadecane and found that  $H_\tau$  is nearly equal to  $H_\eta$  only in Heptane which has slightly lower viscosity. The potential barrier height  $H_\eta$  is always higher than  $H_\tau$ , because while in the process of viscous flow both rotation and translation are involved, the process of dipole orientation involves only rotation.

## ACKNOWLEDGMENT

The authors express their sincerest gratitude to Dr. P. N. Sharma, Head of the Department, for his interest in the work and to Dr. M. C. Saxena, for his constant guidance and valuable suggestions.

## REFERENCES

- Bhanumati, A., 1963, *Ind. J. Pure Appl. Phys.*, **1**, 148.  
 Dakin, T. W., and Works, C. N., 1947, *J. Appl. Phys.*, **18**, 789.  
 Debye, P., 1929, *Polar Molecules*, Reinhold Publishing Corp, New York.  
 Eyring, H., Glasstone, S., and Laidler, K. J., 1941, *The Theory of Rate Process*, McGraw-Hill Co., New York, pp. 548.  
 Franklin, A. D., Heston, W. M., Hennelly, E. J., and Smyth, C. P., 1950, *J. Amer. Chem. Soc.*, **72**, 3447.  
 Gopala Krishna, K. V., 1957, *Trans. Farad. Soc.*, **53**, 767.  
 Hill, N. E., 1954, *Proc. Phys. Soc.*, **67**, 149.  
 Meakins, R. J., 1958, *Proc. Phys. Soc.*, **72**, 283.  
 Pitt, D. A., and Smyth, C. P., 1959, *J. Amer. Chem. Soc.*, **81**, 783.  
 Roberts, S., and von Hippel, A., 1946, *J. Appl. Phys.*, **17**, 610.  
 Sobhanadri, J., 1959, *Ind. J. Phys.*, **33**, 511.  
 Vaughan, W. E., Purcell, W. P., and Smyth, C. P., 1961, *J. Amer. Chem. Soc.* **83**, 571.

# HALL MOBILITY OF TELLURIUM FILMS DEPOSITED ON $\text{BaTiO}_3$ CRYSTAL

A. K. CHOUDHURI AND S. K. DUTTA ROY

DEPARTMENT OF PHYSICS, INDIAN INSTITUTE OF TECHNOLOGY, KHARAGPUR, INDIA

(Received January 15, 1965)

**ABSTRACT.** The measurements of electrical resistivity and Hall coefficient of tellurium films deposited on polarised barium titanate single crystals have been reported; the results on glass and mica substrate are also included for comparison. The results yield a value of surface state density for tellurium to be  $15 \times 10^{14}/\text{cm}^2$  volt and the energy of the surface states 0.09 e.v. below the mid gap position.

## INTRODUCTION

The surface properties of a semiconductor are generally determined from the field effect experiments on evaporated layers of films deposited on glass and mica substrate. It has been observed that if the thickness of the film is of the order of the space charge layer ( $10^{-4}$  to  $10^{-5}\text{cm}$ ), then with the application of a transverse electric field to the surface, part of the induced electric charge is trapped by the surface levels and other part changes the carrier density in the space charge region. At the same time an interaction between the space charge layer of the upper and lower surfaces introduces a large scattering of the carriers and the conductivity and Hall mobility of the film become less than the bulk value.

Recently Aigrain *et al* (1952), Godefroy (1956), and Ghosh (1961) have made detailed investigations of field effect of tellurium films deposited on mica and glass substrate. They have shown that there is a large decrease in field and Hall mobility with the decreasing thickness of the film and this is due to the inclusion of more defects in the thinner films. But it is quite noticeable that the field mobility measurement is more reliable. The changes in Hall mobility with transverse electric field (upto 500 volts/cm) are very small and almost of the order of experimental accuracy.

This paper reports the Hall effect and conductivity measurements of tellurium films deposited on a ferroelectric crystal instead of glass substrate. The film is exposed to intense localised electric field at the semiconductor substrate contact. This would materially affect the density and scattering of the carriers and the changes in Hall mobility would be very large, not only increasing the reliability and sensitivity of the measurements but also the effect of the ferroelectric property of the crystal would be reflected on the results and this property

of the crystal could be easily observed if the polarization of the crystal is gradually increased to saturation. An experiment of this nature has as yet attracted limited attention.

### EXPERIMENTAL

Tellurium films on  $\text{BaTiO}_3$  substrate was prepared using a conventional vacuum coating apparatus. The thicknesses of the films were about  $0.7\mu$  and were determined by the graphical method (Nandi, 1954). The dimension of the films were  $1.0 \times 0.5 \times 7.10^{-5}$  cm. As it is known that the adsorption of a gas on the surface of a semiconductor affects the surface barrier, causing large changes in surface conductance, the films were therefore removed to the experimental chamber within few minutes after preparation and aging of the films were done for more than twenty four hours until the constancy in resistivity was reached. In this way any contamination due to nitrogen and oxygen from air was precluded. The vacuum within the experimental chamber was as low as  $10^{-4}$  to  $10^{-5}$  mms. of mercury. A heater and a Cu-constantan thermocouple were provided in the experimental chamber in order to measure the temperature and also to keep the sample at different fixed temperatures of the bath.

The voltage and current measuring circuits were constructed following the standard circuit given by Pugh and Foner (1953). The Hall and resistive voltages were of the order of 100 microvolts; this was measured very easily with a micro-volt potentiometer with a Liston-Becker chopper amplifier and a wide scale millivoltmeter as output meter. In this arrangement a voltage of the order of

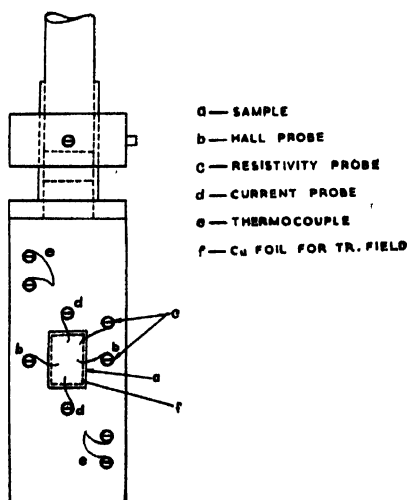


Fig. 1. Sample holder.

$0.1 \mu V$  could be measured. In Hall effect measurement, always the special feature is the construction of a suitable sample holder; the major difficulty

appears at the contact probes, which have a tendency to scratch out the film. After several preliminary trials this difficulty was finally removed by making a sample holder from syndanio board in which phosphor bronze springs were incorporated at predetermined distances (Fig. 1). These springs not only made automatic electrical contacts of current and Hall probes but also kept the sample rigidly in position. But for surity of good electrical contacts minute traces of aquadag were used at the contact points.

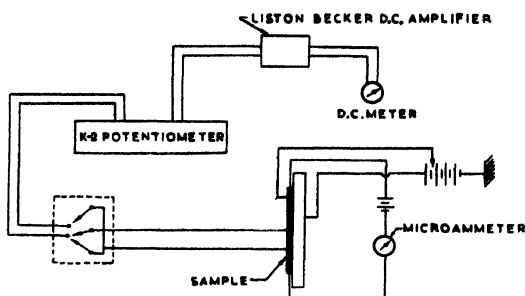


Fig. 2. Circuit diagram.

For field effect measurement (Fig. 2) a thin copper foil was placed underneath the flat face of  $\text{BaTiO}_3$  crystal. This arrangement formed a parallel plate condenser with the tellurium film as the top plate and copper foil as the bottom plate with  $\text{BaTiO}_3$  as dielectric. The electric field could then be applied across the crystal and polarisation of the crystal could be effected by increasing the electric

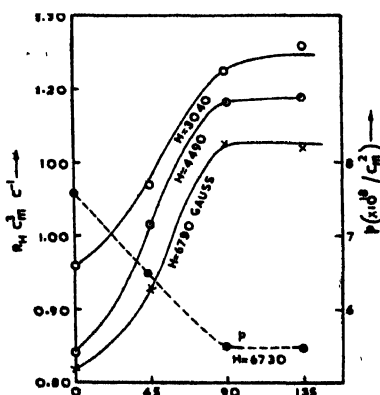


Fig. 3. Variation of  $R_H$  and hole density with transverse electric field.

field at a step of 15 volts upto 220 volts. Arrangements were also provided for depolarising the crystal so that fresh sets of measurements could be taken. The apparatus was standardised with spec pure (Johnson and Matthey) copper foil.



The Hall coefficient at 300°K was found to be  $-5.4 \times 10^{-13}$  volt cm. amp $^{-1}$  gauss $^{-1}$ . This is within one percent of the value quoted by Jan (1955). The electromagnet was of aircooled type and the maximum field for 1.5" pole gap was limited to 8000 gauss. The magnet field was calibrated with a fluxmeter to within one percent.

## RESULTS AND DISCUSSION

Fig. 3 shows the variation of Hall coefficient  $R_H$  and  $P$  (hole density/cm $^2$ ) as a function of the applied field. The number of carriers rapidly decrease with increasing polarisation of the crystal. The magnitude of Hall coefficient for films of tellurium on glass and BaTiO $_3$  substrates (deposited from the same  $p$  type bulk sample) of comparable thickness is different;  $R_H$  is larger in glass substrate almost by a factor of 1.5 (Godefroy's (1956) result with mica substrate is higher than the values of glass and BaTiO $_3$  substrate). This difference is due to the contact of three different dielectrics on the surface of tellurium; this contact difference modifies the structure of tellurium and perhaps the surface states are also altered.

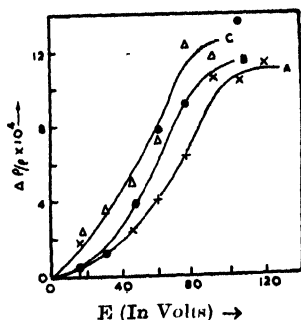


Fig. 4. Variation of  $\Delta\rho/\rho$  with applied transverse electric field.

Fig. 4 shows the variation of resistivity with applied electric field. The curves A, B, C are obtained after depolarising the BaTiO $_3$  crystal in quick succession by applying transverse A.C. voltage. The curves are almost similar in nature,

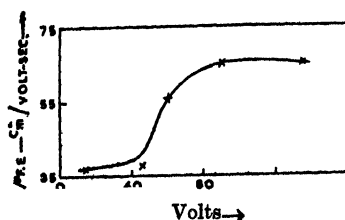


Fig. 5. Variation of field mobility with transverse electric field.

only the saturation field of the crystal is different by about 10 volts. The crystal comes back to its initial unpolarised condition after about twenty four hours.

The field mobility (Fig. 5) is calculated from the expression :

$$\mu_F = \frac{d\Delta\sigma}{dQ}$$

Where  $\Delta\sigma$  is the change in conductivity per unit area of the surface and  $Q$  is the charge induced on the surface.  $dQ$  is found out from the measurement of applied voltage, dimension of the specimen and the capacity between the film and the field plate; the capacity is quite high in the present case because of the high dielectric constant of  $\text{BaTiO}_3$  crystal. This is a particular advantage over the glass substrate samples, because the  $\text{BaTiO}_3$  substrate introduces a reliability in the measurement of capacity which is a common source of error in field effect experiments. The field mobility increases at higher fields. The lowest value of field mobility is higher by a factor of three from the values quoted by Ghosh (1961) for glass substrate samples. The present values compare well with similar results on mica substrate (Godefroy, 1956).

The field mobility results can also be utilised in calculating the surface state density. Shockley and Pearson (1948) have shown that the surface state density of the films of a semiconductor is given by

$$N_s = 1.31 \times 10^{12} \left( \frac{\epsilon\mu}{LV\sigma} \right)^{\frac{1}{2}} \sigma \frac{\delta q}{\delta\sigma}$$

where the units are  $N_s/\text{cm}^2$  volt,  $\mu\text{cm}^2/\text{volt-sec}$ ,  $L$  cm,  $V$  in volts, and  $\sigma$  mhos,  $\delta q$  coulombs/ $\text{cm}^2$ ,  $\epsilon = 30.5$  for tellurium.  $N$  from the present results yields a value  $15 \times 10^{14}/\text{cm}^2$ . volt. This is about twenty times higher than the value for  $p$ -germanium quoted by Pearson and Shockley (1948). Our result is quite expected since tellurium is nearly metallic, so that the density of surface states should be higher than the corresponding value of  $p$ -Ge.

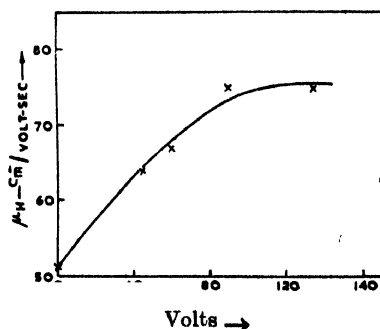


Fig. 6. Variation of Hall mobility with transverse electric field.

Fig. 6 shows the variation of Hall mobility  $\mu$  with applied field.  $\mu$  increases with increasing polarisation of the  $\text{BaTiO}_3$  crystal. Hall mobility is also higher than the field mobility. Both these suggest that the increasing number of

carriers are made to conduct in the space charge layer due to the large scattering of the carriers. It is also interesting to note that the magnetic field variation also shows a large change of  $R_H$  (Fig. 7). This variation is small in glass substrate; but in  $\text{BaTiO}_3$  this variation increases with increasing polarisation of the crystal. The calculation of mean free path from Hall mobility data yields a value of  $10^{-6}$  cm at  $300^\circ\text{K}$ . This is quite small in comparison to the thickness of the film and the size effect of the type suggested by Sondheimer (1950) is not expected. But the nature of magnetic field variation resembles Sondheimer's field variation curves

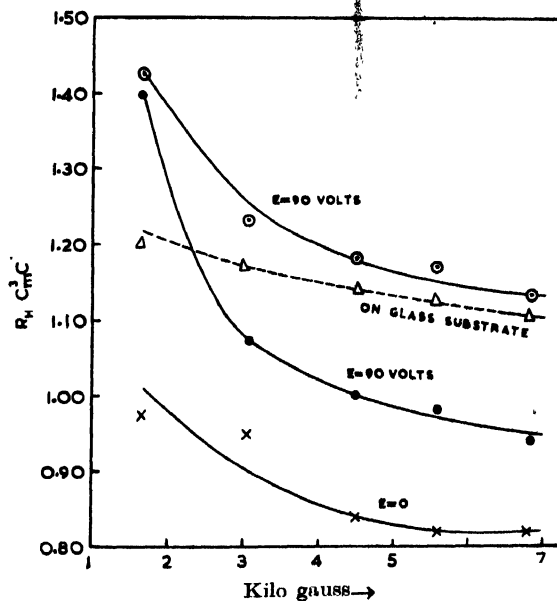


Fig. 7. Variation of  $R_H$  with  $H$ .

for diffuse scattering, though such a large magnitude of field variation (particularly at the saturation field of the crystal) is not accounted for on the basis of Sondheimer's theory alone. This result is at present not well understood.

The ratio  $\mu_H/\mu_F$  shows a slight variation almost of the order of experimental errors. Our value is smaller by a factor of three from the results quoted by

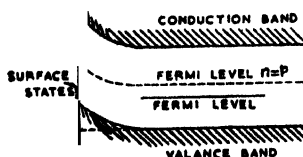


Fig. 8. Band representation showing position of the energy bands at the surface.

Ghosh (1961) on glass substrate. Using the expression for surface state energy as deduced by Godefroy<sup>(2)</sup> (1956) on the basis of discrete energy levels associated

with the surface, the energy of the surface states  $\eta$  as measured from the mid gap position at the surface, yields a value 0.09 e.v. below the mid gap position (Fig. 8). This differs with the value of  $\eta$  in glass substrate as 0.10 e.v. and in mica 0.08 e.v. above the middle of the forbidden energy gap.

The ferroelectric loop of  $\text{BaTiO}_3$  crystal is observed in Hall effect and conductivity results, particularly the onset of saturation beyond 90 volts is clearly indicated in Figs. 4 and 5. The conductance and Hall coefficient variations are proportional to the induced charge hence to the polarisation  $P$ ; both  $R$  and  $\Delta\sigma$  are therefore functions of polarisation.

#### ACKNOWLEDGMENT

The authors are indebted to Prof. H. N. Bose for suggesting the problem and also to Dr. G. B. Mitra and Dr. A. L. Laskar for many helpful discussions.

#### REFERENCES

- Aigrain, P. *et al.*, 1952, *J. Phys. Radium*, **13**, 587.  
Ghosh, S. K., 1961, *Phys. Chem. Solids*, **19**, 61.  
Godefroy, L., 1956, *Prog. in Semiconductors*, **1**, 197.  
Nandi, S., 1954, *Rev. Sci. Inst.*, **25**, 523.  
Jan, J. P., 1955, *Solid State Phys.*, **5**, 1.  
Pugh, E. M. and Foner, S., 1953, *Phys. Rev.*, **91**, 20.  
Pearson, G. L. and Shockley, W., 1948, *Phy. Rev.*, **74**, 232.  
Sondheimer, E. H., 1950, *Phy. Rev.*, **80**, 401.

# HALL EFFECT IN SINGLE CRYSTALS OF GRAPHITE

R. BHATTACHARYA

DEPARTMENT OF MAGNETISM,

INDIAN ASSOCIATION FOR THE CULTIVATION OF SCIENCE,

JADAVPUR, CALCUTTA-32.

**ABSTRACT.** In view of the apparent differences in the results of Hall effect measurements on natural single crystals of graphite by different workers, it has been remeasured with some good crystals before and after the usual chemical purificatory treatments, adopting some special techniques. It has been shown that the Hall coefficient which is more or less independent of the magnetic field before the chemical treatments, shows irregular variations with magnetic field after these treatments and that such irregularities are beyond the limits of experimental errors. Possibility of these anomalies being associated with misalignments produced by chemical treatments has been indicated.

## INTRODUCTION

Recent studies on the Hall effect in single crystals of graphite by Kinchin (1953), Berlincourt and Steele (1955) and Soule (1958) are very important since they could utilise their observations for deducing different electronic parameters of graphite and indicating (Soule 1958) the existence of new types of carriers in it. Kinchin observed that in cases of all the three specimens of single crystals studied by him, Hall coefficient at room temperatures remained always negative and independent of magnetic field down to about 600 oersteds. Soule on the other hand observed that in case of one of the two specimens studied by him Hall coefficient remained negative and practically independent of magnetic field down to about 350 oersteds then began to decrease very sharply and became positive at about 300 oersteds continuing to rise sharply with further decrease of field. But in the case of the other specimen the coefficient remained always negative and practically independent of field down to very low fields (of the order of 100 oersteds). It may be mentioned here that Soule had eleven different specimens at his disposal and he classified them according to their purities on the basis of magnetoresistance measurements but utilised for Hall effect measurements only two which are not the purer ones. The reason for this might be the fact that these two crystals behaved more or less similarly so far as magnetoresistance was concerned. Berlincourt and Steele who confined their measurements in the liquid helium range only and at magnetic fields from 6 to 25 kilo-oersteds obtained an oscillatory field variation of Hall coefficient like Soule under similar conditions of temperature and field but no such behaviour was observed

by Kinchin at similar temperatures and upto the maximum field (10 kilo-oersteds\*) used by him. Again, while Berlincourt and Steele (1955) obtained a negative coefficient for the average field variation of the Hall coefficient at temperatures of liquid helium, that obtained by Soule (1958) under similar conditions is positive and in the case of Kinchin (1953) the Hall coefficient which was always negative at these temperatures first increased with field and then decreased with the further increase of field. Besides these the sign of the Hall coefficient is found by Soule to change from negative to positive for both the specimens at low temperatures and moderate fields and for one specimen at room temperature and very low fields. These low field variations are very important in view of some theoretical predictions (Soule 1958) and need careful consideration. Further, the specimens of natural crystals of graphite used by these authors are subjected to the usual purificatory treatments to remove all foreign impurities which, as has been pointed out by Ray (1959), considerably enhances the mosaicity in structure already present to some extent in these natural crystals, and thereby affects the electrical and magnetic properties appreciably (Bhattacharya, 1959). It is therefore natural to expect that Hall effect in graphite is also affected by these structural defects.

In view of what has been stated above it appears therefore desirable to re-measure the Hall effect in graphite in order to obtain a set of values free from the said apparent contradictions so that the data can safely be utilised for discussion in the light of different theories proposed. The present paper gives an account of these measurements at room temperatures and at moderate fields. The observations at low temperatures which are in progress will be discussed in a subsequent paper.

#### EXPERIMENTAL

The measurements described in this paper were taken with some flakes of well developed single crystals of graphite obtained from Ceylon as also with some thin pieces of extruded samples of graphite having the direction of extrusion either parallel or perpendicular to the plane of the specimen. These specimens were cut into rectangular shapes before mounting them in the requisite holders for Hall effect measurements, taking care that no fresh structural defects are introduced by these cutting and manipulation processes.

It may be mentioned here that for avoiding shorting effect in Hall effect measurements it is essential that the specimens should be cut so as to have their length to breadth ratio not less than 4 (Fig. 1) (Isenberg *et al*, 1948). Since in the present investigation it was not convenient to cut the samples in this manner, we avoided this difficulty by designing our holder in such a way that the distance between the Hall probes can be altered easily. By this process the ratio of the

---

\*From the curves published by Berlincourt and Steele and by Soule it is found that the oscillations are distinctly observable from fields of about 6.5 kilo-oersteds and at about 10 kilo-oersteds these are very prominent.

distance between the two current contacts at the two ends of the specimen to that between the Hall probes can easily be made 4. To be sure that by this process we are able to avoid the shorting effect we measured with such a holder the Hall coefficient of a piece of very pure bismuth for different distances between the Hall probes. The results are represented in Fig. 1 wherefrom it can be seen that the experimental points follow the same curve as that of Isenberg *et al* (1948) and that

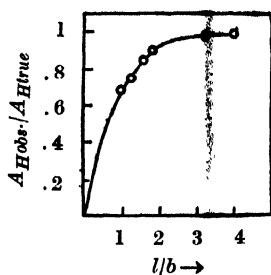


Fig. 1. Variation of Hall Coefficient with different length( $l$ ) to breadth ( $b$ ) ratios. Full line curve is due to Isenberg and the points are from our observations. In our case the abscissa represents the ratio between  $l$  and distance between Hall probes  $\delta$ .

the actual value of the Hall coefficient of bismuth is obtained when the ratio of the distance between current contacts to that between Hall probes is about 4. Under this arrangement the Hall coefficient  $A_H$  is given by

$$A_H = \frac{\Delta V \cdot t}{H \cdot i} \cdot \frac{b}{\delta} \quad 10^9 \text{ c.g.s. e.m.u.}$$

where  $\Delta V$  is the Hall e.m.f. in volts,  $i$  the current through the sample in amperes,  $H$  the magnetic field in oersteds, and  $t$ ,  $b$ , and  $\delta$  are the thickness and the breadth of the sample, and the separation between the Hall probes, respectively, in centimeters.

Hall e.m.f.'s have been measured upto magnetic fields of about 7500 oersteds with a Pye precision vernier potentiometer reading down to 1 micro-volt. The superimposed magnetoresistance, thermal and thermomagnetic effects have been eliminated in the usual way. The magnetic field was kept steady within 1 part in 1000 of any particular value by the manual operation of a fine motion accurate rheostat utilising a standard ammeter reading down to  $10^{-2}$  amperes, the corresponding field being measured with the help of the magneocrystallic anisotropy of a paramagnetic crystal, so that an accuracy of 0.1 per cent (Dutta Ray, 1954) is obtained. The current through the sample was measured by observing the potential drop across a standard one ohm resistance connected in series with the crystal. The thicknesses of the specimens were measured with a standard micrometer and the lengths and breadths with a travelling microscope accurately to one hundredth of a millimeter. In consequence, for different samples, at a given field the values of the Hall coefficients are subjected to a maximum error

of about 5 per cent and the corresponding limit of error in the study of magnetic field variation of the coefficient for a given sample is about 0.3 per cent.

Measurements with each sample of natural graphite crystal was undertaken before and after purification. The process of purification was the same as already described (Ray, 1959). The extruded samples however were not subjected to such purificatory treatments.

In addition to these observations an experiment was performed with a block of graphite made by stacking a number of graphite flakes one above the other and applying pressure on them. Current was passed perpendicular to the layers keeping the magnetic field transverse to the direction of current and Hall probes were placed midway between the two current contacts. The data obtained from observations with such a specimen will no doubt be far from reliable but the sign of Hall coefficient for current perpendicular to the basal plane will obviously be obtained with reasonable amount of definiteness. Experiment was also performed with a plate formed by pressing graphite powder.

#### RESULTS AND DISCUSSIONS

Fig. 2 represents the results of observations with single crystals of graphite before and after chemical purificatory treatments and Fig. 3 those with extruded samples, compressed plate of graphite powder and *c*-axis compact of natural flakes.

It is observed in cases of single crystals that before purification the Hall coefficient is on the average practically independent of magnetic field within the range of fields used, except in one or two cases at higher and lower extremities of the field. But after the usual purification has been done the Hall coefficient in every case vary with the magnetic field, the type of variation being quite different for different samples (see Fig. 2).

In order to explain these irregularities one may be tempted to associate such behaviours with the mosaicities in structure which, as is well known, (Ray, 1959) develop due to the chemical purification processes undertaken to remove foreign impurities from natural graphites. But before accepting such a view we took measurements with some polycrystalline samples of graphite. An extruded sample of graphite with currents parallel to the direction of extrusion, whose electrical conductivity for this direction has more or less the same value as that in the basal plane of a crystal, behaves similarly as an unpurified natural single crystal (Figs. 2 and 3). But with direction of current perpendicular to that of extrusion, in which case the number of misoriented crystalline blocks affecting the electrical resistivity will obviously be larger than in the earlier case, Hall coefficient is again seen to vary like those of purified samples of single crystals (Figs. 2 and 3). The compressed powdered sample which is evidently a highly defective crystal or a polycrystal also shows a variation of the Hall coefficient with field (Fig. 3). One



may therefore suggest that these irregularities in the field variation of Hall coefficient are in some way connected with the crystalline defects. However, to establish a quantitative relation between the defects and the deviations from the normal field variation of Hall coefficient a detailed knowledge of the number of

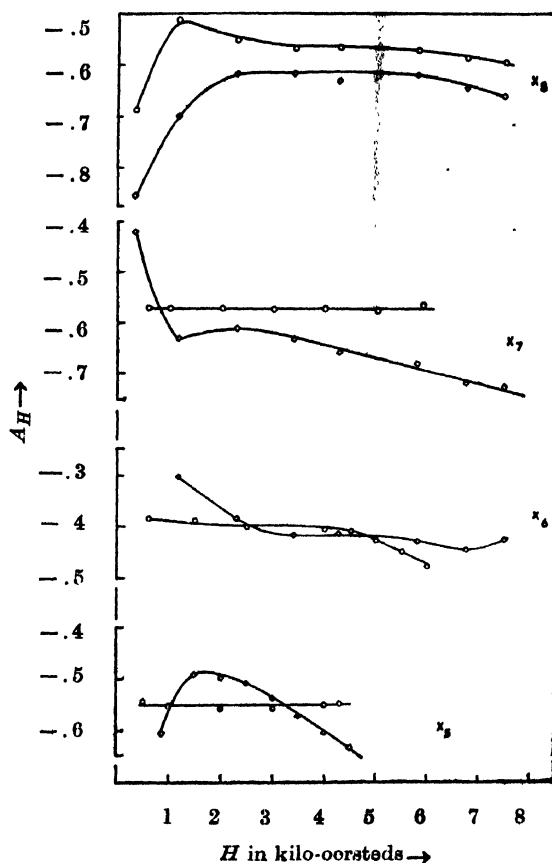


Fig. 2. Magnetic field variation of Hall coefficient of single crystals,  $X_5$ ,  $X_6$ ,  $X_7$  and  $X_8$  before and after chemical treatments.

O — Before chemical treatment  
 □ — After chemical treatment.

misoriented blocks with a particular value of misorientation and the manner in which these can affect the Hall effect is evidently necessary. This indeed is very difficult. However we are trying to do this by utilising the method we have developed for the purpose of finding the values of electrical conductivities and the magnetic susceptibilities of perfect crystals of graphite from a study of these properties of defective ones.

In this connection it would be interesting to reproduce here (Fig. 4) the room temperature observations of a some what similar nature by Soule (1958) who alone

among the earlier workers made such observations. His specimens were, as already pointed out, defective. These irregularities as also their behaviour at low temperatures were explained by him as being due to the presence of some new types of carriers in graphite.

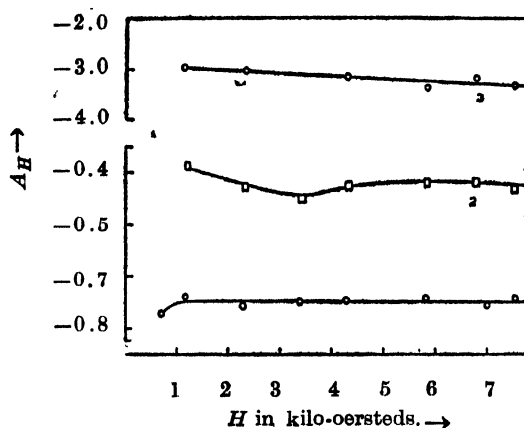


Fig. 3. Magnetic field variation of Hall coefficient of extruded and compressed samples.

Curve 1—extruded sample, direction of extrusion  $\parallel$  to the plane.

„ 2— „do- „  $\perp$  to the plane

„ 3—plate formed of compressed powder.

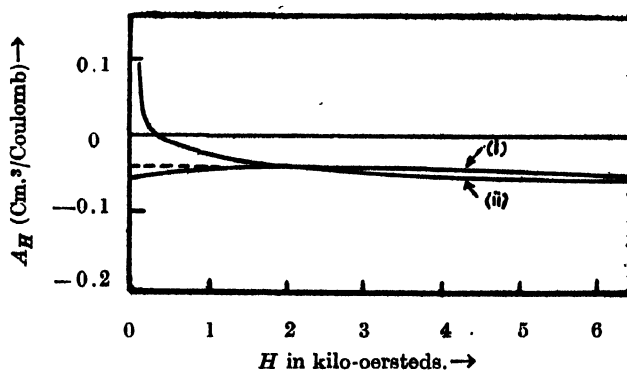


Fig. 4. Magnetic field variation of Hall coefficient of single crystals at room temperatures by Soule.

Curve 1—Specimen  $EP_{14}$

„ 2—Specimen  $EP_7$ .

It therefore becomes apparent that these irregularities which we intend to associate with crystalline defects should also be studied at low temperatures before any definite conclusion is drawn. Work is in progress in this line and the results will be published soon.

It may be mentioned finally that the sign of the Hall coefficient has been found by us to be negative at all fields with all the different types of samples (single crystals, extruded samples, c-axis compact and powdered sample) studied.

## ACKNOWLEDGMENT

In conclusion the author wishes to express his best thanks to Shri A. K. Dutta for suggesting the problem and guidance throughout the course of the work and to Prof. A Bose for his kind interest in the work. Thanks are also due to Mr. L. J. D. Fernando of the Geological Survey Department, Government of Ceylon for kindly presenting us with some crystals of graphite with which some of the measurements described in this paper have been made. The author is also grateful to Prof. E. W.J. Mitchel of the University of Reading for the extruded samples of graphite and to the Workshop of the Association for kindly constructing the different measuring units required in course of these investigations.

## REFERENCES

- Berlincourt T. G. and Steele M. C. 1955, *Phys. Rev.* **98**, 956.  
Bhattacharya R. 1959, *Ind. Jour. Phys.* **33**, 407.  
Dutta Roy S. K. 1954, *Ind. Jour. Phys.* **28**, 183.  
Isenberg I., Russel B. R. and Greene R. F. 1948, *Rev. Sci. Instrum.* **19**, 685.  
Kinchin G. H. 1953, *Proc. Roy. Soc.* **A217**, 9.  
Ray S. 1959, *Ind. Jour. Phys.* **33**, 282.  
Soule D. E. 1958, *Phys. Rev.* **112**, 698.

# CRYSTALLOGRAPHIC DATA FOR NICKEL AND COBALT BIURET COMPLEXES

S. K. GHOSH, R. M. SANYAL AND B. K. BANERJEE

PLANNING AND DEVELOPMENT DIVISION  
FERTILIZER CORPORATION OF INDIA LTD., SINDRI, BIHAR

(Received February 19, 1965)

**ABSTRACT.** The crystallographic properties of nickel biuret and cobalt biuret complexes have been studied by means of X-ray diffraction data. The powder diffraction data showed that both the complexes belong to the monoclinic system. The cell dimensions for nickel biuret is  $a = 10.08 \text{ \AA}$ ,  $b = 9.82 \text{ \AA}$ ,  $c = 4.31 \text{ \AA}$  and  $\beta = 101^\circ 18'$ , while that of cobalt biuret is  $a = 6.06 \text{ \AA}$ ,  $b = 11.05 \text{ \AA}$ ,  $c = 11.23 \text{ \AA}$ , and  $\beta = 110^\circ 55'$ . The systematic extinctions observed are consistent with the space group  $P2_1/a$  with two molecules per unit cell for nickel biuret and  $P2_1/c$  with two molecules per unit cell for cobalt biuret.

## INTRODUCTION

Biuret is an organic compound derived from the products of the thermal decomposition of urea or urea nitrate. Because of its poisonous effect on some plants its presence in urea used as fertilizer is undesirable.

Schiff (1896) first reported the formation of chelate complexes of biuret with Cu and Ni salts. These complex formations subsequently serves a very useful method for the estimation of biuret in a very low concentration in urea. It has also been found that biuret can be estimated most satisfactorily by complex formation with Co-salts (Sanyal and Pal, 1964). The behaviour of chelating molecules and chelate complexes could ultimately be understood if the structure of the molecules are known in detail. Such question as the specificity (or the lack thereof) of a chelating molecule, for inorganic ions, solubility, stability of the salts formed and many other physical properties could be easily answered only when the exact structures are known.

In order to explain such factors a preliminary investigation on the crystallographic properties of these complex salts have been undertaken.

## EXPERIMENTAL

The nickel and cobalt biuret complex samples were prepared in accordance with the method followed by the previous workers in this laboratory (Sanyal and Pal, 1964). The samples were recrystallized from aqueous solution.

X-ray diffraction patterns of the above samples were obtained in Phillips X-ray diffractometer PW1050/51 with Geiger counter as detector. Filtered  $\text{CuK}_\alpha$  radiation and cobalt radiation with iron filter was used. The interplanar

distances of the lattices were calculated from the measurement on X-ray diffraction patterns with maximum accuracy.

The phase identification was done by the usual method of Hanawalt *et al* (1938).

*Interpretation of X-ray data :*

The X-ray data are given in Tables II and IV. The powder pattern was indexed by Ito's method (Ito, 1950 ; Azaroff and Buerger, 1953). The interplanar spacing and corresponding  $Q$  values ( $Q_{hkl} = 1/d_{hkl}^2$ ) are listed in Tables II and IV.

*Nickel biuret :*

The first three lines in the Tables II were first selected as  $Q_{100}$ ,  $Q_{010}$  and  $Q_{001}$ . Then the higher orders of these lines i.e.  $Q_{200}$ ,  $Q_{300}$  etc. were computed. An inspection of the observed  $Q$ 's failed to show the computed values for these higher orders of  $Q$  i.e.,  $Q_{200}$ ,  $Q_{300}$  etc. So it was decided to select other possible values for the pinacoidal  $Q$ 's. Accordingly, the first three lines were selected as  $Q_{200}$ ,  $Q_{020}$  and  $Q_{001}$ . It can be seen that the observed  $Q$ 's are in quite agreement with the calculated  $Q$  values for other higher orders of reflection.

TABLE I  
Selection of  $Q_{200}$ ,  $Q_{020}$  and  $Q_{001}$

$Q_{hkl}$	Computed	Observed	Error in $Q_{hkl}$
$Q_{200}$		.0359	
$Q_{400}$	.1438	.1449	+ .0011/4 = + .0002
$Q_{600}$	.3235	.3235	
$Q_{020}$		.0412	
$Q_{040}$	.1649	.1666	+ .0017/4 = + .0004
$Q_{060}$	.3711		
$Q_{001}$		.0541	
$Q_{002}$	.2163	.2200	+ .0037/4 = + .0009
$Q_{003}$	.4867		

From the table it can be seen that

$$Q_{200} = .0359 + .0002 = .0361 = 2a^{*2}$$

$$Q_{020} = .0412 + .0004 = .0416 = 2b^{*2}$$

$$Q_{001} = .0541 + .0009 = .0550 = c^{*2}$$

The dimensions of the reciprocal cell then becomes,

$$a^* = .0948 \quad \alpha^* = 90^\circ$$

$$b^* = .1019 \quad \beta^* = 78^\circ 41'$$

$$c^* = .2345 \quad \gamma^* = 90^\circ$$

Finally the other  $Q_{hkl}$  values were determined using the equation,

$$Q_{hkl} = h^2 a^{*2} + k^2 b^{*2} + l^2 c^{*2} = 2hka^*b^* \cos \gamma + 2klb^*c^* \cos \alpha^* + 2lhc^*a^* \cos \beta^* \quad (1)$$

TABLE II

Final agreement of observed and computed  $Q_{hkl}$  's for nickel biuret complex

Powder diagram line	$d\text{\AA}$	$Q$ observed	$Q$ computed	$hkl$
1.	5.275	.0359	.0361	200
2.	4.925	.0412	.0416	020
3.	4.300	.0541	.0550	001
4.	3.910	.0654	.0654	011
5.	3.690	.0734	.0734	201
6.	3.427	.0851	.0812	111
7.	3.340	.0896	.0916	310
8.	3.230	.0959	.0966	021
9.	3.160	.1001	.1034	421
10.	3.122	.1026	.1026	130
11.	3.040	.1082	.1082	201
12.	3.000	.1111	.1124	121
13.	2.866	.1217	.1228	320
14.	2.820	.1257	.1297	230
15.	2.772	.1301	.1304	402
16.	2.730	.1342	.1310	132
17.	2.627	.1449	.1438	400
18.	2.522	.1572	.1548	410
19.	2.450	.1666	.1649	040
20.	2.400	.1736	.1748	330
21.	2.327	.1847	.1830	122
22.	2.242	.1989	.1980	321
23.	2.217	.2035	.2025	240
24.	2.132	.2200	.2163	002
25.	2.069	.2336	.2304	012
26.	2.045	.2391	.2372	141
27.	1.930	.2685	.2678	421
28.	1.824	.3006	.2936	212
29.	1.758	.3235	.3235	600
30.	1.681	.3539	.3522	312
31.	1.605	.3882	.3864	042

The direct cell dimensions are as follows :

$$\begin{array}{ll} a = 10.68 \text{ \AA} & \alpha = 90^\circ \\ b = 9.82 \text{ \AA} & \beta = 101^\circ 18' \\ c = 4.31 \text{ \AA} & \gamma = 90^\circ \end{array}$$

The crystal therefore belongs to the monoclinic system. The indexed powder pattern showed the following systematic extinctions.

1.  $0k0$  absent when  $k$  is odd.
2.  $h00$  absent when  $h$  is odd.
3.  $h0l$  absent when  $h$  is odd.

The space group indicated by these data is  $P2_1/a - C^5_{2h}$ .

The observed density of  $2.653 \text{ gm cm}^{-3}$  indicates 2 molecules per unit cell; calculated density =  $2.54 \text{ gm cm}^{-3}$ . The molecules must be centro-symmetrical with nickel atom at symmetry centres.

*Cobalt biuret :*

In this case first three lines in Table IV was selected as  $Q_{100}$ ,  $Q_{020}$  and  $Q_{002}$ . It can be seen that the observed  $Q$ 's are in quite agreement with the calculated  $Q$  values for other higher orders of reflection.

TABLE III  
Selection of  $Q_{100}$ ,  $Q_{020}$  and  $Q_{002}$

$Q_{hkl}$	Computed	Observed	Error in $Q_{hkl}$
$Q_{100}$		.0312	
$Q_{200}$	.1248	.1245	-.0003/4 = -.0000
$Q_{300}$	.2809	.2805	-.0004/9 = -.0000
$Q_{020}$		.0329	
$Q_{040}$	.1317	.1322	+.0005/4 = +.0001
$Q_{060}$	.2964	.2980	+.0016/9 = +.0001
$Q_{002}$		.0365	
$Q_{004}$	.1459	.1457	-.0002/4 = -.0000
$Q_{006}$	.3284	.3280	-.0004/9 = -.0000

From the table it can be seen that,

$$\begin{aligned} Q_{100} &= .0312 + .0000 = .0312 \\ Q_{020} &= .0329 + .0001 = .0330 \\ Q_{002} &= .0364 + .0000 = .0365 \end{aligned}$$

TABLE IV

Final agreement of observed and computed  $Q_{hkl}$  's for cobalt biuret complex

Powder diagram lines	$d\text{\AA}$	$Q$ observed	$Q$ calculated	$hkl$
1.	5.660	.0312	.0312	100
2.	5.510	.0329	.0330	020
3.	5.235	.0364	.0364	002
4.	5.036	.0394	.0394	110
5.	4.990	.0401	.0400	20 $\bar{2}$
6.	4.890	.0419	.0419	021
7.	4.820	.0430	.0430	10 $\bar{2}$
8.	4.780	.0437	.0444	13 $\bar{2}$
9.	4.490	.0496	.0447	012
10.	4.420	.0511	.0481	21 $\bar{2}$
11.	4.160	.0577	.0606	111
12.	3.995	.0627	.0642	120
13.	3.645	.0753	.0728	222
14.	3.310	.0913	.0913	102
15.	3.260	.0941	.0903	013
16.	3.120	.1027	.1000	112
17.	3.060	.1068	.1050	130
18.	3.020	.1096	.1103	032
19.	2.834	.1245	.1248	200
20.	2.785	.1289	.1262	131
21.	2.750	.1322	.1320	040
22.	2.680	.1392	.1403	041
23.	2.620	.1457	.1459	004
24.	2.245	.1984	.1986	230
25.	2.214	.2040	.2096	202
26.	2.114	.2238	.2252	104
27.	1.888	.2805	.2808	300
28.	1.810	.3052	.3013	035
29.	1.796	.3100	.3122	223
30.	1.772	.3185	.3138	320
31.	1.745	.3284	.3284	006



The dimensions of the reciprocal cell thus becomes,

$$\begin{array}{ll} a^* = .1766 & \alpha^* = 90^\circ \\ b^* = .0905 & \beta^* = 69^\circ 4' \\ c^* = .0954 & \gamma^* = 90^\circ \end{array}$$

Finally the other  $Q_{hkl}$  values were determined using the equation (1).

The direct cell dimensions are as follows :

$$\begin{array}{ll} a = 6.06 \text{ \AA} & \alpha = 90^\circ \\ b = 11.05 \text{ \AA} & \beta = 110^\circ 55' \\ c = 11.23 \text{ \AA} & \gamma = 90^\circ \end{array}$$

In case of cobalt biuret complex the crystal belongs to the monoclinic system. The indexed powder pattern showed the following extinctions.

1. *oko* absent when *k* is odd.
2. *ool* absent when *l* is odd.
3. *hol* absent when *l* is odd.

The space group indicated by these data is  $P2_1/c - C^5_{2h}$ .

The observed density of  $2.542 \text{ gm cm}^{-3}$  indicates two molecules per unit cell; calculated density =  $2.436 \text{ gm cm}^{-3}$ .

#### ACKNOWLEDGMENT

Thanks are due to Dr. K. R. Chakravorty, General Manager, Planning and Development Division. for his constant encouragement and kind permission to publish this paper.

#### REFERENCES

- Schiff, H., 1896, *Ber* **29**, 296.  
 Bull of Indian Standard Institution IS 1781-1961 BS. 12.  
 Nowak, K, Jadwiga, W. and Nikiel S., 1964, *Chem. Abst.* **60**, 2292.  
 Sanyal, R. M. and Pal P. K., 1964, *Technology* **1**, 64.  
 Hanawalt, J. D. *et al*, 1938, *Ind. Eng. Chem.*, Anal. Ed. **10**, 457-512.  
 Azaroff, L. V. and Buerger M. J. 1958, *The powder method in X-ray crystallography.*  
 Mc Graw-Hill Book Co. Inc. 106-123.  
 Ito, I, 1950, *X-ray studies of Polymorphism*, Maruzen Co. Ltd., Tokyo, 187-228.

# LIGAND FIELD THEORY OF SUSCEPTIBILITY AND ANISOTROPY IN TRIGONALLY DISTORTED $\text{Fe}^{2+}$ COMPLEXES

A. BOSE AND R. RAI

DEPARTMENT OF MAGNETISM, INDIAN ASSOCIATION FOR THE CULTIVATION OF SCIENCE,  
CALCUTTA-32

(Received February 3, 1965)

**ABSTRACT.** Expressions for susceptibility and anisotropy of trigonally distorted  $\text{Fe}^{2+}$  complexes are deduced on the basis of the molecular orbital theory of Van Vleck (1935), Stevens (1953) and others (Bose *et al.*, 1960) and compared with the experimental results obtained by Mazumder *et al.*, (unpublished) and Jackson (1959) on  $\text{FeSiF}_6 \cdot 6\text{H}_2\text{O}$  consistently with structural and spectroscopic data. It is found that the spin-orbit coupling coefficients have to be decreased anisotropically from its free ion value indicating an anisotropic overlap between the central  $3d$  and ligand  $s$ - and  $p$ -charge clouds. The increase in trigonal field coefficient  $\Delta$  with temperature from a value of  $-1030 \text{ cm}^{-1}$  at  $7.85^\circ\text{K}$  to  $-350 \text{ cm}^{-1}$  at  $300^\circ\text{K}$  in  $\text{FeSiF}_6 \cdot 6\text{H}_2\text{O}$  is probably due to the thermal expansion and relaxation effects of the crystal lattice.

## INTRODUCTION

In  $\text{Fe}^{2+}$  Tutton salts the assumption of a small tetragonal ligand field, comparable in magnitude to the spin-orbit coupling, superposed upon the predominant cubic field acting upon these ions, is found to give reasonable agreement with magnetic susceptibilities and anisotropies (Bose *et al.*, 1961b). Pallumbo (1958) has tried to fit Jackson's (1959) susceptibility measurements of  $\text{FeSiF}_6 \cdot 6\text{H}_2\text{O}$  in the range  $2^\circ\text{K}$  to  $77^\circ\text{K}$  assuming a trigonal distortion of the field and with a formula based on the spin Hamiltonian approximation. This is not very satisfactory and also cannot explain quantitatively the detailed mean susceptibility and anisotropy measured recently in this laboratory. So we have deduced in the present paper expression for magnetic susceptibility and anisotropy of trigonally distorted  $[\text{Fe}^{2+}, 6\text{H}_2\text{O}]$  complex on the basis of molecular orbital theory of Stevens (1953) and Bose *et al.* (1960). The susceptibility measurements of Mazumder *et al.* (unpublished) and Jackson (1959) (accurate to better than 0.5%) have been used to evaluate the theoretical parameters. It may be mentioned here that this salt belongs to the trigonal class (Pauling, 1930) with a single trigonally distorted  $[\text{Fe}^{2+}, 6\text{H}_2\text{O}]$  octahedral complex in the unit cell, so that the principal ionic susceptibilities of this complex  $K_i$  ( $i = \parallel$  or  $\perp$  to the trigonal axis of the complex) can be directly obtained from the measured principal susceptibility values of the crystal.

MOLECULAR ORBITAL THEORY OF TRIGONALLY  
DISTORTED ( $\text{Fe}^{2+}, 6\text{H}_2\text{O}$ ) COMPLEX

Under an octahedral field of the type  $O_h$ ,  $3d^6$  ground state of the free ion  $\text{Fe}^{2+}$  splits up to the extent  $10580 \text{ cm}^{-1}$  (Agnetta *et al* 1962) into a triplet  ${}^5T_2$  and a doublet  ${}^5E$  arising out of the configurations (considering a system consisting of four  $d$  holes)  $(e_g)^2 (t_{2g})^2$  and  $(e_g)^1 (t_{2g})^3$  respectively. The triplet state  ${}^5T_2$  lies lowest, whose determinantal wavefunctions are (considering only the orbital part);

$$\begin{aligned}\psi_1 &= |e_a e_b t_b| \\ \psi_2 &= |e_a e_b t_c| \\ \psi_3 &= |e_a e_b t_a|\end{aligned} \quad \dots \quad (1)$$

which are inclusive of the overlap of the surrounding ligand  $s$ - and  $p$ -orbitals with central  $d$ -orbitals as given by :

$$\begin{aligned}t_a &= N \left[ d_{xy} + \frac{\lambda}{2} (\pi_{x1} + \pi_{y2} + \pi_{x5} + \pi_{y4}) \right] \\ t_b &= N \left[ d_{yz} + \frac{\lambda}{2} (\pi_{x2} + \pi_{y3} + \pi_{x6} + \pi_{y5}) \right] \\ t_c &= N \left[ d_{zx} + \frac{\lambda}{2} (\pi_{x3} + \pi_{y1} + \pi_{x4} + \pi_{y6}) \right] \\ e_a &= N' \left[ d_{x^2-y^2} + \frac{\lambda'}{2} (\sigma_1 + \sigma_4 - \sigma_2 - \sigma_5) \right] \\ e_b &= N' \left[ d_{3z^2-r^2} + \frac{\lambda'}{2\sqrt{3}} (2\sigma_3 + 2\sigma_6 - \sigma_1 - \sigma_4 - \sigma_2 - \sigma_5) \right]\end{aligned} \quad \dots \quad (2)$$

where  $N$ 's are normalizing constants,  $\lambda$ 's are the measure of the amounts of admixtures of the ligand  $s$ - and  $p$ -orbitals with the central  $d$ -orbitals. Here all  $\sigma$ -bonds are described by using  $z$ -coordinates; and  $\pi$ -bonds by using  $x$  and  $y$ -coordinates; all  $z$ -axes of the ligands pointing towards the metal atom.

The appropriate eigen states for the lowest triplet on quantization along the trigonal axis are

$$\begin{aligned}|+\rangle &= -\frac{1}{\sqrt{3}} [w|\psi_2\rangle + w^2|\psi_3\rangle + |\psi_1\rangle] \\ |0\rangle &= \frac{1}{\sqrt{3}} [|\psi_2\rangle + |\psi_3\rangle + |\psi_1\rangle] \\ |-\rangle &= \frac{1}{\sqrt{3}} [w^2|\psi_2\rangle + w|\psi_3\rangle + |\psi_1\rangle]\end{aligned} \quad \dots \quad (3)$$

where  $w = \exp\left(\frac{2\pi i}{3}\right)$  and  $\psi_1$  etc., are given by (1). The overlap of the surrounding ligand  $s$ - and  $p$ -orbitals with the central  $d$ -orbitals introduces two orbital reduction factors defined by Griffiths (1961)

$$\begin{aligned}\langle t_{2\mu} | l_{\lambda} | t_{2\mu'} \rangle &= \kappa \langle t'_{2\mu} | l_{\lambda} | t'_{2\mu'} \rangle \\ \langle t_{2\mu} | l_{\lambda} | e_{\mu'} \rangle &= \kappa' \langle t'_{2\mu} | l_{\lambda} | e'_{\mu'} \rangle \quad \dots \quad (4) \\ \langle e_{\mu} | l_{\lambda} | e_{\mu'} \rangle &= 0\end{aligned}$$

where  $t'_{2\mu}$  and  $e'_{\mu}$  are the original  $d$ -orbitals and  $t_{2\mu}$  and  $e_{\mu}$  are those admixed with the surrounding ligand orbitals.  $\kappa$  and  $\kappa'$  are orbital reduction factors generally unequal. On actual calculations of matrix element  $\langle \psi_m | \vec{L} | \psi_n \rangle$  it is seen that so long as we are confined only to  ${}^5T_2$  state of  $\text{Fe}^{2+}$ , only the factor  $\kappa$  is of importance since  $\kappa'$  does not occur, and the anisotropic reduction in  $\zeta_i$  ( $i = \parallel$  or  $\perp$  to the trigonal axis of the ion) the spin-orbit coupling parameter from its free ion value is mainly due to the overlap of  $\pi$ -orbitals with the central  $d$ -orbitals.

#### FINE STRUCTURE

It can be shown that the set  $|+\rangle$ ,  $|0\rangle$  and  $|-\rangle$  behaves as atomic  $P$ -state having  $l_z = 1, 0, -1$  respectively and so the appropriate Hamiltonian for the lowest triplet state of the ion is (Abragam and Pryce 1951)

$$H = V_{trig} - \alpha \zeta_{\parallel} L_z S_z - \alpha' \zeta_{\perp} (L_{\xi} S_{\xi} + L_{\eta} S_{\eta}) \quad \dots \quad (5)$$

where  $L_z$  is along the trigonal axis of the crystal and  $L_{\xi}$ ,  $L_{\eta}$ ,  $L_z$  form a mutually orthogonal right handed set.  $\alpha$  and  $\alpha'$  are the effective orbital Lande' factors (Abragam and Pryce, 1951; Bose *et al.*, 1961a) parallel or perpendicular to the trigonal axis, respectively, and includes the effect of the excited state  ${}^5E$  upon the lowest  ${}^5T_2$ ;  $\zeta_i$  ( $i = \parallel$  or  $\perp$  to the trigonal axis) is the spin-orbit coupling coefficient reduced from its free ion value of  $-106 \text{ cm}^{-1}$  due to covalency. Operating with the above Hamiltonian upon the atomic  ${}^5P$  term and solving we get the eigen values and the new wavefunctions as follows :

$$\begin{aligned}E_0 &= \frac{1}{2} [(\alpha \zeta_{\parallel} + \Delta) - \{(\alpha \zeta_{\parallel} - \Delta)^2 + 24\alpha'^2 \zeta_{\perp}^2\}^{\frac{1}{2}}] \\ E_1 &= \alpha \zeta_{\parallel} x_1 \\ E_2 &= \frac{1}{2} [(\Delta - \alpha \zeta_{\parallel}) - \{(\Delta + \alpha \zeta_{\parallel})^2 + 8\alpha'^2 \zeta_{\perp}^2\}^{\frac{1}{2}}] \\ E_3 &= \alpha \zeta_{\parallel} x_3 \\ E_4 &= \alpha \zeta_{\parallel} \quad \dots \quad (6)\end{aligned}$$

$$E_5 = \frac{1}{2} [(\alpha\zeta_{||} + \Delta) + \{(\alpha\zeta_{||} - \Delta)^2 + 24\alpha'^2\zeta_{\perp}^2\}^{1/2}]$$

$$E_6 = \alpha\zeta_{||}x_6$$

$$E_7 = \frac{1}{2} [(\Delta - \alpha\zeta_{||}) + \{(\Delta + \alpha\zeta_{||})^2 + 8\alpha'\zeta_{\perp}^2\}^{1/2}]$$

$$E_8 = -2\alpha\zeta_{||}$$

where  $x_j$ 's are the roots of cubic eqn. :

$$x^3 - x^2(2 + \delta) + (2\delta - 5\rho^2)x + 6\rho^3 = 0$$

$$\rho = \frac{\alpha'\zeta_{\perp}}{\alpha\zeta_{||}} ; \quad \delta = \frac{\Delta}{\alpha\zeta_{||}} , \quad (7)$$

and  $\Delta$  is the trigonal field separation between the split components (a doublet and a singlet) of the triplet  ${}^6T_2$ .

The corresponding eigenstates are :-

$$\phi_0 = a_0 |1, -1\rangle + b_0 |0, 0\rangle + a_0' |-1, 1\rangle$$

$$\phi_1 = a_1 |1, 0\rangle + b_1 |0, 1\rangle + c_1 |-1, 2\rangle$$

$$\phi_{1-} = a_1' |-1, 0\rangle + b_1 |0, -1\rangle + c_1 |1, -2\rangle$$

$$\phi_2 = b_2 |1, 1\rangle + a_2 |0, 2\rangle$$

$$\phi_{2-} = b_2' |-1, -1\rangle + a_2 |0, -2\rangle$$

$$\phi_3 = a_3 |1, 0\rangle + b_3 |0, 1\rangle + c_3 |-1, 2\rangle$$

$$\phi_{3-} = a_3' |-1, 0\rangle + b_3 |0, -1\rangle + c_3 |1, -2\rangle \quad \dots \quad (8)$$

$$\phi_4 = \frac{1}{\sqrt{2}} |1, -1\rangle - \frac{1}{\sqrt{2}} |-1, +1\rangle$$

$$\phi_5 = \frac{b_0}{\sqrt{2}} |1, -1\rangle - \sqrt{2}a_0 |0, 0\rangle + \frac{b_0'}{\sqrt{2}} |-1, +1\rangle$$

$$\phi_6 = a_6 |1, 0\rangle + b_6 |0, 1\rangle + c_6 |-1, 2\rangle$$

$$\phi_{6-} = a_6' |-1, 0\rangle + b_6 |0, -1\rangle + c_6 |1, -2\rangle$$

$$\phi_7 = a_2 |1, 1\rangle - b_2 |0, 2\rangle$$

$$\phi_{7-} = a_2 |-1, -1\rangle - b_2 |0, -2\rangle$$

$$\phi_8 = |1, 2\rangle$$

$$\phi_{8-} = |-1, -2\rangle$$

where

$$a_0 = \frac{\sqrt{3}\alpha'\zeta_{\perp}}{(\alpha\xi_{\parallel} - E_0)} b_0; \quad 2a_0^2 + b_0^2 = 1$$

$$a_j = -\frac{\sqrt{3}(2\alpha\xi_{\parallel} - E_j)}{\sqrt{2}E_j} c_j; \quad a_j^2 + b_j^2 + c_j^2 = 1 \quad \dots \quad (9)$$

$$b_j = \frac{2\alpha\xi_{\parallel} - E_j}{\sqrt{2}\xi} c_j \quad j = 1, 3, 6$$

and

$$a_2 = \frac{\sqrt{2}\alpha'\zeta_{\perp}}{\Delta - E_2} b_2; \quad a_2^2 + b_2^2 = 1$$

#### EXPRESSION FOR SUSCEPTIBILITY

As usual calculating the effect of the magnetic perturbations  $\beta H(-\alpha L + 2S)$  upto the second order, we get the expressions for principal magnetic susceptibility  $K_i$  ( $i = \parallel$  or  $\perp$  to the trigonal axis of the crystal) as given below :

$$\begin{aligned} K_{\parallel} = \frac{N\beta^2}{kW} \left[ \frac{1}{T} \left\{ \sum_{j=1,3,6} 2[\alpha\xi_{\parallel}(c_j^2 - a_j^2) + 2b_j^2 + 4c_j^2]^2 \exp\left(-\frac{E_j - E_0}{kT}\right) \right. \right. \\ + 2[b_2^2(2 - \alpha\xi_{\parallel}) + 4a_2^2]^2 \exp\left(-\frac{E_2 - E_0}{kT}\right) \\ + 2[a_2^2(2 - \alpha\xi_{\parallel}) + 4b_2^2]^2 \exp\left(-\frac{E_7 - E_0}{kT}\right) \\ \left. \left. + 2[(4 - \alpha\xi_{\parallel})^2] \exp\left(-\frac{E_8 - E_0}{kT}\right) \right\} \right. \\ \left. + 2k \left\{ \frac{2a_0^2(2 + \alpha\xi_{\parallel})^2}{E_4 - E_0} + G_{22} \exp\left(-\frac{E_1 - E_0}{kT}\right) \right\} \right] \quad \dots \quad (10) \end{aligned}$$

$$\begin{aligned}
 & + \frac{2a_1^2 b_2^2 (2 + \alpha_{\parallel})^2}{E_7 - E_2} \exp \left( - \frac{E_2 - E_0}{kT} \right) + G_{2z}^3 \exp \left( - \frac{E_3 - E_0}{kT} \right) \\
 & + G_{2z}^0 \exp \left( - \frac{E_4 - E_0}{kT} \right) - \frac{b_0^2 (2 + \alpha_{\parallel})}{E_5 - E_4} \exp \left( - \frac{E_5 - E_0}{kT} \right) \\
 & + G_{2z}^6 \exp \left( - \frac{E_6 - E_0}{kT} \right) - \frac{2a_1^2 b_2^2 (2 + \alpha_{\parallel})^2}{E_7 - E_2} \exp \left( - \frac{E_7 - E_0}{kT} \right) \} \}
 \end{aligned}$$

where

$$G_{2z}^1 = R_{31} + R_{61}; \quad G_{2z}^3 = -R_{31} + R_{63}; \quad G_{2z}^0 = -R_{63} - R_{61}$$

$$R_{ij} = \frac{2[\alpha_{\parallel}(c_i c_j - a_i a_j) + 2b_i b_j + 4c_i c_j]^2}{E_i - E_j} \quad \dots \quad (11)$$

$$G_{2z}^0 = - \frac{2a_0^2 (2 + \alpha_{\parallel})^2}{E_4 - E_0} + \frac{b_0^2 (2 + \alpha_{\parallel})^2}{E_5 - E_4} \quad ]$$

$$\begin{aligned}
 W = & \left[ 1 + 2 \exp \left( - \frac{E_1 - E_0}{kT} \right) + 2 \exp \left( - \frac{E_2 - E_0}{kT} \right) + 2 \exp \left( - \frac{E_3 - E_0}{kT} \right) \right. \\
 & + \exp \left( - \frac{E_4 - E_0}{kT} \right) + \exp \left( - \frac{E_5 - E_0}{kT} \right) + 2 \exp \left( - \frac{E_6 - E_0}{kT} \right) \\
 & \left. + 2 \exp \left( - \frac{E_7 - E_0}{kT} \right) + 2 \exp \left( - \frac{E_8 - E_0}{kT} \right) \right] \quad \dots \quad (12)
 \end{aligned}$$

and

$$\begin{aligned}
 K_1 = \frac{2N\beta^2}{W} & \left[ G_{2z}^0 + G_{2z}^1 \exp \left( - \frac{E_1 - E_0}{kT} \right) + G_{2z}^2 \exp \left( - \frac{E_2 - E_0}{kT} \right) \right. \\
 & + G_{2z}^3 \exp \left( - \frac{E_3 - E_0}{kT} \right) + G_{2z}^4 \exp \left( - \frac{E_4 - E_0}{kT} \right) \\
 & + G_{2z}^5 \exp \left( - \frac{E_5 - E_0}{kT} \right) + G_{2z}^6 \exp \left( - \frac{E_6 - E_0}{kT} \right) \\
 & \left. + G_{2z}^7 \exp \left( - \frac{E_7 - E_0}{kT} \right) + G_{2z}^8 \exp \left( - \frac{E_8 - E_0}{kT} \right) \right] \quad \dots \quad (13)
 \end{aligned}$$

$$\phi_7 = a_2 |1, 1\rangle - b_2 |0, 2\rangle$$

$$\phi_{7-} = a_2 |-1, -1\rangle - b_2 |0, -2\rangle$$

$$\phi_8 = |1, 2\rangle$$

$$\phi_{8-} = |-1, -2\rangle$$

where

$$a_0 = \frac{\sqrt{3}\alpha'\zeta_{\perp}}{(\alpha\zeta_{\parallel} - E_0)} b_0; \quad 2a_0^2 + b_0^2 = 1$$

$$a_j = -\frac{\sqrt{3}(2\alpha\zeta_{\parallel} - E_j)}{\sqrt{2}E_j} c_j; \quad a_j^2 + b_j^2 + c_j^2 = 1 \quad \dots \quad (9)$$

$$b_j = \frac{2\alpha\zeta_{\parallel} - E_j}{\sqrt{2}\zeta} c_j \quad j = 1, 3, 6$$

and 
$$a_2 = \frac{\sqrt{2}\alpha'\zeta_{\perp}}{\Delta - E_2} b_2; \quad a_2^2 + b_2^2 = 1$$

#### EXPRESSION FOR SUSCEPTIBILITY

As usual calculating the effect of the magnetic perturbations  $\beta H(-\alpha L + 2S)$  upto the second order, we get the expressions for principal magnetic susceptibility  $K_i (i = \parallel \text{ or } \perp \text{ to the trigonal axis of the crystal})$  as given below :

$$\begin{aligned} K_{\parallel} = \frac{N\beta^2}{kW} & \left[ \frac{1}{T} \left\{ \sum_{j=1,3,6} 2[\alpha\kappa_{\parallel}(c_j^2 - a_j^2) + 2b_j^2 + 4c_j^2]^2 \exp\left(-\frac{E_j - E_0}{kT}\right) \right. \right. \\ & + 2[b_2^2(2 - \alpha\kappa_{\parallel}) + 4a_2^2]^2 \exp\left(-\frac{E_2 - E_0}{kT}\right) \\ & + 2[a_2^2(2 - \alpha\kappa_{\parallel}) + 4b_2^2]^2 \exp\left(-\frac{E_7 - E_0}{kT}\right) \\ & \left. \left. + 2[(4 - \alpha\kappa_{\parallel})^2] \exp\left(-\frac{E_8 - E_0}{kT}\right) \right\} \right. \quad \dots \quad (10) \\ & \left. + 2k \left\{ \frac{2a_0^2(2 + \alpha\kappa_{\parallel})^2}{E_4 - E_0} + G_{22} \exp\left(-\frac{E_1 - E_0}{kT}\right) \right\} \right] \end{aligned}$$



$$\begin{aligned}
 & + \frac{2a_2^2 b_2^2 (2 + \alpha \kappa_{||})^2}{E_7 - E_2} \exp \left( - \frac{E_2 - E_0}{kT} \right) + G_{2z}^3 \exp \left( - \frac{E_3 - E_0}{kT} \right) \\
 & + G_{2z}^0 \exp \left( - \frac{E_4 - E_0}{kT} \right) - \frac{b_0^2 (2 + \alpha \kappa_{||})}{E_5 - E_4} \exp \left( - \frac{E_5 - E_0}{kT} \right) \\
 & + G_{2z}^6 \exp \left( - \frac{E_6 - E_0}{kT} \right) - \frac{2a_2^2 b_2^2 (2 + \alpha \kappa_{||})^2}{E_7 - E_2} \exp \left( - \frac{E_7 - E_0}{kT} \right) \} ]
 \end{aligned}$$

where

$$G_{2z}^1 = R_{31} + R_{61}; \quad G_{2z}^3 = -R_{31} + R_{63}; \quad G_{2z}^6 = -R_{63} - R_{61}$$

$$\begin{aligned}
 R_{ij} &= \frac{2[\alpha \kappa_{||}(c_i c_j - a_i a_j) + 2b_i b_j + 4c_i c_j]^2}{E_i - E_j} \\
 G_{2z}^0 &= - \frac{2a_0^2 (2 + \alpha \kappa_{||})^2}{E_4 - E_0} + \frac{b_0^2 (2 + \alpha \kappa_{||})^2}{E_5 - E_4}
 \end{aligned} \quad \left. \begin{array}{l} \dots \\ \dots \end{array} \right\} \dots \quad (11)$$

$$\begin{aligned}
 W &= \left[ 1 + 2 \exp \left( - \frac{E_1 - E_0}{kT} \right) + 2 \exp \left( - \frac{E_2 - E_0}{kT} \right) + 2 \exp \left( - \frac{E_3 - E_0}{kT} \right) \right. \\
 &+ \exp \left( - \frac{E_4 - E_0}{kT} \right) + \exp \left( - \frac{E_5 - E_0}{kT} \right) + 2 \exp \left( - \frac{E_6 - E_0}{kT} \right) \\
 &\left. + 2 \exp \left( - \frac{E_7 - E_0}{kT} \right) + 2 \exp \left( - \frac{E_8 - E_0}{kT} \right) \right] \dots \quad (12)
 \end{aligned}$$

and

$$\begin{aligned}
 K_1 &= \frac{2N\beta^2}{W} \left[ G_{2x}^0 + G_{2x}^1 \exp \left( - \frac{E_1 - E_0}{kT} \right) + G_{2x}^2 \exp \left( - \frac{E_2 - E_0}{kT} \right) \right. \\
 &+ G_{2x}^3 \exp \left( - \frac{E_3 - E_0}{kT} \right) + G_{2x}^4 \exp \left( - \frac{E_4 - E_0}{kT} \right) \\
 &+ G_{2x}^5 \exp \left( - \frac{E_5 - E_0}{kT} \right) + G_{2x}^6 \exp \left( - \frac{E_6 - E_0}{kT} \right) \\
 &\left. + G_{2x}^7 \exp \left( - \frac{E_7 - E_0}{kT} \right) + G_{2x}^8 \exp \left( - \frac{E_8 - E_0}{kT} \right) \right] \dots \quad (13)
 \end{aligned}$$

where

$$\begin{aligned}
 G_{2x}^0 &= \frac{2A_{01}^2}{E_1 - E_0} + \frac{2A_{03}^2}{E_3 - E_0} + \frac{2A_{06}^2}{E_6 - E_0} \\
 G_{2x}^1 &= -\frac{2A_{01}^2}{E_1 - E_0} + \frac{2B_{21}^2}{E_2 - E_1} + \frac{2A_{41}^2}{E_4 - E_1} + \frac{2A_{51}^2}{E_5 - E_1} + \frac{2B_{71}^2}{E_7 - E_1} \\
 G_{2x}^2 &= -\frac{2B_{21}^2}{E_2 - E_1} + \frac{2B_{23}^2}{E_3 - E_2} + \frac{2B_{26}^2}{E_6 - E_2} + \frac{2(2b_2 - \alpha' \kappa_1 a_2 \sqrt{2})}{E_8 - E_2} \\
 G_{2x}^3 &= -\frac{2A_{03}^2}{E_3 - E_0} - \frac{2B_{23}^2}{E_3 - E_2} + \frac{2A_{43}^2}{E_4 - E_3} + \frac{2A_{53}^2}{E_5 - E_3} + \frac{2B_{73}^2}{E_7 - E_3} \\
 G_{2x}^4 &= -\frac{2A_{41}^2}{E_4 - E_1} - \frac{2A_{43}^2}{E_4 - E_3} + \frac{2A_{46}^2}{E_6 - E_4} \\
 G_{2x}^5 &= -\frac{2A_{51}^2}{E_5 - E_1} - \frac{2A_{53}^2}{E_5 - E_3} + \frac{2A_{56}^2}{E_6 - E_5} \\
 G_{2x}^6 &= -\frac{2A_{06}^2}{E_6 - E_0} - \frac{2B_{26}^2}{E_6 - E_2} - \frac{2A_{46}^2}{E_6 - E_4} - \frac{2A_{56}^2}{E_6 - E_5} + \frac{2B_{76}^2}{E_7 - E_6} \\
 G_{2x}^7 &= -\frac{2B_{71}^2}{E_7 - E_1} - \frac{2B_{73}^2}{E_7 - E_3} - \frac{2B_{76}^2}{E_7 - E_6} + \frac{2 \left( 2a_2 - \frac{\alpha' \kappa_1 b_2}{\sqrt{2}} \right)^2}{E_8 - E_7} \\
 G_{2x}^8 &= -\frac{2 \left( 2a_2 - \frac{\alpha' \kappa_1 b_2}{\sqrt{2}} \right)^2}{E_8 - E_7} - \frac{2 \left( 2b_2 - \frac{\alpha' \kappa_1 a_2}{\sqrt{2}} \right)^2}{E_8 - E_7}
 \end{aligned} \tag{14}$$

where

$$\begin{aligned}
 A_{0j} &= \sqrt{6}(a_0 a_j + b_0 b_j) - \frac{\alpha' \kappa_1}{\sqrt{2}} (a_j b_0 + b_j a_0) + 2c_j a_0 \\
 B_{2j} &= (\sqrt{6} b_2 a_j + 2a_2 b_j) - \frac{\alpha' \kappa_1}{\sqrt{2}} (b_2 b_j + a_2 c_j) \\
 A_{4j} &= \sqrt{3} a_j + \frac{b_j \kappa_1}{2} - \sqrt{2} c_j
 \end{aligned} \tag{15}$$

$$A_{5j} = \sqrt{3}(b_0a_j - 2a_0b_j) - \frac{\alpha'\kappa_1}{2} (b_0b_j - 2a_0a_j) + \sqrt{2}b_0b_j$$

$$B_{7j} = (\sqrt{6}a_2a_j - 2b_2b_j) - \frac{\alpha'\kappa_1}{2} (b_2a_2 - c_2b_2)$$

## g - V A L U E S

If we take  $\Delta$  to be positive, on including the spin-orbit coupling a doublet ( $\phi_1, \phi_{1-}$ ) comes to occupy the lowest position giving  $g_{||} \approx 8$  and  $g_{\perp} \approx 0$  (Bose *et al*, 1961b) which requires  $K_{||}$  to be greater than  $K_{\perp}$ . Recent neutron diffraction studies of the salt (Hamilton, 1962) seem to indicate that the trigonal axis of  $[\text{Fe}^{2+}, 6\text{H}_2\text{O}]$  cluster in this salt is elongated and we would expect a priori that  $g_{||} > g_{\perp}$  as roughly calculated above. On the contrary, the magnetic measurement definitely shows that the trigonal axis of the crystal sets normally to the magnetic field and hence  $\chi_1 > \chi_{||}$  or  $K_{\perp} > K_{||}$  (since the unit cell contains one ion only). This shows that the criterion for  $g_{||} >$  or  $< g_{\perp}$  depends on other factors as well in addition to ligand distances e.g. the charge densities, overlap etc. Also, it is evident that  $\Delta$  must be negative.

For a negative value of  $\Delta$  the wavefunctions, as arranged in (9), are in the order of increasing energies and the singlet  $\phi_0$  lies lowest with doublet ( $\phi_1, \phi_{1-}$ ) close to it. The system behaves for most purposes as with effective spin 1.  $g$ -value expressions are

then

$$g_{||} = [\alpha\kappa_{||}(c_1^2 - a_1^2) + 2b_1^2 + 4c_1^2] \quad \dots (16)$$

$$g_{\perp} = \sqrt{2} \left[ \sqrt{6}(a_0a_1 + b_0b_1) - \frac{\alpha'\kappa_{\perp}}{\sqrt{2}} (a_1b_0 + b_1a_0) + 2c_1a_0 \right]$$

No experimental resonance data for  $g_{||}, g_{\perp}$  on  $\text{FeSiF}_6 \cdot 6\text{H}_2\text{O}$  are available. However the mean  $g$ -value = 3.30 calculated indirectly from susceptibility is close to Low's result ( $\bar{g} = 3.41$ ; Low, 1960) on hexacoordinated  $\text{Fe}^{2+}$  ion embedded in  $\text{MgO}$ . Crystal field in this latter salt is perfectly cubic, which along with spin-orbit coupling alone is not sufficient to remove the degeneracy of the ground level; three-fold degeneracy remains in the ground state, which is responsible for Jahn-Teller instability. An isotropic  $g$ -value is obtained (Low, 1960, Opik and Pryce, 1951). In  $\text{FeSiF}_6 \cdot 6\text{H}_2\text{O}$  however, this degeneracy is partly lifted by the introduction of the trigonal field; the  $g$ -value becomes anisotropic. It appears that the introduction of the trigonal asymmetry in the ligand cluster does not make much difference in the mean  $g$ -value from the above cubic case. These values may be compared with the mean  $g$ -values for  $\Delta = +ve$ , in

$\text{Fe}(\text{NH}_4\text{SO}_4)_2 \cdot 6\text{H}_2\text{O}$  ( $\bar{g} = 3.0$  Bose *et al* 1961b) and  $\text{FeF}_2$  embedded in  $\text{ZnF}_2$  ( $\bar{g} = 2.99$ ; Tinkham, 1955) in which the  $\text{Fe}^{2+}$  ions have approximately tetragonal and orthorhombic symmetry, respectively.

#### DISCUSSIONS ON EXPERIMENTAL MEAN SUSCEPTIBILITIES AND ANISOTROPY

Symmetry considerations of the ligand clusters discussed above apply in general equally to the magnetic susceptibility and anisotropy. The theoretical parameters  $\Delta$ ,  $\alpha\zeta_{||}$ ,  $\alpha'\zeta_{\perp}$  and  $\alpha\kappa_{||}$ ,  $\alpha'\kappa_{\perp}$  fitting the experimental magnetic mean susceptibility and anisotropy have been uniquely calculated within an error of about 0.5% by extensive trial and error method described elsewhere (Bose *et al*, 1964) consistent with spectroscopic absorption data.

The coefficients  $\alpha$ ,  $\alpha'$ ,  $\zeta_{||}$ ,  $\zeta_{\perp}$  and  $\kappa_{||}$ ,  $\kappa_{\perp}$  can not be calculated separately since they appear as products, in the equations mentioned above, though reasonable estimates may be made of the anisotropic reductions in the ideal values of the coefficients, namely  $\zeta_{||} = \zeta_{\perp} = -106 \text{ cm}^{-1}$  for the free ion,  $\alpha = \alpha' = 1$  in a cubic field and  $\kappa_{||} = \kappa_{\perp} = 1$  for no overlap.

The level  $(\phi_1, \phi_{1-})$  just above the ground level  $\phi_0$  starts getting depopulated quickly in the liquid hydrogen temperature range (energy separation being  $\sim 10 \text{ cm}^{-1}$ ), causing a comparatively rapid fall in experimental effective moment square  $\bar{p}^2$  versus  $T$  curve, as also a hump in the  $(p_{\perp}^2 - p_{||}^2)$  versus  $T$  curve in this region. No thermal phase transition has been observed in this salt as in the isomorphous  $\text{Co}^{2+}$  (Bose *et al*, 1965) and  $\text{Cu}^{2+}$  fluosilicates (Mazumder *et al*, unpublished). The experimental data for both mean susceptibility and anisotropy fit nicely with a unique set of theoretical parameters (given in Table I) at each temperature in the entire range  $300^\circ\text{K}$ – $7.85^\circ\text{K}$ , only when  $\Delta$  is made to vary with temperature and a temperature dependent field separation  $\Delta$  with a continuous increase from  $-1025 \text{ cm}^{-1}$  at  $7.85^\circ\text{K}$  to  $-350 \text{ cm}^{-1}$  at  $300^\circ\text{K}$  is taken. The variation in  $\Delta$  is apparently somewhat exaggerated since we assumed the anisotropies in the other parameters though related to  $\Delta$ , as independent of temperature for the sake of keeping the uniqueness of the trial and error calculations. The cubic and the Coulomb fields may of course be reasonably taken to be independent. The said exaggerated variation in  $\Delta$  might be reduced reasonably if we had independent thermal variation data of spectroscopic absorption or para-magnetic resonance. But in the absence of these we are not able to make further refinement for the present.

One apparently anomalous situation needs a further remark or two. As seen in the case of  $\text{FeSiF}_6 \cdot 6\text{H}_2\text{O}$  the relative elongation or contraction of the axial principal directions as observed by neutron-diffraction does not seem to have any direct bearing on the relative magnitudes of the susceptibility tensors, as frequently assumed by many workers. A further example is provided by the recent accurate X-ray investigation (Grimes *et al* 1963) on  $\text{Ni}(\text{NH}_4\text{SO}_4)_2 \cdot 6\text{H}_2\text{O}$ , indicating a strict

tetragonal symmetry of  $[\text{Ni}^{2+}, 6\text{H}_2\text{O}]$  clusters, whereas both the paramagnetic resonance and magnetic anisotropy measurements indicate a rather large orthorhombic symmetry. Moreover, the tetragonal axis found by X-ray is quite different from the approximate tetragonal axis found from anisotropy and resonance calculations, and again the X-ray data gives the tetragonal axis as elongated, whereas, the approximately tetragonal magnetic tensor axis is characterised by

$$K_{\perp}(= K_1 \approx K_2) > K_{\parallel}(= K_3)$$

This is not surprising if we note that the anisotropic ligand field effect upon the central ion is not a function of distance alone but is quite sensitively dependent upon small ligand charge orientations and overlaps.

TABLE I

$\text{FeSiF}_6 \cdot 6\text{H}_2\text{O}$ . Temperature variation of mean moment sq ( $\bar{p}^2$  and) anisotropy ( $p_{\perp}^2 - p_{\parallel}^2$ )

Temp. °K	$\Delta\text{cm}^{-1}$	$p_{\perp}^2 - p_{\parallel}^2$	$p^2$	Mean <i>g</i> -value
300	-350	6.76 (6.73)	27.64 (27.66)	
180	-750	8.84 (8.80)	27.55 (27.53)	
140	-925	9.90 (9.92)	27.40 (27.40)	
20.4	-1000	25.68 (25.64)	24.55 (24.46)	3.30 (3.34)
14.2	-1025	26.71 (26.62)	22.97 (22.99)	
7.85	-1030	26.00 (26.06)	19.86 (19.88)	

The values within parantheses are from experiments of L. C. Jackson (1959) and Mazumdar *et al.*, unpublished.

$$\alpha\zeta_{\parallel} = P_{\parallel} = -104 \text{ cm}^{-1}$$

$$\alpha\kappa_{\parallel} = Q_{\parallel} = 0.50$$

$$\alpha'\zeta_{\perp} = P_{\perp} = -98 \text{ cm}^{-1}$$

$$\alpha'\kappa_{\perp} = Q_{\perp} = 0.70$$

## APPENDIX

Expression for  $\alpha$  and  $\alpha'$  in the case of  $\text{Fe}^{2+}$

Wavefunctions of the lowest triplet state of  $\text{Fe}^{2+}$  under trigonal field, which admixes the excited doublet  $E_g$  with the split doublet component of  $T_{2g}$ , say  $T_{2g}\pm$  is in  $|LM_L\rangle$  scheme are,

$$\begin{aligned}\psi_+ &= \epsilon \left[ \sqrt{\frac{2}{3}} |22\rangle - \sqrt{\frac{1}{3}} |2-1\rangle \right] + \tau \left[ \sqrt{\frac{1}{3}} |22\rangle + \sqrt{\frac{2}{3}} |2-1\rangle \right] \\ \psi_- &= \epsilon \left[ \sqrt{\frac{2}{3}} |2-2\rangle + \sqrt{\frac{1}{3}} |21\rangle \right] + \tau \left[ \sqrt{\frac{1}{3}} |2-2\rangle - \sqrt{\frac{2}{3}} |21\rangle \right] \quad (17) \\ \psi_0 &= |20\rangle\end{aligned}$$

So that a calculation similar to Pryce for  $\text{Co}^{2+}$  (1951) yields

$$\begin{aligned}\alpha &= \epsilon^2 + 2\sqrt{2}\epsilon\tau \\ \alpha' &= \epsilon - \sqrt{2}\tau \quad \dots \quad (18) \\ \epsilon^2 + \tau^2 &= 1\end{aligned}$$

Expression (18) is applicable in all the cases where the lowest state is  $D$ -state and the asymmetric field is a trigonal one.

## REFERENCES

- Abraham, A. and Pryce, M. H. L., 1951, *Proc. Roy. Soc.*, **A206**, 175.  
 Agnetta, G., Garofano, T., Vittorelli, Palma M. B. and Palma, M. U., 1962, *Phil. Mag.*, **7**, 495.  
 Bose, A., Chakraborty, A. S. and Chatterjee, R., 1960, *Proc. Roy. Soc.*, **A255**, 145.  
 Bose, A., Chakraborty, A. S. and Chatterjee, R., 1961a, *Proc. Roy. Soc.*, **A261**, 43.  
 Bose, A., Chakraborty, A. S. and Chatterjee, R., 1961b, *Proc. Roy. Soc.*, **A261**, 207.  
 Bose, A., Chatterjee, R. and Rai, R. 1964, *Proc. Phys. Soc.* **83**, 953.  
 Boe, A., Jackson, L. C. and Rai, R. 1965, *Ind. Jour. Phys.* **39**, 7.  
 Griffiths, J. S., 1961. *The Theory of Transition Metal Ions*, Cambridge University Press. p. 284.  
 Grimes, N. W., K. H. F. and Webb, M. W., 1963, *Acta. Cryst.*, **16**, 823.  
 Hamilton, Walter C., 1962, *Acta. Cryst.*, **15**, 353.  
 Jackson, L. C., 1959, *Phil. Mag.*, **4**, 269.  
 Low, W. and Weger, M., 1960, *Phys. Rev.*, **118**, 1130.  
 Opik, U. and Pryce, M. H. L., 1957, *Proc. Roy. Soc.*, **A238**, 425.  
 Pallumbo, D., 1958, *Nuovo Cim.*, **8**, 271.  
 Pauling, L. C., 1930, *Zeits. f. Krist.*, **72A**, 482.  
 Stevens, K. W. H., 1953, *Proc. Roy. Soc.*, **A219**, 176.  
 Tinkham, M., 1955, *Proc. Roy. Soc.*, **A236**, 535.  
 Van Vleck, J. H., 1935, *J. Chem. Phys.*, **3**, 807.

# DETERMINATION OF THE RELATIVE DISTRIBUTION OF LAYERS IN DENSELY PACKED COLLOIDAL SYSTEMS—WOOL

T. RATHO AND B. C. PANDA

(REGIONAL ENGINEERING COLLEGE, RORKELA)

(Received October 5, 1964; Resubmitted January 21, 1965)

**ABSTRACT.** This paper deals with the determination of the distribution of layers in wool assuming it to belong to the Hohl-raum system, substances packed in layers with free spaces in between. In a paper by one of us, (Ratho, 1964), Guinier methods (1937) have been applied to determine the thickness factor in wool. In the present paper we have assumed a particular thickness factor of  $61\lambda$  or  $94\text{ \AA}$ , for  $\lambda = 1.54\text{ \AA}$ , as the mean thickness of layers which is also the probable mean thickness of different samples of wool belonging to the general micelle system. Porod (1949) in his paper on such systems has introduced a relative fluctuation factor  $\delta$  given by

$\delta = \frac{\Delta}{d_0}$ , where  $d_0$  is the mean distance between layers,  $\Delta = \{(d-d_0)^2\}^{1/2}$  is the root

mean square fluctuation and  $d$  is the distance between any two layers. We have here tried to find out the relative distribution by calculating the theoretical scattering curves with different relative fluctuation factors  $\delta = 0.2, 0.4, 0.6$ , and  $0.8$ , for the thickness factor of  $61\lambda$  and have tried to show the agreement between the theoretical and the experimental results. We have also drawn the theoretical curves with these four fluctuation factors for two other thicknesses of  $40\lambda$  and  $80\lambda$  which are also probable as they give rise to a mean thickness about  $61\lambda$ . It is found that with the mean thickness of  $61\lambda$  alone the theoretical and the experimental scattering curves, agree most in the high intensity region when  $\delta = 0.4$  and in the region of low intensities when  $\delta = 0.8$ . From this one can conclude that the thicker layers in the sample occur more frequently than the thinner ones.

## EXPERIMENT

The substance investigated is a sample of wool of the variety Scottish Black-face from England. The experimental arrangement and the procedures were the same as reported in the paper referred to above (Ratho, 1964). As wool is an oriented substance one can proceed with the smeared-out intensity,  $\tilde{I}$ , no slit correction being necessary. The experimental intensity  $\tilde{I}$  is converted to a scattering function  $\phi(s)_{\text{ex}}$  as after Porod (1949) where we have taken  $\tilde{I} = I_0 S \phi(s)_{\text{ex}}$ .

where  $I_0$  is the incident intensity and  $S$  is a scattering factor ;  $\phi(s)_{Ex}$  represents the experimental value of the scattering function  $\phi(s)$  and

$$s = \frac{4\pi \sin \theta}{\lambda} = \frac{4\pi\theta}{\lambda}, \text{ for } \theta \rightarrow 0.$$

The scattering angle  $\theta$  is represented in terms of  $\mu$  where

$$\mu = 244\pi\theta.$$

The  $\phi(s)_{Ex}$  and  $\mu$  values are shown in the Table I, the angular range studied being from

$$\theta = 0.27 \times 10^{-3} \text{ to } \theta = 3.93 \times 10^{-3} \text{ in radians.}$$

#### THEORY AND DISCUSSION

A large volume of theoretical and experimental works on densely packed colloidal systems have been published by Kratky (1938) and Porod (1949). The scattering of fibrous substances like regenerated cellulose and wool have been treated after Babinet's reciprocal relation in optics and they have come to the conclusion that scattering should not come under particle-scattering while interparticle-scattering plays a predominant role. Porod (1949) in his paper arrived at a scattering function  $\phi(s)_{Th}$ , theoretically which can be split up into two functions  $\phi_1$  and  $\phi_2$  where

$$\phi(s)_{Th} = \phi_1 + \frac{1}{n} \phi_2$$

Here  $\phi_1$  represents the particle-scattering while  $\phi_2$  represents the interparticle scattering.

Assuming the particle scattering to be completely absent one can represent the theoretical scattering function, after certain approximations,

$$\begin{aligned} \phi(s)_{Th} &= \frac{1}{n} \phi_2 \text{ as} \\ \phi(s)_{Th} &= \frac{(1 - \cos \mu \cosh \mu^2 \delta^2 / 2)}{(\cosh \mu^2 \delta^2 / 2 - \cos \mu)^2} \end{aligned}$$

where

$$\mu = s d_0.$$

For small values of  $\theta$  and for a mean thickness  $d_0$  of  $61\lambda$  it can be easily seen that

$$\mu = 244\pi\theta$$

From the experimental measurements one gets the scattering intensity  $\tilde{I}$  which can be represented as

$$\tilde{I} = I_0 S \phi(s)_{Ex}$$



where  $I_0$  is the incident intensity and  $S$  is the scattering factor as before. Since  $I_0 S$  is the same for the same substance and for the same incident radiation, we have taken its value to be 175 so that one of the points of the theoretical curve is made to coincide with the corresponding point on the experimental curve.  $\phi(s)_{Ex}$  values have been compared with  $\phi(s)_{Th}$  values for different values of  $\mu$  according to the above formula in Fig. 1.

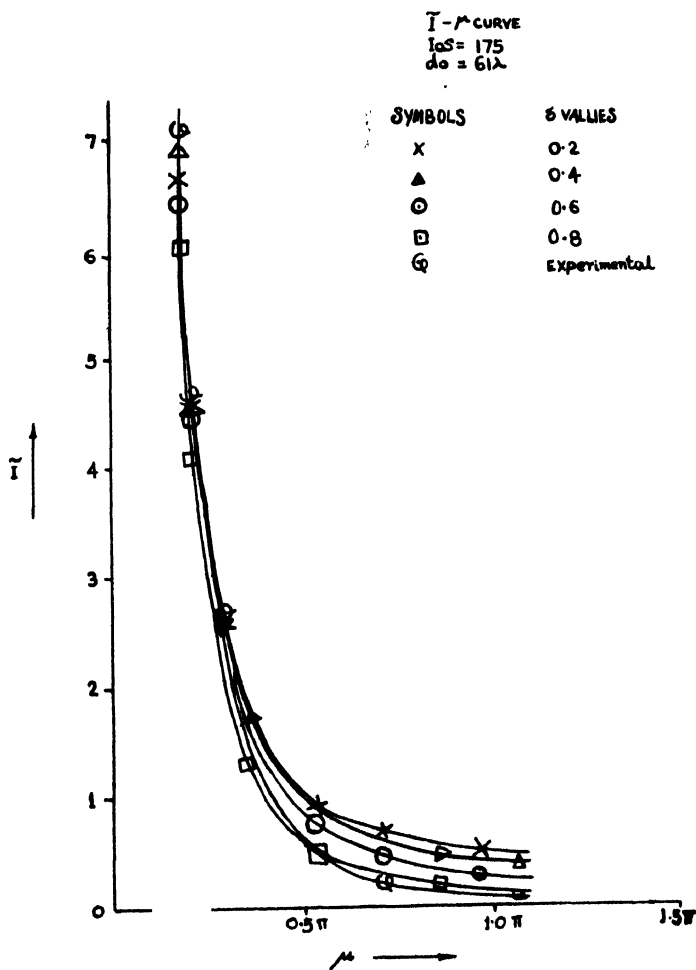


Fig. 1.

We have tried to get a good agreement between the theoretical and the experimental curves by taking four different values of  $\delta$ , the relative fluctuation factor, as equal to 0.2, 0.4, 0.6 and 0.8 for a thickness factor of  $61\lambda$ . For every one of these values the theoretical curves are drawn to the same scale in the same figure along with the experimental curve (Fig. 1, Table I). It is seen from the figure that

when the mean thickness is  $61\lambda$  there is good agreement between the theoretical and the experimental curves in the high intensity region if  $\delta = 0.4$  and in the low intensity region when  $\delta = 0.8$ .

We have also tried to vary the thickness from  $61\lambda$  to  $40\lambda$  and  $80\lambda$ . The theoretical  $\phi(s)_{Th}$  values have been calculated and  $\phi(s)_{Th}$  versus  $\mu$  curves have been drawn for each one of them for the above four values of  $\delta$  along with the experimental curve. These two sets of curves one for each thickness factor are not shown here. Drawn to the same scale with the same constant factor  $I_0 S = 175$  for the experimental curve, in none of these two cases there is found to be good agreement between the theoretical and the experimental curves.

TABLE I

$\mu$	$\phi(s)_{Th}$				$\phi(s)_{Ex}$
	$\delta = 0.2$	$\delta = 0.4$	$\delta = 0.6$	$\delta = 0.8$	
0.178	6.622	6.858	6.416	6.033	7.120
0.213	4.622	4.612	4.437	4.062	4.705
0.284	2.678	2.648	2.493	2.114	2.666
0.320	2.125	2.118	1.972	1.636	1.908
0.355	1.779	1.735	1.598	1.280	1.451
0.426	1.294	1.282	1.115	0.834	0.893
0.533	0.902	0.863	0.735	0.503	0.481
0.622	0.725	0.691	0.563	0.367	0.294
0.711	0.679	0.578	0.457	0.287	0.199
0.834	0.524	0.506	0.354	0.206	0.121
0.960	0.485	0.440	0.299	0.162	0.090
1.067	0.480	0.411	0.245	0.116	0.068

#### DETERMINATION OF RELATIVE DISTRIBUTION

It is seen that the relative fluctuation factor is 0.4 in the high intensity region and 0.8 in the region of low intensities corresponding to low and large angles of scattering respectively. It is wellknown that the inner part of the scattering curve is effected by the particles of large dimensions and the outer part of the scattering curve is effected by particles of small sizes. Again the principle of Statistical Independence after Landau (1958) demands that the relative fluctuation is inversely proportional to the square root of the number of particles in the macroscopic body, given by

$$\delta = \frac{\{(d-d_0)^2\}^{\frac{1}{2}}}{d_0} \propto \frac{1}{N^{\frac{1}{2}}}$$

where  $N$  is the number of particles in the macroscopic body.

The agreement between the experimental and the theoretical curves of scattering is satisfactory on the inner parts when  $\delta = 0.4$ . Since the inner part of the curve is obviously due to large sized particles and since the value of  $\delta$  is small, it means that  $N$  is large, i.e. the large sized particles are more in number. The outer part of the scattering curve corresponding to large angles is effected by particles of smaller dimensions. The very fact that a large value of  $\delta = 0.8$  satisfies the outer region according to the above formula,  $N$  is small. In other words the number of layers corresponding to this region are small. That means the small sized particles are fewer in number. This amounts to saying that the large sized layers are more predominant. Thus the agreement of a large  $\delta$  value in the outer region further supports the abundance of the large particles. Therefore it is very likely that the thicker layers are more predominant than the thinner ones.

It has been pointed out in a paper by one of us (Ratho, 1964) that there exists probably two types of layers of micelle of thickness of about  $60\text{\AA}$  and  $125\text{\AA}$  respectively. A rough relative distribution of layers can however be calculated from the above formula.

If  $N_1$  is the number of thicker layers and  $N_2$  the number of thinner layers and if  $\delta_1$  and  $\delta_2$  are the relative fluctuations for these two types of layers respectively, then from the above formula

$$N_1 = \frac{C}{\delta_1^2}$$

$$N_2 = \frac{C}{\delta_2^2}$$

where  $C$  is the constant of proportionality. Therefore the fraction of the thicker layers in the system is

$$\frac{N_1}{N_1 + N_2} = \frac{\delta_2^2}{\delta_1^2 + \delta_2^2}$$

Since  $\delta_1 = 0.4$  is assigned to the thicker layer and  $\delta_2 = 0.8$  to the thinner layers, we have

$$\frac{N_1}{N_1 + N_2} = \frac{(0.8)^2}{(0.4)^2 + (0.8)^2} = 0.80.$$

Therefore the thicker layers are predominant in the system, being about 80 %.

#### DISCUSSION

The effect of particle scattering on the total scattering can be shown to be negligible and our assumption that  $\phi_1 = 0$  can hence be justified.

It can be easily seen from the expression

$$\phi_2 = \frac{\left(1 - \cos \mu \cdot \cosh \mu^2 \frac{\delta^2}{2}\right)}{\left(\cosh \mu^2 \frac{\delta^2}{2} - \cos \mu\right)^2}$$

that for finite values of  $\delta$  (which is always less than 1) the value of

$$\lim_{\mu \rightarrow 0} \phi_2 = \infty$$

In a paper by Porod (1949) it has also been shown that the particle scattering  $\phi_1$  can be given by

$$\phi_1 = \frac{1 - k^2}{1 - 2k \cos \mu + k^2}$$

where  $k = e^{-\mu^2 \delta^2 / 2}$ ,  $\mu = s d_0$  and  $\delta$  is the relative fluctuation factor as before. Now it can be shown that

$$\lim_{\mu \rightarrow 0} \phi_1 = \delta^2 < 1$$

Therefore in the range of low angles of the order of  $10^{-3}$  the effect of particle scattering on the total scattering, i.e. the effect of  $\phi_1$  on  $\phi = (\phi_1 + 1/n \phi_2)$  is negligible.

## CONCLUSION

The mean thickness factor is more than  $90 \text{ \AA}$ , as it is a densely packed system, this can be taken as the mean distance between the scattering centres. There are about 80% thicker layers in the sample. The particle scattering is negligible and the interparticle scattering is predominant.

## REFERENCES

- Porod, G., (1949) *Acta Physica Austriaca*, **3**, 66; *Kolloid-Z*, 124; (1951) *Band*, 83; (1952) 25, *Band*, 51.  
 Kratky, O., *Naturwiss*, 20, 94(1934); 30, 542(1962); *Z. Elektrochemangew. Physik. Chem.* **46**, 55(1940).  
 Landau, L. D. and E. L. Lifshitz, *Statistical Physics* (1958).  
 Ratho, T. (1964), *Ind. J., Physics*, **38**, 475.  
 Guinier, A. (1937). *Ccunt. Rend.* **204**, 1115.

# A MODIFIED PROCEDURE OF SCANNING NUCLEAR EMULSIONS FOR OBTAINING ABSOLUTE NEUTRON YIELDS OF REACTIONS

J. P. [

PHYSICS DEPARTMENT, UNIVERSITY OF LUCKNOW

(Received September 21, 1964)

**ABSTRACT.** A modified procedure for scanning nuclear emulsions exposed to neutrons has been used, in order to avoid the correction for recoil proton tracks running out of the plate. This procedure has not been previously employed. The absolute yield for the  ${}^7\text{Li} + {}^2\text{H}$  reaction has been obtained.

## INTRODUCTION

In the studies of nuclear reactions where neutrons with energies exceeding 12 Mev constitute the outgoing particles, it has not been possible with nuclear emulsions to obtain their absolute yield. A large number of the recoil proton tracks do not end within the emulsion and hence their range cannot be determined.

For assessing the number of such particles whose tracks run out of the emulsion, a correction has to be applied. This correction which depends on the particle energy, the thickness of the emulsion and the maximum scattering angle for which tracks are accepted, was calculated geometrically by Gibson and Levesoy<sup>1</sup> (1948). It is valid provided the proton range varies with energy according to the Geiger rule. As this rule does not accurately represent the range energy relation for protons, the correction factor is approximate.

Trumpy *et al* (1953) gave the approximate relation

$$f = - \frac{R_0}{48d} \cdot \frac{1 - \cos^6 \alpha}{2\alpha + \sin 2\alpha} \cdot \frac{12\beta + 8 \sin 2\beta + \sin 4\beta}{\sin \beta}$$

where  $R_0$  is the range of a proton in the forward direction,  $\beta$  the angle between the projection of the track on the emulsion plane and the projected neutron direction,  $\alpha$  the angle between the track and its projection on the plane of the emulsion and  $f$  is the fraction of the total number of protons scattered at these angles which are recorded in an emulsion thickness  $d$ .

## EXPERIMENT AND RESULTS

The calculated values of  $f$  at different energies from Trumpy's data, for emulsions of  $400\mu$  thickness, are shown in column 2 (Table 1). The number of tracks escaping from the emulsion can be reduced by choosing a smaller angle of scattering for which tracks are accepted. Calculated values of  $f$  for  $\alpha_1 = 5^\circ$  and  $\beta = 5^\circ$  are shown as  $f_{cal}$  in column 3 (Table I). This correction is however approximate.

TABLE I

Variation in the value of  $f$  with the criterion for selection of tracks and with the neutron energy

$E_n$ Mev	$f$	$f_{cal.}$
11	0.85	0.95
12	0.82	0.94
14	0.76	0.92

In the study of the  ${}^7\text{Li}(d, n){}^8\text{Be}$  reaction, in order to cut down the number of tracks lost from the emulsion surfaces, a modified procedure of scanning was adopted. By considering only those tracks that originated in the region extending from a depth of about  $50\mu$  to about  $250\mu$  below the surface of the  $400\mu$  thick emulsion, the search was limited to about half the thickness of the plate. Thus although a larger area of the plate had to be scanned, a greater thickness of the emulsion was available to the particles whose tracks started in the above mentioned region. Therefore a greater probability of the recoil particles stopping within the emulsion surfaces was expected.

## DISCUSSION

The results show that out of more than 3000 tracks counted, only 15 left the emulsion. As this number is insignificantly small compared to the number of tracks measured, no correction is necessary for the tracks leaving the emulsion. With the normally used scanning procedure the correction would have certainly amounted to more than a hundred lost tracks.

It has thus been possible to obtain with this modified procedure of scanning, the absolute yield of the reaction under investigation. The neutron intensities at the four angles of observation with respect to the deuteron beam, have been shown in Table II.

TABLE II

The absolute neutron yield of  ${}^7\text{Li}+{}^2\text{H}$  reaction at different angles  
(Neutron yields obtained in terms of the number of tracks observed per  $10^9\mu^3$ )

Angle	Neutron yield
$0^\circ$	12.03
$45^\circ$	13.48
$90^\circ$	13.52
$135^\circ$	11.83

## ACKNOWLEDGEMENT

Thanks are due to Dr. M. A. S. Ross of the University of Edinburgh, U. K. for helpful discussions.

## REFERENCES

- Gibson, W. M. and Levesey, E. L., 1948, *Proc. Phys. Soc.*, **A60**, 523.  
 Trumpy, Grottdal and Graue, 1953, *University of Bergen Yearbook*, No. 8.

# INCOHERENT SCATTERING OF 280 KEV GAMMA RAYS

P. V. RAMANA RAO, J. RAMA RAO AND V. LAKSHMINARAYANA

LABORATORIES FOR NUCLEAR RESEARCH, ANDHRA UNIVERSITY, WALTAIR

(Received December 1, 1964)

**ABSTRACT** Incoherent scattering cross-sections  $\sigma_b$  in elements carbon, aluminium, copper and cadmium are determined at the photon energy 280 kev and compared with the corresponding Klein-Nishina cross-section  $\sigma_f$ . Progressively increasing deviation is observed between the two cross-sections with increasing atomic number. This deviation is attributed to the influence of electron binding. The ratio  $(\sigma_b/\sigma_f)$  is computed theoretically on the basis of Thomas-Fermi atomic charge distribution and compared with the experimentally observed ratio. A fair agreement is noticed.

## INTRODUCTION

It is well-known that the incoherent scattering of photons by free electrons is accurately described by Klein-Nishina theory. Atomic electrons can be considered as free if the incident photon energy greatly exceeds the binding energy of the electrons in the atom. When this condition does not obtain, the cross-section for incoherent scattering will be smaller than predicted by Klein-Nishina formula. This diminution in the incoherent scattering cross-section due to electron binding effects is expressed in terms of an incoherent scattering function which is dependent on the momentum transferred to the electron and the atomic number of the scattering medium. Various models of atomic charge distribution are in use to compute the incoherent scattering function theoretically.

It was shown experimentally by Lakshminarayana *et al* (1961) that the 'free electron assumption' holds for light elements at incident photon energies greater than 662 kev. Detailed investigations by Motz *et al* (1961) on the Compton scattering of 662 kev photons by the *K*-shell electrons of tin and gold have shown that even in these elements atomic binding effects are negligible at this energy. However, at lower energies, definite deviations from Klein-Nishina cross-section due to binding effects are qualitatively indicated even for light elements in the work of Lakshminarayana *et al*. The present investigation is an attempt to assess the influence of electron binding in light elements in a quantitative manner at the photon energy 280 kev.

A simple procedure is adopted to obtain the incoherent scattering cross-sections experimentally. The method consists of determining the total atomic cross-

section by transmission experiments and subtracting from it the theoretically computed contributions due to photoelectric and coherent scattering processes. To achieve sufficient accuracy in this 'subtraction technique', the light elements C, Al, Cu and Cd are chosen as the scattering materials in as much as the theoretical computation of photoelectric and coherent scattering cross-sections can be carried out to the desired degree of accuracy in light elements.

#### EXPERIMENTAL DETAILS

A 10 milli-curie mercury—203 source is used to provide the 280 kev gamma rays. A modified narrow-beam geometry identical with that described by Lakshminarayana *et al* (1961) is employed. A Du Mont 6292 photomultiplier with  $3/4" \times 3/4"$  NaI(Tl) crystal is used as the detector. The experimental procedure as well as the method of analysis of obtaining total atomic-cross-sections is just the same as of Lakshminarayana *et al*. The cross-sections are determined with a standard deviation not exceeding 1% in the present investigation.

The photoelectric cross-sections are computed to within an accuracy of 2% using Nagel's formula (1960) whose applicability to low and medium Z elements is established by Parthasarathi, *et al* (1964). The coherent scattering cross-sections are estimated to within an accuracy of 3% making use of the form-factor formalism whose validity is established in the low energy region for light elements.

By subtracting the sum of photoelectric and coherent scattering cross-sections from the total atomic cross-section, the experimental value of the incoherent scattering cross-section  $\sigma_b$  is deduced. The values of  $\sigma_b$  for the various elements are given in column 2 of Table I. For comparison, the corresponding free electron

TABLE I

Element (1)	$\sigma_b$ (in barns/atom) (2)	$\sigma_f$ (in barns/atom) (3)	$(\sigma_b/\sigma_f)$ Exptl. (4)	$(\sigma_b/\sigma_f)$ Theor. (5)
Carbon	$2.12 \pm 0.02$	2.18	$0.98 \pm 0.01$	$0.98 \pm 0.03$
Aluminium	$4.55 \pm 0.05$	4.72	$0.97 \pm 0.01$	$0.97 \pm 0.03$
Copper	$9.80 \pm 0.1$	10.53	$0.93 \pm 0.01$	$0.95 \pm 0.03$
Cadmium	$15.7 \pm 0.4$	17.4	$0.90 \pm 0.02$	$0.92 \pm 0.03$



cross-sections  $\sigma_f$  are computed using Klein-Nishina formula and are given in column 3 of Table I. The values of cross-section given in column 2 refer to the incoherent scattering of photons by all the electrons of the atom integrated over all angles of scattering. The values of cross-section given in column 3 of Table I are obtained by multiplying the integral free electron cross-section by the atomic number. The ratio  $(\sigma_b/\sigma_f)_{exptl}$  given in column 4 provides a quantitative estimate of the influence of atomic binding on the incoherent scattering of 280 kev gamma rays. A theoretical estimate of this ratio is made using the Thomas-Fermi atomic charge distribution. The relevant procedure is outlined as follows : Data on the incoherent scattering function  $S(q, Z)$  as a function of universal variable  $v$  are compiled by Grodstein (1957) and Nelms (1953). The differential Compton scattering cross-sections for a free electron are computed using Klein-Nishina formula at various scattering angles, at intervals of  $10^\circ$ , in the range  $0^\circ$  to  $180^\circ$ . The value of  $S(q, Z)$  corresponding to each of these scattering angles is obtained by graphical interpolation of the data compiled by Grodstein and Nelms. The differential free electron cross-section is then multiplied by the corresponding  $S(q, Z)$  to yield the differential cross-section for bound electron scattering. By a graphical integration of these free electron and bound electron differential cross-sections in the angular interval  $0^\circ$  to  $180^\circ$ , the corresponding integral cross-sections are computed and the ratio  $(\sigma_b/\sigma_f)_{theor}$  is then directly obtained. The overall error involved in the interpolation and integration procedures is estimated to be about 3%. These theoretical ratios are presented in column 5 of Table I.

## R E S U L T S

It can be seen from columns 2 and 3 of Table I that the bound electron cross-sections progressively deviate from the free electron cross-sections. The increasing influence of atomic binding as  $Z$  increases is clearly evident. From the values of  $(\sigma_b/\sigma_f)_{exptl}$  in column 4 of Table I, it can be readily seen that the diminution in the free electron cross-section due to binding effects is  $(2 \pm 1)\%$  for C,  $(3 \pm 1)\%$  for Al,  $(7 \pm 1)\%$  for Cu and  $(10 \pm 2)\%$  for Cd.

A comparison between theory and experiment is provided by the values given in columns 4 and 5 of Table I. It is apparent that there is good agreement between theoretical and experimental values of the ratio  $(\sigma_b/\sigma_f)$ . This agreement, however, has to be considered with some caution in view of the inadequacies of the Thomas-Fermi model for observed distribution. The charge agreement may be due to the fact that at this energy the absolute magnitude of the influence of binding is itself small, so that the deviations, if any, are masked by the combined errors of theory and experiment. It may, however, be possible that the deviations might be noticeable at lower photon energies where the diminution of  $\sigma_f$  due to binding effects will be considerably large. Further investigations at lower photon energies are in progress to test this view-point.

# ACKNOWLEDGMENT

The authors are thankful to Professor Swami Janananda for his keen interest in this work. The award of Research Fellowship by the Council of Scientific and Industrial research to one of them (PVR) is gratefully acknowledged.

# REFERENCES

- Grodstein, G. W., 1957, N.B.S. Circular, 583.
- Lakshminarayana, V., and Janananda, S., 1961, *J. Sci. Industr. Res.*, **20B**, **1**; 1961, *Proc. Phys. Soc.* **77**, 593.
- Motz, J. W., and Missoni, G., 1961, *Phys. Rev.*, **124**, 1458.
- Nagel, C. H., 1960, *Ark. Fys.*, **18**, (No. 1)1.
- Nelms, A. T., 1953, N.B.S. Circular **542**.
- Parthasaradhi, K., Lakshminarayana, V. & Jananananda, S., 1964, *Indian J. Pure & appl Phys*, **2**, 306.

# Letters to the Editor

The Board of Editors does not hold itself responsible for opinions expressed in the letters published in this section. The notes containing short reports of original investigations communicated to this section should not contain many figures and should not exceed 500 words in length. The contributions reaching the Secretary by the 15th of any month may be expected to appear in the issue for the next month. No proof will be sent to the author.

9

## DIMORPHISM OF DL-ASPARTIC ACID

G. S. R. KRISHNA MURTI, R. NATARAJAN AND A. R. DEB

DIVISION OF AGRICULTURAL PHYSICS,

INDIAN AGRICULTURAL RESEARCH INSTITUTE,

NEW DELHI

(Submitted December 27, 1963; Resubmitted December 19, 1964; January 9, 1965),

The occurrence of dimorphism in *DL*-aspartic acid has not been reported previously. The space group and a preliminary structure of this compound has been worked out by earlier workers (Dawson and Mathieson, 1951; Amirthalingam and Ramachandran, 1955) as  $a = 9.18\text{\AA}$ ,  $b = 7.49\text{\AA}$ ,  $c = 15.79\text{\AA}$ ,  $\beta = 96^\circ$ ,  $Z = 8$  and the space group as  $P2_1/a$ . Pure *DL*-aspartic acid obtained from Nutritional Biochemicals Corporation Ltd., U.S.A., was crystallised from an aqueous solution at room temperature ( $34^\circ\text{C}$ ).

The spacings and  $1/d^2$  values calculated from the powder patterns of the crystals of both the modifications are given in Table I. The visually estimated intensities of the reflections are given in parentheses as very strong (*vs*), strong (*s*), medium (*m*), weak (*w*) and very weak (*vw*).

The pattern of modification II was analysed by a modification of Lipson's method (1949) in which the  $1/d^2$  values were used instead of the  $\sin^2 \theta$  values. The values of  $1/d^2$  calculated after fixing the three constants  $A (= 1/a^2)$ ,  $B (= 1/b^2)$  and  $C (1/c^2)$  were compared with the observed values (Table I), within an accuracy of  $\pm 0.0008$ .

### Modification I

The values of  $1/d^2$  calculated from the data of earlier workers agree reasonably well with the observed values of the present investigation (Table I). Hence the unit cell dimensions of the crystal of this modification are:  $a = 9.18\text{\AA}$ ,  $b = 7.49\text{\AA}$ ,  $c = 15.79\text{\AA}$ ,  $\beta = 96^\circ$  and  $Z = 8$ . The space group is  $P2_1/a$ .

## Modification II

The crystal of this modification was found to belong to orthorhombic symmetry with the unit cell dimensions as  $a = 15.00\text{\AA}$ ,  $b = 6.87\text{\AA}$ ,  $c = 10.26\text{\AA}$ , and  $Z = 8$ . The calculated density of 1.67 agrees very well with the accepted value of 1.663. The values of  $1/d^2$  calculated from this data agree very well with the observed values as can be seen from Table I. The probable space group is  $Pmmn(D_{2h}^1)$ .

The authors are grateful to Dr. B. P. Pal and Dr. C. Dakshinamurti for their interest in the work.

TABLE I  
Spacings and  $1/d^2$  values of DL aspartic acid

Modification I				Modification II			
spacing in A. with intensity	values of $1/d^2$		indices	spacing in A. with intensity	values of $1/d^2$		indices
	obs.	calc.			obs.	calc.	
7.91 (w)	0.0160	0.0162	002	7.52 (w)	0.0177	0.0177	200
6.79 (vw)	0.0217	0.0218	011	5.11 (m)	0.0384	$\begin{cases} 0.0380 \\ 0.0390 \end{cases}$	$\begin{cases} 002 \\ 210 \end{cases}$
5.84 (vw)	0.0292	0.0298	110	4.10 (vs)	0.0596	0.0592	012
4.74 (vw)	0.0449	0.0431	$11\bar{2}$	3.95 (m)	0.0641	0.0635	112
4.59 (s)	0.0475	0.0483	200	3.78 (s)	0.0702	$\begin{cases} 0.0707 \\ 0.0710 \end{cases}$	$\begin{cases} 311 \\ 400 \end{cases}$
4.34 (vw)	0.0530	0.0542	013	3.51 (m)	0.0809	0.0806	401
3.95 (m)	0.0640	0.0648	004	3.42 (m)	0.0855	$\begin{cases} 0.0848 \\ 0.0857 \end{cases}$	$\begin{cases} 020 \\ 300 \end{cases}$
3.87 (w)	0.0667	0.0672	$21\bar{1}^{\dagger}$	3.32 (w)	0.0902	0.0908	103
3.75 (ms)	0.0710	$\begin{cases} 0.0707 \\ 0.0711 \end{cases}$	$\begin{cases} 113 \\ 020 \end{cases}$	3.18 (s)	0.0988	$\begin{cases} 0.0988 \\ 0.0993 \end{cases}$	$\begin{cases} 121 \\ 312 \end{cases}$
3.40 (vs)	0.0867	0.0873	022	2.99 (vw)	0.1114	$\begin{cases} 0.1111 \\ 0.1114 \\ 0.1122 \end{cases}$	$\begin{cases} 500 \\ 113 \\ 221 \end{cases}$
3.27 (vw)	0.0934	$\begin{cases} 0.0935 \\ 0.0938 \end{cases}$	$\begin{cases} 203 \\ 21\bar{3} \end{cases}$	2.89 (s)	0.1199	0.1194	501
3.15 (vw)	0.1013	$\begin{cases} 0.1012 \\ 0.1015 \end{cases}$	$\begin{cases} 005 \\ 20\bar{4} \end{cases}$	2.80 (w)	0.1273	0.1279	122

TABLE I (contd.).

modification I				modification II			
spacing in A. with intensity	values of $I/d^2$		indices	spacing in A. with intensity	values of $I/d^2$		indices
	obs.	calc.			obs.	calc.	
2.92 (m)	0.1170	0.1190	015	2.62 (m)	0.1462	0.1469	313
2.84 (w)	0.1240	$\begin{cases} 0.1238 \\ 0.1240 \end{cases}$	$\begin{matrix} 11\bar{5} \\ 123 \end{matrix}$	2.57 (m)	0.1518	0.1525	004
2.72 (w)	0.1350	$\begin{cases} 0.1350 \\ 0.1359 \end{cases}$	$\begin{matrix} 20\bar{5} \\ 024 \end{matrix}$	2.42 (s)	0.1702	$\begin{cases} 0.1695 \\ 0.1703 \end{cases}$	$\begin{matrix} 601 \\ 204; 512 \end{matrix}$
2.63 (w)	0.1438	0.1471	223	2.38 (w)	0.1770	0.1774	413
2.55 (m)	0.1538	0.1538	114	2.29 (m)	0.1913	$\begin{cases} 0.1905 \\ 0.1915 \end{cases}$	$\begin{matrix} 611 \\ 214 \end{matrix}$
2.46 (vw)	0.1649	$\begin{cases} 0.1642 \\ 0.1647 \end{cases}$	$\begin{matrix} 031; 205 \\ 223 \end{matrix}$	2.24 (w)	0.2003	$\begin{cases} 0.2004 \\ 0.2009 \end{cases}$	$\begin{matrix} 031 \\ 700 \end{matrix}$
2.41 (m)	0.1734	$\begin{cases} 0.1721 \\ 0.1724 \end{cases}$	$\begin{matrix} 130 \\ 025 \end{matrix}$	2.19 (vw)	0.2085	0.2086	230
2.36 (s)	0.1797	$\begin{cases} 0.1795 \\ 0.1798 \end{cases}$	$\begin{matrix} 32\bar{1} \\ 320 \end{matrix}$	2.12 (vw)	0.2227	$\begin{cases} 0.2222 \\ 0.2235 \end{cases}$	$\begin{matrix} 710 \\ 404 \end{matrix}$
2.35 (s)	0.1815	0.1806	016	2.08 (w)	0.2313	$\begin{cases} 0.2310 \\ 0.2316 \end{cases}$	$\begin{matrix} 330 \\ 701 \end{matrix}$
2.29 (w)	0.1910	$\begin{cases} 0.1912 \\ 0.1915 \end{cases}$	$\begin{matrix} 132 \\ 401 \end{matrix}$	2.06 <sub>5</sub> (m)	0.2343	0.2340	522
2.20 (w)	0.2050	$\begin{cases} 0.2042 \\ 0.2058 \end{cases}$	$\begin{matrix} 13\bar{3} \\ 313 \end{matrix}$	2.05 (m)	0.2373	0.2373	024
2.16 (m)	0.2149	0.2153	231	2.04 (m)	0.2396	$\begin{cases} 0.2390 \\ 0.2403 \end{cases}$	$\begin{matrix} 702 \\ 331 \end{matrix}$
2.11 (w)	0.2247	0.2263	207	1.99 (vw)	0.2533	0.2540	621
2.05 <sub>6</sub> (w)	0.2366	$\begin{cases} 0.2360 \\ 0.2372 \end{cases}$	$\begin{matrix} 23\bar{3} \\ 12\bar{6} \end{matrix}$	1.96 (vw)	0.2595	$\begin{cases} 0.2593 \\ 0.2603 \end{cases}$	$\begin{matrix} 015 \\ 712 \end{matrix}$
2.01 <sub>6</sub> (w)	0.2460	0.2473	403	1.92 (m)	0.2708	0.2713	413
1.97 (w)	0.2569	0.2548	126	1.88 <sub>6</sub> (m)	0.2814	$\begin{cases} 0.2810 \\ 0.2816 \end{cases}$	$\begin{matrix} 133 \\ 523 \end{matrix}$
1.92 <sub>8</sub> (vw)	0.2708	0.2714	127				
1.89 <sub>5</sub> (vw)	0.2785	0.2772	331				
1.87 (w)	0.2859	$\begin{cases} 0.2848 \\ 0.2850 \end{cases}$	$\begin{matrix} 234 \\ 217 \end{matrix}$				

TABLE I (*contd.*).

modification I				modification II			
spacing in A. with intensity	values of $I/d^2$		indices	spacing in A. with intensity	values of $I/d^2$		indices
	obs.	calc.			obs.	calc.	
1.82 <sub>4</sub> (w)	0.3007	0.2998 0.3007 0.3009	226 042 118	1.82 (m)	0.3021	0.3020	530
1.78 (w)	0.3173	0.3163	326	1.81 (m)	0.3050	0.3056	810
1.73 <sub>7</sub> (vw)	0.3318	{ 0.3307 0.3314	128 511	1.76 (vw)	0.3236	{ 0.3229 0.3238	025 722
1.71 <sub>8</sub> (vw)	0.3388	{ 0.3383 0.3397	227 241, 416	1.71 <sub>8</sub> (m)	0.3395	{ 0.3393 0.3400	040 532
1.67 <sub>8</sub> (m)	0.3560	{ 0.3555 0.3556	144, 225 317	1.71 (m)	0.3425	0.3430	600
1.65 (vw)	0.3676	{ 0.3672 0.3678	144 219	1.65 <sub>8</sub> (m)	0.3647	0.3642	016
1.60 (m)	0.3879	{ 0.3863 0.3876 0.3887	237 523 236	1.64 (m)	0.3718	0.3715	723

## REFERENCES

- Amirthalingam, V. and Ramachandran, G. N. 1955, *Curr. Sci.*, **24**, 294.  
 Dawson, B. and Mathieson, A. M. 1951. *Acta Cryst.*, **4**, 475.  
 Lipson, H. 1949, *Acta Cryst.*, **2**, 43.

# THERMAL CONDUCTIVITY AND COMPOSITION PROFILE OF A CHEMICALLY REACTING GAS MIXTURE PLACED IN A HOT-WIRE CELL

T. K. RAI DASTIDAR AND A. K. BARUA

INDIAN ASSOCIATION FOR THE CULTIVATION OF SCIENCE, CALCUTTA-32, INDIA.

(Received March 30, 1965)

**ABSTRACT.** A simple method is given for obtaining the actual compositions at the hot and the cold surfaces of a hot-wire thermal conductivity cell in which a chemical reaction of intermediate rate is proceeding. These compositions are related to the rates of formation ( $R_f$ ) and destruction ( $R_d$ ) of a particular species involved in the chemical reaction. ( $R_f - R_d$ ) is a measure of the departure of the system from the condition of local chemical equilibrium.

## INTRODUCTION

The heat flux in a chemically reacting gas mixture placed in a thermal conductivity cell can be divided into two parts, viz., (1) the usual flux in the absence of chemical reactions and (2) the heat flux due to diffusional transport of chemical enthalpies of the reactants and the products. If the reaction rates are so fast that the composition at every point in the conductivity cell is at equilibrium with the local temperature, the thermal conductivity of the reacting gas mixture may be written as (Butler and Brokaw, 1957)

$$\lambda_e = \lambda_f + \lambda_R \quad \dots (1)$$

where  $\lambda_f$  is the thermal conductivity of the 'frozen' (absence of chemical reaction) mixture and  $\lambda_R$ , the contribution due to chemical reaction. A generalised expression for  $\lambda_R$  in this case has been obtained by Butler and Brokaw (1957) and further simplified by Brokaw (1960). Again if the reaction is very slow, it has been shown by Secrest and Hirschfelder (1961) that the composition in the cell becomes almost uniform and the contribution of  $\lambda_R$  to the total thermal conductivity is negligible.

It is most difficult to tackle theoretically the problem of heat conduction when the reaction rate is intermediate. In this case, the heat conductivity becomes a function of the reaction rate and the geometry of the apparatus. Consequently for such a system the usual term 'coefficient of thermal conductivity' has no significance. However, we can still talk about an 'effective thermal conductivity' for such a system placed in a thermal conductivity cell. For such a system an elaborate treatment has been given by Brokaw (1961) which permits an evaluation of the 'effective co-efficient of thermal conductivity' of a reacting gas mixture when the temperature difference between the hot and the cold surfaces of the

conductivity cell is not large (e.g. in a hot-wire cell). When there is local chemical equilibrium, the rates  $R_f$ ,  $R_d$  of the formation and the destruction, respectively, of a particular species involved in a chemical reaction, are equal. When the reaction rate is not fast enough to maintain the condition of local chemical equilibrium,  $R_f \neq R_d$ , and the magnitude of the quantity  $(R_f - R_d)$  is a measure of the departure of the system from local chemical equilibrium.  $(R_f - R_d)$  can be expressed in terms of the actual compositions in the conductivity cell which are different from the local chemical equilibrium compositions. However, from Brokaw's formulation (1961), it is not possible to find directly the actual compositions and effects of relaxation of chemical energy remain obscure. Seerest and Hirschfelder (1961) have attempted to obtain the composition profile in a conductivity cell. However, their method is suitable in cases where there is a large temperature difference in the cell and it also requires laborious numerical techniques.

In the present paper we have attempted to give a comparatively simple method of obtaining the actual compositions of a reacting gas mixture at the hot and the cold surfaces of a hot-wire cell. Experiments performed on the basis of this method are expected to throw some direct light on the actual physical conditions in the cell in which a reacting gas mixture has been placed.

#### THEORETICAL CONSIDERATIONS

We shall limit our present considerations to a unimolecular dissociation reaction given by,



placed in a hot-wire thermal conductivity cell. We shall designate the quantities corresponding to the species  $B$  without any suffix and those corresponding to species  $A$  by the suffix  $A$ . Let  $G_i$  denote the molar flux of the species  $i$  crossing unit length of a cylinder of radius  $r$ . Then, at equilibrium,

$$G_A = -2G \quad \dots (3)$$

For the present case, the equations of multi-component diffusion can be written as

$$2\pi r \frac{dx}{dr} = (nD)^{-1}(xG_A - x_A G) \quad \dots (4)$$

$D$  is the binary diffusion coefficient between  $B$  and  $A$  and  $n = p/RT$ . From Eq. (3) and since  $x + x_A = 1$ , we get

$$2\pi r \frac{dx}{dr} = -(nD)^{-1}(1+x)G \quad \dots (5)$$

and

$$2\pi r \frac{dx_A}{dr} = (nD)^{-1}(1+x)G \quad \dots (6)$$

Eqs. (5) and (6) give

$$\frac{dx}{1+x} = -\frac{(nD)^{-1}}{2\pi} G \frac{dr}{r} \quad \dots (7)$$



When the reaction is fast enough so that the condition of local chemical equilibrium is valid, the heat flux through unit length of the hot-wire cell is given by

$$q = 2\pi\lambda_e \frac{(T_H - T_C)}{\ln r_C/r_H} \quad (8)$$

where  $r_C$ ,  $r_H$  are the radii of the cell and the hot-wire respectively and  $T_C$  and  $T_H$  are the temperatures of the walls of the cell. We shall neglect temperature jump at the walls of the cell and surface chemical reactions.

However, if the local chemical equilibrium condition does not hold, the actual heat flux  $q^*$  is less than  $q$  and we have

$$q^* = 2\pi\lambda^* \frac{(T_H - T_C)}{\ln r_C/r_H} \quad (9)$$

where  $\lambda^*$  is the effective value of the thermal conductivity for the particular cell.

The heat flux  $q$  may also be represented as (Secrest and Hirschfelder, 1961),

$$q = -2\pi r \lambda_f \frac{dT}{dr} - GQ \quad (10)$$

where  $Q$  is the heat of reaction. By using Eqs (7), (9) and (10) and integrating between the hot and the cold surfaces of the cell, we get

$$\lambda_e(T_H - T_C) = \lambda_f(T_H - T_C) + \frac{Q}{\Delta} \ln \left( \frac{x_{Ce} + 1}{x_{He} + 1} \right) \quad (11)$$

$$\text{and} \quad \lambda^*(T_H - T_C) = \lambda_f(T_H - T_C) + \frac{Q}{\Delta} \ln \left( \frac{x_C + 1}{x_H + 1} \right) \quad (12)$$

where  $\Delta = (nD)^{-1}$ . The subscript  $e$  denotes the local chemical equilibrium value. Combining Eqs. (11) and (12) and denoting  $\lambda_e - \lambda^* = \Delta\lambda$  we have

$$\Delta\lambda(T_H - T_C) = \frac{Q}{\Delta} \left[ \ln \left( \frac{x_{Ce} + 1}{x_{He} + 1} \right) - \ln \left( \frac{x_C + 1}{x_H + 1} \right) \right] \quad (13)$$

Eq. (13) expresses the difference between the effective coefficient of thermal conductivity and  $\lambda_e$  in terms of the actual and the local chemical equilibrium compositions at the walls of the cell.

In the reaction



where  $k_f$  and  $k_r$  are the rate constants we have

$$R_f = k_f x \frac{p}{RT}$$

$$R_d = k_r(1-x)^2 \frac{p^2}{R^2T^2} \quad (15)$$

Therefore, for example, at the hot surface of the cell,

$$(R_f - R_d)T_H - k_r \frac{p}{RT} \left[ K_C x_H - \frac{p}{RT} (1 - x_H)^2 \right] \quad \dots \quad (16)$$

Thus if we know  $x_H$  and  $T_H$  the quantity  $(R_f - R_d)$  can be directly obtained. As stated earlier, for local chemical equilibrium  $R_f = R_d$ . Thus the magnitude of  $(R_f - R_d)$  will be a measure of the departure of the system from the condition of local chemical equilibrium.

#### DETERMINATION OF THE ACTUAL COMPOSITIONS AT THE WALLS OF THE THERMAL CONDUCTIVITY CELL

Let the bath temperature  $T_C$  be kept constant and the temperature of the hot-wire be varied slightly from  $(T_H)_1$  to  $(T_H)_2$ . Then from Eq. (13)

$$\Delta\lambda_1[(T_H)_1 - T_C] = \frac{Q}{\Delta} \left( \ln \frac{x_{Ce1} + 1}{x_{He1} + 1} - \ln \frac{x_{C1} + 1}{x_{H1} + 1} \right) \quad \dots \quad (17)$$

$$\Delta\lambda_2[(T_H)_2 - T_C] = \frac{Q}{\Delta} \left( \ln \frac{x_{Ce2} + 1}{x_{He2} + 1} - \ln \frac{x_{C2} + 1}{x_{H2} + 1} \right) \quad \dots \quad (18)$$

the subscripts 1 and 2 correspond to  $(T_H)_1$  and  $(T_H)_2$  respectively. In a hot-wire cell the difference between  $T_C$  and  $T_H$  is not large and  $(T_H)_1$  and  $(T_H)_2$  are also quite close to each other so that it is reasonable to assume that

$$(x_{Ce1} - x_{C1}) = (x_{Ce2} - x_{C2}) \quad \dots \quad (19)$$

$$(x_{He1} - x_{H1}) = (x_{He2} - x_{H2}) \quad \dots \quad (20)$$

Since  $T_C$  is kept constant,  $x_{Ce1} = x_{Ce2}$ ,

$$\text{or} \quad x_{C1} = x_{C2} \quad \dots \quad (21)$$

Thus by knowing  $\Delta\lambda_1$ ,  $\Delta\lambda_2$ ,  $x_{Ce1}$ ,  $x_{He1}$ ,  $x_{He2}$  and using Eqs. (20), (19) and (21)  $x_C$  and  $x_H$  values can be obtained from Eqs. (17) and (18). The equilibrium compositions can be calculated from the experimentally determined equilibrium constants. The values of  $(R_f - R_d)$  can be obtained from Eq. (16).

Experiments on the system  $\text{N}_2\text{O}_4 \rightleftharpoons 2\text{NO}_2$  by utilising the method described above are in progress.

#### ACKNOWLEDGMENT

The authors are grateful to Prof. B. N. Srivastava for his kind interest and encouragement.

#### REFERENCES

- Brokaw, R. S., 1960, *J. Chem. Phys.*, **32**, 1005.  
 Brokaw, R. S., 1961, *J. Chem. Phys.*, **35**, 1569.  
 Butler, J. N., and Brokaw, R. S., 1957, *J. Chem. Phys.*, **26**, 1636.  
 Secrest, D., and Hirschfelder, J. O., 1961, *Phys. Fluids*, **4**, 61.

# ESTIMATION OF AIR-FRACTION, SPECIFIC SURFACE AND OTHER PARAMETERS OF MICELLE SYSTEMS— WOOL—LOW ANGLE X-RAY METHODS

T. RATHO AND B. C. PANDA

REGIONAL ENGINEERING COLLEGE, ROURKELA

(Received February 15, 1965)

**ABSTRACT.** This paper deals with the estimation of the percentage of air, the specific surface, the length of coherence, the range of inhomogeneity and the characteristic number of a sample of wool, Scottish Blackface, from England. The low angle scattering camera after Kratky (1958) was used for the experimental measurements. The calculations are similar to those applied by Porod (1951) to two phase systems.

## INTRODUCTION

The analysis of the diffraction pattern obtained under small angle scattering is due to Guinier (1937, 1939 and 1943). He introduced the idea of "Particle scattering," continuous low angle scattering considered to be a non-coherent scattering of the individual particles. It can be easily seen that this theory will apply only to dilute systems. During the same period, however, Kratky and his co-workers made an attempt to explain the scattering effects of densely packed colloidal systems on the basis of interparticular interference. This led to a good treatment of some of the micelle systems by Kratky (1938, 1942 and 1949) and also by Porod (1949 and 1951). A large volume of work has also appeared in recent years (Kratky 1962 Porod 1961). We have in this paper followed the considerations of Kratky to find out the parameters of the sample of wool belonging to the densely packed systems.

For a thorough analysis of low angle scattering the following assumptions have also been made.

(i) The incoherent Compton scattering is neglected as we are here concerned with very low angles of the order of  $10^{-3}$  of a radian. Further as this is a densely packed system, the coherent scattering effects are very high compared to the very low effects due to Compton scattering.

(ii) The Babinet's reciprocal relation in Optics is assumed to be valid.

Low angle treatments of the micelle systems allow only the estimation of such parameters common to both the phases and also of the statistical mean values of certain lengths known as the range of inhomogeneity " $l_r$ " and the distance of heterogeneity or the extent of coherence  $l_c$  according to Porod (1961). We have

here tried to find out these above quantities from our experimental observations on this particular sample of wool. It is also very interesting to find out the percentage of air fraction in it, while this may throw light on the textile properties of the substance.

## EXPERIMENTAL

The source of x-rays was a Philips unit fitted with a copper target. The low angle scattering camera of Kratky (1958) fitted with photographic arrangement was set up along with a crystal monochromator after Johanson-Guinier (1956) to record the scattered intensities. The sample of wool investigated was of the type Scottish Blackface from England. The density of the compact material is assumed to be 1.35 gm/cc, while the sample had an apparent density of 0.376 gm/cc. The experimental details regarding the purification of the sample and its mode of setting up in the Kratky camera are the same as reported in a paper by us (T. Ratho *et al.* 1965). The process of obtaining the scattered intensity was also the same as in the above paper. It may be mentioned here that for recording a particular angular range of scattering only a single photographic record is necessary, since a monochromator is used. From these measurements therefore it is possible to obtain the scattering angle and the corresponding scattered intensity values. For convenience the angle of scattering  $2\theta$  has been represented by  $x$  where  $x$  is given by

$$x = 2\phi(ap)$$

Here  $a$  is the film sample distance and  $p$  is the transformation factor of the densitometer curves.

As the sample under investigation has some degree of orientation, it is not necessary to make any slit correction and one can proceed with the smeared-out intensity  $\bar{I}$  values. In order to calculate the integrated primary intensity  $P_0$ , the primary beam was recorded on a film twice, once for 15 seconds and again for 25 seconds with a reduction factor of 100/3. After microphotometry of these records the areas of the primary beam cross-sections were found out with the help of a planimeter.

## THEORY AND DISCUSSION

### (a) Calculation of $P_0$

The two areas of the primary beam cross-sections obtained for times of exposure 15 and 25 seconds were 21.22 cm<sup>2</sup> and 34.95 cm<sup>2</sup> respectively. As the sample was exposed for 6 hours and as the reduction factor of the primary beam is 100/3, we can easily calculate the average value of  $P_0$ . It is given by

$$P_0 = \text{Area under the curve} \times \frac{\text{Time of exposure of sample}}{\text{Time of exposure of primary beam}}$$

Therefore, on substituting the above value, we have

$$P_0(15) = \left( \frac{3600 \times 6}{15} \right) \quad 21.22 \quad \left( \frac{100}{3} \right) = 1019 \times 10^3$$

$$P_0(25) = \left( \frac{3600 \times 6}{25} \right) \quad 34.95 \quad \left( \frac{100}{3} \right) = 962 \times 10^3$$

Therefore the average value of  $P_0$  is  $991 \times 10^3$ .

(b) *The invariant Q*

For calculating the value of the specific surface it is necessary to find out the value of the quantity  $Q$  known as the invariant. According to the theories of Debye and Bueche (1949) as well as of Porod (1951), in the case of a two phase system, the invariant  $Q$  of a scattering curve is independent of the shape and size of the particles responsible for scattering. On the other hand, it depends on the scattering power of the system. It, however, is not independent of the primary beam intensity. This invariant  $Q$  is given by

$$Q = \int_0^{\infty} I(x)x^2 dx$$

for a slit corrected intensity ;

or, 
$$\tilde{Q} = \int_0^{\infty} \tilde{I}(x)x dx$$

for intensity not corrected for collimation error as in the present case. The value of  $\tilde{Q}$  is obtained after drawing  $\tilde{I}(x)x$  versus  $x$  curve and planimetrying the area under it. The value obtained in the present case is  $978 \text{ cm}^2$  and is represented as  $\tilde{Q}_{exp}$ , meaning thereby the experimental value of the invariant.

(c) *Invariant and air-fraction*

The effective sample thickness is given by  $D$

where, 
$$D = \frac{d_a}{d_c} \cdot \phi.$$

Here the density of (compact) wool is assumed to be

$$d_c = 1.35$$

and the apparent density is

$$d_a = 0.376$$

where  $\phi$  is the diameter of the Mark capillary container and has a value  $1.69 \text{ mm}$ .

On substituting the above values we have

$$D = 0.047065 \text{ cm}.$$

The electron density of wool is represented by  $\rho$  which is expressed as

$$\rho = d_e \frac{\Sigma O}{\Sigma A} = 1.35(0.535) = 0.7223$$

where,  $\Sigma O$  is the sum of the atomic numbers and  $\Sigma A$  is the sum of the atomic weights.

This  $\frac{\Sigma O}{\Sigma A} = 0.535$  is taken here, in the case of wool, to have the same value as proteins.

In order to interpret the invariant  $\tilde{Q}_{exp}$  given by  $\tilde{Q}_{exp} = \int_0^\infty \tilde{I}(x) \times dx$  whose estimated value is  $978 \text{ cm}^2$ , we assume that the system contains air.

The theoretical invariant comparable with  $\tilde{Q}_{exp}$ , is given by

$$\tilde{Q}_{Th} = \frac{7.9 \times 10^{-26}}{2\pi} \cdot \lambda^3 N^2 P_0 D(ap) \rho^2 \omega_1 \omega_2$$

for  $\lambda = 1.54 \text{ \AA}$ ,  $N$  being the Avogadro's number,  
 $p_0$  is the integrated primary intensity,  
 $\omega_1$  is the volume fraction of air, and  
 $\omega_2$  is the volume fraction of wool.

On substituting the values of  $a = 20.8$ ,  $\rho = 25.4$ ,  $P_0 = 0.991 \times 10^6$ ,  $\rho^2 = 0.5216$  and  $D = 0.047$ , we get

$$\tilde{Q}_{Th} = 2.1469 \times 10^5 \omega_1 \omega_2.$$

From  $\tilde{Q}_{Th} = \tilde{Q}_{exp}$  follows,

$$\omega_1 \omega_2 = 4.5572 \times 10^{-3}.$$

That means  $\omega_1 \sim 4.5572 \times 10^{-3}$

and  $\omega_2 \sim 1$ .

Therefore the system contains about 0.5% air.

#### (d) Specific surface

In the case of a two phase system it is at times very convenient to exploit the tail portion of the scattering curve corresponding to high angles of scattering. According to Porod (1951) the tail portion of a smeared-out scattering curve of a general two phase system as in the present case has a decrease proportional to  $x^{-3}$ . The tail portion however follows a course  $x^{-4}$  for a curve corrected for length collimation error. Homogeneous electron density distribution however is assumed within each phase. The  $\tilde{I}(x)x^3$  versus  $x$  curve should show therefore an asymptotic behaviour for large values of  $x$  in our present case.

We can therefore write

$$\lim \tilde{I}(x)x^3 = \tilde{k}, \text{ where } \tilde{k} \text{ is a constant.}$$

The relative curve is plotted in Fig. 1 after our experimental observations from Table I, where the value of  $\tilde{k}$  is obtained as 380. This value is related to the

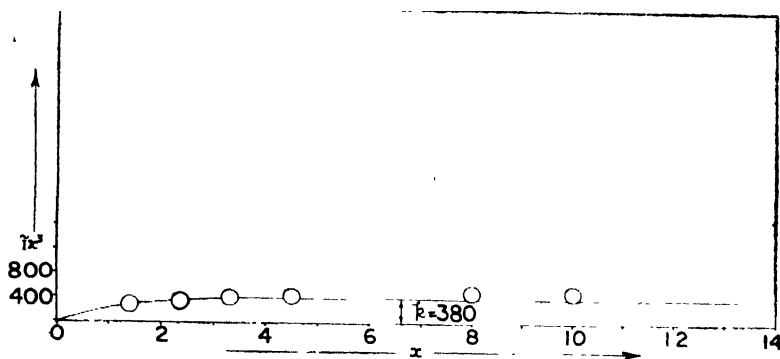


Fig. 1

specific inner surface, i.e. the phase boundary area per unit volume of dispersed phase.

This behaviour of the scattering curve can also be verified by drawing the double logarithmic plot, i.e.  $\log I(x)$  as a function of  $\log x$  which should lead to a straight line of slope—3. This is shown in Fig. 2 where a slope of —2.97 is obtained, while the dotted line is the line of slope—3.

The specific surface (per  $\text{\AA}^3$  sample volume) is given by Porod (1952) as

$$\frac{O}{V} = \frac{8\pi}{\lambda \mu p} \times \frac{\tilde{k}}{\tilde{Q}_{exp}} \cdot \omega_1 \omega_2 = \frac{16.32}{a p} \times \frac{\tilde{k}}{\tilde{Q}_{exp}} \cdot \omega_1 \omega_2 \quad (\text{for } \lambda = 1.54 \text{\AA})$$

with  $\tilde{k} = 380$  and  $\omega_1 \omega_2$  as calculated before we get, on substitution,

$$\frac{O}{V} = \frac{16.32 \times 380 \times 4.5572 \times 10^{-3}}{20.8 \times 25.4 \times 978} = 5.4702 \times 10^{-5} \text{ cm}^2/\text{\AA}^3.$$

The mean dimensions  $\bar{l}_1$  and  $\bar{l}_2$  of the sample are calculated therefore to be

$$\bar{l}_1 = \frac{4V\omega_1}{O} = 333.28 \text{\AA}$$

and

$$\bar{l}_2 = \frac{4V\omega_2}{O} = 7.3131 \times 10^4 \text{\AA}.$$

In this case  $\bar{l}_1$  is practically identical with the reduced length  $l_r$ , defined by, according to Porod (1953),

$$\frac{1}{l_r} = \frac{1}{\bar{l}_1} + \frac{1}{\bar{l}_2}$$

and for example  $l_r = \frac{4V\omega_1\omega_2}{\alpha}$  ; since  $\omega_2 = 1$

( $l_r$ , the range of inhomogeneity given by the above formula corresponds to that of reduced mass in Mechanics. In interpreting certain results Porod introduces the length  $l_r$  known as the "range of inhomogeneity". This is symmetrical with respect to the two average dimensions of the specimen occupied by matter and is built up in the same manner as the reduced mass in Mechanics).

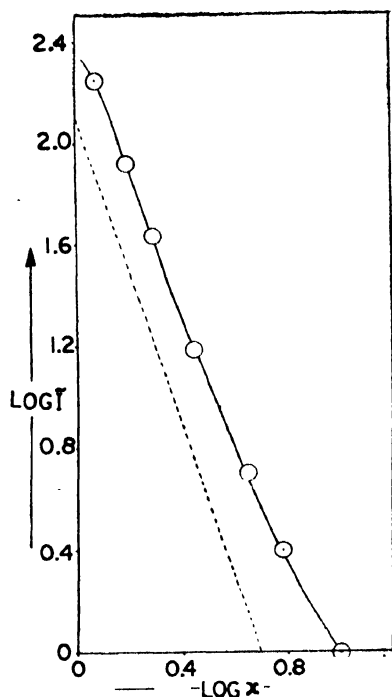


Fig. 2

(e) *Length of coherence  $l_c$*

The integrated scattered energy is given by

$$\tilde{E} = \int_0^{\infty} \tilde{I}(x) dx$$

In order to get the value of  $\tilde{E}$  the  $\tilde{I}(x)$  versus  $x$  curve is drawn and the area under the curve is found out with the help of a planimeter. The value of  $\tilde{E}$  obtained



in the present case is 1188.0 cm<sup>2</sup>. The length of coherence  $l_c$  is derived from the smeared-out scattering curve according to the relation

$$l_c = \frac{\lambda}{\pi} ap \frac{\int_0^\infty \tilde{I}(x) dx}{\int_0^\infty \tilde{I}(x) x dx} = 0.490 ap \frac{\tilde{E}}{\tilde{Q}_{exp}}$$

On substituting the values of  $E$ ,  $a$  and  $p$  as  $\tilde{E} = 1188.0$ ,  $a = 20.8$  and  $p = 25.4$  and  $\tilde{Q}_{exp} = 978.0$  we get

$$l_c = 314.48 \text{ \AA.}$$

(f) *The characteristic number  $f$*

The characteristic number " $f$ " is given by

$$f = \frac{1}{2} \frac{l_c}{l_r} = \frac{1}{2} \frac{l_c}{l_1} = 0.47181.$$

TABLE I  
(Experimental measurements)

$x$	$\tilde{I}$	$\tilde{I}x^3$	$\log x$	$\log \tilde{I}$
1.2	176.0	304.09	0.07918	2.24551
1.30	125.6	275.93	0.11394	2.09895
1.40	105.2	288.66	0.14613	2.02200
1.55	83.6	311.31	0.19033	1.92221
1.70	65.6	322.26	0.23045	1.81690
1.95	43.4	321.81	0.29003	1.63749
2.20	26.9	286.42	0.34242	1.42975
2.35	23.0	298.47	0.37107	1.36173
2.50	18.8	293.76	0.39794	1.27416
2.80	15.2	333.66	0.44716	1.18184
3.05	12.8	363.18	0.48430	1.10721
3.30	11.5	413.24	0.51851	1.06070
3.50	10.0	428.75	0.54407	1.00000
4.00	7.1	454.40	0.60206	0.85126
4.50	5.0	455.62	0.65321	0.69897
5.00	3.9	487.50	0.69897	0.59106
6.00	2.5	540.00	0.77815	0.39794

Although this value is slightly low it is almost the probable value for densely packed systems where the independent micelle are arranged in layers with free space, in between.

### CONCLUSION

The specific surface per  $\text{\AA}^3$  sample volume is found to be  $5.47 \times 10^{-5} \text{ cm}^2/\text{\AA}^3$ . The sample contains about 0.5% of air. The range of inhomogeneity  $l_r$  is 333.28  $\text{\AA}$ . The length of coherence  $l_c$  is 314.48  $\text{\AA}$ . The characteristic number  $f$  of the system is 0.472. Further experiments are being undertaken to find out the relation of these quantities with the textile properties of the sample.

### ACKNOWLEDGMENT

The authors wish to express their sincere thanks to Prof. Dr. O. Kratky Graz University, Austria, for some very helpful suggestions.

### REFERENCES

- Debye, P. and Bueche, A. M., 1949, *J. Appl. Phys.*, **20**, 518.  
 Guinier, A. 1937, *C. R. Hebd. Seances Acad. Sci.*, **204**, 1115.  
 ——— 1939, *Ann. Physique*, **12**, 161.  
 ——— 1943, *J. Chem. Physique*, **40**, 133.  
 Kratky, O., 1942, *Naturwiss.*, **30**, 542.  
 ——— 1938, *Naturwi. Naturwiss.*, **26**, 94.  
 Kratky, O. and Scala, Z., 1958, *Z. Elektrochemie*, **62**(1), 66.  
 Kratky, O., Sekora, A. and Treer, R., 1942, *Z. Elektrochemie*, **48**, 587.  
 Kratky, O. and Porod, G., 1949, *J. Colloid Sci.*, **4**, 35.  
 Kratky, O., 1962, In *Moderne Methoden der Pflanzenanalyse*, Verlag-Springer, Berlin.  
 Porod, G., 1949, *Acta Physica Austriaca*, **3**, 66.  
 ——— 1951, *Kolloid, Z.*, **124**, 83; **125**, 51.  
 ——— 1952, *Kolloid- Z.*, **125**, 51.  
 ——— 1961, *Fortschr. Hochpol. Forsch.*, **2**, 363.  
 Ratho, T., Sahu, N. C., Misra, T. and Panda, B. C., 1965, *Ind. J. Pure and Appl. Phys.*,  
 (Under publication).

GAMMA-GAMMA ANGULAR CORRELATION IN  $\text{Sn}^{125}$ 

A. K. NIGAM AND R. BHATTACHARYYA

SAHA INSTITUTE OF NUCLEAR PHYSICS, CALCUTTA, INDIA.

(Received January 15, 1965)

**ABSTRACT.** Spin assignment to the 2.23, 1.98, 1.88, 1.41 and 1.07 MeV levels of  $\text{Sb}^{125}$  has been made from directional angular correlation measurements.

## INTRODUCTION

The levels of  $\text{Sb}^{125}$  excited through the decay of  $\text{Sn}^{125}$  have been previously studied by several authors (Nuclear Data Sheets, 1964, Devare *et al.*, 1964). The spin-parities of these levels were ascertained mainly from the knowledge of the beta-decay log ft-values. In the present work the spins of some of the levels have been determined from  $\gamma$ - $\gamma$  angular correlation experiments.

The experimental sources were prepared in small thin-walled perspex containers from chemically processed  $\text{Sn}^{125}$  obtained from the Oak Ridge National Laboratory. The 9.4 min activity of  $\text{Sn}^{125}$  was allowed to decay sufficiently before the chemical separation was carried out in order to get rid of some  $\text{Sb}^{125}$  activity formed therefrom. The activity of  $\text{Sb}^{125}$  accumulating from the decay of the 9.7d  $\text{Sn}^{125}$ , was not large enough to disturb our measurements within the short time in which the experiments were performed.

## EXPERIMENTS AND RESULTS

$\gamma$ - $\gamma$  angular correlation between five cascades, shown in Table I has been measured. The spins of the 2.23, 1.98, 1.88, 1.41 and 1.07 MeV levels were determined. As it was not possible to study the short lived isomer of  $\text{Sn}^{125}$ , the spins of the levels at 0.325, 0.640, 0.910, 1.470, 1.720, 1.940 MeV could not be determined. The summation technique of Hoogenboom (1958) was used to separate the peaks more effectively from the general Compton background and from other adjoining peaks. Fig. 1 shows some of the representative spectra measured with the help of this method. The spectrum of Fig. 1(a) was recorded with the sum channel set at 1.8-2.1 MeV region. As both of 0.81 and 0.91 MeV  $\gamma$ -rays are in coincidence with the 1.07 MeV  $\gamma$ -ray, they, with their respective intensities, contribute to the area under the 1.07 MeV peak. The prominent peak in Fig. 1(b) is due to the coincidence between the sum-pulses at 1.41 MeV ( $= 1.07 + 0.34$ ) and 0.34 MeV  $\gamma$ -ray. The second peak in the same spectrum arises due to the straightforward coincidence between the 0.47 MeV  $\gamma$ -ray and the  $\gamma$ -ray of 1.41 MeV energy selected

along with the sum-pulses. In order to increase the area under the 1.16 MeV peak shown in Fig. 1(d), a broad selection was made in the sum channel (2—2.3MeV) which admitted some of the sum-pulses of the 0.81—1.07 and 0.91—1.07 MeV cascades resulting in an increase in the area under the 1.07 MeV peak.

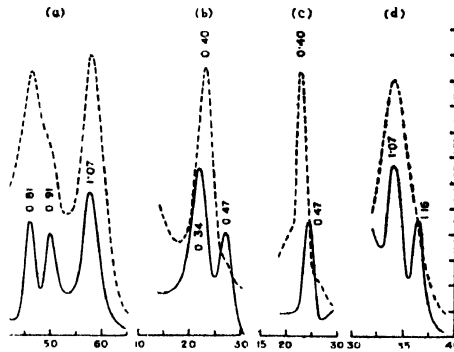


Fig. 1. Solid Curves : Hoogenboom-spectra of the  $\gamma$  rays of  $\text{Sb}^{123}$ . Cotted Curves: Spectra recorded in the straightforward manner. Spectra in the region of interest have been Shown.

The correlation experiment performed with these spectra in the channels need little correction due to other perturbing radiations. However, for the weak intensity cascades, statistical accuracy in the result could not be increased sufficiently. Measurements were also conducted using the conventional slow-fast coincidence method for all the cascades except the 1.16—1.07 MeV one and essentially same results were obtained. The  $A_2$  and  $A_4$  coefficients were calculated according to the formulation of Rose (1953). Geometry correction was made from the curves by Stanford and Rivers (1959).

TABLE I  
Experimental results

Cascade MeV	Sum channel setting	$A_2$ Exp.	$A_4$ Exp.	Possible Assignment
0.81—1.07	1 80—2.00	$0.131 \pm 0.032$	$-0.046 \pm 0.05$	$13/2(3)7/2(1)7/2$
0.91—1.07	1 90—2.10	$0.176 \pm 0.031$	$-0.111 \pm 0.05$	$11/2(2)7/2(1)7/2$
0.34—1.07	1.35—1.45	$0.031 \pm 0.036$	$0.037 \pm 0.05$	$11/2(2)7/2(1)7/2$
0.47—1.41	1.80—2.00	$-0.078 \pm .078$	$-0.026 \pm 0.12$	$13/2(1)11/2(2)7/2$
1.16—1.07	2 00—2.30	$0.084 \pm 0.083$	$0.019 \pm 0.10$	$\left\{ \begin{array}{l} 11/2(2)7/2(1)7/2 \\ 11/2(2)9/2(1)7/2 \\ 9/2(2)9/2(1)7/2 \end{array} \right.$

## DISCUSSION

The ground state of  $\text{Sn}^{125}$  and  $\text{Sb}^{125}$  have been assigned on the basis of single particle shell model (Goldhaber and Hill, 1952). The beta spectrum of  $9.7d$   $\text{Sn}^{125}$  was also measured with a Siegbahn-Slätis spectrometer. The end-energies

and log  $ft$ -values were found to be in accord with these previous results (Devare *et al.*, 1964). The spin assignments to the levels of  $\text{Sb}^{125}$  from the present measurements shown under  $J[\gamma\gamma(\theta)]$  in Fig. 2. are compatible with both log  $ft$  and angular correlation data.

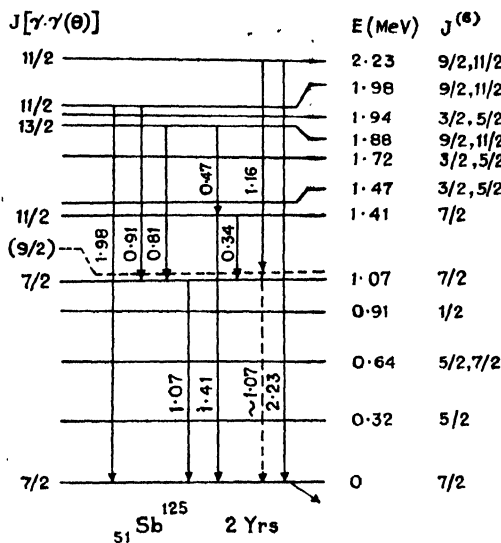


Fig. 2. Proposed level-scheme of  $\text{Sb}^{125}$ .

Explanation of the level spectrum of  $\text{Sb}^{125}$  was suggested by Silverberg (1961) on the basis of the coupling between the  $g_{7/2}$  and  $d_{5/2}$  odd protons with the harmonic vibration of the  $2^+$  one phonon excitation of the even-even core. However the centre of gravity rule does not seem to hold good there. In order to make the C. G. Rule fit into this scheme we require two sets of states arising due to these couplings. For the  $g_{7/2}$ ,  $2^+$  coupling the C. G. lies at 1.15 MeV considering the 0.640, 1.075, 1.41 and 1.47 MeV levels of Fig. 2, in which a  $9/2^+$  level has been left out. In Table 1 the 1.16–1.075 MeV cascade shows the possibility of a  $9/2^+$  intermediate level at or near 1.075 MeV, not resolved from the  $7/2^+$  1.075 MeV line in the spectrum. This would, however, suggest a mode of decay for the 2.23 MeV level and a  $9/2^+$  level very nearly at 1.075 MeV. When this level is taken into consideration the above values of C. G. comes out to be at 1.11 MeV, fairly in agreement with the energy of the  $2^+$  state of  $\text{Sn}^{124}$  at 1.13 MeV. Some of the other levels belong to the  $d_{5/2}$ – $2^+$  coupling. At the present stage the set for this scheme cannot be completed. Moreover, the levels at 1.88, and 1.98 MeV have high spin values whose origin cannot be connected to any of the above mode of couplings.

## ACKNOWLEDGMENT

The authors are grateful to Prof. A. K. Saha for his encouragement during the progress of the work. They are also thankful to Mr. S. Shastry and Mr. B. B. Roy for their help.

## REFERENCES

- Devare, S. H. and Devare, H. G., 1964, *Phys. Rev.*, **133**, No. 3B, B568.  
Goldhaber M. and Hill, R. D., 1952, *Revs. Modern Phys.*, **24**, 179.  
Hoogenboom, A. M., 1958, *Nuclear Instruments and Methods*, **3**, 57.  
*Nuclear Data Sheets*, National Academy of Sciences, National Research Council, Washington D. C. (1964)  
Rose, M. E., 1953, *Phys. Rev.*, **91**, 610.  
Silverberg, Lars, 1961. *Arkiv Fysik*, **20**, 341.  
Stanford, A. L. and Rivers, W. K., Jr., 1959, *Revs. Scientific Instruments*, **30**, 719.

# IONIZATION CROSS-SECTIONS OF ATOMS AND MOLECULES BY ELECTRON IMPACT

A. K. BATABYAL, A. K. BARUA AND B. N. SRIVASTAVA

INDIAN ASSOCIATION FOR THE CULTIVATION OF SCIENCE, CALCUTTA-32.

(Received March 30, 1965)

**ABSTRACT.** Apparent ionization cross-sections of several atoms and molecules for 70 ev electrons have been measured with the help of a mass spectrometer. By introducing a simple correction an attempt has been made to improve the method of Otvos and Stevenson for the calculation of the ionization cross-sections of atoms and molecules. With this correction, the additivity postulate for the molecular ionization cross-sections appears to hold better.

## INTRODUCTION

The knowledge of ionization cross-sections of atoms and molecules has various practical applications in problems of physics and astro-physics. This is of particular interest and importance in the analytical applications of mass spectrometry. The ionization cross-section is intimately related to the electronic structure of atoms and molecules. However, till now reliable data on the ionization cross-sections are very scanty. The earliest absolute measurements of the ionization cross-sections are those of Bleakney (1930), Smith (1930) and Tate and Smith (1932). More recently, Otvos and Stevenson (1956), to be subsequently referred to as O and S, and Lampe, Franklin and Field (1957) subsequently referred to as L.F. and F have used mass spectrometers to obtain the total cross-sections of a large number of atoms and molecules using 75 ev electrons as the ionizing agent in the source of the mass spectrometer. The agreement between the two sets of data is not quite satisfactory. The methods available at present for the calculation of the ionization cross-sections are at best approximate. By considering their own experimental data O and S have suggested that the molecular ionization cross-sections can be calculated as a purely constitutive property of the gaseous substance. This suggestion of O and S has been critically analysed and compared by L. F. and F with their own experimental data. They have arrived at the conclusion that the seeming agreement between O and S calculated and experimental values is a consequence of compensating errors and therefore reservations have been expressed regarding the validity of additivity postulate for calculating molecular ionization cross-sections. The present state of our knowledge of ionization cross-sections of atoms and molecules has been reviewed by Haissinsky (1961). It is clear that further independent experimental measurements are needed to resolve the discrepancies between various sets of data

which will also help in formulating a better theoretical method for the calculation of molecular ionization cross-sections. With this end in view we have measured the ionization cross-sections of several atoms and molecules by bombarding them with 70 ev electrons at the source of our MS3 mass spectrometer (manufactured by Messrs Associated Electrical Industries Ltd., U.K.).

In the second half of the paper, attempt has been made to introduce a simple correction and thereby improve the method of calculation of molecular ionization cross-sections as suggested by O and S. With this correction the additivity postulate for molecular ionization cross-section appears to hold better.

### EXPERIMENTAL

In a mass spectrometer if ' $i$ ' is the electron current and ' $i^+$ ' is the positive ion current,  $N$  the number density of the atoms and ' $l$ ' the path length of the electrons then Massey (1956)

$$i^+/i = NlQ_i^{app} \quad \dots (1)$$

where  $Q_i^{app}$  is the apparent ionization cross-section which may be written as

$$Q_i^{app} = Q_i^{(1)} + 2Q_i^{(2)} + 3Q_i^{(3)} + \dots \quad \dots (2)$$

where  $Q_i^{(1)}$ ,  $Q_i^{(2)}$  .... are the cross sections for single, double ... etc. ionization. For effusive flow, if we determine total ion current as a function of the reservoir pressure in the mass spectrometer, a straight line should be obtained by plotting the total ion current ' $i^+$ ' against reservoir pressure, with the slope proportional to the ionization cross-section. By taking the absolute ionization cross section of a substance from some other source (e.g. Smith, 1930 and Tate and Smith 1932) as standard, one can find the apparent ionization cross-section  $Q_i^{app}$  for any other substance.

Experimental measurements were made with the MS3 mass spectrometer which is a 90°-sector type instrument, with a tube radius of 4 in. The ion source was run with 2kv ion accelerating voltage, 70 ev electron accelerating voltage, 3V ion repeller voltage and 85 $\mu$ A trap current. Peaks were tuned by magnetic scanning and very small variation of the ion accelerating voltage. The gas reservoir of the mass spectrometer was slightly modified to include a McLeod gauge for measuring the reservoir pressure accurately. The gases He, Ne, A, Kr, Xe, N<sub>2</sub> and O<sub>2</sub> were supplied by Messrs British Oxygen Co., as spectroscopically pure.

The total ion current was determined by adding up the specific intensities of the ions in the resolved mass spectra. The total mass spectral sensitivity, however, has not been corrected for the mass discrimination effect as this is minimised to a large extent by employing magnetic scanning in our mass spectrometer and whatever discrimination still remains will be more pronounced in case of fragment ions



with large initial kinetic energies formed as a result of dissociation of molecules. Thus the effect of neglecting mass discrimination in calculating the relative total ionization cross-section from the total mass spectral sensitivity data can be considered to be minor especially in the case of monatomic gases. The absolute ionization cross section of argon at 70 ev which is used as standard is taken to be  $3.58 \times 10^{-16} \text{ cm}^2$ , which is the value of ionization efficiency of argon at 70 ev (12.75 positive ions/cm path/mm pressure at 0°C) as reported by Smith (1930) multiplied by the conversion factor  $2.81 \times 10^{-17}$  to get the cross section in  $\text{cm}^2$  unit. The results thus obtained are shown in Table I. For the sake of comparison we have also given the value of 75 ev as obtained by O and S and L. F. and F with a slight correction. The value of the ionization cross section of argon at 75 ev has been taken as  $3.62 \times 10^{-16} \text{ cm}^2$  as reported by Smith (1930) and not  $3.52 \times 10^{-16} \text{ cm}^2$ . The ionization cross section of other atoms and molecules have increased slightly due to this change in the value of the standard.

**TABLE I**  
Ionization Cross Sections of Atoms and Molecules  
( $Q_i \times 10^{16} \text{ cm}^2$ )

Substance	70 ev electrons		75 ev electrons		
	This work	Absolute measurement	Absolute measurements	O & S (1956) Expt.	L.F. & F. (1957) Expt.
He	0.309	0.312 <sup>a</sup>	0.322 <sup>c</sup>	0.299	0.397
Ne	0.553	0.593 <sup>a</sup>	0.622 <sup>c</sup>	0.579	0.633
A	3.58	3.58 <sup>a</sup>	3.62 <sup>c</sup>	3.62	3.62
Kr	5.17	—	—	5.55	5.33
Xe	6.68	—	—	—	7.53
N <sub>2</sub>	2.47	2.67 <sup>b</sup>	2.74 <sup>d</sup>	2.72	2.96
O <sub>2</sub>	2.51	2.63 <sup>b</sup>	2.70 <sup>d</sup>	2.34	2.58

a Smith (1930)

b Massey, H.S.W. and Burhop, E.A., *Electronic and Ionic Impact Phenomena*, p. 265, Oxford University Press, Oxford, 1952.

c Interpolated values from Smith (1930).

d Interpolated values from Tate & Smith (1932).

It may be seen that the agreement between our measurements and those of Tate and Smith (1932) is fairly good. For krypton and xenon no data are available for 70 ev electrons. It is possible that due to the presence of various electrostatic fields and secondary electrons in the source of the mass spectrometer

some uncertainty will occur in the determination of the ionization cross section by this method.

# THEORETICAL CALCULATION OF THE IONIZATION CROSS-SECTIONS

Bethe's (1930) formula for the total ionization cross-section may be written as

$$Q_{nl}^i = \frac{2\pi e^4}{mv^2} \cdot \frac{c_{nl}}{E_{nl}} \cdot Z_{nl} \log \left( \frac{2mv^2}{C_{nl}} \right) \quad \dots (3)$$

where  $e$  is the charge,  $m$  the mass and  $V$  is the velocity of the electrons.  $E_{nl}$  is the ionization potential and  $Z_{nl}$  the nuclear charge corresponding to the  $nl$  shell.  $C_{nl}$  is an energy of the order of the ionization potential and  $c_{nl}$  is given by

$$c_{nl} = (Z_{eff}^2/n^2a_0^2) \int |x_{nl,k}|^2 dk. \quad \dots (4)$$

$|x_{nl,k}|^2$  is one-third the mean square radius of the electron and  $dk$  corresponds to a range of energy such that  $k$  lies between  $k$  and  $k+dk$ .  $K$  is related to  $E_k$ , the energy of the level, by the relation,

$$E_k = k^2\hbar^2/8\pi^2m. \quad \dots (5)$$

However, it is not possible to apply Eq. (3) satisfactorily to atoms more complex than helium. In order to calculate the ionization cross-sections of atoms, O and S have modified Bethe's (1930) formula. According to the modified method, the ionization cross-section is calculated as the sum of the outer or valence electrons weighted by the mean square radii of those electron, as calculated from hydrogenlike wave functions.

In order to calculate molecular ionization cross-sections, O and S have used the additivity postulate according to which the ionization cross-section is the sum of the cross-sections of the constituent atoms. In a subsequent publication L.F. and F have analysed their own data on the ionization cross-sections of a large number of atoms and molecules as well as those of O and S. Their analysis shows that the agreement between the experimental and the theoretical values of the total ionization cross-sections calculated by the O and S method is not satisfactory and the additivity postulate does not hold well.

A look at Table II shows that for the atoms the difference between the calculated and the experimental values of the total ionization cross-section increases with the increase of the atomic number  $Z$ . It has also been pointed out by O and S that due to the method of calculation, the values of the mean-square radius become too large for the outer or valence electrons for higher  $Z$  values. This error in calculating the mean-square radii results in too high values of the ionization cross-sections calculated by the O and S method,

TABLE II

Experimental and calculated atomic ionization cross sections,  
( $Q_i \times 10^{16} \text{ cm}^2$ )

Substance	Z	O & S (1956) (Expt.)	O & S (1956) (Calc.)	Deviation
He	2	0.299	0.347	+0.048
Ne	10	0.579	0.875	+0.296
A	18	3.62	5.45	+1.83
Kr	36	5.55	8.70	+3.15
Xe	54	7.53 <sup>a</sup>	12.1	+4.57
<sup>a</sup> Expt. value of L.F. & F (1957)				

In order to test the validity of the additivity postulate for calculating molecular ionization cross-sections, it is essential to have correct atomic ionization cross-sections. For this we assume the difference between the calculated and the experimental values of the atomic ionization cross-sections to be function of  $Z$  only i.e.,

$$Q_{i,corr} = Q_{i,calc} - C(Z) \quad (6)$$

where  $C(Z)$  is the correction factor.

In Fig. 1, we have plotted the difference between the calculated and the experimental values of O and S of the total ionization cross-section ( $Q_{i,calc}$

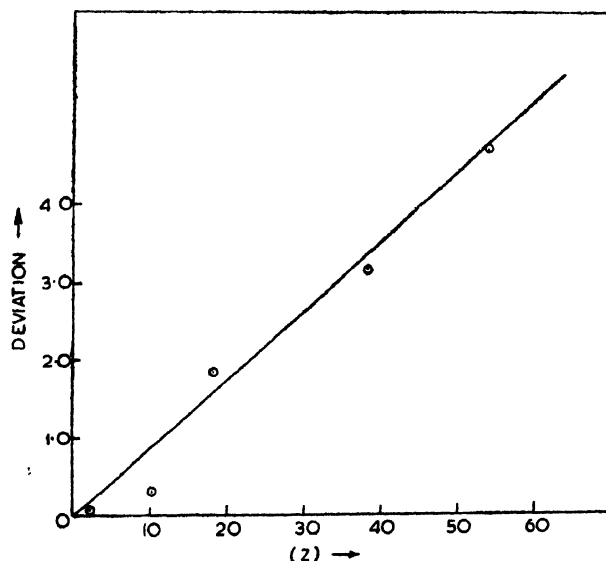


Fig. 1. Difference of the O & S (1956) calculated and experimental values of the total ionization cross-section, as a function of  $Z$ .

$Q_{i_{\text{expt}}}$  as a function of  $Z$ . There is some uncertainty in the calculated values for Ne, consequently, we have considered only the point for He, Ar, Kr and Xe. It will be seen that the plot is a straight line passing through the origin and therefore  $C(Z)$  may be represented as

$$C(Z) = AZ \quad \dots (7)$$

with  $A = 0.09$ .

Although at present it is not possible to explain quantitatively the increase of the correction factor  $C(Z)$  with increasing  $Z$ , a qualitative explanation may however, be given. The expression for the mean square-radius of the electron ( $n, l$ ) may be written as,

$$\bar{r}_{nl}^2 = a_0^2 n'^4 (Z - S_{nl})^{-2} - 1 + \frac{3}{2} \left( 1 - \left\{ \frac{l(l+1) - 1/3}{n'^2} \right\} \right). \quad \dots (8)$$

where  $a_0$  is the Bohr radius,  $n'$  the effective quantum number and  $S_{nl}$  the Slater's screening constant. In the ionization process the screening is complete only when the energy of the ejected electron is less than the energy of the scattered electron, Bates (1962). As the atomic number  $Z$  increases, the ionization potential of the outermost electrons decreases with a consequent increase of energy of the ejected electron. Hence, the probability of the energy of the ejected electron to be higher than the energy of the scattered electron increases with increasing  $Z$ . This means that the values of  $S_{nl}$  should be taken less than Slater's value as  $Z$  increases, which will result in lower values of  $\bar{r}_{nl}^2$ . In the O and S method the effect of incomplete screening has not been considered in calculating the value of  $\bar{r}_{nl}^2$ , and hence difference between the calculated and experimental values of ionization cross-section increases with increasing  $Z$ . Another probable source of error in the method of O and S as pointed by Haisinsky (1961) is their association of the ionization cross-section  $Q_i$  with  $\Sigma \langle r^2 \rangle$ . Actually  $\Sigma \langle r^2 \rangle$  is proportional to the sum of the ionization cross-sections and the excitation cross-section  $Q_e$ , i.e.

$$Q_i + Q_e \propto \Sigma \langle r^2 \rangle$$

or

$$Q_i = K \Sigma \langle r^2 \rangle - Q_e$$

Thus the success of  $\Sigma \langle r^2 \rangle$  in correlating the observed ionization cross-sections depends on the constancy of the proportion of inelastic collision which results in excitation. If the proportion of  $Q_e$  increases with increasing  $Z$  the difference between the experimental and the values of  $Q_i$  as calculated by the O and S method will also increase.

By using Eqs. (6) and (7) it is possible to correct the calculated values of the atomic ionization cross-sections arrived at by O and S method. We have then calculated the molecular ionization cross-sections as the sum of the corrected

constituent atomic ionization cross-sections. The results for some inorganic and hydrocarbon molecules are shown in Table III. It may be seen that the agreement between the experimental values of O and S and their calculated values after correction is reasonably good thereby supporting the view that the total ionization cross-section of molecules are constitutive molecular properties. This is also in agreement with the quantum mechanical calculations of Watanabe (1961), who showed that for impinging electrons having energy greater than 80 ev the additivity postulate should hold within 20%.

**TABLE III**  
Molecular ionization cross-sections ( $Q_i$ )  
 $Q_i(H_2) = 1$

Molecule	O & S (1956) Calc.	O & S (1956) Expt.	O & S (1956) corrected calc.
N <sub>2</sub>	3.84	2.64	2.58
O <sub>2</sub>	3.29	2.20	1.85
CO	3.73	2.66	2.47
CO <sub>2</sub>	5.37	3.46	3.39
H <sub>2</sub> S	7.40	4.23	5.78
HCl	6.40	3.68	4.78
CH <sub>4</sub>	4.08	2.84	3.18
C <sub>2</sub> H <sub>4</sub>	6.16	4.17	4.72
C <sub>2</sub> H <sub>6</sub>	7.15	4.91	5.53
C <sub>3</sub> H <sub>6</sub>	9.24	6.20	7.08
C <sub>3</sub> H <sub>8</sub>	10.2	6.85	7.86
i-C <sub>4</sub> H <sub>8</sub>	12.3	8.37	9.42
n-C <sub>4</sub> H <sub>10</sub>	13.3	8.91	10.24
i-C <sub>5</sub> H <sub>10</sub>	15.4	10.1	11.80
n-C <sub>5</sub> H <sub>12</sub>	16.4	11.1	12.62
C <sub>6</sub> H <sub>6</sub>	15.5	10.8	11.72
Cyclo-C <sub>6</sub> H <sub>12</sub>	18.5	11.5	14.18
n-C <sub>6</sub> H <sub>14</sub>	19.5	12.8	15.00
CH <sub>3</sub> Cl	9.48	5.26	7.14

In conclusion we may state that reasonably good values of the molecular ionization cross-sections can be obtained quite simply by applying the correction suggested by us to the values obtained by O and S method and using additivity postulate.

# REFERENCES

- Bates, D. R., 1962, *Atomic and Molecular Processes*, 391, Academic Press, New York.
- Bethe, H., 1930, *Ann. Physik*, **5**, 325.
- Bleakney, W., 1930, *Phys. Rev.*, **36**, 1303.
- Huassinsky, M., 1961, *Actions Chimiques et Biologiques des Radiations*, Vth Series, Masson et Cie, Paris.
- Lampe, F. W., Franklin, J. L., and Field, F. H., 1957, *J. Am. Chem. Soc.*, **79**, 6129.
- Massey, H.S.W., 1956, *Handbuch der Physik*, **36A**, Tom II.
- Otvos, J. W., and Stevenson, D. P., 1956, *J. Am. Chem. Soc.*, **78**, 546.
- Smith, P. T., 1930, *Phys. Rev.*, **36**, 1293.
- Tate, T. T., and Smith, P. T., 1932, *Phys. Rev.*, **39**, 270.
- Watanabe, T., 1961, *J. Phys. Soc., Japan*, **16**, 529.

# ON THE REPRESENTATION OF THE DISTORTIONS IN $1s$ ORBITALS IN THE BONDING MOLECULAR ORBITAL OF A HOMONUCLEAR DIATOMIC MOLECULE

S. CHATTERJEE AND A. K. BARUA

INDIAN ASSOCIATION FOR THE CULTIVATION OF SCIENCE, CALCUTTA-32.

(Received March 10, 1965)

**ABSTRACT.** The energy of the lowest state ( $2\Sigma_g^+$ ) of  $H_2^+$  has been calculated by using Inui-Nordsieck type orbitals. The results show that this type of orbitals are flexible enough to give a very satisfactory representation of the distortions in  $1s$  orbitals in the bonding orbital of a homonuclear diatomic molecule.

## INTRODUCTION

The success of the *ab initio* calculation of the molecular energies depends largely on the choice of molecular wave functions. Till now, mostly linear combinations of Slater type orbitals (S.T.O.'s) have been used for constructing molecular orbitals. However, a serious drawback of these orbitals is the inability to represent adequately and economically the distortion in the atomic charge cloud when it becomes a part of the molecular system. This aspect of the problem has recently been discussed in some detail by Geller, Frost and Lykos (1962) and Miller and Lykos (1962). They have shown that the main effect in the electron cloud of an atom when it forms a part of a molecule is the 'charge shift' which means the movement of the centre of electron density from around the attractive nucleus in an atom to a region between the nuclei in a diatomic system. A second order effect is the deformation of the charge cloud associated with a particular nucleus as it is stretched along the internuclear axis.

It has been pointed out by Harris (1960) and Barua and Chatterjee (1964) that attempts to represent the deformations in molecular orbitals by using S.T.O.'s of added complexities may not be worth while. For diatomic molecules, wave functions in the ellipsoidal coordinates with the nuclei at the foci, though quite simple in form, are expected to represent the distortion of the atomic orbitals to a large degree. The success of this approach has been proved by the recent calculation of the repulsive energy of the H-He system by using Inui-Nordsieck type orbitals (Barua and Chatterjee, 1964).

The Inui-Nordsieck type orbitals have been used by Sakamoto and Ishiguro (1956) for the calculation of the repulsive energy of the He-He system which was

not quite successful. The reason for this has been shown by Huzinaga (1957) to be the failure of the same set of parameter for both the bonding and anti-bonding orbitals to represent properly the distortions of the atomic orbitals. For a hetero-nuclear system like H-He, the sets of parameters for the atomic orbitals of the two atoms are independently variable and the limitation found in the case of He-He is not present.

For the calculation of the lowest  $^2\Sigma_g^+$  state of  $\text{H}_2^+$  molecule only the bonding orbital is to be used. It is interesting to see how far the Inui-Nordsieck type orbitals can represent the distortions in the  $1s$  orbitals of the bonding molecular orbital. With this end in view, in this paper we have made sample calculations of the energy of the  $^2\Sigma_g^+$  state of  $\text{H}_2^+$ . It is also expected that the use of different sets of parameters for the  $1s$  orbitals will make it possible to represent the distortions in the antibonding state properly.

#### CALCULATION OF ENERGY INTEGRALS

For the  $^2\Sigma_g^+$  state of  $\text{H}_2^+$  molecule, the molecular orbital may be represented as,

$$\psi = \chi_a + \chi_b \quad \dots (1)$$

$\chi_a$  and  $\chi_b$  being the atomic orbitals of the two nuclei of  $\text{H}_2^+$  and are given as

$$\left. \begin{aligned} \chi_a &= e^{-\alpha\xi - \beta\eta} \\ \chi_b &= e^{-\alpha\xi + \beta\eta} \end{aligned} \right\} \quad \dots (2)$$

$\alpha$  and  $\beta$  being the parameters of the atomic orbitals and

$$\left. \begin{aligned} \xi &= (r_a + r_b)/R \\ \eta &= (r_a - r_b)/R \end{aligned} \right\} \quad \dots (3)$$

where  $R$  is the distance between two nuclei,  $r_a$  and  $r_b$  are the distances of the electron from the nuclei  $a$  and  $b$  respectively.

The Hamiltonian of the system, in atomic units is given by

$$H = -\nabla^2 - \frac{1}{r_a} - \frac{1}{r_b} + \frac{1}{R} \quad \dots (4)$$

The energy of the system may be written as

$$E = \frac{\int \psi^* H \psi d\tau}{\int \psi^* \psi d\tau} \quad \dots (5)$$

We define the following integrals

$$\left. \begin{aligned} \int \chi_a^2 d\tau &= \frac{\pi R^3}{4} E \\ \int \chi_a \chi_b d\tau &= \frac{\pi R^3}{4} F \end{aligned} \right\} \quad \dots (6)$$



$$\left. \begin{aligned}
 \int \chi_a(-\nabla^2)\chi_a d\tau &= \int \chi_b(-\nabla^2)\chi_b d\tau = \pi R(I) \\
 \int \chi_a(-\nabla^2)\chi_b d\tau &= \int \chi_b(-\nabla^2)\chi_a d\tau = \pi R(I) \\
 \int \chi_a^2 \frac{1}{r_a} d\tau &= \frac{\pi R^2}{2} K \\
 \int \chi_a^2 \frac{1}{r_b} d\tau &= \frac{\pi R^2}{2} L \\
 \int \chi_a \chi_b \frac{1}{r_a} d\tau &= \frac{\pi R^2}{2} M \\
 \int \chi_a \chi_b \frac{1}{r_b} d\tau &= \frac{\pi R^2}{2} N
 \end{aligned} \right\} \dots (7)$$

The expressions for the integrals in Eq. (6) have been given in the Appendix.

In terms of (7) the energy may be written as,

$$E(\alpha, \beta; R) = \frac{X}{R} + \frac{Y}{R^2} \quad \dots (8)$$

with

$$X = 2[-(K+L+M+N)/(E+F)] + 1 \quad \dots (9a)$$

$$Y = 2(G+I)/(E+F) \quad \dots (9b)$$

For a particular value of  $R$ , the values of  $\alpha, \beta$  are to be varied till the minimum value of the energy is obtained. First, the parameters were varied at an interval of 0.125 by using the tables of Miller *et al.* (1958). The exact values of  $\alpha, \beta$  which gave the minimum value of  $E$  were obtained by the method of Sakamoto and Ishiguro (1956).

TABLE I  
Energy of the  $^2\Sigma_g^+$  state of  $H_2^+$  for  $R = 2au$

Wave function	Values of the parameters	Energy $-E au$
One parameter <sup>a</sup>	$\zeta = 1$	0.55377
One parameter <sup>a</sup>	$\zeta = 1.293$	0.58651
Two parameter <sup>a</sup>		0.59980
Three parameter <sup>a</sup>		0.60183
Present	$\alpha = 1.3625$ $\beta = .9100$	0.60228
Bates et. al. (1953) (actual)		0.60262

<sup>a</sup> Miller and Lykos (1962)

## RESULTS AND DISCUSSION

The results of our calculation at  $R = 2$  *au* are shown in Table I together with the result of a few other accurate calculations including the exact values obtained by Bates *et al.* (1954). It may be seen that our values obtained with only a two-parameter wavefunction is in better agreement with the exact values of Bates *et al.* (1954) than even the values obtained with three parameter hybrid orbitals used by Miller and Lykos (1962). The present sample calculations show that the Inui-Nordsieck orbitals are flexible enough to represent adequately the distortions in the  $1s$  orbitals in the bonding orbital of a homonuclear diatomic molecule. In fact, they represent the atomic charge clouds in a molecule better than the complicated combinations of different S.T.O.'s. Further studies of the representation of the distortion of atomic orbitals in molecular orbitals on the basis of Inui-Nordsieck type orbitals are in progress.

The authors are grateful to Professor B. N. Srivastava for his interest and encouragement.

## REFERENCES

- Bates, D. R., Ledsham, K., and Stewart, A. L., 1953, *Phil. Trans. Roy. Soc. (London)*, **A 246**, 215.  
Barua, A. K., and Chatterjee, S., 1964, *Mol. Phys.*, **7**, 443.  
Geller, M., Frost, A. A., and Lykos, P. G., 1962, *J. Chem. Phys.*, **36**, 2693.  
Harris, F. E., 1960, *J. Chem. Phys.*, **32**, 3.  
Huzinaga, S., 1957, *Prog. Theor. Phys.*, **17**, 169.  
Miller, R. V., and Lykos, P. G., 1962, *J. Chem. Phys.*, **37**, 993.  
Miller, J., Gerhauser, J. M., and Matsen, F. A., 1958, *Quantum Chemistry Integrals and Tables* (Austin: University of Texas Press).  
Sakamoto, M., and Ishiguro, E., 1956, *Prog. Theor. Phys.*, **15**, 37.

# DEHYDROXYLATION REACTION KINETICS OF SOME INDIAN KAOLINITIC CLAYS

J. PRASAD\* AND B. M. BISHUI

CENTRAL GLASS AND CERAMIC RESEARCH INSTITUTE, CALCUTTA-32, INDIA.

(Received February 5, 1965 ; Resubmitted March 10, 1965)

**ABSTRACT.** The kinetic parameters for the dehydroxylation process of five Indian kaolinitic clays have been found out experimentally. The results obtained by thermogravimetric and differential thermal analysis methods showed fair agreement. The dehydroxylation reaction for all the clays obeyed first order kinetics. Activation energy for Bhandak clay was found to be highest indicating it to be most well crystallised kaolinite.

## INTRODUCTION

When a kaolinitic clay is heated there is loss of structural hydroxyls between about 500-700°C. This process is known as dehydroxylation, since during this operation the neighbouring (OH) radicals in the kaolinite structure coalesce together to form water vapour.

A prior knowledge about the dehydroxylation characteristics of a clay is of much advantage to the ceramic industry where during manufacture, the body is almost invariably heated beyond this temperature range, and the strength which is rendered to the ware, before and after firing, is one of the principal considerations in selecting a clay for a particular purpose.

Work on the dehydroxylation reaction kinetics of a large number of clays has been reported previously by several authors (Murray and White, 1949, 1955; Vaughan, 1955, 1958; Brindley and Nakahira, 1957). No work in this direction on Indian clays has come to the notice of the authors.

In the present communication results on the dehydroxylation kinetics of a few Indian kaolinitic clays are presented, obtained by using thermogravimetric and differential thermal analysis methods and the activation energy and frequency factors for the reaction calculated.

## THEORETICAL CONSIDERATIONS

### *Thermogravimetric method*

Weight loss measurements as a function of time at different temperatures in the dehydroxylation peak region were used for determining kinetic parameters by the thermogravimetric method.

\* Present address—Central Scientific Instruments Organisation, Chandigarh.

Let  $w$  be the amount of clay present at any instant  $t$  and  $K_T$  the corresponding rate constant at temperature  $T$ . Assuming that the dehydroxylation process obeyed first order kinetics, and employing the general principle laid by Guggenheim (1926), it follows that

$$\frac{dw}{dt} = -K_T w \quad \dots (1)$$

or 
$$w = w_0 e^{-K_T t} \quad \dots (2)$$

where  $w_0$  is the amount of the reacting material present at time  $t = 0$ . If  $\Delta L$  represents loss in weight of the clay during the time interval  $\Delta t$ , then at time  $(t + \Delta t)$  we have

$$w - \Delta L = w_0 e^{-K_T(t + \Delta t)} \quad \dots (3)$$

Combining (2) and (3)

$$\log_{10} \Delta L = -(0.4343 K_T) t + \log_{10} w_0 (1 - e^{-K_T \Delta t}) \quad \dots (4)$$

Hence if  $\log_{10} \Delta L$  vs  $t$  plot for a certain constant time interval  $\Delta t$ , at any experimental temperature  $T$ , gives a straight line a first order kinetics is indicated and from the slope  $K_T$  can be evaluated. Equation (4) thus enables the rate constants at different temperatures to be evaluated graphically.

From Arrhenius equation 
$$K_T = A e^{-E/RT} \quad \dots (5)$$

or 
$$\log_{10} K_T = \frac{(0.4343 E)}{R} \cdot \frac{1}{T} + \log_{10} A \quad \dots (6)$$

where  $E$  is the activation energy and  $\log_{10} A$  the frequency factor. Equation (6) indicates that the plot of  $\log_{10} K_T$  vs  $1/T$  should be a straight line, and from the attributes of the same  $E$  and  $\log_{10} A$  can be evaluated.

#### *Differential thermal analysis method*

The variation in dehydroxylation peak temperature with different heating rates was used for determining the kinetic parameters by differential thermal analysis method.

Combining equations (1) and (5) above dealt already under thermogravimetric method

$$\frac{dw}{dt} = -A w e^{-E/RT} \quad \dots (7)$$

or 
$$\frac{d^2 w}{dt^2} = -A e^{-E/RT} \frac{dw}{dt} + \frac{E}{RT^2} \frac{dw}{dt} \frac{dT}{dt} \quad \dots (8)$$

At peak maximum ( $T_m$ ) in the differential thermal analysis curve  $\frac{d^2 w}{dt^2} = 0$

Hence 
$$\ln \frac{\beta}{T_m^2} = \frac{(-E)}{R} \cdot \frac{1}{T_m} + \ln \frac{AR}{E} \quad \dots (9)$$

where  $\beta = dT/dt$  (heating rate).

Thus if the dehydroxylation process obeyed first order kinetics  $\ln \frac{\beta}{T_m^2}$  vs  $\frac{1}{T_m}$  plot should be a straight line, from which  $E$  and frequency factor  $\log_{10} A$  can be evaluated.

## EXPERIMENTAL

### Thermogravimetric analysis

The thermogravimetric analysis was done with the apparatus described by Sen (1958). The buoyancy correction for the heating cycle of thermobalance was determined by using calcined alumina as the reference material. The samples were first preheated at 410°C to constant weight, transferred in a platinum boat, keeping the same exposed area through all experiments, and readings of the weight loss taken as a function of time at different temperatures in the dehydroxylation peak region.

### Differential thermal analysis

For D.T.A. curves, the apparatus described by Atma Ram *et al.*, (1955) was used, which enabled any heating rate between 1–15°C/min, to be adjusted within an accuracy of  $\pm 0.1^\circ\text{C}$ . Before taking D.T.A. run, the samples were agitated to pass through 200 mesh Tyler, and stand in vacuum for at least four days over a saturated solution of  $\text{Mg}(\text{NO}_3)_2 \cdot 6\text{H}_2\text{O}$ . Calcined alumina of equal fineness was used as the reference inert material. The temperature thermocouple was located in the inert material and peak temperatures obtained reported as such.

## RESULTS

Isothermal dehydration curves of Beldanga clay at 6 different temperatures in the dehydroxylation peak region are given in Fig. 1.  $\log_{10} \Delta L$  vs  $t$  plots for this clay are given in Fig. 2.

D.T.A. curves at different heating rates of the clays are given in Fig. 3. Utilizing equations (6) and (9), Fig. 4 shows the Arrhenius plots for the different clays. The calculated values of the activation energy and frequency factor for the dehydroxylation process of the different clays are given in Table I.

## DISCUSSION

Fig. 4 shows that  $\log_e \frac{\beta}{T_m^2}$  vs  $\frac{1}{T_m}$  plots for all the clays under study are linear indicating that their dehydroxylation obey first order kinetics.

Amongst all the kaolins under study, that from Bhandak region showed the highest activation energy (42.36 K Cal/mol/°K) (Table I). This indicates a stronger

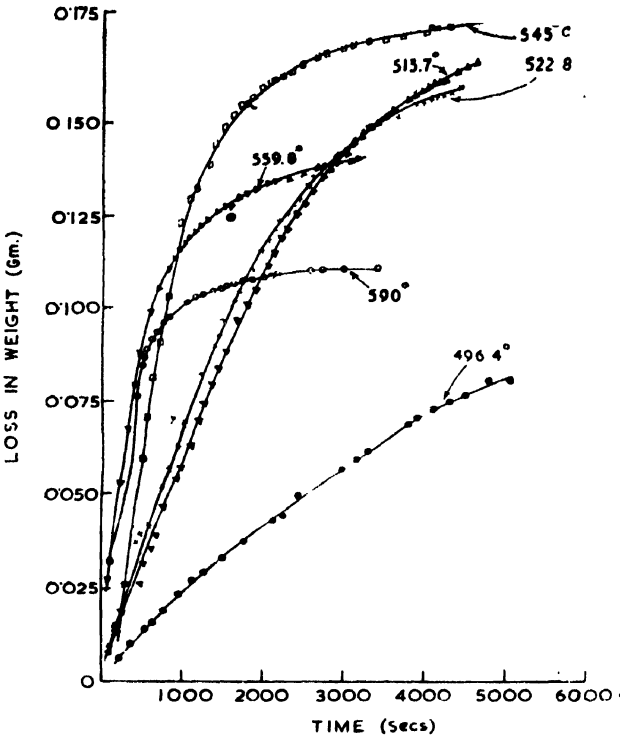


Fig. 1. Isothermal dehydration curves of Beldanga clay at different temperatures.

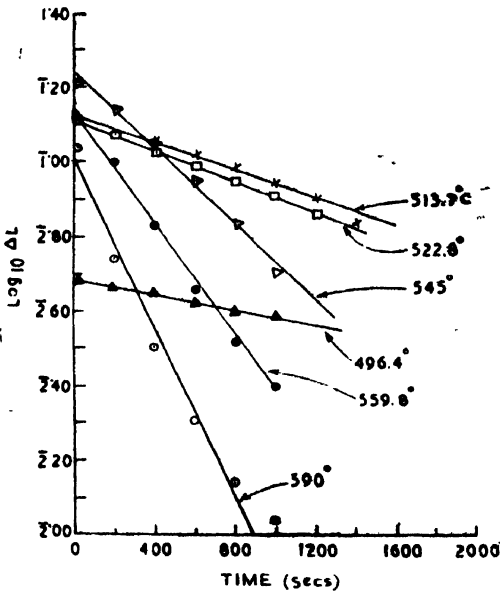


Fig. 2.  $\log_{10} \Delta L$  vs  $t$  plots of Beldanga clay at different temperatures  
(Derived from Fig. 1 taking  $\Delta t = 2400$  secs.)

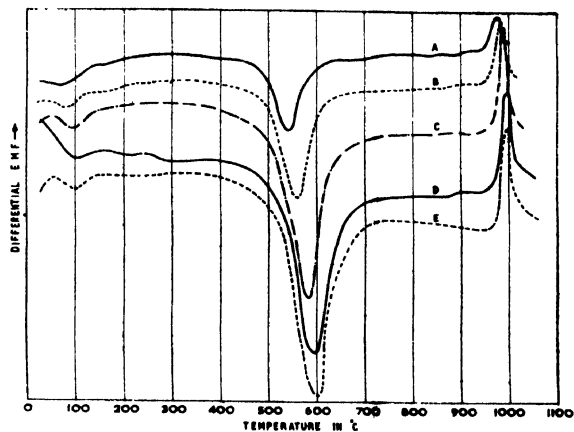


Fig. 3. (1) A, B, C, D, E Curves at 3, 6, 9, 12 and 15°C/min. respectively.

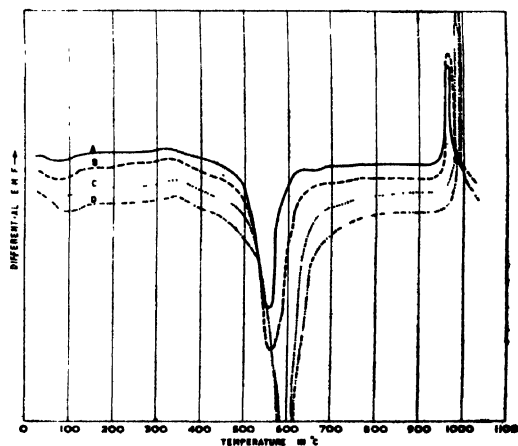


Fig. 3. (2) A, B, C, D—curves at 6, 9, 12 and 14.6°C/min. respectively.

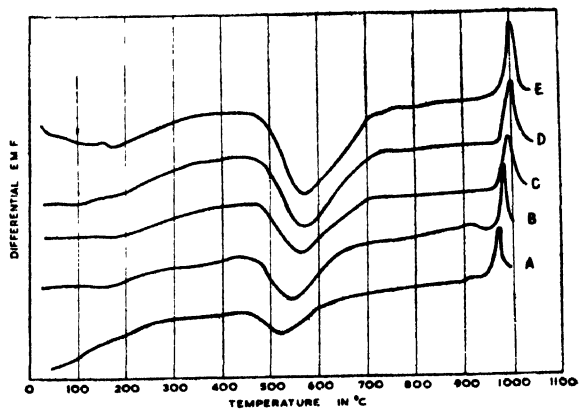


Fig. 3. (3) A, B, C, D, E—curves at 3, 6, 9, 12 and 14.9°C/min. respectively.

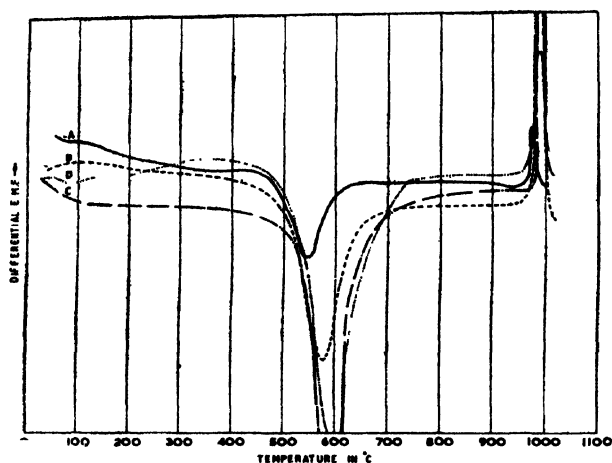


Fig. 3. (4) A, B, C, D —curves at 6, 9, 12 and 14.6°C/min. respectively.

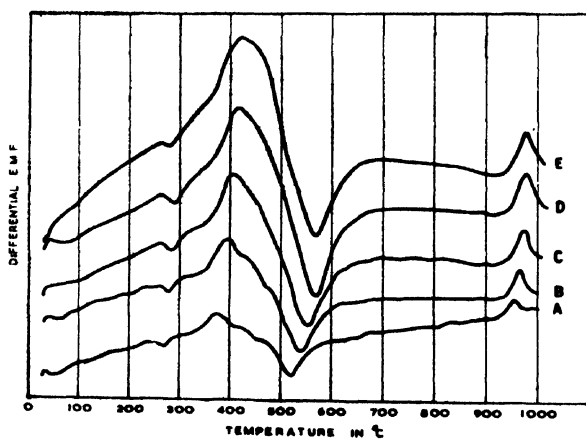


Fig. 3. (5) A, B, C, D, E —curves at 3, 6, 9, 12 and 14.9°C/min. respectively.

TABLE I

Activation energy and frequency factor for the dehydroxylation process for some Indian clays

Clay	Activation energy, $E$ ( $K$ cal/mol/°K)	Frequency factor, $\log_{10} A$
Kusumpur	37.18	9.00
Kot Ransipur	30.53	7.03
Bhandak	42.36	10.60
Rajmahal	39.74	9.57
Beldanga	38.79	9.66



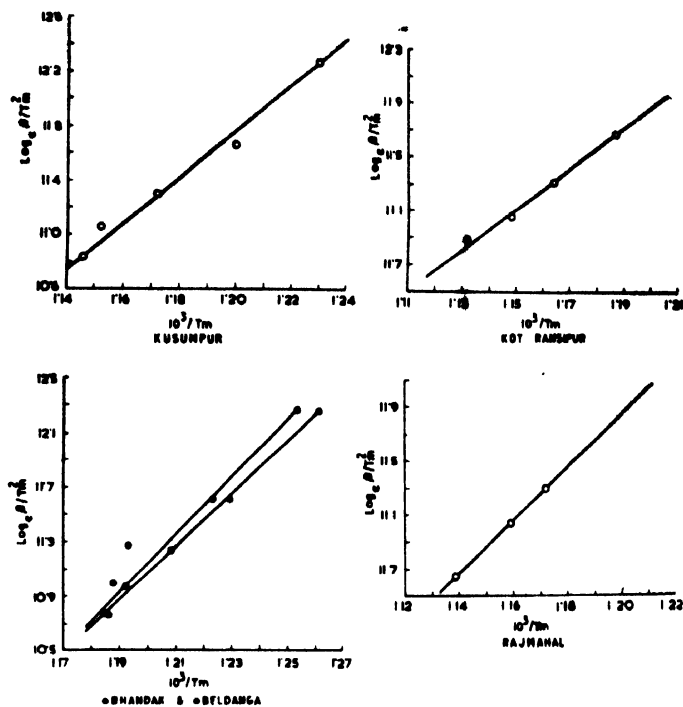


Fig. 4 Arrhenius plots of some Indian clays.  
(A) D.T.A. method,

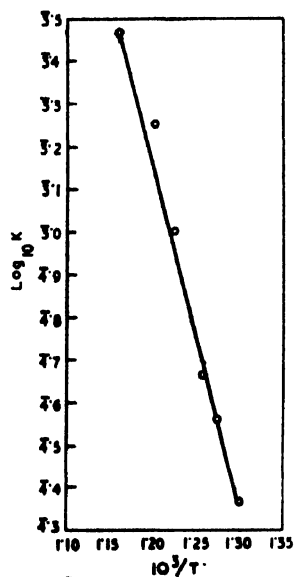


Fig. 4. (B) Thermogravimetric method

bonding and more ordered structure in it, which evidence is also corroborated from X-ray analysis and electron microscopy results (Bishui and Prasad, 1959; Prasad, 1961).

A comparison of the results obtained for  $E$  and  $\log_{10}A$  of Beldanga clay by thermogravimetric and differential thermal analysis methods (Fig. 4) showed fair agreement between them. This suggests that for evaluating kinetic parameters of kaolinitic clays, less time consuming D.T.A. method may be preferred in place of thermogravimetric method wherein considerable computation work is involved.

The dehydroxylation of kaolinite is not instantaneous but spreads over a fairly large temperature interval. This indicates that possibly the frequency factor in the dehydroxylation of kaolinite is related to the probability with which the (OH) radicals in the kaolinite structure combine when a certain threshold energy has been given to the system.

#### ACKNOWLEDGEMENT

The authors are thankful to Dr. Atma Ram, Director of the Institute, for his keen interest in the work and kind permission to publish the paper.

#### REFERENCES

- Bishui, B. M., and Prasad, J., 1959, *Cent. Glass. Ceram. Res. Inst. Bull.*, **6**, 76.  
Brindley, G. W., and Nakahira, M., 1957, *J. Amer. Ceram. Soc.*, **40**, 346.  
Guggenheim, E. A., 1926, *Phil. Mag.*, **2**, 538.  
Murray, P., and White, J., 1949, *Trans. Brit. Ceram. Soc.*, **48**, 187.  
Murray, P., and White, J., 1955, *Trans. Brit. Ceram. Soc.*, **54**, 137.  
Prasad, J., 1961, *Physico-chemical properties of some Indian Clays and Related Minerals*.  
D. Phil (Science) Thesis, Calcutta University.  
Ram, A., Banerjee, J. C., and Nandi, D. N., 1955, *Trans. Ind. Ceram. Soc.*, **14**, 169.  
Sen, S., 1958, *Cent. Glass Ceram. Res. Inst. Bull.*, **5**, 93.  
Vaughan, F., 1955, *Clay. Min. Bull.*, **2**, 265.  
Vaughan, F., 1958, *Trans. Brit. Ceram. Soc.*, **57**, 38.

# ELASTIC SCATTERING AND POLARIZATION OF ELECTRONS BY ATOM IN SECOND BORN APPROXIMATION

G. CHATTERJEE AND N. C. SIL

DEPARTMENT OF THEORETICAL PHYSICS,  
INDIAN ASSOCIATION FOR THE CULTIVATION OF SCIENCE,  
JADAVPUR, CALCUTTA-32.

(Received March 31, 1965)

**ABSTRACT.** In the present paper, the differential cross section of scattering and the asymmetry after double scattering for electrons of energy 121 kev by screened field of the gold atom have been calculated by the Born method in second approximation, the theoretical findings have been compared with the exact results obtained by numerical computation. The comparison allows us to re-examine the degree of validity of the Born method in scattering process. It is found that the second Born approximation gives fairly good results for scattering cross section of 121 kev electrons, but for polarization effect, the second approximation is inadequate.

## INTRODUCTION

In recent years, the study of scattering and polarization of electrons in the field of a heavy atom has assumed importance because of the relevancy of the latter to  $\beta$ -decay interactions theories. There are two main difficulties, one of them is the choice of a suitable representation of the screened field surrounding the atomic nucleus and the other is the limited range within which the analytical methods are valid. Because of the latter difficulty, recourse to numerical computation is now almost a common practice. Apart from mathematical nicety the analytical method often allows us to probe the problem step by step. With that in view we have calculated by second Born approximation the cross section of scattering and the consequent polarization of electrons in the field of the gold atom.

The nucleus of a heavy atom is surrounded by an electronic cloud; the effective field of such a system is usually given by the Thomas-Fermi or Hartree-Fock method; in our calculations we have taken the 'two term field' of Mohr and Tassie (1954) which reproduces the Hartree field for gold very well.

Bartlet and Welton (1941) have calculated the cross section of scattering of electrons of energy 100 kev and 230 kev in the screened field of mercury atom by three methods : (1) Integration with differential analyser, (2) W. K. B. method, and (3) First order Born approximation. They have found that the first order Born approximation is not so good as the other two. It is with a view to seeing

whether second Born approximation improves the theoretical findings we have done the calculation both for scattering as well as for polarization effects when electrons of energy 121 kev impinge on gold atom.

Mohr and Tassie (1954) have calculated the differential cross section and polarization effects of electrons scattered by gold by a semi-analytic method. Without making rigorous calculations with Dirac equation, they have added the influence of spin as a correction by assuming that the difference in the phase values when spin is taken and neglected is the same for the coulomb and the screened coulomb.

Sherman and Nelson (1959) have obtained by numerical computation, scattering cross section and polarization asymmetry for electron scattering by gold using Dirac equation, but they have neglected the screening.

Very recently Lin (1964) has made numerical computation for scattering cross section and polarization of electrons of 121 kev energy by screened gold atom. According to his estimate, the error in the calculation is less than 1%. On comparing our results with those of Lin we find that the differential scattering cross section results calculated by second Born approximation method agrees fairly well with values obtained by numerical computations, specially for smaller angles; however, the second Born approximation is found to be inadequate for polarization results.

#### MATHEMATICAL FORMULATION

The Dirac equation for an electron of energy  $E$ , rest mass  $m$ , moving in the field  $ZeV$  of an atom may be written as

$$[E - i\hbar(\boldsymbol{\alpha} \cdot \mathbf{grad}) + \beta mc^2]\psi = -Ze^2V\psi$$

where  $\boldsymbol{\alpha}, \beta$  are the Dirac matrices and wave function  $\psi$  has the four-component column form.

If we operate on both sides of the above equation by

$$D = [E + i\hbar(\boldsymbol{\alpha} \cdot \mathbf{grad}) + \beta mc^2]$$

we obtain

$$[\nabla^2 + k^2]\psi = -\frac{Ze^2}{c^2\hbar^2} DV\psi \quad \dots (1)$$

where

$$k^2 = \frac{1}{\hbar^2 c^2} [E^2 - m^2 c^4]$$

We seek a solution of Eqn. (1) the asymptotic form of which is

$$\psi = ae^{i\mathbf{k}_0 \cdot \mathbf{r}} + u \frac{e^{ikr}}{r} \quad \dots (2)$$

$\mathbf{k}_0$  denotes propagation vector along the incident direction,  $|\mathbf{k}_0|^2 = k^2$ .

The first part represents the incident wave which consists of particles having an arbitrary spin direction. If the incident particles move in the  $Z$  direction, then  $a$  can be written in the form

$$\frac{-c\hbar k A}{E + mc^2}$$

$$\frac{c\hbar k B}{E + mc^2}$$

$$A$$

$$B$$

where  $\frac{-B}{A} = \cot \frac{\chi}{2} e^{i\omega}$ ,  $(\chi, \omega)$  being the spherical polar angle of the arbitrary spin direction of the incident wave.

The current due to the incident wave depends on  $|A|^2 + |B|^2$ ,  $A, B$  being the 3rd and 4th element of  $a$ . In the same way the current due to the scattered wave depends on  $|u_3|^2 + |u_4|^2$ .

The elastic scattering cross section is

$$\frac{d\sigma}{d\Omega} = \frac{|u_3|^2 + |u_4|^2}{|A|^2 + |B|^2}$$

If we choose  $|A|^2 + |B|^2 = 1$ , the scattering cross section is

$$\frac{d\sigma}{d\Omega} = |u_3|^2 + |u_4|^2 \quad \dots \quad (3)$$

The scattered wave is evaluated by Born approximation upto second order. In view of the asymptotic condition (2) the differential equation (1) may be converted into the following integral equation :

$$\psi(r) = ae^{ik_0 \cdot r} - \frac{Ze^2}{\hbar^2 c^2} \int G(\mathbf{r}, \mathbf{r}') D' V(r') \psi(r') d' \quad \dots \quad (4)$$

where 
$$G(\mathbf{r}, \mathbf{r}') = -\frac{4\pi}{|\mathbf{r} - \mathbf{r}'|} e^{ik|\mathbf{r} - \mathbf{r}'|},$$

is the appropriate Green's function.

For the first Born approximation, we replace  $\psi(r')$  in the above integral by incident unperturbed wave function,  $ae^{ik_0 \cdot r}$ .

Thus as a first approximation, we obtain

$$\psi^I_{sc} = \frac{e^{ikr}}{r} u^I = \frac{e^{ikr}}{r} \frac{Ze^2}{c^2 \hbar^2} \frac{1}{4\pi} (\mathbf{k}_1 | \mathbf{V} | \mathbf{k}_0) (E - c\hbar \boldsymbol{\alpha} \cdot \mathbf{k}_1 - \beta mc^2) a$$

$\mathbf{k}_1$  denotes propagation vector in the scattered direction,  $|\mathbf{k}_1|^2 = k^2$ .

On simplification we have

$$u^I = \begin{pmatrix} u^I_1 \\ u^I_2 \\ u^I_3 \\ u^I_4 \end{pmatrix} = \begin{pmatrix} \dots\dots\dots \\ \dots\dots\dots \\ Af_1 - Bg_1 e^{-i\varphi} \\ Bf_1 + Ag_1 e^{i\varphi} \end{pmatrix},$$

$$\text{where } f_1 = \frac{Ze^2}{c^2 \hbar^2} \frac{1}{4\pi} (\mathbf{k}_1 | \mathbf{V} | \mathbf{k}_0) [(E - mc^2) \cos \theta + (E + mc^2)]$$

$$g_1 = \frac{Ze^2}{c^2 \hbar^2} \frac{1}{4\pi} (\mathbf{k}_1 | \mathbf{V} | \mathbf{k}_0) [(E - mc^2) \sin \theta]$$

$$a_1 = \frac{1}{4\pi} (\mathbf{k}_1 | \mathbf{V} | \mathbf{k}_0) = \frac{1}{4\pi} \int e^{-i\mathbf{k}_1 \mathbf{r}} V e^{i\mathbf{k}_0 \mathbf{r}} d\mathbf{r}.$$

For the second Born approximation, we iterate the above Eqn. (4) once again and obtain

$$\begin{aligned} \psi^{\text{II}}_{sc} &= \frac{e^{ikr}}{r} u^{\text{II}} \\ &= \frac{e^{ikr}}{r} \left( \frac{Ze^2}{c^2 \hbar^2} \right)^2 (E - c\hbar \boldsymbol{\alpha} \cdot \mathbf{k}_1 - \beta mc^2) [(E - \beta mc^2) a_2 - a_3 \boldsymbol{\alpha} \cdot (\mathbf{k}_0 + \mathbf{k}_1)] a \end{aligned}$$

Expressing the amplitude as a column matrix, we have

$$u^{\text{II}} = \begin{pmatrix} u^{\text{II}}_1 \\ u^{\text{II}}_2 \\ u^{\text{II}}_3 \\ u^{\text{II}}_4 \end{pmatrix} = \begin{pmatrix} \dots\dots\dots \\ \dots\dots\dots \\ Af_2 - Bg_2 e^{-i\varphi} \\ Bf_2 + Ag_2 e^{i\varphi} \end{pmatrix}$$

where  $f_2$  and  $g_2$  are given by

$$f_2 = \left( \frac{Ze^2}{c^2 \hbar^2} \right)^2 \left[ \{ (E - mc^2)^2 \cos \theta + (E + mc^2) \} a_2 + (E^2 - m^2 c^4) (1 + \cos \theta) \frac{2a_3}{\hbar c} \right]$$

$$g_2 = \left( \frac{Ze^2}{c^2 \hbar^2} \right)^2 \left[ (E - mc^2)^2 \sin \theta \cdot a_2 + (E^2 - m^2 c^4) \sin \theta \frac{2a_3}{\hbar c} \right]$$

$$\text{where, } a_2 = \frac{1}{4\pi(2\pi)^3} \int_c \frac{(\mathbf{k}_1 | \mathbf{V} | \mathbf{k})(\mathbf{k} | \mathbf{V} | \mathbf{k}_0)}{k^2 - k_0^2} d^3k.$$

$$a_3 = \frac{\hbar c}{4\pi(2\pi)^3} \int_c \frac{(\mathbf{k}_1 | \mathbf{V} | \mathbf{k})[(\mathbf{k}_0 + \mathbf{k}_1) \cdot \mathbf{k}](\mathbf{k} | \mathbf{V} | \mathbf{k}_0)}{|\mathbf{k}_0 + \mathbf{k}_1|^2 (k^2 - k_0^2)} d^3k.$$

From Eqn. (3) the scattering cross section is given by

$$\frac{d\sigma}{d\Omega} = |f|^2 + |g|^2 + (fg^* - f^*g)(-AB^*e^{i\varphi} + A^*Be^{-i\varphi})$$

where,

$$f = f_1 + f_2, \quad g = g_1 + g_2$$

For scattering of an unpolarized beam, we have to average over all spin directions. Thus retaining terms upto the order  $(Ze^2/\hbar c)^3$ , we get the scattering crosssection as

$$\begin{aligned} \frac{d\sigma}{d\Omega} &= |f|^2 + |g|^2 \\ &= |f_1|^2 + |g_1|^2 + 2(f_1 \text{Re} f_2 + g_1 \text{Re} g_2) \\ &= \frac{d\sigma_1}{d\Omega} + \frac{d\sigma_2}{d\Omega} \end{aligned}$$

$d\sigma_1$  is the usual scattering cross section in first Born approximation and is given by

$$\frac{d\sigma_1}{d\Omega} = 4 \left( \frac{Ze^2}{\hbar c} \right)^2 \left[ \frac{1}{4\pi} (\mathbf{k}_1 | \mathbf{V} | \mathbf{k}_0) \right]^2 k^2 \cos^2 \frac{\theta}{2} \left( 1 + \frac{m^2 c^2}{k^2 \hbar^2} \sec^2 \frac{\theta}{2} \right) \dots \quad (5)$$

and  $d\sigma_2$  is the additional contribution to scattering cross section from second Born approximation.  $d\sigma_2$  is given by

$$\begin{aligned} \frac{d\sigma_2}{d\Omega} &= 8 \left( \frac{Ze^2}{\hbar c} \right)^3 \frac{1}{\hbar c} \left[ \frac{1}{4\pi} (\mathbf{k}_1 | \mathbf{V} | \mathbf{k}_0) \right] Ek^2 \cos^2 \frac{\theta}{2} \\ &\quad \left[ \text{Re} a_2 + \frac{1}{\hbar c} \text{Re}(2a_3) + \frac{2m^2 c^2}{k^2 \hbar^2} \sec^2 \frac{\theta}{2} \text{Re} a_2 \right] \dots \quad (6) \end{aligned}$$

The asymmetry after double scattering of an initial unpolarized beam is given by

$$2\delta = 2 |D(\theta)|^2 / \left[ \frac{d\sigma}{d\Omega}(\theta) \right]^2$$

where  $D = (fg^* - f^*g)$

$$= 4mic^2 \left( \frac{Ze^2}{\hbar c} \right)^3 \frac{1}{\hbar c} \frac{1}{4\pi} (\mathbf{k}_1 | \mathbf{V} | \mathbf{k}_0) k^2 \sin^2 \theta \left[ \text{Im} a_2 - \text{Im} \frac{2a_3}{\hbar c} \right] \dots \quad (7)$$

neglecting  $\left( \frac{Ze^2}{\hbar c} \right)^4$  and higher order terms.

Thus we find that for the calculation of scattering cross section we need the real parts of  $a_2$  and  $a_3$  and of the asymmetry factor, their imaginary parts.

The above expressions (5), (6) and (7) are derived for any general potential which tends to zero faster than  $1/r$ . Particularly, for the case of gold atom we take the form of the potential as

$$ZeV = \frac{Ze^2}{r} (\alpha_1 e^{-\lambda_1 r} + \alpha_2 e^{-\lambda_2 r})$$

With this potential, the values of  $a_1$ ,  $a_2$  and  $a_3$  take a simple form,

$$\begin{aligned} a_1 &= -\frac{\alpha_1}{4k^2 \sin^2 \frac{\theta}{2} + \lambda_1^2} + \frac{\alpha_2}{4k^2 \sin^2 \frac{\theta}{2} + \lambda_2^2} \\ a_2 &= \frac{4\pi}{(2\pi)^3} \left[ \frac{\alpha_1^2}{k^3} M_3(\lambda_1, \lambda_1) + \frac{2\alpha_1\alpha_2}{k^3} M_3(\lambda_1, \lambda_2) + \frac{\alpha_2^2}{k^3} M_3(\lambda_2, \lambda_2) \right] \\ a_3 &= \frac{4\pi}{(2\pi)^3} \frac{\hbar c}{|\mathbf{k}_0 + \mathbf{k}_1|^2} \left[ \frac{\alpha_1^2}{k^3} (2k^2 + \lambda_1^2) M_3(\lambda_1, \lambda_1) + \frac{\alpha_1\alpha_2}{k^3} (4k^2 + \lambda_1^2 + \lambda_2^2) M_3(\lambda_1, \lambda_2) \right. \\ &\quad \left. + \frac{\alpha_2^2}{k^3} (2k^2 + \lambda_2^2) M_3(\lambda_2, \lambda_2) + \frac{\alpha_1^2}{k} M_2(\lambda_1, \lambda_1) \right. \\ &\quad \left. + \frac{\alpha_2^2}{k} M_2(\lambda_2, \lambda_2) + \frac{2\alpha_1\alpha_2}{k} M_2(\lambda_1, \lambda_2) - \alpha_1^2 I_1 - \alpha_1\alpha_2(I_1 + I_2) - \alpha_2^2 I_2 \right] \end{aligned}$$

The values of real parts of  $M_3$ ,  $M_2$ ,  $I_1$  and  $I_2$  have been calculated by Lewis (1956); we have further extracted the imaginary parts of these expressions and a list of all of them is inserted in the appendix.

The scattering cross sections and asymmetry factors for coulomb field, may be easily deduced from the expression (5), (6) and (7), noting that  $\alpha_1 = 1$ ,  $\lambda_1 = 0$  and  $\alpha_2 = 0$  for coulomb field. The results are found to be identical with the corresponding results in Dalitz's paper (1951).

## RESULTS AND DISCUSSIONS

Numerical calculation has been made for the differential cross section and polarisation of electrons of energy 121 Kev scattered by gold atom. The values of the parameters occurring in the expression for the potential are, as given by Mohr and Tassie,

$$\alpha_1 = \frac{20}{79}, \alpha_2 = \frac{59}{79}, \lambda_1 = \frac{1.3}{a_0}, \lambda_2 = \frac{6}{a_0}$$

( $a_0$  being the first Bohr radius).

We have compared our results with those of Sherman and Nelson (1959) and Lin *et al.* (1963,64). Sherman *et al.*, have calculated the scattering cross section and



the asymmetry factor for unscreened coulomb field of gold by numerical computation of a large number of phase shifts. Lin *et al.* have further included the effect of screening in his extensive numerical computation.

The Born series converges very slowly in the present case as  $\left(\frac{Ze^2}{\hbar v}\right)$  is equal to 0.97. Therefore, though the present calculation has been extended upto second order, the third and higher order terms are of considerable importance. For scattering cross section the first term dominates over the higher order terms but for asymmetry the contribution from the first term is zero, whereas the second and higher order terms are nearly of the same order of magnitude. Hence the neglect of higher order terms, affects the polarization more seriously than it does the scattering cross section.

In Fig. 1 we give the results of our numerical calculation of scattering cross section together with those of Sherman *et al.* and of Lin *et al.* A comparison shows

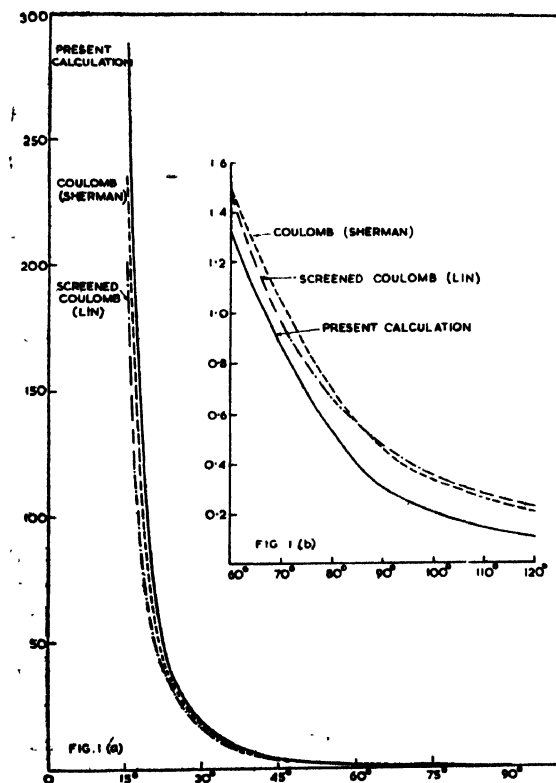


Fig. 1 (a) Differential scattering cross section in units of  $10^{-20} \text{ cm.}^2$ , against angle.

(b) The same with scales enlarged 100 times.

that the Born approximation gives fair agreement with the results of exact numerical calculations specially at small scattering angles, in the present case.

The numerical results for asymmetry in double scattering are shown in Figure 2.

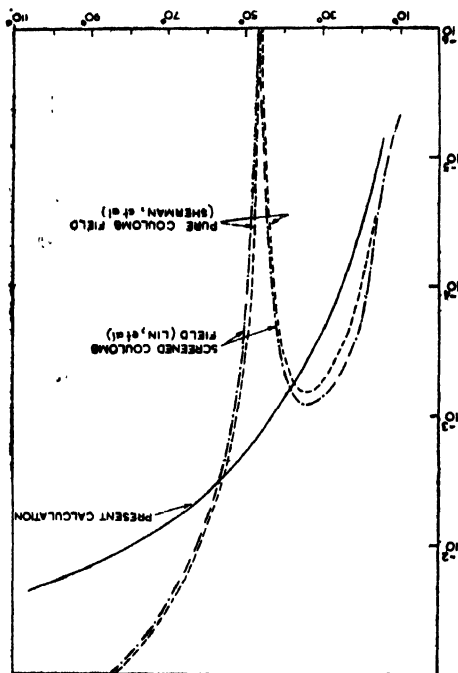


Fig. 2. The asymmetry  $2\delta = 2 \frac{|D(\theta)|^2}{\left[ \frac{d\sigma}{d\Omega}(\theta) \right]^2}$  after double scattering.

The value of the asymmetry after double scattering has a gradual tendency to increase with the increase of angles. The present calculation does not show the sudden fall in the asymmetry near  $45^\circ$  as observed by Sherman and Lin which according to them is due to the change of sign of the asymmetry factor.

It is to be noted that the accuracy of the method of calculation matters more than the inclusion of the screening effect.  $fg^* - f^*g$  is so sensitive to small inaccuracies in the calculation of  $f$  and  $g$  that for a difference of 2% in the values of  $f$  and  $g$  leads to a difference of 15% in the asymmetry factor, as has been remarked by Sherman.

The main source of error in the present calculation is the neglect of higher order terms in the Born series and it is expected that our analytical calculation will show a better agreement for elements of small atomic number in which case the higher order terms have less importance,

# APPENDIX

The following values of  $M_3$ ,  $M_2$ ,  $I_1$  and  $I_2$  have been utilized in the calculation of  $a_2$  and  $a_3$  given in (3).

$$Re M_3(\mu, \nu) = \frac{\pi^2 k^3}{R} \left[ \tan^{-1} \frac{S+R}{T} - \tan^{-1} \frac{S-R}{T} \right]$$

$$Im M_3(\mu, \nu) = \frac{\pi^2 k^3}{R} \frac{1}{2} \left[ l_n \frac{T^2 + (R+S)^2}{T^2 + (R-S)^2} \right]$$

where,

$$R = [k^2(K^2 + \mu^2 + \nu^2)^2 - P^2 \mu^2 \nu^2]^{\frac{1}{2}}$$

$$S = k[K^2 + (\mu + \nu)^2]$$

$$T = \mu \nu (\mu + \nu)$$

$$\mathbf{K} = \mathbf{k}_0 - \mathbf{k}_1$$

$$\mathbf{P} = \mathbf{k}_0 + \mathbf{k}_1$$

$$Re M_2(\mu, \nu) = \frac{2\pi^2 k}{|\mathbf{K}|} \tan^{-1} \frac{|\mathbf{K}|}{\mu + \nu}$$

$$Im M_2(\mu, \nu) = 0$$

$$Re I_i = \frac{\pi^2}{k} \tan^{-1} \frac{2k}{\lambda_i}$$

$$Im I_i = \frac{\pi^2}{k} l_n \frac{(4k^2 + \lambda_i^2)^{\frac{1}{2}}}{\lambda_i}$$

# ACKNOWLEDGMENT

The authors are thankful to Prof. D. Basu for his kind interest and valuable discussions, throughout the progress of the work. Thanks are due also to Sri S. Sirkar for some valuable remarks.

# REFERENCES

- Dalitz, A. H., 1951, *Proc. Roy. Soc., A* **206**, 509.
- Lewis, R. R., 1956, *Phys. Rev.*, **102**, 537.
- Lin, S. R., 1964, *Phys. Rev.*, **133**, A 965.
- Lin, S. R., Sherman, N., and Percus, J. K., 1963, *Nucl. Phys.* **45**, 492.
- Mott, N. F., 1929, *Proc. Roy. Soc., A* **124**, 425.
- Mohr, C. B. O. and Tassie, L. J., 1954, *Proc. Phys. Soc.*, **67**, 711.
- Sherman, N., and Nelson, D. F., 1959, *Phys. Rev.* **114**, 1541.
- Vachaspati, 1954, *Phys. Rev.*, **93**, 502.

# Letters to the Editor

*The Board of Editors does not hold itself responsible for opinions expressed in the letters published in this section. The notes containing short reports of original investigations communicated to this section should not contain many figures and should not exceed 500 words in length. The contributions reaching the Secretary by the 15th of any month may be expected to appear in the issue for the next month. No proof will be sent to the author.*

9

## ON MEASUREMENT OF ELECTRON DENSITY OF PLASMA

A. K. GHOSHAL, S. K. SEN AND J. BASU\*

INSTITUTE OF RADIO PHYSICS AND ELECTRONICS

UNIVERSITY OF CALCUTTA

(Received January 9, 1965)

The usual methods for determining the electron density in a narrow plasma column are :

(a) Perturbation method, —to note the detuning of a cavity due to introduction of a coaxial plasma in it. The mode of the cavity, used most often, is  $TM_{010}$  mode. For a  $TM_{010}$  mode in a cylindrical cavity the change in the resonant frequency of the cavity is related to the electron density in Plasma as shown by Agdur and Enander (1962).

(b) Admittance method, —to note the admittance offered by the plasma column when placed in a waveguide parallel to the microwave electric field vector of  $TE_{10}$  mode. The relation between the admittance and electron density is given by Davidson and Farvis (1962).

However, both the above methods have certain limitations. The perturbation method is assumed to be valid if  $N/N_c < 1 + (\lambda/2\pi r_1)^2$  (Buchsbaum, Mower, and Brown, 1960), where  $N$  is the electron density in plasma,  $N_c$  is the critical electron density corresponding to the wavelength of microwave radiation  $\lambda$ , and  $r_1$  is the radius of the plasma column. The admittance method is assumed to be applicable if  $r_1/a \ll 1$  (Davidson and Farvis, 1962), where  $a$  is the width of the waveguide. Nevertheless the results given by the methods are somewhat approximate. Besides, in both the methods the effect of the plasma container, viz. a quartz or pyrex glass tube, is not properly taken into consideration.

---

\*Present Address :—Saha Institute of Nuclear Physics, Calcutta.

To assess the accuracy of the results and for comparison with the results as given by the perturbation and admittance methods for a typical plasma, a more accurate method termed, in this report, the exact method, has been developed. With the plasma placed coaxially in it, the cylindrical cavity operating in  $TM_{010}$  mode is tuned. Maxwell's equations for the different media in the cavity, viz. plasma, its container and air (air assumed equivalent to free space), are solved, and the following transcendental equations relating the operating frequency  $f$  and the electron density  $N$  are obtained by applying proper boundary conditions (Sen, Basu, and Ghoshal, 1964)

For  $N < N_c$ ,

$$\left[ J_0(\beta_2 r_2) - \sqrt{\frac{\epsilon_2}{\epsilon_0}} A J_1(\beta_2 r_2) \right] \left[ Y_0(\beta_2 r_1) J_1(\beta_1 r_1) - \sqrt{\frac{\epsilon_2}{\epsilon_1}} J_0(\beta_1 r_1) Y_1(\beta_2 r_1) \right] \\ = \left[ \sqrt{\frac{\epsilon_2}{\epsilon_0}} A Y_1(\beta_2 r_2) - Y_0(\beta_2 r_2) \right] \left[ \sqrt{\frac{\epsilon_2}{\epsilon_1}} J_0(\beta_1 r_1) J_1(\beta_2 r_1) - J_1(\beta_2 r_1) J_1(\beta_1 r_1) \right] \dots \quad (1a)$$

For  $N > N_c$ ,

$$\left[ J_0(\beta_2 r_2) - \sqrt{\frac{\epsilon_2}{\epsilon_0}} A J_1(\beta_2 r_2) \right] \left[ Y_0(\beta_2 r_1) I_1(\beta_1 r_1) - \sqrt{\frac{\epsilon_2}{\epsilon_1}} I_0(\beta_1 r_1) Y_1(\beta_2 r_1) \right] \\ = \left[ \sqrt{\frac{\epsilon_2}{\epsilon_0}} A Y_1(\beta_2 r_2) - Y_0(\beta_2 r_2) \right] \left[ \sqrt{\frac{\epsilon_2}{\epsilon_1}} I_0(\beta_1 r_1) J_1(\beta_2 r_1) - J_0(\beta_2 r_1) I_1(\beta_1 r_1) \right] \dots \quad (1b)$$

Where

$$A = \frac{J_0(\beta_0 r_2) Y_0(\beta_0 r_3) - J_0(\beta_0 r_3) Y_0(\beta_0 r_2)}{J_1(\beta_0 r_2) Y_0(\beta_0 r_3) - J_0(\beta_0 r_3) Y_1(\beta_0 r_2)}$$

$\beta_0$  = propagation constant corresponding to  $f$

$\beta_1$  = propagation constant in plasma =  $\beta_0 \sqrt{\frac{\epsilon_1}{\epsilon_0}} = \beta_0 (1 - N/N_c)^{1/2}$

$\beta_2$  = propagation constant in the medium constituting the plasma container  
 $= \beta_0 \sqrt{\frac{\epsilon_2}{\epsilon_0}}$

$\epsilon_0, \epsilon_1, \epsilon_2$  are the permittivities of free space, plasma and its container respectively.

$r_1, r_2$  are the inner and outer radii of the container,

$r_3$  is the radius of the cavity.

$J_0, J_1$  are the Bessel functions of the first kind ;  $Y_0, Y_1$  are the Bessel functions of the second kind,

$I_0, I_1$  are the modified Bessel functions of the first kind.

Experiments have been carried out, at *S*-band frequency, on a typical mercury discharge plasma column of radius  $r_1 = 3.89$  mm, for discharge currents ranging from 0 to 500 mA. The plasma is contained in a pyrex glass tube of thickness 1.1 mm and dielectric constant 4.58, the latter being determined by the method, the authors have described elsewhere (Sen, Basu, and Ghoshal, 1964). The cavity radius  $r_3$  is 38.37 mm., and the width of the waveguide  $a$  is 72 mm. Pressure in the plasma was of the order of  $1\mu$ .

The electron densities at various discharge currents have been determined by the perturbation, admittance method and by the exact method using equations (1a) and (1b). The electron density at the maximum current was of the order of  $1.7 \times 10^{11}$  per c.c., corresponding to  $N/N_c \simeq 1.5$ . Compared with the results given by the exact method, those by the perturbation and admittance methods were within 15% and 20% respectively. It appears that, of the perturbation and admittance methods, the former is somewhat more accurate.

The authors are indebted to Prof. J. N. Bhar, D.Sc., F.N.I. for his keen interest in the work and for helpful discussions.

#### REFERENCES

- Agdur, B., and Enander, B., 1962, *Journal of Applied Physics*, **33**, 575.  
Buchsbaum, S. J., Mower, Lyman., and Brown, S. C., 1960, *Physics of Fluids*, **3**, 806.  
Davidson, C. W., and Farvis, W. E. J., 1962, *Physical Review*, **127**, 1858.  
Sen, S. K., Basu, J., and Ghoshal, A. K., 1964, *Ind. Jour. of Phys.* **38**, 601.

# COPPER-MOLYBDENITE THERMO-COUPLE

A. K. DUTTA AND R. BHATTACHARYA

DEPARTMENT OF MAGNETISM,  
INDIAN ASSOCIATION FOR THE CULTIVATION OF SCIENCE,  
JADAVPUR, CALCUTTA 32.

(Received March, 15, 1965)

Molybdenite ( $\text{MoS}_2$ ), the well known anisotropic semi-conducting crystal occurs in nature in the form of thin flakes parallel to the basal plane. In addition to its interesting electrical and magnetic properties its thermo-electric properties are also remarkable. The value of the thermo-electric power against copper is about a few hundred microvolts (Ogawa, 1928; Pierce, 1909) per degree within a range  $0^\circ\text{C}$  to  $200^\circ\text{C}$ , whereas that of a copper-constantan thermocouple is about  $40\mu\text{v}/\text{degree}$  near the room temperature. In order, therefore to investigate the possibility of using such a thermocouple for sensitive temperature measurement in connection with our studies of magnetic and electrical properties of solids, we constructed one  $\text{Cu-MoS}_2\text{-Cu}$  thermocouple.

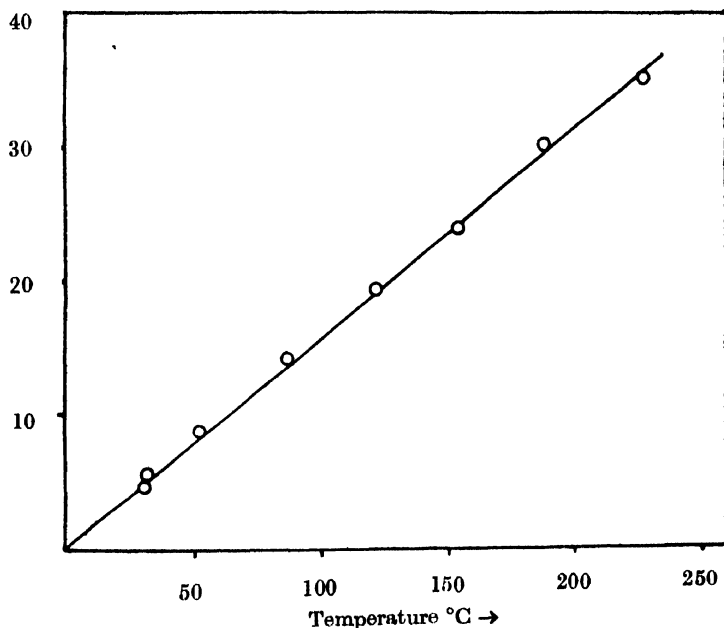


Fig. 1. Temperature Variation of Thermo E. M. F. in  $\text{MoS}_2$ .

A thin flake of a crystal of molybdenite of length of about 6 cms. was electroplated with copper at the two ends and two copper wires of thermocouple variety

were soldered at the two plated ends using soft solder. One junction of this thermocouple was kept at 0°C and the temperature of the other was suitably varied, the entire length of the crystal excepting the plated portions being thoroughly lagged. The thermo e.m.f.'s were recorded potentiometrically upto a temperature of about 250°C and are represented in the adjoining figure. It is evident from the figure that the thermoelectric power is practically constant within this range of temperature and has a value of about  $160\mu v/\text{degree}$ . Such a thermocouple may therefore be profitably utilised upto about 250°C. The possibility of its utilisation in low temperature measurements is under investigation and will be reported as soon as reliable results are obtained.

The authors are thankful to Prof. A. Bose for his kind interest in the work.

#### R E F E R E N C E S

- Ogawa, W. 1928, *J. Soc. Chem. Ind. (Japan)*, **31**, 476.  
Pierce, G. W., 1909, *Phys. Rev.*, **28**, 151.



# AN OBSERVATION ON A NEW TYPE OF DISTORTION IN NUCLEAR EMULSIONS.\*

PREM K. ADITYA

INDIAN INSTITUTE OF TECHNOLOGY,  
NEW DELHI 16.

(Received August 26, 1964)

**ABSTRACT.** An event demonstrating the correlation between spurious scattering and the distortion peculiar to pellicles is described. It is shown that the origin of distortion is non-planarity of the pellicle rather than differential shear as generally understood.

## INTRODUCTION

In recent years considerable attention has been paid to the presence of spurious scattering in nuclear emulsions. From an earlier investigation on the causes of spurious scattering (Aditya *et al* 1961, 1963) and subsequent work (Aditya 1962) it became abundantly clear that the origin of spurious scattering lay in the peculiar type of distortion present in emulsion pellicles as a result of their flexibility. In recent works (Aditya and Puri, 1964; Aditya 1964) we have described the characteristics of this distortion and methods of its measurement.

During the course of these investigations measurements were made on a high energy event initiated by cosmic radiation, the very star which had been used by Biswas *et al* (1955) to describe the peculiar nature of spurious scattering; the origin of spurious scattering was not investigated by them. Our measurements have allowed an interpretation of the event in terms of the distortion investigated by us. The analysis is very revealing and is described in the present note.

## THE EVENT

A high energy heavy primary nucleus (energy per nucleon  $\sim 2 \times 10^{10}$  eV) traversing a stack of stripped emulsions entered at the surface-stuck-to-glass of a pellicle. At a few microns within the pellicle the heavy primary underwent a fragmentation into six narrowly collimated  $\alpha$ -particles. Soon after one of the  $\alpha$ -particles produced a second interaction. The collimated beam of five  $\alpha$ -particles, followed through the pellicle, was found to leave again at the same face of the pellicle at which the primary had entered. The maximum depth to which an  $\alpha$ -particle went into the pellicle was  $\sim 70 \mu\text{m}$ , measured in terms of original

(\*) This paper is the revised version of a manuscript submitted for publication in August 1963 and which remained unpublished due to inadvertent circumstances. Some amendments have been made by giving references to further work carried out by the author.

thickness assumed to be  $600\mu\text{m}$ . The tracks had experienced, obviously, some sort of a severe distortion in the depth direction.

Coordinate measurements on the  $z$  and  $y$  coordinates of the  $5\alpha$ -particles have been made at  $500\mu\text{m}$  interval on the  $x$ -axis, along which the event was aligned. These have been plotted in Figs. 1. and 2, for the depth and projected plane respectively.

From the plot in depth (1-a), the nature of distortion has been obtained by superimposition (1-b), thereby yielding the contour common to all tracks (1-c). The contour obtained by the method of algebraic mean (Aditya 1964) has been found to be similar to that shown here. Since the deviations due to multiple

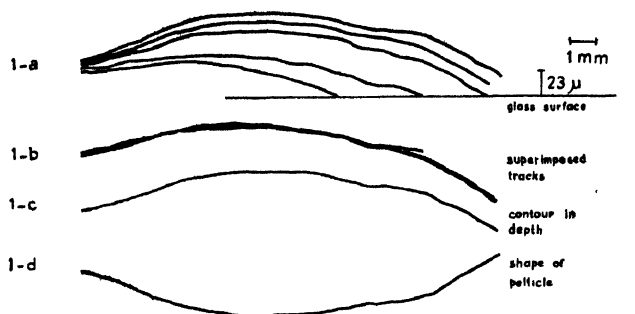


Fig. 1. Profile in depth.



Fig. 2. Profile in projection.

scattering are random there could be no component of scattering in the common contour. Moreover the true scattering is negligibly small and the common contour should be a straight line in the absence of any distortion. It is evident that the contour 1-d, which is a mirror image of the contour 1-c, represents the shape of the lower surface of the pellicle, or that of the pellicle as a whole if the thickness is assumed to be uniform. The pellicle was thus not plane at the time of exposure.

This event is particularly favourable since it has been possible to locate the source of the dislocation in depth. The pellicle formed part of a stack, described by Daniel *et al* (1954), in which an  $18\mu\text{m}$  thick nylon-thread grid, irradiated with pollonium, had been used to mark emulsions for pellicle alignment. The position of the threads as seen in the two sections, elevation and plan, are shown in Fig. 3(a) and (b), respectively. It is clear that the shape of the pellicle as derived

at 1-*d*, has resulted from the presence of the marking grid between pellicles. The two sets of grids have so pressed the pellicle that a cup has been formed. It was pointed out also by Daniel *et al* (1954) that the gap height, measured experimentally by following tracks, varies from 25 $\mu$ m to 35 $\mu$ m within the stack pellicles, which means that the pellicles were non-plane to the extent indicated by them and is substantiated by our measurements.

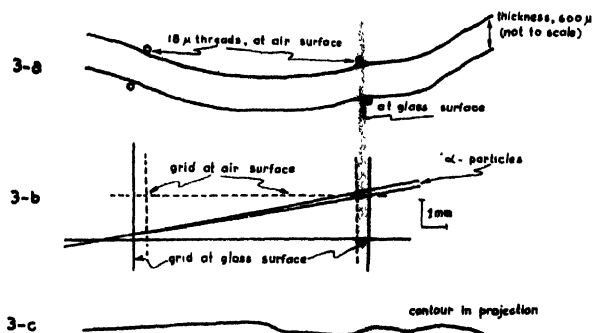


Fig. 3. The scale of (a) is same as in Fig. 1, and of (c) same as in Fig. 2.

The influence of this type of distortion on the shape of the tracks as seen in the projected plane may now be considered. From the plot, in projection, of the  $\alpha$ -particles Fig. (2a), the common contour 2-*b* has been obtained after superimposition. The contour is highly complicated and has no resemblance with the conventional *C* or *S*-shape distortion, which one may normally expect. This contour is reproduced at the bottom of Fig 3 to let a comparison be made with the shape of the pellicle as referred to the position of the grid threads. A point to point correspondence is apparent.

# DISCUSSION

The nature and origin of distortion described above is different from that conventionally understood, viz., due to differential shear between various layers of emulsion. A large number of investigations (Cosyns *et al*, 1950; Major, 1952; Apostolakis *et al*, 1957) have been devoted to the determination of this type of distortion, on account of which a straight track is assumed to take a *C*-shape or at worst an *S*-shape. Measurements are conventionally made on fast dipping tracks. The distortion described in this work is not due to differential shear. In the region of emulsion containing this event, for example, Biswas *et al* found the distortion determined by conventional methods to be moderate, (50 covans). We have, instead, shown the distortion to be severe; this is not astonishing because a different mechanism has been considered as the origin and a different method used for the determination of its magnitude.

The correlation between this distortion and the level of spurious scattering will now be demonstrated. The contribution of distortion to the mean second

difference,  $\bar{D}_d$  (for definition see Aditya 1962) and  $\bar{D}_{ss}$  (as obtained by conventional methods) are tabulated in Table. 1, for different sections of the tracks,

TABLE I

Section	Cell length	$\bar{D}_{ss} (\mu m)$	$\bar{D}_d (\mu m)$	$\bar{D}_{ss}/\bar{D}_d$
First cm	500 $\mu$ m	0.245	0.20	1.23
	1000 $\mu$ m	0.375	0.21	1.78
Second cm	500 $\mu$ m	0.865	0.58	1.49
	1000 $\mu$ m	1.06	1.5	0.71
Total Track	500 $\mu$ m	0.53	0.38	1.39
	1000 $\mu$ m	0.96	0.91	1.06

as well as for the entire length. It is seen that  $\bar{D}_d$  behaves in the same manner as  $\bar{D}_{ss}$ . Such a correlation has been demonstrated for a wide variety of samples in another work (Aditya *et al.* 1964; Fig. 5).

## ACKNOWLEDGMENTS

Thanks are due, to Dr. R. R. Daniel, Tata Institute of Fundamental Research Bombay, for the loan of emulsions.

## REFERENCES

- Aditya, P. K., 1962, *Korpuskularphotographie*, **4**, 513; Proceedings of IV International Conference on Nuclear Photography Munchen, September 1962.
- Aditya, P. K., 1964, *Ind. J. Phys.*, **38**, 326.
- Aditya, P. K., Bhatia, V. S. and Sood, P. M., 1963, *Nuovo Cimento* **29**, 577; results reported earlier, 1961, Minutes of informal meeting held at Bombay, 1961.
- Aditya, P. K., and Puri, R. K., 1964; *Journal Sci. Inst. (London)*, **41**, 529.
- Apostolakis, A. J., and Major, J. V., 1957, *Brit. J. Appl. Phys.*, **8**, 9.
- Biewas, S., Peters, B., and Rama, 1955, *Proc. Ind. Acad. Sci.*, **41**, 154.
- Cosyns, M., and Vanderhaeghe, G., Bulletin du Centre de Physique Nucleaire, No. 15, 1950.
- Daniel, R. R., Friedman, G., Lal, D., Pal, Y., and Peters, B., 1954, *Proc. Ind. Acad Sci.*, **40**, 151.
- Major, J. V., 1952, *Brit. J. Appl. Phys.*, **3**, 309.

# FOURTH-ORDER ELASTIC COEFFICIENTS FOR SOME CRYSTAL CLASSES\*†

P. B. GHATE

DEPARTMENT OF ENGINEERING PHYSICS AND MATERIALS SCIENCE, CORNELL UNIVERSITY  
ITHACA, NEW YORK

(Received February 25, 1964)

**ABSTRACT.** The fourth-order elastic coefficients form an eight-order tensor containing 6561 components of which 126 are independent for a triclinic system. Using symmetry arguments it is shown that there are 70, 42, 25, and 11 independent constants for monoclinic (2, 2/m, m), orthorhombic (222, 2mm, mmm), tetragonal (4mm, 42m, 422, 4/mmm) and cubic (43m, 432, m3m) crystals respectively.

## INTRODUCTION

In the classical theory of elasticity the strains are treated as infinitesimal and the elastic energy of a body initially under no stresses, is a quadratic function of the strain. The stress-strain relationships and the scheme of the second-order elastic coefficients are quite well known (Huntington, 1958). In those cases where the strains may not be considered as infinitesimal, it is necessary to include higher order terms. An elegant treatment of the finite deformation of an elastic solid has been given by Murnaghan (1951). The elastic energy  $\phi$  is analyzed into a sum

$$\phi = \phi_2 + \phi_3 + \phi_4 + \dots$$

of terms of different degrees in the elements of  $\eta$ . The  $\eta$ 's are the symmetrized Lagrangian strain components (Birch, 1947). It is possible to express  $\phi_2$  and  $\phi_3$  as

$$\begin{aligned}\phi_2 &= 1/2 C'_{ijkl} \eta_{ij} \eta_{kl} \\ \phi_3 &= C'_{ijklmn} \eta_{ij} \eta_{kl} \eta_{mn}\end{aligned}$$

where  $i, j, k, l, m, n$  take the values 1, 2, 3. Repeated indices imply the usual summation convention. The coefficient 1/2 in the expression for  $\phi_2$  is conventional. The expression for  $\phi_3$  follows that given by Hearmon (1953). Here the  $C'_{ijklmn}$

\*Work supported by the Advanced Research Projects Agency through the Cornell Materials Science Center.

†After this article was prepared, it was brought to the attention of the author of a recent communication by Krishnamurty (1963) on fourth-order elastic coefficients in crystals. For the crystal classes considered in this article, the results agree with those given by Krishnamurty.

are the third order elastic coefficients which are the components of a sixth-order tensor. Group theory has been used to determine the number of independent components of the sixth-order tensor (Bhagavantam and Suryanarayan, 1947, 1949; Jahn, 1949). Fumi (1951, 1952, 1953) has carried out an extensive investigation on "Matter Tensors" up to the sixth-order, and has given the relations between the actual components. The scheme of the third-order elastic coefficients given by Hearmon (1953, 1956) agrees with those given by Birch (1947) for cubic crystals and by Bhagavantam and Suryanarayan (1947, 1949), Jahn (1949), and Fumi (1951, 1952, 1953) for other crystal classes. The sixth-order tensor with 729 components gives only 56 independent third-order elastic coefficients for a triclinic system. This number is reduced considerably for crystals with higher symmetry. Recently, these considerations have been extended to investigate the fourth-order elastic coefficients (Ghate, 1964). In the present article, the fourth-order elastic coefficients for some crystal classes, using symmetry arguments, are enumerated.

#### ELASTIC ENERGY $\phi_4$ AND THE FOURTH-ORDER ELASTIC COEFFICIENTS

Let us express  $\phi_4$  as follows :

$$\phi_4 = C_{ijklmnop} \eta_i \eta_j \eta_k \eta_l \eta_m \eta_n \eta_o \eta_p$$

where  $i, j, k, l, m, n, o, p$  take the values 1, 2, 3. The  $\eta$ 's are the Lagrangian strain components and the  $C_{ijklmnop}$ 's are the fourth-order elastic coefficients which are the components of an eighth-order tensor containing 6561 components. However, the tensor is symmetrical with respect to the interchange of  $i$  and  $j$ ,  $k$  and  $l$ ,  $ij$  with  $kl$ , and so on. The number of independent tensor components then reduce to 126. The components of the elastic coefficients are conventionally contracted as follows :

$$\begin{array}{ccc} 11-1 & 22-2 & 33-3 \\ 23-4 & 31-5 & 12-6 \end{array}$$

then  $\phi_4 = C_{pqrs} \eta_p \eta_q \eta_r \eta_s$  where  $p, q, r, s$  take the values 1, 2, 3, 4, 5, 6 and  $C_{pqrs}$  are the fourth-order elastic coefficients. For a triclinic system, there are in all 126 fourth-order elastic coefficients. These are listed in Column I of Table I. Here  $C_{1111}$ ,  $C_{1112}$ , etc. are written as 1111, 1112, and so on for convenience.

The contraction of the indices of  $C_{ijklmnop}$  to give  $C_{pqrs}$  needs a little explanation. It may be recalled that

$$C_{pqrs} = C_{qprs} = C_{pqsr} = C_{psqr}, \text{ etc.}$$

It is convenient to define a ratio  $R$  such that

$$R = \frac{C_{nnss}}{C_{ijklmnop}}$$

which gives the possible number of combinations of the indices. This point can be illustrated as follows :

$$C_{1112} = C_{11\ 11\ 11\ 22}$$

Because of the symmetry with respect to the interchange of the indices, we have

$$C_{11\ 11\ 11\ 22} = C_{11\ 11\ 22\ 11} = C_{11\ 22\ 11\ 11} = C_{22\ 11\ 11\ 11}$$

$$\therefore R = \frac{C_{1112}}{C_{11\ 11\ 11\ 22}} = 4.$$

Similarly it can be verified that

$$C_{1122} = 6C_{11\ 1122\ 22}.$$

The values of  $R$  for all the 126 fourth-order elastic coefficients are listed in column " $R$ " of Table I. The sum of all the values of " $R$ " is 6561, as it should be.

TABLE I

Hermann-Mauguin symbols of the crystal classes are used at the top of each column

	Triclinic	Monoclinic			Orthorhombic	Tetragonal	Cubic
	1	2			222	4mm	43m
	1	2/m			— —	42m	432
		m			mmn	422	m3m
		Mirror plane = $x_2x_3$	Mirror plane = $x_3x_1$	Mirror plane = $x_1x_2$		4/mmm	
		Twofold axis = $x_1$	Twofold axis = $x_2$	Twofold axis = $x_3$			
	(126)	(70)	(70)	(70)	(42)	(25)	(11)
R	I	II	III	IV	V	VI	VII
1	1111	1111	1111	1111	1111	1111	1111
4	1112	1112	1112	1112	1112	1112	1112
4	1113	1113	1113	1113	1113	1113	1112
8	1114	1114	0	0	0	0	0
8	1115	0	1115	0	0	0	0
8	1116	0	0	1116	0	0	0
6	1122	1122	1122	1122	1122	1122	1122
12	1123	1123	1123	1123	1123	1123	1123
24	1124	1124	0	0	0	0	0
24	1125	0	1125	0	0	0	0
24	1126	0	0	1126	0	0	0
6	1133	1133	1133	1133	1133	1133	1122
24	1134	1134	0	0	0	0	0
24	1135	0	1135	0	0	0	0
24	1136	0	0	1136	0	0	0
24	1144	1144	1144	1144	1144	1144	1144
48	1145	0	0	1145	0	0	0
48	1146	0	1146	0	0	0	0

TABLE I (contd.)

R	I	II	III	IV	V	VI	VII
24	1155	1155	1155	1155	1155	1155	1155
48	1156	1156	0	0	0	0	0
24	1166	1166	1166	1166	1166	1166	1155
4	1222	1222	1222	1222	1222	1112	1112
12	1223	1223	1223	1223	1223	1123	1123
24	1224	1224	0	0	0	0	0
24	1225	0	1225	0	0	0	0
24	1226	0	0	1226	0	0	0
12	1233	1233	1233	1233	1233	1233	1123
48	1234	1234	0	0	0	0	0
48	1235	0	1235	0	0	0	0
48	1236	0	0	1236	0	0	0
48	1244	1244	1244	1244	1244	1244	1244
96	1245	0	0	1245	0	0	0
96	1246	0	1246	0	0	0	0
48	1255	1255	1255	1255	1255	1244	1244
96	1256	1256	0	0	0	0	0
48	1266	1266	1266	1266	1266	1266	1266
4	1333	1333	1333	1333	1333	1333	1112
24	1334	1334	0	0	0	0	0
24	1335	0	1335	0	0	0	0
24	1336	0	0	1336	0	0	0
48	1344	1344	1344	1344	1344	1344	1244
96	1345	0	0	1345	0	0	0
96	1345	0	1346	0	0	0	0
48	1355	1355	1355	1355	1355	1355	1266
96	1356	1356	0	0	0	0	0
48	1366	1366	1366	1366	1366	1366	1244
32	1444	1444	0	0	0	0	0
96	1445	0	1445	0	0	0	0
96	1446	0	0	1446	0	0	0
96	1455	1455	0	0	0	0	0
102	1456	1456	1456	1456	1456	1456	1456
96	1466	1466	0	0	0	0	0
32	1555	0	1555	0	0	0	0
96	1556	0	0	1556	0	0	0
96	1566	0	1566	0	0	0	0
32	1666	0	0	1666	0	0	0
1	2222	2222	2222	2222	2222	1111	1111
4	2223	2223	2223	2223	2223	1113	1112
8	2224	2224	0	0	0	0	0
8	2225	0	2225	0	0	0	0
8	2226	0	0	2226	0	0	0
6	2233	2233	2233	2233	2233	1133	1122
24	2234	2234	0	0	0	0	0



TABLE I—(contd.)

R	I	II	III	IV	V	VI	VII
24	2235	0	2235	0	0	0	0
24	2236	0	0	2236	0	0	0
24	2244	2244	2244	2244	2244	1155	1155
48	2245	0	0	2245	0	0	0
48	2246	0	2246	0	0	0	0
24	2255	2255	2255	2255	2255	1144	1144
48	2256	2256	0	0	0	0	0
24	2266	2266	2266	2266	2266	1166	1165
4	2333	2333	2333	2333	2333	1333	1112
24	2334	2334	0	0	0	0	0
24	2335	0	2335	0	0	0	0
24	2336	0	0	2336	0	0	0
48	2344	2344	2344	2344	2344	1355	1266
96	2345	0	0	2345	0	0	0
96	2346	0	2346	0	0	0	0
48	2355	2355	2355	2355	2355	1344	1244
96	2356	2356	0	0	0	0	0
48	2366	2366	2366	2366	2366	1366	1244
32	2444	2444	0	0	0	0	0
96	2445	0	2445	0	0	0	0
96	2446	0	0	2446	0	0	0
96	2455	2455	0	0	0	0	0
192	2456	2456	2456	2456	2456	1456	1456
96	2466	2466	0	0	0	0	0
32	2555	0	2555	0	0	0	0
96	2556	0	0	2556	0	0	0
96	2566	0	2566	0	0	0	0
32	2666	0	0	2666	0	0	0
1	3333	3333	3333	3333	3333	3333	1111
8	3334	3334	0	0	0	0	0
8	3335	0	3335	0	0	0	0
8	3336	0	0	3336	0	0	0
24	3344	3344	3344	3344	3344	3344	1155
48	3345	0	0	3345	0	0	0
48	3346	0	3346	0	0	0	0
24	3355	3355	3355	3355	3355	3344	1155
48	3356	3356	0	0	0	0	0
24	3366	3366	3366	3366	3366	3366	1144
32	3444	3444	0	0	0	0	0
96	3445	0	3445	0	0	0	0
96	3446	0	0	3446	0	0	0
96	3455	3455	0	0	0	0	0
192	3456	3456	3456	3456	3456	3456	1456
96	3466	3466	0	0	0	0	0
32	3555	0	3555	0	0	0	0

TABLE I (contd.)

R	I	II	III	IV	V	VI	VII
96	3556	0	0	3556	0	0	0
96	3566	0	3566	0	0	0	0
32	3666	0	0	3666	0	0	0
16	4444	4444	4444	4444	4444	4444	4444
64	4445	0	0	4445	0	0	0
64	4446	0	4446	0	0	0	0
96	4455	4455	4455	4455	4455	4455	4455
192	4456	4456	0	0	0	0	0
96	4466	4466	4466	4466	4466	4466	4455
64	4555	0	0	4555	0	0	0
192	4556	0	4556	0	0	0	0
192	4566	0	0	4566	0	0	0
64	4666	0	4666	0	0	0	0
16	5555	5555	5555	5555	5555	4444	4444
64	5556	5556	0	0	0	0	0
96	5566	5566	5566	5566	5566	4466	4455
64	5666	5666	0	0	0	0	0
16	6666	6666	6666	6666	6666	6666	4444

Finally we note that the  $n$ -th order elastic coefficients form a  $2n$ -order-tensor with  $3^{2n}$  components. It is easy to convince oneself that the number of independent coefficients is given by

$$\frac{6(6+1) \dots (6+n-1)}{n!}$$

#### FOURTH-ORDER ELASTIC COEFFICIENTS FOR SOME CRYSTAL CLASSES

If the crystal possesses certain symmetry properties, then the elastic energy should be invariant with respect to these symmetry operations. In the following discussion, the primed axes will imply the new set of axes obtained after a symmetry operation.

*Monoclinic Crystals* (2,  $2/m.m$ ): We take a coordinate system with  $x_2x_3$  as the plane of symmetry. On reflection in this plane, we obtain the new set of axes.

$$x_1' = -x_1; x_2' = x_2; x_3' = x_3.$$

The primed and the unprimed strain components are related to each other in the following manner :

$$\eta_1' = \eta_1, \eta_2' = \eta_2, \eta_3' = \eta_3; \eta_4' = \eta_4, \eta_5' = -\eta_5, \eta_6' = -\eta_6.$$

The elastic energy should be invariant with respect to this operation and therefore

$$\phi_4 = C_{pqrs}\eta_p\eta_q\eta_r\eta_s = C_{ijkl}\eta_i'\eta_j'\eta_k'\eta_l'$$

where  $p, q, r, s, i, j, k, l$  take the values 1, 2, 3, 4, 5, 6. It follows that :

$$C_{1113}\eta_1^3\eta_5 = -C'_{1113}\eta_1^3\eta_5; \therefore C'_{1115} = 0.$$

All the nonvanishing coefficients can be found in a similar manner. These are listed in column II of Table I. In all there are 70 independent fourth-order elastic coefficients. In columns III and IV, the coefficients are listed for those cases where  $x_3x_1$  and  $x_1x_2$  are the planes of symmetry.

*Orthorhombic Crystals* (222, 2mm mmm): Take the three planes of symmetry as the coordinate planes. It can be easily verified that only those coefficients which are common to columns 2, 3 and 4 are the required ones. Thus we find that there are only 42 independent fourth-order elastic coefficients for an orthorhombic system. These are listed in column V of Table I.

*Tetragonal Crystals* (4mm, 42m, 422, 4/mmm): In the case of the tetragonal crystals there is a four-fold axis in addition to the three planes of symmetry, which are taken as the coordinate planes. The " $x_3$ " axis is chosen as the four-fold axis. It is evident that we have to examine the 42 coefficients of the orthorhombic system for further interrelationships. For a rotation of  $\pi/2$  about the " $x_3$ " axis, the primed and the unprimed strain components are related to each other as follows :

$$\eta_1' = \eta_2, \eta_2' = \eta_1, \eta_3' = \eta_3; \eta_4' = -\eta_5, \eta_5' = \eta_4, \eta_6' = -\eta_6.$$

The elastic energy  $\phi_4$  must be insensitive to this covering operation. The following relations are then obtained :

$$1111 = 2222; 1112 = 1222; 1113 = 2223; \text{ and so on.}$$

There are in all 25 independent coefficients which are listed in column VI of Table I. The other equivalent coefficients, for example, 1456 = 2456, can be easily obtained from Table I.

*Cubic Crystals* (43m, 432, m3m): Take the cartesian coordinate axes ( $x_1, x_2, x_3$ ) as coinciding with a set of cubic axes. Note that each cubic axis is a four-fold axis and hence has the tetragonal symmetry. Thus it is necessary to examine only the independent coefficients of the tetragonal system for additional interrelationships. It is further noted that each body diagonal is a three-fold axis. A rotation of  $2\pi/3$  about the body diagonal defines a new set of axis such that  $x_1'$  coincides with  $x_2$ ,  $x_2'$  coincides with  $x_3$ , and  $x_3'$  coincides with  $x_1$ . The primed and the unprimed strain components are related to each other in the following manner :

$$\eta_1' = \eta_2, \eta_2' = \eta_3, \eta_3' = \eta_1; \eta_4' = \eta_5, \eta_5' = \eta_6, \eta_6' = \eta_4.$$

The elastic energy  $\phi_4$  has to be invariant for these symmetry operations. It is found that,

$$1111 = 2222 = 3333$$

$$1112 = 1113 = 1222 = 1333 = 2223 = 2333$$

and so on. There are in all 11 independent coefficients for a cubic crystal and these are listed in column VII of Table I.

### Elastic Energy $\phi_4$

The use of the table in writing the terms of the elastic energy  $\phi_4$  for a cubic crystal will now be illustrated. For a particular constant, say 1244, scan the column VII downwards and find out how many times it appears. Every time 1244 is found, look for the corresponding coefficient in the column for the triclinic system. Note that,  $1244 = 2366 = 1344 = 1366 = 2355 = 1255$ . That part of the elastic energy with coefficient  $C'_{1244}$ , can now be written as

$$C'_{1244}(\eta_1\eta_2(\eta_4^2 + \eta_5^2) + \eta_2\eta_3(\eta_5^2 + \eta_6^2) + \eta_1\eta_3(\eta_6^2 + \eta_4^2)).$$

The total elastic energy  $\phi_4$  can now be easily written as follows :

$$\begin{aligned}\phi_4 = & C_{1111}(\eta_1^4 + \eta_2^4 + \eta_3^4) \\ & + C_{1112}(\eta_1^3(\eta_2 + \eta_3) + \eta_2^3(\eta_3 + \eta_1) + \eta_3^3(\eta_1 + \eta_2)) \\ & + C_{1122}(\eta_1^2\eta_2^2 + \eta_2^2\eta_3^2 + \eta_3^2\eta_1^2) \\ & + C_{1123}(\eta_1^2\eta_2\eta_3 + \eta_2^2\eta_3\eta_1 + \eta_3^2\eta_1\eta_2) \\ & + C_{1144}(\eta_1^2\eta_4^2 + \eta_2^2\eta_5^2 + \eta_3^2\eta_6^2) \\ & + C_{1155}(\eta_1^2(\eta_5^2 + \eta_6^2)\eta_2^2(\eta_4^2 + \eta_6^2)\eta_3^2(\eta_4^2 + \eta_5^2)) \\ & + C_{1244}(\eta_1\eta_2(\eta_4^2 + \eta_5^2) + \eta_2\eta_3(\eta_5^2 + \eta_6^2) + \eta_1\eta_3(\eta_6^2 + \eta_4^2)) \\ & + C_{1266}(\eta_1\eta_2\eta_6^2 + \eta_2\eta_3\eta_4^2 + \eta_3\eta_1\eta_5^2) \\ & + C_{1456}(\eta_4\eta_5\eta_6(\eta_1 + \eta_2 + \eta_3)) \\ & + C_{4444}(\eta_4^4 + \eta_5^4 + \eta_6^4) \\ & + C_{4455}(\eta_4^2\eta_5^2 + \eta_5^2\eta_6^2 + \eta_6^2\eta_4^2).\end{aligned}$$

Table I can be used to write  $\phi_4$  for other crystal classes. It may be remarked, however, that the independent fourth-order elastic coefficients for the hexagonal and trigonal systems can be deduced, starting from the 70 independent coefficients of the monoclinic system, except for the formidable algebra involved.

### ACKNOWLEDGMENT

The author wishes to thank Dr. A. L. Ruoff for many valuable discussions.

### REFERENCES

- Bhagavantam, S. and Suryanarayan, D., 1947, *Nature*, Lond. **160**, 750 ; *Acta Cryst.*, 1949, **2**, 21.  
 Birch, F., 1947, *Phys. Rev.* **71**, 809.  
 Fumi, F. G., 1951, *Phys. Rev.*, **83**, 1274 ; 1952, *Phys. Rev.*, **86**, 561 ; 1952, *Acta Cryst.* **5**, 691 ; 1952, *Nuovo Cimento* **9**, 739 ; 1953, *Nuovo Cimento* **10**, 865.  
 Ghate, P. B., 1964, *J. Appl. Phys.* **35**, 337. Also available as Materials Science Center Report No. 124, Cornell University, Ithaca, New York.  
 Hearmon, R. F. S., 1953, *Acta Cryst.* **6**, 331 ; 1956, *Advances in Phys.*, **5**, 323.  
 Huntington, H. B., *Solid State Physics*, Edited by F. Seitz and D. Turnbull (Academic Press, Inc., New York, Vol. 7, pp. 213-351, 1958).  
 Jahn, H. A., 1949, *Acta Cryst.* **5**, 691.  
 Krishnamurty, T. S. G., 1963, *Acta Cryst.* **16**, 839.  
 Murnaghan F. D., *Finite Deformation of an Elastic Solid* (John Wiley & Sons, Inc., New York, 1951).

# NON-RADIATIVE TRANSITIONS DURING THE DECAY OF A PHOSPHOR

Y. L. ARORA

DEFENCE RESEARCH LABORATORY (STORES) KANPUR

(Received August 30, 1963)

**ABSTRACT.** The decay of zinc sulphide phosphors at different temperatures using ultraviolet excitation has been measured. It is found that the decay constant decreases with temperature. This is theoretically explained by using the idea of non-radiative transitions during the decay. Efficiency of phosphorescence during decay is also discussed.

## INTRODUCTION

Randall and Wilkins (1945) and Garlick and Gibson (1948) developed a theory to explain the various phenomena of phosphorescence by assuming the storage of excited electrons in metastable energy levels due to traps arising from the co-activator atoms or lattice defects of the crystal. The existence of these electron traps is responsible for the slow rise of fluorescence, of phosphorescence of glow emission, of infra-red stimulation and quenching. In spite of extensive studies in the field of solid-state luminescence by various workers, it has not yet been possible to explain the luminescence phenomena satisfactorily. The present experiments were conducted to study the decay properties at different temperatures and also the efficiency of phosphorescence.

## EXPERIMENTAL

### (A) *Preparation of zinc sulphide phosphor*

Zinc sulphide of high purity was prepared. Triply distilled water and pyrex containers were used throughout. Small quantities of copper in the form of copper sulphate (Analar B.D.H.) were added to the zinc sulphide and then dried at 110°C in an oven. The dried material was put in a clean fireclay boat and placed in the hottest zone of a tubular silica furnace. A constant stream of pure dry  $H_2S$  was allowed to flow through this furnace and the temperature maintained at 1100°C for half-an-hour. Under these conditions the phosphors produced were of reasonably reproducible quality.

### (B) *Apparatus* . . .

The phosphor was excited by a mercury discharge bulb operated by a stabilized voltage supply. By the use of proper filters the 3600 Å line was allowed to fall

\*Present Address : Century Rayon, Kalyan.

on the phosphor. To measure the intensity of phosphorescence and its decay, a RCA 931 A photomultiplier was used in conjunction with a Hilger galvanometer. A wratten 2A filter was placed in front of the photo-multiplier to exclude the direct light from the mercury bulb. For work at room temperature and above the phosphor was painted on a 1"×1" copper plate with sodium silicate as binder. The plate was held at an angle of 45° to the incident beam. The temperature of the phosphor was measured by a copper-constantan thermocouple and potentiometer arrangement.

*Experiment I:* Decay at different temperatures.

## RESULTS AND DISCUSSIONS

The variation of the intensity of phosphorescence,  $I$  with time  $t$  was observed at different temperatures. The intensity was measured in terms of the galvanometer deflection  $\theta$  and plotted against  $1/t$  which gave a straight line (Fig. I.)

$$\text{i.e. } \propto I\alpha\theta = \frac{B}{t}$$

Where  $B$  is the decay constant and is given by the slope of the straight line. The various values of the slope at different temperatures are given in Table I.

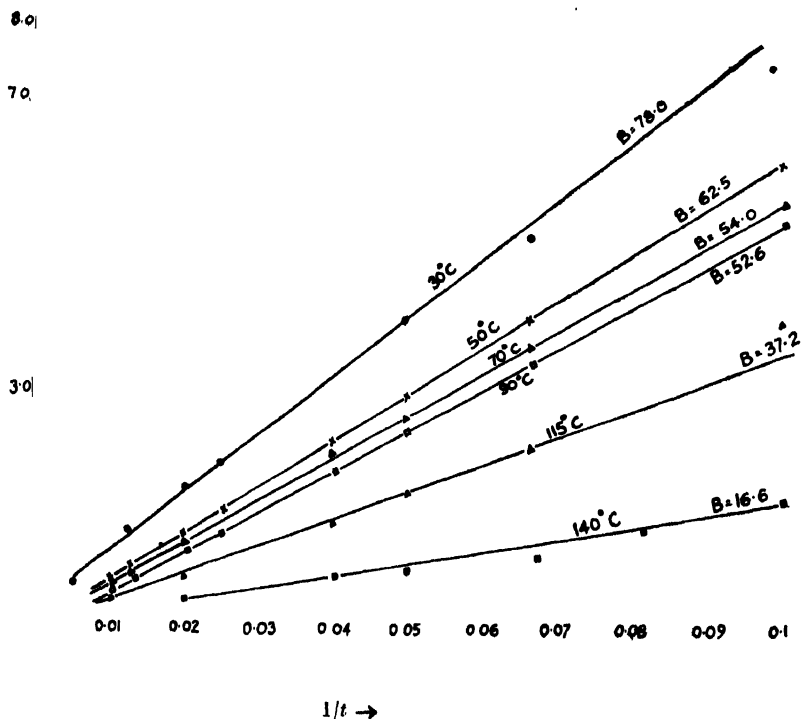


Fig. 1. Decay of ZnS phosphor at different temperatures.

From Table I we find that as the temperature increases the slope  $B$  decreases. This cannot be explained by the existing equation (3),(4) of decay,

$$I = \frac{N_E k T}{t}$$

Where  $T$  is the temperature in absolute units

$k$  is Boltzman constant

$N_E$  is the number of electrons in each trap.

TABLE I  
Calculated values of slope at different temperatures

S/No.	Name of phosphor	Temperature	Value of slope
1		30°C	78.0
2		50°C	62.5
3	Zns	70°C	54.0
4	'a'	90°C	52.6
5		115°C	37.3
6		140°C	16.6

#### EFFECT OF NON-RADIATIVE TRANSITIONS

Assuming that during the decay non-radiative transitions are also  $\delta$  taking place, it is explained that the decay constant decreases with temperature as follows. The general equation for the light emission during decay may be written as :

$$0 = L + Q + \frac{dn_t}{dt} + \frac{dn_c}{dt} \quad \dots (1)$$

where  $L$  = number of electrons/cm<sup>3</sup> recombining per second radiatively.

$Q$  = number of electrons/cm<sup>3</sup> recombining per second non-radiatively.

$n_t$  = number of electrons/cm<sup>3</sup> in traps

$n_c$  = number of electrons/cm<sup>3</sup> in the conduction band

for  $n_t \gg n_c$

$$0 = L + Q + \frac{dn_t}{dt} \quad \dots (2)$$

It can be shown that during decay non-radiative transitions are proportional to radiative transitions at any instant.

i.e.  $Q_{(\tau)} = KL_{(\tau)}$  where  $K$  is a constant.

Thus equation (2) will become

$$0 = L + KL + \frac{dn_t}{dt}$$

or 
$$\frac{dn_i}{dt} = -L[1+K]$$

Now 
$$L = nse^{-E/kT}$$

where  $s$  is a escape frequency

$k$  = Boltzman constant

$T$  = Temperature in absolute unit.

$\therefore \frac{dn}{dt} = -ns(1+k)e^{-E/kT}$

Integrating and putting  $t = 0, n = n_0$  we get

$$n = n_0 \exp[-st(1+K)e^{-E/kT}] \quad \dots (3)$$

Now, the intensity of phosphorescence during decay is,

$$L = nse^{-E/kT} \quad \dots (4)$$

substituting the value of  $n$  from (3) we get

$$L = n_0 s \text{Exp}[-st(1+K)e^{-E/kT}]e^{-E/kT}$$

If there are  $N_E dE$  traps with energy lying between  $E$  and  $E+dE$ , then the phosphorescence intensity ( $I_t$ ) at time  $t$ , after cessation of excitation, will be

$$I_t = N_E s \int_0^\infty \text{Exp}[-st(1+K)e^{-E/kT}]e^{-E/kT} dE \quad \dots (5)$$

or 
$$I_t = \frac{N_E kT}{(1+K)t}$$

or 
$$\theta = \frac{N_E kT}{c(1+K)t} = \frac{B}{t} \quad \text{where } c \text{ is a constant}$$

or 
$$B = \frac{N_E kT}{c(1+K)} \quad \dots (6)$$

The value of constant  $B$  does not vary linearly with temperature as  $K$ , the ratio of non-radiative and radiative transitions is also affected by temperature. If the different values of  $B$  from Table I and their corresponding temperatures are substituted in (6), we get the values of  $c(1+K)/kN_E$  at different temperature as listed in Table II.

From Table II, it becomes clear that  $K$  can be expected to increase with temperature and thus it is easy to see that  $B$  the decay constant might decrease with temperature.



TABLE II

S/No.	$T$ in absolute unit	$C(1+K)/N_E k$
1	303	3.8
2	323	5.1
3	343	6.3
4	363	6.9
5	388	10.4
6	413	24.8

*Experiment II : Efficiency of phosphorescence*

Zinc sulphide phosphor was first de-excited completely by heating and by infra-red. The phosphor was then excited at room temperature until the maximum intensity was reached. The excitation was then removed and the phosphor was allowed to decay for some time, and then excitation was recommenced. The ratio of the phosphorescent area  $P$  to the deficiency area  $D_P$  (Fig. 2) obtained

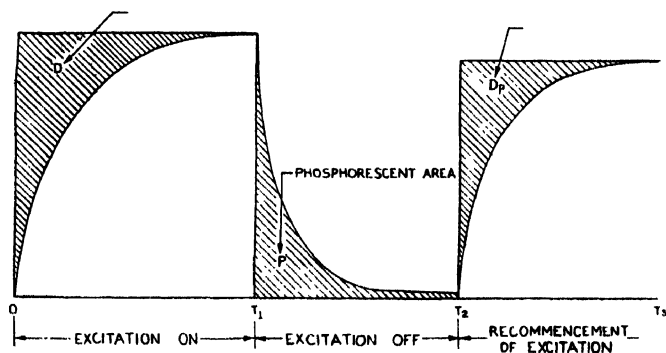


Fig. 2. Experiment of the deficiency area during the rise following the decay (Deflection vs time in second)

TABLE III

Ratio of phosphorescent area of zinc sulphide phosphor to corresponding deficiency area after recommencement of excitation at room temperature

S.No.	Time of decay	$P$ def. sec.	$D$ def. sec.	$D_P$ def. sec.	$\frac{P}{D_P}$
1	15 seconds	40	620	42	.95
2	$\frac{1}{2}$ minute	64	620	70	.90
3	1 minute	74	620	99.2	.82
4	3 minutes	94	620	125	.75

during the rise following the decay was determined. Results of this experiment are summarized in Table III, where  $D$  is the deficiency area for the completely de-excited sample.

#### DISCUSSION

The value of  $P/D_P$  is nearly one for 15 seconds decayed-phosphor and then decreases with the increase of the decay period. From this result it can be concluded that the efficiency of phosphorescence at room temperature in the beginning of the decay is of the same value as that of fluorescence. The decrease of  $P/D_P$  with prolonged-decay period may be due to the increase of non-radiative transitions during recommencement of excitation.

#### ACKNOWLEDGMENT

The Author is indebted to Dr. J. N. Nanda, Director Defence Research Laboratory, for suggesting the problem and for valuable guidance and discussions. The author is obliged to Shri S. N. Singhal for assisting in experimental work. The author is also grateful to Dr. C. B. Sharma for encouragement received from him.

#### REFERENCES

- Garlick, C. F. J. *Luminescent Materials*, 1949, Oxford University Press New York, P. 33.
- Garlick, C. F. J. and Gibson A. F. 1948, *Proc. Phys. Soc.*, Lond., **60**, 574.
- Handbuck Der Physik edited by S. Flugge Band **XXVI**, 1959, P. 65.
- Randall, J. T. and Wilkins, M. H. F., 1945, *Proc. Roy. Soc. A***184**, 365.
- Shionoya, S. Kullman, H. and Kramer, B., 1961, *Phys. Rev.* **121**, 1610.

# DECAY OF OSCILLATIONS OF A SPHERE AND CYLINDER IN A LIQUID—A NEW METHOD OF DETERMINING VISCOSITY

J. C. KAMESVAR RAV AND J. RAMAKRISHNA

PHYSICAL LABORATORIES, HYDERABAD SCIENCE SOCIETY, HYDERABAD

(Received September 23, 1963; Resubmitted December 7, 1964)

**ABSTRACT.** With the help of the dissipation function, it is deduced that the modulus of decay of torsional oscillations of a sphere of radius  $r$  and moment of inertia  $I$  about a diameter, in a liquid of viscosity  $\eta$  is given by  $8\pi r^3/I$  and that of a cylinder of radius  $a$  immersed in a liquid, to a depth  $l$ , contained in a concentric cylinder of radius  $b$  is given by  $2\pi\eta l \frac{a^2b^2}{I(b^2 - a^2)}$  where  $I$  is the moment of inertia of the cylinder about its axis of suspension. By knowing the logarithmic decrement the viscosity of a liquid can be found. The experimental values are found to agree with standard values.

## INTRODUCTION

Among the methods of finding the viscosity of liquids are Poiseuille's capillary tube method, rotating cylinder (Couette 1890, Searle 1912) and Stoke's (1851) method for highly viscous liquids. Measurement of modulus of decay of liquids in vessels or of solids in liquids was used by Helmholtz (1850) and Meyer (1891) for the determination of viscosity. But these require corrections which are complicated. A comparative method of measuring viscosity was first given by Mennerette (1911), who studied the decay of oscillations of liquids in a  $U$ -tube. By making use of the dissipation function Venkataraman (1933) deduced an expression for the modulus of decay in the above case and thus made it an absolute method. Christopherson and others (1938) made a study of the forced oscillations of a liquid in a  $U$ -tube and after elaborate mathematical analysis obtained expressions for the viscosity. Recently Choudhary and Trivedi (1961) described a method by which the viscosities can be compared by noting the damping of rotation of a symmetrical body in a liquid. This method is, however, useful only in the case of a very viscous liquids. In the concentric cylinder method, it is necessary to maintain a uniform motion of the external cylinder to get a constant deflection of the inner cylinder. This difficulty can be avoided by measuring the modulus of decay of the oscillations of the inner cylinder when it is twisted through a small angle and allowed to execute free oscillations. The same method can be used in the case of the sphere. This is what is attempted in this investigation.

## T H E O R Y

The modulus of decay of oscillations can be found from the dissipation function which was first given by Stokes (1851) and used by Lamb (1911) in the solution of some problems in hydrodynamics.

The dissipation function suitable for the rotational oscillations of a sphere in a liquid can be written as

$$2F = \eta \iiint (\omega_x^2 + \omega_y^2 + \omega_z^2) dx dy dz \quad \dots (1)$$

where  $\eta$  is the viscosity of the liquid,  $\omega_x$ ,  $\omega_y$ ,  $\omega_z$  are the components of the angular velocity. The integration is to be taken over the whole volume of the liquid. The dissipation is equal to the rate of decay of the total energy  $\epsilon$  i.e.,  $d\epsilon/dt$ . In the case of a sphere, suspended in a liquid by a long thin wire attached to a chuck fixed to a stand, the kinetic energy  $= \frac{1}{2} I \omega^2$  where  $\omega$  is the angular velocity of the sphere and  $I$  is the moment of inertia of the sphere about an axis passing through its centre. If the angular velocity is variable, it is equal to  $\frac{1}{2} I (d\theta/dt)^2$  where  $\theta$  is the angular displacement. Since the sphere is executing harmonic oscillations, its total energy is twice this, i.e.,

$$I \left( \frac{d\theta}{dt} \right)^2 \quad \dots (2)$$

*Sphere in an infinite liquid*

The dissipation function for a sphere in an infinite liquid can be easily found. In the case of a sphere rotating uniformly about its diameter in a liquid of viscosity  $\eta$  the moment of the couple acting on it is given by (Lamb 2, 1916)

$$C' = 8\pi\eta a^3 \omega \quad \dots (3)$$

The dissipation function given in (1) is therefore

$$2F = 8\eta a^2 \omega^2 \quad \dots (4)$$

when the angular velocity is varying, it is given by  $8\pi\eta a^3 (d\theta/dt)^2$ . Equating the rate of decay of total energy to dissipation, we get

$$\frac{d}{dt} \left[ I \left( \frac{d\theta}{dt} \right)^2 \right] = -8\pi\eta a^3 \left( \frac{d\theta}{dt} \right)^2 \quad \dots (5)$$

writing

$$x \text{ for } \left( \frac{d\theta}{dt} \right)^2, \quad \text{we have}$$

$$I \left( \frac{dx}{dt} \right) = -8\pi\eta a^3 x$$

Integrating this we get

$$\log x = - \frac{8\pi\eta a^3 t}{I} + \text{const} \quad \dots (6)$$

If we put the boundary condition  $x = x_0$  when  $t = 0$ , the above becomes

$$x = x_0 \exp[-8\pi a^3 \eta t / I]. \quad \dots (7)$$

Substituting  $(d\theta/dt)^2$  for  $x$ , equation (7) can be written as

$$\frac{d\theta}{dt} = \theta' \exp[-4\pi \eta a^3 t / I];$$

when this is integrated we obtain

$$\theta = \theta_0 \exp[-4\pi \eta a^3 t / I]$$

where  $\theta_0$  is a new constant, thus the logarithmic decrement is

$$-4\pi \eta a^3 / I \quad \dots (8)$$

### *Concentric cylinders*

In the case of a cylinder of radius  $a$  executing rotational oscillations in a liquid contained in another concentric cylinder of radius  $b$  the viscous couple on the inner cylinder, when the outer cylinder rotates with uniform angular velocity  $\omega$  is given by (Lamb 3, 1916).

$$4\pi \eta \frac{a^2 b^2}{b^2 - a^2} l \omega \quad \dots (9)$$

Where  $l$  is the length of the immersed portion of the cylinder in the liquid. As before, the dissipation function in this case is

$$4\pi \eta \frac{a^2 b^2}{b^2 - a^2} l \omega^2 \quad \dots (10)$$

Thus equating the rate of decay of total energy to dissipation we get an equation corresponding to (5)

$$\frac{d}{dt} \left[ I \left( \frac{d\theta}{dt} \right)^2 - 4\pi \eta l \frac{a^2 b^2}{b^2 - a^2} \left( \frac{d\theta}{dt} \right)^2 \right]$$

Integrating the equation as in the previous case we get

$$\theta = \theta_0 \exp \left[ - \frac{2\pi \eta l}{I} \cdot \frac{a^2 b^2}{b^2 - a^2} t \right].$$

Thus the modulus of decay is

$$- \frac{2\pi \eta l a^2 b^2}{I(b^2 - a^2)} \quad \dots (11)$$

Equation (8) and (11) form the basis of the measurement of viscosity by finding the modulus of decay of a sphere in a liquid and a cylinder in a liquid contained in a concentric cylinder.

## EXPERIMENTAL ARRANGEMENT

For finding the logarithmic decrement a steel sphere is suspended by a long thin wire whose other end is fixed to a heavy stand. A small mirror is fixed to the wire to note the deflections by means of a telescope and scale arrangement. The length is measured by a cathetometer. The entire set-up is shielded from draught by enclosing it in a glass case. The sphere is fully immersed in a liquid contained in a beaker. A thermoregulator was used to keep the temperature constant.

The sphere is given an angular displacement and the oscillations are observed with the help of a telescope and scale. The maximum time taken for a set of reading is 5 or 6 minutes. From the first and final quarter swings (to the same side) the logarithmic decrement is computed. If  $\alpha_1$  and  $\alpha_{n+1}$  are the first and  $(n+1)$  the deflections, say, to the right side, then the logarithmic decrement is given by

$$\lambda = \frac{1}{n} \log \frac{\alpha_1}{\alpha_{n+1}}$$

or, if logarithm to the base 10 are used

$$\lambda = \frac{2.3026}{n} \log_{10} \frac{\alpha_1}{\alpha_{n+1}} \quad \dots (12)$$

from relation (8) we get

$$\lambda = \frac{1}{2} K \eta I \quad \dots (13)$$

where  $K = 4\pi\gamma^3/I$ . Substituting  $\frac{2}{5}Mr^2$  for  $I$ , where  $M$  is the mass of the sphere, we get

$$K = \frac{10\pi r}{M}$$

The coefficient of viscosity is therefore, given from (12) and (13) by

$$\eta = \frac{4.6052}{\eta K T} \log_{10} \frac{\alpha_1}{\alpha_{n+1}} \quad \dots (14)$$

where  $T$  is the periodic time. The time for 25 oscillations was measured to 0.2". The time is of the order of 5 or 6 minutes and the time for one oscillation is calculated and is given to two decimal places.

The results are given in Table I.

*Cylinder in a liquid contained in a coaxial cylinder*

Just as in the above case the inner cylinder, of radius 'a' is suspended by a wire and is immersed in a liquid contained in an outer cylinder of radius 'b'.

TABLE I

Logarithmic decrement and viscosity of liquids with a sphere  
(using a sphere 1" in diameter).

Sl. No.	Liquid	Period $T$ (in seconds)	Logarithmic Decrement	Coefficient of viscosity in centipoises	
				Expt. at 25°C.	Standard at 25°C.
1.	Toluene	11.01	1.519	0.525	0.525
2.	Benzene	11.00	1.794	0.622	0.604
3.	Water	11.28	2.624	0.886	0.893
4.	Carbon tetra chloride	11.28	2.738	0.922	0.905
5.	Acetic Acid	11.30	3.442	1.160	1.113
6.	Olive Oil*	1.80	21.640	66.0	68.0
7.	Mobiloil SAE 40*	1.84	67.370	217.0	214.0

\*using a sphere 2.0" in diameter.

We get for the angular displacement as shown above

$$\theta = \theta_0 \exp \left[ - \frac{2\pi a^2 b^2 \eta l}{(b^2 - a^2) I} \cdot t \right]$$

The decrement for one oscillation is therefore

$$\lambda = \frac{2\pi a^2 b^2 \eta l}{(b^2 - a^2) I} \cdot \frac{T}{2} \quad \dots (13a)$$

where  $T$  is the periodic time.

The coefficient of viscosity is given from (13a) and (12) by the relation

$$\eta = \frac{2.3026}{\eta T K'} \log_{10} \frac{\alpha_1}{\alpha_{n+1}} \quad \dots (15)$$

where

$$K' = \frac{\pi a^2 b^2}{b^2 - a^2} \cdot \frac{l}{I}$$

The experimental set-up is the same as in the previous case; the sphere is replaced by the cylinder. The outer vessel, containing the liquid is also a cylinder with a perfectly flat bottom. The cylinder used here is a brass cylinder. In order to eliminate the effects of viscous forces on the ends of the suspending cylinder another cylinder of the same diameter as the suspending cylinder is placed right below and the length of the wire is so adjusted that the space between the two is less than 0.5mm. and the top end of the suspending cylinder is about 5mm. above the surface of the liquid. The outer cylinder is a glass cylinder so

as to enable one to measure the length of the cylinder immersed in the liquid and also to check the parallelism of the suspending cylinder and the guard cylinder.

The temperature of the liquid was kept constant at 30°C (which happens to be the room temperature during the experiment), with the help of the thermo-regulator. The procedure is the same as in the case of a sphere. The lengths are measured by a reading microscope reading up to 0.01 mm.

*Results :* The results, after using relation (5), are given in Table II.

TABLE II

Logarithmic decrement and viscosity of liquids with concentric cylinders  
(using a cylinder of diameter of 2.55 cms).

Sl. No.	Liquid	Length in cms.	Period 'T' in seconds	Logarithmic decrement	Coeff. of viscosity in centipoises	
					Expt. at 30°C.	Std. value at 30°C.
1.	Acetic Acid	2.20	25.30	3.608	1.039	1.040
2.	Carbon tetra chloride	2.25	25.40	2.945	0.826	0.848
3.	Benzene	2.30	25.40	2.052	0.563	0.561
4.	Ethyl Acetate	2.20	25.40	1.417	0.406	0.407
5.	Olive Oil*	2.62	9.00	35.0	49.60	52.00
6.	Mobil oil SAE 40*	2.48	9.20	71.4	208.0	212.1
7.	" " 30*	2.52	9.15	95.9	278.0	290.0

\*using cylinder of diameter of 3.82 cms.

TABLE III

Variation of log. decrement with depth of liquid between cylinders

Liquid	Spacing in mm	Length of cylinder immersed	log. decrement $\times 10^{-2}$	Viscosity in CP at 30°C.	Standard value at 30°C.
Acetic Acid	5.45	2.22	3.642	1.040	1.040
	4.18	2.20	3.635	1.047	
	2.40	2.20	3.630	1.045	
	1.14	2.23	3.628	1.045	
	0.48	2.20	3.625	1.043	
	0.35	2.20	3.624	1.043	
Carbon Tetra-Chloride	5.50	2.25	2.973	0.834	0.828
	4.22	2.26	2.969	0.833	
	2.50	2.25	2.964	0.831	
	1.10	2.24	2.963	0.831	
	0.50	2.22	2.960	0.830	
	0.34	2.25	2.960	0.830	
Benzene	5.30	2.28	2.070	0.568	0.561
	4.10	2.30	2.068	0.568	
	2.45	2.30	2.065	0.567	
	1.20	2.28	2.064	0.566	
	0.47	2.28	2.062	0.566	
	0.36	2.30	2.062	0.566	



In order to find the effect of the spacing the liquid below the inner cylinder and the bottom of the outer cylinder on the logarithmic decrement and consequently on the viscosity, a detailed study was made for some liquids for spacings between 5.5 mm. and 0.35 mm. The results are given below.

From the above table, it is easily seen that the change in viscosity is only in the third decimal place and the value of  $\eta$  is practically constant and reached the standard value when the spacing between the bottom of the cylinders is about 2mm.

### DISCUSSION

Above is described a method of measuring the viscosity of a liquid by measuring the logarithmic decrement of the rotational motion of a sphere or a cylinder immersed in a liquid. This method can be used for all liquids, viscous as well as mobile and is absolute. It is convenient for measuring the effect of temperature, as the apparatus is of small dimensions, unlike the previous types used for the purpose.

In order to get the sphere and cylinder to execute harmonic angular oscillation and to get a reasonable value for the logarithmic decrement, for very viscous liquid, the oscillating masses must be large. They must be made of steel or brass. For mobile liquids, aluminium can be used. It was shown experimentally that the energy taken up by the layers of liquid below the inner cylinder is negligible. Recently an estimate of this was given by Roscoe (1962). But it can be used only in the case of cylinder in uniform rotation.

### REFERENCES

- Choudhary, K. R. and Trivedi, G. K., 1961, *J. Sci. Indust. Res.* **20B**, 470.  
Christopherson, D. C., Gemart, A., Hogg, H. A. and South Well, R. M., 1938, *Proc. Roy. Soc.* **163A**, 351.  
Helmholtz, H. V. and Peotrowski, G. V., 1860, *Wien. Bar*, **50**, 107.  
Lamb A (1) 1916 *Hydrodynamics*, 575.  
Lamb A (2)                -do-                582.  
      (3)                -do-                580.  
Mennerotte, M., 1911, *J. Phys. Radium* **1**, 753.  
Meyer O. E., 1891, *Wied. Ann.* **43**.  
Searle G. F., Champton and Davy—*Properties of Matter* 251.  
Stokes G. G., Champion, F. C. and Davy, N. *Properties of Matter*, 253.  
Venkataraman, S., 1933, *Ind. Jour. Phys.* **8**, 26.

# VISCOSITY OF POLAR-NONPOLAR GAS MIXTURES EMPIRICAL METHOD

S. MATHUR AND S. C. SAXENA

PHYSICS DEPARTMENT, RAJASTHAN UNIVERSITY, JAIPUR

(Received November 24, 1964; Resubmitted March 4, 1965)

**ABSTRACT.** The adequacy of the familiar Sutherland expression for the viscosity of gas mixtures is tested successfully for binary mixtures involving one component as polar. The limited calculations of this paper also reveal that the co-efficients of the Sutherland expression may be treated as approximately temperature independent. This interesting result may find great use in predicting values at high temperatures where no direct measurements are available.

## INTRODUCTION

In spite of the fact that viscosity is the best theoretically understood transport property we still lack enough in our knowledge to be able to predict it with reliance for complicated systems such as polar gas mixtures. This is primarily because of the complicated nature of the interatomic forces of polar gas molecules, in general. Some calculations have recently been reported by Mason and Monchick (1962) for a somewhat over simplified potential model. This is about the best that has been achieved so far, unfortunately. Mathur and Saxena (1964a) have recently examined the Chapman-Enskog expression for the viscosity of a binary gas mixture,  $\eta_{mix}$ , in a fashion analogous to that of Gambhir and Saxena (1964) for nonpolar gas mixtures. This study revealed that most of the simple polar gases are amenable to treatment on the general theory of Chapman-Enskog except the collision cross-sections may require still more sophisticated angular averaging than given by Monchick and Mason (1961). This encouraged us to look into the procedures analogous to the approximate method of Wilke (1950) and semiempirical method of Saxena and Gambhir (1963a, 1963b). All these calculations, which are still to be published, indicated that the over-all accuracy of such calculations is the same as that obtained for nonpolar gases.

The purpose of this article is to look into the possibility of being able to correlate the experimental  $\eta_{mix}$  data on the basis of the following equation, Sutherland (1895) :

$$\eta_{mix} = \sum_{i=1}^n \frac{\eta_i}{1 + \sum_{\substack{j=1 \\ j \neq i}}^n \phi_{ij} \frac{X_j}{X_i}}, \quad \dots \quad (1)$$

where  $\eta_i$  and  $X_i$  are the coefficient of viscosity and mole fraction respectively of the pure component of molecular weight  $M_i$ , and  $\phi_{ij}$  is a constant which as shown by Mathur and Saxena (1964a) is a complicated function of  $T$  (temperature),  $M_i$ ,  $X_i$ , and collision integrals. They also showed that the dependence of  $\phi_{ij}$  on temperature and composition is feeble. Here we will treat  $\phi_{ij}$  as disposable parameters to be determined from the knowledge of  $\eta_{mix}$ . This endeavour holds a great promise in predicting the  $\eta_{mix}$  values at high temperatures, as well as values of multicomponent gas mixtures.

## CALCULATION OF VISCOSITIES

If the two pure viscosities and the mixture viscosity values be known at two compositions of a binary system,  $\phi_{12}$  and  $\phi_{21}$  can be evaluated directly on the basis of Eq. (1). If the form of Eq. (1) is correct then it should be possible to correlate

TABLE I

Comparison of the calculated and experimental  $\eta_{mix}$  values of  $H_2-NH_3$  system and some other pertinent data

Temp°.K	$\times_{polar}$	$10^7 \times \eta_{mix}(\text{gm/cm sec})$ Exptl.	Calc.	%dev.	$\phi_{12}$	$\phi_{21}$	$\eta_{NH_3} \times 10^7$ (gm/cm Sec.)	$\eta_{H_2} \times 10^7$ (gm/cm. Sec.)
293.16	0.9005	1004	1005	(+0.1)	0.307	1.659	(a, c, d) 982	(b) 881
	0.7087	1047	1047	(+0.0)				
	0.5177	1080	1080	(+0.0)				
	0.2975	1087	1087	(+0.0)				
	0.2239	1072	1072	(+0.0)				
	0.1082	1011	1012	(+0.1)				
373.16	0.9005	1299	1302	(+0.2)			1279	1035
	0.7087	1333	1341	(+0.6)				
	0.5177	1354	1367	(+1.0)				
	0.2975	1329	1349	(+1.5)				
	0.2239	1299	1320	(+1.6)				
	0.1082	1204	1224	(+1.7)				
473.16	0.9005	1660	1668	(+0.5)			1646	1217
	0.7087	1680	1703	(+1.4)				
	0.5177	1676	1718	(+2.5)				
	0.2975	1610	1669	(+3.7)				
	0.2239	1560	1620	(+3.8)				
	0.1082	1432	1479	(+3.3)				
523.16	0.9005	1825	1836	(+0.6)			1814	1303
	0.7087	1837	1869	(+1.7)				
	0.5177	1823	1879	(+3.1)				
	0.2975	1737	1817	(+4.6)				
	0.2239	1678	1760	(+4.9)				
523.16	0.9005	1825	1826(a)	(+0.1)	0.376	1.605	1814	1303
	0.7087	1837	1837	(+0.0)				
	0.5177	1823	1822	(-0.1)				
	0.2975	1737	1737	(+0.0)				
	0.2239	1678	1678	(+0.0)				

(a) Utilising  $\phi_{ij}$  calculated at this very temperature. a, b, c, and d stand for the same references as given in the foot-note of Table 2.

TABLE II

Comparison of the calculated and experimental  $\eta_{mix}$  values of  $N_2-NH_3$  system and some other pertinent data

Temp. °K	$\times polar$	$\eta_{mix} \times 10^7$ (gm./cm-sec)			$\varphi_{12}$	$\varphi_{21}$	$\eta_{N_2} \times 10^7$	$\eta_{NH_3} \times 10^7$
		Exptl.	Calc.	%dev			(gm/cm-sec)	(gm/cm-sec)
293.16	0.8883	1092	1093	(- 0.1)	0.954	0.839	1758	982
	0.7147	1254	1254	(+ 0.0)				
	0.5638	1383	1383	(+ 0.0)				
	0.2920	1885	1585	(+ 0.0)				
	0.1111	1690	1698	(+ 0.5)				
373.16	0.8883	1398	1407	(+ 0.6)			2145	1279
	0.7147	1569	1591	(+ 1.4)				
	0.5638	1710	1736	(+ 1.5)				
	0.2920	1920	1961	(+ 2.1)				
	0.1111	2031	2082	(+ 2.5)				
473.16	0.8883	1768	1787	(+ 1.1)			2560	1646
	0.7147	1946	1988	(+ 2.1)				
	0.5638	2085	2145	(+ 2.9)				
	0.2920	2296	2380	(+ 3.7)				
	0.1111	2408	2501	(+ 3.9)				
523.16	0.8883	1939	1960	(+ 1.1)			2740	1814
	0.7147	2112	2167	(+ 2.6)				
	0.5638	2250	2327	(+ 3.4)				
	0.2920	2460	2564	(+ 4.2)				
	0.1111	2572	2683	(+ 4.3)				
293.16	0.8883	1092	1090	(- 0.2)	0.533	2.401	1758	982
	0.7147	1254	1254	(+ 0.0)				
	0.5638	1383	1385	(+ 0.1)				
	0.2920	1585	1585	(+ 0.0)				
	0.1111	1690	1697	(+ 0.4)				
373.16	0.8883	1398	1392	(- 0.4)			2145	1279
	0.7147	1569	1572	(+ 0.2)				
	0.5638	1710	1718	(+ 0.5)				
	0.2920	1920	1946	(+ 1.4)				
	0.1111	2031	2074	(+ 2.1)				
473.16	0.8883	1768	1753	(- 0.8)			2560	1646
	0.7147	1946	1937	(- 0.5)				
	0.5638	2085	2092	(+ 0.3)				
	0.2920	2296	2340	(+ 1.9)				
	0.1111	2408	2482	(+ 3.1)				
523.16	0.8883	1939	1916	(- 1.2)			2740	1814
	0.7147	2112	2100	(- 0.6)				
	0.5638	2250	2257	(- 0.3)				
	0.2920	2460	2512	(+ 2.1)				
	0.1111	2572	2659	(+ 3.4)				

(a) Braune, H. and Linke, R., 1930, *Z. Phys. Chem.*, **A148**, 195.

(b) Hirschfelder, J. O., Bird, R. B., and Spotz, E. L., 1948, *J. Chem. Phys.*, **16**, 968.

(c) Trautz, M. and Heberling, R., 1931, *Ann. Physik.*, **10**, 155.

(d) Van Cleave, A. B. and Maass, O., 1935, *Canadian J. Res.*, **13**, 140.

the entire composition range in this way. As this approach has proved very successful for the binary combinations of nonpolar gases it will be interesting to see how far this procedure holds when polar gases are involved. To check this we consider the specific systems  $\text{H}_2\text{-NH}_3$  and  $\text{N}_2\text{-NH}_3$  for which elaborate data are available as a function of composition at various temperatures. It may be pointed out that the procedure for  $\phi_{ij}$  determination suggested above will, in general, lead to two sets of coupled  $\phi_{ij}$  values. In certain cases it may be possible to discard one in favour of the other but sometimes it may not be. In Table I, we list the calculated values for  $\text{H}_2\text{-NH}_3$  while in Table II for  $\text{N}_2\text{-NH}_3$ . Only one set of appropriate  $\phi_{ij}$  values were found in the case of  $\text{H}_2\text{-NH}_3$  system but in the case of  $\text{N}_2\text{-NH}_3$  system two sets were found. It may be possible to decide about their relative appropriateness by the degree of agreement between the calculated and experimental values. Thus, for the  $\text{N}_2\text{-NH}_3$  system the first set of  $\phi_{ij}$  values, reproduce the  $\eta_{\text{mix}}$  values within the average absolute deviation of 2.5%, while for the latter set this number drops to 1.3% only. However, the other relatively rigorous procedures of evaluating  $\phi_{ij}$  lead to values closer to the first set (Mathur and Saxena, 1964a, 1964b) and therefore this particular set should be preferred over the second set. A little enhanced discrepancy found in the values using this set when compared with the experimental values should not matter much for  $\phi_{ij}$  are also dependent on  $M_i$  and to some extent on the temperature, composition and nature of molecular interactions. The other set owes its origin to the fact that a large number of coupled  $\phi_{ij}$ 's are possible which will reproduce the data almost equally well (Gray and Wright, 1961). Here, of course, we are looking for such values of  $\phi_{ij}$ , which are independent of temperature, composition and nature of potential energy functions.

Cowling (1961) gave a simple but approximate interpretation of the physical significance of  $\phi_{ij}$ . According to him  $\phi_{ij}$  is the ratio of the efficiencies with which molecules  $j$  and molecules  $i$  separately impede the transport of momentum by molecules  $i$ . Thus, on this picture one should get only one set of  $\phi_{ij}$  values. The fact that we get here two sets is not necessarily a contradiction. The reason for this anomaly lies in the assumptions made in arriving at this simple definition for  $\phi_{ij}$ . As pointed out by Cowling (1961) Eq. (1) with this meaning for  $\phi_{ij}$  assumes the interaction between molecules of different gases purely as opposition to transport of momentum and neglects other interactions, for example, the one most important arises from the transfer of momentum transport from one gas to another at collisions. This has been discussed by Cowling, Gray and Wright (1963) and when this effect is also included much more complicated expressions result for  $\phi_{ij}$  and its simple definition is found to be no more valid. Therefore, the only criterion of choosing one set of  $\phi_{ij}$  values amongst many should be the concordance of their actual values with those obtained on the basis of rigorous theory (Mathur and Saxena, 1964a).

To investigate the adequacy of the temperature independent  $\phi_{ij}$  for purposes of prediction at high temperatures we also compute  $\eta_{mix}$  at high temperatures where direct measured values are available. The  $\phi_{ij}$  were always evaluated at the lowest temperature and it is interesting that the reproduction even at the highest temperature is not bad. A somewhat better correlation is possible if  $\phi_{ij}$  are calculated at the same temperature. Thus for  $H_2-NH_3$ , where calculations were repeated at  $T = 523.16^\circ K$ , it was found that the values get reproduced within the maximum deviation of 0.1%

#### CONCLUSIONS

As for nonpolar binary and higher order mixtures, the Sutherland form seems adequate to correlate the data even when polar gases are involved. Numerical calculations performed here for the two systems indicate that Sutherland's expression holds the promise of being extended to high temperatures with  $\phi_{ij}$  values determined at a lower temperature. By this analogy one may expect the generalised Sutherland formula to be adequate also for multicomponent mixtures involving polar gases though no checks could be made because of the lack of experimental data.

#### REFERENCES

- Cowling, T. G., Gray, P., and Wright, P. G., 1963, *Proc. Roy. Soc.* **A276**, 69.  
Gambhir, R. S., and Saxena, S. C., 1964, *Trans. Faraday Soc.*, **60**, 38.  
Gray, P., and Wright, P. G., 1961, *Proc. Roy. Soc.* **A263**, 161.  
Mason, E. A. and Monchick, L., 1962, *J. Chem. Phys.*, **36**, 2746.  
Mathur, S. and Saxena, S. C., 1964a, *Appl. Sci. Res. (Netherland)*, (In Press).  
Mathur, S. and Saxena, S. C., 1964b, *Brit. J. Appl. Phys.*, **16**, 389.  
Monchick, L., and Mason, E. A., 1961, *J. Chem. Phys.*, **35**, 1676.  
Saxena, S. C., and Gambhir, R. S., 1963a, *Proc. Phys. Soc.*, **81**, 788; 1963b *Indian J. Pure and Applied Phys.*, **1**, 208.  
Sutherland, W., 1895, *Phil. Mag.*, **40**, 421.  
Wilke, C. R., 1950, *J. Chem. Phys.*, **18**, 517.

# AN ANALYSIS OF THE $J$ -DISCONTINUITY IN SCATTERED X-RAYS—PART-III

HIRENDRA KUMAR PAL

DEPARTMENT OF PURE PHYSICS, CALCUTTA UNIVERSITY, CALCUTTA.

(Received May 31, 1965)

**ABSTRACT.** The paper discusses the cause of a discontinuity of the second kind which constitutes a significant feature of the  $J$ -phenomenon. It has been shown that the occurrence of this discontinuity and the associated characteristics may be accounted for in terms of an irregular fluctuation of the percentage modification during scattering. A possible interpretation has also been suggested for the 'levels' of X-ray activity postulated by Barkla.

## INTRODUCTION

In two previous papers, Parts I and II (Pal, 1964 and 1965) an attempt had been made to give an interpretation of the  $J$ -discontinuity of one kind and some aspects of the  $J$ -phenomenon, on the basis of established theory and simple acceptable assumptions. In the present paper, the other aspects, with particular reference to the  $J$ -discontinuity of a second kind are studied analytically. The experiments on the  $J$ -phenomenon with which the present analysis is concerned were performed in the following way : Keeping the penetrating power of the incident X-radiation constant the scattered beam in a particular direction  $\phi$  was compared either to the primary beam or to another scattered beam in a different direction  $\theta$ . For this purpose, the two beams compared were each passed through equal thickness  $x$  of any absorbing substance (generally  $Al$ ) and the corresponding ratio of ionisations  $(S'/P')_{90^\circ}$  or  $S'_\theta/S'_\phi$  due to the intercepted beams determined, as they were progressively filtered, and plotted against increasing thickness  $x$ . The experiments were conducted by Barkla in collaboration with Khastgir (1925 a, b) Watson (1926), Mackenzie (1926 a, b), Sen Gupta (1929), Kay (1933) and others including the writer (1935-37). Khastgir, Watson and Kay compared the scattered radiation at an angle  $90^\circ$  with the primary, whereas Mackenzie compared the two scattered beams at angles  $60^\circ$  and  $120^\circ$  respectively. When the graph  $(S'/P')_{90^\circ}$  or  $S'_{120^\circ}/S'_{60^\circ}$  plotted against  $x$ , was drawn, it was found, in general, to be *either*, a continuous curve with a descending course *or*, a graph (which might be horizontal i.e. parallel to the  $x$ -axis) showing one or more discontinuities (i.e. steps).

The discontinuities observed in the latter alternative were also termed  $J$ -discontinuities and they occurred seemingly at definite critical value of the mass-

---

\*Present Address, A-91, H. B. Town, P. O. Sodpur, 24 Parganas, W.B. India.

absorption coefficient  $(\mu/\rho)_{Al}$  of the transmitted radiation. Each discontinuity ( $J_1, J_2, J_3 \dots$ ), as postulated by Barkla, signified a transformation from one 'level' of X-ray activity to another, there being altogether several such (absorption) levels and such a transformation was called by him the  $J$ -transformation. It was not, however, possible to predict which of the two alternative types of graph mentioned above, one was going to get; for, strangely, the discontinuity occurred and did not occur under what appeared to be identical experimental conditions. For a comprehensive perusal, the reader is especially referred to the original papers by Barkla *et al.*

### THEORETICAL

#### A. The ratio $(S'/P')_{90^\circ}$ :

In the previous paper, Part II, (Pal, 1965) it was shown that

$$(S'/P')_{90^\circ} = K' \left[ 1 - 3C'_{90^\circ} \left\{ \frac{B}{2} x \lambda^3 \left( r_x + \frac{\delta\lambda_{90^\circ}}{\lambda} \right) + \left( \frac{\delta\lambda_{90^\circ}}{\lambda} - r_x \right) \right\} + (A - A')x \right] \dots (1)$$

where

$K'$  = a constant depending on the scattering material.

$C'_{90^\circ}$  = percentage modification of the scattered rays in the direction  $\phi = 90^\circ$ .

$A, B$  = constants depending on the absorbing element.

$A'$  = the modified value of  $A$  (for the scattered rays) depending on the geometry of the apparatus.

$\lambda$  = average incident wavelength.

$\delta\lambda_{90^\circ}$  = the Compton-change of wavelength for  $\phi = 90^\circ$ .

$x$  = thickness of the absorber.

and  $r_x$  = 'disparity' -term for  $\phi = 90^\circ$ .

Further, when the ratio  $(S'/P')_{90^\circ}$  is plotted against small values of  $x$ , for Al-absorber, the graph should (if  $C'_{90^\circ}$  is not zero) be a descending curve. Experimentally also, when the  $J$ -discontinuity was not in evidence, this was the type met with. In exceptional circumstances, however, as in the case of Ag- or Sn-absorber, the graph may sometimes be horizontal straight lines parallel to the  $x$ -axis.

#### B. The ratio $S'_{120^\circ}/S'_{60^\circ}$ :

In the previous paper referred to above (Pal, 1965), it was also shown that by neglecting absorption inside the scatterer, we can write

$$(S'/P')_\phi = K' f(\phi, \lambda) [\exp \{(A - A')x\}] \left[ 1 + C_\phi \int_\phi^{f_\phi} \delta\lambda_\phi \right. \\ \left. - \frac{3B}{2} x \lambda^3 \left\{ \frac{\Delta_\phi}{\lambda} + p_x + C_\phi \left( q_x - p_x + \frac{\delta\lambda_\phi}{\lambda} \right) \right\} + 3 \left\{ p_x + C_\phi \left( q_x - p_x - \frac{\delta\lambda_\phi}{\lambda} \right) \right\} \right] \dots (2)$$



where

$$f_{\varphi} = f(\phi, \lambda) = (1 + \cos^2 \phi) \{1 + \psi(\phi, \lambda)\}$$

and  $\{1 + \psi(\phi, \lambda)\}$  = a factor representing the enhancement of the scattered intensity due to interference.

$\Delta_{\varphi}$  = increase in the scattered wavelength in the direction  $\phi$ , due to interference  
 $p_x, q_x$  = the 'disparity'—terms corresponding respectively to interference and to the combination of the Compton effect and the interference effect at an angle  $\phi$ . The other terms are as previously explained.

If there is no interference at the scattering angle  $\theta$  then  $\psi(\theta, \lambda) = 0$ , and  $f(\theta, \lambda) = 1 + \cos^2 \theta$

Also 
$$f'_{\theta} = \frac{\partial f_{\theta}}{\partial \lambda} = 0, \quad \Delta_{\theta} = 0 \text{ and } p_x = 0.$$

so that from (2) we have

$$(S'/P')_{\theta} = K'f(\theta, \lambda) \exp\{(1 - A')x\} \left[ 1 - \frac{3B}{2} x \lambda^3 \left\{ C'_{\theta} \left( s_x - \frac{\delta \lambda_{\theta}}{\lambda} \right) \right\} - 3 \left\{ C'_{\theta} \left( s_x - \frac{\delta \lambda_{\theta}}{\lambda} \right) \right\} \right] \dots (3)$$

where  $s_x$  = the 'disparity'-term due to the Compton effect in the direction  $\theta$ .

Now putting  $\phi = 60^\circ$  and  $\theta = 120^\circ$ ,

we get,  $f(\phi, \lambda) = (1 + \cos^2 60^\circ) \{1 + \psi(60^\circ, \lambda)\} = 5 \{1 + \psi(60^\circ, \lambda)\}/4$

and  $f(\theta, \lambda) = (1 + \cos^2 120^\circ) = 5/4$

so that dividing (3) by (2) and substituting the values of  $f(\phi, \lambda)$  and  $f(\theta, \lambda)$  we get approximately

$$S'_{120^\circ}/S'_{60^\circ} = K'' \left[ 1 - C'_{\varphi} \frac{f'_{\varphi}}{f_{\varphi}} \delta \lambda_{\varphi} - \frac{3B}{2} x \lambda^3 M(x) + 3 \{M(x) - N\} \right] \dots (4)$$

where  $K'' = \{1 + \psi(60^\circ, \lambda)\}^{-1} = \text{Const. (independent of } x\text{)}.$

$$M(x) = \left\{ C'_{\theta} \left( s_x + \frac{\delta \lambda_{\theta}}{\lambda} \right) - \frac{\Delta_{\theta}}{\lambda} - p_x - C'_{\varphi} \left( q_x - p_x + \frac{\delta \lambda_{\varphi}}{\lambda} \right) \right\}$$

and  $N = 2C'_{\theta} \frac{\delta \lambda_{\theta}}{\lambda} - \frac{\Delta_{\varphi}}{\lambda} - 2C'_{\varphi} \frac{\delta \lambda_{\varphi}}{\lambda} = \text{const. (independent of } x\text{)}.$

When the ratio  $S'_{120^\circ}/S'_{60^\circ}$  is plotted against  $x$ , the course of the graph will be determined by  $x.M(x)$  and  $M(x)$ . In the case of a light scatterer like paraffin wax,  $p_x$  is small and  $M(x)$  is positive ( $\delta \lambda_{\theta} > \delta \lambda_{\varphi}$  and  $s_x > q_x$ ). Also,  $x \cdot M(x)$

increases initially and  $M(x)$  diminishes, as  $x$  increases. This means that the ratio falls initially with an increase in  $x$ . Hence in such a case a curve descending in the direction of increasing  $x$  is expected. This is corroborated by graph No. 13, p. 545 of the paper by Barkla and Mackenzie (1926a).

The unintercepted ratio may be deduced from equation (4) by putting  $x = 0$ . Thus

$$S_{120^\circ}/S_{60^\circ} = K'' \left[ 1 - C'_\varphi \int_\varphi^{f'_\varphi} \delta\lambda_\varphi + 3 \left\{ M(0) - N \right\} \right] \quad \dots (5)$$

where

$$M(0) = 2 \left( C'_\theta \frac{\delta\lambda_\theta}{\lambda} - \frac{\Delta_\theta}{\lambda} - C'_\varphi \frac{\delta\lambda_\varphi}{\lambda} \right) = \text{const.} \quad \dots (6)$$

In Barkla and Mackenzie's experiments, the course of the graphs depicting the discontinuities was, however generally straight and horizontal.

The conditions for the horizontal graph may be deduced as follows: For horizontality the ratio  $S''_{120}/S'_{60}$  should be independent of  $x$ . This requires that  $M(x)$  in equation (4) should be equal to zero

$$\text{i.e., } -\{C'_\theta s_x - p_x - C'_\varphi(q_x - p_x)\} = C'_\theta \frac{\delta\lambda_\theta}{\lambda} - \frac{\Delta_\theta}{\lambda} - C'_\varphi \frac{\delta\lambda_\varphi}{\lambda} = \alpha \text{ (const.)}$$

for all values of  $x$  concerned. Clearly this identity is fulfilled if the constant  $\alpha$  is equal to 0; i.e.,

$$C'_\theta \delta\lambda_\theta - \Delta_\theta - C'_\varphi \delta\lambda_\varphi = 0 \quad \dots (7)$$

and

$$C'_\theta s_x - p_x - C'_\varphi(q_x - p_x) = 0 \quad \dots (8)$$

for all values of  $x$  concerned.

The relations (7) and (8) provide the conditions necessary for a horizontal graph. It is, however, noted that (8) transforms into (7) when  $x = 0$ . Hence the general condition for the horizontality is contained in (8) which must be true for all values of  $x$  concerned, from zero upward.

From equations (6) and (7) the value of  $M(0)$  is found to be equal to 0 — (when the graph is horizontal).

Corollary 1. For large values of  $p_x$  the condition (8) reduces to

$$p_x \approx C'_\theta \cdot s_\theta$$

Corollary 2. When  $p_x$  is negligible, i.e. when interference is absent, the condition (8) cannot be satisfied and there can be no horizontal graph then.

Corollary 3. When  $x \geq x_c$  (corresponding to  $s_x$ ), the condition (8) is automatically satisfied; for, each term then is separately equal to zero; and (7) is the surviving condition which should be fulfilled.

Referring to equation (5), the constant ratio for the horizontal graph is obtained by substituting the value of  $M(0)$  and  $N$  in that equation. Thus

$$S'_{120^\circ}/S'_{60^\circ} = S_{120^\circ}/S_{60^\circ} = K'' \left[ 1 - C'_\varphi \frac{f'_\varphi}{f_\varphi} \delta\lambda_\varphi - 3 \frac{\Delta_\varphi}{\lambda} \right] \quad \dots (9)$$

$$\left. \begin{array}{l} \text{Now} \quad \delta\lambda_\varphi = \delta\lambda_{90^\circ} \text{ vers } 60^\circ = \delta\lambda_{90^\circ}/2 \\ \text{and} \quad \delta\lambda_\theta = \delta\lambda_{90^\circ} \text{ vers } 120^\circ = 3\delta\lambda_{90^\circ}/2 \end{array} \right\} \quad \dots (10)$$

Substituting these values of  $\delta\lambda_\varphi$  and  $\delta\lambda_\theta$  in eqn. (7)

$$\Delta_\varphi = (3C_\theta - C'_\varphi) \delta\lambda_{90^\circ}/2 \quad \dots (11)$$

From (9), (10) and (11) the constant ratio can also be written down as :

$$S'_{120^\circ}/S'_{60^\circ} = S_{120^\circ}/S_{60^\circ} = K'' \left[ 1 - \frac{3}{2} \left\{ 3C_\theta - C'_\varphi \left( 1 - \frac{\lambda f'_\varphi}{3f_\varphi} \right) \right\} \frac{\delta\lambda_{90^\circ}}{\lambda} \right] \dots (12)$$

For a light scatterer like paraffin for which interference in the direction  $\phi = 60^\circ$  is small and so also its rate of variation with  $\lambda$ , (vide Pal 1948) the term  $\lambda f'_\varphi/3f_\varphi \ll 1$ , so that the above ratio reduces to

$$K'' \left[ 1 - \frac{3}{2} \{ 3C_\theta - C'_\varphi \} \frac{\delta\lambda_{90^\circ}}{\lambda} \right]$$

### C. The discontinuity :

Equations (1) and (12) respectively show that the intercepted ratios  $(S'/P')_{90^\circ}$  and  $(S'_{120^\circ}/S'_{60^\circ})$  are each a function of  $C$  i.e. of the percentage modification of the scattered rays in the direction or directions concerned. Consequently any perturbation of this quantity is expected to affect the ratio. If  $C$  increases the ratio suffers a diminution.

A small change in  $C$ , of the order of a few per cent only is, however, not likely to upset appreciably the balance in equations (7) and (8), which happen to be the conditions for horizontality of the graph in (12); for, a variation in  $C$  is attended with a variation in  $\Delta_\varphi$  or  $p_x$  in the same sense.

A sudden small increase occurring in the  $C$ -value during experiment can only mean an abrupt discontinuity appearing in the graph concerned, at the proper place there being no change in the nature of the same, except that its subsequent course is bodily lowered down. Obviously, such an occurrence is detectable by its effect on absorption.

Yet the origin of this kind of discontinuity, according to the present view, is fundamentally in the material of the scatterer and not in the absorber, as may be supposed on the evidence furnished by the mass-absorption coefficients.

The discontinuities observed by Barkla with Khastgir, Mackenzie and others may be explained in the manner suggested above.

# EVIDENCES AND DISCUSSION GENERAL CONSIDERATIONS

From what has already been said it will appear that the discontinuity arising from a sudden variation of  $C$ , i.e., of the percent modification on scattering is essentially associated with the scattered radiation. One must therefore look to the scattered radiation alone for the realisation of this kind of discontinuity.

Let us now examine the soundness of the idea put forward. The percentage modification in Compton scattering is determined by the number of free electrons which recoil from the parent atom due to the impact of the incident photons. When high-energy quanta, generated at high exciting voltage are scattered, practically all the loosely bound electrons are ejected from the atom, with the result that modification is complete i.e., cent per cent. On the contrary, at low exciting voltages the energy of the colliding photon is wholly inadequate to release any electron from the atom, so that the scattered rays are unmodified. With medium exciting voltage, however, only a few of the electrons are emitted. This means a partial modification of the scattered rays. It is in this case, that under the action of continued impulses from the incident photons, a few more electrons than normally\* at the outset, may be expected to recoil from the scattering atom in a given time, particularly when it is a light one. In addition, the possibility may not be ruled out that some slight and appropriate changes of a casual nature, occurring in the microscopic structure of the primary radiation itself may also contribute to the same effect.\*\* In the circumstances, one may expect a slightly greater percentage modification than previously. It thus appears reasonable that such a process may occasionally be in actual operation, suddenly stepping up the modification by a few per cent. A reversion due to 'fatigue' may also be conceived.

This concept gets strong support from the experimental observation of Barkla and Kay (1933) that medium exciting voltages around 60KV(peak) were the most favourable for the occurrence of the  $J$ -discontinuity—a fact which was confirmed by the writer also (unpublished). It should be mentioned here, that the discontinuities in the experiments of Barkla and Watson (1926) were also obtained with 60KV. (peak), while those in Barkla and Mackenzie's (1926a) with about 40KV. (peak).

---

\*It may as well be that, owing to some kind of 'inertia' or lag, the normal number of electrons may not, at times be emitted till the atom has been irradiated for some time depending on the energy of the incident quanta.

\*\*Barkla and Mackenzie (1926b) found that a certain frequency of interruption of the induction coil used for generating high voltage applied to the X-ray tube was more favourable for the occurrence of the  $J$ -discontinuity than any other frequency of interruption, greater or less. The composition of the primary beam from the X-ray tube is determined to some extent by the rate of interruption of the induction. The rate of interruption may therefore create a condition favourable or otherwise for the discontinuity to occur.

The intermediate frequency of interruption of the induction coil which was found most favourable for the  $J$ -discontinuity of the second kind to appear, is also consistent with the observation that such discontinuities are usually obtained with medium exciting voltages.

(a) *Multiple discontinuities:*

Granting the possibility of a sudden change (increase) in the  $C$ -value under favourable circumstances, there is no reason why more than one such change should not be admissible in an unsteady state. Each change will correspond to a discontinuity. In this way, several discontinuities, named  $J_1, J_2, \dots$  have been actually observed in course of a single experiment. For example, Barkla and Watson reported as many as four discontinuities, whereas Barkla and Mackenzie obtained generally upto two. With more extensive filtration of the beams concerned, the number might increase to three.

(b) *Drop in the ratio:*

In the filtering experiments of Barkla and Mackenzie performed with aluminium and paraffin scatterers, (*vide* Barkla and Mackenzie, 1926a, Fig. 4, p. 547), the drop in the ratio at each discontinuity, was about 7.5% for aluminium and about 10% for paraffin. The greater drop for paraffin is very significant, being another evidence in support of the idea advanced. For, paraffin being lighter than aluminium, the probability of modification produced by the former should be greater than that produced by the latter; so also the probability of any fluctuation of the same\*. That the percentage modification diminishes with an increase in the (i) atomic number of the scattering element and (ii) incident wavelength, was experimentally verified by Backhurst (1934) at  $\phi = 150^\circ$  and also by others.

According to Barkla, the scattered beam in the direction,  $\theta = 120^\circ$ , was mainly responsible for the abrupt fall in the ratio at the discontinuity in the experiment of Barkla and Mackenzie (1926a). This would correspond to a variation in  $C_\theta$  causing the major portion of the fall. It should, indeed, be so, according to our analysis also. (*Vide* eqn. 12).

(c) *The shift of the discontinuity in progressive filtering experiments :*

Barkla and Mackenzie (1926a) and later Barkla and Kay (1933) found that the effect of softening the primary beam was to shift the discontinuity towards a higher value of  $x$ ; that is to say, for the discontinuity to be observed, filtering had to proceed a little further than previously. The reverse (i.e., a shift of the discontinuity towards a lower value of  $x$ )—was found when the primary beam was hardened. The shift to a higher value of  $x$  may be regarded as due to a longer exposure necessary for the softer radiation (at the lower voltage) to excite the scattering atom into that critical state at which a few extra or more electrons are ejected per unit time. This is because, a softer radiation means lesser average

\*For the same reason again, the probability of occurrence of a  $C$ -change should be greater for paraffin-scatterer than for aluminium. This was substantiated by the experiments of Barkla and Mackenzie and also of Barkla and Watson, where paraffin usually gave a greater number of discontinuities than aluminium. (*Vide* Barkla and Mackenzie, 1926 a, Fig. 3., p. 545).

energy for the incident quanta. The required longer exposure generally carries the experimenter through a greater distance from the origin in the graph. With a more penetrating radiation—say a filtered one—a shorter exposure is expected to bring about the necessary condition, resulting in an earlier occurrence of the discontinuity, if it occurs at all. The same remark holds good generally irrespective of the sequence in which the different exciting voltages are applied, provided they are of the right magnitude. (*Vide* Barkla and Kay, 1933, Fig. 6, p. 471).

(d) *Critical absorbability*

With regard to the critical absorbabilities, at which the  $J$ -discontinuities of the second kind were expected to appear, it may be said that the values obtained by different investigators and under different experimental conditions\* reveal a wide divergence amongst themselves, thereby detracting much from the 'critical' character of the quantity, which should have been, otherwise, well-defined. For instance, obtained with aluminium absorber,  $(\mu/\rho)$  for  $J_2$  varied from 1.8. (Barkla and Khastgir) to 2.2 (Barkla and Kay). Watson got figures higher still (2.35). This works out to a divergence from the mean value, of about 10% or even more.  $(\mu/\rho)_{Al}$  for  $J_1$  had been observed to range from *mean* 3.6 (Barkla and Mackenzie) to 3.8 (Barkla and Khastgir), which means a divergence of about 6%. The divergence for  $J_3$  is also of the same order. These divergences certainly far exceed the limits of accuracy—usually about  $\pm 2\%$  (Barkla and Mackenzie, 1926a) claimed for the absorption coefficient in this type of experiments. Furthermore, as many as eight discontinuities have to be accommodated within a span extending from  $(\mu/\rho)_{Al} = .34$  to  $(\mu/\rho)_{Al} = 3.8$ , the corresponding wavelengths being  $0.23 \text{ \AA.U.}$  and  $0.63 \text{ \AA.U.}$  respectively. The so-called 'critical' mass-absorption coefficients are, therefore, deprived of a considerable portion of the weights attached to them. According to the present view, on the contrary, the above discontinuities are the outcome of random fluctuations in the electron-emission from the scattering atom—fluctuations which apparently know no law except the law of chance. The proximity to certain values of  $(\mu/\rho)_{Al}$  (in the region of medium wavelength) however, is more conducive to the initiation of the process suggested.

The discontinuity  $J_3$  in the light of this analysis, also belongs to a different category and was discussed elsewhere, (Pal, 1964).

The chance character of the discontinuity is more convincingly brought out by the appearance of new discontinuities between the so-called  $J_1$  and  $J_2$  and between  $J_2$  and  $J_3$  in the experiments of Barkla and Watson (1926).

(e) *Occurrence and non-occurrence of a discontinuity:*

A very interesting and yet puzzling aspect of the  $J$ -phenomenon had been brought to light by experiments of Barkla and Kay (1933). They took two scatterers  $A$  and  $B$ , made of the same material (filter paper or paraffin wax) and alike

\*Large variations with variations in the tube current were recorded by Watson (1926),

in dimensions. *A* was an old scatterer which was in use for a long time past and *B*, a newly-made one, previously unexposed to radiations. The two specimens *A* and *B* were then irradiated and observations made, as usual, sometimes alternately on the same day. Specimen *B* of filter paper and *A* of paraffin wax consistently exhibited the discontinuity day after day, while no discontinuity was observed with the other specimen of the same material. This state of affairs persisted for quite a long time, till the scatterer hitherto giving the discontinuity all right, also ceased to give it any longer. With a view to make the test as stringent as possible, the experiment was repeated by placing the two specimens *A* and *B* of paraffin wax in the same position alternately, corresponding to each absorbing thickness of the series. But this made no difference in the nature of the result previously observed.

Obviously, a behaviour of this kind cannot be reconciled with any probable variation in the radiation alone. The unescapable presumption therefore, is that so far as the occurrence of the discontinuity is concerned, it is intimately linked up with the scattering process and yet the chemical composition of the scatterer is not the only deciding factor. Something more is needed. It may be some particular 'state' of or in the scatterer as suggested by Barkla; the state itself being dependent on or dominated by the whole associated history.

The evidence cited, does not upset the hypothesis of extra electron-emission, if it is conceded that two scatterers though chemically and in all external appearances identical, may yet differ substantially in their reaction towards X-ray stimuli; though in what way exactly, it is not possible to say. The necessary responsiveness was actually present, in the beginning, in one specimen but never in the other. This responsive feature again was not of a permanent character, in as much as it disappeared after some time. Neither could the irresponsive scatterer, though in use all the while, be thrown into the hypersensitive state in which a few more electrons could recoil per unit time, even under continued exposure. It thus appears that neither previous over-exposure nor absolute non-exposure is decisive. The precise nature of the influence that helps or prevents the necessary peculiar disposition of the scatterer is yet unknown.

(f) *The C-levels:*

When the percentage of modification i.e. *C* has undergone a change, it may or may not settle down to its new value. There may be further sudden and localized changes including even a reversion to the old value. The experiments of Barkla and Watson and also of Barkla and Mackenzie bear testimony to the former kind of behaviour and our experience with a Müller tube (hot-cathode, water-cooled) to the latter. Instances are also on record, depicting how the plots

on the graph, systematically choose between two (or amongst three) distinct levels indicating preferred values for  $C$ . In this connection, we can refer to our Fig. 1

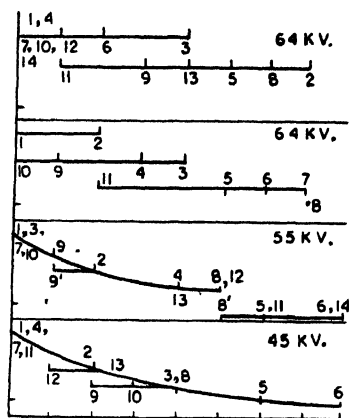


Fig. 1. Illustrating the fluctuation of percentage modification of the scattered X-rays in the unsteady state.

and to the results of Barkla and Khastgir (1925) (*Vide* Figs. 2, 3 and 4, pp. 1119-1123) where the stratified graphs illustrate how  $C$  changed by jumps between well-defined levels at the same wavelength. In this context, some truth may be sensed in the postulate of 'levels' of X-ray activity with which Barkla associated the  $J$ -phenomenon. The  $J$ -levels may be identified with the  $C$ -levels, in view of the fact that an increase in  $C$  is attended with a greater absorption of the scattered rays.

#### (g) *Superposition of X-rays:*

Barkla and Mackenzie (1926a) and later Barkla and Sen Gupta (1929) performed experiments with one beam of X-rays superposed on another by which they sought to establish that the  $J$ -absorption and all the associated phenomena depended on the whole of a complex beam and not on individual harmonic constituents of the radiation considered separately. This view, however, was not established. We shall outline here the experiments of Mackenzie and of Sen Gupta with Barkla and the results obtained by them. We shall also give an explanation which seems satisfactory and consistent.

#### (i) *Experiments of Barkla and Mackenzie on progressive filtering of the two beams.*

The position of the  $J$ -discontinuity was at first found with a thin sheet of aluminium acting as a scatterer. On interposing a second thicker sheet of the same material behind and in contact with the first, so that the rays scattered by it, were superposed on those scattered by the first scatterer, it was found that the discontinuity was displaced to the left, i.e. toward a lower value of the thickness  $x$  of the filter.



The result of these experiments can be explained as follows : After the second sheet had been interposed, the incident radiation being filtered through deeper layers, of the scatterer became, on the average, more penetrating than previously and hence the incident quanta became more energetic. The discontinuity if it appears, should therefore, appear earlier.

(ii) Experiments of Barkla and Sen Gupta.

Two scattering slabs of paraffin wax —  $R_1$  and  $R_2$  — were placed in parallel positions separated by a distance in the path of the primary rays. The scattered radiation from  $R_2$  could be superposed whenever desired, on that from  $R_1$ , upon and inside the absorbing sheets  $A_2$  only. In the experimental set-up, it could be so arranged that the primary rays were received by (i)  $R_2$  first and (ii)  $R_1$  first. (*Vide* Barkla and Sen Gupta, 1929, Figs. 1 and 2).

On superposition it was observed that the discontinuity was displaced to the right in case (i) and to the left in case (ii).

The superposed scattered radiation from  $R_2$ , in each case, evidently could not directly affect the ionization inside the ionization chamber due to the radiation scattered from  $R_1$  except through a tertiary contribution due to scattering by  $A_2$ . This tertiary contribution must necessarily have been of a negligible magnitude. This fact was borne out by the plots on the graph being actually identical with the superposed beam 'on' or 'off', except near the discontinuity. In the circumstances, it is not quite clear why there should be an exception with regard to the discontinuity itself, if it had fundamentally originated in an absorption process.

We are, however, inclined to the view that, as in Barkla and Mackenzie's experiments, here also, the observed fact was not a superposition effect. It is suggested that in the experiments of Barkla and Sen Gupta, the position of the discontinuity and also the number of such discontinuities were determined solely by chance. The appearance of a second discontinuity to the right of the original one, besides the one to the left (*Vide* Barkla and Sen Gupta, 1929, Fig. 3, graph 2) suggests a random character of the phenomenon.

(h) *The unsteady state*

A casual variation in  $C$ , as described above, should always be recognized as an unsteady state of affairs departing from the ideal. A steady  $C$  yields a continuous curve, whereas abrupt deviations in its value give rise to the well-known steps or discontinuities, whatever the degree of heterogeneity of the rays concerned.

In further support of what has been stated in connection with abrupt fluctuation of  $C$ , a few illustrative samples of graphs, obtained by the present writer (with Al\* as the absorbing substance) are furnished in Figure 1. They speak for themselves. The numbers assigned to the plots show the sequence in which observations were made. It should be pointed out here, that any change in  $C$

---

\*The purity of Al. used was not chemically tested.

should not theoretically affect the unintercepted ratio, i.e.  $(S'/P')_{90^\circ}$  corresponding to  $x = 0$ , as will be evident from Eqn. (1). In practice, however, even when  $x = 0$  the rays have yet to pass through one foil of Al ( $x = 0.1$  mm) which covers the window of the ionization chambers. A zero thickness in the graph is really a thickness of 0.1 mm. Other thicknesses are to be amended accordingly.

#### SUMMARY AND CONCLUSION

The ratio of ionizations,  $S'_{120^\circ}/S'_{60^\circ}$ , as a function of the thickness  $x$  of the absorbing substance placed in each beam, has been theoretically obtained and the condition of horizontality of the graph showing  $S'_{120^\circ}/S'_{60^\circ}$  against  $x$  has been deduced. The experimental results showing the graph to have a downward slope in the direction of increasing thickness or to be a horizontal straight line parallel to the  $x$ -axis, have thus been explained. The discontinuity observed by Barkla and Mackenzie (1926a) in this graph or in the  $(S'/P')_{90^\circ} - x$  graph of Barkla and Khastgir (1925a) has been ascribed to an abrupt increase in the percentage modification associated with the Compton scattering\*. The sudden variation of the proportion of the modified rays has been attributed to a casual excess electron-recoil from the scattering atom. Such a discontinuity is, therefore, of a second kind, as distinguished from that of the first kind discussed in a previous paper (Part I, Pal, 1964). It may be recalled that the discontinuity of the first kind was shown to be linked with what was called the 'D-point' which was governed by the character of the heterogeneous radiation concerned and the nature of the absorbing substance.\*\*

The concept of excess electron-recoil successfully explains (i) the necessity of medium voltage of excitation of X-rays for the occurrence of the discontinuity of the second kind, (ii) the occurrence of multiple discontinuities, (iii) the greater drop in the ratio,  $S'_{120^\circ}/S'_{60^\circ}$  or  $(S'/P')_{90^\circ}$ , and a greater number of such discontinuities in a lighter substance (paraffin) than for a relatively heavier substance (aluminium) used as scatterer and (iv) the shift of the discontinuity towards a higher or a lower value of  $x$ , according as the beam is less or more penetrating.

As the values obtained experimentally for the critical absorability at which a  $J$ -discontinuity of the second kind was expected to occur, showed a wide range, the critical character of the mass-absorption coefficient loses its significance and it is believed that the position of such a discontinuity is only a matter of chance.

\*If there is truth in this concept, it seems probable that in suitable circumstances, the associated discontinuity should also appear with monochromatic X-rays.

\*\*The discontinuity of the first kind may be obtained with scattered radiations also. An abrupt change in the  $C$ -value, depending on the casual excess electron-recoil during the scattering process and causing a discontinuity of the second kind may have an indirect influence on the 'D-point'. This complication may perhaps account for the capricious appearance and disappearance of the  $J$ -discontinuity (first kind) in the case of scattered radiations under apparently identical experimental Conditions—(Vide Pal, 1964, p. 76).

The puzzling experimental results of Barkla and Kay (1933) regarding the occurrence and non-occurrence of a discontinuity of the second kind, obtained with an old and a newly-made scatterer seem to suggest that the chemical composition of the scatterer is not the only deciding factor: a condition of matter determined by its previous history and also the composition and character of the radiation depending to some extent on the frequency of interruption of the induction coil appear to play an important role.

The *J*-absorption 'level' postulated in this connection by Barkla receive in a restricted sense a possible interpretation in the concept of the fluctuation of the electron-emission from the scattering atom. Also the element of uncertainty involved in the process explains the dubious character of the *J*-discontinuity of the second kind.

The effect of superposition of two beams of X-rays as observed by Barkla and Mackenzie (1926a) and also by Barkla and Sen Gupta (1929) has also been discussed and interpreted.

#### ACKNOWLEDGMENT

The author wishes to acknowledge his indebtedness to late Prof. C. G. Barkla, F.R.S., N.L., for affording him all facilities for experimental research in his laboratory at Edinburgh University and for giving him helpful guidance during the period 1935-37. His best thanks are also due to Prof. S. R. Khastgir, D.Sc., F.N.I., Head of the Dept. of Physics, Bose Institute, Calcutta, for valuable discussions.

#### REFERENCES

- Backhurst, I., 1934, *Phil. Mag.* **XVII**, 321.
- Barkla, C. G., 1918, *Phil. Trans. Roy. Soc., A*, **CCXVII**, 315.
- 1924, *Nature*, **CXIV**, 753.
- 1925, *Phil. Mag.*, **XLIX**, 1033.
- 1926, *Nature*, **CXVII**, 448.
- 1927, *Nature*, **CXIX**, 778.
- 1928, *Phil. Mag.* **V**, 1164.
- 1929, *International Critical Tables*, **VI**, 1.
- 1931, *Nature*, **CXXVII**, 877.
- 1933, *Nature*, **CXXXI**, 166.
- Barkla, C. G., and Kay, J. S., 1933, *Phil. Mag. (Suppl. Aug.)* **XVII**, 457.
- Barkla, C. G., and Khastgir, S. R., 1925a, *Phil. Mag.* **XLIX**, 251.
- 1925b, *Phil. Mag.* **I**, 1115.
- 1926, *Nature*, **CXVII**, 228.
- 1926, *Phil. Mag.*, **II**, 642.
- 1927, *Phil. Mag.* **IV**, 735.
- Barkla, C. G., and Mackenzie, G. I., 1925, *Nature*, **CXV**, 942.
- 1926a, *Phil. Mag.* **I**, 542.
- 1926b, *Phil. Mag.* **II**, 1116.

- Barkla, C. G., and Sen Gupta, M. M., 1929, *Phil. Mag.* **VII**, 737.  
Barkla, C. G., and Watson, W. H., 1926, *Phil. Mag.* **II**, 1122.  
Khastgir, S. R., and Watson, W. H., 1925, *Nature*, **CXV**, 604.  
——— 1925, *Nature*, **CXVI**, 47.  
Khastgir, S. R., 1932, *Phil. Mag.* **XIV**, 99.  
Pal, H. K., 1948, *Ind. Jour. Phys.* **22**, 291.  
——— 1949, *Ind. Jour. Phys.* **23**, 111.  
——— 1964, *Ind. Jour. Phys.* **38**, 61.  
——— 1965, *Ind. Jour. Phys.* **39**, 108.  
Watson, W. H., 1925, *Proc. Roy. Soc. (Edinburgh)* **XIV**, 48.  
——— 1928, *Phil. Mag.* **V**, 1146.

# Letters to the Editor

*The Board of Editors does not hold itself responsible for opinions expressed in the letters published in this section. The notes containing short reports of original investigations communicated to this section should not contain many figures and should not exceed 500 words in length. The contributions reaching the Secretary by the 15th of any month may be expected to appear in the issue for the next month. No proof will be sent to the author.*

11

## EFFECT OF RESONANCE ON NEUTRON SCATTERING BY CARBON

PARESH KUMAR BISWAS

DEPARTMENT OF THEORETICAL PHYSICS,

INDIAN ASSOCIATION FOR THE CULTIVATION OF SCIENCE,  
JADAVPUR, CALCUTTA-32.

(Received March 31, 1965)

Recently Ganguly and Sil (1963) have obtained the elastic scattering cross-section of neutrons by  $C^{12}$  at 4.1 and 2.7 Mev energy (laboratory system) by calculating the phases by the Brysk (1962) method with a complex potential of Woods-Saxon (1954) form. As the agreement of theoretical results with experimental values was not good, we have recalculated the same problem taking into account the resonance level of the  $C^{13}$  nucleus at 3.38 Mev (centre of mass system) which has the width  $\Gamma = 1$  Mev (Landolt-Börnstein, 1961), we have neglected other resonances as their widths are much less compared with the above. As the level ascribed to it is  $D_{3/2}$  the phase shift corresponding to this level will be, according to Breit-Wigner formula, changed to

$$\delta_{3/2,2} = \delta_{3/2,2}^0 + \tan^{-1}[\Gamma/2(E_R - E)]$$

where  $\delta_{3/2,2}^0$  is the ordinary phase shift without the resonance effect.  $E_R$  and  $E$  are respectively the energies of the resonance level and the incident particle expressed in C.M. system.  $E$  in C.M. system will be 3.77 and 2.48 Mev corresponding to energies 4.1 and 2.7 Mev in the Laboratory system.

The phases of Ganguly and Sil (1963) did not depend on spin, as such they were labelled as  $\delta_0$ ,  $\delta_1$  and  $\delta_2$ . Now in view of the fact that the resonance level depends on the spin value, we rewrite the previous phases as  $\delta_0 \rightarrow \delta_{1/2,0}$ ,

$\delta_1 \rightarrow \delta_{1/2,1}^0 = \delta_{3/2,1}^0$  and  $\delta_2 \rightarrow \delta_{5/2,2}^0 = \delta_{3/2,2}^0$ . Because of the resonance, only the phase  $\delta_{3/2,2}$  gets changed as follow :

Energy $E$	$\tan \delta_{3/2,2}^0$	$\tan \delta_{3/2,2}$
3.77	$-0.1092 + 0.0036 i$	$-1.6223 + .0129 i$
2.48	$-0.0340 + 0.0012 i$	$+0.5126 + .0016 i$

Neglecting contribution from partial waves with  $l > 2$  we may write the expression for the scattering cross-section (vide Wu and Ohmura, 1962) as

$$\sigma(\theta) = K^{-2} |A_0 + 3A_1 \cos \theta + (3A_2 + 2A'_2)P_2(\cos \theta)|^2 + K^{-2} |A_2 - A'_2|^2 \cdot 9 \sin^2 \theta \times \cos^2 \theta,$$

where  $A_l = \frac{\tan \delta_l}{1 - i \tan \delta_l}$ ,  $l = 0, 1$  and  $2$ ;  $A'_2 = \frac{\tan \delta_{3/2,2}}{1 - i \tan \delta_{3/2,2}}$ .

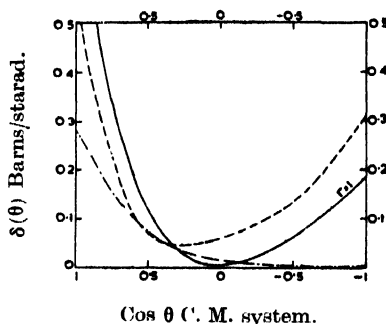


Fig. 1. Elastic scattering of 4.1 Mev neutrons by  $C^{12}$ . The solid curve represents the theoretical results due to the inclusion of the effect of the resonance level; the dash-dot-dash curve is the theoretical findings of Ganguly and Sil and the dashed curve is the experimental results of Walt and Beyster.

The results as obtained are compared with experimental values (Walt and Beyster, 1955; Little *et al.*, 1955) in Figs. 1 and 2. The agreement for the case of

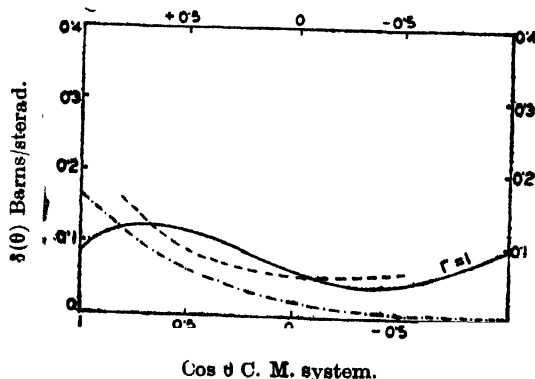


Fig. 2. Elastic scattering of 2.7 Mev neutrons by  $C^{12}$ . The notations are the same as those of Figure 1. Experimental results are due to Little *et al.*,

3.77 Mev is good but for 2.48 Mev it is not so particularly at small angles of scattering.

The author is thankful to Professor D. Basu, Ph.D., for his keen interest in the work and to Dr. N. C. Sil for his guidance throughout this work.

## REFERENCES

Brysk, H., 1962, *Phys. Rev.*, **126**, 1589.

Ganguly, C. and Sil, N. C., 1963, *Ind. Jour. Phys.*, **37**, 389.

Landolt-Börnstein, 1961, New Series 1/1, Energy levels in Nuclei, Pp. 1-39, Springer-verlag.

Little, Leonard, Pruddhomme and Vincent, 1955, *Phys. Rev.*, **98**, 634.

Walt, M. and Beyster, J. R., 1955, *Phys. Rev.*, **98**, 677.

Woods, R. D. and Saxon, D. S., 1954, *Phys. Rev.*, **95**, 577.

Wu, Ta-You, and Ohmura, Takashi, 1962, Quantum Theory of Scattering, Section J, Printice-Hall.

# QUANTITATIVE ESTIMATION OF MISALIGNMENT OF THE LAYERS IN NATURAL CRYSTALS OF GRAPHITE

S. RAY and R. BHATTACHARYA

DEPARTMENT OF MAGNETISM,  
INDIAN ASSOCIATION FOR THE CULTIVATION OF SCIENCE,  
JADAVPUR, CALCUTTA 32.

(Received March 29, 1965)

It has been shown from X-ray observations (Ray, 1959) that the misalignments between the different crystal blocks, inevitably present in natural crystals of graphite, are further enhanced by the purificatory treatments usually undertaken before the actual measurements of any of their electronic properties. It has also been shown that such enhancement of the misalignments produces appreciable change in these properties (Bhattacharya, 1959). Hence none of the existing measurements of such properties, which have all been made with purified natural crystals, represent the true values for perfect single crystals of graphite, and are suitable for discussion in relation to any of the proposed theories.

The correct values of the electronic properties for perfect crystals can only be obtained, if some quantitative estimation of the nature of the misalignments of the crystals is made. To determine the amount of misalignment, a distribution function  $I(\phi)$  is defined, such that the number of normals to basal planes inclined at angle between  $\phi$  and  $\phi + d\phi$  to the  $c$ -axis of the crystal in  $2\pi I(\phi) \sin \phi d\phi$ .

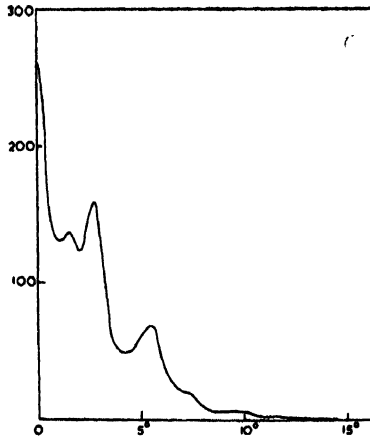


Fig. Variation of  $I(\phi)$  with  $\phi$

In a rotation photograph of a natural crystal of graphite rotating about the  $a$ -axis, the 0002 and 0004 spots are found to be elongated into almost Debye-



Scherrer lines (Ray, 1959). The other spots however, are not affected in this manner, showing thereby that the particular nature of the basal spots is due solely to the misalignment of the basal planes of the different blocks in the crystal. The intensity occurring at any point on the 'tail' of a basal reflection is due to the planes misaligned at a particular angle  $\phi$  with respect to the axis of rotation. If now a zero-layer Weissenberg photograph is obtained, the basal spots are elongated along the  $\omega$ -direction and the intensity at each value of  $\omega$  (which is simply related to  $\phi$ ) is proportional to the number of misaligned planes whose normals are at angle  $\phi$  with the  $c$ -axis of the crystal, that is, proportional to  $I(\phi)$ . From a multiple film exposure, distribution of intensity along the  $\omega$ -direction of the spots can be obtained, which evidently gives a plot of  $I(\phi)$  against  $\phi$  (Fig.).

Different electronic properties of a perfect crystal of graphite have been calculated utilising this method of estimation of the misalignments and the results are going to be published soon.

The authors express their best thanks to Shri A. K. Dutta for suggesting the problem and to Prof. A. Bose for his interest in the work. Thanks are also due to Dr. R. K. Sen for some valuable discussions.

## REFERENCES

- Bhattacharya R. 1959, *Ind. Jour. Phys.* **33**, 407.  
Ray S. 1959, *Ind. Jour. Phys.* **33**, 282.

## ROLE OF RELAXATION IN AN ADIABATIC CHANGE

M. P. SAKSENA AND S. C. SAXENA

PHYSICS DEPARTMENT, RAJASTHAN UNIVERSITY, JAIPUR, INDIA

(Received June 9, 1964; Resubmitted September 19, 1964)

Whenever rapid changes of energy occur in polyatomic gases, the phenomenon of relaxation is called into play. This is because the internal degrees of freedom do not readily acquire the temperature of the external degrees of freedom but take an appreciable time, the relaxation time. The purpose of this note is to examine the possibility of using an adiabatic compression (or expansion) of a gas for the study of relaxation.

Consider a polyatomic gas suddenly compressed adiabatically. It is reasonable to assume that the external degrees of freedom will attain equilibrium almost instantaneously with the external conditions thereby increasing the temperature. By external degrees we mean here the translational and all such degrees which instantaneously acquire equilibrium with the external conditions. On the other hand the internal degrees exhibit a lag and it is only through some slow process that energy flows from external to internal degrees and equilibrium is attained. In this process the temperature of the external degrees falls while those of internal rises.

Let us also assume that the adiabatic change is quite fast and its duration is much smaller than the relaxation time of the gas. Under such conditions the total specific heat of the gas,  $C_p$ , is not effective and the energy transfer fails to follow the quick adiabatic change. We denote the contributions of the external degrees of freedom to the total specific heat of the gas by  $C_e$  and  $C_i$ , respectively. We have therefore

$$C_p = C_e + C_i \quad (1)$$

Let  $T_0$  and  $V_0$  be the initial temperature and volume of the gas respectively, and after the adiabatic compression the temperature rises to  $T_1$  while the volume reduces to  $V_1$ . We also presume that this adiabatic change is so fast that only the external degrees participate and the internal degrees remain unexcited. However, as the time passes the exchange of energy occurs between the external and internal modes and finally they get into equilibrium and at this stage let  $T_2$  be the temperature of the gas. Applying the law of conservation of energy we get

$$C_e(T_1 - T_2) = C_i(T_2 - T_0). \quad (2)$$

Further, for the adiabatic change

$$T_0 V_0^{\gamma-1} = T_1 V_1^{\gamma-1}. \quad \dots (3)$$

Here,  $\gamma$  is the ratio of the two specific heats of the gas with the internal degrees of freedom frozen and we take  $\gamma$  to be constant in the small temperature range,  $(T_1 - T_0)$ . In writing equation (3) it is assumed that the equation of state depends only on the temperature  $T_1$ . This, however, seems reasonable in view of the success of a similar assumption in the study of the dispersion and absorption of ultrasonic waves. (Herzfeld, 1955). Eliminating  $T_1$  from equations (2) and (3) we get,

$$C_i = C_v \left[ 1 + \frac{(T_2 - T_0) V_2^{-\gamma}}{(T_0 V_0^{\gamma-1} - T_1 V_1^{\gamma-1})} \right]. \quad (4)$$

Thus, the knowledge of the initial temperature and volume of the gas and their values after the adiabatic change, will enable to estimate  $C_i$ , and therefore the extent of participation of the internal modes at that temperature.

In the above treatment we have assumed the gas to be perfect which, however, is not true and therefore we replace the perfect gas equation by the following equation of state :

$$PV = RT[1 + B(T)/V]. \quad \dots (5)$$

Here,  $P$ ,  $V$  and  $T$  represent the pressure, volume and temperature of the gas, respectively,  $R$  is the gas constant and  $B(T)$  the second virial coefficient of the gas at the temperature  $T$ . Consideration of equation (5) modifies equation (3) to

$$T_0 V_0^{\gamma-1} [1 + B(T_0)/V_0]^{\gamma-1} = T_1 V_1^{\gamma-1} [1 + B(T_1)/V_1] \quad (6)$$

Combining equations (2) and (6) and eliminating  $T_1$  we get

$$C_i = C_v \left[ 1 + \frac{(T_2 - T_0) V_0^{\gamma-1} [1 + B(T_0)/V_0]^{\gamma-1}}{T_0 V_0^{\gamma-1} [1 + B(T_0)/V_0]^{\gamma-1} - V_1^{\gamma-1} [1 + B(T_0)/V_0]^{\gamma-1}} \right]$$

instead of equation (4).

The slow energy exchange between the external and internal degrees of freedom is characterised by the relaxation time,  $\tau$ . It is possible to derive an expression for  $\tau$  adopting a treatment similar to that of Herzfeld (1955). However, unlike Herzfeld we prefer to express  $\tau$  in terms of the temperature of the external degrees of freedom since it is directly measurable. The final result is :

$$T(t) = T_2 + \frac{C_i}{C_v - C_i} (T_2 - T_0) e^{-\frac{C_v}{C_i} \frac{t}{\tau}} \quad (8)$$

In equation (8)  $T(t)$  is the temperature of the external modes at a certain time  $t$ , and if its values be determined as a function of  $t$ ,  $\tau$  can be evaluated directly.

The application of equation (8) is in general handicapped because of the short relaxation times, which range between  $10^{-3}$  to  $10^{-9}$  sec. or so. A practical though indirect way to use it, is to study the changes in volumes corresponding

to the changes in temperatures at a constant pressure as a function of time. Such an experiment can be conducted making use of an apparatus technically called as ERMA (expansion rate measuring apparatus). This essentially consists of a hollow cylinder closed at one end, with a light piston. Through the wall of the barrel a number of electrical contacts are located whose position can be accurately determined. As the piston moves it shorts the electrical contacts one after the other and generates electrical signals. It had been possible to measure the position of the piston at intervals of a few microseconds with such an arrangement. (Siegel, 1952).

Another example where the theory developed here will find application is the study of the state of a gas in a weak shock wave. When a weak shock wave from an explosion or shock tube has passed a certain distance in a gas, the gas adiabatically to return to the original pressure. For such an expansion equation (4) will get modified to

$$C_i = C_r \left[ 1 - \frac{(T_0 - T_2)V_1^{\gamma-1}}{T_0(V_1^{\gamma-1} - V_0^{\gamma-1})} \right], \quad \dots (9)$$

or in an alternative form in terms of the pressure as

$$C_i = C_r \left[ 1 - \frac{(T_0 - T_2)}{T_0 \left\{ 1 - \left( \frac{p_1}{p_0} \right)^{\frac{\gamma-1}{\gamma}} \right\}} \right]. \quad \dots (10)$$

Here  $T_0$ ,  $V_0$  and  $p_0$  represent the temperature, volume and the pressure of the gas in the presence of the shock wave and  $T_2$ ,  $V_1$  and  $p_1$  the corresponding quantities after the adiabatic expansion had subsided.

The various quantities involved in the above equations are measurable. Such an experiment apart from being of practical value in the determination of  $C_i$ , will also be of great theoretical importance in verifying the assumption viz., the equation of state depends only on the temperature of the external degrees of freedom. This assumption, though successfully applied and tested to some extent from the study of ultrasonic waves, still awaits a more direct confirmation and support from as straightforward experiments as mentioned and proposed here.

We are thankful to Prof. M. F. Soonawala for his kind interest in this work.

#### REFERENCES

- Herzfeld, K. F., 1955, Section H, *Thermodynamics and Physics of Matter*, Edited by Rossini, G. D. (Princeton University Press, New Jersey, U.S.A.), p. 646.  
 Siegel, A. E., 1952, Ph.D. Thesis, *The Rapid Expansion of Compressed Gases behind a Piston*, University of Amsterdam.

# A NOTE ON BROKEN $SU(3)$ SYMMETRY

P. GHOSE

INDIAN ASSOCIATION FOR THE CULTIVATION OF SCIENCE, JADAVPUR, CALCUTTA

S. SEN

SAHA INSTITUTE OF NUCLEAR PHYSICS, CALCUTTA

(Received July 17, 1965)

The  $J^P = 3/2^+$  baryon decuplet decay into a baryon and a pseudoscalar meson octet has been studied using the  $U$ -spin technique within the framework of broken  $SU(3)$ . The relevant Hamiltonian transforms like the  $I = 0$ ,  $Y = 0$  member of a unitary octet, thus conserving isospin  $I$  and hypercharge  $Y$ . For the processes considered the decay amplitudes obtained by using the Wigner-Eckart theorem occur in terms of three parameters. The novel feature of our treatment is the estimation of the ratio of two of them from the observed decuplet mass splittings. This is essentially a dynamical assumption. A second relation between the parameters is obtained from the experimental decay widths  $\Gamma$ .\*

The results are tabulated below :

Process	Theoretical		Expt.	Reference
	$SU(3)$	Broken $SU(3)$		
$\Gamma(N^{*-} \rightarrow \pi^- n) / \Gamma(Y_1^{*-} \rightarrow \Lambda \pi^-)$	2.4	2	$\sim 2$	Rosenfeld <i>et al.</i> R.M.P. 36, 977 (1964)
$\Gamma(\Xi^{*-} \rightarrow \Xi^- \pi) / \Gamma(Y_1^{*-} \rightarrow \Lambda \pi^-)$	0.5	0.09	$0.13 \pm 0.05$	
$\Gamma(Y_1^{*-} \rightarrow \Sigma \pi) / \Gamma(Y_1^{*-} \rightarrow \Lambda \pi^-) \sim 16\%$	$\sim 0\%*$		$2 \pm 2\%$	

\*We have taken  $\Gamma(Y_1^{*-} \rightarrow \Sigma \pi) \approx 0$

Note that the type of broken  $SU(3)$  considered accommodates the puzzling  $Y_1^{*-}$  (1385) branching ratio.

We are grateful to Professor R. H. Capps, Dr. P. K. Roy and Dr. B. Datta Roy for valuable suggestions and criticisms. Fellowships granted to (P. G.) by Prof. S. N. Bose and to (S. S.) by Prof. M. K. Banerjee have enabled the present work to be undertaken and are gratefully acknowledged.

## SU(3) SYMMETRY IN A BOOTSTRAP MODEL

T. ROY

JADAVPUR UNIVERSITY, CALCUTTA

P. GHOSE

INDIAN ASSOCIATION FOR THE CULTIVATION OF SCIENCE, JADAVPUR, CALCUTTA

(Received July 17, 1965)

Cutkowsky's (1963) idea of the VVV bootstrap has been further explored following the remarks of Gell-Mann, Ne'eman (1964) and Zachariasen (1964). Starting from the interaction Lagrangian

$$L = g_c K^{*0} K^{*-} \rho^+ + g_c K^{*0} K^{*+} \rho^- + g_0 (K^{*+} K^{*-} - K^{*0} K^{*0}) \rho^0 + h (K^{*+} K^{*-} + K^{*0} K^{*0}) \phi^0 + f \rho^+ \rho^- \phi^0$$

a possible self-consistent solution of the  $K^*$  and  $\rho$  straps yields the  $SU(2)_I$  solutions for the coupling constants and masses of  $K^*$  and  $\rho$ . The bootstrap conditions also generate another  $SU(2)_I$  invariance and mass degeneracy among such  $SU(2)_V$  multiplets. These considerations finally lead to full mass degeneracy among the eight physical vector mesons ( $\rho$ ,  $K^*$ ,  $\phi^0$ ) and the  $SU(3)$  solutions for the coupling constants :

$$L = g \left[ K^{*0} K^{*-} \rho^+ + K^{*+} \bar{K}^{*0} \rho^- + \frac{1}{\sqrt{2}} (K^{*0} K^{*0} - K^{*+} K^{*-}) \rho^0 \right. \\ \left. - \frac{1}{\sqrt{6}} (K^{*0} \bar{K}^{*0} + K^{*+} K^{*-}) \phi^0 + \frac{2}{\sqrt{6}} \rho^+ \rho^- \phi^0 \right]$$

The calculation is essentially an extension of the method of Abers, Zachariasen and Zemach (1963). We emphasize that our main result shows that Cutkowsky's and Capps' (1963) assumption of mass degeneracy can be removed.

We are indebted to Professor R. H. Capps and Mr. S. Mallik for valuable discussions. One of the authors (P. G.) is grateful to Professor S. N. Bose for granting him a fellowship.

## REFERENCES

- Abers, E., Zachariasen, F., Zemach, C. 1963, *Phys. Rev.*, **132**, 1831.  
 Cutkowsky, R. E. 1963, *Phys. Rev.*, **131**, 1888.  
 Capps, R. H. 1963, *Phys. Rev.*, **10**, 312.  
 Gell-Mann, M. Ne'eman, Y. 1964, "The Eightfold Way", (W. A. Benjamin, INC., N.Y., Amsterdam) 282.  
 Zachariasen, F. 1964, 'Bootstraps'. Scottish Summer School Lectures.

# X-RAY STUDY OF A SECOND DEHYDRATED PHASE OF COPPER AMMONIUM SULPHATE HEXAHYDRATE

GOURI RAY (née Bhowmik)

DEPARTMENT OF MAGNETISM,

INDIAN ASSOCIATION FOR THE CULTIVATION OF SCIENCE,

CALCUTTA-32.

(Received May 26, 1965)

**ABSTRACT.** The existence of a second dehydration product of  $\text{Cu}(\text{NH}_4\text{SO}_4)_2 \cdot 6\text{H}_2\text{O}$ , viz.  $2[\text{Cu}(\text{NH}_4\text{SO}_4)_2]\text{H}_2\text{O}$  has been reported. The powder photograph of this phase has been indexed by De Wolff's method. The unit cell dimensions of this monoclinic phase are  $a = 16.35\text{\AA}$ ,  $b = 12.88\text{\AA}$ ,  $c = 8.77\text{\AA}$ ,  $\beta = 103.19^\circ$ . It contains 4 molecules per unit cell and the probable space groups are P2, Pm or P2/m.

## INTRODUCTION

In a previous paper (Bhowmik 1961), the results of the X-ray study of  $\text{Cu}(\text{NH}_4\text{SO}_4)_2 \cdot 2\text{H}_2\text{O}$ , a dehydrated phase of  $\text{Cu}(\text{NH}_4\text{SO}_4)_2 \cdot 6\text{H}_2\text{O}$  occurring at  $65^\circ\text{C}$  was reported. The thermal dehydration curve for  $\text{Cu}(\text{NH}_4\text{SO}_4)_2 \cdot 6\text{H}_2\text{O}$  showed another dehydrated phase which forms at  $105^\circ\text{C}$  and is stable upto  $160^\circ\text{C}$ . The dihydrate phase lost weight corresponding to a further loss of  $1\frac{1}{2}$  molecules of water so that the new phase at  $105^\circ\text{C}$  contained  $\frac{1}{2}$  molecule of water of crystallisation per formula unit. The molecular formula  $2[\text{Cu}(\text{NH}_4\text{SO}_4)_2]\text{H}_2\text{O}$  was assigned to it and it was further confirmed by chemical analysis.

## EXPERIMENTAL

Informations regarding the crystal structure of this phase was obtained from x-ray powder photograph, since it could not be obtained as single crystals. To prepare the powder sample, a capillary tube packed with finely powdered  $\text{Cu}(\text{NH}_4\text{SO}_4)_2 \cdot 6\text{H}_2\text{O}$  was treated in the furnace at  $110^\circ\text{C}$  for 24 hours, so that the hemihydrate was obtained. The tube was sealed at both ends while still in the furnace, and a powder photograph was taken with a 19 cm. Unicam camera using filtered copper radiation from a Machlett tube running at 40 KV. 15mA.

The powder photograph thus obtained was entirely different from that of the hexahydrate or the dihydrate. Also there was no spacing common with any of the following substances:  $\text{CuSO}_4 \cdot \text{H}_2\text{O}$ ,  $(\text{NH}_4)_2\text{SO}_4$  or  $\text{CuSO}_4$  anhydrous. Hence it was confirmed to be that of the new double salt  $2[\text{Cu}(\text{NH}_4\text{SO}_4)_2]\text{H}_2\text{O}$ .

*Analysis of the powder pattern:* Attempts were made to index the powder lines in terms of cubic, tetragonal or hexagonal systems. Since the data did not

fit with any of these systems. Lipson's method (Lipson 1949) was tried, which also did not give sufficient number of constant differences. The only remaining possibilities then were those of the salt belonging to the monoclinic or the triclinic system. In such cases of lower symmetry, both Ito's method (Ito 1950) as well as De Wolffe's method (De Wolffe 1957) may be successfully applied.

De Wolffe has shown that certain algebraic relations may be derived from Ito's equation of reciprocal lattice. With the help of these relations among the existing  $Q(=1/d^2)$  values one can explore the complete reciprocal net and all its different levels.

According to the procedure of De Wolffe, we have utilised the following theoretical relations between the  $Q$  values :—(1) The relation between reflections of different orders from a common lattice plane

$$n^2Q(m\mathbf{h}) = m^2Q(n\mathbf{h}) \quad \dots (1)$$

where  $Q(\mathbf{h})$  denotes the  $Q$  value corresponding to the reciprocal lattice point with radius vector  $\mathbf{h}$ ;  $m$  and  $n$  are integers.

(2) Relations for a zone of lattice planes

$$\begin{aligned} \text{(a)} \quad Q(\mathbf{h}+\mathbf{h}') + Q(\mathbf{h}-\mathbf{h}') &= 2[Q(\mathbf{h}) + Q(\mathbf{h}')] \\ \text{(b)} \quad Q(\mathbf{h}+2\mathbf{h}') - Q(\mathbf{h}-2\mathbf{h}') &= 2[Q(\mathbf{h}+\mathbf{h}') - Q(\mathbf{h}-\mathbf{h}')] \\ \text{(c)} \quad Q(\mathbf{h}+3\mathbf{h}') - Q(\mathbf{h}) &= 3[Q(\mathbf{h}+2\mathbf{h}') - Q(\mathbf{h}+\mathbf{h}')] \\ \text{(d)} \quad Q(\mathbf{h}+x\mathbf{h}') - Q(\mathbf{h}-x\mathbf{h}') &= x[Q(\mathbf{h}+\mathbf{h}') - Q(\mathbf{h}-\mathbf{h}')] \end{aligned}$$

Searching for relations like (1) it was observed that  $4Q_2 = Q_{18}$ ,  $9Q_2 = Q_{32}$  and  $9Q_1 = Q_{23}$ , (subscripts of  $Q$ 's refer to serial number of lines). Further, it was seen that if  $1/4Q_1$  is taken as  $Q(\mathbf{h}_1)$  and  $1/4Q_2$  as  $Q(\mathbf{h}_2)$  then  $Q_1 = Q(2\mathbf{h}_1)$ ,  $Q_6 = Q(3\mathbf{h}_1)$  and  $Q_{23} = Q(6\mathbf{h}_1)$ ; again  $Q_2 = Q(2\mathbf{h}_2)$ ,  $Q_{11} = Q(3\mathbf{h}_2)$ ,  $Q_{18} = Q(4\mathbf{h}_2)$ ,  $Q_{25} = Q(5\mathbf{h}_2)$ , and  $Q_{32} = Q(6\mathbf{h}_2)$ .

Thus the lines  $h = 0$  and  $l = 0$  in the array shown below could be written down. The figures placed at the reciprocal lattice points represent  $1/d^2 \times 1000$  calculated. Those in bold types represent the  $Q$  values actually observed in the powder photograph.

Now in 2(a) we may put  $\mathbf{h} = \mathbf{h}_1$  and  $\mathbf{h}' = 2\mathbf{h}_2$  and since  $Q_5 + Q_2 = 2Q(\mathbf{h}_1) + Q(2\mathbf{h}_2)$ , we recognise  $Q_2$  and  $Q_5$  as  $Q(\mathbf{h}_1 - 2\mathbf{h}_2)$  and  $Q(\mathbf{h}_1 + 2\mathbf{h}_2)$ . (The former being a case of double index).

Having obtained  $Q(\mathbf{h}_1 + 2\mathbf{h}_2)$  and  $Q(\mathbf{h}_1 - 2\mathbf{h}_2)$  we can find  $Q(\mathbf{h}_1 + \mathbf{h}_2)$ ,  $Q(\mathbf{h}_1 - \mathbf{h}_2)$ , because  $Q(\mathbf{h}_1 + \mathbf{h}_2) + Q(\mathbf{h}_1 - \mathbf{h}_2) = 2[Q(\mathbf{h}_1) + Q(\mathbf{h}_2)] = 2(39 + 63\frac{1}{2}) = 205$  and  $Q(\mathbf{h}_1 + \mathbf{h}_2) - Q(\mathbf{h}_1 - \mathbf{h}_2) = \frac{1}{2}[Q(\mathbf{h}_1 + 2\mathbf{h}_2) - Q(\mathbf{h}_1 - 2\mathbf{h}_2)] = \frac{1}{2}[339 - 249] = 45$  whence  $Q(\mathbf{h}_1 + \mathbf{h}_2) = 125$  and  $Q(\mathbf{h}_1 - \mathbf{h}_2) = 80$ .

From these two, values of  $Q(2\mathbf{h}_1 + 2\mathbf{h}_2)$ ,  $Q(3\mathbf{h}_1 + 3\mathbf{h}_2)$  etc. and  $Q(2\mathbf{h}_1 - 2\mathbf{h}_2)$ ,  $Q(3\mathbf{h}_1 - 3\mathbf{h}_2)$  etc. were obtained using relation (1).



Now, using the various special cases of the general relation (2d), a zone of the reciprocal lattice could be built up, in which 15 of the observed  $Q$  values appeared.

$k = 0$													
$l = 6$			2224	2165	2185	<b>2284</b>	2462	2719	3056				
5	2356	2035	1795	1634	1552	1549	<b>1625</b>	1780	2014	2328	2719	3191	3742
4	1884	1540	1276	1103	988	961	<b>1014</b>	1146	1357	1639	2016	2462	2992
3	1579	1212	936	718	590	541	<b>571</b>	680	868	1134	1470	1906	2411
2	1400	1001	<b>700</b>	471	320	<b>249</b>	<b>253</b>	<b>339</b>	500	747	1070	1473	1955
1	1349	936	<b>603</b>	<b>350</b>	175	80	63.5	125	<b>268</b>	<b>489</b>	788	1167	1626
0	1424	975	632	356	158	39	0	39	<b>158</b>	<b>356</b>	632	975	<b>1424</b>
$h =$	$\bar{6}$	$\bar{5}$	$\bar{4}$	$\bar{3}$	$\bar{2}$	$\bar{1}$	0	1	2	3	4	5	6

Searching now for a value of  $Q(h_3)$  it was observed that  $\frac{1}{4}Q_9 = \frac{1}{8}Q_{18} = 131$ , which however did not appear very promising. But just to test whether the lattice is monoclinic or not, zones were constructed adding  $131, 4 \times 131, 9 \times 131, 16 \times 131$  and  $25 \times 131$  to the zone obtained before. In the five new zones respectively 8, 10, 9, 1 and 1 observed  $Q$  values appeared and thus all the observed values were accounted for.

$k = 1$											
$l = 3$	1343	1067	849	721	672	<b>701</b>	<b>811</b>	999	1265	1601	2542
3	1132	831	<b>602</b>	452	<b>380</b>	<b>385</b>	470	631	<b>878</b>	1103	2086
1	1067	734	481	<b>306</b>	211	194.5	<b>256</b>	399	620	919	1757
0	1106	763	487	289	170	131	170	289	487	763	1106
$h =$	$\bar{5}$	4	3	$\bar{2}$	1	0	1	2	3	4	5

$k = 2$											
$l = 4$	2064	1800	<b>1627</b>	1512	1485	<b>1538</b>	2304	2538	2852	<b>3243</b>	3715
3	1736	1460	1242	1114	1065	1095	1670	1881	2163	2540	<b>2986</b>
2	1525	1224	995	844	773	779	863	1024	1271	1596	1997
1	1460	1127	874	<b>699</b>	<b>604</b>	587.5	<b>649</b>	792	1013	1412	<b>1691</b>
0	1499	1156	880	682	563	<b>524</b>	563	682	<b>880</b>	1156	1499
$h =$	$\bar{5}$	$\bar{4}$	3	$\bar{2}$	$\bar{1}$	0	1	2	3	4	5

$k = 3$										
$l = 4$	2455	<b>2282</b>	2167	2140	<b>2193</b>	<b>2325</b>	2536	2818	3195	
3	2115	1897	1769	1720	1750	<b>1859</b>	2047	2313	2649	
2	1879	<b>1650</b>	1499	<b>1428</b>	<b>1432</b>	1518	1679	1926	2251	
1	1782	1529	1354	1259	1243	1304	1447	1668	1967	
0	1811	<b>1535</b>	1337	1218	<b>1179</b>	1218	1337	<b>1535</b>	1811	
$h =$	$\bar{4}$	$\bar{3}$	$\bar{2}$	$\bar{1}$	0	1	2	3	4	

$k = 4$

$l = 2$	2796	2567	2416	2345	2349	2435	2596	2843	3168
1	2699	2446	2271	2176	2159.5	2221	2364	2585	2884
0	2728	2452	2254	<b>2185</b>	2096	<b>2185</b>	2254	2452	2728
$h =$	$\bar{4}$	$\bar{3}$	$\bar{2}$	$\bar{1}$	0	1	2	3	4

$k = 5$

$l = 2$	3524	3528	3614
1	<b>3355</b>	3338.5	3400
0	3314	3275	3314
$h = 1$	$\bar{1}$	0	1

The calculated and observed  $Q$  values appear in the table.

No. of lines	Intensity	$d\text{\AA}$	$Q$ obs.	$Q \cdot 1/d^2$ calc.	Indices
1.	s	8.031	.0155	.0158	200
2.	w	6.318	.0251	.0253	002
				.0249	10 $\bar{2}$
				.0256	111
3.	s	6.134	.0266	.0268	201
4.	w	5.729	.0305	.0306	21 $\bar{1}$
5.	w	5.475	.0334	.0339	102
6.	ms	5.308	.0355	.0356	300
				.0350	30 $\bar{1}$
7.	vw	5.115	.0382	.0385	012
8.	w	4.495	.0494	.0489	301
9.	vw	4.373	.0523	.0524	020
10.	s	4.285	.0545	.0541	103
11.	w	4.186	.0571	.0571	003
12.	vw	4.066	.0605	.0604	12 $\bar{1}$
				.0603	40 $\bar{1}$
				.0602	312
13.	ms	3.914	.0653	.0649	121
14.	s	3.785	.0698	.0702	013
				.0700	40 $\bar{2}$
				.0699	22 $\bar{1}$
15.	w	3.496	.0816	.0811	113
16.	vw	3.367	.0882	.0880	320
				.0878	312
17.	vs	3.231	.0956	.0961	10 $\bar{4}$
18.	ms	3.133	.1019	.1014	004
				.1024	222

No. of lines	Intensity	$d\text{\AA}$	$Q = 1/d^2$ obs.	$Q = 1/d^2$ calc	Indices
19.	vs	3.049	.1076	.1072	402
20.	vw	2.914	.1178	.1179	030
21.	vvw	2.824	.1254	.1259	13 $\bar{1}$
22.	vw	2.744	.1331	.1334	030
				.1335	204
23.	vvw	2.642	.1430	.1432	032
				.1428	13 $\bar{2}$
				.1424	600
24.	vvw	2.551	.1537	.1538	024
				.1535	330
25.	vw	2.482	.1623	.1626	601
				.1625	005
				.1627	32 $\bar{4}$
26.	w	2.425	.1695	.1691	521
27.	vvw	2.322	.1855	.1859	133
28.	vw	2.287	.1910	.1914	205
				.1906	503
29.	vvw	2.225	.2020	.2016	404
30.	vw	2.167	.2130	.2135	140
31.	ms	2.133	.2188	.2185	10 $\bar{6}$
				.2193	034
32.	vvw	2.096	.2279	.2282	33 $\bar{4}$
				.2284	006
33.	w	2.072	.2329	.2325	134
				.2328	305
34.	vvw	1.829	.2989	.2986	523
35.	w	1.756	.3243	.3243	424
36.	w	1.726	.3357	.3355	15 $\bar{1}$

Thus we have finally established a monoclinic cell, the dimensions of the unit cell being  $a = 16.35\text{\AA}$ ,  $b = 12.88\text{\AA}$ ,  $c = 8.77\text{\AA}$ ,  $\beta = 103^\circ 19'$ .

No evidence of existence of glide planes and screw axes is depicted by the indices. So the possible space-group may be any of the following,  $P2$ ,  $Pm$ ,  $P2/m$ .

The density of the hemihydrate determined by a method described previously (Bhowmik loc. cit.) comes out as 2.20 gms per c.c. It agrees fairly well with the density 2.16 gms per c.c. calculated on the basis of 4 molecules per unit cell.

## DISCUSSION

From the meagre data of a powder photograph it is not possible to throw any light on the structure of the substance. However, it may be noted that as was observed in the case of the dihydrate (orthorhombic,  $b = 12.52 \text{ \AA}$ , Bhowmik, loc. cit), the value of  $b$  remains very similar to that of the hexahydrate (monoclinic,  $b = 12.50 \text{ \AA}$ ) in the case of the hemihydrate also.

## ACKNOWLEDGMENT

The author expresses her sincerest thanks to Professor A. Bose, D.Sc., F.N.I., for suggesting the problem and his keen interest throughout the progress of the work. She is also thankful to Shri S. Ray, Research Officer, for general supervision and helpful discussions.

## REFERENCES

- Bhowmik G., 1961., *Ind. J. Phys.*, **35**, 499.  
Ito, T., 1950, X-ray studies in Polymerphism, Maruzen Tokyo.,  
Lipson, H., 1949, *Act. Cryst.* **2**, 43.  
Wolffe, P. M. De., 1957, *Acta Cryst.* **10**, 590.

# SINGLET→TRIPLET ABSORPTION IN META- AND PARACHLOROTOLUENE

D. K. MUKHERJEE, P. K. BISHTUI AND S. C. SIRKAR

INDIAN ASSOCIATION FOR THE CULTIVATION OF SCIENCE,  
CALCUTTA-32.

(Received June 14, 1965)

**ABSTRACT.** The absorption spectra of semi-transparent thick masses of *p*-chlorotoluene and *m*-chlorotoluene obtained by lowering the temperature of the liquids slowly upto about  $-130^{\circ}\text{C}$  have been investigated. In the case of the first compound five broad bands at 26200, 26810, 27230, 27750 and 28260  $\text{cm}^{-1}$  have been observed. Taking the first band as the (0, 0) band, the excited state vibration frequencies 610, 1030 and 1550  $\text{cm}^{-1}$  have been derived. It has been pointed out that these frequencies correspond respectively to the frequencies 634, 1090 and 1596  $\text{cm}^{-1}$  of the unsymmetrical modes of the molecule in the ground state and that in the fluorescence spectrum the 0, 0 band is absent.

In the case of metachlorotoluene only four weak bands at 24885, 25830, 26775 and 27720  $\text{cm}^{-1}$  have been observed. The position of the first band is almost the same as that of the first broad band in the fluorescence spectrum of the molecule and if this band is taken as the 0, 0 band, a progression of the excited state frequency 945  $\text{cm}^{-1}$  is given by the other bands. This corresponds to the frequency 996  $\text{cm}^{-1}$  of the symmetric mode of the molecule in the ground state. It has been concluded that when the substitutions take place at positions which make the ring unsymmetrical the symmetric mode of the ring is coupled predominantly to the singlet-triplet transition in absorption and in the case of the para-substituted molecule vibration modes asymmetric to some two-fold axes of the ring are coupled to the transition.

## INTRODUCTION

It was observed by Paul and Sirkar (1963) that the absorption spectrum of solid mass of *p*-bromotoluene of thickness about 7 mm. obtained by cooling the liquid very slowly to low temperatures shows weak absorption bands in the region 4045Å—3603Å. They concluded from the analysis of the bands that they are due to singlet→triplet transition. From a comparison of the positions of the bands with those of the fluorescence bands reported by previous workers they pointed out that the 0, 0 band does not appear in the fluorescence spectrum of this compound and that the vibration frequency 1516  $\text{cm}^{-1}$  is coupled to the electronic transition in absorption. As chlorotoluenes in the solid state at low temperatures also exhibit strong luminescence which is excited by radiation of wavelengths shorter than 3750Å but longer than 3000Å (Roy, 1959), the luminescence is produced by excitation from the singlet state to the triplet state followed by transition to the singlet state again. The liquid, however, shows only continuous absorption in the region on the longer wavelength side of 3300Å (Roy,

1960). It was, therefore, thought worthwhile to find out whether bands are produced in the absorption spectra also of these compounds in the solid state at low temperatures. The results of investigations on the absorption spectra of *m*-chlorotoluene and *p*-chlorotoluene in the solid state at about  $-130^{\circ}\text{C}$  have been discussed in the present paper.

## EXPERIMENTAL

As the singlet $\rightarrow$ triplet absorption is very weak, a cell of thickness about 10mm. had to be used in each case. The cell was made of Pyrex glass and the thin windows were made by blowing the ends of a tube. When *m*-chlorotoluene or *p*-chlorotoluene contained in such a cell is frozen by immersing the cell in liquid oxygen an opaque mass is obtained. Attempts were therefore made to obtain at least a semi-transparent frozen mass in each case by cooling the liquid slowly to a temperature just above the melting point of the crystal and then by slowly lowering the temperature a few degrees below the freezing point. No single crystal was produced by this method, but almost a transparent mass with a few internal cracks was obtained. The liquids were of chemically pure quality supplied by B.D.H. of London. The vertical straight portion of a 250-watt coiled tungsten filament lamp was used as the source of light and it was focussed with a lens on one of the windows of the cell. The light transmitted through the other window was focussed on the slit of an Adam Hilger medium quartz spectrograph giving an inverse dispersion of about 10Å/mm in the 3500Å region. An exposure of about eight hours was required to photograph the absorption spectrum. On each spectrogram iron arc spectrum was also photographed as a comparison.

Microphotometric records of the spectrograms were taken using a Moll self-recording microphotometer. Two sharp scratches made with a razor blade along two chosen iron lines on each of the spectrograms were extended across the absorption spectrum and the wavelengths of the absorption maxima were measured from the microphotometer records of the absorption and iron arc spectra by measuring the distances of the maxima from the positions of the chosen iron lines and finding out the wavelengths of the iron lines at such distances on the record of the iron arc spectrum. As the bands were found to be broad, care was taken to locate the positions of the maxima with reasonable accuracy.

## RESULTS AND DISCUSSION

Microphotometric records of the absorption spectra are reproduced in Fig. 1. The record of the spectrum of the incident light photographed with suitable exposure is also reproduced in the figure. The wave numbers of the bands are given in Table I.

TABLE I

Metachlorotoluene			Parachlorotoluene		
No.	$\nu$ in $\text{cm}^{-1}$	Assignment	No.	$\nu$ in $\text{cm}^{-1}$	Assignment
A	24885	0,0	A	26200	0,0
B	25830	0+945	B	26610	0+610
C	26775	0+2 $\times$ 945	C	27230	0+1030
D	27720	0+3 $\times$ 945	D	27750	0+1550
			E	28260	0+2 $\times$ 1030

*Metachlorotoluene*

The band at  $24885\text{ cm}^{-1}$  (4017.4A) is very weak but it is definitely present in the different spectrograms obtained for *m*-chlorotoluene. The frequency of this band is very near to that of the first broad fluorescence band at  $24862\text{ cm}^{-1}$  reported by Biswas (1956a). Thus in this case the 0,0 singlet-triplet transition is allowed weakly both in absorption and in fluorescence. The other three bands in the absorption spectrum at  $25830$ ,  $26775$  and  $27720\text{ cm}^{-1}$  form a progression of the excited state vibrational frequency  $945\text{ cm}^{-1}$ . Probably the corresponding ground state frequency is  $996\text{ cm}^{-1}$ , as can be seen from the fact that the strong Raman line  $996\text{ cm}^{-1}$  is assigned to the breathing mode of the ring. Thus this symmetric mode is coupled to the singlet-triplet transition in this molecule which as a whole has neither a centre of symmetry nor a strict two-fold axis.

It would be of interest to find out what vibrational frequencies are associated with the singlet  $\leftarrow$  triplet emission. The frequencies of first three fluorescence bands reported by Biswas (1956a) are  $24862$ ,  $23578$  and  $23115\text{ cm}^{-1}$ . All these bands are very broad and the third is the strongest. If the centre of the second band would be taken at  $23646\text{ cm}^{-1}$  the difference of the first two frequencies would agree with the Raman frequency  $1216\text{ cm}^{-1}$  which is due probably to the mode 2 of the ring. The next band would then be assigned as  $\nu_0 - (1216 + 531)$ . The frequency  $531\text{ cm}^{-1}$  would then agree fairly with the Raman frequency  $522\text{ cm}^{-1}$  due to mode 6B of the ring (Pitzer and Scott, 1943). A very feeble band at  $4107\text{A}$  is visible in the spectrogram reproduced by him (Biswas, 1956a). Thus the modes associated in the emission spectrum are different from those associated in the corresponding singlet-triplet absorption in this case.

*Parachlorotoluene*

In this case the first band is at  $26200\text{ cm}^{-1}$  which is at a distance of  $1442\text{ cm}^{-1}$  on the shorter wavelength side from the first fluorescence band at  $24758\text{ cm}^{-1}$  (Biswas, 1956b). It appears that in this case the 0,0 transition in fluorescence does not occur. Probably, the emission is induced by the vibrational mode corresponding to  $\nu_{10u}$  of the ring. The other bands of the absorption spectrum

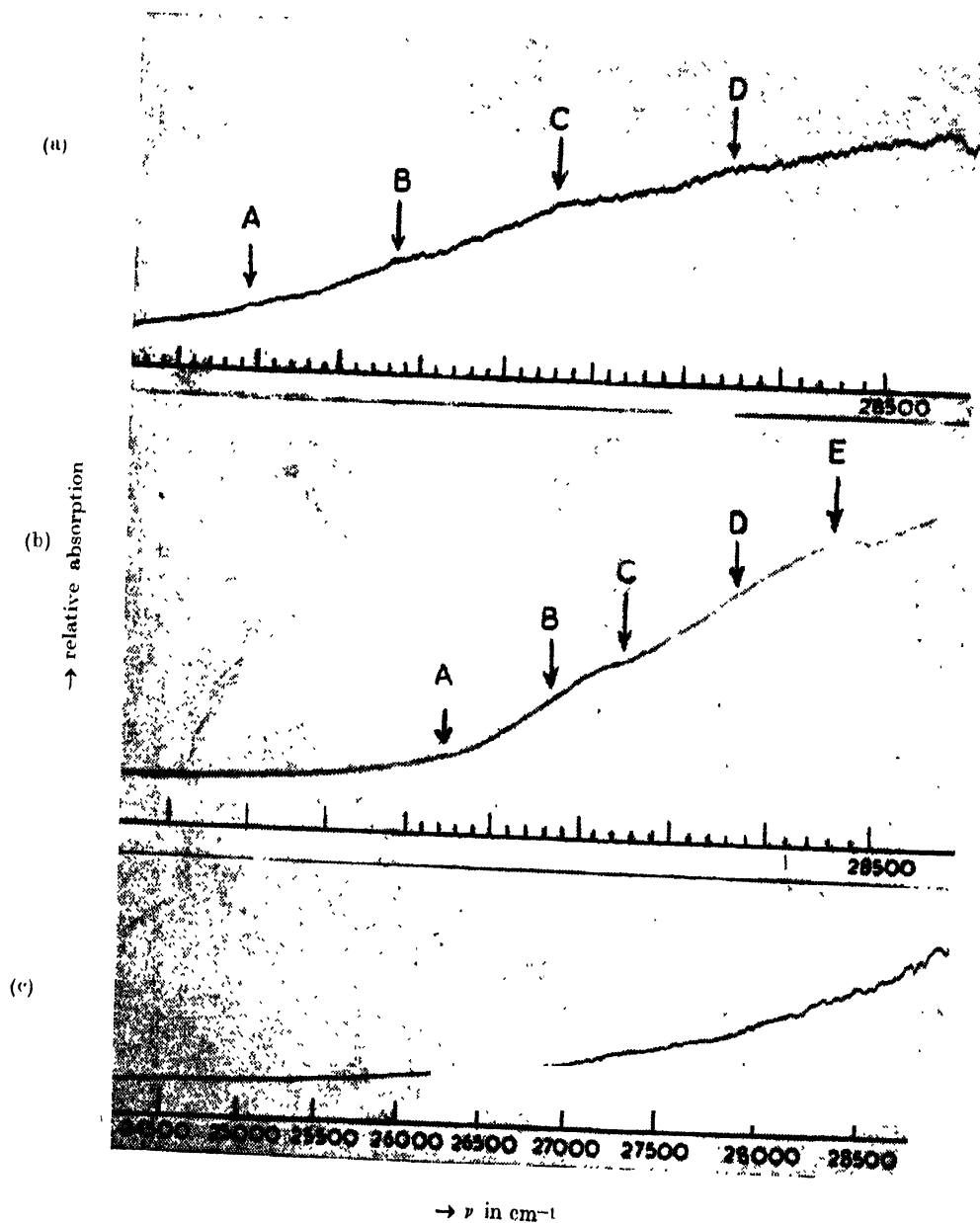


Fig. 1. Microphotometric records of absorption spectra.

(a) Metachlorotoluene at about  $-130^{\circ}\text{C}$ .

(b) Para chlorotoluene

(c) Spectrum of incident light.



shown in Table I give the excited state vibration frequencies 610, 1050 and 1550  $\text{cm}^{-1}$  respectively. The Raman spectrum of the crystal shows (Sanyal, 1953) strong lines at 630, 1090 and 1590  $\text{cm}^{-1}$  and a weak line at 1454  $\text{cm}^{-1}$  was also reported by previous workers for the liquid (Magat, 1936). The three lines 630  $\text{cm}^{-1}$ , 1090  $\text{cm}^{-1}$  and 1590  $\text{cm}^{-1}$  are assigned (Mecke-Kerkhof, 1951) respectively to the modes  $\nu_{6B}$ ,  $\nu_{10A}$  and  $\nu_{8B}$  (Pitzer and Scott, 1943). In that case the excited state frequencies 617, 1050 and 1566  $\text{cm}^{-1}$  would correspond to the ground state frequencies of modes  $\nu_{6B}$ ,  $\nu_{10A}$  and  $\nu_{8B}$  respectively. So, it is found that these modes which make the ring asymmetric to a two fold axis of the ring are coupled to the singlet→triplet transition. In the luminescence spectrum also Biswas (1956b) observed a vibrational frequency 1062  $\text{cm}^{-1}$  which might be the frequency 1090  $\text{cm}^{-1}$  observed in the Raman effect.

A comparison of these results with those observed in the case of metachlorotoluene leads to the conclusion that asymmetric electronic structure of the ring is the essential requirement for the singlet→triplet transition in absorption and this is produced in the case of metachlorotoluene by the substitution itself and in the case of parachlorotoluene by some asymmetric modes of vibration of the ring.

#### ACKNOWLEDGMENT

The work was done under a scheme sanctioned by the Council of Scientific and Industrial Research and two of the authors (S.C.S. and P.K.B.) are thankful to the Council for the financial help. They are also indebted to the authorities of the Indian Association for the Cultivation of Science for kindly offering facilities for carrying out the investigation.

#### REFERENCES

- Biswas, D. C., 1956a, *Ind. J. Phys.*, **30**, 565.
- Biswas, D. C., 1956b, *Ind. J. Phys.*, **30**, 143.
- Magat, M., 1936, *Annual Tables of Constants and Numerical data*, p. 77.
- Mecke-Kerkhof, 1951, *Landolt Börnstein Tables*, Auf. 6, Band I. Teil 2.
- Paul, A. R. and Sirkar, S. C., 1963, *Ind. J. Phys.*, **37**, 252.
- Pitzer, K. S. and Scott, D. W., 1943, *J. Amer. Chem. Soc.*, **65**, 803.
- Roy, J. K., 1959, *Ind. J. Phys.*, **33**, 209.
- Roy, J. K., 1960, *Ind. J. Phys.*, **34**, 331.
- Sanyal, S. B., 1953, *Ind. J. Phys.*, **27**, 447.

# MOLECULAR ORBITAL THEORY OF THE LIGAND FIELD IN $[\text{NiHal}_4]^{2-}$ COMPLEXES

A. BOSE, R. RAI AND S. MITRA

DEPARTMENT OF MAGNETISM

INDIAN ASSOCIATION FOR THE CULTIVATION OF SCIENCE,

JADAVPUR, CALCUTTA-32.

(Received May 17, 1965)

**ABSTRACT** An expression for magnetic susceptibility for  $[\text{NiHal}_4]^{2-}$  complexes is deduced on the basis of the molecular orbital procedure of Stevens, Bose *et al.* and others, and compared with the experimental results on single crystals of  $[\text{Et}_4\text{N}]_2[\text{NiBr}_4]$ . An anisotropic reduction in spin-orbit coupling coefficient is found, which indicates an anisotropic overlap of ligand  $\sigma$ - and  $p$ - charge clouds with the central  $d$ -charge clouds and also admixture of  $3d^{74p}$  with  $3d^8$  configurations. A sharper fall in the theoretical  $p^2f-T$  curve below 200 in contrast to the experimental curve and nearly 7% discrepancy between the two at the lowest temperature (100°K) suggest an appreciable change of the trigonal field coefficient  $\Delta$  with temperature.

## INTRODUCTION

In the tetrahedrally co-ordinated  $\text{Ni}^{2+}$  complexes the cubic ligand field energy pattern, into which the free ion ground level  $3d^8\ ^3F$  is split up, consists of the levels  $^3T_1$ ,  $^3T_2$  and  $^3A_2$ , in increasing order of magnitude, which is just the reverse of the octahedral complexes, and the separation of the levels in the former case is 4/9 of the latter (Van Vleck, 1932; Gorter, 1932; Bleaney and Stevens, 1953). The X-ray studies by Peter Pauling (unpublished, reference by Gill *et al.*, 1959) of a series of isomorphous organometallic halides of  $\text{Ni}^{2+}$  e.g.  $(\text{Ph}_3\text{MeAs})_2(\text{NiHal}_4)$  and  $[(\text{Et}_4\text{N})]_2 \cdot [(\text{NiHal}_4)]$  indicate that in all these salts the  $\text{Ni}^{2+}$  ion is tetrahedrally co-ordinated. This is supported by the optical absorption measurements in the latter salts (Gill *et al.*, 1959; Goodgame *et al.*, 1961) which give bands round about  $12500\text{ cm}^{-1}$  ( $^3T_1(F) \rightarrow ^3T_1(P)$ ) and  $6900\text{ cm}^{-1}$  ( $^3T_1(F) \rightarrow ^3A_2(F)$ ) as against  $25000\text{ cm}^{-1}$  ( $^3A_2 \rightarrow ^3T_1(P)$ ) and  $14000\text{ cm}^{-1}$  ( $^3A_2 \rightarrow ^3T_1(F)$ ) respectively, in the octahedral salts (Bose *et al.*, 1963). Also, the mean magnetic susceptibility measurements (Gill *et al.*, 1959; Bose *et al.*, 1965) yield a high magnetic moment (about 3.6–4.0 Bohr magnetons) compared to the spin only value of 2.83, indicating the presence of large orbital contributions which is reasonable to expect if the  $^3T_1$  triplet lies lowest in the Stark pattern.

X-ray measurements further indicate that the salts which form cubic crystal (space group  $P2_1/3$ ) with four ions in the unit cell,  $a = 15.5\text{ \AA}$ ) have a trigonal distortion of the halogen tetrahedron round the  $\text{Ni}^{2+}$  ion, the trigonal axis passing

through one halogen at the vertex of the tetrahedron and the central  $\text{Ni}^{2+}$  ion, and normal to the base formed by the other three equivalent halogens. Thus the  $\text{Ni}^{2+}$  may be taken as under a small trigonal field superposed upon the predominant cubic field, so that a further splitting of the energy levels will occur and the  $[(\text{NiHal}_4)]^{2-}$  complex will be magnetically anisotropic, the effect of which will be appreciable even in the mean susceptibility of the crystal (the crystal being cubic will not show magnetic anisotropy), in the higher order terms particularly at low temperature.

We have therefore derived a theoretical expression of the mean susceptibility of  $(\text{NiHal}_4)^{2-}$  complexes on the basis of the molecular orbital theory of Van Vleck (1935), Stevens (1953), Bose *et al.* (1960) and compared it with the recent experimental values by one of the co-authors (S.M.) on  $[(\text{C}_2\text{H}_5)_4\text{N}]_2\text{NiBr}_4$  the details of which will be published in a separate paper.

# MOLECULAR ORBITAL THEORY OF TETRAHEDRAL $\text{Ni}^{2+}$ COMPLEXES

In addition to the splitting of the ground state of  $\text{Ni}^{2+}$  ion by the tetrahedral field of the type  $T_d$  we have also to consider the effect of the excited  $^3P$  state on  $^3T_1(F)$  which arises from the same electron configuration. The lowest triplet  $^3T_1(F)$  contains an admixture of  $^3P$ , which itself remains unsplit under the said field and spans the same representation  $^3T_1$  of the point group  $T_d$ .

A  $\text{Ni}^{2+}$  ion under a point group  $T_d$  can be treated as a system consisting of two  $d$ -holes, in which the three lowest states  $^3T_1(F)$ ,  $^3T_2(F)$  and  $^3A_2(F)$  arise out of  $(t_2)^2$ ,  $(t_2)^1 \cdot (e)^1$  and  $(e)^2$  configurations, respectively. Following the usual notations  $t_a = |xy\rangle$ ,  $t_b = |yz\rangle$ ,  $t_c = |xz\rangle$  the determinantal wavefunctions of the lowest triplet  $^3T_1(F)$  including the admixture of the ligand  $s$ - and  $p$ - orbitals with the central  $\text{Ni}^{2+}$   $d$ -orbitals can be written as :

$$\begin{aligned}\psi_1 &= |t_c t_a| \\ \psi_2 &= |t_a t_b| \\ \psi_3 &= |t_b t_c|\end{aligned} \quad \dots \quad (1)$$

where  $t_a$ ,  $t_b$  and  $t_c$  are single electron or hole orbitals in  $t_2$  configuration. To include the effect of spon-orbit coupling, which takes the form  $\Sigma(us)_i$  (Bose *et al.* 1960) we note that

$$\begin{aligned}\langle \psi_1 | u_{z_1} + u_{z_2} | \psi_2 \rangle &= \langle \psi_2 | u_{x_1} + u_{x_2} | \psi_3 \rangle \\ &= \langle \psi_3 | u_{y_1} + u_{y_2} | \psi_1 \rangle = i\zeta_i \quad \dots \quad (2)\end{aligned}$$

where  $\zeta_i$  is the spin-orbit coupling coefficient modified by covalency overlap, a result similar to Stevens (1953) for single  $d$ -electron case. Here  $u_{r_1}$  and  $u_{r_2}$  are the  $r$ -th component of operator for hole number 1 and 2 respectively.

Further, the absence of a centre of inversion in these tetrahedral complexes introduces a feature which does not occur with octahedral, which is that  $3d^7 4p$  configuration can be admixed with  $3d^8$ , the consequence of which may be considered to be that the holes are not in pure  $3d$ -orbitals but in orbitals which are an admixture of a  $3d$ - with a  $4p$ -wavefunction. Then following Bates *et al.* (1962), Bates (1963), Wolfsberg and Helmholz (1952) and taking this admixture the orbitals  $|xy\rangle$ ,  $|yz\rangle$  and  $|xz\rangle$  used in (1) are finally written as :

$$\begin{aligned}
 t_a = |xy\rangle &= N \left[ \frac{1}{(1+\gamma^2)^{\frac{1}{2}}} \left\{ dxy + \gamma |z\rangle \right\} + \frac{\lambda_1}{2} (\sigma_1 + \sigma_4 - \sigma_2 - \sigma_3) \right. \\
 &\quad \left. + \frac{\lambda_2}{2} \left\{ \frac{1}{2} (\pi_{x_3} + \pi_{x_2} - \pi_{x_1} - \pi_{x_4}) + \frac{\sqrt{3}}{2} (\pi_{y_4} + \pi_{y_1} - \pi_{y_2} - \pi_{y_3}) \right\} \right] \\
 t_b = |yz\rangle &= N \left[ \frac{1}{(1+\gamma^2)^{\frac{1}{2}}} \left\{ dyz + \gamma |x\rangle \right\} + \frac{\lambda_1}{2} (\sigma_1 + \sigma_3 - \sigma_2 - \sigma_4) \right. \\
 &\quad \left. + \frac{\lambda_2}{2} \left\{ \frac{1}{2} (\pi_{x_4} + \pi_{x_2} - \pi_{x_1} - \pi_{x_3}) + \frac{\sqrt{3}}{2} (\pi_{y_4} + \pi_{y_2} - \pi_{y_1} - \pi_{y_3}) \right\} \right] \\
 t_c = |xz\rangle &= N \left[ \frac{1}{(1+\gamma^2)^{\frac{1}{2}}} \left\{ dxz + \gamma |y\rangle \right\} + \frac{\lambda_1}{2} (\sigma_1 + \sigma_2 - \sigma_3 - \sigma_4) \right. \\
 &\quad \left. + \frac{\lambda_2}{2} (\pi_{y_1} + \pi_{y_2} - \pi_{y_3} - \pi_{y_4}) \right] \quad \dots \quad (3)
 \end{aligned}$$

in which  $N$  is the normalizing factor and  $\lambda$ 's are measures of admixture of ligand  $s$ - and  $p$ -orbitals with the central  $Ni^{2+}d$ -orbitals;  $dxy$  etc., represent the major  $3d$  contributions and  $\gamma|z\rangle$  etc. the  $3d^7 4p$  contributions.

Taking the trigonal axis of the complex as the axis of quantization, the appropriate trigonal orbital states for lowest triplet are :

$$\begin{aligned}
 + &> = - \frac{1}{\sqrt{3}} \left[ \omega |\psi_1\rangle + \omega^2 |\psi_2\rangle + |\psi_3\rangle \right] \\
 0 &> = \frac{1}{\sqrt{3}} \left[ |\psi_1\rangle + |\psi_2\rangle + |\psi_3\rangle \right] \quad \dots \quad (4) \\
 - &> = \frac{1}{\sqrt{3}} \left[ \omega^2 |\psi_1\rangle + \omega |\psi_2\rangle + |\psi_3\rangle \right]
 \end{aligned}$$

where  $\omega = \exp \left( \frac{2\pi i}{3} \right)$

so that inclusive of covalency the non-zero matrix elements of  $u_\xi, u_\eta, u_\zeta$  are given by ( $\zeta$  is the direction along the trigonal axis and with  $\xi$  and  $\eta$  form a right handed orthogonal system of coordinates).

$$\begin{aligned} \langle + | u_\zeta | + \rangle &= - \langle - | u_\zeta | - \rangle = - \frac{\zeta_{||}(d) - \gamma_{\perp}^2 \zeta_{||}(p)}{(1 + \gamma_{\perp}^2)} = - \zeta_{||} \\ \langle + | u_\xi | 0 \rangle &= \langle 0 | u_\xi | - \rangle = - \frac{1}{\sqrt{2}} \frac{\zeta_{\perp}(d) - \gamma_{||} \gamma_{\perp} \zeta_{\perp}(p)}{(1 + \gamma_{\perp}^2)^{1/2} (1 + \gamma_{||}^2)^{1/2}} = - \frac{1}{\sqrt{2}} \zeta_{\perp} \\ \langle + | u_\eta | 0 \rangle &= \langle 0 | u_\eta | - \rangle = \frac{i}{\sqrt{2}} \frac{\zeta_{\perp}(d) - \gamma_{||} \gamma_{\perp} \zeta_{\perp}(p)}{(1 + \gamma_{\perp}^2)^{1/2} (1 + \gamma_{||}^2)^{1/2}} = \frac{i}{\sqrt{2}} \zeta_{\perp} \dots \quad (5) \end{aligned}$$

where the spin-orbit coupling coefficients  $\zeta_i(d)$  ( $||$  and  $\perp$  to trigonal axis) are for  $3d^8$  configuration and  $\zeta_i(p)$  are for  $3d^7 4p$  configuration, inclusive of the reduction due to covalency overlap of surrounding  $s$ - and  $p$ -ligand orbitals and  $\gamma_{||}$  and  $\gamma_{\perp}$  are the  $3d^8 - 3d^7 4p$  admixtural coefficients associated with the states  $|0\rangle$  and  $|+\rangle, |-\rangle$  of eqn.(4), respectively),  $\zeta_{||}$  and  $\zeta_{\perp}$  can then be taken as effective spin-orbit coupling coefficients along and normal to the trigonal axis.

## FINE STRUCTURE

The set  $|+\rangle, |0\rangle$  and  $|-\rangle$  behaves as an atomic  $p$ -state having  $M'_L = 1, 0, -1$  respectively so that the appropriate Hamiltonian for the lowest triplet is given by

$$H = V_{trig} - \alpha U_\zeta S_\zeta - \alpha' (U_\xi S_\xi + U_\eta S_\eta) \quad (6)$$

where  $\alpha, \alpha'$  are the effective orbital Landé  $g$ -factors (Abragam and Pryce, 1951)  $||$  and  $\perp$  to the trigonal axis, respectively and takes into account the admixture of the upper levels. Under the trigonal field  ${}^3T_1(P)$  breaks up into  $\pi_{xy}$  (doublet) and  $\pi_z$  (singlet),  ${}^3A_2$  remains unsplit ( $\chi$ )  ${}^3T_2(F)$  into  $\psi_{xy}$  (doublet) and  $\psi_z$  (singlet) and the ground triplet  ${}^3T_1(F)$  into  $\phi_{xy}$  (doublet) and  $\phi_z$  (singlet) (Abragam and Pryce 1951). The energy separation of the split components of the ground triplet  ${}^3T_1(F)$  is such that the doublet  $\phi_{xy}$  lies at  $-(1/3)\Delta$  and the singlet  $\phi_z$  at  $(2/3)\Delta$  where  $\Delta$  is the trigonal field separation. Operating with Hamiltonian (6) over a  ${}^3P$  term and solving the secular determinant we get the energies as

$$E_0 = \frac{1}{2} \left[ \frac{\Delta}{3} + \alpha \zeta_{||} - S_0 \right]$$

$$E_1 = \frac{1}{2} \left[ \frac{\Delta}{3} - S_1 \right]$$

$$\begin{aligned}
 E_2 &= -\frac{\Delta}{3} + \alpha \zeta_{\parallel} \\
 E_3 &= \frac{1}{2} \left[ \frac{\Delta}{3} + S_0 + \alpha \zeta_{\parallel} \right] \\
 E_4 &= \frac{1}{2} \left[ \frac{\Delta}{3} + S_1 \right] \quad \dots \quad (7) \\
 E_5 &= -\frac{\Delta}{3} - \alpha \zeta_{\parallel}
 \end{aligned}$$

where,

$$\begin{aligned}
 S_0 &= [(\Delta - \alpha \zeta_{\parallel})^2 + 8\alpha'^2 \zeta_{\perp}^2]^{\frac{1}{2}} \\
 S_1 &= [\Delta^2 + 4\alpha'^2 \zeta_{\perp}^2]^{\frac{1}{2}}
 \end{aligned}$$

and the wavefunctions as

$$\begin{aligned}
 \phi_0 &= a \left| 1, -1 \right\rangle + b \left| 0, 0 \right\rangle + a \left| -1, 1 \right\rangle \\
 \phi_1 &= c \left| 1, 0 \right\rangle + d \left| 0, -1 \right\rangle \\
 \phi'_1 &= c \left| -1, 0 \right\rangle + d \left| 0, -1 \right\rangle \\
 \phi_2 &= -\frac{1}{\sqrt{2}} \left| -1, 1 \right\rangle + \frac{1}{\sqrt{2}} \left| 1, -1 \right\rangle \quad \dots \quad (8) \\
 \phi_3 &= \frac{b}{\sqrt{2}} \left| 1, -1 \right\rangle - \sqrt{2} a \left| 0, 0 \right\rangle + \frac{b}{\sqrt{2}} \left| -1, 1 \right\rangle \\
 \phi_4 &= d \left| 1, 0 \right\rangle - c \left| 0, 1 \right\rangle \\
 \phi'_4 &= d \left| -1, 0 \right\rangle - c \left| 0, -1 \right\rangle \\
 \phi_5 &= \left| 1, 1 \right\rangle \\
 \phi'_5 &= \left| -1, -1 \right\rangle
 \end{aligned}$$

where,

$$\begin{aligned}
 a &= \frac{2\alpha' \zeta_{\perp}}{\alpha \zeta_{\parallel} + \Delta + S_0} \cdot b ; & 2a^2 + b^2 &= 1 \\
 d &= \frac{2\alpha' \zeta_{\perp}}{\Delta + S_1} c ; & c^2 + d^2 &= 1
 \end{aligned}$$

In the above expressions since  $\alpha$  and  $\xi_{||}$  also  $\alpha'$  and  $\xi_1$  appear as products we may replace these by  $P_{||}$  and  $P_1$ .

If the trigonal field coefficient  $\Delta$  is positive the relative positions of the energy levels including the effect of the spin-orbit coupling in ascending order will correspond to the sequence of wave functions  $\phi_0, \phi_2, (\phi_1, \phi'_1), (\phi_5, \phi'_5), (\phi_4, \phi'_4), \phi_3$ . For negative value of  $\Delta$  the arrangement of the wavefunctions in (8) holds good in the order of increasing energy. Since in the former case two non-magnetic singlets  $\phi_0$  and  $\phi_2$  come successively, in the two lowermost positions where in the latter case a magnetic doublet  $(\phi_1, \phi'_1)$  lies immediately above  $\phi_0$ , the effective magnetic moment should be comparatively smaller in the former. Assuming  $\Delta$  negative to start with and calculating the first and second order magnetic perturbations for only the lowest  $\phi_0$  and  $\phi_1, \phi'_1$  levels, since rest of the levels lie too high above about  $1000 \text{ cm}^{-1}$ , to give appreciable contribution to the susceptibility we get the expression for the mean susceptibility as follows :

$$K = \frac{N\beta^2}{3k} B \left[ \frac{2A^2}{T} + \frac{16B_1^2k}{D} \left\{ \exp \left( \frac{D}{kT} \right) - 1 \right\} \right. \\ \left. + \frac{N\beta^2}{3} B \left[ \left\{ \frac{8(c + \frac{1}{2}\alpha'\kappa_1 d)^2}{E_2 - E_1} \right\} + \frac{8\{bc - 2ad + \frac{\alpha'\kappa_1}{2}(2ac - bd)\}^2}{E_3 - E_1} \right. \right. \\ \left. \left. + \frac{4c^2d^2(\alpha\kappa_{||} + 2)^2}{E_4 - E_1} + \frac{16(c - \alpha'\kappa_1 d)^2}{E_5 - E_1} \right\} \right. \\ \left. + \left\{ \exp \left( \frac{D}{kT} \right) \left( \frac{4a^2(\alpha\kappa_{||} + 2)^2}{E_2 - E_0} + \frac{16\{ad - bc + \frac{\alpha'\kappa_1}{2}(ac - bd)^2\}}{E_4 - E_0} \right) \right\} \right]$$

where,

$$A = 2d^2 - \alpha\kappa_{||} c^2$$

$$B_1 = \left[ \left\{ ac + bd - \frac{\alpha'\kappa_1}{2} (bc + ad) \right\} + \left\{ bc\nu_5 - ac\nu_3 + bd\nu_2 \right\} \right]$$

$$B = \left[ 2 + \exp \left( \frac{D}{kT} \right) \right]^{-1}$$

$$\kappa_{||} = \frac{1 - \gamma_1^2}{1 + \gamma_1^2} \kappa'_{||}$$

$$\kappa_1 = \frac{1 - \gamma_{||}\gamma_1}{(1 + \gamma_1^2)(1 + \gamma_{||}^2)^{\frac{1}{2}}} \cdot \kappa_1$$

$\kappa_{||}$  and  $\kappa'_{\perp}$  are the actual orbital reduction factors due to covalency,  $\kappa_{||}$  and  $\kappa_{\perp}$  can be taken as effective reduction factors inclusive of the effect of  $3d^7$   $4p$ -admixture. Here again in (9) we can replace  $\alpha\kappa_{||}$  and  $\alpha'\kappa_{\perp}$  by  $Q_{||}$  and  $Q_{\perp}$  respectively.

In the expression for  $B_1$  the second term within braces is the contribution from upper  $\pi_{xy}$ ,  $\pi_z$ ,  $\chi$ ,  $\psi_{xy}$  and  $\psi_z$  levels coming directly through the lowest level  $\phi_0$  of (6) calculated similar to Abragam and Pryce (1951) where

$$\begin{aligned} v_2 &= \left( \frac{5f_z^2}{24\psi'_{xy}} - \frac{2q_z^2}{\pi'_{xy}} \right) \zeta \\ v_3 &= \left( \frac{2q_z^2}{\pi'_z} + \frac{2q_z^2}{\chi'} \right) \bar{\zeta} \\ v_5 &= \left( \frac{5f_z f_5}{\sqrt{2} \psi'_{xy}} \right) \zeta \end{aligned} \quad \dots \quad (10)$$

in which  $f$ 's are very near to 1 and  $q$ 's are about 0.1. The denominators in (10) stand for the energy spacing of various states from the ground level. In the absence of the fine structure absorption spectra results we have taken these to be pure cubic field energy spacings. The situation here is formally similar to the octahedrally co-ordinated  $V^{3+}$  salts (Bose *et al.*, 1964), where also after the introduction of spin-orbit coupling there is a lowest singlet with a doublet above it. However, in that case  $D$  the energy separation between these two lowest levels is less than  $10 \text{ cm}^{-1}$  and the system behaves as with effective spin = 1, though only  $g_{||}$  value has been observed by paramagnetic resonance method (Zverev and Prokhorov, 1958) since the transition for  $g_{\perp}$  can be spanned experimentally only by waves of length  $\sim 1 \text{ mm}$ . In the present case from calculations that follow,  $(\phi_1, \phi'_1)$  will be appreciably populated at ordinary temperatures and matrix elements corresponding  $\langle \phi_1 | L_x + 2S_x | \phi_1 \rangle$ ,  $\langle \phi'_1 | L_z + 2S_z | \phi'_1 \rangle$ , will have non-zero values, while the matrix elements for  $\langle \phi_1 | -2S_x | \phi'_1 \rangle$ , and  $|\langle \phi_1 | L_y + 2S_y | \phi'_1 \rangle|$  are zero, so that the p.m.r. absorption spectrum corresponding to  $g_{||}$  can be obtained, though with a decreased intensity, while  $g_{\perp}$  will be zero. The arrangement of energy levels resembles in some respects that in Cu-acetate where resonance signal comes from a triplet lying  $\sim 315 \text{ cm}^{-1}$  above a non-magnetic singlet (Bleaney and Bowers, 1952) though it must be remembered that in the two cases the mechanisms of the splitting are physically quite different. The expression for  $g$  values are as usual

$$\begin{aligned} g_{||} &= 2[2d^2 - \alpha\kappa_{||}c^2] \\ g_{\perp} &= 0 \end{aligned} \quad \dots \quad (11)$$

but as yet no p.m.r. data are available.



## COMPARISON WITH EXPERIMENTAL MEAN SUSCEPTIBILITY AT DIFFERENT TEMPERATURE

While comparing with experimental results we note that  $P_{||}$ ,  $P_{\perp}$ ,  $Q_{||}$ ,  $Q_{\perp}$  are five adjustable parameters whose values can be decided by fitting with the mean susceptibility at five temperatures (theoretically three since the relative magnitudes of  $P_{||}$ ,  $P_{\perp}$  and  $Q_{||}$ ,  $Q_{\perp}$  are dependent on  $\Delta$ ), if the value of  $\Delta$  is assumed to remain constant with temperature. However, in view of the large number of earlier experimental findings (Bose *et al.*, 1960, 1961, 1964, 1965) it is very unlikely that  $\Delta$  should be constant. But since we do not have any anisotropy or resonance data we are not able to find the values of  $\Delta$  at different temperatures from mean susceptibility, which only was measured for the cubic crystal. On attempting to fit the experimental values on mean susceptibility it is found that no single set of above parameters can bring the fitting within the limits of experimental error at all the temperatures. When the closest approach to one value at a given temperature is made with a given set of parameters the values at other show systematic increasing differences. Since the room temperature experimental mean moment value is always treated as standard we found out the set of the values of the parameters which gave the calculated moment at this temperature very close to the experimental value and also gives nearest approach to the moments at other temperatures. This set of the values of the parameters are  $P_{||} = -240 \text{ cm}^{-1}$ ,  $P_{\perp} = -375 \text{ cm}^{-1}$ ,  $Q_{||} = .7$ ,  $Q_{\perp} = 1.624$  and  $\Delta = -1020 \text{ cm}^{-1}$ . Under the present circumstances we are unable to separately calculate  $\alpha$ 's,  $k$ 's and  $\zeta$ 's from  $P$ 's and  $Q$ 's.  $P_{||}$  and  $P_{\perp}$  can further be written as  $P_{||} = \alpha R_{||} \zeta$  and  $P_{\perp} = \alpha' R_{\perp} \zeta$ , where  $\zeta (= -325 \text{ cm}^{-1}$ ; Bose *et al.*, 1963) is the free ion spin-orbit coupling coefficient for  $\text{Ni}^{2+}$  and so  $\alpha R_{||} = 0.74$  and  $\alpha' R_{\perp} = 1.15$ ;  $R_i$  ( $i = ||$  or  $\perp$ ) is the reduction factor associated with the matrix elements for spin-orbit interaction. These reductions (given by  $k_i$ ,  $R_i$  are due to the anisotropic overlap of the surrounding  $s$ - and  $p$ -ligand charge clouds with the central  $d$ -charge clouds and the admixture of  $3d^7 4p$  configuration with  $3d^8$ .

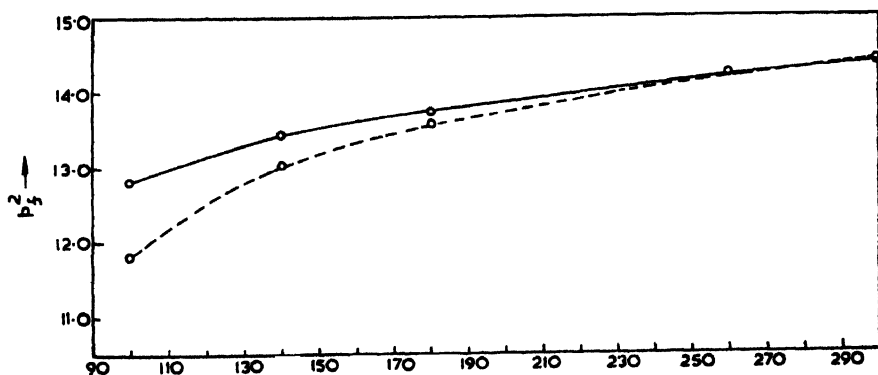


Fig. 1 The full and the dotted curves represent the experimental and theoretical values respectively.

The systematic increasing difference between the experimental and theoretical results as shown in the table (1.2% at 200°K,  $\sim 3.1\%$  at 140°K and  $\sim 7.0\%$  at 100°K) gives a clear evidence of the inadequacy of treating the anisotropic parameters as independent of temperature. In particular the parameter  $\Delta$  might change appreciably from the room temperature value of  $-1026\text{ cm}^{-1}$  in order to wipe out the 7% disagreement in mean susceptibility at low temperatures, since the mean susceptibility is not very sensitive to the changes of  $\Delta$ . Of course as  $\Delta$  changes it is only natural that the relative values of  $P_{\parallel}$ ,  $P_{\perp}$  and  $Q_{\parallel}$ ,  $Q_{\perp}$  will also change correspondingly, thus sharing the task of wiping out the discrepancy between them. This is particularly true for the tetrahedral complexes in which the anisotropic field admixtures and overlaps are comparatively larger than in octahedral complexes and temperature variation of  $\Delta$  may have greater influence on  $(P_{\parallel}, P_{\perp})$  and  $(Q_{\parallel}, Q_{\perp})$ . This effect, in cases where sufficient experimental data on anisotropy and resonance at different temperatures are available, can be introduced as a *second* approximation, the *first* being the calculation of  $P_{\parallel}$ ,  $P_{\perp}$ ,  $Q_{\parallel}$  and  $Q_{\perp}$  as constant and  $\Delta$  as the only variable with temperature as done at present.

One interesting point is that the theoretical  $p_f^2$  versus  $T$  curve (figure) (considering  $\Delta = \text{constant}$ ) shows a rather quicker fall below 200°K ( $kT \sim 140\text{ cm}^{-1}$ ) owing to the fact that (1) the lowest level  $\phi_0$  is non-magnetic and (2) the next higher level  $(\phi_1, \phi'_1)$  is about  $150\text{ cm}^{-1}$ . The experimental data above room temperature is not available. But those below show a steady fall of magnetic moment with temperature down to 100°K instead of a sharp fall. Evidently the theoretical sharp fall is counteracted in practice by the appreciable temperature dependence of the anisotropic part of the field. Finally, we considered the case when  $\Delta$  is

TABLE I

$$\begin{aligned} P_{\parallel} &= -240\text{ cm}^{-1} & P_{\perp} &= -375\text{ cm}^{-1} \\ Q_{\parallel} &= 0.700 & Q_{\perp} &= 1.624 \\ \Delta &= -1020\text{ cm}^{-1} \end{aligned}$$

Temperature °K	Experimental values		Theoretically calculated values	
	$\bar{K} \times 10^8$	$p_f^2$	$\bar{K} \times 10^8$	$p_f^2$
300	5986	14.36	6008	14.41
260	6840	14.22	6840	14.22
180	9536	13.72	9421	13.56
140	11909	13.33	11643	13.03
100	15997	12.79	14759	11.80

positive. But the mean moment in that case would be very much smaller and practically of the higher frequency type which does not agree with experimental magnetic results.

# REFERENCES

- Abragam, A., and Pryce, M. H. L., 1951, *Proc. Roy. Soc. A* **206**, 173.
- Bates, C. A., 1963, *Proc. Phys. Soc.* **83**, 465.
- Bates, C. A., Moore, W. S., Standley, K. J., and Stevens, K. W. H., 1962, *Proc. Phys. Soc.*, **79**, 73.
- Bleaney, B., and Stevens, K. W. H., 1953, *Rep. Prog. Phys.*, **16**, 108.
- Bleaney, B., and Bowers, K. D., 1952, *Proc. Roy. Soc.*, **A214**, 451.
- Bose, A., Mitra, S., and Rai, R., 1965, *Indian J. Phys.*, (In press).
- Bose, A., Chakravarty, A. S., and Chatterjee, R., 1960, *Proc. Roy. Soc.*, **A255**, 145.
- Bose, A., Chatterjee, R., and Rai, R. 1964, *Proc. Phys. Soc.*, **83**, 959.
- Bose, A., Chakravarty, A. S. and Chatterjee, R., 1961(a) *Proc. Roy. Soc. A* **261**, 43.  
-Do- 1961(b) *Proc. Roy. Soc. A* **261**, 207.
- Bose, A. and Chatterjee, R. 1963 *Proc. Phys. Soc.*, **82**, 23.
- Bose, A., Jackson, L.C. and Rai, R. 1965, *Indian J. Phys.* **39**, 7.
- Bose, A. and Rai, R. 1965, *Indian J. Phys.* **39**, 176.
- Gill, N. S., and Nyholm, R. S., 1959, *J. Chem. Soc.*, 2997.
- Goodgame, D. M. L., and Cotton, F. A., 1961, *J. Am. Chem. Soc.*, **83**, 4161.
- Gorter, C. J., 1932, *Phys. Rev.*, **42**, 427.
- Stevens, K. W. H., 1953, *Proc. Roy. Soc.*, **A219**, 542.
- Van Vleck, J. H., 1932, *Phys. Rev.* **41**, 208.  
-Do- 1935, *J. Chem. Phys.* **3**, 807.
- Wolfsberg, M. and Helmholz, L., 1952, *J. Chem. Phys.*, **20**, 837.
- Zverev, G. M. and Prokhorov, A. M., 1958, *J. Exptl. Theo. Phys.* (U.S.S.R.) **34**, 10

# ABSORPTION OF 7.7 mm MICROWAVES BY SOLUTIONS OF SOME SUBSTITUTED NITROBENZENES IN DIFFERENT NON-POLAR SOLVENTS

(Miss) B. SINHA, S. B. ROY AND G. S. KASTHA

OPTICS DEPARTMENT,

INDIAN ASSOCIATION FOR THE CULTIVATION OF SCIENCE,  
CALCUTTA-32.

(Received May 11, 1965)

**ABSTRACT.** The absorption of 7.7 mm microwaves by some substituted nitrobenzenes in solutions in  $\text{CCl}_4$ ,  $\text{C}_6\text{H}_6$ , *n*-hexane and paraffin at different temperatures has been investigated and the  $\tau$ -values for the various polar compounds have been determined. It has been found that while the values of  $\frac{\tau T}{\eta}$  in all the cases do not remain constant and increase with increase of temperature, the values of  $\frac{\tau T}{\eta \gamma}$  (where  $\gamma$  is the ratio of the molar heats of activation for dielectric relaxation and viscous flow) for each of the compounds in solutions in different solvents are found to be constants. From these results, it has been concluded that  $\eta \gamma$  may be taken to be a measure of internal friction.

## INTRODUCTION

In deriving the relation  $\tau = \frac{4\pi\eta_{int} \cdot a^3}{kT}$  between the time of relaxation ( $\tau$ ) at a certain temperature ( $T$ ), the internal viscosity ( $\eta_{int}$ ) and the radius of the rotating dipole ( $a$ ), Debye assumed that the moment of the frictional force acting on the rotating dipole is proportional to its angular velocity and the constant of proportionality  $\zeta$  is given by  $\zeta = 8\pi\eta_{int}a^3$ . The values of ' $a$ ' calculated from the experimentally observed  $\tau$ -values in many cases differ widely from the dimension of the rotor obtained from the chemical bond data. This difference is attributed to (1) non-sphericity of most of the polar molecules, (2) the inadequacy of the macroscopic viscosity ( $\eta$ ) as a measure of the internal friction and (3) non-applicability of the hydrodynamic model of uniform fluid to the solutions possessing macroscopic structure. Fischer (1939, 1949) used the Perrin's (1934) modification of the Debye relation in the case of ellipsoidal molecules and a coefficient of internal friction  $\eta_{int} = \text{const. } \eta$  to calculate the  $\tau$ -values for some polar molecules from the dimensions of the molecules and found some agreement with the experimental values of the time of relaxation for these compound in solution in a certain non-polar solvent at a fixed temperature. The agreement is, however, lost when the solvent is changed (Whiffen, 1950; Hase, 1953). Wirtz and his co-workers

(1953a, b) obtained an expression for  $\zeta$  in case of solutions of spherical polar molecules in solvents composed of spherical molecules in terms of the macroscopic viscosity of the solutions and the ratio of the radii of the two types of molecules. Hill (1954) derived an expression for  $\zeta$  which depended in a complicated way on the macroscopic viscosities of the solvents, the solute and the solution and also on the various parameters of the solvent and solute molecules. Hase (1953) proposed an empirical relation  $\eta_{int} = \eta \exp\left(-\frac{AV_1}{V_2}\right)$ , where  $V_1$  and  $V_2$  respectively are the volumes of the molecules of the solvent and the solute and  $A$  is a constant. However, none of the above mentioned authors have explicitly studied the compatibility of the new expressions for  $\tau$  which they use with the constancy in the values of  $\tau T/\zeta$  at different temperatures. Recently, (Sinha *et al.*, 1964) from a study of the temperature dependence of  $\tau$ -value of nitrobenzene and metanitrotoluene in dilute solutions in medicinal paraffin, it has been suggested that  $\eta^\gamma$  (where  $\gamma$  is the ratio of the molar activation energies for dielectric relaxation and viscous flow) may be a measure of the internal friction. In order to test the general validity of this suggestion and also to find out how the times of relaxation are related to the macroscopic viscosity, the present investigation on the measurement of dielectric loss in dilute solutions of some substituted nitrobenzenes in different non-polar solvents having high as well as low macroscopic viscosity at different temperatures was undertaken in the frequency region of 38.8 KMc/s. The results obtained are discussed in this paper.

#### EXPERIMENTAL

All the substituted nitrobenzenes (*o*-, *m*- and *p*-nitrotoluene, *o*-, *m*- and *p*-chloronitrobenzenes, 2,5-dichloronitrobenzene and 1-Cl-2,4-dinitrobenzene) studied in the present investigation were of chemically pure quality. The liquid compounds were fractionally distilled and the proper fractions were dried by usual method while the solid compounds were purified by repeated crystallisations. The solvents used were  $\text{CCl}_4$ ,  $\text{C}_6\text{H}_6$ , *n*-hexane and medicinal paraffin. The dried solvents showed negligible loss in the frequency region investigated. The experimental arrangements and the method of calculation of loss tangent ( $\tan \delta$ ) were the same as described in an earlier paper (Bhattacharyya *et al.*, 1964).

#### RESULTS AND DISCUSSION

The values of times of relaxation ( $\tau$ ) for the various compounds in solutions in different solvents and at different temperatures ( $T$ ) have been calculated from the experimental  $\tan \delta$  values with the help of the Debye equation for dilute solutions,

$$\tan \delta = \frac{(\epsilon' + 2)^2}{\epsilon'} \cdot \frac{4\pi N c \mu^2}{9}$$

where the various symbols have their usual significance. The values of the dipole moments ( $\mu$ ) of the different polar compounds and the dielectric constant ( $\epsilon'$ ) of the solvents have been taken from the standard literature. The calculated values of  $\tau$  together with the values of temperature ( $T$ ) and loss tangent ( $\tan \delta$ ) are given in Tables I-IX.

The values of molar heats of activation  $\Delta H_\tau$  and  $\Delta H_\eta$  for dielectric relaxation and viscous flow respectively (Eyring *et al.*, 1941) have been determined from the plots of  $\log(T\tau)$  and  $\log \eta$  against  $1/T$  as usual. Some of the graphs are shown in Fig. 1a, 1b and 1c.

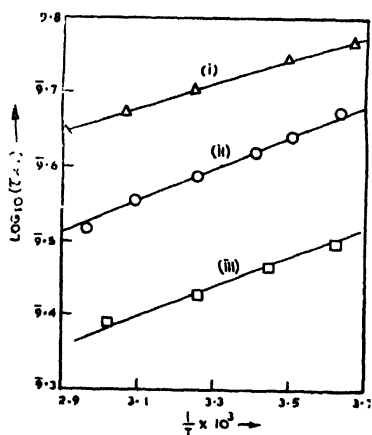


Fig. 1a. Plots of  $\log_{10}(\tau T)$  vs  $1/T$   
 Curve (i) Solution of orthochloronitrobenzene in  $\text{CCl}_4$ .  
 Curve (ii) Solution of orthochloronitrobenzene in  $\text{C}_6\text{H}_6$ .  
 Curve (iii) Solution of orthochloronitrobenzene in  $\text{C}_6\text{H}_{14}$ .

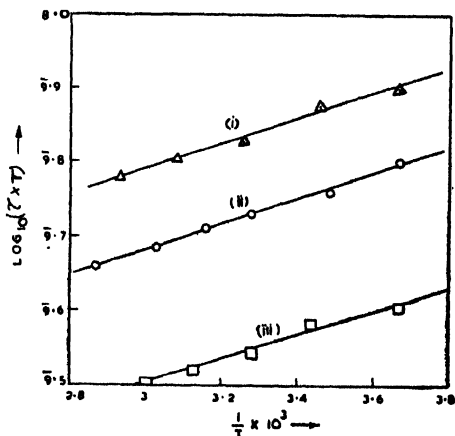


Fig. 1b. Plots of  $\log_{10}(\tau T)$  vs  $1/T$ .  
 Curve (i) Solution of metanitrotoluene in  $\text{CCl}_4$   
 Curve (ii) Solution of metanitrotoluene in  $\text{C}_6\text{H}_6$   
 Curve (iii) Solution of metanitrotoluene in  $\text{C}_6\text{H}_{14}$

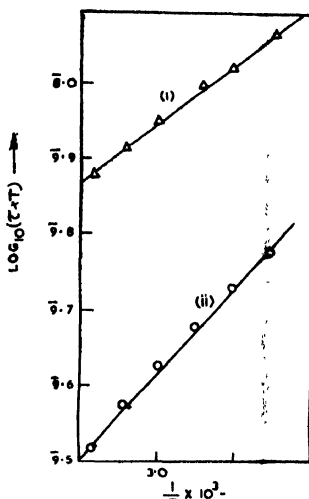


Fig. 1c. Plots of  $\log_{10} (\tau T)$  vs  $1/T$

Curve (i) Solution of metanitrotoluene in medicinal paraffin

Curve (ii) Solution of orthochloronitrobenzene in medicinal paraffin.

The value of  $\Delta H_\tau$  for a particular compound in a given solvent together with the value of  $\Delta H_\eta$  for the solvent are given at the foot of the table for the particular compound.

It can be seen from the Tables that the  $\tau$ -values for a given compound at any temperature in different solvents, increase in the order  $\tau_{CCl_4} > \tau_{C_6H_6} > \tau_{C_6H_{14}}$  for all the nitrobenzenes. From the Debye relation  $\tau = \frac{\zeta}{2KT}$ , it is evident that  $\zeta_{CCl_4} > \zeta_{C_6H_6} > \zeta_{C_6H_{14}}$ . Since the macroscopic viscosities of the solvents increase in the same order viz  $\eta_{CCl_4} > \eta_{C_6H_6} > \eta_{C_6H_{14}}$ , it may reasonably be concluded that  $\zeta$  is functionally dependent on  $\eta$ . However, this dependence is not a linear one because the values of  $\frac{\tau T}{\eta}$  for the different compounds in solutions in the various solvents do not remain constant but increase with increase of temperature or decrease in the value of viscosity. We may, therefore, put  $\zeta = \phi(\eta)$ . Substituting this value in the relation  $\tau = \frac{\zeta}{2KT}$ , we get  $\frac{\tau T}{\phi(\eta)} = \frac{1}{2K} = \text{const.}$  and therefore,  $\frac{d}{dT} \left[ \frac{\tau T}{\phi(\eta)} \right] = 0$ . This equation in conjunction with the relations due to Eyring *et al* (1941).

$$\tau = \frac{A}{T} \cdot e^{\Delta H_\tau / RT} \quad (1)$$

$$\eta = B \cdot e^{\Delta H_\eta / RT} \quad (2)$$

TABLE I  
o-Chloronitrobenzene

Sol. in $\text{CCl}_4$ ( $1.7 \times 10^{-4}$ mole/cc)				Sol. in $\text{C}_6\text{H}_6$ ( $1.7 \times 10^{-4}$ mole/cc)				Sol. in $\text{C}_6\text{H}_{14}$ ( $1.7 \times 10^{-4}$ mole/cc)			
$T^\circ\text{K}$	$\tan \delta \times 10^3$	$\tau \times 10^{12}$ Sec.	$\frac{\tau \cdot T}{\eta \gamma} \times 10^7$	$T^\circ\text{K}$	$\tan \delta \times 10^3$	$\tau \times 10^{12}$ Sec.	$\frac{\tau \cdot T}{\eta \gamma} \times 10^7$	$T^\circ\text{K}$	$\tan \delta \times 10^3$	$\tau \times 10^{12}$ Sec.	$\frac{\tau \cdot T}{\eta \gamma} \times 10^7$
273	33.5	21.46	26.80	275	40.9	17.2	20.81	276	57.1	11.4	16.49
286	34.9	19.48	27.23	285	43.5	15.3	20.38	290	59.4	10.1	16.46
308	37.9	16.38	27.10	293	45.0	14.2	20.48	307	61.7	8.8	16.54
326	39.8	14.50	27.08	307	47.5	12.6	20.43	331	63.0	7.5	16.79
344	41.6	12.88	27.10	323	50.2	11.0	20.45	—	—	—	—

 $\Delta H_f = 0.73\text{K Cal/mole}$  $\Delta H_\eta = 2.44\text{K Cal/mole}$  $\Delta H_f = 0.97\text{K Cal/mole}$  $\Delta H_\eta = 2.53\text{K Cal/mole}$  $\Delta H_f = 0.90\text{K Cal/mole}$  $\Delta H_\eta = 1.84\text{K Cal/mole}$



TABLE II  
*m*-Chloronitrobenzene

Sol. in CCl <sub>4</sub> ( $1.27 \times 10^{-4}$ mole/cc)				Sol. in C <sub>6</sub> H <sub>6</sub> ( $1.27 \times 10^{-4}$ mole/cc)				Sol. in C <sub>6</sub> H <sub>14</sub> ( $1.27 \times 10^{-4}$ mole/cc)			
T°K	tan $\delta \times 10^3$	$\tau \times 10^{12}$ Sec	$\frac{\tau \cdot T}{\eta} \times 10^7$	T°K	tan $\delta \times 10^3$	$\tau \times 10^{12}$ Sec	$\frac{\tau \cdot T}{\eta} \times 10^7$	T°K	tan $\delta \times 10^3$	$\tau \times 10^{12}$ Sec	$\frac{\tau \cdot T}{\eta} \times 10^7$
274	15.2	20.74	20.13	273	19.0	16.20	19.19	273	28.4	9.80	11.62
288	15.8	18.73	21.10	284	19.7	14.89	19.66	286	29.7	8.59	11.48
298	16.3	17.50	21.64	294	20.6	13.60	19.75	294	30.1	7.99	11.61
308	17.4	15.63	21.00	307	21.7	12.43	20.10	308	30.6	7.13	11.82
320	18.3	14.10	20.95	320	22.6	10.90	19.55	319	31.1	6.38	11.70
331	18.7	13.16	21.22	336	23.5	9.75	20.04	338	31.5	5.14	11.08
345	19.2	12.15	21.85	352	24.6	8.35	19.12	—	—	—	—
$\Delta H_\tau = 0.97\text{K Cal/mole.}$				$\Delta H_\tau = 0.96\text{K Cal/mole.}$				$\Delta H_\tau = 1.13\text{K Cal/mole.}$			
$\Delta H_\eta = 2.44\text{K Cal/mole.}$				$\Delta H_\eta = 2.53\text{K Cal/mole.}$				$\Delta H_\eta = 1.84\text{K Cal/mole.}$			

TABLE III  
p-Chloronitrobenzene

Sol. in CCl <sub>4</sub> ( $2.13 \times 10^{-4}$ mole/cc)					Sol. in C <sub>6</sub> H <sub>6</sub> ( $1.94 \times 10^{-4}$ mole/cc)					Sol. in C <sub>6</sub> H <sub>14</sub> ( $1.27 \times 10^{-4}$ mole/cc)					
T°K	tan $\delta \times 10^3$	$\tau \times 10^{12}$ Sec	$\frac{\tau \cdot T}{\eta^2} \times 10^7$	T°K	tan $\delta \times 10^3$	$\tau \times 10^{12}$ Sec	$\frac{\tau \cdot T}{\eta^2} \times 10^7$	T°K	tan $\delta \times 10^3$	$\tau \times 10^{12}$ Sec	$\frac{\tau \cdot T}{\eta^2} \times 10^7$	T°K	tan $\delta \times 10^3$	$\tau \times 10^{12}$ Sec	$\frac{\tau \cdot T}{\eta^2} \times 10^7$
275	11.5	28.6	35.38	273	11.8	25.5	33.75	274	14.9	12.0	14.42				
286	11.9	26.6	36.29	287	12.1	23.4	35.22	285	15.7	10.7	14.20				
296	12.3	24.8	36.80	295	13.1	21.0	33.90	295	16.5	9.5	13.96				
307	13.0	22.3	35.86	307	13.3	19.8	34.90	309	16.9	8.6	14.35				
317	13.4	21.0	36.39	320	13.7	18.4	35.78	319	17.3	7.8	14.30				
333	13.7	19.8	38.15	333	14.0	17.4	37.03	334	17.7	6.8	14.15				
347	14.5	17.4	36.75	348	14.4	14.8	34.91	—	—	—	—				
$\Delta H_\tau = 0.76\text{K Cal/mole.}$					$\Delta H_\tau = 0.83\text{K Cal/mole.}$					$\Delta H_\tau = 1.12\text{K Cal/mole.}$					
$\Delta H_\eta = 2.4\text{K Cal/mole.}$					$\Delta H_\eta = 2.53\text{K Cal/mole.}$					$\Delta H_\eta = 1.85\text{K Cal/mole.}$					

TABLE IV  
*o*-Nitrotoluene

Sol. in CCl <sub>4</sub> (1.69 × 10 <sup>-4</sup> mole/cc)				Sol. in C <sub>6</sub> H <sub>6</sub> (1.69 × 10 <sup>-4</sup> mole/cc)				Sol. in C <sub>6</sub> H <sub>14</sub> (1.69 × 10 <sup>-4</sup> mole/cc)			
T°K	tan δ × 10 <sup>3</sup>	τ × 10 <sup>12</sup> Sec	$\frac{\tau \cdot T}{\eta^2} \times 10^7$	T°K	tan δ × 10 <sup>3</sup>	τ × 10 <sup>12</sup> Sec	$\frac{\tau \cdot T}{\eta^2} \times 10^7$	T°K	tan δ × 10 <sup>3</sup>	τ × 10 <sup>12</sup> Sec	$\frac{\tau \cdot T}{\eta^2} \times 10^7$
275	26.8	21.5	11.33	280	36.5	13.1	12.14	279	53.3	9.8	10.65
284	27.9	19.9	11.91	286	38.2	12.3	12.30	289	54.6	8.8	10.64
298	32.3	16.0	11.65	295	39.9	10.9	12.22	297	55.9	8.3	10.99
308	35.3	13.9	11.37	308	41.5	9.7	12.29	308	56.4	7.2	10.60
319	36.6	12.7	11.81	323	44.3	8.2	12.24	325	60.9	5.7	10.01
328	38.6	11.5	11.66	328	49.8	7.9	12.13	—	—	—	—
341	40.2	10.4	12.12	—	—	—	—	—	—	—	—
$\Delta H_\tau = 1.55\text{K Cal/mole.}$ $\Delta H_\eta = 2.44\text{K Cal/mole.}$				$\Delta H_\tau = 1.35\text{K Cal/mole.}$ $\Delta H_\eta = 2.53\text{K Cal/mole.}$				$\Delta H_\tau = 1.33\text{K Cal/mole.}$ $\Delta H_\eta = 1.84\text{K Cal/mole.}$			

TABLE V  
m-Nitrotoluene

Sol. in $\text{CCl}_4$ ( $1.7 \times 10^{-4}$ mole/cc)				Sol. in $\text{C}_6\text{H}_6$ ( $1.7 \times 10^{-4}$ mole/cc)				Sol. in $\text{C}_6\text{H}_{14}$ ( $1.7 \times 10^{-4}$ mole/cc)			
T <sup>m</sup>	$\tan \delta \times 10^3$	$\tau \times 10^{12}$ Sec	$\frac{\tau \cdot T}{\eta \gamma} \times 10^7$	T <sup>c</sup> K	$\tan \delta \times 10^3$	$\tau \times 10^{12}$ Sec.	$\frac{\tau \cdot T}{\eta \gamma} \times 10^7$	T <sup>c</sup> K	$\tan \delta \times 10^3$	$\tau \times 10^{12}$ Sec	$\frac{\tau \cdot T}{\eta \gamma} \times 10^7$
273	25.0	29.17	34.58	273	30.4	23.02	31.80	273	46.9	14.77	22.76
289	26.2	26.06	35.72	287	32.6	20.15	31.50	291	48.0	13.20	23.30
307	29.0	21.95	34.51	305	34.8	17.60	31.64	305	51.7	11.45	22.53
324	30.4	19.68	35.02	318	35.9	16.21	32.01	320	53.31	10.33	22.74
341	31.8	17.73	35.46	330	37.6	14.72	31.49	333	54.10	9.56	22.86
$\Delta H_f = 0.78\text{K Cal/mole.}$ $\Delta H_\eta = 2.44\text{K Cal/mole.}$				$\Delta H_f = 0.79\text{K Cal/mole.}$ $\Delta H_\eta = 2.53\text{K Cal/mole.}$				$\Delta H_f = 0.78\text{K Cal/mole.}$ $\Delta H_\eta = 1.84\text{K Cal/mole.}$			

TABLE VI  
*p*-Nitrotoluene

Sol. in CCl <sub>4</sub> ( $1.46 \times 10^{-4}$ mole/cc)				Sol. in C <sub>6</sub> H <sub>6</sub> ( $1.46 \times 10^{-4}$ mole/cc)				Sol. in C <sub>6</sub> H <sub>14</sub> ( $1.46 \times 10^{-4}$ mole/cc)			
T°K	$\tan \delta \times 10^3$	$\tau \times 10^{12}$ Sec.	$\frac{\tau \cdot T}{\eta \gamma} \times 10^7$	T°K	$\tan \delta \times 10^3$	$\tau \times 10^{12}$ Sec.	$\frac{\tau \cdot T}{\eta \gamma} \times 10^7$	T°K	$\tan \delta \times 10^3$	$\tau \times 10^{12}$ Sec.	$\frac{\tau \cdot T}{\eta \gamma} \times 10^7$
275	18.9	36.55	40.74	273	22.9	29.7	38.48	273	38.9	19.1	28.24
288	20.8	31.71	40.17	288	25.1	25.3	37.51	288	40.6	17.2	28.64
307	23.0	26.69	39.41	307	27.3	21.8	37.72	307	44.2	14.6	28.21
328	24.5	23.30	40.24	320	28.0	20.2	38.77	329	46.5	12.6	28.51
343	26.0	20.83	40.13	334	30.2	17.8	36.61	—	—	—	—
—	—	—	—	350	32.4	15.6	36.71	—	—	—	—

 $\Delta H_\tau = 0.85\text{K Cal/mole.}$   
 $\Delta H_\eta = 2.44\text{K Cal/mole.}$ 
 $\Delta H_\tau = 0.86\text{K Cal/mole.}$   
 $\Delta H_\eta = 2.53\text{K Cal/mole.}$ 
 $\Delta H_\tau = 0.82\text{K Cal/mole.}$   
 $\Delta H_\eta = 1.84\text{K Cal/mole.}$

TABLE VII  
2, 5-dichloronitrobenzene

Sol. in $\text{CCl}_4$ ( $1.331 \times 10^{-4}$ mole/cc)				Sol. in $\text{C}_6\text{H}_6$ ( $1.321 \times 10^{-4}$ mole/cc)				Sol. in $\text{C}_6\text{H}_{14}$ ( $1.081 \times 10^{-4}$ mole cc)			
T°K	$\tan \delta \times 10^3$	$\tau \times 10^{12}$ Sec.	$\frac{\tau \cdot T}{\eta} \times 10^7$	T°K	$\tan \delta \times 10^3$	$\tau \times 10^{12}$ Sec.	$\frac{\tau \cdot T}{\eta} \times 10^7$	T°K	$\tan \delta \times 10^3$	$\tau \times 10^{12}$ Sec.	$\frac{\tau \cdot T}{\eta} \times 10^7$
277	10.8	35.8	17.58	275	14.2	26.9	27.38	278	19.8	14.3	12.92
288	11.6	31.3	18.21	286	15.2	23.5	26.95	288	21.3	12.6	12.80
297	13.2	26.5	17.46	297	16.2	21.1	27.19	296	22.6	11.3	12.65
307	14.5	23.0	17.04	307	17.6	18.5	26.21	308	23.7	10.6	13.24
320	15.5	20.5	17.81	319	18.4	17.0	26.81	319	24.7	8.9	13.20
327	16.3	18.9	17.74	331	19.0	15.7	27.45	333	26.9	7.2	12.31
337	16.9	17.6	18.40	347	20.2	13.8	27.71	—	—	—	—
$\Delta H_r = 1.67\text{K Cal/mole.}$ $\Delta H_\eta = 2.44\text{K Cal mole.}$				$\Delta H_r = 1.17\text{K Cal/mole.}$ $\Delta H_\eta = 2.53\text{K Cal/mole.}$				$\Delta H_r = 1.57\text{K Cal/mole.}$ $\Delta H_\eta = 1.84\text{K Cal mole.}$			

TABLE VIII  
1-Chloro, 2,4-dinitrobenzene

Sol. in $\text{CCl}_4$ ( $9.97 \times 10^{-5}$ mole/cc)				Sol. in $\text{C}_6\text{H}_6$ ( $1.25 \times 10^{-4}$ mole/cc)			
T°K	$\tan \delta \times 10^3$	$\tau \times 10^{12}$ Sec	$\frac{\tau \cdot T}{\eta \gamma} \times 10^7$	T°K	$\tan \delta \times 10^3$	$\tau \times 10^{12}$ Sec.	$\frac{\tau \cdot T}{\eta \gamma} \times 10^7$
277	7.0	33.4	17.70	276	9.6	30.7	17.78
288	7.9	28.6	17.88	285	10.6	26.8	17.74
295	8.5	25.9	17.78	292	11.5	24.0	17.77
304	9.3	22.6	17.37	297	12.1	22.2	17.74
313	9.7	20.9	17.74	305	13.4	19.6	17.32
321	10.1	19.4	18.05	315	14.3	17.7	17.68
332	11.1	16.9	17.56	323	15.3	15.7	17.45
345	11.7	15.1	18.13	335	16.2	14.1	17.78

 $\Delta H_\tau = 1.58\text{K Cal/mole.}$  $\Delta H_\eta = 2.44\text{K Cal/mole.}$  $\Delta H_\tau = 1.85\text{K Cal/mole.}$  $\Delta H_\eta = 2.53\text{K Cal/mole.}$ 

TABLE IX  
3% Solution in Paraffin

Metanitrotoluene				Orthochloronitrobenzene			
T°K	$\tan \delta \times 10^3$	$\tau \times 10^{12}$ Sec	$\frac{\tau \cdot T}{\eta \gamma} \times 10^7$	T°K	$\tan \delta \times 10^3$	$\tau \times 10^{12}$ Sec	$\frac{\tau \cdot T}{\eta \gamma} \times 10^7$
303	25.8	38.4	27.09	304	38.5	19.8	7.46
313	28.4	33.6	27.72	313	42.4	17.2	7.81
321	30.3	30.7	28.08	323	46.9	14.8	8.04
333	33.3	26.8	28.26	333	51.9	12.7	8.00
343	35.9	24.0	28.32	343	56.4	11.0	8.07
353	38.5	21.6	28.04	353	61.4	9.4	7.79

 $\Delta H_\tau = 1.83\text{K Cal/mole.}$  $\Delta H_\eta = 6.33\text{K Cal/mole.}$  $\Delta H_\tau = 2.66\text{K Cal/mole.}$  $\Delta H_\eta = 6.33\text{K Cal/mole.}$

yields

$$\frac{d\phi}{\phi} = \gamma \cdot \frac{d\eta}{\eta}$$

where

$$\frac{\Delta H\tau}{\Delta H_n}.$$

In equation (2) the factor  $B$  is assumed to be independent of temperature within the range under investigation.

Integration of this equation gives  $\phi(\eta) = D\eta^\gamma$  where  $D$  is a constant. Thus  $\zeta = D\eta^\gamma = \frac{D}{\eta^{1-\gamma}} \cdot \eta$  and since  $\zeta$  has the dimension of erg. sec. and  $\eta$  that of poise ( $ML^{-1}T^{-1}$ ) it is seen that  $D/\eta^{1-\gamma}$  must have the dimension of a volume ( $L^3$ ).

It is evident that  $D$  contains a factor which has the same dimension as that of  $\eta^{1-\gamma}$  and another factor having the dimension of volume. So  $D$  may be written as  $D = C\eta_0^{1-\gamma}$  where  $C$  and  $\eta_0$  are constants for a particular compound in a particular solvent.  $C$  has the dimension of volume and  $\eta_0$  is in poise so that  $\left(\frac{\eta_0}{\eta}\right)^{1-\gamma}$  is a pure fraction.

Thus  $\zeta = D\eta^\gamma = C\left(\frac{\eta_0}{\eta}\right)^{1-\gamma} \eta = 2\tau KT$ . and

$$\frac{\tau T}{\eta^\gamma} = \frac{C}{2K} \eta_0^{1-\gamma} \quad (3)$$

The above equation shows that  $\frac{\tau T}{\eta^\gamma}$  should be a constant for a given polar solute in solution in a given non-polar solvent for all temperatures. Actually, it is found from the Tables that the values of  $\frac{\tau T}{\eta^\gamma}$  are constants which are different in different cases. The values of  $C$  and  $\eta_0$  can not be determined at present but if  $\gamma = 1$ , it is seen that  $\tau = \frac{C \cdot \eta}{2KT}$  which has the same form as the usual expression for  $\tau$  viz  $\tau = \frac{3V}{KT} \cdot \eta$ . For other values of  $\gamma$  if  $\left(\frac{\eta_0}{\eta}\right)^{1-\gamma} \cdot \eta$  is put equal to  $\eta_{int}$ ,  $\tau$  can be written in the form  $\tau = \frac{C}{2KT} \cdot \eta_{int}$ . This expression for  $\eta_{int}$  at once shows why the value of the constant in Fischer's assumption  $\eta_{int} = \text{const.}$   $\eta$  has to be different for different solvents. From these consideration it may be concluded that  $\eta^\gamma$  may be taken to be a measure of internal frictions as has been suggested earlier (Sinha *et al*, 1964). But it should be noted that the value of  $\gamma$  in the latter case is different from that in the present case.



R E F E R E N C E S

- Bhattacharyya, J., Sinha, B. Roy, S. B. and Kastha, G. S., 1964, *Ind. J. Phys.*, **38**, 413.  
Fischer, E., 1939, *Phys. Z.*, **40**, 645.  
-----, 1949, *Z. Phys.*, **127**, 49.  
Gierer, A. and Wirtz, K., 1953a, *Z. Naturf.*, **8a**, 532.  
Glasstone, S., Laidler, K. J. and Eyring, H., 1941, *The Theory of Rate Process* (McGraw Hill Book Company, Inc.)  
Hase, H., 1953, *Z. Naturf.*, **8a**, 695.  
Hill, N. E., 1954, *Proc. Phys. Soc.*, B, **67**, 149.  
Perrin, F., 1934, *J. de Phys.* (7), **5**, 497.  
Sinha, B., Roy, S. B., and Kastha, G. S., 1964, *J. Phys. Soc., Japan*, **19**, 2355.  
Spernol, A. and Wirtz, K., 1953b, *Z. Naturf.*, **8a**, 522.  
Whiffon, D. H., 1950, *Trans. Farad. Soc.*, **46**, 130.

# PRINCIPAL SUSCEPTIBILITIES OF $\text{Eu}^{+++}$ ION IN THE CRYSTAL OF $\text{Eu}_2(\text{SO}_4)_3 \cdot 8\text{H}_2\text{O}$ AT LOW TEMPERATURES

D. NEOGY\* AND A. MOOKHERJI

PHYSICS LABORATORY,  
THE UNIVERSITY, BURDWAN.

(Received May 6, 1965)

**ABSTRACT.** Principal magnetic susceptibilities of  $\text{Eu}_2(\text{SO}_4)_3 \cdot 8\text{H}_2\text{O}$  single crystals have been measured from 300°K to 85°K. It is observed that the magnetic anisotropy is .16 at 300°K which increases to .66 at 85°K. A qualitative explanation of some of the salient magnetic properties have been attempted on the assumption of a crystal field of tetragonal symmetry acting on the  $\text{Eu}^{+++}$  ion.

## INTRODUCTION

The magnetic behaviour of  $\text{Eu}^{+++}$  ion is quite distinct from the rest of the rare earth ions. The only other ion which occupies a similar position is  $\text{Sm}^{+++}$  ion. The ground state for  $\text{Eu}^{+++}$  ion is  ${}^7\text{F}_0$ . The separations of the nearest two levels,  $J = 1$  and  $J = 2$  from the lowest state  $J = 0$  are  $340 \text{ cm}^{-1}$  and  $1000 \text{ cm}^{-1}$  respectively; as a result unlike other ions the multiplet intervals are comparable to  $kT$  in this case. Hence the concentrations of the electrons in higher  $J$ -states at ordinary temperature will not be negligible. Thus the susceptibility for this ion should be calculated for the low-lying levels individually and their statistical average taken. The relative population of these levels will depend upon temperature and hence the effective variation of susceptibility will be a complicated one.

The multiplet intervals being close the interactions among different states will be quite large and hence the second order Zeeman terms will have a major contribution to make for this ion. Laporte (1928) showed that without this term the effective magnetic moment for  $\text{Eu}^{+++}$  ion is only 1.7 instead of 3.53 at 300°K as calculated by Van Vleck and Frank (1929). This portion of susceptibility does not depend on temperature and hence there will be wide departure from Curie Law.

Frank (1935) has discussed theoretically the magnetic behavior of  $\text{Eu}^{+++}$  ion in the crystal of  $\text{Eu}_2(\text{SO}_4)_3 \cdot 8\text{H}_2\text{O}$  under the influence of a crystal field. She

\*Now at Kamerlingh and Onnes Laboratory, Lieden.

finds that a crystal field of cubic symmetry could explain the mean effective moment values as observed by Selwood (1933) and that the rhombic field had very little effect on the mean moment.

It must be pointed out here that owing to the averaging out, the effect of the noncubic part of the field is not so very conspicuous with crystal powder values. It is the measurement with single crystals which can reveal the noncubic field effect precisely. Hence we have measured the principal magnetic susceptibilities of single crystals of  $\text{Eu}_2(\text{SO}_4)_3 \cdot 8\text{H}_2\text{O}$  from 300°K to 85°K. The results are discussed in the light of a crystal field of tetragonal symmetry.

## EXPERIMENTAL

Europium sulphate was prepared from a spectroscopic pure variety of Europium oxide supplied by Johnson and Mathey Co., London. The crystals were grown out of an aqueous solution by slow evaporation at room temperature.

The magnetic anisotropy and the absolute susceptibility at room temperature were measured respectively by the well-known method of Krishnan and Banerji (1935) and by a microbalance as devised by Neogy and Lal (1962).

Low temperature measurements were carried out following the procedure of Krishnan *et al* (1939). The temperature within the experimental tube was held constant at any desired value by the help of a liquid bath type of cryostat (Bose *et al* 1963).

## RESULTS

The crystal is monoclinic.  $X_3$  represents the gram molecular susceptibility along 'b' crystallographic axis, while greater of the two in the (010) plane is denoted by  $X_1$  and the smaller by  $X_2$ .  $\theta$  is the angle which  $X_2$ -axis makes with 'a' axis. The unit adopted is  $10^{-6}$  C.G.S.E.M.U. The mean effective Bohr magneton number  $2\bar{\mu}$  is  $\sqrt{3kT\bar{K}/N\beta^2}$  where  $\bar{\mu} = \sqrt{2\bar{\mu}_1^2 + \bar{\mu}_2^2}/3$  and  $\bar{K} = K_{\parallel} + 2K_{\perp}/3$ . The results are collected in Table I.

## DISCUSSION

### a) Magnetic anisotropy in relation to crystal structure

X-ray studies (Zachariasen 1935) show that the crystal is monoclinic in the space group  $C_{2h}^6$  with eight paramagnetic complexes in the unit cell of the crystal. Out of these eight, four are oriented parallel to the other four and shifted to a glide plane. The four units in any set are related amongst themselves by a two-fold axis 'b' and a plane of reflexion (010). Thus magnetically there will be two inequivalent complexes per unit cell. This is in agreement with the PMR findings of Bogle and Heine (1954) on  $\text{Gd}_2(\text{SO}_4)_3 \cdot 8\text{H}_2\text{O}$  single crystals which is isomorphous with  $\text{Eu}_2(\text{SO}_4)_3 \cdot 8\text{H}_2\text{O}$ .

reasonable as  $V_2^0$  depends on the shape of the unit cell and atomic position coordinates; but nothing can be said conclusively till rigorous theoretical calculations are undertaken.

## REFERENCES

- Bethe, H., 1929, *Ann. der. Physik* **3**, 133.  
Bose, A., Dutta Roy, S. K., Ghose, P. K. and Mitra, S. 1963, *Ind. J. Phys.* **35**, 505.  
Boglic, G. S. and Heine, V., 1954, *Proc. Roy. Soc.* **67**, 734.  
Chachra, S. P., 1965, *Ind. J. Pure and Appl. Phys.* (Communicated).  
Frank, A., 1935, *Phys. Rev.* **48**, 771.  
Krishnan, K. S. and Banerji, S., 1935, *Philos. Trans.* **234**, 265.  
Krishnan, K. S., Mookherji, A. and Bose A., 1939, **238**, 125.  
Laporte, 1928, *Zeits. F. Physik*, **47**, 761.  
Mookherji, A., 1945, *Ind. J. Phys.* **19**, 63.  
Neogy, D. 1963, *Physica*, **29**, 974.  
Neogy, D. and Mookherji, A., 1965, *Physica* (accepted).  
Neogy, D. and Lal, R. B., 1962, *J. Sci. Ind. Res.* **21B**, 103.  
Selwood P. W., 1933, *J. Am. Chem. Soc.* **55**, 3161.  
Steven, K. W. H., 1952, *Proc. Phys. Soc.* **65**, 209.  
Syre, E. V. and Freed, S., 1958, *J. Chem. Phys.* **24**, 1211.  
Van Vleck, J. H. and Frank, A., 1929, *Phys. Rev.* **34**, 1494.  
Zachariasen, W. H., 1935, *J. Chem. Phys.* **3**, 197.

# SCATTERING OF ELECTROMAGNETIC WAVES BY PLASMA

R. M. KHAN AND T. P. KHAN

DEPARTMENT OF PHYSICS

JADAVPUR UNIVERSITY

CALCUTTA-32

(Received June 7, 1965)

**ABSTRACT.** In this paper we have treated the case of reflection and refraction of plane electromagnetic wave by plasma in an applied magnetic field. The component of the magnetic field perpendicular to the plane of incidence in the reflected wave provides an easy means of analysing the physical features of the plasma.

## INTRODUCTION

The physical characteristics of a homogeneous plasma can be determined in various ways. We propose a simple way which utilises the anisotropic behaviour of plasma under an applied magnetic field. The external magnetic field thus as if removes the degeneracy. The various micro-effects are however not taken separately but their net effect is considered macroscopically. Thus the whole of the uniform plasma behaves like an anisotropic medium under the externally applied magnetic field. The co-efficients of anisotropy are dependent on the physical characteristics of the plasma. Thus the experimental determination of the field components of scattered electromagnetic fields from such a plasma will go to determine some of its internal details.

## THE PLANE WAVES

Consider a semiinfinite homogeneous plasma. We choose our co-ordinates in such a way that

$Z = 0$  is the plasma boundary,

$Z > 0$  is plasma region,

$Z < 0$  is vacuum.

Let us suppose that there is an imposed external homogeneous magnetic field  $H$  parallel to the  $Z$ -direction. Under these circumstances the plasma region may be approximated as an anisotropic medium of dielectric tensor  $\epsilon$  where

$$\epsilon = \begin{bmatrix} \epsilon_1 & \epsilon^* & 0 \\ \epsilon & \epsilon_2 & 0 \\ 0 & 0 & \epsilon_3 \end{bmatrix} \quad \dots (1)$$

We now consider the propagation of a plane electromagnetic wave towards the plasma region where it will suffer reflection and refraction. The case when the incident wave will have the magnetic field perpendicular to the plane of incidence may be taken to discuss the situation. Calling the incident plane to be the  $x-z$  plane we have

$$\vec{H} \text{ incident} = \vec{B}_0 e^{i\omega \left( t - \frac{\vec{r} \cdot \vec{n}_0}{c} \right)} \quad \dots (2)$$

$$\vec{H} \text{ reflected} = \vec{B}_1 e^{i\omega \left( t - \frac{\vec{r} \cdot \vec{n}_1}{c} \right)} \quad \dots (3)$$

and 
$$\vec{H}' \text{ refracted} = \vec{B}_2 e^{i\omega \left( t - \frac{\vec{r} \cdot \vec{n}_2}{v_2} \right)} \quad \dots (4)$$

$$\vec{H}'' \text{ refracted} = \vec{B}_3 e^{i\omega \left( t - \frac{\vec{r} \cdot \vec{n}_3}{v_3} \right)} \quad \dots (5)$$

where  $\vec{n}_i = \sin \theta_i \cos \phi_i \vec{i} + \sin \theta_i \sin \phi_i \vec{j} + \cos \theta_i \vec{k}$ . ( $\vec{i}, \vec{j}, \vec{k}$  are the unit vectors)  $c$  and  $v$  are the velocities of wave propagation in vacuum and plasma.

#### FIELD COMPONENTS

For the incident wave putting  $\vec{B}_0 = \vec{B} \vec{j}$  and  $\theta_0 = \theta =$  the angle of incidence and  $\phi_0 = 0$  by choice, we obviously find from the continuity conditions of the magnetic field

$$\theta_1 = \theta, \quad \phi_1 = 0 \quad \text{and} \quad \frac{\sin \theta}{c} = \frac{\sin \theta_2}{v_2} = \frac{\sin \theta_3}{v_3} \quad \dots (6)$$

also

$$B + B_1 = B_2 + B_3 \quad \dots (7)$$

$$C_1 \cos \theta = -C_2 \cos \theta_2 - C_3 \cos \theta_3 \quad \dots (8)$$

$$C_1 \sin \theta = C_2 \sin \theta_2 + C_3 \sin \theta_3 \quad \dots (9)$$

We have called  $B_i$  and  $C_i$  the components of  $\vec{B}_i$  in the incident plane and perpendicular to that plane respectively.

The electric displacement vector  $\vec{D}$  will have its normal component continuous because of (7). We have the electric field vector

$$\vec{E} = -\frac{c}{v} \vec{E}^{-1} [\vec{n} \times \vec{H}] \quad \dots (10)$$

The continuity of tangential components of  $\vec{E}$  leads to

$$B \cos \theta - B_1 \cos \theta = \frac{c}{v_2} (a_1 B_2 \cos \theta_2 + a^* C_2) + \frac{c}{v_3} (a_1 B_3 \cos \theta_3 + a^* C_3) \dots \quad (11)$$

and

$$C_1 = \frac{c}{v_1} (a B_2 \cos \theta_2 + a_2 C_2) + \frac{c}{v_1} (a B_3 \cos \theta_3 + a_2 C_3) \dots \quad (12)$$

Where

$$\epsilon^{-1} = \begin{bmatrix} a_1 & a^* & 0 \\ a & a_2 & 0 \\ 0 & 0 & a_3 \end{bmatrix}$$

we have further from Maxwell's equations.

$$\frac{v_2^2}{c^2} C_2 = a B_2 \cos \theta_2 + a_2 C_2 \quad (13)$$

$$\frac{v_3^2}{c^2} C_3 = a B_3 \cos \theta_3 + a_2 C_3 \quad \dots \quad (14)$$

$$\frac{v_2^2}{c^2} B_2 = a_1 B_2 \cos^2 \theta_2 + a^* C_2 \cos \theta_2 + a_3 B_2 \sin^2 \theta_2 \quad \dots \quad (15)$$

$$\frac{v_3^2}{c^2} B_3 = a_1 B_3 \cos^2 \theta_3 + a^* C_3 \cos \theta_3 + a_3 B_3 \sin^2 \theta_3 \quad \dots \quad (16)$$

The six quantities  $B_i$  and  $C_i$  can be obtained from the seven equations (7), (8), (9), (11), (12), (13) and (14) in terms of the incident intensity  $B$ . Equations (13) and (15) lead to the same equation as equations (14) and (16), e.g.

$$\{1 + (a_1 - a_3) \sin^2 \theta\} \frac{v^4}{c^4} - \{a_1 + a_2 + (a_1 a_2 - a_2 a_3 - a a^*) \sin^2 \theta\} \frac{v^2}{c^2} + a_1 a_2 - a a^* = 0 \dots (17)$$

which really determine the two velocities inside the plasma,  $v_2$  and  $v_3$  and these along with equation (6) give the angle of refractions  $\theta_2$  and  $\theta_3$ . From (17) we obtain

$$\frac{v^2}{c^2} = [a_1 + a_2 + (a_1 a_2 - a_2 a_3 - a a^*) \sin^2 \theta \pm \sqrt{\{a_1 + a_2 + (a_1 a_2 - a_2 a_3 - a a^*) \sin^2 \theta\}^2 - 4(a_1 a_2 - a a^*)\{1 + (a_1 - a_3) \sin^2 \theta\}}] / 2\{1 + (a_1 - a_3) \sin^2 \theta\} \quad \dots \quad (18)$$

From equations (7) - (14) we get

$$B_1 = \frac{C_1}{2 \sin(\theta_2 - \theta_3)} \left[ \frac{1}{a} \left( \frac{v_2^2}{c^2} - a_2 \right) \sin(\theta + \theta_3) \left( \frac{1}{\cos \theta_2} - \tan \theta \frac{a_1}{\sin \theta_3} \right) \right]$$

$$\begin{aligned}
& -\frac{1}{a} \left( \frac{v_3^2}{c^2} - a_2 \right) \sin(\theta + \theta_2) \left( \frac{1}{\cos \theta_3} - \tan \theta \frac{a_1}{\sin \theta_3} \right) \\
& - a^* \tan \theta \left\{ \frac{\sin(\theta + \theta_3)}{\sin \theta_2} - \frac{\sin(\theta + \theta_2)}{\sin \theta_3} \right\} \quad \dots \quad (19)
\end{aligned}$$

$$\begin{aligned}
\text{and } C_1 &= 2B \sin(\theta_2 - \theta_3) \left/ \left[ \frac{1}{a} \left( \frac{v_2^2}{c^2} - a_2 \right) \sin(\theta + \theta_3) \left( \frac{1}{\cos \theta_2} + \tan \theta \frac{a_1}{\sin \theta_2} \right) \right. \right. \\
& - \frac{1}{a} \left( \frac{v_3^2}{c^2} - a_2 \right) \sin(\theta + \theta_2) \left( \frac{1}{\cos \theta_3} + \tan \theta \frac{a_1}{\sin \theta_3} \right) \\
& \left. \left. + a^* \tan \theta \left\{ \frac{\sin(\theta + \theta_3)}{\sin \theta_2} - \frac{\sin(\theta + \theta_2)}{\sin \theta_3} \right\} \right] \right. \quad \dots \quad (20)
\end{aligned}$$

We particularly focus our attention to the reflected wave, since it will be outside the plasma and can be easily measured.

When the anisotropy will be small as is usually the case in the plasma under consideration we may make first order approximations and equations (18), (19) and (20) give

$$v_2 = c \left\{ 1 - \frac{1}{2} \eta + \frac{1}{4} (\eta + \delta) \sin^2 \theta + \frac{1}{4} \times \right\} \quad \dots \quad (21)$$

$$v_3 = c \left\{ 1 - \frac{1}{2} \eta + \frac{1}{4} (\eta + \delta) \sin^2 \theta - \frac{1}{4} \times \right\} \quad \dots \quad (22)$$

$$B_1 = B \left\{ -\frac{1}{4} \eta \sec^2 \theta + \frac{1}{2} (\eta + \delta) \tan^2 \theta \sin^2 \theta \right\} \quad \dots \quad (23)$$

$$C_1 = -B \frac{\epsilon}{\cos \theta} \quad \dots \quad (24)$$

where

$$\epsilon = \begin{bmatrix} 1 + \eta & \epsilon^* & 0 \\ \epsilon & 1 + \eta & 0 \\ 0 & 0 & 1 - \delta \end{bmatrix}$$

$\eta, \delta, \epsilon$  are first order small quantities and

$$X = \sqrt{\{(\eta + \delta)^2 \sin^4 \theta + 4\epsilon\epsilon^* \cos^2 \theta\}}$$



## MEASUREMENTS

If the plasma be kept without any applied field, no anisotropy occurs and  $C_1$  in (24) is necessary zero. Applying a magnetic field, sending a polarized wide beam and subsequently measuring  $C_1$  with a tuned coil (measuring the induced voltage) one can verify the result (24) and also get  $|\epsilon|$ . The waves should not be near grazing incidence as then (24) will not hold. This  $|\epsilon|$  is

$$\sum_k \frac{\Omega_k \omega_k}{\omega(\omega_k^2 - \omega^2)}$$

A plot of (25) or even the induced voltage in the coil against the frequency will have peaking at  $\omega_k$ . Also the values of  $(\omega^2 - \omega_k^2)|\epsilon|$  near  $\omega_k$ 's will give the values of  $\Omega_k$ . In the strict sense however one can not take  $\epsilon$  to be given by (24) at the poles rather one should use (20). The expressions of  $\Omega_k$  and  $\omega_k$  being<sup>(1)</sup>

$$\Omega_k^2 = n_k e^2 / m_k \quad \dots \quad (26)$$

$$\omega_k = e_k B / m_k. \quad \dots \quad (27)$$

The determinations of these give the values of the ionized masses and the fraction ionized, the state of ionization.

## REFERENCE

Astrom 1951, *Arkiv fur Physik.* **2**.

# Letters to the Editor

The Board of Editors does not hold itself responsible for opinions expressed in the letters published in this section. The notes containing short reports of original investigations communicated to this section should not contain many figures and should not exceed 500 words in length. The contributions reaching the Secretary by the 15th of any month may be expected to appear in the issue for the next month. No proof will be sent to the author.

16

## VARIATION OF THE RELAXATION TIME AND THE MOLAR FREE ENERGY OF ACTIVATION WITH THE C-AXIS SPACING ( $d_{001}$ ) OF SOME COMPLEXES OF BENTONITE

SABITA GHOSH

KHATRA LABORATORY OF PHYSICS,

UNIVERSITY COLLEGE OF SCIENCE, CALCUTTA.

(Received May 10, 1965)

### Plate—II

The clay mineral montmorillonite (commonly called bentonite) displays an expansion in *c*-axis spacing depending on size and the charge of the exchangeable cations (Barshad, 1950) and the adsorbed water molecules (Grim, 1953) between the negatively charged silicate layers. The extent of expansion depends on the interaction between the binding force, which acts from layer to layer through the interlayer cations, and the expansion force created by the adsorption of the water molecules on the interlayer surfaces (Jonas, *et al* 1960).

In the present note, it is reported how the dielectric properties vary with the *c*-axis expansion in different complexes of bentonite brought about by the cation exchange process. To observe the variation in the *c*-axis spacing ( $d_{001}$ ) the powdered raw sample (England) was sieved through a 200-mesh screen and brought in suspension in water. The complexes of the mineral with  $H^+$ ,  $Li^+$ ,  $Na^+$ ,  $K^+$ ,  $Mg^{2+}$ ,  $Ca^{2+}$  and  $Ba^{2+}$  ions were made by percolating the suspension through different columns of the cation exchange resin (IR 120, Amberlite) previously converted into the desirable cation forms. All the samples were dried under same relative humidity and the X-ray photographs were taken with  $CuK_{\alpha}$  radiation (using Ni-filter) in a Debye-Scherrer camera of radius 9.956 cm. One such photograph is shown in Fig. 1.



Fig. 1.—X-ray Photograph for Mg. Complex



The loss-tangent ( $\tan \delta$ ) and the dielectric constant ( $\epsilon'$ ) of the above clay-complexes were measured at 30°C with the help of a Q-meter within the range of frequencies from 100 Kc/sec to 4 Mc/sec following the same method as adopted previously by the author (Ghosh, 1962). The relaxation times ( $\tau$ ) for these samples were then determined from the frequency of maximum absorption and hence the values of molar free energy of activation for dipole relaxation were calculated

from the formula,  $\frac{1}{\tau} = \frac{kT}{h} \exp \frac{-\Delta G^*}{RT}$  where  $\Delta G^*$  is the molar free energy of

activation and the other symbols have their usual significance. The values of relaxation time for H, Li, Na, K, Mg, Ca and Ba complexes are  $6.10 \times 10^{-7}$  sec.,  $7.53 \times 10^{-7}$  sec.,  $1.03 \times 10^{-6}$  sec.,  $1.05 \times 10^{-6}$  sec.,  $4.81 \times 10^{-7}$  sec.,  $6.10 \times 10^{-7}$  sec. and  $7.53 \times 10^{-7}$  sec. respectively.

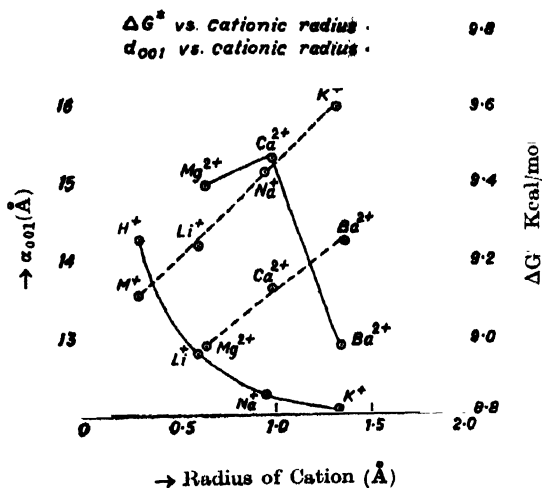


Fig. 2. Variation of  $d_{001}$  and  $\Delta G^*$  with cationic radius.

The observed variations of the  $c$ -axis spacing ( $d_{001}$ ) and activation energy ( $\Delta G^*$ ) with the radius of the cations is shown in Fig. 2 for monovalent and divalent cation complexes and can be understood in the following manner: Since the molar free energy of activation is found to increase with the cationic radii, it can be said that the binding with the two silicate layers is stronger for the larger cations and for more polarizable ones in these cases. This is consistent with the observation that there is a gradual decrease in  $c$ -axis spacing with the cationic radii in the case of monovalent and divalent cations except for Ca<sup>2+</sup>-ion. This decrease of spacing indicates that the binding force, acting through the charged material between the silicate layers, gradually increases with the radius of the cations. In case of Ca-complex (having larger spacing than Mg-complex) the increase in activation energy may be due to the fact that Ca<sup>2+</sup> is more polarizable than Mg<sup>2+</sup> which increases the activation energy.

A significant feature is to be noted from Fig. 2. Considering the valencies of the cations having nearly the same size, viz., ( $\text{Mg}^{2+}$ ,  $\text{Li}^+$ ), ( $\text{Ca}^{2+}$ ,  $\text{Na}^+$ ), ( $\text{Ba}^{2+}$ ,  $\text{K}^+$ ) etc., it can be seen that the activation energy for the divalent cation is less than that for monovalent cation for each of the Sepairs. This indicates lowering of binding between the silicate layers in case of divalent cations. This lowering of binding energy is evidently due to the increase of spacing by the greater adsorption of water molecules between the silicate layers for divalent cation-complex.

My sincere thanks are due to Professor S. R. Khastgir, under whose guidance the present work was carried out.

#### R E F E R E N C E S

- Barshad, I., 1950, *Am. Min.*, **35**, 225.  
Ghosh, S., 1962, *J. Chem. Phys.*, **37**, 199.  
Grim, R. E., *Clay Mineralogy*, (McGraw-Hill Book Company, Inc., 1953), pp. 257-260.  
Jonas, E. and Roberson Herman E., 1960, *Am. Min.*, **45**, 828.

## BOOK REVIEW

**A STAR CALLED THE SUN**—G. Gamow, 35 sh. net, McMillan and Co., London.

This modernized version of Gamow's older book is welcome not only as another popular presentation of a vast mass of modern scientific facts relating to stars in general and the sun in particular, to which the author's own contribution is considerable, but also as an outstanding piece of literature which one expects from the facile pen of Gamow. Perusing the explanatory expositions of the many basic principles connected with the solar theories a layman may have once or twice the feeling of going astray in the maze. But Gamow pulls him right back at the right moment with not much of a jerk and sets him again on the road to the goal.

It is hardly necessary to go into the merits of a book coming from Gamow but drawbacks should be pointed out to prevent the layman from stumbling and looking askance. For example, an obvious oversight on page 58 in joining together lithium and fluorine and giving lithium hydrate as the progeny will tickle the chemical geneticists. Taking the next few lines about the manner of formation of water from hydrogen and oxygen in the context of the ionic mechanism of combination of lithium and fluorine given in the preceding lines, may lead to admonitive headshakes from the same quarters.

On page 125, a layman expected a little more in the way of an explanation of the paradox of  $\alpha$ -particles tunnelling in and out through the potential hill, instead of simply referring to Quantum Mechanics, as the solver of the paradox.

On page 151, 5th and 6th line the statement on ordinate and abscissa is likely to confuse a layman, with his usual knowledge of graphic representation.

It is indeed very satisfying that amongst the shining galaxy of astrophysicists of the world at least three of my countrymen are given prominent positions in Gamow's book. But I wish that on pages 147 and 176 the obvious typographic misspelling of the name of Prof. Meghnad Saha be corrected.

A. Bose

# LIGAND FIELD THEORY OF MAGNETIC SUSCEPTIBILITY AND ANISOTROPY IN $\text{CoSiF}_6 \cdot 6\text{H}_2\text{O}$

A. Bose, L. C. Jackson AND R. Rai

Vol. 39 No. 1, January, 1965

Page 11 eqn. (8) fourth line from the bottom—

instead of  $2(3a_s a_s - \alpha \kappa_{||} b_s b_s + b_s b_s)$

read :  $\frac{3a_s a_s - \alpha \kappa_{||} b_s b_s + b_s b_s}{E_s - E_g}^2$

Page 11 eqn. (8) fifth line from the bottom

instead of  $2(3 - \alpha \kappa_{||})$

read ;  $2(3 - \alpha \kappa_{||})^2$

Page 13 eqn. (11)

instead of  $g_{||} = 2\{2\alpha \kappa_{||}(a^2 - c^2) + 3a^2 + b^2 + c^2\}$

$g_{\perp} = 2\{-\sqrt{2}bc\alpha'\kappa_{\perp} + 2\sqrt{3}ac + 2b^2\}$

read :  $g_{||} = 2\{\alpha \kappa_{||}(a_1^2 - c_1^2) + 3a_1^2 + b_1^2 - c_1^2\}$

$g_{\perp} = 2\{-\sqrt{2}b_1c_1\alpha'\kappa_{\perp} + 2\sqrt{3}a_1c_1 + 2b_1^2\}$

## LIGAND FIELD THEORY OF SUSCEPTIBILITY AND ANISOTROPY IN TRIGONALLY DISTORTED $\text{Fe}^{2+}$ COMPLEXES

A. Bose AND R. Rai

Vol. 39, No. 4, April 1965

Page 179 eqn. (6)

instead of:  $E_7 = \frac{1}{2} [(\Delta - \alpha s_{||}) + \{(\Delta + \alpha s_{||}) + 8\alpha'^2 s_{\perp}^2\}^{\frac{1}{2}}]$

read  $E_7 = \frac{1}{2} [(\Delta - \alpha s_{||}) + \{(\Delta + \alpha s_{||})^2 + 8\alpha'^2 s_{\perp}^2\}^{\frac{1}{2}}]$

Page 182 eqn. (14) fourth and fifth lines from the bottom—

instead of :  $2\left(2a_s - \frac{\alpha'\kappa_{\perp}}{\sqrt{2}}b_s\right)^2$

read :  $2\left(2a_s + \frac{\alpha'\kappa_{\perp}}{\sqrt{2}}b_s\right)^2$

Page 183 eqn. (15) first line from the top—

instead of :  $A_{sj} = \sqrt{3}(b_s a_j - 2a_s b_j) - \frac{\alpha'\kappa_{\perp}}{2}(b_s b_j - 2a_s a_j) + \sqrt{2}b_s b_j$

read :  $A_{sj} = \sqrt{3}(b_s a_j - 2a_s a_j) - \frac{\alpha'\kappa_{\perp}}{2}(b_s b_j - 2a_s a_j) + \sqrt{2}b_s a_j$



# ERRATA

(An Analysis of the *J*-Phenomenon in Scattered X-rays, Part II)

March Issue 1965.

Page 110	line 16	read (1925b, 1926b, 1927)	instead of 1925b), 26b, 27)
" 111	" 33	read $\lambda + \delta\lambda_\phi$	" " $\lambda + \delta\lambda_\rho$
" 114	" 16	delete 'to' after signifies	
	last line	read verified	instead of varified
" 117	line 9	read $I_x$	" " $I_x$
	" 11	read $I_x =$	" " $I_x =$
" 118	" 5		
	(denominator)	read $\omega$	" " $\omega'$
	line 17	read $\Delta\phi$	" " $\Delta\rho$
" 119	lines 10 and 11	read (	" " ( (
	line 11	insest an asteris $k'$ after]	
" 121	" 13	read} instead of (	
		and delete} near $+(A_2 - A'_2)y$	
" 122	" 20	read $C_\phi$	instead of $C\phi$
	" 21	read $\delta\lambda_\phi$	" " $\delta\lambda_\xi$
" 124	" 11	delete 'short'	
" 125	" 21	read $\phi$ as a subscript to $(S'/P')$	
	" 26	read wax	instead of was
" 126	foot note	read $x_\phi$	" " $x_\phi$
" 127	" 12	read (1926b)	" " (1962b)
	" 21	delete {and}	
	" 22		
	(denominator)	read $(S'/P')_\phi$	$(S'P')_\phi$
	line 28	read $(S'/P')_{30^\circ}$	$(S'P')_{30^\circ}$
		read $(S/P)_{32^\circ}$	$(S^\circ/P)_{30^\circ}$
" 128	" 1	read equality	quality °
	" 37	delete asterik*	after (30)
Pages 129 &			
130	" 20	read $x_\phi$	instead of $x_\phi$
Page 130	" 19	insert small at the end	
Page 130	foot note	read .015	0.15
" 131	line 25	raise 'ratio falls' to the	beginning of the previous line.
" 132	" 11	read $A_1'$	instead of $A'_y$





# LIGAND FIELD THEORY OF MAGNETIC SUSCEPTIBILITY AND ANISOTROPY IN $\text{CoSiF}_6 \cdot 6\text{H}_2\text{O}$

A. Bose, L. C. Jackson AND R. Rai

Vol. 39 No. 1, January, 1965

Page 11 eqn. (8) fourth line from the bottom—

instead of  $2(3a_s a_s - \alpha \kappa_{||} b_s b_s + b_s b_s)$

read :  $\frac{2}{E_s - E_s} (3a_s a_s - \alpha \kappa_{||} b_s b_s + b_s b_s)^2$

Page 11 eqn. (8) fifth line from the bottom

instead of  $2(3 - \alpha \kappa_{||})$

read ;  $2(3 - \alpha \kappa_{||})^2$

Page 13 eqn. (11)

instead of :  $g_{||} = 2\{2\alpha \kappa_{||}(a^2 - c^2) + 3a^2 + b^2 + c^2\}$

$g_{\perp} = 2\{-\sqrt{2}bc\alpha' \kappa_{\perp} + 2\sqrt{3}ac + 2b^2\}$

read :  $g_{||} = 2\{\alpha \kappa_{||}(a_1^2 - c_1^2) + 3a_1^2 + b_1^2 - c_1^2\}$

$g_{\perp} = 2\{-\sqrt{2}b_1 c_1 \alpha' \kappa_{\perp} + 2\sqrt{3}a_1 c_1 + 2b_1^2\}$

## LIGAND FIELD THEORY OF SUSCEPTIBILITY AND ANISOTROPY IN TRIGONALLY DISTORTED

$\text{Fe}^{3+}$  COMPLEXES

A. Bose AND R. Rai

Vol. 39, No. 4, April 1965

Page 179 eqn. (6)

instead of:  $E_7 = \frac{1}{2} [(\Delta - \alpha s_{||}) + \{(\Delta + \alpha s_{||}) + 8\alpha'^2 s_{\perp}^2\}^{\frac{1}{2}}]$

read  $E_7 = \frac{1}{2} [(\Delta - \alpha s_{||}) + \{(\Delta + \alpha s_{||})^2 + 8\alpha'^2 s_{\perp}^2\}^{\frac{1}{2}}]$

Page 182 eqn. (14) fourth and fifth lines from the bottom—

instead of :  $2\left(2a_z - \frac{\alpha' \kappa_{\perp}}{\sqrt{2}} b_z\right)^2$

read :  $2\left(2a_z + \frac{\alpha' \kappa_{\perp}}{\sqrt{2}} b_z\right)^2$

Page 183 eqn. (15) first line from the top—

instead of :  $A_{sj} = \sqrt{3}(b_s a_j - 2a_s b_j) - \frac{\alpha' \kappa_{\perp}}{2}(b_s b_j - 2a_s a_j) + \sqrt{2}b_s b_j$

read :  $A_{sj} = \sqrt{3}(b_s a_j - 2a_s a_j) - \frac{\alpha' \kappa_{\perp}}{2}(b_s b_j - 2a_s a_j) + \sqrt{2}b_s c_j$

# ERRATA

(An Analysis of the J-Phenomenon in Scattered X-rays, Part II)

March Issue 1965.

Page 110	line 16	read (1925b, 1926b, 1927) instead of 1925b), 26b, 27)
" 111	" 33	read $\lambda + \delta\lambda_\phi$ " " $\lambda + \delta\lambda_\rho$
" 114	" 16	delete 'to' after signifies
	last line	read verified instead of varified
" 117	line 9	read $I_x$ " " $I_x$
	" 11	read $I_x =$ " " $I_x =$
" 118	" 5	
	(denominator)	read $\omega$ " " $\omega'$
	line 17	read $\Delta_\phi$ " " $\Delta_\rho$
" 119	lines 10 and 11	read ( " " ( (
	line 11	insert an asterisk $k^*$ after]
" 121	" 13	read } instead of ( and delete } near $+ (A_2 - A'_2)y$
" 122	" 20	read $C_\phi$ instead of $C\phi$
	" 21	read $\delta\lambda_\phi$ " " $\delta\lambda_\xi$
" 124	" 11	delete 'short'
" 125	" 21	read $\phi$ as a subscript to $(S'/P')$
	" 26	read wax instead of was
" 126	foot note	read $x_e$ " " $\pi_e$
" 127	" 12	read (1926b) " " (1962b)
	" 21	delete {and}
	" 22	
	(denominator)	read $(S'/P')_\phi$ " " $(S'P')_\phi$
	line 28	read $(S'/P')_{30^\circ}$ " " $(S' P')_{30^\circ}$
		read $(S/P)_{32^\circ}$ " " $(S^\circ/P)_{30^\circ}$
" 128	" 1	read equality " " quality $^\circ$ .
	" 37	delete asterik* after (30)
Pages 129 &		
	130 " 20	read $x_0$ instead of $x_\phi$
Page 130	" 19	insert small at the end
Page 130	foot note	read .015 " " 0.15
" 131	line 25	raise 'ratio falls' to the beginning of the previous line.
" 132	" 11	read $A_1'$ instead of $A'y$



# MAGNETIC STUDIES OF SINGLE CRYSTALS CONTAINING TETRAHEDRALLY CO-ORDINATED $\text{Cu}^{2+}$ , $\text{Ni}^{2+}$ AND $\text{Co}^{2+}$ IONS BETWEEN 300°K AND 90°K

A. BOSE, S. MITRA AND R. RAI

DEPARTMENT OF MAGNETISM, INDIAN ASSOCIATION FOR THE CULTIVATION OF SCIENCE,  
JADAVPUR, CALCUTTA-32

(Received, August 28, 1965)

**ABSTRACT.** The paper reports the measurements on the single crystals of the salts of tetrahedrally co-ordinated  $\text{Cu}^{2+}$ ,  $\text{Ni}^{2+}$  and  $\text{Co}^{2+}$  ions in  $\text{Cu}(\text{C}_2\text{H}_3\text{Cl}_4)_2$ ,  $\{(\text{C}_2\text{H}_3\text{Cl}_4)_2\}_2$ ,  $\text{NiBr}_4$  and  $\text{Co}(\text{C}_3\text{Cl}_5)_2$  respectively between 300°K and 90°K. The improved methods of measurements of magnetic anisotropy and mean susceptibility have been described in short. The results have been explained on the basis of refined ligand field theories of these ions developed recently by Bose *et al* (1965), taking the help of the optical and paramagnetic resonance studies. It has been shown that the experimental results can not be fully explained on the basis of the inversion of Stark pattern alone but have to be considered against the background of present refined theories which take into consideration the configurational interaction, overlap of the ligand and metal charge clouds and the variation of the crystalline electric field with temperature.

## INTRODUCTION

Magnetic anisotropy and susceptibility of octahedrally co-ordinated ionic complexes of iron group of salts have been very extensively studied in our laboratory and elsewhere (Krishnan *et al* 1936, 1938, Mookherji, 1945, Bose, 1947, 1948; Guha, 1951, Jackson, 1927) to elucidate the various aspects of crystalline electric field theory. But very little work seems to have been done on the tetrahedrally co-ordinated salts (except  $\text{CoCs}_2\text{Cl}_4$  and  $\text{CoCs}_3\text{Cl}_5$ , Krishnan and Mookherji, 1938; Bose, 1948) although their studies are sure to prove equally instructive. In the recent years a large number of such salts of  $\text{Cu}^{2+}$ ,  $\text{Ni}^{2+}$  and  $\text{Co}^{2+}$  ions has been prepared and studied by X-ray and other physico-chemical methods.

It is well known that in the similarly co-ordinated salts of the transition group the cubic ligand field Stark patterns for the ions with  $d^n$  and  $d^{5+n}$  configurations are inverted with respect to the reciprocally related ions with  $d^{5-n}$  and  $d^{10-n}$  configurations (Van Vleck, 1932; Gorter, 1932). The same kind of inversion again takes place from an octahedrally to a tetrahedrally co-ordinated salt of the same ion, and in the latter case the overall cubic susceptibility and anisotropy behaviours of the tetrahedrally co-ordinated salts may be very different from the octahedral salts of the same ion and resemble to some extent the octahedral salts

of the reciprocally related ions. A study of these properties, especially of the anisotropy and its variation with temperature provides very sensitive indications of the details of such behaviours and throws more light upon their causes.

In view of the above, we have undertaken detailed experimental investigation of the magnetic anisotropy and susceptibility of three tetrahedrally co-ordinated complexes of  $\text{Cu}^{2+}$ ,  $\text{Ni}^{2+}$  and  $\text{Co}^{2+}$  in the single crystals  $\text{CuCs}_2\text{Cl}_4$ ,  $[(\text{C}_2\text{H}_5)_4\text{N}]_2[\text{NiBr}_4]$  and  $\text{CoCs}_3\text{Cl}_5$  respectively, between  $300^\circ\text{K}$  and  $90^\circ\text{K}$ . The details of the methods of measurements have been published earlier (Bose *et al*, 1963; Dutta Roy 1958). So only a summary of the methods is given here. The details of processing the experimental data for fitting the recent theories of the anisotropic tetrahedrally co-ordinated ions (Bose *et al*, 1965) are given and the results of such fittings are discussed.

#### EXPERIMENTAL TECHNIQUES OF MAGNETIC MEASUREMENTS

##### (a) Anisotropy

The apparatus for measuring the magnetic anisotropy of single crystals of the salts, consists of a circular 10 cm. diameter vernier torsion head reading rotations accurately to  $0.1^\circ$ . The crystal specimen with any desired orientation at the center of homogeneous magnetic field, is attached with 'Poligom' or pure shellac cement to the lower end of a thin pyrex glass rod about 12 cm length and 0.5 mm. diameter, which is in its turn is suspended from the torsion head with a fine quartz fibre of about the same length and 0.01 mm diameter. A hexagonal set of small mirrors is attached to the upper end of the glass rod showing above the cryostat chamber. The image of an illuminated scale from one or other of the mirrors can always be observed as the crystal is rotated and gives the orientation of the crystal in the field accurately. The crystal is mounted to the fibre system removed outside the cryostat, with a known plane or axis horizontal or vertical as the case may be, with the help of a two circle goniometer and then replaced in proper position inside the crystal, mounted between the poles of a strong electromagnet. The magnetic field required is about 1000–3000 oersteds, produced between the plane parallel rectangular pole pieces (10 cm.  $\times$  15 cm) of the electromagnet, energised by current (2 to 3 amps.) from a D.C. 220 volt 15 KW stabilized generator.

When the magnetic field is switched on, the crystal in general, tends to set with its maximum susceptibility direction in the horizontal plane along the field, and any torsion produced thereby in the fibre is released by turning the torsion head. In this position there is no couple acting on the crystal and no rotation on switching on or off the magnetic field, as observed very accurately by the mirror and scale arrangement. With the magnetic field off, the torsion head is rotated to bring the crystal at  $45^\circ$  to the above 'zero couple position'. Now the crystal will experience the maximum couple due to the field. The position of the light spot on the scale and the reading of the torsion head is very carefully noted and



the magnetic field is switched on. The crystal is strongly deflected but is slowly brought back to its original position by rotating the torsion head, as can be checked by the return of the light spot. If  $\alpha$  be the angle in degrees through which the torsion head is rotated from 45° position of the crystal,  $C$  the torsion constant of the fibre,  $H$  the magnetic field,  $M$  and  $m$  the molecular weight and mass of the crystal respectively, then the *gm.* molecular magnetic anisotropy  $\Delta\chi$  in the horizontal plane of the crystal is given by

$$\Delta\chi = \frac{2\alpha M C'}{180 m H^2} \quad \dots (1)$$

The superiority of the above method (Dutta Roy, 1958) over that of Krishnan and Banerjee (1936) is quite obvious. The present one being a null method, the experimental conditions can be maintained constant with a much greater precision, and the large uncertain correction factor for small angles of rotation of the head (less than 300°), with small anisotropies of the crystals or large torsion constant of the fibres, in the earlier method is avoided.

The accurate determinations of  $H$ ,  $C$  etc. have been dealt at length by Datta (1954) and Dutta Roy (1958). The field is further checked by a proton resonance meter recently built here (Ghosh *et al.* 1964). Corrections for the shape anisotropies of crystals are made with the help of empirically obtained data by Majumdar (1962). Small crystals are accurately weighed upto  $10^{-6}$  gms with a Mettler microbalance. Use of dust free and air-conditioned chambers and other standard procedures for crystal preparation, crystal identifications polarographic check and accurate suspension of the crystals with the help of a goniometer, etc., have been discussed in details by Datta (1954).

In the case of small paramagnetic anisotropies of crystals a diamagnetic anisotropy correction needs to be made to a sufficiently good approximation from the measurements of anisotropies of isomorphous diamagnetic crystals using the method followed by Krishnan *et al.* (1936) in the crystalline anisotropies themselves, or at a later stage when ionic anisotropies have been calculated.

For anisotropy measurements at any desired low temperature in the range 300°K to 90°K, the automatic gas flow type cryostat of Bose (1947) was used.

#### (b) Mean Susceptibility

The mean susceptibility was measured with the help of a very sensitive Curie-balance but of robust construction (Bose *et al.*, 1963). Vertical suspension of the balance beam being of moderately thick phosphor bronze strip, the deflectional sensitivity has to be increased several thousand times by using a balanced pair of photo-electric cells, connected across a galvanometer and actuated by extremely small differences of illumination on the cells by a light spot, reflected from a mirror attached at the centre of the horizontal balance beam. The sample is

suspended vertically from one arm of the beam with a torsionless silk fibre in the central part of a Sucksmith type inhomogeneous horizontal magnetic field, with a small gradient at right angles to the field in the same plane (Dutta Roy, 1955).

In the central region,  $H \frac{dH}{dx}$  is sensibly constant over about  $1 \text{ cm}^3$  volume. The crystal can freely turn round to have its maximum susceptibility axis in the horizontal plane along the field, and at the same time move bodily along the gradient. The effect of anisotropy of shape upon the rotation is eliminated by cutting the crystal in a square or cylindrical shape about the vertical axis, where necessary. The translational force on the sample is balanced electro-dynamically by the force exerted on a small current bearing coil of insulated copper wire, rigidly attached to the same arm of the beam, as the crystal, with a long thick glass rod and placed with the coil parallel to the field, close to the sample. In practice, the potential drop across a suitable series of standard resistances for the requisite current in the coil (usually a few milliamperes) is measured with a Leeds and Northrup potentiometer with an accuracy of 0.1%.

The sample is enclosed in a new type of liquid oxygen cryostat (Bose *et al*, 1963) in which any desired temperature between  $400^\circ\text{K}$  and  $65^\circ\text{K}$  may be kept automatically constant within  $0.01^\circ\text{K}$  by isolating the experimental chamber from the cooling refrigerant liquid, the experimental chamber being a mirrored glass Dewar jacket the degree of vacuum in which can be changed by an adjustable air leak in the continuous high vacuum pumping system. A small heater is incorporated within the chamber so as to accurately balance the small heat leakage across the vacuum interspace. The refrigerant liquid is itself kept in a wide mouthed narrow tailed Dewar in which the experimental chamber is inserted. A constant volume air thermometer inserted in the experimental chamber and connected with a mercury contact magnetic relay operates the heater automatically.

The mass susceptibility of the sample at room temperature is calculated from the expression

$$\chi = \frac{e}{e_s} \left( \chi - \frac{k_s}{\rho_s} \right) \cdot \frac{m_s}{m} + \frac{k_a}{\rho} \quad \dots \quad (2)$$

in which  $\chi$ 's are the mass susceptibilities of the samples along the field direction (mean value in case of powdered sample),  $e$ 's the potential drops across a fixed resistance for the currents needed to balance the magnetic forces on the samples, corrected for the force upon the suspension system (including empty containers in the case of powders),  $m$ 's their masses,  $\rho$ 's densities; symbols with and without the subscript 's' refer to the standard (chromium potassium sulphate alum, Dutta Roy, 1955) and the unknown samples respectively;  $k_a$  is the volume susceptibility of surrounding air. Then knowing by comparison the susceptibility of the

unknown sample at a convenient reference temperature (say, 300°K), the susceptibility value at any other temperature ( $T$ ) can be obtained by the relation

$$\chi_T = \chi \cdot \frac{eT}{e_{300}} \left[ 1 - \frac{K_a}{K_{300}} (1 - \gamma \cdot 300) \left( 1 - \frac{300}{T} \right) \right] \quad (3)$$

where  $K$  is the volume susceptibility of the crystal at 300°K,  $\gamma$  its volume coefficient of expansion. Suffixes  $T$  and 300 indicate values for the samples at  $T^\circ\text{K}$  and 300°K respectively. The measurements have been taken at 15°, 10° or even closer temperature intervals when necessitated by a preliminary run to follow the temperature-susceptibility curve closely in a desired region. Since the room temperature in different seasons and times of the day will vary sometimes by more than 25°, it has been our practice to plot the value of  $e \cdot T$  against  $T$ , giving a very nearly linear extra- or intrapolation near room temperatures to get the actual values at 300°K for both the standard and unknown samples. The values of  $\chi_i$  at different temperatures are then calculated from the smoothed out values of  $e$  by graphical interpolation at short convenient intervals of temperatures.

A similar method of intrapolation is also adopted to get the values of anisotropy at the same set of temperatures from a graph of  $\alpha \cdot T$  against  $T$  from measurements described in the previous section.

The gram molecular susceptibilities ( $\chi_M$ ) at any temperature are corrected for diamagnetism of the molecule and the square of the effective gram ionic moments ( $p_f^2$ ) in Bohr magneton are calculated from

$$p_f^2 = \frac{3k}{N\beta^2} \chi_M \cdot T - 7.995\chi_M T^*. \quad (4)$$

$N, \beta, k$  having the usual significances.

The notations for principal crystalline tensors are the usual ones used by magnetic workers. In the orthorhombic crystals the magnetic susceptibility axes coincide with the crystallographic axes and  $\chi_a, \chi_b, \chi_c$  denote the susceptibilities along  $a, b, c$  axes corresponding to  $\chi_i = 1, 2, 3$  respectively. In the case of crystals with uniaxial symmetry (e.g. tetragonal, trigonal),  $\chi_{||}$  and  $\chi_{\perp}$  denote the crystalline susceptibilities along and perpendicular to  $c$ , the crystalline symmetry axis, corresponding to  $\perp = 1, 2$ , and  $|| = 3$ . Ionic susceptibilities on the simplifying assumption that the ions have approximate uniaxial symmetry are given by  $K_{||}$  and  $K_{\perp}$  along and perpendicular to the ionic symmetry axis corresponding to  $\perp = x, y$  and  $|| = z$  respectively. The method of calculation of  $K_{||}$  and  $K_{\perp}$  using crystalline values are shown later

### (c) Preparation of the Crystals :

The single crystals of  $\text{CuOs}_2\text{Cl}_4$  were grown from an aqueous solution of  $\text{CuCl}_2$

\* The values of the physical constants have been taken from Dumond and Cohen (1948).

and CsCl mixed in equimolecular proportions. The crystal generally grows in brownish orange colour in the form of elongated prisms along  $b$  axis.

Green tetraethylammonium nickel boride crystals were prepared by slow evaporation of an equimolecular absolute alcohol solution of nickel bromide and tetraethylammonium bromide.

The deep blue crystals of  $\text{CoCs}_2\text{Cl}_5$  were prepared from an aqueous solution of  $\text{CoCl}_2$  and CsCl in appropriate quantity at room temperature (about  $30^\circ\text{C}$ ).

The reagents used were of the extra pure or guaranteed reagent quality of Merck or B.D.H.

#### STRUCTURAL DATA

(a) The structural analysis of  $\text{CuCs}_2\text{Cl}_4$  by Helmholtz and Kruh (1952) shows that the crystal belongs to the orthorhombic system (space group  $\text{Pnma}$ ) with following parameters

$$a = 9.7 \text{ \AA}$$

$$b = 7.6 \text{ \AA}$$

$$c = 12.35 \text{ \AA}$$

Each  $\text{Cu}^{2+}$  ion is at the centre of a tetrahedron formed by four Cl atoms at its vertices at an average distance of  $2.22 \text{ \AA}$  from the  $\text{Cu}^{2+}$  ion. The  $[\text{CuCl}_4]^{2-}$  cluster is a tetragonal sphenoid having a four fold inversion symmetry about one of the line through central  $\text{Cu}^{2+}$  ion joining the middle points of two pairs of Cl atoms. This tetragonal symmetry axis is appreciably shorter in length than the other two such equal and mutually perpendicular bisectors lying in the plane normal to the said axis.

The unit cell of the crystal contains two pairs of the "magnetically inequivalent"  $[\text{CuCl}_4]^{2-}$  clusters. From the detailed X-ray data on the various atoms in the unit cell, it is possible to calculate the direction cosines of the tetragonal axes of one pair of the  $[\text{CuCl}_4]^{2-}$  clusters with respect to  $a, b, c$  axes of the crystals which are :

$$\alpha = 0.59307$$

$$\beta = 0$$

$$\gamma = 0.80543$$

The direction cosines of the tetragonal axes of the other pair of the  $[\text{CuCl}_4]^{2-}$  cluster is same but with opposite signs. Since direction cosines occur as squares in the calculation of ionic susceptibilities, their signs do not matter. We shall need in the next section how these direction cosine values are utilized for the calculation of ionic susceptibilities.

(b) The X-ray studies by Peter Pauling (as quoted by Gill and Nyholm, 1959) of a series of isomorphous organometallic halides of  $\text{Ni}^{2+}$  like  $[(\text{C}_2\text{H}_5)_4]_2\text{NiBr}_4$  indicate that the crystal belongs to the cubic system (space group  $\text{P2}_1/3$ )

with four molecules in the unit cell of dimension  $a = 15.5 \text{ \AA}$ . The X-ray results also show that the  $\text{Ni}^{2+}$  ion is tetrahedrally co-ordinated with four halogens forming a trigonally distorted tetrahedron round the  $\text{Ni}^{2+}$  ion. The trigonal axis passes through the halogen at one of the vertices of the tetrahedron and the central  $\text{Ni}^{2+}$  ion, and is normal to the base formed by other three halogens. Evidently, this trigonal axis is a body diagonal of the unit cell. But the detailed results of the structure are not known since the X-ray results of Peter Pauling do not appear to have been published. However, since the crystal is cubic we can only measure the mean susceptibility of the crystal and do not require X-ray data for correlation with the ionic mean susceptibility.

(c) The structural analysis of  $\text{CoCl}_3\cdot 4\text{H}_2\text{O}$  by Powell and Wells (1935) reveals that in this salt the  $\text{Co}^{2+}$  ion is tetrahedrally co-ordinated with four chlorine atoms at an average distance of  $2.34 \text{ \AA}$  from the central  $\text{Co}^{2+}$  ion. The crystal belongs to the tetragonal system (space group  $D_{4h}^{16}$ ) with four molecules in the unit cell of dimensions

$$a = 9.18 \text{ \AA} \quad c = 14.47 \text{ \AA}$$

The tetrahedron is slightly distorted along one of the axes which is a four fold inversion axis and passes through the midpoints of two pairs of adjacent chlorine atoms and the central  $\text{Co}^{2+}$  ion. The tetragonal axes of the four molecules being all parallel to the 'c' axis of the crystal, the crystalline ellipsoid coincides with the molecular ellipsoid and hence no structural parameters are required to get the ionic susceptibilities.

#### CALCULATION OF IONIC SUSCEPTIBILITIES IN $\text{CuCl}_2\cdot 2\text{H}_2\text{O}$

The ionic susceptibilities of  $\text{CuCl}_2\cdot 2\text{H}_2\text{O}$  have been calculated following the method of Ghosh and Mitra (1964). A short outline of the method is given below. The direction cosines of the three principal ionic susceptibility tensors ( $K_1, K_2, K_3$ ) with respect to an arbitrary orthogonal system ( $x, y, z$ ) is given as

$$\begin{array}{c|ccc} & x & y & z \\ \hline K_1 & \alpha_1 & \beta_1 & \gamma_1 \\ K_2 & \alpha_2 & \beta_2 & \gamma_2 \\ K_3 & \alpha_3 & \beta_3 & \gamma_3 \end{array}$$

If  $\chi_{\max}$  and  $\chi_{\min}$  represent the maximum and minimum susceptibilities in a given horizontal section of the crystalline ellipsoid in which magnetic measurement is to be made, having Millerian indices ( $h, k, l$ ), then for  $n$  inequivalent ions in the unit cell,

$$\chi_{\max} + \chi_{\min} = K_1 \left[ 1 - \frac{1}{n} \sum \{ (\alpha_1^2 \xi^2 + \beta_1^2 \eta^2 + \gamma_1^2 \zeta^2) + 2(\alpha_1 \beta_1 \xi \eta + \alpha_1 \gamma_1 \xi \zeta + \beta_1 \gamma_1 \zeta \eta) \} \right]$$

$$+ K_2 \left[ 1 - \frac{1}{n} \sum \{ (\alpha_2^2 \xi^2 + \beta_2^2 \eta^2 + \gamma_2^2 \zeta^2) + 2(\alpha_2 \beta_2 \xi \eta + \alpha_2 \gamma_2 \xi \zeta + \beta_2 \gamma_2 \eta \zeta) \} \right] \\ + K_3 \left[ 1 - \frac{1}{n} \sum \{ (\alpha_3^2 \xi^2 + \beta_3^2 \eta^2 + \gamma_3^2 \zeta^2) + 2(\alpha_3 \beta_3 \xi \eta + \alpha_3 \gamma_3 \xi \zeta + \beta_3 \gamma_3 \eta \zeta) \} \right] \quad \dots \quad (5)$$

where  $\xi, \eta, \zeta$  are the direction cosines of the normal to the given  $(h, k, l)$  plane relative to  $x, y$ , and  $z$ . And,

$$\chi = \frac{1}{3} (\chi_1 + \chi_2 + \chi_3) = \frac{1}{3} (K_1 + K_2 + K_3) = K$$

For  $\text{CuCl}_2\text{Cl}_4$  which is an orthorhombic crystal with a uniaxial symmetry of the ion,  $x, y$  and  $z$  are taken to coincide with  $a, b$  and  $c$  axes of the crystal respectively, and

$$K_1 = K_2 = K_{\perp} \text{ and } K_3 = K_{\parallel}$$

Hence the equation (5) with 'b' axis vertical (for magnetic measurement to be made [010] plane) reduces to ( $\eta = 1, \xi = \zeta = 0$ )

$$\chi_e + \chi_a = K_{\parallel}(1 - \beta_3^2) + K_{\perp}(1 + \beta_3^2) \quad \dots \quad (6)$$

$$\chi = \frac{K_{\parallel} + 2K_{\perp}}{3}$$

where  $\beta_3$  is the direction cosine of the tetragonal axis of the ion with respect to 'b' axis obtained from X-ray measurement and is, as we calculated earlier, equal to zero. ( $\chi_e + \chi_a$ ) can be determined from two anisotropy and the mean susceptibility measurements by the methods described earlier ( $K_{\parallel} \sim K_{\perp}$ ) and  $K$  may be obtained from equation (6). The same equation also determines uniquely whether ( $K_{\parallel} - K_{\perp}$ ) is positive or negative. The data for the crystalline anisotropies and mean susceptibilities at different temperatures are given in the 2nd, 3rd and 4th columns of the table I and the ionic anisotropies are shown in column 7-th. In the absence of structural data at all temperatures, we have to assume that the direction cosine in equation (6) remains constant with temperature. Since the tetragonal axis of the  $\text{Cu}^{2+}$  ion lies in the (010) plane with  $\beta = 0$ , such an assumption is justified so long as this special symmetry is unchanged.

#### STARK PATTERNS AND INFORMATION ON THEM OBTAINED FROM OPTICAL ABSORPTION STUDIES OF TETRAHEDRALLY CO-ORDINATED COMPLEXES

From what has been said earlier about the inversion of the Stark pattern for tetrahedral complexes, the pattern under the predominant cubic part of the crystal field in such  $\text{Cu}^{2+}$  complexes will consist of an orbital doublet  ${}^2E_g$  and a triplet  ${}^2T_g$  with the triplet lying lowest. The superimposed tetragonal component of the field will break this triplet into a single Kramers spin doublet and a pair of coincident doublets, separated by  $\Delta \text{ cm}^{-1}$  where  $\Delta$  is the anisotropic field splitting.

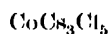
TABLE I  
 $\text{CuCs}_2\text{Cl}_4$ 

Temp. $^{\circ}\text{K}$	$(\chi_c - \chi_b) \times 10^6$	$(\chi_c - \chi_a) \times 10^6$	$\chi \times 10^6$	$K_{\parallel} \times 10^6$	$K_{\perp} \times 10^6$	$(K_{\parallel} - K_{\perp}) \times 10^6$
300	341	156	1680	2031	1505	526
290	351	161	1733	2094	1552	542
280	263	167	1790	2161	1604	557
270	374	173	1853	2237	1661	576
260	385	178	1918	2313	1720	593
250	398	184	1989	2401	1783	618
240	412	190	2068	2495	1854	641
230	425	196	2151	2594	1929	665
220	443	203	2244	2703	2015	688
210	461	210	2345	2817	2109	708
200	481	218	2420	2945	2211	734
190	501	226	2578	3085	2325	760
180	525	236	2713	3242	2445	797
170	549	247	2866	3417	2586	831
160	587	260	3037	3621	2745	876
150	607	275	3231	3845	2922	923
140	638	290	3452	3103	3127	976
130	674	308	3709	4100	3363	1037
120	715	330	4007	4748	3636	1112
110	769	352	4361	4818	3633	1185
100	811	376	4784	5628	4362	1266
90	869	401	5321	6220	4870	1350

TABLE II  
 $\sqrt{[(\text{C}_2\text{H}_5)_4\text{N}]_2\text{NiBr}_4}$ 

Temperature $^{\circ}\text{K}$	$\chi_M \times 10^6$	$\mu g^2$
300	5986	14.36
290	6193	14.34
280	6387	14.30
270	6601	14.26
260	6840	14.22
240	7348	14.10
230	7646	14.06
220	7959	14.00
210	8302	13.94
200	8674	13.87
190	9008	13.81
180	9536	13.72
170	10223	13.69
160	10639	13.61
150	11809	13.54
140	11909	13.33
130	12777	13.28
120	13696	13.28
110	14758	12.98
100	16010	12.80
90	17358	12.49

TABLE III



Temp °K	$(\gamma_{\parallel} - \gamma_{\perp}) \times 10^6$	$K_{\delta} \times 10^6$	$K_{\parallel} \times 10^6$	$K_{\perp} \times 10^6$	$(K_{\parallel} - K_{\perp}) \times 10^6$
300	652	9093	9528	8876	652
290	666	9407	9851	9185	666
280	689	9732	10192	9502	689
270	718	10083	10562	9844	718
260	750	10481	10981	10231	750
250	790	10875	11402	10612	790
240	833	11303	11858	11025	833
230	883	11752	12341	11458	883
220	937	12235	12860	11923	937
210	998	12704	13369	12371	998
200	1073	13300	14008	12935	1073
190	1154	13947	14716	13562	1154
180	1240	14634	15461	14221	1240
170	1338	15395	16322	14985	1338
160	1448	16268	17233	15785	1448
150	1561	17274	18328	16747	1581
140	1737	18453	19758	17841	1737
130	1907	19862	21133	19226	1907
120	2089	21421	22814	20725	2089
110	2337	23155	24713	22376	2337
100	2677	25176	26961	24284	2677
90	3245	27807	30002	26757	3345

The recent optical absorption studies of  $\text{CuCs}_2\text{Cl}_4$  at 77°K by Ferguson (1964, see Fig. 1a) have revealed that this anisotropic field splitting is as high as  $5000 \text{ cm}^{-1}$  and is comparable in magnitude with the cubic field separation which is  $9000 \text{ cm}^{-1}$ . Such a high anisotropic field splitting appears to be rather rare amongst the iron group of salts. The polarised spectral studies of Lawson and Morrison (1961) also reveal such high magnitude of anisotropic field separation in this salt. It is also observed that the cubic field splitting is nearly 3/4 of  $12300 \text{ cm}^{-1}$ , that observed in octahedral  $\text{Cu}^{2+}$  complex in the hydrated halides (Dreich and Trommer, 1937) instead of 4/9 as expected from theory. As we shall presently see, there are enough indications to show that the magnetic behaviour of the  $\text{Cu}^{2+}$  ion in this case is quite different from what is to be expected from the inversion of Stark pattern alone. The magnetic behaviour depends sensitively upon whether the singlet or the doublet component of the triplet  $^2T_2$  lies lowest in the Stark pattern and hence decides whether  $\Delta$  will be positive or negative. The spin-orbit coupling in  $\text{Cu}^{2+}$  is the highest in the iron group and considerable admixtures the various levels will take place under its action.



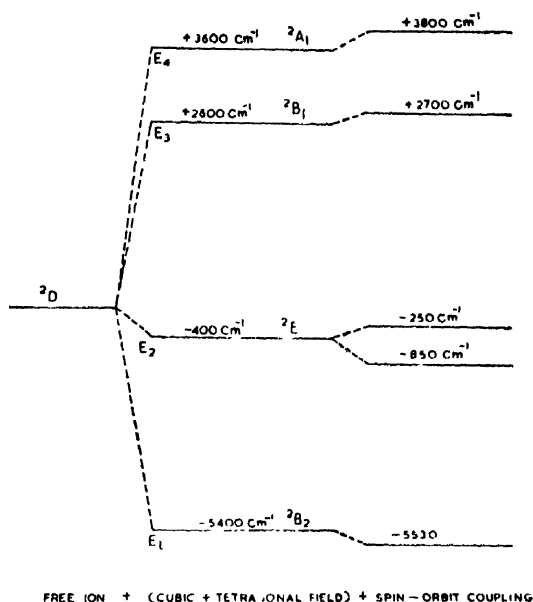


Fig. 1(a) Stark Pattern of Tetrahedrally Co-ordinated  $\text{Cu}^{2+}$  ion in  $\text{Cu}(\text{S}_2\text{Cl}_4)$  (Ferguson, 1964). (Not to Scale).

In the case of the  $\text{Ni}^{2+}$  tetrahedral complex in the salt the predominant cubic ligand field breaks up the  $^3F$  ground state of the free ion into two triplets  $^3T_1$  and  $^3T_2$  and a singlet  $^3A_2$  arranged in ascending order of energy. The small superposed trigonal component of the field further splits up the lowest triplet  $^3T_1$  into a doublet ( $^2E_2$ ) and a singlet  $^3A_1$ , separated by  $\Delta \text{ cm}^{-1}$ , the anisotropic field splitting. Which of these two ( $^2E_2$ ,  $^3A_1$ ) will lie lowest, depends upon the sign of  $\Delta$  and is to be decided from the experimental data. These levels will be further split up by the spin-orbit coupling which will mix up the different states and new states will be obtained. The Stark pattern of this complex is shown diagrammatically in figure (1b). In the figure the  $^3P$  level is also shown since this will give admixtural contributions to the ground state as also high frequency type contributions.

The optical absorption of an isomorphous tetrahedral  $\text{Ni}^{2+}$  salt in mull has been studied by Gill and Nyholm (1959) and Goodgame *et al* (1961) at room temperature. They have observed bands round about  $12,000 \text{ cm}^{-1}$  and  $6900 \text{ cm}^{-1}$ . The former is assigned to be due to the transition  $^3T_1(F) \rightarrow ^3T_1(P)$  and latter to  $^3T_1(F) \rightarrow ^3A_2$ . This gives the cubic field coefficient ( $Dq$ ) as nearly  $-380 \text{ cm}^{-1}$ . The cubic field coefficient ( $Dq$ ) for octahedrally co-ordinated  $\text{NiSiF}_6 \cdot 6\text{H}_2\text{O}$  is nearly  $1000 \text{ cm}^{-1}$  (Pryce *et al*, 1964). It has been shown by Jorgenson (1956) that a reduction in  $Dq$  of  $\sim 25\%$  occurs while going from water to halogen ligands with the same paramagnetic ion. This indicates that in the present case  $Dq$  of tetrahedral

$\text{Ni}^{2+}$  ion is about 4/9th that of the octahedral one as expected from theory, after allowing for the reduction due to chlorine ligands.

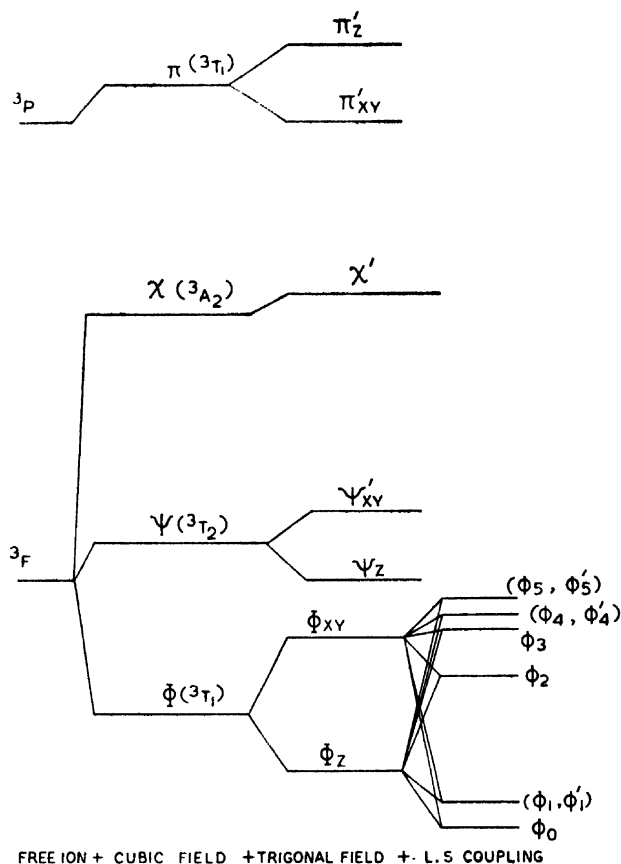


Fig 1(b) Energy Level Diagram for  $\text{Ni}^{2+}$  ion in Tetrahedral Co-ordination.  
(Not Drawn to Scale.)

The Stark pattern of the tetrahedral  $\text{Co}^{2+}$  ion in the cubic field will be similar to that of octahedral  $\text{Ni}^{2+}$  with an orbital singlet lying lowest. The  $^4\text{F}$  ground state of free  $\text{Co}^{2+}$  ion is split up by the predominant cubic field of the ligand tetrahedron into an orbital singlet ( $^4\text{A}_2$ ) and two triplets  $^4\text{T}_2$  and  $^4\text{T}_1$  arranged in ascending order of energy. In the superimposed tetragonal field, the above triplets break into a singlet and a doublet to the extent of about  $500\text{ cm}^{-1}$  (Bose *et al*, 1965c). With the spin-orbit interaction included, the lowest  $^4\text{A}_2$  level splits up into two Kramers doublet with a separation of about  $9\text{ cm}^{-1}$  (Hall and Hayes, 1960). The Stark pattern of the tetrahedral  $\text{Co}^{2+}$  ion is shown in figure 1(c).

Cotton *et al*, (1961) have done extensive investigations of the spectra of  $[\text{CoCl}_4]^{2-}$  complexes in different solution and mulls. In the spectra of  $\text{CoCl}_3\text{Cl}_5$

in hexachlorobutane mull, which may be taken to represent the spectra of the salt itself, band are observed near  $5580\text{ cm}^{-1}$  and  $14000\text{ cm}^{-1}$  owing to the transitions

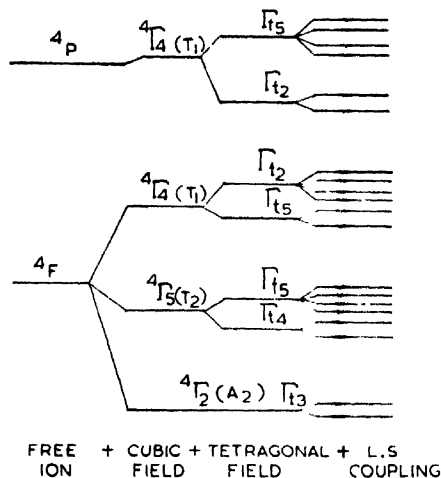


Fig. 1(c) Energy Level Diagram for  $\text{Co}^{2+}$  ion in Tetrahedral Co-ordination.  
(Not to Scale)

${}^4A_2 \rightarrow {}^4T_1(F)$  and  ${}^4A_2 \rightarrow {}^4T_1(P)$  respectively. They have also been able to resolve these bands into five and four components respectively. The value of  $Dq$  as found by Cotton *et al* (1961) is  $325\text{ cm}^{-1}$ . It may be mentioned that the  $Dq$  for the octahedral hydrated  $\text{Co}^{2+}$  complexes (Pappalardo, 1954) is nearly  $980\text{ cm}^{-1}$  which is about  $9/4$  times the former when we remember that a reduction of  $Dq$  by  $\sim 25\%$  occurs while going from the water to halogen co-ordination (Jorgenson, 1956).

Since the cubic field separation in tetrahedral complex is less than half that of the octahedral co-ordination in the former case the effect of second order perturbation terms becomes relatively more important. Moreover, in the tetrahedral case the absence of a centre of symmetry may justify the retention of odd order harmonics in the expression for the ligand field potential. As a consequence configurational interaction between the  $3d$  and  $4p$  orbitals of the metal ion arises and modifies the  $3d$  wavefunctions. The effect of configurational interaction is to modify the orbital overlap factors ( $\kappa$ ) and spin-orbit coupling coefficient ( $\xi$ ) in the crystal. Hence the reduction in  $\kappa$  and  $\xi$  in tetrahedral case is not only due to the scrambling of the metal and ligand orbitals as in the octahedral case, but also partly to the configurational interaction though according to Low (1960) and Weakliem (1962) this latter part appears to be rather small in comparison to the former. It is also important to note that such reductions are essentially anisotropic in character.

Recently the expressions for the magnetic anisotropy and susceptibility of these tetrahedrally co-ordinated complexes, of  $\text{Cu}^{2+}$ ,  $\text{Ni}^{2+}$  and  $\text{Co}^{2+}$  have been

deduced in our laboratory taking into account the special features of the present case and fitted with the experimental values. The details of the theory are under publication (Bose *et al.*, 1965a, 1965b, 1965c). In the present paper we give the theoretical expressions of the susceptibilities and describe the trial and error method of calculating the various physical parameters arising in the said theoretical expressions from the magnetic anisotropy and mean susceptibility data given in an earlier section, and checking them with spectroscopic and paramagnetic resonance data wherever available.

# THEORETICAL EXPRESSIONS FOR THE IONIC SUSCEPTIBILITIES FOR THE TETRAHEDRALLY CO-ORDINATED $\text{Cu}^{2+}$ , $\text{Ni}^{2+}$ AND $\text{Co}^{2+}$ COMPLEXES

## (i) $\text{Cu}^{2+}$ ion

The expressions for the ionic susceptibilities of the tetrahedrally co-ordinated  $\text{Cu}^{2+}$  ion in  $\text{CuCl}_2\cdot 2\text{H}_2\text{O}$  have been deduced by Bose *et al.* (1965a) following Pryce's Spin Hamiltonian formalism (1950). The expressions are

$$K_{\parallel} = \frac{8N\beta^2\kappa_{\parallel}^2}{E_3 - E_1} + \frac{N\beta^2}{4\kappa} \cdot \frac{G_{\parallel}^2}{T}$$

$$K_{\perp} = 2N\beta^2 \left[ \frac{k_{\perp}^2}{E_2 - E_1} - \frac{\zeta R_{\perp} k_{\parallel}}{(E_2 - E_1)^2} \right] + \frac{N\beta^2}{4k} \cdot \frac{G_{\perp}^2}{T} \quad \dots (7)$$

where  $K_{\parallel}$  and  $K_{\perp}$  are the gram ionic susceptibilities along and perpendicular to the tetragonal axis. The explicit expressions for the different parametral symbols are given in the theoretical paper (Bose *et al.*, 1965a). It can be mentioned here that  $E$ 's are the energy values (shown in the Fig. 1a) which involve the cubic field parameter  $G$  and anisotropic field parameters  $H$  and  $I$ . Other physical parameters involved in the expression are the spectroscopic splitting factors  $G_{\parallel}$ ,  $G_{\perp}$  in the crystal, orbital reduction factors ( $\kappa_{\parallel}$ ,  $\kappa_{\perp}$ ) and spin-orbit coupling reduction factors ( $R_{\parallel}$ ,  $R_{\perp}$ ), subscripts  $\parallel$ ,  $\perp$  refer to the quantities parallel and perpendicular to the tetragonal axis. The factor  $R_{\parallel}$  in this expression does not enter in the 2nd order terms with the square brackets but is involved in the expression for  $G_{\parallel}$ .

## (ii) $\text{Ni}^{2+}$ ion

The expression of mean susceptibility which could only be measured in this case, has been deduced by Bose *et al.* (1965b) on molecular orbital approximation. The expression is :

$$K = \frac{N\beta^2}{3k} B_1 \left[ \frac{2A^2}{T} + \frac{16B^2k}{D} \left\{ \exp \left( \frac{D}{kT} \right) - 1 \right\} \right]$$

$$\begin{aligned}
& + \frac{N\beta^2}{3} B_1 \left[ \left\{ \frac{8(c + \frac{1}{2}\alpha'k_{\perp}d)^2}{E_2 - E_1} + \frac{8\{bc - 2ad + \frac{\alpha'k}{2}(2ac - bd)\}^2}{E_3 - E_1} \right. \right. \\
& \left. \left. + \frac{4c^2d^2(\alpha k_{\parallel} + 2)^2}{E_4 - E_1} + \frac{16(c - \frac{1}{2}\alpha'k_{\perp}d)^2}{E_5 - E_1} \right\} \right. \\
& \left. + \left\{ \exp\left(\frac{D}{kT}\right) \left( \frac{4a^2(\alpha k_{\parallel} + 2)^2}{E_2 - E_0} + \frac{16\left\{(ad - bc) + \frac{\alpha'k_{\perp}}{2}(ac - bd)\right\}^2}{E_4 - E_0} \right) \right\} \right] \quad (8)
\end{aligned}$$

The explicit expressions for the different parameter symbols in the above expression is given in the theoretical paper (Bose *et al*, 1965b). It is seen from there that there are five physical parameters in this case ( $\Delta$ ,  $P_{\parallel}$ ,  $P_{\perp}$ ,  $Q_{\parallel}$ ,  $Q_{\perp}$ ) where  $\Delta$  is the anisotropic field coefficient and  $P_{\parallel} = \alpha R_{\parallel} \zeta$ ,  $P_{\perp} = \alpha' R_{\perp} \zeta$ ,  $Q_{\parallel} = \alpha k_{\parallel}$ ,  $Q_{\perp} = \alpha' k_{\perp}$ ;  $\alpha$ ,  $\alpha'$  being the Lande factors along and perpendicular to the symmetry axis of the ion.  $\zeta$  is the free ion spin-orbit coupling coefficient and  $R_i$  ( $i = \parallel$  or  $\perp$ ) are the reduction factors associated with the matrix element for spin-orbit coupling.  $\kappa_{\parallel}$ ,  $\kappa_{\perp}$ ,  $R_{\parallel}$ ,  $R_{\perp}$  are as before the orbital reduction overlap factors and spin orbit coupling reduction factors parallel and perpendicular to trigonal axis.

### (iii) $\text{Co}^{2+}$ ion

The expressions for the ionic susceptibilities of the tetrahedrally co-ordinated  $\text{Co}^{2+}$  ion have been deduced by Bose *et al* (1965c) by spin Hamiltonian formalism. The expressions for  $K_{\parallel}$  and  $K_{\perp}$  are given below

$$\begin{aligned}
K_{\parallel} &= 8N\beta^2 \alpha_{\parallel} k_{\parallel}^2 + \frac{15}{32} \frac{g_{\parallel}^2}{T} + \frac{3D}{8kT^2} \cdot g_{\parallel}^2 \\
K_{\perp} &= 8N\beta^2 \alpha_{\perp} k_{\perp}^2 + \frac{15}{32} \frac{g_{\perp}^2}{T} + \frac{3D}{16kT^2} \cdot g_{\perp}^2 \quad (9)
\end{aligned}$$

Here  $\alpha$ 's are the inverse of energy difference and involve the usual field parameters,  $D_q$ ,  $H$  and  $I$ . The other parameters involved in the expressions already explained earlier are  $k_i$  and  $\zeta_i$  ( $i = \parallel$  and  $\perp$ ).  $D$  is the 'Zero-field splitting' and  $g_i$  ( $i = \parallel$  and  $\perp$ ) are the spectroscopic splitting factors. The detailed expressions are given in the theoretical paper (Bose *et al*, 1965c).

### CALCULATION OF THE PHYSICAL PARAMETERS IN THE EXPRESSIONS FOR THE SUSCEPTIBILITIES FROM EXPERIMENTAL DATA

While fitting the experimental results already given with the theoretical expressions in the cases where an orbital singlet is lying lowest (i.e. in tetrahedral  $\text{Co}^{2+}$  and  $\text{Cu}^{2+}$ ), we notice that there are seven adjustable parameters viz.  $D_q$  (or

$G$ ),  $H$ ,  $I$ ,  $k_{\parallel}$ ,  $k_{\perp}$ ,  $\xi_{\parallel}$  and  $\xi_{\perp}$ . Theoretically all these parameters are independent; the relative values of  $k_{\parallel}$  and  $k_{\perp}$ ,  $\xi_{\parallel}$  and  $\xi_{\perp}$  dependent on the lower symmetric field parameters.  $H$  and  $I$ , although they may not be explicitly expressible in terms of them; so that there are, effectively, only five independent parameters. We can then decide uniquely the values of these parameters by fitting with the mean susceptibility data alone for at most seven (theoretically five) temperatures, if all these parameters are assumed to remain constant with temperature. In this particular case we have the anisotropy data as well. Hence a unique choice of the parameters is always possible with at most four pairs of anisotropy and mean susceptibility data at four temperatures provided the parameters do not vary with temperature. With this assumption holding strictly valid, these values of the parameters should be consistent not only with the mean susceptibility and anisotropy data at other temperatures but also with the paramagnetic resonance data and the fine structure optical absorption data.

In actual practice, owing to the complicated nature of the equations, we had to use a trial and error method to find the values of the parameters and it became immediately obvious that no single set of parameters could be consistent with all the available data. Hence the conclusion is that the given set of parameters obtained for magnetic data at the requisite number of temperatures can be a unique solution for data these only at the given temperatures, and for no other data; so that the set of parameters cannot have much physical significance, and hence the assumption that they are independent of temperature is not valid. Finally, we proceeded as follows to bring out properly the systematic discrepancy in fitting the data with the theory. In the case of  $\text{Co}^{2+}$  it is seen that the optical fine structure data of Cotton *et al* (1961) are available only at room temperature whereas the paramagnetic resonance data of Bowers and Owen (1955) are for 90°K. Since the room temperature magnetic anisotropy and susceptibility data are always taken as standard and also the energy levels of the optical absorption are of primary importance in the calculation of susceptibilities, we found out by extensive trial the set of values which gave practically exact fit with the experimental mean susceptibility and anisotropy data at room temperature, consistent with optical absorption data. These data are enough to give a unique solution of the parameters at room temperature only and will have a physical reality for this temperature. In the case of  $\text{Cu}^{2+}$ , since the  $g$ -values (Sharnoff, 1964) and fine structure optical absorption data of Ferguson (1964) are available at 77°K and are not supposed to change appreciably at 90°K, the lowest temperature of our magnetic measurements, we found out as above the set of parameters which gave practically exact fit with experimental susceptibility and anisotropy at this temperature, consistent with the paramagnetic resonance and optical absorption data. If these sets of parameters for  $\text{Co}^{2+}$  and  $\text{Cu}^{2+}$  had been constant with temperature, then it could be expected that they would give good fit with the magnetic data at all other temperatures.

But in both cases systematic deviations are found to occur which is especially prominent in anisotropy. While fitting the experimental data in the case of  $\text{Ni}^{2+}$  with the expression of mean susceptibility (eqn. 8), we notice that there are five adjustable parameters ( $\Delta, P_{\parallel}, P_{\perp}, Q_{\parallel}, Q_{\perp}$ ) whose values can be uniquely decided by fitting with the mean susceptibility data at five temperatures (theoretically three since the relative magnitudes of  $P_{\parallel}, P_{\perp}$  and  $Q_{\parallel}, Q_{\perp}$  are dependant on  $\Delta$ ), if the parameters are assumed to remain constant with temperature. However, in view of the large number of earlier experimental findings (Bose *et al.*, 1960, 1961a, 1961b, 1964), it is very unlikely that the anisotropic field coefficient  $\Delta$  should remain constant with temperature even if the others are assumed to be so as a first approximation. But since we do not have any anisotropy or resonance data, we are not able to find the values of  $\Delta$  at different temperatures from mean susceptibility alone, which could only be measured for this cubic crystal. On attempting to fit the experimental values on mean susceptibility, it is found that no single set of the above parameters can bring the fitting within the limits of experimental error at all temperatures. When the closest approach to one values at a given temperature is made with a given set of parameters, the values at other temperatures show systematic increasing differences. Since the room temperature experimental mean moment is always treated as standard, we found out the set of values of the parameters which gave a very close approach to it within the limits of experimental errors with the calculated mean value. The causes of these discrepancies will be discussed in due course.

## DISCUSSIONS

### (a) $\text{Cu}^{2+}$ ion

#### (i) Room Temperature Mean Moment and Magnetic Anisotropy

As we have seen earlier, the magnetic behaviour of tetrahedrally co-ordinated  $\text{Cu}^{2+}$  ion ( $3d^9$ ) should be somewhat similar to the octahedrally co-ordinated  $\text{Fe}^{2+}$  ( $3d^6$ ) or  $\text{Ti}^{3+}$  ( $3d^1$ ) if all other considerations are identical. The mean moment of  $\text{Cu}^{2+}$  ion in  $\text{CuCs}_2\text{Cl}_4$  is 2.02 (Table I) whereas for octahedral  $\text{Cu}^{2+}$  in  $\text{Cu}(\text{NH}_4\text{SO}_4)_2 \cdot 6\text{H}_2\text{O}$  it is 1.95 (Bose, 1948), both values being at  $300^\circ\text{K}$ . The spin only value for the  $^2\text{D}$  state of  $\text{Cu}^{2+}$  ion is 1.73. Thus the orbital contributions in the case of tetrahedral and octahedral  $\text{Cu}^{2+}$  are about 16 and 13 percents respectively. The mean magnetic moment of octahedral  $\text{Fe}^{2+}$  ion in  $\text{Fe}(\text{NH}_4\text{SO}_4)_2 \cdot 6\text{H}_2\text{O}$  at  $300^\circ\text{K}$  is 5.66 (Bose, 1948) as against the spin only value of 4.89, thus showing an orbital contribution of the order 17 percent. It should be remembered that although the Stark pattern in both the tetrahedral  $\text{Cu}^{2+}$  and octahedral  $\text{Fe}^{2+}$  should be similar with a triplet lying lowest, the actual magnetic behaviour in  $\text{CuCs}_2\text{Cl}_4$  is rather different owing to three reasons. Firstly the spin-orbit coupling in  $\text{Cu}^{2+}$  is about eight times that in  $\text{Fe}^{2+}$ , giving more admixture with upper levels. Secondly, the spin contribution to the moment is about 3 times larger in  $\text{Fe}^{2+}$  making the percentage orbital contribution appear smaller. Thirdly, as has been mentioned

earlier the optical absorption spectra of  $\text{CuCs}_2\text{Cl}_4$  show that under the action of the total ligand field the lowest orbital singlet with two fold Kramers spin degeneracy is separated from the next higher level by  $5000\text{ cm}^{-1}$ . On the other hand the axial field separation of the lowest cubic triplet in octahedral  $\text{Fe}^{2+}$  is only  $600\text{ cm}^{-1}$  (Bose *et al.*, 1961). Thus although the spin-orbit coupling in tetrahedral  $\text{Cu}^{2+}$  is nearly eight times the octahedral  $\text{Fe}^{2+}$ , and the cubic field separation being comparable (the cubic field separation in octahedral  $\text{Fe}^{2+}$  is about  $10300\text{ cm}^{-1}$ ; Dreisch and Kallschener, 1944), the orbital contributions are nearly equal. In the octahedral  $\text{Cu}^{2+}$ , the cubic field separation is about  $12000\text{ cm}^{-1}$  and the tetragonal separation of the lower 'non-magnetic' orbital doublet is about  $1000\text{ cm}^{-1}$ . Orbital contribution thus comes only from the upper orbital triplet through spin-orbit coupling. It is then difficult to understand why the orbital contributions are apparently about the same in the two cases, unless it is assumed that a strong covalency effect reduces the normally expected orbital contributions in the tetrahedral case. Again though octahedral  $\text{Ti}^{3+}$  ion is very similar to tetrahedral  $\text{Cu}^{2+}$  in respect of orbital as well as spin degeneracy, the higher ionic charge and consequent larger cubic separation  $20,000\text{ cm}^{-1}$  and much smaller positive spin-orbit coupling gives much smaller negative orbital contribution (about 5%) to the moment.

We shall next consider the anisotropy of the  $\text{Cu}^{2+}$  ion. It will be seen from the Table I that at  $300^\circ\text{K}$  the ionic anisotropy and mean susceptibility data for the tetrahedral  $\text{Cu}^{2+}$  are

$$K_{\parallel} - K_{\perp} = 526 \times 10^{-6}$$

$$K = 1680 \times 10^{-6}$$

which show that the anisotropy of the ion is quite high, i.e.  $526/1680$ , nearly 30 percent. The ionic anisotropy and mean susceptibility of octahedrally co-ordinated  $\text{Fe}^{2+}$  ion in the salt  $\text{Fe}(\text{NH}_4\text{SO}_4)_2 \cdot 6\text{H}_2\text{O}$  at  $300^\circ\text{K}$  (Bose, 1948) are

$$K_{\parallel} - K_{\perp} = 4229 \times 10^{-6}$$

$$K = 12698 \times 10^{-6}$$

which indicate that the octahedral  $\text{Fe}^{2+}$  ion also shows a high anisotropy i.e. nearly 33 percent. Thus we observe that the anisotropies of tetrahedral  $\text{Cu}^{2+}$  and octahedral  $\text{Fe}^{2+}$  are of the same order. As we remarked at the beginning, all the considerations in the two cases are not identical. For example, as we have seen earlier, the spin-orbit coupling is nearly eight times in  $\text{Cu}^{2+}$ , the mean magnetic moment is roughly three times less and anisotropic field itself is very large in  $\text{Cu}^{2+}$ . So that the magnetic anisotropy should have been much more in tetrahedral  $\text{Cu}^{2+}$ . Even between the octahedral and tetrahedral  $\text{Cu}^{2+}$  where both these factors are the same, the latter should have a much larger anisotropy because of the inversion of the doublet and triplet. But this is not found to be the case.



So it appears that the anisotropic behaviours here are more complicated than can be explained by a simple inversion of the levels and has to be considered against the background of complicated theoretical expressions involving a number of contributing factors.

### (ii) Variation of Ionic Moments with Temperature

From the figure (2), we observe that the ionic moment perpendicular to the tetragonal axis shows a smaller temperature dependence and the curve  $(K_{\perp} \cdot T)$  is almost a straight line with small slope to the temperature axis, whereas the ionic moment along the parallel direction shows a much larger temperature dependence with a small curvature. This is reasonable since the orbital moment along the

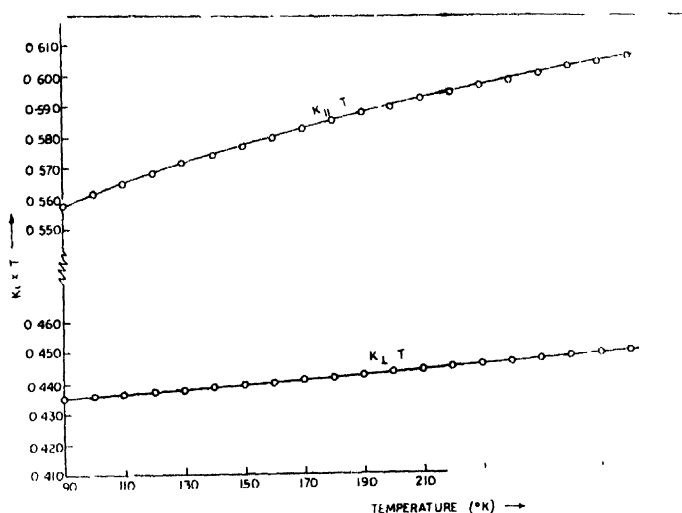


Fig. 2. The Variation of  $K_{\perp} \cdot T$  with Temperature in  $\text{CuCs}_2\text{Cl}_4$

perpendicular direction is quenched to a much larger extent than along the parallel direction, the actual values of changes of ionic moments in our temperature range being 9 and 3 percents respectively. The corresponding changes in ionic moments along and perpendicular to the tetragonal axis in octahedral  $\text{Fe}^{2+}$  ion (Bose, 1948) are 43 and 20 percents respectively. Thus we observe that the variations in the ionic moments in  $\text{CuCs}_2\text{Cl}_4$  ion are very small in comparison to the octahedral  $\text{Fe}^{2+}$  ion. In octahedral  $\text{Cu}^{2+}$  ion the temperature variation of the moment is also very small. These facts are consistent with the spectral findings that in  $\text{Cu}_2\text{Cs}_2\text{Cl}_4$  an orbital singlet lies lowest, with a large separation with the next higher level.

### (iii) Variation of 'Anisotropic Moment' $(\Delta k \cdot T)$ with Temperature :

The plot of  $(K_{\parallel} - K_{\perp}) \cdot T$  against  $T$  (Fig. 3) for  $\text{CuCs}_2\text{Cl}_4$  shows that the  $(K_{\parallel} - K_{\perp}) \cdot T$  decreases with temperature with a large curvature. The change in the values of  $\Delta k \cdot T$  between  $300^\circ\text{K}$  and  $90^\circ\text{K}$  is nearly 23 percent. A similar

plot for octahedral  $\text{Cu}^{2+}$ , say in  $\text{Cu}(\text{KSO}_4)_2 \cdot 6\text{H}_2\text{O}$  (Bose *et al.*, 1957) shows that the curve has a small slope to the temperature axis and with smaller curvature.

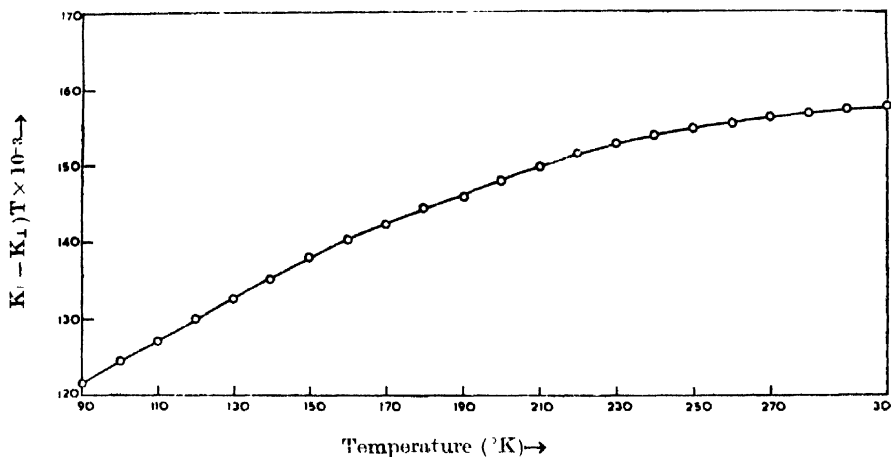


Fig. 3. Variation of  $(K_{||} - K_{\perp}) \cdot T$  with Temperature in  $\text{CuCs}_2\text{Cl}_4$

In the case of  $\text{Cu}(\text{NH}_4\text{SO}_4)_2 \cdot 6\text{H}_2\text{O}$  such curvature is very large and anomalous. The variation of  $\Delta k \cdot T$  in the same temperature range is nearly 9 percent. It is thus clear that the thermal behaviour of the anisotropic moment in this as in the  $\text{Cu}(\text{NH}_4\text{SO}_4)_2 \cdot 6\text{H}_2\text{O}$  is inconsistent with a theory in which the field and other parameters are constants with temperature.

(iv) *Fitting of the Mean Susceptibility and Anisotropy Data with Detailed Theory :*

The results of the fitting of the experimental data by the trial and error method already described in detailed, with the expressions of ionic susceptibilities are given in Table IV. From the Table IV we find that in order to fit the experimental data between our temperature range, the orbital factors are reduced anisotropically to  $\kappa_{||} = .81$  and  $\kappa_{\perp} = .72$  and the spin-orbit coupling coefficient along and perpendicular to the tetragonal axis is reduced by 27 and 30 percents respectively from its free ion value of  $-829 \text{ cm}^{-1}$ . Thus it indicates a large anisotropic covalency overlap between the  $3d$  orbital of the  $\text{Cu}^{2+}$  ion and the  $s$ - and  $p$ -orbitals of the ligand chlorines. The values of the second and fourth order tetragonal field parameters,  $H$  and  $I$ , have been chosen consistently with the other field parameters as  $H = 300 \text{ cm}^{-1}$  and  $I = 240 \text{ cm}^{-1}$ . It is also observed that the fitting of the mean susceptibility data at all temperatures is fairly close, though a small systematic departure of about 0.5% above experimental errors ( $\pm 0.2\%$ ) is observed at higher temperatures. A good fit might have been obtained with the mean susceptibility at all temperatures by adjusting the parameters slightly. But in view of what follows, this matters very little. The fitting of the anisotropy data at  $90^\circ\text{K}$  is well within experimental errors, as it should be, but systematic

TABLE IV

$G = 900 \text{ cm}^{-1}$	$\kappa_{\parallel} = 0.81$	$R_{\parallel} = 0.73$
$H = 300 \text{ cm}^{-1}$	$\kappa_{\perp} = 0.72$	$R_{\perp} = 0.70$
$I = 240 \text{ cm}^{-1}$	$\zeta = -829 \text{ cm}^{-1}$ (free ion value)	

## (1) Spectroscopic energy levels

	Theoretical	Experimental (at 77°K)
$E_2 - E_1$	5100 $\text{cm}^{-1}$	5000 $\text{cm}^{-1}$
$E_3 - E_1$	8100 $\text{cm}^{-1}$	7900 $\text{cm}^{-1}$
$E_4 - E_1$	9300 $\text{cm}^{-1}$	9050 $\text{cm}^{-1}$

(2)  $g$ -values :

	Theoretical	Experimental (at 77°K)
$G_{\parallel} =$	2.410	$G_1 = 2.384 \pm 0.006$
$G_{\perp} =$	2.141	$G_2 = 2.083 \pm 0.001$ $G_3 = 2.105 \pm 0.006$

## (3) Magnetic Susceptibility and Anisotropy

Temperature	Experimental		Theoretical	
	$K \times 10^6$	$(K_{\parallel} - K_{\perp}) \times 10^6$	$K \times 10^6$	$(K_{\parallel} - K_{\perp}) \times 10^6$
300	1680	526	1660	495
250	1973	618	1898	572
200	2420	734	2441	689
150	3231	934	3222	882
90	5321	1350	5352	1347

large departures are observed as the temperature increases, so that at 300°K or near the disagreement between the calculated and experimental values is about 7 percent. Attempts to adjust the parameters to reduce this departure in anisotropy caused an increased misfit in mean susceptibility. Elaborate trial and error calculations show that no single set of parameters could fit all values of both anisotropies and mean susceptibilities at all temperatures and also remain consistent with optical and paramagnetic resonance data. The fitting shown in the Table IV is the closest, with the set of parameters given in round numbers. The reason of this discrepancy is as follows. We have assumed all the parameters to remain constant with temperature. But there are experimental findings to suggest

that at least the anisotropic field parameters do vary with temperature, often considerably (Bose *et al.*, 1960, 1961a, 1961b, 1964). The large deviation of our anisotropy curve mentioned above indicates the same. A consideration of the variation of the above field parameters may lead to a better fitting of the susceptibility and anisotropy data at all temperatures, but then if both  $H$  and  $I$ , the independent anisotropic field parameters are assumed to change with temperature, our set of mean susceptibility and anisotropy data would not be enough to give unique solution of their values at different temperatures. Relative values of  $\kappa_{||}$ ,  $\kappa_{\perp}$  and  $R_{||}$ ,  $R_{\perp}$  are dependent on  $H$  and  $I$  though not explicitly and need not be considered as varying independently. For this purpose more detailed data on optical absorption or paramagnetic resonance at different temperatures would be necessary. In our present calculations since we would not consider such variations in  $H$  and  $I$ , it is to be expected that the fixed set of parameters used should not be able to give a unique fitting with the mean susceptibilities and anisotropies at all temperatures, consistent with the optical fine structure and resonance data. The very perceptible discrepancy in the fitting of the magnetic anisotropy can be then ascribed to a large extent to the temperature dependence of the parameters  $H$  and  $I$  and the concomitant dependance of  $\kappa_{||}$ ,  $\kappa_{\perp}$ ,  $R_{||}$ ,  $R_{\perp}$ . There is another point to be considered. While calculating the ionic anisotropies at different temperatures, we have used the direction cosines and assumed it to be constant with temperature because in calculating  $(K_{||} - K_{\perp})$  we have used only the direction cosine of  $K_{||}$  against  $b$  axis,  $\beta = 0$ , which is not likely to change because of the peculiarity of symmetry requirement in the arrangement of the  $\text{Cu}^{2+}$  ions in the unit cell. This may not be quite correct and present deviation between the calculated and experimental anisotropy data may be partly due to this neglect. In any case, such a variation of the direction cosine with the temperature may be inherently connected with changes in the anisotropic coefficients since that would change the packing in the unit cell and cause an induced distortion in the primary Jahn-Teller Cluster  $(\text{CuCl}_4)^{2-}$  (Van Vlec, 1939). Since the direction cosines and field parameters appear independently, it is not possible in the absence of low temperature X-ray data to calculate the effect of these changes of one upon the other. The apparent changes in the anisotropic fields are obviously brought about by anisotropic thermal expansion of the lattice which would not only change orientations and distances of the ligand charges but also changes the direction cosines referred to. Moreover, the spin-lattice relaxation process acting through the ligand fields, and responsible for keeping the equilibrium of the spin orientation energy with the lattice vibrational and rotational energy may change considerably with temperature and might cause an appreciable change in Jahn-Teller anisotropy effect. It has been assumed here that the cubic field and the covalency overlap are independent of temperature. Though this is not stringtly correct, the effects of these are perhaps very much smaller than the effect of thermal changes of the anisotropic field upon the magnetic anisotropy.

(v) *Fitting of the Paramagnetic Resonance Data :*

The paramagnetic resonance study of this crystal has been done very recently by Sharnoff (1964). Measurements were carried out at 77°K. Though the unit cell of this crystal contains two pairs of magnetically inequivalent ions, the p.m.r. spectrum consists of a single line for all orientations of the crystal in the external magnetic field. The presence of one line in the p.m.r. spectrum has been ascribed to the exchange interaction which couples the spins of the paramagnetic ions. In order to confirm this and to obtain correct principal ionic  $g_i$ -values, he studied  $\text{CuCs}_2\text{Cl}_4$  diluted with isomorphous  $\text{ZnCs}_2\text{Cl}_4$  and obtained two lines.

The experimental principal ionic  $g$ -values at 77°K and theoretical values calculated with our choice of parameters at 90°K are given below for comparison

Calculated	Experimental
$g_{\parallel} = 2.410$	$g_1 = 2.38 \pm .006$
$g_{\perp} = 2.141$	$\begin{cases} g_2 = 2.08 \pm .006 \\ g_3 = 2.105 \pm .006 \end{cases}$

The p.m.r. spectrum indicates that the  $(\text{CuCl}_4)^{2-}$  cluster is really orthorhombic though as is apparent from the above values  $g_2$  and  $g_3$ , the departure from tetragonality is rather small so as to justify our tetragonal approximation. It is also evident that the mean of  $g_2$  and  $g_3$  about 2.093 is somewhat different from our  $g_{\perp} = 2.141$  and  $g_{\parallel} = 2.41$  from  $g_1 = 2.38$ . These are to be expected since (1) the temperatures of measurements for the two sets are somewhat different, (2) the mixed salt used to get proper resolution of p.m.r. spectra though isomorphous with the pure salt should have appreciably different anisotropic ligand fields (3) and for the reason noted in previous section namely that our choice set of the parameters is to some extent dependent on the errors in spectroscopic fine structure data, until full consideration of their temperature variation has been allowed for (4) the direction cosine data used in magnetic results was calculated for room temperature. However, the fairly close agreement serves as a check for our result and limiting the labour in the trial and error calculation, by giving at once the orders of magnitudes of the parameters to start with.

(iv) *Fitting of the Fine structure Optical Absorption Data :*

As has been already discussed though the above choice of parameters  $H$  and  $I$  near 90°K is not compatible with magnetic data at all temperatures, these are quite consistent with the fine structure optical absorption data of Ferrguson (1964) at low temperature. The table IV shows that the agreement between the calculated and observed values of the energy levels are not quite perfect. This may be just owing to rounding off of the values of  $H$  and  $I$  in magnetic calculations. It is also to be noted that a small actual difference may exist between the separations of the levels at the temperature of observation 77°K and at our temperature of magnetic fitting 90°K.

(b)  $Ni^{2+}$ (i) *Mean Moment and Its Variation with Temperature :*

As we have remarked earlier the magnetic behaviour of tetrahedrally co-ordinated  $Ni^{2+}$  salts should be somewhat similar to the octahedrally co-ordinated  $Co^{2+}$  salts, showing a high anisotropy, high orbital contribution to the magnetic moment and large deviation from Curie law. Unfortunately the present crystal being of cubic class, we could not study the magnetic anisotropy directly. However a scrutiny of its mean moment may provide some information in this respect through the higher order terms involving the anisotropic splittings. The effective mean moment ( $p_f$ ) of this ion in  $[(C_2H_5)_4N]_2[NiBr_4]$  at  $300^\circ K$  is 3.79 as against 3.17 of octahedrally co-ordinated  $Ni^{2+}$  ion in  $Ni(KSO_4)_2 \cdot 6H_2O$  (Bose, 1948). The spin only value for the  $^3F$  ground state of  $Ni^{2+}$  ion is 2.83. The  $p_f$  value for octahedrally co-ordinated  $Co^{2+}$  ion in  $CoSiF_6 \cdot 6H_2O$  at  $300^\circ K$  is 5.01 (Majumdar *et al*, 1965), the spin only value being 3.87. Thus the tetrahedral  $Ni^{2+}$  ion shows nearly 34% orbital contribution compared to about 32% for octahedral  $Co^{2+}$  and about 12% for octahedral  $Ni^{2+}$ , as is to be expected. In  $Ni^{2+}$  the higher value of spin orbit coupling compared to  $Co^{2+}$  is no doubt responsible for a large orbital contribution, even if the energy level separation had been the same which is surely not the case since  $D_q$  is 4/9 times less in magnitude.

Again the variation of experimental  $p_f^2$  value of the tetrahedral  $Ni^{2+}$  with temperature (Fig. 4) shows a large deviation from the Curie law similar to octahedral  $Co^{2+}$  ion but unlike the octahedral  $Ni^{2+}$  ion in which the magnetic moment roughly obeys a Curie law. The experimental  $p_f^2$ -curve (Fig. 4) shows that the

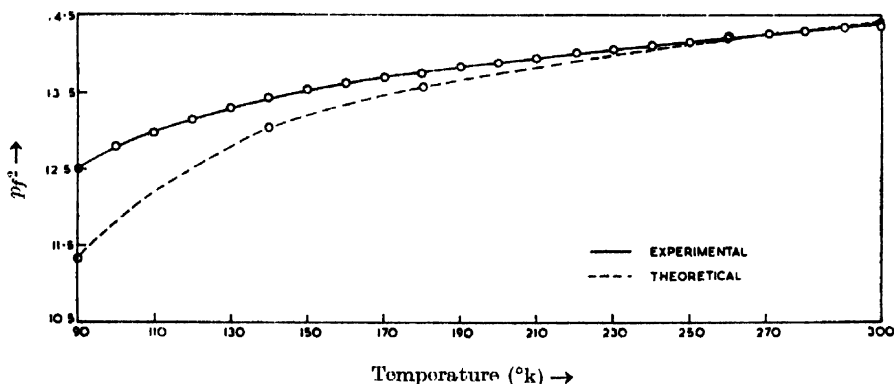


Fig. 4. Variation of  $p_f^2$  with temperature in  $[(C_2H_5)_4N]_2NiBr_4$ .

$p_f^2$  value first gradually decreases with a slope to the temperature axis and then after about  $200^\circ K$  the graph has an increasing curvature.

It is seen from the Stark pattern of the tetrahedral  $Ni^{2+}$  ion (Fig. 1b; see Bose *et al*, 1965b) that after the spin-orbit coupling, a singlet  $\phi_0$  lies lowest. Just

above that is a doublet ( $\phi_1, \phi'_2$ ) at about  $140 \text{ cm}^{-1}$  and the next higher level  $\phi_2$  (singlet) lies much higher, at nearly  $1000 \text{ cm}^{-1}$ .  $\phi_0$  is a non-magnetic level and so its own contribution to the magnetic moment is zero. The contribution of ( $\phi_1, \phi'_1$ ) is proportional to  $eD/kT$  where  $D$  is the energy separation of this level from the  $\phi_0$ . The next higher level ( $\phi_2$ ) is too high above to be populated at ordinary temperatures, and the contribution of such level will be of the high frequency type only. When the temperature decreases, the upper doublet ( $\phi_1, \phi'_1$ ) will gradually be depopulated and a steady fall in magnetic moment will result so long as  $D < kT$ . When  $D \approx kT$  the rate of decrease will be faster and for any further lowering of temperature ( $D > kT$ , i.e. below  $\sim 200^\circ\text{K}$ ) a steep fall in magnetic moment tending to zero except for high frequency contributions will result. This is very beautifully illustrated in the case of octahedral  $\text{V}^{3+}$  ion which has qualitatively the same ligand field pattern except as modified by the facts that the values of  $D$  is only  $\sim 8 \text{ cm}^{-1}$  and  $\zeta = 106 \text{ cm}^{-1}$ , with a very steep fall in the  $\mu_f^2 - T$  curve below  $10^\circ\text{K}$  (Seigert and Vandon Handel, 1937; Chakravarty, 1959). In the present case, however, the experimental curve does not show such a steep fall, of magnetic moment in our temperature range for mainly two reason. The first is that the range of temperature between  $200^\circ\text{K}$  to  $0^\circ\text{K}$  is sufficient to cause a more gradual fall and the high frequency contributions are of more importance. The other more interesting reason is that the anisotropic field may change with temperature in such a way as to counteract the rate of decrease of the moment. This will be discussed in details below.

(ii) *Fitting of the mean susceptibility data with the Detailed Theory :*

By fitting the experimental data with the expression of susceptibility given in equation (8) as discussed earlier, we find (Table V) that the set of values of the parameters so obtained are :  $P_{||} = -240 \text{ cm}^{-1}$ ,  $P_{\perp} = -375 \text{ cm}^{-1}$ ,  $Q_{||} = 0.7$ ,  $Q_{\perp} = 1.024$  and  $\Delta = -1020 \text{ cm}^{-1}$ . Under the present circumstances, we are not

TABLE V

$$\begin{aligned} P_{||} &= -240 \text{ cm}^{-1} & Q_{||} &= 0.700 \\ P_{\perp} &= -375 \text{ cm}^{-1} & Q_{\perp} &= 1.624 \\ \Delta &= -1029 \text{ cm}^{-1} \end{aligned}$$

Temperature °K	Experimental		Theoretical		Deviations m K
	$\bar{K} \times 10^6$	$\mu_f^2$	$\bar{K} \times 10^6$	$\mu_f^2$	
300	5986	14.36	6008	14.41	- 22
260	6840	14.22	6840	14.22	0
180	9536	14.72	9421	13.56	+ 115
140	11909	13.33	11643	13.03	+ 266
90	17358	12.49	15732	11.32	+ 1626

able to separately calculate  $\alpha_i$ 's,  $k_i$ 's,  $\zeta_i$ 's from  $P$ 's and  $Q$ 's.  $P_{||}$  and  $P_{\perp}$  can then be further written as  $P_{||} = \alpha R_{||} \zeta$  and  $P_{\perp} = \alpha' R_{\perp} \zeta$  where  $\zeta$  ( $= -325 \text{ cm}^{-1}$ ) is the free ion value and so  $\alpha R_{||} = 0.74$  and  $\alpha' R_{\perp} = 1.15$ .  $R_2( || \text{ or } \perp )$  is the reduction factor associated with the matrix elements for spin-orbit coupling. These reductions are due to the anisotropic overlap of the surrounding  $s$ - and  $p$ -charge clouds and the admixture of  $3d^7 4p$  and  $3d^8$  configuration.  $\alpha, \alpha'$  are the effective Landé' splitting factors in the crystal and are different from the value  $3/2$  for the case of an isotropic field.

From the Table V we find that at  $300^\circ\text{K}$  and at  $260^\circ\text{K}$  the agreement between the experimental and theoretically calculated values is well within the experimental errors. But at lower temperatures, this difference increases beyond experimental error, e.g., at  $180^\circ\text{K}$  it is 1.2%, at  $140^\circ\text{K} \sim 3.0\%$  and at  $90^\circ\text{K} \sim 9\%$ . This shows that there is a systematic increase in the difference between the experimental and theoretically calculated values. In the  $p_f^2-T$  plot, the theoretical curve as we have discussed earlier shows a steeper fall after  $200^\circ\text{K}$  than the experimental curve. This discrepancy is evidently only due to the fact that we have assumed  $\Delta$ , the anisotropy field coefficient as constant with temperature, the other factors controlling the curvature mentioned before namely the range of temperature through which the population of the level ( $\phi_1, \phi'_1$ ) is drained into the lowest state  $\phi_0$  and high frequency contribution being already taken into account in the theory. From what we have discussed earlier, this variation of  $\Delta$  with temperature is just as much as is required to wipe out this discrepancy at the different temperatures and evidently must be occurring in this salt as in the other cases. Of course, as  $\Delta$  changes, the relative values of  $P_{||}, P_{\perp}$  and  $Q_{||}, Q_{\perp}$  also change with temperature, thus sharing the task of wiping out the discrepancy and keeping the apparent variation of  $\Delta$  to reasonable magnitudes. This is particularly true for the tetrahedral complexes in which the anisotropic field admixtures and overlaps are comparatively larger than in the octahedral complexes and temperature variation of  $\Delta$  may have greater influence on ( $P_{||}, P_{\perp}$ ) and ( $Q_{||}, Q_{\perp}$ ) than in the later case, however, as we have discussed earlier, we could not calculate the actual temperature variations of the parameters because then we could not decide the values of the parameters uniquely with the help of optical absorption and means susceptibility data alone, which are rather insensitive to the variations of the anisotropic field with temperature. So we have to remain satisfied by giving only the systematic deviation between the experimental and theoretical values.

(c)  $\text{Co}^{2+}$

(i) *Room Temperature Mean Moment and Anisotropy :*

As we have seen earlier, the magnetic behaviours of the tetrahedrally coordinated  $\text{Co}^{2+}$  should be similar to octahedral  $\text{Ni}^{2+}$ . The effective mean moment of tetrahedral  $\text{Co}^{2+}$  ion is  $300^\circ\text{K}$  in  $\text{CoCs}_2\text{Cl}_5$  is 4.67, the spin only value being 3.87, so that the orbital contribution is about 20 percent. This contribution



in the case of octahedral  $\text{Co}^{2+}$  and  $\text{Ni}^{2+}$  have been already calculated to be about 30 and 12 percents respectively. Thus we observe that the orbital contribution in tetrahedral  $\text{Co}^{2+}$  lies in between octahedral  $\text{Ni}^{2+}$  and  $\text{Co}^{2+}$ . It is to be remembered that the spin-orbit coupling in  $\text{Co}^{2+}$  is less than half of  $\text{Ni}^{2+}$  so that orbital contribution in the former should have been smaller. But on the other hand, the cubic field separation in the tetrahedral  $\text{Co}^{2+}$  is less than half of octahedral  $\text{Ni}^{2+}$  which obviously more than makes up the deficiency. This very likely arises from the appreciable difference in the contributions from the higher order terms in equation (9) and is also from differences in the anisotropic field constants, covalency factors and spin orbit coupling reductions in the two cases.

Again the magnetic anisotropy and mean susceptibility of tetrahedral  $\text{Co}^{2+}$  ion (Table III) at  $300^\circ\text{K}$  are

$$K_{\parallel} = K_{\perp} = 652 \times 10^{-6}$$

$$K = -9093 \times 10^{-6}$$

The above data show that the anisotropy is small, only about 7 percent. The magnetic data for octahedral  $\text{Co}^{2+}$  ion in  $\text{Co}(\text{KSO}_4)_2 \cdot 6\text{H}_2\text{O}$  at  $300^\circ\text{K}$  (Bose, 1948) are

$$K_{\parallel} = K_{\perp} = 3090 \times 10^{-5}$$

$$K = -10514 \times 10^{-6}$$

showing an anisotropy of nearly 30 percent. But the corresponding values for octahedral  $\text{Ni}^{2+}$  in  $\text{Ni}(\text{KSO}_4)_2 \cdot 6\text{H}_2\text{O}$  at  $300^\circ\text{K}$  (Bose *et al*, 1958) are

$$K_{\parallel} = K_{\perp} = 262 \times 10^{-6}$$

$$K = -4393 \times 10^{-6}$$

so that the anisotropy is only about 6 percent. All these facts are in accord with the theory of Van Vleck (1932).

After this work was completed and while this detailed report of the work was being prepared, Figgis *et al* (June, 1964) published a paper on the magnetic measurements of this crystal. A preliminary report of our work was, however, already sent by us in February 1964 for reading at the International conference on Magnetism, held at Nottingham. It would be seen that the mean susceptibility data of Figgis *et al* (1964) and that of ours are in good agreement but the anisotropy data at room temperature differs nearly by 6 percent. The reason of this difference may be due to three factors.

(a) They have measured the anisotropy taking  $\text{K}_3\text{Fe}(\text{CN})_6$  as secondary and have taken its room temperature anisotropy values from Guha (1950) who had taken the standard room temperature data from the earlier works of Krishnan *et al* (1936) when the anisotropy method was yet to be well standardised. It has been actually shown by Stout and Griefel (1950) and Datta (1954) by more

accurate measurements that the values obtained by them in many cases differed widely from the earlier measurements of Krishnan *et al* (1934, 1936) and hence the high values obtained by Figgis *et al* (1964) may be due to this reason. It can be mentioned that our anisotropy data agrees well with Krishnan *et al* (1938) when their method was much improved.

(b) Figgis *et al* (1964) have adopted the old critical couple method, which is in many ways inferior to our present null method particularly for low anisotropies shown by Dutta-Roy (1958) and has been already discussed at length.

(c) Anisotropies of shape and diamagnetism have not been corrected for by Figgis *et al* (1964) which may be important for crystals with low magnetic anisotropy.

(ii) *Variation of Ionic Moments and Ionic Anisotropy Moment with Temperature :*

The ionic moments ( $K_i \cdot T$ ) parallel and perpendicular to the tetragonal axis have been plotted against temperature in Fig. 5. The temperature variations

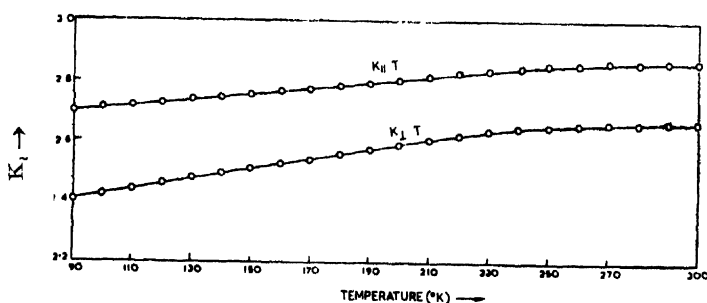


Fig. 5. Variation of  $K_i T$  with Temperature in  $\text{CoCs}_3\text{Cl}_5$ .

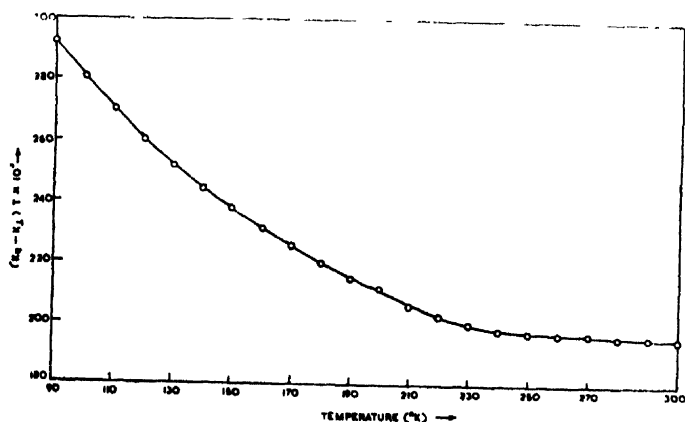


Fig. 6. Variation of  $(K_{\parallel} - K_{\perp})$  with temperature in  $\text{CoCs}_3\text{Cl}_5$ .

of ionic moments for both the directions are nearly similar and obey the Curie-Weiss law with small different values of Weiss constant. The ionic moments of octahedrally co-ordinately  $\text{Ni}^{2+}$  salts also show similar behaviour.

The curve of  $(K_{\parallel} - K_{\perp}) \cdot T$  against (Fig. 6) shows that the values of  $(\Delta K \cdot T)$  increases with temperature, as in octahedrally co-ordinated  $\text{Ni}^{2+}$  ion, though the increment in the latter case is less than in the former. This value in the case of octahedral  $\text{Co}^{2+}$  ion also increases with temperatures.

(iii) *Fitting of the Mean Susceptibility and Anisotropy Data with the Detailed theory :*

The results of the fitting of the experimental data with the expressions of ionic susceptibilities are given in Table VI. From the table we find that in order

TABLE VI

$$\begin{aligned} D_q &= 325 \text{ cm}^{-1} & \zeta_{\parallel} &= -148 \text{ cm}^{-1} & k_{\parallel} &= 0.920 \\ H &= 173 \text{ cm}^{-1} & \zeta_{\perp} &= -153 \text{ cm}^{-1} & k_{\perp} &= 0.906 \\ I &= -26 \text{ cm}^{-1} \end{aligned}$$

(1) Paramagnetic Resonance Data

Experimental (at 90°K)	Theoretical
$g_{\parallel} = 2.32 \pm 0.04$	$g_{\parallel} = 2.377$
$g_{\perp} = 2.27 \pm 0.04$	$g_{\perp} = 2.324$
$2D = -9.0 \text{ cm}^{-1}$	$2D = -6.0 \text{ cm}^{-1}$

(2) Magnetic Susceptibility and Anisotropy data :

Temperature °K	Experimental		Theoretical	
	$K \times 10^6$	$(K_{\parallel} - K_{\perp}) \times 10^6$	$\bar{K} \times 10$	$(K_{\parallel} - K_{\perp}) \times 10^6$
300	9093	652	9106	654
250	10875	790	10872	799
200	13300	1073	13396	1037
150	17264	1581	17676	1496
90	27807	3248	29115	3084

to fit the experimental data between our temperature range, the orbital reduction factors have to be taken as  $\kappa_{\parallel} = 0.920$  and  $\kappa_{\perp} = 0.906$  and the spin-orbit coupling coefficient as  $\zeta_{\parallel} = -148 \text{ cm}^{-1}$  and  $\zeta_{\perp} = -153 \text{ cm}^{-1}$ , the free ion value being  $-180 \text{ cm}^{-1}$ . These reductions indicate an appreciable anisotropic convalency overlap between the  $3d$  orbitals of  $\text{Co}^{2+}$  ion and the  $s$ - and  $p$ -orbitals of the ligand chlorines. The values of the second and fourth order tetragonal field parameters,  $H$  and  $I$  have been chosen, consistent with spectroscopic data, as  $H = 173 \text{ cm}^{-1}$

and  $I = 26 \text{ cm}^{-1}$ . It is observed that the fitting of both the anisotropy and mean susceptibility data is within the experimental errors at  $300^\circ\text{K}$ , but increased differences between the experimental and theoretically calculated values are observed at lower temperatures, so much so that at  $90^\circ\text{K}$ , this difference is about 5 percent, and much beyond the limit of experimental errors. The reason of this discrepancy is as follows. We have assumed all the parameters to remain constant with temperature. But there are adequate experimental findings to show that at least the anisotropic field parameters do vary with temperature, often considerably (Bose *et al.*, 1960, 1961a, 1961b, 1964). A consideration of the variation of the above field parameters may lead to a better fitting of the mean susceptibility and anisotropy at all temperatures. If  $H$  and  $I$ , the independent anisotropic field parameters, are assumed to vary with temperature, our set of mean susceptibility and anisotropy data would be just enough to give a unique solution of their values at other temperatures, consistent with the room temperature values of parameters fitting the spectroscopic data. But then it would not be possible to vary  $k_{\parallel}$ ,  $k_{\perp}$  and  $\xi_{\parallel}$ ,  $\xi_{\perp}$  which though dependent on  $H$  and  $I$  are not explicitly related to them. It is then evident that the room temperature parameters though uniquely determined from magnetic and spectroscopic data can not fit at low temperatures. We could have exactly fitted the entire range of values of susceptibility and anisotropy with a hypothetical fixed set of parameters using only the magnetic measurements since we have enough magnetic data for this purpose, but this set of parameters would not be consistent with spectroscopic or resonance data. In our present calculation since we could not consider such variation in  $H$  and  $I$  as well as  $k_{\parallel}$ ,  $k_{\perp}$ ,  $\xi_{\parallel}$ ,  $\xi_{\perp}$  in the absence of temperature variation data on spectroscopic absorption and paramagnetic resonance, we had to remain satisfied by showing that the fixed set of parameters consistent with spectroscopic absorption data at room temperature could not give unique fitting with the experimental data at all temperatures. This is further brought out by the fact that the zero-field splitting ( $-6 \text{ cm}^{-1}$ ) calculated uniquely at room temperature is appreciably different from the experimental value  $-9 \text{ cm}^{-1}$  at low temperature. The very perceptible and consistently increasing discrepancy in the fitting of anisotropy and mean susceptibility at other temperatures can then be ascribed to a large extent to the temperature dependence of the parameters  $H$  and  $I$  and concomitant dependence of  $k_{\parallel}$ ,  $k_{\perp}$ ,  $\xi_{\parallel}$ ,  $\xi_{\perp}$ . Evidently the fixed set of parameters at all temperatures and a zero-field splitting as large as  $-20 \text{ cm}^{-1}$  postulated by Figgis *et al.* (1964) is against all experimental facts even if the large errors in their anisotropy values is overlooked. They have further postulated a weak super exchange interaction ( $J \sim 0.5 \text{ cm}^{-1}$ ) between  $\text{Co}^{2+}$  ions through the nearest intermediary chlorines to close up the still existing discrepancy with the theory. It is of course possible that such a small exchange interaction exists though p.m.r. (Hall and Hayes, 1960) and Zeeman field splitting studies (Judd, 1964) do not report any. But even taking into account this interaction, causing a small departure from Curie Law, the whole

from this law can not be covered unless a very unlikely observed departure value of zero-field splitting is taken as done by Figgis *et al* (1964) on an adhoc basis.

(iv) *Fitting of the Paramagnetic Resonance Data :*

Paramagnetic resonance measurements on the single crystals of  $\text{CoCs}_2\text{Cl}_6$  were done by Bowers and Own (1955) and by Hall and Hyes (1960) at 90 K. The set of the theoretical parameters which gives good fit with the susceptibility and anisotropy data at room temperature was utilised to calculate the 'g' and 'D' values. The experimental and theoretical values are given below :

Experimental	Theoretical
$g_{\parallel} = 2.32 \pm 0.04$	$g_{\parallel} = 2.377$
$g_{\perp} = 2.28 \pm 0.04$	$g_{\perp} = 2.325$
$2D = -9.0 \text{ cm}^{-1}$	$2D = -6.0 \text{ cm}^{-1}$

It would be seen that there is a small but appreciable difference between the experimental and theoretical values particularly the  $D$  value. This difference between them is due to the fact that we have calculated the  $g_i$  and  $D$  with the help of parameters which give good fit with the mean susceptibility and anisotropy data only at room temperature. Hence the calculated  $g_i$  and  $2D$  values refer to the values at room temperature whereas the experimental values are for 90K. This shows a variation of the 'g' and  $2D$  values in this temperature region indicating a change in the crystal field as we had anticipated earlier. It is to be noted that Figgis *et al*'s value for  $2D$  is  $-20 \text{ cm}^{-1}$  which does not agree in magnitude with the resonance values.

(v) *Fitting of the Optical Absorption Data .*

As had already been discussed, although the above choice of parameters derived from susceptibility and anisotropy data, is not compatible with the magnetic data at all temperatures, these are quite consistent with the fine structure optical absorption data at room temperature. Considering cubic and tetragonal fields and spin-orbit coupling, the main bands  $\nu_2$  and  $\nu_3$  break into six components which are in good agreement with the experimental fine structure levels (Cotton *et al*, 1961).

# AN APPARENT DISCREPANCY BETWEEN STRUCTURAL ANALYSIS AND MAGNETIC MEASUREMENTS IN $\text{CuCs}_2\text{Cl}_4$

As we have seen earlier, the structural analysis of  $\text{CuCs}_2\text{Cl}_4$  by Helmholz and Kruh (1952) reveals that the tetrahedron of four chlorine atoms is compressed along the tetragonal axis and the other two perpendicular axes are equal. Hence the field along this direction might have been considered to be stronger than along the former would have been quenched to a greater extent than in the perpendicular

direction; consequently  $K_{\perp}$  would appear to be greater than  $K_{\parallel}$ . But we experimentally observe that  $K_{\parallel}$  is greater than  $K_{\perp}$ . This is supported by the spectroscopic studies (Ferguson, 1964) showing that the singlet  ${}^2B_2$  is below the doublet  ${}^2E_2$  as is to be expected in this case and also directly by the e.s.r. studies of Sharnoff (1964) giving  $G_{\parallel} > G_{\perp}$ . A similar result has been obtained recently in  $\text{FeSiF}_6 \cdot 6\text{H}_2\text{O}$  (trigonal crystal, space group  $C_{3i}^2$  with one molecule in the unit cell) where neutron diffraction studies (Hamilton, 1961) indicate the  $(\text{Fe}(\text{6H}_2\text{O}))^{2+}$  octahedron to be elongated, whereas magnetic measurements of Jackson (1959) and Bose and Rai (1965) uniquely show that  $K_{\perp} > K_{\parallel}$ .

A qualitative explanation of the present discrepancy was given by Mitra (1964) who tried to account for this on the basis of anisotropic covalency overlap of the orbitals of the ligands and the metal ion, which in consequence may cause an anisotropic reduction of the orbital moment in a sense opposite to that of the flattening of the tetrahedron. A look at the ligand field parameters given in Table V indicates that the orbital factor  $K_{\perp}$  has been reduced anisotropically to  $\kappa_{\parallel} = 0.81$  and  $\kappa_{\perp} = 0.72$  along and perpendicular to the tetragonal axis, respectively, thus showing that the covalency overlap along the perpendicular direction is 28 percent. The effect of covalency overlap in general is to reduce the orbital moment. Hence the reduction of the orbital moment in the perpendicular direction of the orbital moment in the perpendicular direction is nearly 9 percent more than in the parallel direction, and this in spite of the squatness of the tetrahedron may reduce the susceptibility along the perpendicular direction so much so that it becomes smaller than the susceptibility along the parallel direction i.e.  $K_{\perp}$  becomes less than  $K_{\parallel}$ .

#### REFERENCES

- Bose, A., 1947, *Ind. J. Phys.*, **21**, 275.  
 Bose, A., 1948, *Ind. J. Phys.*, **22**, 74, 195, 483.  
 Bose, A., Mitra, S. C. and Datta, S. K., 1957, *Proc. Roy. Soc.*, **A239**, 165.  
 Bose, A., Mitra, S. C. and Datta, S. K., 1958, *Proc. Roy. Soc.*, **A248**, 153.  
 Bose, A., Chakravarty, A. S. and Chatterji, R., 1960, *Proc. Roy. Soc.*, **A255**, 145.  
 Bose, A., Chakravarty, A. S. and Chatterji, R., 1961, *Proc. Roy. Soc.*, **A261**, 43, 207.  
 Bose, A. and Chatterji, R., 1963, *Proc. Phys. Soc.*, **82**, 23.  
 Bose, A., Chatterji, R. and Rai, R., 1964, *Proc. Phys. Soc.*, **83**, 959.  
 Bose, A., Dutta Roy, S. K., Ghosh, P. K. and Mitra, S., 1963, *Ind. J. Phys.*, **38**, 505.  
 Bose, A., Lahiri, S. and Ghosh, U. S., 1965a, *J. Phys. Chem. Solids* (In press).  
 Bose, R., Rai, R. and Mitra, S., 1965b, *Ind. J. Phys.*, **39**, 318.  
 Bose, A., Rai, R., Kumar, S. and Mitra, S., 1965c, *Physica*, (Communicated).  
 Bowers, K. D., and Owen, J., 1955, *Rep. Prog. Phys.*, **18**, 304.  
 Cotton, F. A., Goodgame, D. M. L. and Goodgame, M., 1961, *J. Am. Chem. Soc.*, **83**, 46900.  
 Datta, S. K., 1954, *Ind. J. Phys.*, **28**, 239.  
 Dutta Roy, S. K., 1954, *Ind. J. Phys.*, **28**, 183.  
 Dutta Roy, S. K., 1958, D.Phil. Thesis, C.U.  
 Dumon J. W. M. and Cohen, E. R. 1948, *Rev. Mod. Phys.* **20**, 82.

- Ferguson, J., 1964, *J. Chem. Phys.*, **40**, 3406.
- Figgis, B. N., Gerloch, M. and Mason, R., 1964, *Proc. Roy. Soc.*, **A279**, 210.
- Ghosh, U. S. and Mitra, S., 1964, *Ind. J. Phys.*, **38**, 19.
- Gill, N. S. and Nyholm, R. S., 1959, *J. Chem. Soc.*, 3997.
- Goodgame, D. M. S. and Cotton, F. A., 1961, *J. Am. Chem. Soc.*, **83**, 4161.
- Gorter, C. J., 1932, *Phys. Rev.*, **42**, 437.
- Guha, B. C., 1951, *Proc. Roy. Soc.*, **A206**, 353.
- Hall, J. P. P. and Hayes, W., 1960, *J. Chem. Phys.*, **32**, 1871.
- Hamilton, W. C., 1962, *Acta Cryst.*, **15**, 353.
- Helmholz, L. and Kruh, R. F., 1952, *J. Am. Chem. Soc.*, **74**, 1176.
- Jackson, L. C., 1959, *Phil. Mag.*, **4**, 554.
- Jackson, L. C. 1957, *Phil. Trans.* **227**, 107
- Jorgensen, C. K., 1956 Kgl. Danske. Videnskab Selskab. *Mat-fys. Medd.*, **29**, 11.
- Judd, B. R., 1964, *Proc. Phys. Soc.*, **83**, 1036.
- Krishnan, K. S. and Banerji, S., 1936, *Phil. Trans.*, **A232**, 99.
- Krishnan, K. S. and Mookherji, A., 1938, *Phil Trans.*, **A237**, 135.
- Low, W., 1960, Paramagnetic Resonance in Solids (Solid State Phys., Suppl. 2)
- Mookherji, A., 1945, *Ind. J. Phys.*, **19**, 63.
- Mitra, S., 1964, *Ind. J. Pure & Appl. Phys.*, **2**, 333.
- Powell, H. M. and Wells, A. F., 1935, *J. Chem. Soc.*, 359.
- Pryce, M. H. L., 1950, *Proc. Phys. Soc.*, **A63**, 25.
- Rai, R., and Mitra, S., 1964, *Ind. J. Phys.*, **38**, 121.
- Sharnoff, M., 1964, *J. Chem. Phys.*, **41**, 2203.
- Vanden, Handel, J. and Seigert, A., 1937, *Physica*, **4**, 871.
- Van Vleck, J. H., 1932, *Phys. Rev.*, **41**, 208.
- Van Vleck, J. H., 1939, *J. Chem. Phys.*, **7**, 61, 72.
- Weakliem, H. A., 1962, *J. Chem. Phys.*, **36**, 2116.

INFRARED AND RAMAN STUDY OF PARA-  
CHLORONITROBENZENE

K. C. MEDHI

OPTICS DEPARTMENT,

INDIAN ASSOCIATION FOR THE CULTIVATION OF SCIENCE,  
CALCUTTA-32.

(Received October 10, 1964)

## Plate III

**ABSTRACT.** The infrared absorption spectrum in the 4000–630  $\text{cm}^{-1}$  region in the solid state at 26°C and in solution in carbon tetrachloride and the Raman spectrum in the liquid state at 90°C have been reported for para-chloronitrobenzene. A complete assignment of the observed frequencies is given.

## I N T R O D U C T I O N

In a previous paper (Medhi, 1964) the infrared and Raman spectra of the three isomers of fluoronitrobenzene were presented and a complete assignment of the vibrational frequencies given. In continuation of that work the investigation has been extended to para-chloronitrobenzene. The infrared spectrum of this compound was studied previously by Lecomte (1938) over the limited range 1400–500  $\text{cm}^{-1}$  and by Mooney (1964). Earlier works on the Raman spectrum of this molecule relate to those of High (1931), Manzoni-Ansidei (1935), Reitz and Stockmair (1936) and Wittek (1942), and only a partial assignment of some of the fundamentals is given in Landolt-Börnstein Table (1951).

In the present investigation a detailed study of the infrared and the Raman spectrum of para-chloronitrobenzene has been made. Several new Raman lines which were not detected by the earlier workers have been observed. Essentially complete vibrational assignments, based largely on comparison with those proposed for para-fluoronitrobenzene (Medhi, 1964) are given.

## E X P E R I M E N T A L

The pure sample of para-chloronitrobenzene was supplied by Riedel-de Haen A. G. It was purified by fractional distillation. The fractions boiling at 242°C were collected and distilled again under reduced pressure before use.

A Perkin-Elmer Model 21 spectrophotometer equipped with sodium chloride prism was used to record the infrared absorption spectrum in the region 4000–630  $\text{cm}^{-1}$ . The instrument was calibrated with the standard atmospheric water vapour and carbon dioxide bands. The spectrum was obtained using a thin polycrystalline film grown by melting the substance between two NaCl



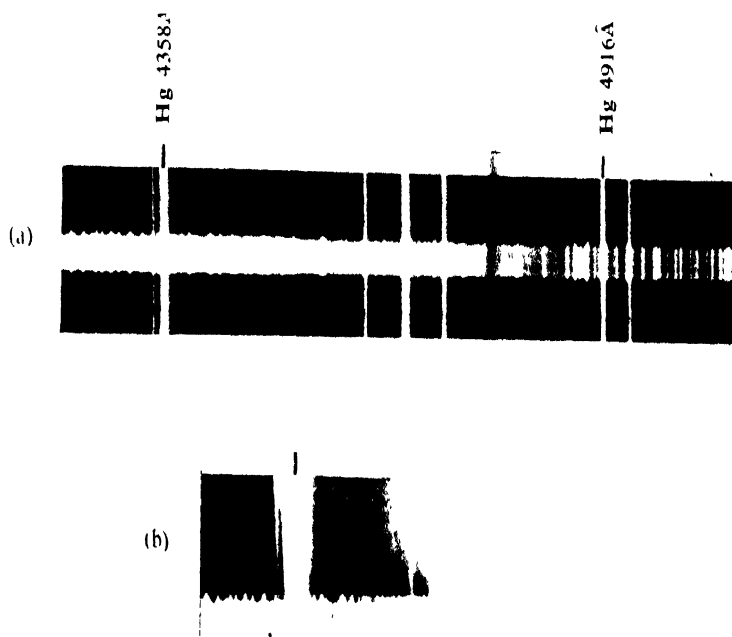


Fig. 2.—Raman Spectrum of Para-chloronitrobenzene.

(a) Short exposure.

(b) Long exposure.



plates and cooling the specimen slowly to room temperature. The infrared spectrum in the frequency region  $3400\text{--}1600\text{ cm}^{-1}$  was also measured in solution in carbon tetrachloride.

The Raman spectrum was recorded photographically using a Fuess glass spectrograph (dispersion  $19\text{ \AA/mm}$  in the  $4358\text{ \AA}$  region) in the liquid state at  $90^\circ\text{C}$  (i.e. at a temperature slightly above the melting point). The spectrum was excited by the Hg  $4358\text{ \AA}$  line. The compound being slightly yellowish in colour there is strong absorption in the region near  $4358\text{ \AA}$ . A fairly long exposure was necessary to record the low-lying Raman frequencies. The study of the polarisation of the Raman lines was also made by the method described elsewhere (Medhi, 1964).

## RESULTS AND DISCUSSION

The observed infrared and Raman frequencies of para-chloronitrobenzene and their approximate intensities are given in Table I. The assignment of the fundamental frequencies is given in the fourth column of the table. Fig. 1 shows the infrared spectrum in the range  $1800\text{--}630\text{ cm}^{-1}$ . The Raman spectrum is reproduced in Fig. 2, Plate III.

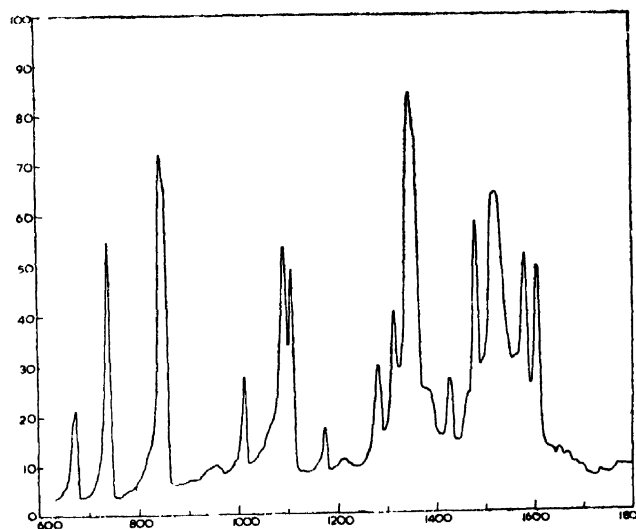


Fig. 1. Infrared spectrum of parachloronitrobenzene

The parachloronitrobenzene molecule is assumed to have  $C_{2v}$  symmetry. It should thus have thirty-six fundamental modes of vibration which are distributed over the four symmetry species as follows

In-plane vibrations

$13 a_1$  (infrared and Raman active) +  $12 b_1$  (infrared and Raman active).

Out-of-plane vibrations

TABLE I  
Infrared and Raman frequencies of *p*-chloronitrobenzene

Infrared, $\nu$ in $\text{cm}^{-1}$ . Solid at 26°C	Raman, $\Delta\nu$ in $\text{cm}^{-1}$ . Liquid at 90°C	Assignment		Remarks
		Species	Corresponding modes of benzene	
	212 (0b)	$b_2$	16B	
	276 (2) dp	$b_2$	11	
	314 (1)	$a_1$	6A	
	367 (0) ?	$b_2$	4	
	415 (0)	$a_2$	16A	
	444 (0)	$b_1$		NO <sub>2</sub> rocking
467†		$b_1$	18B	
535†	530 (1)	$b_2$		NO <sub>2</sub> out of plane rocking.
	569 (0)	$b_2$	10B	
	597 (0)	$b_2$	17B	
645 (sh)	623 (3) dp	$b_1$	6B	
670 (sh)				
674 (m)	677 (0)	$a_1$		NO <sub>2</sub> bending
740 (vs)	734 (2) dp	$b_1, a_1$	9B, 18A	
	790 (0)	$b_2$	5	
820 (sh)	826 (0)			
846 (vs)		$a_1$	12	
854 (vs)	855 (5) p	$a_1, a_2$	1, 10A	
935 (w)				
955 (w)	960 (1)			
1013 (m)	1015 (0)	$a_2$	17A	
1045 (sh)				
1065 (sh)	1056 (2b) dp ?	$b_1$	15	
1093 (s)	1095 (3) p	$a_1$	19A	
1109 (s)	1110 (6) p	$a_1$	2	
	1148 (0)			
1174 (w)	1174 (2) p	$a_1$	9A	
1213 (vw)	1214 (0)			
1231 (vw)	1249 (0)			
1283 (m)	1290 (2)	$b_1$	3	
1314 (m)		$b_1$	14	
1347 (vs)	1347 (10) p	$a_1$		NO <sub>2</sub> stretching
1355 (sh)				
1380 (sh)	1387 (2) dp			
1426 (m)	1426 (3) p	$a_1$	20A	
1464 (sh)		$a_1$	13	
1481 (vs)	1480 (3) p	$a_1$	7A	
1514 (sh)		$b_1$	19B	
1526 (vs)	1523 (3) dp	$b_1$		NO <sub>2</sub> asymmetric stretching
1564 (vw)				

TABLE I (contd.)

Infrared, $\nu$ in $\text{cm}^{-1}$ . Solid at $26^\circ\text{C}$	Raman, $\Delta\nu$ in $\text{cm}^{-1}$ . Liquid at $90^\circ\text{C}$	Assignment		Remarks
		Species	Corresponding modes of benzene	
1581 (s)	1577 (8) dp	$a_1$	8A	
1607 (s)	1605 (2) dp	$b_1$	8B	
1630 (w)				
1660 (w)*				
1690 (sh)*				
1705 (sh)*				
1730 (vvw)*				
1780 (w)*				
1828 (vw)*				
1840 (vw)*				
1880 (sh)*				
1920 (w)*				
1974 (vw)*				
2030 (vvw)*				
2090 (vvw)*				
2135 (vvw)				
2215 (sh)*				
2228 (vw)*				
2291 (w)*				
2454 (w)*				
2570 (sh)*				
2595 (vw)*				
2630 (vvw)*				
2690 (vw)*				
2757 (vw)*				
2855 (w)*				
2930 (vw)*				
3050 (sh)*		$b_1$	7B	
3085 (sh)*	3087 (3) p			
3110 (m)*		$b_1$	20B	
3157 (sh)*				
3205 (sh)*				
3300 (sh)*				
3580 (vvw)*				
3665 (sh)*				
3690 (vvw)*				
3718 (sh)*				
3825 (vvw)*				
3920 (vvw)*				

(s)=strong; (m)=medium; (w)=weak; (vw)=very weak (sh)=shoulder; (b)=broad;  
p=polarised; dp=depolarised.

†Taken from Mooney (1964).

\*Frequency observed in  $\text{CCl}_4$  solution.

4  $a_2$ (Raman active) | 7 $b_2$  (infrared and Raman active).

The species  $a_1$  would give rise to polarised Raman lines and the remaining species to depolarised Raman lines

*Species  $a_1$*  The eleven  $a_1$  modes taking  $\text{NO}_2$  as a single group are derived from the modes 1, 2, 6A, 7A, 8A, 9A, 12, 13, 18A, 19A and 20A of benzene (Wilson, 1934). In the disubstituted benzenes with the substituents in the para positions, the frequencies of the Modes 1, 6A, 7A, 8A, 12, 13, 18A, 19A and 20A are expected to be lowered considerably due to the presence of the heavy atoms in the para positions. The probable values of the frequencies which can be assigned to these modes are shown in the last but one column of Table I. The intense polarised Raman line  $855\text{ cm}^{-1}$  has been assigned to  $\nu_1$ . Its appearance also as a strong infrared band may be due to the difference in the two substituents. The polarised line  $1480\text{ cm}^{-1}$  is assigned to  $\nu_{7A}$  and the strong infrared band at  $1481\text{ cm}^{-1}$  may be due to superposition of the bands due to modes  $\nu_{7A}$  and  $\nu_{10B}$ . The other polarised line  $1426\text{ cm}^{-1}$  is assigned to  $\nu_{20A}$  and the infrared frequency  $1964\text{ cm}^{-1}$  may be due to  $\nu_{13}$ . The intense depolarised Raman line  $1577\text{ cm}^{-1}$  is evidently due to  $\nu_{8A}$  and the weak line  $314\text{ cm}^{-1}$  is due to  $\nu_{6A}$ , as suggested by Mocke-Korkhof (1951). The strong polarised line  $1110\text{ cm}^{-1}$  is assigned to  $\nu_2$  and the polarised Raman line  $1174\text{ cm}^{-1}$  to  $\nu_{9A}$ , because this latter mode is not affected by the substitution in the para position. The strong infrared band at  $846\text{ cm}^{-1}$  is assigned to  $\nu_{12}$  and it may have also appeared feebly as a weak unresolved companion of the line  $855\text{ cm}^{-1}$  in the Raman spectrum. The strong infrared band at  $740\text{ cm}^{-1}$  may be due to  $\nu_{18A}$  and the polarised line  $1095\text{ cm}^{-1}$  is probably due to  $\nu_{19A}$  as suggested by Mocke-Kherkhof (1951). The other two modes of this species are the symmetric stretching and bending vibrations of  $\text{NO}_2$  group giving the Raman lines  $1347\text{ cm}^{-1}$  and  $677\text{ cm}^{-1}$  respectively.

*Species  $b_1$*  Out of the twelve modes of this species ten are derived from the modes 3, 6B, 7B, 8B, 9B, 14, 15, 18B, 19B and 20B of benzene respectively and the remaining two are contributed by the  $\text{NO}_2$  group. The frequencies of the modes 6B, 8B, 7B and 20B remain unchanged on substitution. So, the Raman lines  $623$  and  $1605\text{ cm}^{-1}$  are assigned to  $\nu_{6B}$  and  $\nu_{8B}$  respectively and the infrared bands at  $3110\text{ cm}^{-1}$  and  $3050\text{ cm}^{-1}$  are assigned to the modes  $\nu_{20B}$  and  $\nu_{7B}$  respectively. The Raman line  $1290\text{ cm}^{-1}$  may be due to  $\nu_3$ . The Raman line at  $3087\text{ cm}^{-1}$  may be due to one of the two modes which can be derived from a superposition of  $\nu_2$  and  $\nu_{8B}$ . The depolarised Raman line  $734\text{ cm}^{-1}$  is assigned to  $\nu_{9B}$  and the weak band at  $467\text{ cm}^{-1}$  to  $\nu_{18B}$ . As mentioned earlier, the infrared band at  $1481\text{ cm}^{-1}$  is due to  $\nu_{19B}$ . The infrared bands at  $1314\text{ cm}^{-1}$  and  $1056\text{ cm}^{-1}$  may be assigned tentatively to  $\nu_{14}$  and  $\nu_{15}$  respectively, as the destruction of centre of symmetry makes these modes weakly allowed in the infrared. The remaining two modes of this species are due to the asymmetric

stretching and rocking vibrations of the  $\text{NO}_2$  group giving the depolarised line  $1523\text{ cm}^{-1}$  and the weak line  $444\text{ cm}^{-1}$  respectively.

*Species  $a_2$ .* There are three vibrations of this molecule belonging to species  $a_2$  corresponding to the modes  $\nu_{10A}$ ,  $\nu_{16A}$  and  $\nu_{17A}$  of benzene. The frequency of  $\nu_{10A}$  should be  $849\text{ cm}^{-1}$  as benzene gives a Raman line of this frequency but it is not possible to resolve this line from the strong line at  $855\text{ cm}^{-1}$ . The line  $415\text{ cm}^{-1}$  is given by the mode  $\nu_{16A}$  and probably the weak line  $1015\text{ cm}^{-1}$  is due to  $\nu_{17A}$ , the corresponding infrared band  $1013\text{ cm}^{-1}$  being of medium strength. The fourth vibration arises from  $\text{NO}_2$  twisting which has not appeared in the spectra.

*Species  $b_2$ .* Six modes of this species arise from the modes  $\nu_1$ ,  $\nu_5$ ,  $\nu_{10B}$ ,  $\nu_{11}$ ,  $\nu_{16B}$  and  $\nu_{17B}$  of benzene. All these modes are expected to have frequencies lower than the corresponding frequencies of benzene. The Raman lines  $212$ ,  $276$  and  $367\text{ cm}^{-1}$  can be assigned to  $\nu_{16B}$ ,  $\nu_{11}$  and  $\nu_4$  respectively. The Raman lines  $569$  and  $597\text{ cm}^{-1}$  may be assigned to  $\nu_{10B}$  and  $\nu_{17B}$  respectively and the line  $790\text{ cm}^{-1}$  may be due to  $\nu_5$ . The seventh vibration arises from  $\text{NO}_2$  out of plane rocking and is assigned to the frequency  $530\text{ cm}^{-1}$  appearing both in the Raman and infrared spectra.

Besides the frequencies mentioned above numerous bands, mostly very weak have been observed in the infrared spectrum of the solution in the region from  $1630\text{ cm}^{-1}$  to  $3920\text{ cm}^{-1}$ . The bands are evidently due to combinations of some of the fundamental modes mentioned above.

#### ACKNOWLEDGMENT

The author is grateful to Dr. G. S. Kastha, D.Sc., for his helpful discussions.

#### REFERENCES

- High, M. E., 1931, *Phys. Rev.*, **38**, 1837.  
 Lecomte, J., 1938, *J. Phys. Radium*, **9**, 13.  
 Manzoni-Ansidei, R., 1935, *Gazz. Chim. Ital.*, **65**, 871.  
 Mecke-Korkhof, 1951 Landolt-Bornstein Tables, Auflage 6, Band 1.  
 Medhi, K. C., 1964, *Spectrochim. Acta.*, **20**, 675.  
 Moonoy, E. F., 1964, *Spectrochim. Acta.*, **20**, 1021.  
 Reitz, A. W. and Stockmair, 1936, *Monatsh. Chem.*, **67**, 92.  
 Wilson, E. B., 1934, *Phys. Rev.*, **45**, 706.  
 Wittek, H., 1942, *Z. Physik. Chem. B* **52**, 153, 315.

# LIGHT ABSORPTION IN $\text{NO}_3$ ION IN STATE OF SOLUTION

## (Part III.—Effect of Cation)

A MOOKHERJI AND S. P. TANDON\*\*

PHYSICAL LABORATORIES, UNIVERSITY OF BURDWAN, BURDWAN, (W.B.)  
INDIA

**ABSTRACT.** 200  $m\mu$  band, which is an allowed  $\pi \rightarrow \pi^*$  transition, has been studied in five monovalent nitrates. The blue shift of the band has been found to be proportional to the inverse of the cationic radius.

### INTRODUCTION

In the preceding part (Part II) of the present series of papers, a systematic study of the characteristics and assignment of the 200 $m\mu$  band of nitrate ion has been reported (Mookherji and Tandon, 1965).

Absorption bands are observed to suffer a shift towards shorter wavelength due to the effect of environment known as blue shift. In the state of solution the factors which presumably affect the position of the electronic bands are ion-ion and ion-solvent interactions. The former has not been studied in the case of 200 $m\mu$  band of the nitrate ion while the latter has been studied in some details (McConnell, 1952, Strickler, 1961, Strickler and Kasha, 1961) and will be discussed in the next paper of the series.

In dilute solutions ion-ion interactions are expected to be very weak and are usually masked by the ion-solvent effect. Ion-ion interactions are of two types, anion-cation and anion-anion. The later interactions are so weak that they can not be recorded. So there is a possibility of studying only the former by investigating the spectral shifts, keeping all other parameters constant and varying the cation. The importance of this lies in the expectation that it may become a tool for making direct measurements of intermolecular interactions.

The present communication reports a systematic study of the effect of cation on the energy of the 200 $m\mu$  band, which has been assigned to  $D_{3h}$  symmetry allowed  $\pi \rightarrow \pi^*$  transition of the nitrate ion (Mookherji and Tandon, 1962, 1965) in state of aqueous solution. The results have been discussed in the light of the work of Mott and Gurney, (1948), Meyerstein and Treinin, (1961) and Smith and Boston (1961).

---

\*\*Present address : Physical Laboratories, University of Jodhpur, Jodhpur, Rajasthan, India.



# EXPERIMENTAL RESULTS

The results of measurements of absorption with UVISPEK spectrophotometer reported earlier (Mookherji and Tandon, 1965) have been used. Energy in electron volts of these peaks- (A, B, C, D and E of  $200\text{m}\mu$ ) against inverse of the radius of five monovalent cations, —lithium, sodium, potassium, silver and ammonium, have been given in Fig. 1.

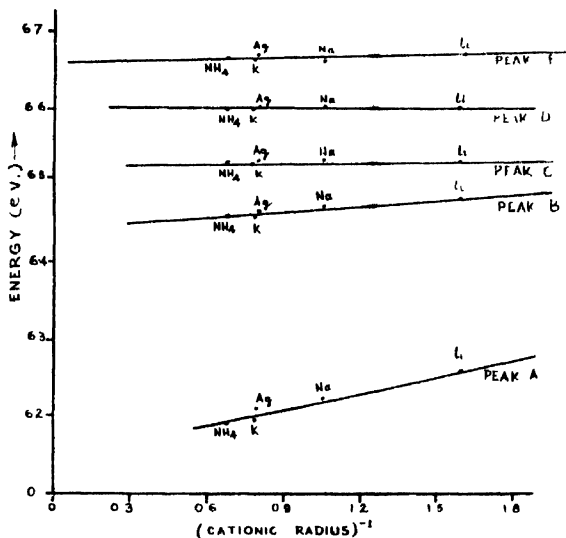


Fig. 1. Variation of energy of peaks A, B, C, D and E of  $200\text{m}\mu$  band of nitrate ion with  $(\text{Cationic radius})^{-1}$ .

# DISCUSSION

A study of Fig. 1 reveals a blue shift with decrease of cation radius for the nitrates studied. To explain such band shifts due to environment several theories have been proposed (Griffiths and Symons, 1960a) in connection with the electron transfer spectra. In an aqueous solution there is also possibility of ion-pairs formation. An internal transition in an anion, brings about only a limited expansion of the electronic orbital, and hence will be probably affected only by the external polarizing effect of the cations (Kortum, 1944; Griffiths and Symons, 1960b) suggesting that the cation would affect the spectrum of anion only at contact approach. But in the present case of nitrate ion, it is possible for the cationic effect to be conveyed (Meyerstein and Treinin, 1961) through the first hydration layer. In dilute aqueous solutions solvated cations which have the nitrate ions as nearest neighbours may be attached quite firmly to the cation. This is the case of local hydrolysis (Diamond, 1958), and is an extreme case of polarization. The polarized water must be more H-bonded to nitrate ion and thus will act as a more polar solvent than ordinary water. The magnitude of the ionic effects

will depend on the charge on the cation, distance and mode of approach to the nitrate ion. Thus the cations having only one water molecule separating them from nitrate ion are expected to have an effect decreasing with increasing cationic radii. This is what has been observed. But this mechanism of band shift is analogous to that of electron transfer spectra. It has already been proved (Mc Ewen, 1961; Strickler and Kasha, 1961; Mookherji and Tandon, 1962, 1965) that the spectrum of the nitrate ion is not due to electron transfer, but due to an allowed  $\pi \rightarrow \pi^*$  transition, which shifts the electronic charge density from the region round oxygen atoms to the region around nitrogen atom. Consequently the blue shift may be explained as follows :

In solution (Mott and Gurney, 1948) like crystal and melt (Smith and Boston, 1961) there exist two types of forces, Coulomb and Overlap forces. The Coulomb forces of the other ions give rise to the external electrostatic potential,  $V$ , arising from pairwise electrostatic interaction between ions. For solutions containing  $N$  ions, we have then

$$V(r_{NO_3}) = \sum_{i=1}^{N-1} \frac{e}{D} \int \frac{\rho_i(r_i)}{r_{NO_3} - r_i} dV_i \quad \dots (1)$$

Where  $r_{NO_3}$  is the vector position of the volume element ( $dV_{NO_3}$ ) in the nitrate ion that becomes excited,  $r_i$  is the vector position of a volume element  $dV_i$  in the  $i$ -th ion,  $\rho_i(r_i)$  is the charge density function of the  $i$ -th ion,  $e$  is the electronic charge and  $D$  is effective dielectric constant. The term  $r_{NO_3} \cdot r_i$  is the scalar distance between  $dV_{NO_3}$  and  $dV_i$ .

The external electrostatic potential  $V$  is positive because nitrate ion is negative. The dipole and higher terms in  $V$  are produced primarily by neighbouring ions. Therefore it is useful to divide the ions into two groups : those ions which lie nearest to a given nitrate ion and those ions which are more remote. The nearest neighbours are cations and are assumed to have rare-gas-electronic configurations, with small polarization terms ignored. These cations can be represented as point charges and the following change made in equation (1) :

$$V(r_{NO_3}) = \sum_{i=1}^C \frac{e}{D} \int \frac{Z_i}{(r_{NO_3})_i} dV_{NO_3} + V_{other} \quad \dots (2)$$

Where  $Z_i$  is the net charge or electrostatic valence of the  $i$ -th cation,  $(r_{NO_3})_i$  is the scalar distance from the centre of the  $i$ -th cation to the volume element  $dV_{NO_3}$  of the nitrate ion, the summation is over the  $C$ -cations of the nearest neighbour shell, and  $V$  is the term similar to equation (1) but is summed from  $(C+1)$  through  $(N-1)$ . The dipole and higher terms in equation (2) are of greatest magnitude near the neighbour cations where they increase as the cationic  $Z/r_0$  increase.

The potential  $V$  as discussed above contributes to the transition energy in a way approximately described by (Smith *et al*, 1961).

$$(h\nu)_{\max} = (h\nu)_0 + e\int (|\psi_{er}|^2 - |\psi_{gr}|^2)VdV \quad \dots \quad (3)$$

where  $(h\nu)_0$  represents the transition energy for a nitrate ion separated to infinity including the effect of repulsive overlap forces and the integral represents the change in interaction energy between  $V$  and the electronic charge cloud of the nitrate ion in going from the ground to the excited states  $|\psi_{gr}|^2$  and  $|\psi_{er}|^2$  are the electronic density functions of the ground and the excited states respectively, and the integral is over the volume of the nitrate ion since dipole and higher terms in equation (2) are of great magnitude near the neighbouring cations, where they increase as the cationic  $Z/r_0$  increase. Consequently the interaction integral in equation (3) changes when  $Z/r_0$  changes. This explains the observed dependence of energy of the  $200\text{m}\mu$  band on  $1/r_0$ .

#### R E F E R E N C E S

- Diamond, R. M., 1958, *J. Amer. Chem. Soc.*, **80**, 4808  
 Griffith, T. R. and Symons, M. C. R., 1960a, *Trans. Faraday Soc., London*, **56**, 1125.  
 Griffith, T. R. and Symons, M. C. R., 1960b, *Mol. Phys.*, **3**, 90.  
 Kortum, G., 1944, *Z. Electrochem.*, **50**, 144.  
 McConnell, H., 1952, *J. Chem. Phys.*, **20**, 700.  
 McEwen, K. L., 1961, *J. Chem. Phys.*, **34**, 547.  
 Myerstein, D. and Troinin, A., 1961, *Trans. Faraday Soc., London*, **57**, 2104.  
 Mookerji, A. and Tandon, S. P., 1962, *Ind. J. Phys.*, **36**, 211.  
 Mookherji, A. and Tandon, S. P., 1965, *Ind. J. Phys.*, **39**, 137  
 Mott, N. F. and Gurney, R. W., 1948, *Electronic Processes in Ionic crystals* Oxford University Press, New York, 2nd Ed.  
 Smith, G. P. and Boston, C. R., 1961, *J. Chem. Phys.*, **34**, 1396.  
 Strickler, S. J., 1961 Ph.D. Dissertations, Florida State University.  
 Strickler, S. J. and Kasha, M., 1961, *J. Chem. Phys.*, **34**, 1077.

# Letters to the Editor

The Board of Editors does not hold itself responsible for opinions expressed in the letters published in this section. The notes containing short reports of original investigations communicated to this section should not contain many figures and should not exceed 500 words in length. The contributions reaching the Secretary by the 15th of any month may be expected to appear in the issue for the next month. No proof will be sent to the author.

17

## MATRIX RELATIONS BETWEEN DIRECTION COSINES AND MILLERIAN INDICES

J. K. GHOSE

DEPARTMENT OF PHYSICS, ST JOHN'S COLLEGE, AGRA.

(Received May 15, 1965)

For magnetic measurements in triclinic crystals, directions are usually specified by the Millerian indices of one or two planes, while for many calculations, the direction cosines with reference to some orthogonal axes  $x, y, z$ , are necessary. As an example, suppose the  $z$  axis coincides with the crystallographic  $c$  axis and the  $x$  axis lies in the  $a-c$  plane close to the  $a$  axis. The cosines of the angles between the various axes are as follows.

	a	b	c
$x$	$\sin \beta$	$(\cos \gamma - \cos \alpha \cos \beta) / \sin \beta$	0
$y$	0	$M / \sin \beta$	0
$z$	$\cos \beta$	$\cos \alpha$	1

where  $M = (1 - \cos^2 \alpha - \cos^2 \beta - \cos^2 \gamma - 2 \cos \alpha \cos \beta \cos \gamma)^{1/2}$  and is positive. The matrix  $[J]$  of transformation from  $x, y, z$  to  $a, b, c$ , is the matrix formed by the trigonometrical quantities as arranged in the above table (Ghose, 1964). These coordinates  $x, y, z$ , have a slight advantage compared to those discussed by U. S. Ghosh and Mitra (1965), because the determinant of  $[J]$  is positive. The values of  $[J]$  and  $[J]^{-1}$  need be calculated only once for a particular variety of crystal. It may be verified that

$$[J]^{-1} = \begin{bmatrix} 1 & \cos \alpha \cos \beta - \cos \gamma & 0 \\ \sin \beta & M \sin \beta & 0 \\ 0 & \frac{\sin \beta}{M} & 0 \\ -\frac{\cos \beta}{\sin \beta} & \frac{\cos \beta \cos \gamma - \cos \alpha}{M \sin \beta} & 1 \end{bmatrix}$$

As shown by Ghose (1964), a unit vector  $[\xi \eta \zeta]$  in  $x, y, z$  coordinates, transforms to a unit covariant vector  $[V_p]$  and a unit contravariant vector  $[V^p]$  in  $a, b, c$  coordinates such that

$$[\xi \eta \zeta] = [V_a V_b V_c][J]^{-1} = [J][V^a V^b V^c]' \quad \dots (1)$$

It may be noted that  $V_a, V_b, V_c$  are cosines of the angles made by the unit vector with  $a, b, c$  axes while  $\xi, \eta, \zeta$  are those made with the orthogonal  $x, y, z$  axes.

If  $a:b:c$  be the axial length ratio and  $(hkl)$  be the Miller indices of a plane, then any contravariant vector lying in this plane, is given by

$$[U^a U^b U^c] = \left[ (m+n) \frac{a}{h} - \frac{mb}{k} - \frac{nc}{l} \right]$$

where  $m$  and  $n$  are any two numbers. For a covariant unit vector  $[V_p]$  normal to this plane,  $[V_p][U^p]$  is zero for all values of  $m$  and  $n$ . Hence we get

$$[V_a V_b V_c] = Q \begin{bmatrix} h & k & l \\ a & b & c \end{bmatrix} \quad \dots (2)$$

where  $Q$  is a suitable multiplier to make the magnitude of the vector equal to unity.

Again if two planes  $(hkl)$  and  $(h'k'l')$  are both kept perpendicular to the plane of measurement, then the normal to the latter lies in both  $(hkl)$  and  $(h'k'l')$  planes and is given by the contravariant vector

$$[V^a V^b V^c]' = Q_1 [a(kl' - k'l) \ b(lh' - l'h) \ c(hk' - h'k)]' \quad \dots (3)$$

where  $Q_1$  is a suitable multiplier.

Values of  $\xi, \eta, \zeta$  may be found by combining either eq. (2) or eq. (3) with eq.(1). If  $\xi_1, \eta_1, \zeta_1$  are the values obtained when  $Q$  or  $Q_1$  is arbitrarily taken as 1, then the actual value of  $Q$  or  $Q_1$  is  $(\xi_1^2 + \eta_1^2 + \zeta_1^2)^{-1/2}$ . When only the ratio of two direction cosines is required,  $Q$  need not be calculated.

This matrix method of calculating the direction cosines seems to be simpler and quicker than other methods.

#### REFERENCES

- Ghose, J. K., 1964, *Ind. Jour. pure appl. Phys.*, **2**, 94.  
 Ghosh, U. S. and Mitra, S., 1964, *Ind. J. Phys.*, **39**, 19.

# THE INTRINSIC DIELECTRIC CONSTANT OF SALICYLIC ACID AND BENZOIC ACID

TATHAGATA SEN

MACROWAVE LABORATORY, PHYSICS DEPARTMENT, ANDHRA UNIVERSITY, WALTAIR.

(Received July 23, 1965; Communicated by Prof K. Rangadhama Rao)

The experimental arrangement\* consists of a slotted coaxial transmission line fed by an ultra high frequency unit oscillator of General Radio Company. The powdered sample is packed into a specially designed dielectric cell terminating one end of the transmission line.

The measurements are made by the standing wave method of Roberts and von Hippel (1946). The technique of square wave amplitude modulation is employed to improve the sensitivity of measurements.

Experiments are conducted over a range of volume fractions for each of the two organic substances. The apparent dielectric constants are then computed by the formula of Dakin and Works (1947). To evaluate the intrinsic dielectric constant  $\epsilon_i$  from the logarithmic formula of Rabinovitch (1964),

$$\log \epsilon_A = P \log \epsilon_i + K$$

graphs are drawn for the two substances taking  $P$ , the volume fraction, on the  $X$  axis and the apparent dielectric constant  $\epsilon_A$  on the  $Y$  axis. Linear plots shown in Fig. 1(a) and (b) are obtained. The intercept (not shown in the figures) on the

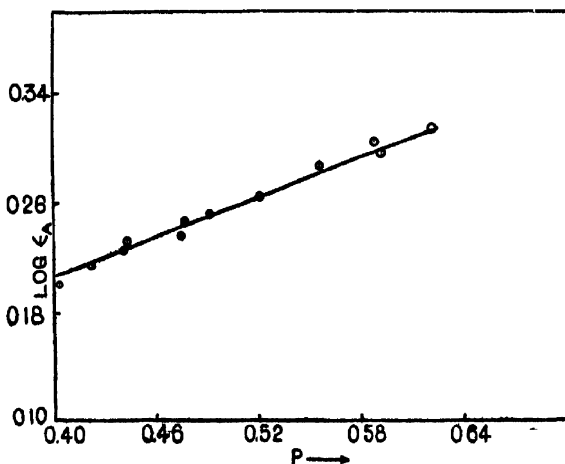


FIGURE 1(a)

Variation of  $\log \epsilon_A$  with  $P$  for Benzoic acid.

\* K. S. Ramakrishna Rao collaborated with the author in setting up this arrangement.

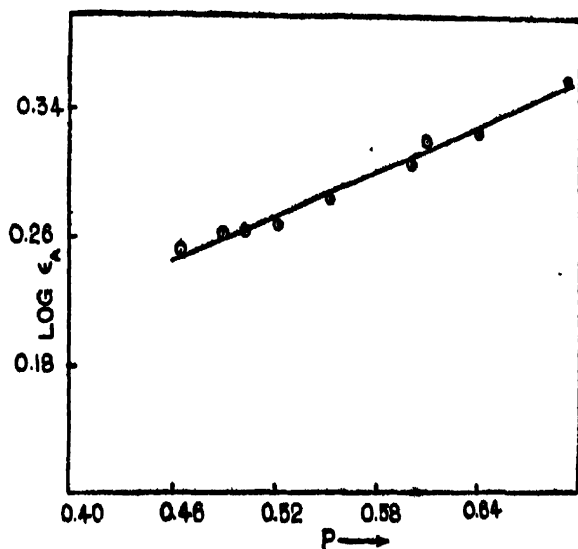


FIGURE 1(6)

Variation of  $\log \epsilon_A$  with  $P$  for Salicylic acid.

$Y$  axis gives the value of ' $k$ '. The intrinsic dielectric constants obtained are given in Table I. Details of the experimental method will be reported shortly.

TABLE I.

Substance	Intrinsic dielectric constant
Benzoic Acid	3.02
Salicylic Acid	2.95

The author is greatly indebted to Prof. K. R. Rao, for his invaluable guidance and to the Council of Scientific and Industrial Research for the award of fellowship.

## REFERENCES

- Dakin, T. W. and Works, C. N., 1947, *J. Appl. Phys.*, **18**, 789.  
 Rabinovitch, M., 11 May, 1964, *C. R. Acad. Sci. (France)*, **258**, 19, 4663-5.  
 Roberts, S. and Von. Hippel, A., 1946, *J. Appl. Phys.*, **17**, 610.

## BOOK REVIEW

IR —THEORY AND PRACTICE OF INFRARED SPECTROSCOPY —by  
Herman A. Szymanski. Pp. XIV+375. Plenum Press, New York, 1964.  
Price \$ 15.00.

The present book under review is, as mentioned on the jacket "a single ready reference to the technology of infrared spectroscopy". It is suitable for beginners as well as for those who have started research works in this subject. The chapter on instrumentation by Nelson L. Alpert, Chief Engineer, Product Design and Development, Perkin-Elmer Corporation is highly gratifying, because it has come from such a source which has provided the various scientific institutions with highly versatile instruments. However, the space devoted seems to be inadequate and the inclusion of the working of an actual spectrophotometer would have been very useful. The chapters dealing with theoretical considerations in infrared spectroscopy contain all the essential topics. But it appears that the section on group theory could have been reduced to give more space to topics like Fermi and Coriolis Perturbations, Inversion doubling l-type doubling and Band contours of the symmetric and asymmetric rotors. The chapter on the use of characteristic group frequencies in Structural Analysis extends over 100 pages of which those dealing with the structural units  $\text{CH}_3$ ,  $\text{CH}_2$ ,  $\text{CH}$ ,  $\text{C}=\text{C}$  cover about seventy pages. This is out of proportion to the pages devoted for all other important and characteristic groups. This may be considered to be a defect. The topic of Quantitative Analysis has been given a place but however, some important topics such as hydrogen bonding, solvent shifts in solutions etc. have not been properly dealt with.

Though there is a special chapter devoted to different methods of documentation, abstracting and reference service, the number of references in the text is not large.

A novel feature of this book is the examples of spectra, many of which have been run on high resolution instruments, contained in a separate packet. The many illustrations, charts, graphs and examples have increased the usefulness of the book.

G. S. K.



# MEAN AMPLITUDES OF VARIATION, BASTIANSEN-MORINO SHRINKAGE EFFECT AND MOLECULAR POLARIZABILITIES FOR THE DIHALIDES OF SOME GROUP IIA ELEMENTS

G. NAGARAJAN

DEPARTMENT OF CHEMISTRY, UNIVERSITY OF MARYLAND, COLLEGE PARK,  
MARYLAND, U.S.A.

(Received May 19, 1965; Resubmitted August 6, 1965)

**ABSTRACT.** A brief survey of the vibrational and dimensional analysis is given for the gaseous dihalides of some group IIA elements possessing a linear symmetrical structure with the symmetry point group  $D_{\infty h}$ . The transferability of vibrational frequencies among related molecules is discussed. Mean-square amplitude quantities, generalized mean-square amplitudes (mean-square parallel amplitudes, mean-square perpendicular amplitudes and mean cross products) and mean amplitudes of vibration for the bonded as well as nonbonded atom pairs have been evaluated by the Cyvin method utilizing symmetry coordinates at the temperatures  $T = 500^\circ\text{K}$ ,  $T = 1000^\circ\text{K}$  and  $T = 1500^\circ\text{K}$ . The values of Bastiansen-Morino shrinkage effect have been computed at these temperatures. The bond and molecular polarizabilities have also been calculated by the Lippincott-Stutman method employing the delta-function model of chemical binding. The calculated values of the molecular polarizabilities are in good agreement with the available experimental ones.

## INTRODUCTION

The dihalides of group IIA elements were for many years subjected to several vibrational and structural investigations in deciding whether they have a linear configuration with the symmetry point group  $D_{\infty h}$  or a bent one with the symmetry point group  $C_{2v}$ . However, the recent investigations have very categorically confirmed that these metal dihalides possess only a  $D_{\infty h}$  symmetry and not a  $C_{2v}$  one. It is aimed here to evaluate the mean amplitudes of vibration and Bastiansen-Morino shrinkage effect for these dihalides with help of the recent vibrational and structural data by the Cyvin method (1959) at the temperatures  $T = 500^\circ\text{K}$ ,  $T = 1000^\circ\text{K}$  and  $T = 1500^\circ\text{K}$  with a view that the results of the present investigation would be very helpful for the interpretation of the results of electron diffraction studies. Lippincott and Stutman (1964) recently applied the delta-function potential model to the calculation of bond and molecular polarizabilities of various diatomic and polyatomic molecules having their elements only from and beyond the IVA-group of the periodic table and their results are in good agreement with the experimental ones obtained from molar refractions, dielectric constants etc. through the well-known relations such as Langevin-Debye

and Lorentz-Lorentz equations. Such a model has not been so far applied to molecules having their elements from below the IVA-group and B-group of the periodic table. In the way of further testing the accuracy of the delta-function model of chemical binding, it is also aimed here to calculate the bond and molecular polarizabilities for the dihalides and compare the calculated molecular polarizabilities with the available experimental values.

#### VIBRATIONAL AND STRUCTURAL ANALYSIS

Braune and Knocke (1933), Gregg *et al* (1937) and Akishin *et al* (1957, 1958) confirmed from their electron diffraction studies a linear symmetrical structure for the dihalides of the second group elements. Warton *et al* (1963) recently explained by the deflection of beams of alkaline-earth halides by inhomogeneous electric fields that barium halides, strontium fluoride, strontium chloride and calcium fluoride have permanent electric dipole moments, which implies that they do not have a center of symmetry. No polarity was observed for the higher members of calcium and strontium families. This observation is most naturally interpreted as implying a non-linear equilibrium geometry. The general trend found in the alkaline-earth dihalides was that large metal atoms and small halogens favoured a rather bent configuration. Later, Buehler *et al* (1964) re-examined the deflection of mass spectrometrically detected beams of the fluorides and chlorides of many metals and found that all were nonpolar except calcium fluoride thereby lending support to the results of earlier electron diffraction studies (1933, 1937, 1957, 1958) as well as vibrational and electronic spectral studies (1964).

The vibrational frequencies, molecular structure and molecular weight yield to the calculation of the vibrational, rotational and translational contributions to the free energy functions of the gaseous molecules. Where sufficient vibrational data is unavailable for a molecular system, vibrational frequencies from related molecules having similar chemical bonds may be substituted, or the frequencies lacking may be estimated from force constants of related molecules by employing a suitable potential energy function. In cases of simple triatomic molecules, the vibrational frequencies may well be evaluated from the frequencies observed for related diatomic molecules by using a suitable valence force model. The values of the free energy functions thus calculated spectroscopically may be compared with those of the experimental ones. Several investigators have successfully applied this method for many molecules and a detailed account has been given by Nagarajan (1964). Following this method and with help of the available spectroscopic data cited above (1964), Brewer *et al* (1963) evaluated the unassigned fundamental frequencies for the dihalides of beryllium, magnesium, calcium, strontium, barium, zinc, cadmium, mercury, titanium, vanadium, chromium, manganese, iron, cobalt, nickel, copper, tin, and lead by the process of transferring the characteristic frequencies, force constants and internuclear distances from related molecules having similar chemical bonds, calculated the free energy func-

tions and compared them with those experimentally observed. On the basis of the principle postulated by Cyvin (1959), the mean amplitudes of vibration and Bastiansen-Morino shrinkage effect were evaluated by Nagarajan (1964) for these molecules except for the dihalides of calcium, strontium and barium by using the vibrational and structural data described above. The fundamental frequencies in  $\text{cm}^{-1}$  and internuclear distances in Å for the dihalides of calcium, strontium and barium are, in accordance with the recent vibrational and structural studies cited above, given in Table I.

#### MEAN AMPLITUDES OF VIBRATION

A linear symmetrical triatomic molecule  $i-j-i$  possessing the symmetry point group  $D_{\infty h}$  gives rise, according to the relevant symmetry considerations and selection rules (1960), to four vibrational degrees of freedom constituting only three fundamental frequencies under the various irreducible representations as follows  $\Sigma_g^+ + \pi_u + \Sigma_u^+$  where the gerade mode is Raman active only and symmetric with respect to the center of symmetry while the ungerade modes are infrared active only and asymmetric with respect to the center of symmetry. The frequency  $\nu_1$  corresponds to a totally symmetrical stretching mode under the symmetry species  $\Sigma_g^+$ ,  $\nu_2$  to a bending mode under the species  $\pi_u$  and  $\nu_3$  to an asymmetrical stretching mode under the species  $\Sigma_u^+$ . The vibrations coming under the species  $\Sigma_g^+$  and  $\Sigma_u^+$  are nondegenerate and parallel vibrations while the remaining under the species  $\pi_u$  is a doubly degenerate and perpendicular one. A schematic representation of the normal modes of oscillation for a molecule of the present study has already been given by Herzberg (1960).

Cyvin (1959) was, in the analysis of molecular vibrations, the first to introduce the symmetry coordinates into the evaluation of mean-square amplitudes of vibration. On the basis of the principle postulated by Cyvin (1959), a theory for the determination of mean-square amplitudes of vibration for a molecule of the present study has already been developed by Cyvin himself (1959, 1960) and applied to many molecules. The same method has been adopted here and one may refer to Cyvin (1959-1960) for the detailed theoretical considerations and calculations. The secular equations giving the normal frequencies in terms of the mean-square amplitude quantities were constructed with help of the fundamental frequencies and internuclear distances in wave numbers and Angstrom units given in Table I and  $\Sigma$  and  $G$  matrices at the temperatures  $T = 500^\circ\text{K}$ ,  $T = 1000^\circ\text{K}$  and  $T = 1500^\circ\text{K}$  for the dihalides of calcium, strontium and barium. Since all the experiments will be done only at very high temperatures, the secular equations were constructed here above  $500^\circ\text{K}$ . Since the secular equation is, on account of the greater symmetry of the molecular system, singular under every symmetry species, the three fundamental frequencies are well sufficient to evaluate the three vibrational constants, namely,  $\Sigma_{11}$ ,  $\Sigma_{22}$  and  $\Sigma_{33}$ . From those three symmetrized mean-square amplitude matrices, the mean-square amplitude quantities were

calculated and their values in  $\text{\AA}^2$  are given in Table II for all the molecules studied at the temperatures  $T = 500^\circ\text{K}$ ,  $T = 1000^\circ\text{K}$  and  $T = 1500^\circ\text{K}$  where  $\sigma_r$  is the mean-square amplitude quantity due to the bonded atom pair  $i-j$ ,  $\sigma_{rr}$  the quantity due to the interaction of the bonded atom pairs and  $\sigma_\theta$  the quantity due to the bending of the molecule. The generalized mean-square amplitude quantities (mean-square parallel amplitudes  $\langle\Delta z^2\rangle$ , mean-square perpendicular amplitudes  $\langle\Delta x^2\rangle$  and  $\langle\Delta y^2\rangle$  and mean cross products  $\langle\Delta x\Delta y\rangle$ ,  $\langle\Delta y\Delta z\rangle$  and  $\langle\Delta z\Delta x\rangle$ ) are given in Table III in  $\text{\AA}^2$  for the bonded as well as nonbonded atom pairs at the temperatures  $T = 500^\circ\text{K}$ ,  $T = 1000^\circ\text{K}$  and  $T = 1500^\circ\text{K}$ . The corresponding calculated values of the mean amplitudes of vibration in  $\text{\AA}$  are given in Table IV at the three temperatures for the bonded and nonbonded distances.

The mean-square amplitude of vibration due to the bending of the molecule is in general very much greater than that due to the bonded atom pair and the quantity due to the interaction of the bonded atom pairs is negligibly small in many cases (see Table II). By symmetry of the molecular system, the mean-square perpendicular amplitudes of vibration for the bonded atom pair and the mean cross products for the bonded as well as nonbonded atom pairs become vanished. Hence the mean cross products are not listed in Table III.

The mean amplitude of vibration for the nonbonded atom pair is in general greater than that of the bonded atom pair for all the molecules (see Table IV). This shows that larger the distance between the atoms greater will be the value for the mean amplitude of vibration. Further, the mean amplitude of vibration for the bonded as well as nonbonded atom pairs are in the increasing order at any temperature toward the higher members in the halogen series of the elements studied. This evidently shows that the replacement of end atoms with atoms of higher atomic weight to the molecular system causes a decrease in the fundamental frequencies (see Table I) and an increase in the mean amplitudes of vibration for the bonded and nonbonded distances. The situation is reversed in the cases of corresponding force constants. Though the electron diffraction studies were made for all the molecules studied, the values of mean amplitudes of vibration were not reported such that a comparison could be made here. However, the results of the present investigation would be very useful for the interpretation of the results of electron diffraction studies when undertaken again for these molecules.

#### BASTIANSEN-MORINO SHRINKAGE EFFECT

The distance between the oxygen atoms in carbon dioxide observed from electron diffraction studies by Karle and Karle (1949) was not exactly twice the value for the carbon-oxygen distance but less. The apparent shortening or shrinkage of the longer distances in several linear chains of atoms was observed by Bastiansen *et al* (1956, 1960) and the effect was confirmed as due to the out-of-linearity vibrations. A theory has been established by Morino (1960) for

this effect in terms of intramolecular motions using the generalized mean-square amplitudes (1955). The theory is based on a power series expansion for the shrinkage effects of linear as well as non-linear conformations as developed by Morino *et al* (1962) and Cyvin (1961, 1962). In the case of a linear conformation, the shrinkage is mainly due to the perpendicular displacements of the nuclei and the anharmonic terms are cancelled. In the case of a non-linear conformation, two kinds of shrinkages have been defined viz., the "natural" and "practical" shrinkages. They are shown to be identical to the first order approximation (1961, 1962). The anharmonic terms, in contrast to the linear conformations, may not necessarily be cancelled out in the non-linear conformations except for highly symmetrical molecules having no totally symmetrical bending modes in the ground electronic states. Later, the name, "Bastiansen-Morino Shrinkage Effect" has been introduced on this aspect by many investigators (1965) in their spectroscopic calculations.

An analytical expression for the mean value of an arbitrary internuclear distance  $r_{ij}^0$  obtained from electron diffraction studies for an atom pair  $i, j$  can simply be related to the equilibrium distance  $r_{ij}^e$  in terms of the mean-square perpendicular amplitudes of vibration as follows.

$$r_{ij}^0 = \langle r_{ij} \rangle = r_{ij}^e + \langle \Delta z_{ij} \rangle + (1/2r_{ij}^e)(\langle \Delta x_{ij}^2 \rangle + \langle \Delta y_{ij}^2 \rangle)$$

where  $\langle \Delta z_{ij} \rangle$  is the so-called anharmonic term which will be vanished when purely harmonic vibrations alone are considered. The Bastiansen-Morino shrinkage effect for a molecule of the present investigation is given by taking the difference of  $r_{ij}^0$  minus the sum of the individual bond lengths  $r_{ij}^e$  and  $r_{ji}^e$  composing it.

$$\delta = r_{ii}^0 - (r_{ij}^0 + r_{ji}^0) = r_{ii}^0 - 2r_{ij}^0 = 2 \cdot \Delta x_{ij}^2 / r_{ij}^e$$

where the mean-square perpendicular amplitudes of vibration  $\langle \Delta x_{ii}^2 \rangle$  and  $\langle \Delta y_{ii}^2 \rangle$  for the nonbonded atom pair  $i, i$  are vanished by symmetry of the molecular system and the mean-square perpendicular amplitudes of vibration  $\langle \Delta x_{ij}^2 \rangle$  and  $\langle \Delta y_{ij}^2 \rangle$  are identical for the bonded atom pair  $i, j$ . The shrinkage begins mainly with the second order terms in the expression for the Bastiansen-Morino shrinkage effect as the linear term completely vanishes. The calculation for the Bastiansen-Morino shrinkage effect needs the values of the mean-square perpendicular amplitudes of vibration and internuclear distances at the equilibrium configuration. High precision values of the internuclear distances at the equilibrium configuration are not required for such calculation. However, approximate values of the internuclear distances obtained from other sources such as microwave, x-ray diffraction or infrared absorption studies will quite be sufficient as the second order terms are only the correction terms.

Using the internuclear distances in Å given in Table I and the mean-square perpendicular amplitudes of vibration in Å<sup>2</sup> given in Table III, the Bastiansen-Mormo shrinkage effects at the temperatures  $T = 500^\circ\text{K}$ ,  $T = 1000^\circ\text{K}$  and  $T = 1500^\circ\text{K}$  were calculated and their values in Å are given in Table V for all the molecules studied. The shrinkage effects, as in the cases of mean amplitude of vibration, are in the increasing order toward the higher members of the halogen group of the calcium strontium and barium families. Though these values appear small in magnitude, they are real. These are to be added at the appropriate temperatures to those of the observed nonbonded distances from electron diffraction experiments in order to obtain the actual values at the equilibrium configuration, thereby compensating the apparent shortening in the internuclear distances.

### MOLECULAR POLARIZABILITIES

In order to test how far the polarizability could be a useful criterion for testing the accuracy of wave functions adopted, many investigations in recent years have been made and developed in several ways to compute the atomic and molecular polarizabilities on the basis of quantum mechanical models for many molecules and ions. Of the various potential models so far developed, the most recent one is the delta-function potential model initiated by Frost (1954, 1955, 1956) and developed by Lippincott (1955, 1957). Recently, Lippincott and Stutman (1964) applied this semi-empirical model to develop a method of generating component polarizabilities in order to compute the molecular or average polarizabilities. This model gives explicit expressions for the parallel and perpendicular components and mean polarizabilities for diatomic as well as polyatomic molecules having their elements only from and beyond the IVA-group of the periodic table. The molecular polarizability is composed mainly of the bond parallel components obtainable from molecular delta-function model and bond perpendicular components obtainable from the atomic delta-function polarizabilities. The polarizability contributions from the bond region electrons and those from the nonbond region electrons have been clearly distinguished. In addition, corrections to the parallel and perpendicular components are made to compensate for polarity effects. The same method has been adopted for the dihalides of beryllium, magnesium, calcium strontium and barium to compute the bond and molecular polarizabilities and one may refer to Lippincott and Stutman (1964) for the detailed theoretical considerations and computations.

The delta-function strengths  $A$ 's in atomic units, atomic polarizabilities  $\alpha$ 's in  $10^{-25} \text{ cm}^3$  and  $c$ 's in atomic units were, according to Lippincott and Dayhoff (1960) and Lippincott and Stutman (1964), derived and their values are given as follows:  $A_{Be} = 0.538$ ,  $A_{Mg} = 0.414$ ,  $A_{Ca} = 0.337$ ,  $A_{Sr} = 0.319$ ,  $A_{Ba} = 0.289$ ,  $A_F = 1.065$ ,  $A_{Cl} = 0.753$ ,  $A_{Br} = 0.633$ ,  $A_I = 0.584$ ,  $\alpha_{Be} = 38.02$ ,  $\alpha_{Mg} = 83.70$ ,  $\alpha_{Ca} = 154.76$ ,  $\alpha_{Sr} = 182.42$ ,  $\alpha_{Ba} = 245.84$ ,  $\alpha_F = 4.90$ ,  $\alpha_{Cl} = 13.88$ ,  $\alpha_{Br} = 19.41$ ,

$\alpha_I = 29.72$ ,  $c_{Be} = 1.522$ ,  $c_{Mg} = 1.434$ ,  $c_{Ca} = 1.35$ ,  $c_{Sr} = 1.427$ ,  $c_F = 5.635$ ,  $c_{Cl} = 4.88$ ,  $c_{Br} = 4.737$  and  $c_I = 4.886$ . From the electron diffraction studies by Akishin *et al* (1957, 1958), the following values of the internuclear distances in Å were used here for the dihalides of beryllium and magnesium: 1.40 for Be—F, 1.75 for Be—Cl, 1.91 for Be—Br, 2.10 for Be—I, 1.77 for Mg—F, 2.18 for Mg—Cl, 2.34 for Mg—Br, 2.52 for Mg—I. The internuclear distances for other dihalides were used from Table I.

TABLE I  
Fundamental frequencies in  $\text{cm}^{-1}$  and internuclear distances in Å for the dihalides of some group IIA elements.

Molecule	$\nu_1(\Sigma_g^+)$	$\nu_2(\pi_u)$	$\nu_3(\Sigma_u^+)$	$r$ (Å)
CaF <sub>2</sub>	484	95	675	2.10
CaCl <sub>2</sub>	268	63	446	2.51
CaBr <sub>2</sub>	164	52	367	2.67
CaI <sub>2</sub>	118	45	321	2.88
SrF <sub>2</sub>	454	77	543	2.20
SrCl <sub>2</sub>	254	48	342	2.67
SrBr <sub>2</sub>	156	37	262	2.82
SrI <sub>2</sub>	111	31	219	3.03
BaF <sub>2</sub>	439	70	496	2.32
BaCl <sub>2</sub>	248	43	302	2.82
BaBr <sub>2</sub>	154	32	226	2.99
BaI <sub>2</sub>	109	26	184	3.20

TABLE II  
Mean-square amplitude quantities in Å<sup>2</sup> for the dihalides of some group IIA elements.

Molecule	Symbol	Mean-square amplitude quantity		
		T = 500 K	T = 1000 K	T = 1500°K
CaF <sub>2</sub>	$\sigma_r$	0.0032176	0.0055453	0.0081942
	$\sigma_{rr}$	—0.0001936	—0.0000939	0.0000815
	$\sigma_\theta$	0.2616924	0.5208368	0.7286038
	$\sigma_r$	0.0050031	0.0094965	0.0139979
CaCl <sub>2</sub>	$\sigma_{rr}$	0.0002245	—0.0000445	—0.0002704

TABLE II (contd.)

Molecule	Symbol	Mean-square amplitude quantity		
		T 500°K	T 1000°K	T 1500°K
CaBr <sub>2</sub>	$\sigma_u$	0.4658179	0.9414614	1.3941088
	$\sigma_f$	0.0056859	0.0110253	0.0161107
	$\sigma_{rr}$	0.0002223	0.0002519	0.0000071
	$\sigma_v$	0.5475689	1.0125188	1.6869917
	$\sigma_t$	0.0068722	0.0137669	0.0207138
CaI <sub>2</sub>	$\sigma_{rr}$	-0.0001852	0.0003382	0.0003271
	$\sigma_u$	0.7226042	1.4438660	1.9489571
	$\sigma_f$	0.0035048	0.0064617	0.0091216
	$\sigma_r$	0.0054142	0.0103934	0.0157682
SrF <sub>2</sub>	$\sigma_{rr}$	0.0000852	0.0001020	0.0000929
	$\sigma_v$	0.3016469	0.6064996	0.9588259
	$\sigma_f$	0.0054142	0.0103934	0.0157682
	$\sigma_{rr}$	0.0001249	0.0001210	-0.0000900
SrCl <sub>2</sub>	$\sigma_u$	0.5130009	1.0043116	1.3746590
	$\sigma_f$	0.0062587	0.0122298	0.0179449
	$\sigma_{rr}$	-0.0000115	0.0001164	0.0003521
	$\sigma_v$	0.6447195	1.1512319	1.6106553
SrBr <sub>2</sub>	$\sigma_f$	0.0075913	0.0151840	0.0233595
	$\sigma_{rr}$	-0.0000645	-0.0001895	0.0006004
	$\sigma_u$	0.7686537	1.5366728	2.3382931
	$\sigma_r$	0.0036807	0.0066716	0.0097318
BaF <sub>2</sub>	$\sigma_{rr}$	-0.0000599	0.0000543	0.0000316
	$\sigma_u$	0.3247989	0.6479921	0.9445528
	$\sigma_f$	0.0056936	0.0108984	0.0163300
	$\sigma_{rr}$	-0.0001384	-0.0001298	-0.0002725
BaCl <sub>2</sub>	$\sigma_u$	0.5596818	1.1183238	1.6772341
	$\sigma_f$	0.0063352	0.0126196	0.0190220
	$\sigma_{rr}$	-0.0000068	-0.0001132	0.0005841
BaBr <sub>2</sub>	$\sigma_u$	0.6424226	1.2841889	2.1401817
	$\sigma_f$	0.0078850	0.0155887	0.0236551
	$\sigma_{rr}$	-0.0002018	-0.0003191	0.0007444
	$\sigma_u$	0.8977888	1.4555268	2.4742529



TABLE III  
Generalized mean-square amplitude quantities in  $\text{\AA}^2$  for the dihalides of some group IIA elements.

Molecule	Mean-square amplitude quantity	$i-j$		$i-i$		
		T = 500°K	T = 1000°K	T = 1500°K	T = 500°K	T = 1000°K T = 1500°K
CaF <sub>2</sub>	$\langle \Delta x^2 \rangle$	0.0032176	0.0053453	0.0081942	0.0064352	0.0110906 0.0163884
	$\langle \Delta x^2 \rangle = \langle \Delta y^2 \rangle$	0.0054321	0.01302092	0.1821509	0	0 0
CaCl <sub>2</sub>	$\langle \Delta x^2 \rangle$	0.0050031	0.0094965	0.0139979	0.0100062	0.0189930 0.0279958
	$\langle \Delta x^2 \rangle = \langle \Delta y^2 \rangle$	0.1164545	0.2353654	0.3485272	0	0 0
CaBr <sub>2</sub>	$\langle \Delta x^2 \rangle$	0.0076859	0.0110253	0.0161107	0.0113718	0.0220506 0.0322214
	$\langle \Delta x^2 \rangle = \langle \Delta y^2 \rangle$	0.1368922	0.2531297	0.4217479	0	0 0
CaI <sub>2</sub>	$\langle \Delta x^2 \rangle$	0.0088722	0.0137669	0.0207138	0.0137444	0.0275338 0.0414276
	$\langle \Delta x^2 \rangle = \langle \Delta y^2 \rangle$	0.1806511	0.3609665	0.4872393	0	0 0
SrF <sub>2</sub>	$\langle \Delta x^2 \rangle$	0.0035048	0.0064617	0.0091216	0.0070096	0.0120234 0.0185432
	$\langle \Delta x^2 \rangle = \langle \Delta y^2 \rangle$	0.0754117	0.1516249	0.2397065	0	0 0
SrCl <sub>2</sub>	$\langle \Delta x^2 \rangle$	0.0054142	0.0103934	0.0157682	0.0108254	0.0207868 0.0312524
	$\langle \Delta x^2 \rangle = \langle \Delta y^2 \rangle$	0.1282502	0.2510779	0.3436648	0	0 0

TABLE III—(contd).

Molecule	Mean-square amplitude quantity	$\bar{r}^2$				$\bar{r}^2$		
		T = 500°K	T = 1000°K	T = 1500°K	T = 500°K	T = 1000°K	T = 1500°K	
SrBr <sub>2</sub>	$\langle \Delta x^2 \rangle$	0.0062587	0.0122298	0.0179449	0.0125174	0.0244596	0.0358898	
	$\langle \Delta x^2 \rangle = \langle \Delta y^2 \rangle$	0.1611799	0.2878080	0.4026638	0	0	0	
SrI <sub>2</sub>	$\langle \Delta x^2 \rangle$	0.0075913	0.0151840	0.0233595	0.0151826	0.0303680	0.0467190	
	$\langle \Delta x^2 \rangle = \langle \Delta y^2 \rangle$	0.1921634	0.3841682	0.5845733	0	0	0	
BaF <sub>2</sub>	$\langle \Delta x^2 \rangle$	0.0036807	0.0066716	0.0097318	0.0073614	0.0133432	0.0194636	
	$\langle \Delta x^2 \rangle = \langle \Delta y^2 \rangle$	0.0811997	0.1619980	0.2361382	0	0	0	
BaCl <sub>2</sub>	$\langle \Delta x^2 \rangle$	0.0056936	0.0108984	0.0163300	0.0113872	0.0217968	0.0326600	
	$\langle \Delta x^2 \rangle = \langle \Delta y^2 \rangle$	0.1399250	0.2795810	0.4193085	0	0	0	
BaBr <sub>2</sub>	$\langle \Delta x^2 \rangle$	0.0063352	0.0126196	0.0190220	0.0126704	0.0242392	0.0380440	
	$\langle \Delta x^2 \rangle = \langle \Delta y^2 \rangle$	0.1606056	0.3210472	0.5350454	0	0	0	
BaI <sub>2</sub>	$\langle \Delta x^2 \rangle$	0.0078850	0.0155887	0.0236551	0.0157700	0.0311774	0.0473102	
	$\langle \Delta x^2 \rangle = \langle \Delta y^2 \rangle$	0.2244472	0.3638817	0.6185632	0	0	0	

TABLE IV

Mean amplitudes of vibration in Å for the dihalides of some group IIA elements.

Molecule	Distance	Mean amplitude of vibration		
		T = 500°K	T = 1000°K	T = 1500°K
CaF <sub>2</sub>	Ca-F	0.0567	0.0745	0.0905
	F-F	0.0802	0.1052	0.1280
CaCl <sub>2</sub>	Ca-Cl	0.0707	0.0974	0.1183
	Cl-Cl	0.1000	0.1378	0.1673
CaBr <sub>2</sub>	Ca-Br	0.0754	0.1051	0.1270
	Br-Br	0.1066	0.1485	0.1795
CaI <sub>2</sub>	Ca-I	0.0829	0.1173	0.1439
	I-I	0.1172	0.1659	0.2035
SrF <sub>2</sub>	Sr-F	0.0592	0.0804	0.0955
	F-F	0.0834	0.1137	0.1351
SrCl <sub>2</sub>	Sr-Cl	0.0736	0.1020	0.1256
	Cl-Cl	0.1041	0.1442	0.1776
SrBr <sub>2</sub>	Sr-Br	0.0791	0.1106	0.1340
	Br-Br	0.1119	0.1564	0.1894
SrI <sub>2</sub>	Sr-I	0.0872	0.1232	0.1529
	I-I	0.1232	0.1743	0.2162
BaF <sub>2</sub>	Ba-F	0.0607	0.0817	0.0987
	F-F	0.0858	0.1155	0.1395
BaCl <sub>2</sub>	Ba-Cl	0.0755	0.1044	0.1277
	Cl-Cl	0.1068	0.1477	0.1807
BaBr <sub>2</sub>	Ba-Br	0.0796	0.1124	0.1379
	Br-Br	0.1126	0.1557	0.1951
BaI <sub>2</sub>	Ba-I	0.0888	0.1248	0.1538
	I-I	0.1256	0.1766	0.2175

TABLE V

Bastiansen-Morino shrinkage effect in Å for the dihalides of some group IIA elements.

Molecule	Bastiansen-Morino shrinkage effect		
	T = 500°K	T = 1000°K	T = 1500°K
CaF <sub>2</sub>	0.06231	0.12401	0.17348
CaCl <sub>2</sub>	0.09280	0.18754	0.27771
CaBr <sub>2</sub>	0.10254	0.18961	0.31592
CaI <sub>2</sub>	0.12545	0.25067	0.33836
SrF <sub>2</sub>	0.06856	0.13784	0.21792
SrCl <sub>2</sub>	0.09607	0.18807	0.25743
SrBr <sub>2</sub>	0.11431	0.20412	0.28559
SrI <sub>2</sub>	0.12684	0.25358	0.38586
BaF <sub>2</sub>	0.06999	0.13965	0.20357
BaCl <sub>2</sub>	0.09923	0.19828	0.29738
BaBr <sub>2</sub>	0.10743	0.21475	0.35789
BaI <sub>2</sub>	0.14028	0.22743	0.38660

TABLE VI

Observed and calculated polarizabilities in  $10^{-25}$  cm<sup>3</sup> for the dihalides of some group IIA elements

Molecule	$\Sigma\alpha_{  p}$	$\Sigma 2\alpha_{\perp}$	$\Sigma\alpha_{  n}$	$\alpha_M(\text{calcd})$	$\alpha_M(\text{obsd})$
BeF <sub>2</sub>	5.833	42.455	8.400	18.896	16.167
BeCl <sub>2</sub>	31.907	99.373	23.794	51.691	
BeBr <sub>2</sub>	47.450	130.472	33.274	70.399	
BeI <sub>2</sub>	78.487	185.917	50.949	105.118	
MgF <sub>2</sub>	8.834	49.218	8.400	22.151	18.426
MgCl <sub>2</sub>	50.409	113.278	23.794	62.494	53.851
MgBr <sub>2</sub>	76.794	147.732	33.274	85.933	
MgI <sub>2</sub>	122.923	210.336	50.949	128.069	
CaF <sub>2</sub>	11.746	56.647	8.400	25.598	24.964
CaCl <sub>2</sub>	69.922	127.768	23.794	73.828	
CaBr <sub>2</sub>	99.921	165.147	33.274	99.447	
CaI <sub>2</sub>	164.632	233.893	50.949	149.825	
SrF <sub>2</sub>	14.019	61.676	8.400	28.032	30.195
SrCl <sub>2</sub>	81.456	136.503	23.794	80.584	70.126
SrBr <sub>2</sub>	121.547	175.097	33.274	109.973	
SrI <sub>2</sub>	197.356	246.187	50.949	164.831	
BaF <sub>2</sub>	19.991	65.089	8.400	31.160	38.516
BaCl <sub>2</sub>	93.753	143.212	23.794	86.919	79.806
BaBr <sub>2</sub>	132.460	183.194	33.274	116.309	
BaI <sub>2</sub>	215.809	257.234	50.949	174.664	

The molecular polarizability is composed of mainly from bond parallel and bond perpendicular components. The bond parallel component is obtained from the contributions of two sources, namely, bond region electrons and nonbond region electrons according to the valence bond interpretation. The contribution to the parallel component by the bond region electrons is calculated using a linear combination of atomic delta-function wave functions representing the two nuclei involved in the bond from the following expression given as  $\alpha_{\parallel b} = 4nA_{12}(1/a_0) \langle x^2 \rangle^2$  where  $n$  is the bond order,  $A_{12}$  the root mean-square delta function strength of the two nuclei involved in the bond,  $a_0$  the radius of the first Bohr orbit of atomic hydrogen and  $\langle x^2 \rangle$  the mean-square position of a bonding electron which may be expressed as  $\langle x^2 \rangle = (R^2/4) + (1/2cR_{12}^2)$  where  $R$  is the internuclear distance at the equilibrium configuration. In the case that the bond is of the heteronuclear type, a polarity correction is necessary to produce the ionic character believed to exist and then the expression for the parallel component of the polarizability is written as  $\alpha_{\parallel p} = \alpha_{\parallel b}\sigma$  where  $\sigma = \exp [-(1/4)(X_1 - X_2)^2]$ . Here  $X$  is Pauling's electronegativity (1960). The calculated values of the sum of the bond parallel components,  $\Sigma\alpha_{\parallel p}$  in  $10^{-25}$  cm<sup>3</sup> by the bond region electron for all the molecules are given under the second column of Table VI. The contribution to the parallel component by the nonbond region electrons is calculated from the expression  $\alpha_{\parallel n} = f_j\alpha_j$  where  $f_j$  is the fraction of electrons in the valence shell of the  $j$ -th atom not involved in bonding and  $\alpha_j$  the atomic polarizability of the  $j$ -th atom obtainable from the delta-function strength  $A_j$ . In a molecule of the present study, the valence electrons of the central atom are completely shared in bonding while there are six valence electrons are left unshared on each end atom. The calculated values of the sum of the bond parallel components,  $\Sigma\alpha_{\parallel n}$  in  $10^{-25}$  cm<sup>3</sup> by the nonbond region electrons for all the molecules are given under the fourth column of Table VI. Thus the contributions by the bond region electrons as well as nonbond region electrons to the parallel component of the polarizability are clearly distinguished.

The perpendicular component of a diatomic molecule is assumed to be the sum of the two atomic polarizabilities, i.e.  $\alpha_{\perp} = 2\alpha_A$  for a nonpolar diatomic molecule,  $A_2 = 2(X_A^2\alpha_A + X_B^2\alpha_B)/(X_A^2 + X_B^2)$  for a molecule  $A - B$  where  $X$  stands for the electronegativity on the Pauling scale and  $\alpha$  for the atomic polarizability. Extending this principle, the sum of the perpendicular components of all the bonds in a polyatomic molecule is given as  $\Sigma 2\alpha_{\perp} = n_{df}(\Sigma X_j^2\alpha_j)/(\Sigma X_j^2)$  where  $n_{df}$  is the number of residual atomic polarizability degrees of freedom and the other quantities are known. The number of residual atomic polarizability degrees of freedom is obtained directly from the structure of a molecule. Every isolated atom is allowed to possess three atomic polarizability degrees of freedom, and every bond which is formed between two atoms removes two of three degree of freedom, with the exception that (1) if two bond are formed from the same atom and exist in a linear configuration, then only three atomic polarizability degrees of freedom

are lost, and (2) if three bonds are formed from the same atom and exist in a plane, then only five atomic polarizability degrees of freedom are lost. Extending this principle, a linear molecule of the present study has only six residual atomic polarizability degrees of freedom (see Fig. 1). The calculated values of the sum of the perpendicular components,  $\Sigma 2\alpha_{\perp}$  in  $10^{-25} \text{ cm}^3$  for all the molecules are given under the third column of Table VI.

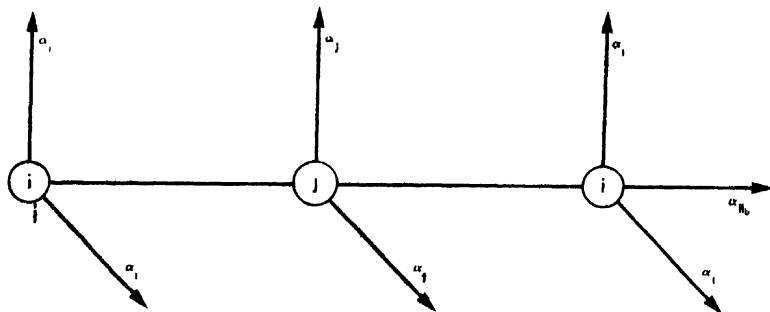


Fig. 1. Residual atomic polarizability degrees of freedom for a linear symmetrical triatomic molecule.

The average or mean molecular polarizability is obtained from the following expression  $\alpha_M = (1/3)(\Sigma\alpha_{\parallel p} + \Sigma\alpha_{\parallel n} + \Sigma 2\alpha_{\perp})$ . The calculated values of the molecular polarizabilities in  $10^{-25} \text{ cm}^3$  for all the molecules are given under the fifth column of Table VI. The experimental values of molar refractions given by Batsanov (1961) for some of the molecules of present study were substituted into the Lorentz-Lorentz equation to obtain the molecular polarizabilities and their values in  $10^{-25} \text{ cm}^3$  are given under the sixth column of Table VI. It is seen what the calculated molecular polarizabilities are in good agreement with the available experimental values. Thus the present investigation further testifies that the delta-function potential model enables us to evaluate the bond and molecular polarizabilities not only for non-metals but also for metals, thereby establishes that it is the most satisfactory one among the various models so far developed.

In considering various potential models so far developed, they have been very limited to atoms, ions and simple diatomic systems but not been extended to even simple polyatomic molecules and may be observed from the following: Hasse (1930, 1931) evaluated the polarizabilities for the helium atom and lithium ion by using the Lennard-Jones 6-12 potential model involving several types of ground state as well as perturbed state wave functions in terms of the perturbing potential. Hirschfelder (1935) computed the polarizabilities of molecular hydrogen and the diatomic hydrogen ion by applying the variational method of Hylleraas (1930) and Hasse (1930, 1931) upon the eigenfunctions proposed by Rosen (1931) and Wang (1928). It was found that the Kirkwood (1932) formula was applicable to the diatomic hydrogen ion and polarizabilities were obtained for may

internuclear separations by using the eigenfunction developed by Guillemin and Zener (1929). The calculated values by Hirschfelder (1935) were compared with those of Mrowka (1932) and Steensholt (1935) but they are not in good agreement with each other. Van Vleck (1932) and Atanasoff (1930) pointed out from their investigations that the Hylleraas method (1930) is not strictly applicable to approximate eigenfunctions and may yield results either too small or too large. The approach of Buckingham (1937) based on the Kirkwood's variational method (1932) and involved heavier atoms leads to complex determinantal self-consistent field wave functions from his calculations of atomic polarizabilities for Ne, Na<sup>+</sup>, Cl<sup>-</sup>, A, K<sup>+</sup>, Kr and Cs<sup>+</sup>. Bell and Long (1950) calculated the polarizabilities of H<sub>2</sub><sup>+</sup> and H<sub>2</sub> molecules from six different unperturbed wave functions but the results are not sensitive to the wave functions adopted, especially for the unperturbed molecules. Abbott and Bolton (1952-1953) studied H<sub>2</sub><sup>+</sup>, H<sub>2</sub> and N<sub>2</sub> molecules and used the polarizability as a criterion for determining the molecular wave function of a system by a self-consistent field method. Kolker and Karplus (1963) calculated the electric polarizability tensor  $\bar{\alpha}$  with 'ab initio' wave functions for a series of first row diatomic molecules such as H<sub>2</sub>, Li<sub>2</sub>, N<sub>2</sub>, LiH, HF, LiF and CO. Since these methods have not been extended to polyatomic molecules, such calculations have not been carried out here to make a comparison with the results of delta-function potential model and the experimental values. On studying all the potential models so far developed, the delta-function potential provides the feasibility of obtaining explicit expression for the parallel and perpendicular components and the mean polarizabilities for the diatomic as well as polyatomic systems. The sum of the perpendicular components of all the bonds in a molecule  $\sum 2\alpha_{\perp}$  is a linear combination of atomic polarizabilities and is independent of the internuclear distance whereas the bond parallel component is dependent on the internuclear distance. Hence the perpendicular component will always be transferable from one molecular system to another having similar chemical bonds irrespective of the accuracy in the values of the internuclear distances in both systems but such a transfer in the case of parallel component would be possible only when the internuclear distances are nearly identical in the two systems considered. Since the nonbond region electrons also contribute to the parallel component, such a transfer would be possible for the bonds formed by the atoms with identical lone pairs of electrons. From the previous investigations as well as with the present one it is felt that the delta-function potential model is a very satisfactory one for such calculations of bond and molecular polarizabilities and a further work on this aspect for various polyatomic molecules having their elements from the B-group is in progress.

## REFERENCES

- Abbott, J. A. and Bolton, H. C., 1952, 1953, *J. Chem. Phys.*, **20**, 762; *Proc. Roy. Soc. London*, **A216**, 477.  
 Almenningen, A., Bastiansen, O. and Munthe-Kaas, T., 1956, *Acta Chem. Scand.*, **10**, 261.

- Almenningen, A., Bastianson, O. and Traetteberg, M., 1956, *Acta Chem. Scand.*, **13**, 1699.
- Akishun, P. A. and Spiridonov, V. P., 1957, *Kristallografiya*, **2**, 475.
- Akishun, P. A., Spiridonov, V. P., Sobolev, G. A. and Naumov, V. A., 1957, 1958, *Zh. Fiz. Khim.*, **31**, 461, 648; **32**, 58.
- Akishun, P. A., Spiridonov, V. P. and Sobolev, G. A., 1958, *Doklady Akad. Nauk. S.S.S.R.*, **118**, 1134.
- Atanasoff, J. V., 1930, *Phys. Rev.*, **36**, 1242.
- Bastianson, O. and Traetteberg, M., 1960, *Acta Cryst.*, **13**, 1108.
- Batsanov, S. S., 1961, *Refractometry and Chemical Structure*, Translated by Sutton, P. P. from Russian to English, Consultants Bureau, New York
- Bell, R. P. and Long, D. A., 1950, *Proc. Roy. Soc., London*, **A203**, 464.
- Breed, H., Bastiansen, O. and Almenningen, A., 1960, *Acta Cryst.*, **13**, 1108.
- Braune, H. and Knoeke, S., 1933, *Z. Physik. Chem.*, **B23**, 163.
- Brewer, L., Somayajulu, G. R. and Bruckett, E., 1963, *Chem. Rev.*, **62**, 111.
- Buchler, A., Stauffer, J. L. and Klemperer, W., 1964, *J. Chem. Phys.*, **40**, 3471.
- Buckingham, R. A., 1937, *Proc. Roy. Soc., London*, **A160**, 94
- Cyvin, S. J., 1959, *Spectrochimica Acta.*, **15**, 828.
- Cyvin, S. J., 1959, *Spectrochimica Acta.*, **15**, 341, 958.
- Cyvin, S. J., 1960, *Acta Polytechnica Scandinavica.*, Ph. No. 6 (279).
- Cyvin, S. J., 1961, 1962, *Tidsskr. Kjemi. Bergvesen, Metallurgi.*, **21**, 236; **22**, 44, 73.
- Frost, A. A., 1954, 1955, 1956, *J. Chem. Phys.*, **22**, 1613; **23**, 985; **25**, 1150.
- Gregg, A. H., Hampson, G. C., Jenkins, G. I., Jones, P. L. F. and Sutton, L. E., 1937, *Trans. Faraday Soc.*, **33**, 852.
- Guillemin, V. and Zener, C., 1929, *Pro. Natl. Acad. Sci.*, **15**, 4, 314.
- Hasse, H. R., 1930, 1931, *Pro. Camb. Phil. Soc.*, **26**, 542; **27**, 66.
- Herzberg, G., 1960, *Infrared and Raman Spectra of Polyatomic Molecules*, D. Van Nostrand Company, New York.
- Hirschfelder, J. O., 1935, *J. Chem. Phys.*, **3**, 555
- Hylleraas, E. A., 1930, *Z. Physik.*, **65**, 209.
- Karle, I. and Karle, J., 1949, *J. Chem. Phys.*, **17**, 1052
- Kirkwood, J. G., 1932, *Physik. Z.*, **33**, 2, 57.
- Kolkor, H. J. and Karplus, M., 1963, *J. Chem. Phys.*, **39**, 2011.
- Lippincott, E. R., 1955, 1957, *J. Chem. Phys.*, **23**, 603; **26**, 1678.
- Lippincott, E. R. and Dayhoff, M. O., 1960, *Spectrochimica Acta.*, **16**, 807
- Lippincott, E. R. and Stutman, J. M., 1964, *J. Phys. Chem.*, **68**, 2926.
- Morino, Y. and Hirota, E., 1955, *J. Chem. Phys.*, **23**, 737.
- Morino, Y., 1960, *Acta Cryst.*, **13**, 1107.
- Morino, Y., Nakamura, J. and Moore, P. W., 1962, *J. Chem. Phys.*, **36**, 1050.
- Morino, Y., Kuchitsu, K. and Oka, T., 1962, *J. Chem. Phys.*, **36**, 1108.
- Morino, Y., Cyvin, S. J., Kuchitsu, K. and Ijima, T., 1962, *J. Chem. Phys.*, **36**, 1109.
- Mrowka, B., 1932, *Z. Physik.*, **76**, 300.
- Nagarajan, G., 1964, *J. Mol. Spectroscopy.*, **13**, 361.
- Nagarajan, G. and Lippincott, E. R., 1965, *J. Chem. Phys.*, **42**, 1809.
- Pauling, L., 1960, *The Nature of the Chemical Bond.*, Cornell University Press, Ithaca, New York.
- Rosen, N., 1931, *Phys. Rev.*, **38**, 2099.
- Steenholt, G., 1935, *T. Physik.*, **93**, 620; **94**, 770.
- Van Vleck, J. H., 1932, *Electric and Magnetic Susceptibilities*, Oxford Press, London, p. 205.
- Wang, S., 1928, *Phys. Rev.*, **31**, 579.
- Warton, L., Berg, R. A. and Klemperer, W., 1963, *J. Chem. Phys.*, **39**, 2023.



# AN X-RAY STUDY OF COIR FIBRE

P. K. RAY AND S. B. BANDYOPADHYAY

TECHNOLOGICAL RESEARCH LABORATORIES

INDIAN CENTRAL JUTE COMMITTEE

12, REGENT PARK, CALCUTTA-40

(Received April 20, 1965)

**ABSTRACT.** The changes in spiral angle, Hermans' average angle of orientation and crystallinity with extension of coir fibre have been studied by X-ray diffraction method. It is found that the spiral angle and the angle of orientation decrease with extension and the two angles differ more in the extended state than in the unextended state and that the crystallinity increases by about 3% after extension to rupture.

## INTRODUCTION

Coir is the fibre obtained from coconut husk. High extensibility (about 37%) and high lignin content (40%) of the fibre distinguish it from other cellulosic fibres. The spiral structure of the microfibrils in the secondary wall of the fibre has been studied by Athury (1943) and Preston (1952) while Stern and Stout (1954) tried to relate the spiral angle with Herman's orientation angle. Stern (1957) has shown that high extensibility of coir fibre is chiefly because the microfibrils in the cell wall lie in perfect helical spirals, extension of the fibre being related with the changes of the spiral angle, that is, the angle which a microfibril element makes with the fibre axis. He did not however examine the changes in crystallinity of the fibre although he noticed that about 4% of the extension remains as permanent even though the extended fibre is drastically treated. The object of this work is to study how far the lateral order of cellulose chains in the fibre is affected by extension. The nature of change in the spiral angle as well as the angle of orientation has also been examined.

## EXPERIMENTAL

In the first series of experiments each individual fibre was extended to the maximum limit (about 30-4%) by loading it gradually on a pendulum type fibre strength tester till it broke in about a minute. The extended portions of all the fibres were then first examined for spiral angle and the angle of orientation in the form of parallel bundles and then cut to pieces for preparing randomised pellet for measurement of crystallinity. In each case unextended fibres were similarly examined under X-rays.

In another series of experiments the behaviour of the fibres at extension below maximum was checked. A bundle of coir fibre was carefully mounted on a pair of fibre clamps so that all the fibres were apparently straight. The clamps were mounted on a pendulum type cloth strength tester and load was gradually increased; the movement of the clamps was arrested after a desired amount of extension, left for 48 hours and then released, immediate relaxation being measured. It was found that the fibres retained about 80% extension. These fibres were then used for crystallinity measurement.

*Spiral angle and angle of orientation* : A parallel fibre bundle was kept just taut by means of a clamp in front of a collimator of 2 mm. diameter and 5 cm. length through which Ni-filtered  $\text{CuK}_\alpha$  radiation was allowed to pass from a Philips sealed X-ray tube and fibre to film distance was 5 cm. An exposure of 3 hrs. with 25 KV. and 15 mA. was used. The exposure time, development technique etc. were kept as constant as possible for all the photographs.

Following Hermans (1946) *et al* and Meredith (1951) a series of microphotometer curves for (002) interferences were recorded starting from the equatorial lines of the diffraction photographs and proceeding along radial lines at angular intervals of  $5^\circ$ . Since the films were of low photographic density it was assumed that the X-ray intensity was proportional to the blackening and was thus linearly related to the logarithm of the intensity of the transmitted light, or of the photometer reading, since the calibration was linear over the range of measurement.

*Crystallinity* : As coir shows a considerably high value of extensibility it was expected that extension in coir would draw the chain molecules into parallelism and may increase the crystallinity. In finding the crystallinity the orientation effects were eliminated by a randomised preparation of the fibres forming pellets with a very small quantity of adhesive. The pellet was then introduced into a mould, a hole of  $\frac{1}{2}$  mm. diameter drilled in a brass plate 1 cm. thick. The other end of the hole was temporarily closed by a screwed plate. A constant pressure was exerted on the pellet with a steel piston having a flat end just fitting the hole. The pellet was then taken out of the hole from the other end after unscrewing the plate. The density of the pellets was kept fairly constant by using weighed amounts of fibre in each case. The pellet was then mounted in the camera for X-ray photographs, which were taken under similar conditions.

## RESULTS AND DISCUSSION

Figs. 1 and 2 are the typical X-ray photographs for parallel bundles and randomised pellets respectively, (a) and (b) indicating unextended and extended fibres.

The widely drawn out interference arcs of Fig 1 (a, b) with two maxima on either side of the equator are the special features of the photographs of fibres with spirally laid microfibrils. X-ray intensity when plotted against the angular

distance from the equator gave graphs as shown in Fig. 3(a, b). Half of the angular separation between the maxima was taken as the vertical spiral angle.

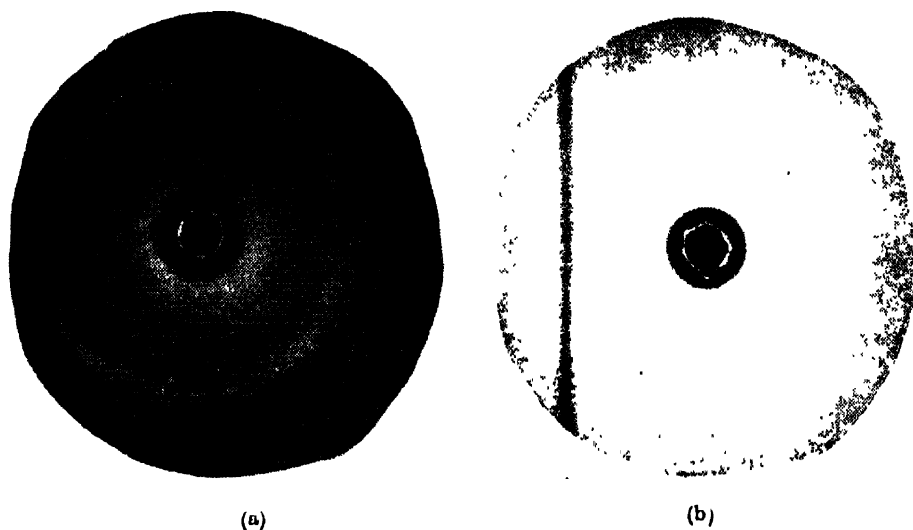


Fig. 1(a, b) X-ray photographs of parallel bundles of coir fibre: (a) Unextended; (b) Extended.

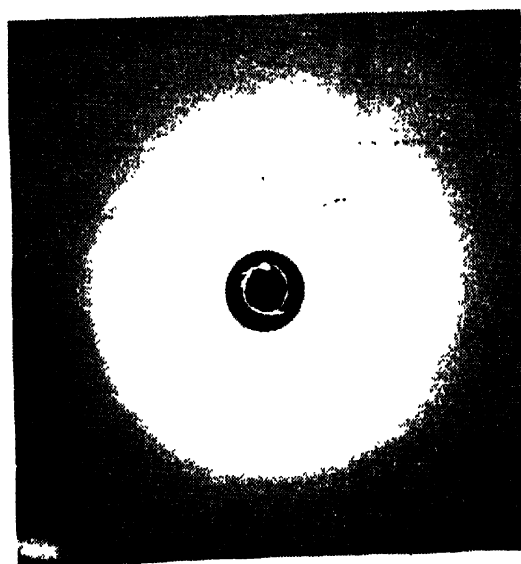


Fig. 2(a)  
Fig. 2(a) Unextended, (b) Extended.

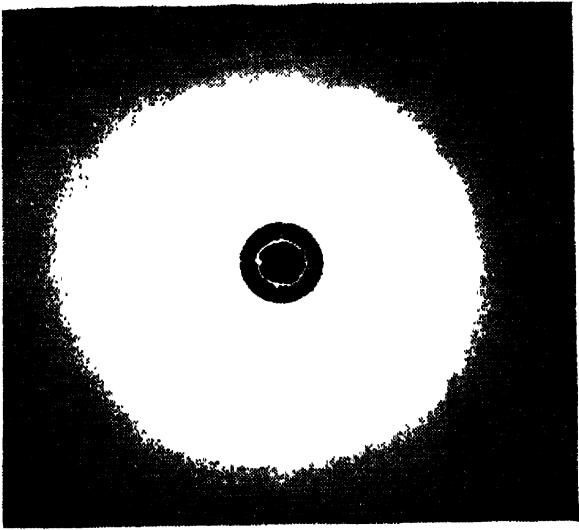


Fig. 2(b) X-ray photograph of randomised pellet :

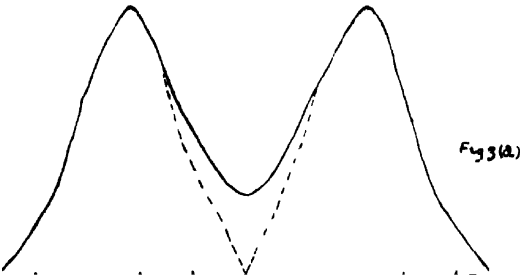


Fig. 3(b)  
(a) Unextended, (b) Extended.

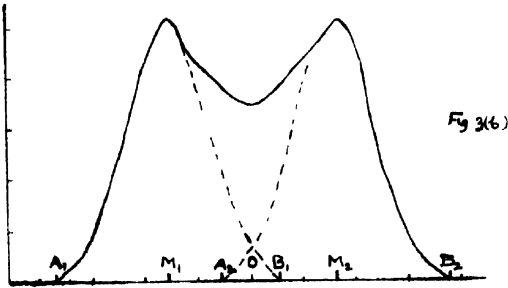


Fig. 3(a, b) Intensity distribution along (002) arc of X-ray photographs of parallel fibres :

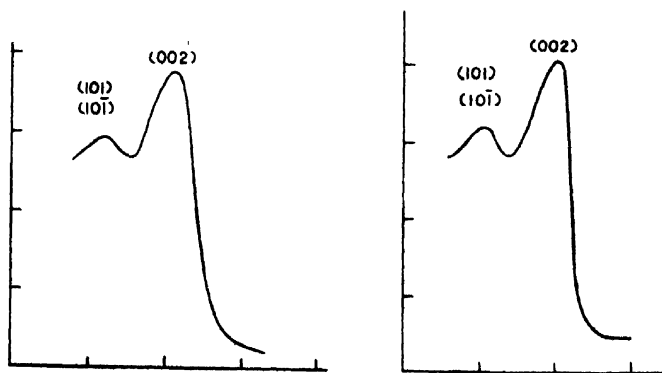


Fig. 4(a,b) Radial intensity distribution of X-ray photographs of roundised fibres (a) Unextended (b) Extended

Taking the intensity  $I(\alpha)$  of (002) arc for different values of angle( $\alpha$ ) from the equator from Fig. 3, the Hermans <sup>(2)</sup> average angle of orientation has been calculated from the equation

$$\sin^2 \alpha_m = 2 \frac{\int_0^{\pi/2} I(\alpha) \sin^2 \alpha \cos \alpha \, d\alpha}{\int_0^{\pi/2} I(\alpha) \cos \alpha \, d\alpha}$$

The integrals were evaluated graphically using a planimeter to measure the areas under the curves  $I(\alpha) \sin^2 \alpha \cos \alpha$  Vs.  $\alpha$  and  $I(\alpha) \cos \alpha$  Vs.  $\alpha$ . The values are given in Table I

TABLE I

Sample	Spiral Angle ( $\delta$ )		Average Angle of orientation ( $\alpha_m$ )		Cr. I	
	Unextended (U)	Extended (E)	Unextended (U)	Extended (E)	U	E
1	45°0'	30°0'	46°48'	37°0'	27.4%	30.3%
2	45°0'	32°30'	46°0'	38°0'	33.0%	36.3%

In Fig. 2, as a result of randomisation the contributions of the crystalline regions have been uniformly distributed over 360° giving rings of uniform intensity in place of the double humped arcs of Fig. 1. These photographs were radially scanned at intervals of 90° and a typical average intensity curve is shown in Fig. 4.

Considering the height  $I_{002}$  of the peak of (002) reflection above the background as the contribution of the crystalline regions and  $I_{am}$ , the height of the minimum between the (002) and the composite (101 and 101) peaks as the contribution of the amorphous portion, the following equation has been taken as the crystallinity index. CrI, after Segal *et al.*, (1959) and Ingersoll (1946)

$$CrI = \frac{I_{002} - I_{am}}{I_{002}} \times 100$$

The values of crystallinity index for the first series are given in Table I and those of second series in Table II. Each figure is based on observations on at least two pellets the difference between duplicates being on an average 1%.

Although, by condition of experiment, only part of the strain was retained in the fibre during X-ray examination, results in Table I clearly indicate that the extension of the fibre reduces the spiral angle ( $S$ ), as observed by Stern (1957) the average angle ( $\alpha_m$ ) of orientation is also reduced but to a much smaller extent so as to increase the difference ( $\alpha_m - S$ ) from  $1^\circ$  in the unextended state to  $7^\circ$  in the extended state. Since the spirality is reduced, this change in the ( $\alpha_m - S$ ) may at first appear to be due to increased dispersion of crystallites within the microfibrils but Fig. 3 shows that the fibre elongation reduces the extent of the tail ends beyond the maximum points  $M_1$  and  $M_2$ , that is, the value of  $\frac{M_1A_1 + M_2B_2}{2}$

from  $45^\circ$  to  $41^\circ$  indicating according to Sisson (1935) reduced dispersion of the crystallites within a microfibril or the microfibrils within a bundle of such. Actually, however, this depended on the method of calculating  $\alpha_m$ , because in Fig. 3 when the dotted curves about the mean positions  $M_1$  and  $M_2$ , representing half of the distribution of crystallites are considered it will be found that in obtaining a value of  $\alpha_m$  for the left hand position  $OM_1A_1$  the tail end  $OB_1$  beyond 0 (equator) was rejected while  $OA_2$  on the left side of the equator was taken into account this enhanced the value of  $\alpha_m$ , as  $M_1$  and  $M_2$  come closer. Moreover, the microfibrils near the edge of the spiral being not much inclined to the fibre axis also contribute towards increasing the value of  $\alpha_m$ .

As regards crystallinity, Table I shows that the CrI of extended fibres was about 3% more than that of the unextended fibres for both samples. This may be explained if it is supposed that breaking extension not only reduces the angle which the microfibrils make with the fibre axis and the dispersion amongst the existing crystallites within the microfibrils but also produces somewhat better alignment amongst the long chain molecules within the microfibrils and better planar regularity so as to assume a better lateral order, that is, to increase crystallinity. This is further verified when it is found from Table II that extension upto 10% do not produce any observable change in crystallinity index, the

Table II  
Sample 3

Extension	Cr. I
0%	18%
10%	18%
20%	21%
Break	21.8%

the closeness of packing of the molecules being probably not sufficient to produce a permanent change in lateral order. On further extension however, CrI gradually increases, till at break the difference reaching the maximum value of 3.8% which is nearly the same as obtained for the previous series. Such increase in crystallinity on stretching has also been reported by M. Ruck-Florjancic (1960) *et al.* in case of regenerated fibres.

These results thus provided an explanation for the retention of about 4% even after drastic treatment as obtained by Stern and also for the properties introduced in the fibre by preconditioning under stress

#### ACKNOWLEDGMENT

The authors are thankful to Dr. A. C. Chakraborty, S.S.O., for many suggestions. Authors' thanks are also due to Dr. P. B. Sarkar, D.Sc., F.N.I., Director, for his keen interest in the work and to Indian Central Jute Committee for providing facilities for work and according permission to publish these results.

#### REFERENCES

- Astbury, W. T., 1943, *Textile Fibres under the X rays* Imperial Chemical Industries Ltd., 27.
- Hermans, P. H., 1946, *Contrib to the Physics of Cellulose fibres*, Amsterdam Elsevier Press p. 198.
- Ingersoll, H. G., 1946, *J Appl Phys* **17**, 924.
- Meredith, R., 1951, *J. Text Inst.*, **42** T275, T291
- Preston, R. D., 1952, *The molecular architecture of plant cell walls*, 120. London, Chapman and Hall.
- Ruck-organjancic, M., and Ruck, H., 1960, *Svensk Papperstidn* **63**, 845, *Rev. Textile Progress* **13**, 42
- Stern, F., 1957, *J. Text. Inst.* **48**, T21
- Stern, F., and Stout, H. P., 1954, **45**, T896.
- Sisson, W. A., 1935, *Ind. Eng. Chem.*, **26**, 51
- Segal, L., Creely, J. J., Manton, A. E., and Conrad, C. M., 1959, *Text. Res. J.*, **29**, 786.

# FINITE SPHERICAL INHOMOGENEITIES IN CONCENTRIC SHELLS

R. D. BHARGAVA AND D. PANDE

INDIAN INSTITUTE OF TECHNOLOGY, KANPUR, INDIA

CHRIST CHURCH COLLEGE, KANPUR, INDIA

(Received May 11, 1965).

**ABSTRACT** Inclusion and inhomogeneity problems in infinitesimal elasticity have been studied by various authors, but such problems in finite elasticity have not been attempted so far. The present paper is concerned with spherical inhomogeneities when the elastic deformation is large. The shells considered are isotropic and incompressible. The problem has been solved for two shells and later generalised for  $n$  shells embedded within each other. Further, the outermost and the inner-most boundaries of the system have been subjected to uniform normal pressures. It will be observed that the final equation determining the parameter giving the equilibrium boundary has irrational roots and could be solved numerically or graphically. Because of the complete symmetry with respect to  $r$ , the elastic field would be function of  $r$  only. If  $W$  be the elastic potential density at  $r$ ,  $U$  the complete elastic potential  $r$ , and  $T_{ij}$  the stress components then

$$U = \int_{R_1}^{R_2} 4\pi R^2 W(R) dR.$$

$$-\frac{4}{3}\pi(R_1^3 - r_1^3)U = -\frac{4}{3}\pi(R_2^3 - r_2^3)U = U + \frac{4}{3}\pi r_1^3 W(R_1) - \frac{4}{3}\pi r_2^3 W(R_2) \quad \dots (1)$$

$$T_{ij} = \phi g_{ij} + \psi B_{ij} + p G_{ij} \quad \dots (2)$$

Equation (1) is a very important relation between boundary pressures, boundary displacements and the predetermined strain-energy of the body. Equation (2) gives the stress field everywhere. For derivation of these equations etc., please refer to [3].

## SPHERICAL INCLUSION

### Two shells case

Let a homogeneous, isotropic spherical shell made of incompressible material with its outer and inner radii  $a_1(1+\delta)$ ,  $\delta$  being finite, and  $a_2$  respectively be embedded into another similar shell of a different incompressible material with outer and inner radii  $a_0$  and  $a_1$  respectively. The former shell will be called 'inclusion' and the latter 'matrix'. Further, let the outer boundary of the matrix be subjected to a uniform normal pressure  $p_0$  and the inner boundary of the inclusion be subjected to a similar pressure  $p_i$  in the equilibrium position. It is further assumed that no relative slipping takes place between the two shells. Due to misfit both the shells will be stressed. Let  $r$  be the inner radius of the inclusion and  $R$  the outer radius of matrix in the strained state, similarly



let  $a_1(1+\epsilon)$ ,  $\epsilon$  finite, be the radius of the common interface. Let  $p$  be the pressure at the equilibrium boundary. Let  $W_i$ ,  $U_i$  respectively be the elastic potential per unit volume and the total elastic potential of the inclusion in the undeformed state and  $W_m$ ,  $U_m$  the corresponding quantities in the case of the matrix.

From (1), for the inclusion we have

$$\begin{aligned} \frac{4}{3} \pi(r^3 - a_2^3)p_i - \frac{4}{3} \pi a_1^3 \{(1+\epsilon)^3 - (1+\delta)^3\} \\ = U_i + \frac{4}{3} \pi a_2^3 W_i(r) - \frac{4}{3} \pi a_1^3 (1+\delta)^3 W_i\{a_1(1+\epsilon)\} \end{aligned} \quad (3)$$

The incompressibility condition gives

$$r^3 - a_2^3 = a_1^3 \{(1+\epsilon)^3 - (1+\delta)^3\} \quad (4)$$

Hence from equations (3) and (4)

$$a_1^3 \{(1+\epsilon)^3 - (1+\delta)^3\} (p_i - p) = \frac{3}{4\pi} \{U_i + a_2^3 W_i(r) - a_1^3 (1+\delta)^3 W_i\{a_1(1+\epsilon)\}\}$$

The right hand side of the above equation is a known quantity say  $I$ , where

$$I = \frac{3}{4\pi} \{U_i + a_2^3 W_i(r) - a_1^3 (1+\delta)^3 W_i\{a_1(1+\epsilon)\}\}.$$

Hence

$$a_1^3 \{(1+\epsilon)^3 - (1+\delta)^3\} (p_i - p) = I \quad (5)$$

For the matrix in the deformed state the inner boundary is  $a_1(1+\epsilon)$  and the outer boundary is  $R$ . As in the case of inclusion we shall have

$$a_1^3 \{(1+\epsilon)^3 - 1\} (p - p_0) = M \quad (6)$$

where

$$M = \frac{3}{4\pi} \{U_m + a_1^3 W_m\{a_1(1+\epsilon)\} - a_0^3 W_m(R)\}$$

Eliminating  $p$  from (5) and (6)

$$a_1^3 (p_i - p_0) = \frac{I}{(1+\epsilon)^3 - (1+\delta)^3} + \frac{M}{(1+\epsilon)^3 - 1}$$

$$\begin{aligned} \text{or } a_1^3 (p_i - p_0) (1+\epsilon)^3 - \{a_1^3 (p_i - p_0) \{(1+\delta)^3 - 1\} + I + M\} (1+\epsilon)^3 \\ + \{a_1^3 (p_i - p_0) + M\} (1+\delta)^3 + I = 0 \end{aligned} \quad (7)$$

This will give the value of  $\epsilon$  in terms of known quantities

$$\delta, p_i, p_0, I, M$$

The equilibrium pressure  $p$  can also be determined from (5) and (6)

$$2p = p_0 - p_i + \frac{M}{(1+\epsilon)^3 - 1} - \frac{I}{(1+\epsilon)^3 - (1+\delta)^3} \quad (8)$$

where  $\epsilon$  is given by (7).

### HOOP STRESS ON THE EQUILIBRIUM BOUNDARY

For the inclusion, at the equilibrium boundary, let

$$Q = \frac{1 + \delta}{1 + \epsilon}$$

The Hoop stress  $\sigma_i^{22} = R^2 T_i^{22}$  for inclusion is given by

$$\sigma_i^{22} = R^2 \left[ \left\{ \left( \frac{1 + \epsilon}{1 + \delta} \right)^2 - \left( \frac{1 + \delta}{1 + \epsilon} \right)^4 \right\} \phi_i + \left\{ \left( \frac{1 + \epsilon}{1 + \delta} \right)^4 - \left( \frac{1 + \delta}{1 + \epsilon} \right)^2 \right\} \psi_i + I - p \right]$$

Similarly, for the matrix  $Q = \frac{1}{1 + \epsilon}$  then

$$\sigma_m^{22} = R^2 \left[ \left\{ (1 + \epsilon)^2 - \frac{1}{(1 + \epsilon)^4} \right\} \phi_m + \left\{ (1 + \epsilon)^4 - \frac{1}{(1 + \epsilon)^2} \right\} \psi_m + M - p \right] \quad \dots (10)$$

The jump in hoop stress at the equilibrium boundary is given by

$$\begin{aligned} \sigma_m^{22} - \sigma_i^{22} = R^2 \left[ \left\{ (1 + \epsilon)^2 - \frac{1}{(1 + \epsilon)^4} \right\} \phi_m - \left\{ \left( \frac{1 + \epsilon}{1 + \delta} \right)^2 - \left( \frac{1 + \delta}{1 + \epsilon} \right)^4 \right\} \phi_i \right. \\ \left. + \left\{ (1 + \epsilon)^4 - \frac{1}{(1 + \epsilon)^2} \right\} \psi_m - \left\{ \left( \frac{1 + \epsilon}{1 + \delta} \right)^4 - \left( \frac{1 + \delta}{1 + \epsilon} \right)^2 \right\} \psi_i + M - p \right] \quad (11) \end{aligned}$$

The ratio of hoop-stress at the equilibrium boundary

$$\frac{\sigma_m^{22}}{\sigma_i^{22}} = \frac{\left\{ (1 + \epsilon)^2 - \frac{1}{(1 + \epsilon)^4} \right\} \phi_m + \left\{ (1 + \epsilon)^4 - \frac{1}{(1 + \epsilon)^2} \right\} \psi_m + M - p}{\left\{ \left( \frac{1 + \epsilon}{1 + \delta} \right)^2 - \left( \frac{1 + \delta}{1 + \epsilon} \right)^4 \right\} \phi_i + \left\{ \left( \frac{1 + \epsilon}{1 + \delta} \right)^4 - \left( \frac{1 + \delta}{1 + \epsilon} \right)^2 \right\} \psi_i + I - p} \quad (12)$$

Special cases of solid incompressible and rigid inclusions can be deduced from (5) and (6). In both these cases it may easily be shown that the equilibrium boundary will coincide with the outer boundary of the inclusion, i.e.  $\epsilon = \delta$ , which is obvious on physical grounds. When the matrix is rigid the equilibrium boundary will again coincide with the inner boundary of the matrix, i.e.  $\epsilon = -\delta$  and the equilibrium pressure is given by (6). Assuming the strain energy form to be that given by linear elasticity, and assuming the infinitesimal displacements, it can be easily verified that  $\epsilon$  and  $p$  as deduced from equations (7) and (8) are the same as obtained in [1], [2], [3].

It may be observed that the solutions given above require the knowledge of nature of the elastic potentials of the materials used for both the inclusion and the matrix. Mooney [1940] has empirically formulated the expression for some materials like rubber. It is

$$W = C_1(I_1 - 3) + C_2(I_2 - 3).$$

where  $C_1$  and  $C_2$  are known constants of the material and  $I_r$  ( $r = 1, 2$ ) are the strain invariants.

Hence for Mooney materials it may be verified that

$$\begin{aligned} \Pi_1 - \Pi_1 = & C_1(Q_2^4 + 4Q_2^2) + 2C_2\left(Q_2^2 - \frac{2}{Q_2}\right) - C_1\left(\frac{1}{\lambda_1^4} - \frac{4}{\lambda_1^2}\right) \\ & - 2C_2\left(\frac{1}{\lambda_1^2} - 2\lambda_1\right), \end{aligned}$$

$$\text{where } Q_1 = \frac{1}{\lambda_1} = \frac{r_1}{R_1} \quad \text{and} \quad Q_2 = \frac{r_2}{R_2}. \quad \dots (13)$$

In the present problem for such inclusion materials we have

$$\begin{aligned} K_1(R_2) = & C_1 \frac{1}{1+\epsilon} \left\{ \left( \frac{1+\delta}{1+\epsilon} \right)^3 + 4 \right\} + 2C_2 \frac{1}{1+\delta} \left\{ \left( \frac{1+\delta}{1+\epsilon} \right)^3 - 2 \right\} \\ & - \frac{a_2 C_1}{\{a_1^3(1+\epsilon)^3 - a_1^3(1+\delta)^3 + a_2^3\}^{1/3}} \left\{ a_1^3(1+\epsilon)^3 - a_1^3(1+\delta)^3 + a_2^3 + 4 \right\} \\ & - \frac{2C_2\{a_1^3(1+\epsilon)^3 - a_1^3(1+\delta)^3 + a_2^3\}^{1/3}}{a_2} \left\{ a_1^3(1+\epsilon)^3 - a_1^3(1+\delta)^3 + a_2^3 - 2 \right\} \end{aligned} \quad (14)$$

where

$$\begin{aligned} K(R) &= \int_{Q_1}^{Q_2} \left[ (Q^2 + 1)\phi + \left( Q - \frac{1}{Q^2} \right) \psi \right] dQ; \\ K(R_1) &= 0, \quad Q = \frac{r}{R} \end{aligned}$$

$$\text{since } Q_2 = \frac{1+\delta}{1+\epsilon}, \quad Q_1 = \frac{1}{\lambda_1}$$

$$= \frac{a_2}{\{a_1^3(1+\epsilon)^3 - a_1^3(1+\delta)^3 + a_2^3\}^{1/3}}$$

For the matrix we have

$$\begin{aligned} k_m(R_2) = & \frac{a_0 C_1}{\{a_1^3(1+\epsilon)^3 - a_1^3 + a_0^3\}^{1/3}} \left\{ \frac{a_0^3}{a_1^3(1+\epsilon)^3 - a_1^3 + a_0^3} + 4 \right\} + \\ & + \frac{2C_2\{a_1^3(1+\epsilon)^3 - a_1^3 + a_0^3\}^{1/3}}{a_0} \left\{ \frac{a_0^3}{a_1^3(1+\epsilon)^3 - a_1^3 + a_0^3} - 2 \right\} - \\ & - \frac{C_1}{1+\epsilon} \left\{ \frac{1}{(1+\epsilon)^3} + 4 \right\} - 2C_2(1+\epsilon) \left\{ \frac{1}{(1+\epsilon)^3} - 2 \right\}, \end{aligned} \quad \dots (15)$$

since

$$Q_2 = \{a_1^3(1+\epsilon)^3 - a_1^3 + a_0^3\}^{1/3}, Q_1 = \frac{1}{\lambda_1} = \frac{1}{1+\epsilon}.$$

Finally we have

$$p_i - p_0 = k_i(R_2) + k_m(R_2) \quad \dots (16)$$

Substituting for  $k_i(R_2)$   $K_m(R_2)$  and simplifying we get

$$\begin{aligned} p - p_0 = & C'_1 \frac{1+\delta}{1+\epsilon} \left\{ \left( \frac{1+\delta}{1+\epsilon} \right)^3 + 4 \right\} + 2C'_2 \frac{1+\epsilon}{1+\delta} \left\{ \left( \frac{1+\delta}{1+\epsilon} \right)^3 - 2 \right\} \\ & - \left\{ a_1^3(1+\epsilon)^3 - a_1^3(1+\delta)^3 + a_2^3 \right\}^{1/3} \left\{ a_1^3(1+\epsilon)^3 - a_1^3(1+\delta)^3 + a_1^3 + 4 \right\} \\ & - \frac{2C'_2 \{a_1^3(1+\epsilon)^3 - a_1^3(1+\delta)^3 + a_2^3\}^{1/3}}{a_2} \left\{ a_1^3(1+\epsilon)^3 - a_1^3(1+\delta)^3 + a_2^3 - 2 \right\} \\ & + \left\{ a_1^3(1+\epsilon)^3 - a_1^3(1+\delta)^3 + a_0^3 \right\}^{1/3} \left\{ \frac{a_0^3}{a_1^3(1+\epsilon)^3 - a_1^3 + a_0^3} + 4 \right\} \\ & + \frac{2C''_2 \{a_1^3(1+\epsilon)^3 - a_1^3(1+\delta)^3 + a_0^3\}^{1/3}}{a_0} \left\{ a_1^3(1+\epsilon)^3 - a_1^3 + a_0^3 - 2 \right\} \\ & - \frac{C''_1}{1+\epsilon} \left\{ \frac{1}{(1+\epsilon)^3} + 4 \right\} - 2C''_2(1+\epsilon) \left\{ \frac{1}{(1+\epsilon)^3} - 2 \right\}. \end{aligned} \quad (17)$$

which gives  $\epsilon$  and the equilibrium boundary is determined. Further, the equilibrium pressure is given by

$$2p = p_0 - p + K_m(R_2) - K_i(R_2) \quad \dots (18)$$

#### *n Shells' Case*

The problem can be extended to the case of  $n$  elastic shells embedded within each other. Let an isotropic, incompressible, spherical shell  $A_1$  with outer and inner radii  $a_0, a_1$  respectively have another similar shell  $A_2$  of different material and outer and inner radii  $a_1(1+\delta_1), a_2$  respectively embedded within it. Further let a third shell  $A_3$  with outer and inner radii  $a_2(1+\delta_2), a_3$  respectively be embedded in  $A_2$ . Like this, let the shell  $A_{r+1}$  with outer and inner radii  $a_r(1+\delta_r), a_{r+1}$ , be embedded in  $A_r$  whose outer and inner radii are  $a_{r-1}(1+\delta_{r-1}), a_r$  respectively. Finally, let the outer and inner radii of  $A_n$  be  $a_{n-1}(1+\delta_{n-1}), a_n$  respectively it is assumed that  $\delta_r$  are finite. Let the outer boundary of  $A_1$  be subjected to uniform compressive pressure  $p_0$  and the inner boundary of  $A_n$  be subjected to a similar pressure  $p_i$ . It is assumed that all the shells are homogeneous isotropic and made

of different incompressible materials. Due to misfits strains will develop in the system. Let the outer radius of  $A_1$  in the deformed state be  $R$  and the inner one of  $A_n$  in the same state be  $r$ , also let the equilibrium boundaries of  $A_r$  and  $A_{r+1}$  be  $a_r(1+\epsilon_r)$ ,  $\epsilon_r$  being finite and  $r = 1, 2, \dots, n-1$ . Let the equilibrium pressures on the interfaces be  $p_r$  ( $r = 1, 2, \dots, n-1$ ). The problem gives rise to  $2n$  unknown quantities, viz.,  $\epsilon_r$ ,  $p_r$  ( $r = 1, 2, \dots, n-1$ ),  $r$  and  $R$ . Which are determined by the equations connecting the boundary pressures and the strain energy of the  $n$  shells  $A_r$  alongwith another set of  $n$  equations giving the incompressibility conditions as shown below

For  $A_1$  we have from (11)

$$a_1^3\{(1+\epsilon_1)^3-1\}p_1 - (R^3-a_0^3)p_0 = \frac{3}{4\pi} U_1 + a_1^3 W_1\{a_1(1+\epsilon_1)\} - a_0^3 W_1(R) \quad \Omega_1 \quad (\text{say}) \quad (1)$$

$$\text{The incompressibility condition gives } a_0^3 = a_1^3 (R^3 - a_1^3 (1+\delta_1)^3) \quad (1')$$

Similarly for  $A_2$  we have

$$a_2^3\{(1+\epsilon_2)^3-1\}p_2 - a_0^3\{(1+\epsilon_1)^3 - (1+\delta_1)^3\}p_1 = \Omega_2 \quad (2)$$

and

$$a_1(1+\delta_1)^3 - a_2^3 = a_1^3 (1+\epsilon_1)^3 - a_2^3(1+\epsilon_2)^3 \quad (2')$$

For  $A_r$

$$a_r^3\{(1+\epsilon_r)^3-1\}p_r - a_{r-1}^3\{(1+\epsilon_{r-1})^3 - (1+\delta_{r-1})^3\}p_{r-1} = \Omega_r \quad \dots \quad (r)$$

and from incompressibility condition

$$a_{r-1}^3(1+\delta_{r-1})^3 - a_r^3 = a_{r-1}^3(1+\epsilon_{r-1})^3 - a_r^3(1+\epsilon_r)^3 \quad \dots \quad (r')$$

$$\text{where } \Omega_r = \frac{3}{4\pi} U_r + a_r^3 W_r\{a_r(1+\epsilon_r)\} - a_{r-1}^3 W_r\{a_{r-1}(1+\epsilon_{r-1})\}$$

Finally for  $A_n$  we have

$$(r^3 - a_n^2)p_n - a_{n-1}^3\{(1+\epsilon_{n-1})^3 - (1+\delta_{n-1})^3\}p_{n-1} = \Omega'_n \quad \dots \quad (n)$$

and

$$a_{n-1}^3(1+\delta_{n-1})^3 - a_n^3 = a_{n-1}^3(1+\epsilon_{n-1})^3 - r^3 \quad \dots \quad (n')$$

$$\text{where } \Omega'_n = \frac{3}{4\pi} U_n + a_n^3 W_n(r) - a_{n-1}^3 W_n\{a_{n-1}(1+\epsilon_{n-1})\}.$$

This set of  $2n$  equations completely determines the  $2n$  unknowns  $\epsilon_r$ ,  $p_r$  ( $r = 1, 2, \dots, n-1$ ),  $r$  and  $R$ .

#### REFERENCES

- Bhargava, R. D., 1962, *App. Sci. Res.*, **A11**, 80.  
 Bhargava, R. D. and Pande, D., 1963, Misfitting Elastic Shells under uniform Pressures, *J. Sci. and Eng. Res. Kharagpur, (India)*, **7**, 2.  
 Green and Zerna, 1960, *Theoretical Elasticity*, Oxford Univ. Press.  
 Mooney, M., 1940, Theory of Large elastic Deformations, *Jour. of App. Phys.*, **11**.  
 Mott, N. F. and Nabarro, F. R. N., 1940, *Proc. Phys. Soc.*, **52**.

# ON A NEW TRANSFORMATION SCHEME RELATED TO A 4-DIMENSIONAL LORENTZ TRANSFORMATION\*

N. N. GHOSH

INDIAN ASSOCIATION FOR THE CULTIVATION OF SCIENCE,

CALCUTTA-32.

(Received June 16, 1965)

**ABSTRACT.** In a four-space  $R_4$  a new real transformation scheme has been so framed that a new representation of a four-dimensional Lorentz transformation is obtained showing the connection between the respective transformation coefficients. The method is a modification of that used in an earlier paper where the representation of a five-dimensional Lorentz transformation was considered. It is to be noted that under this new transformation scheme one can set up a system of 'Dirac Equations'.

## INTRODUCTION

In a recent paper (Ghosh 1964) a new representation of a five dimensional Lorentz transformation was obtained by utilizing the real transformation coefficients of a new transformation scheme defined in a four-space  $R_4$  with coordinates  $x^0, x^1, x^2, x^3$  which leaves invariant an elementary antisymmetric tensor  $C'_{pq}$  with 4 non-vanishing components  $C'_{01} = C'_{10} = 1$ ,  $C'_{23} = C'_{32} = 1$ . The object of the present paper is to modify the transformation scheme so that the representation corresponds to a four-dimensional Lorentz transformation both proper and improper. Further, it is shown how under this transformation scheme one can set up a system of Dirac Equations derived from an invariant divergence equation.

1. Starting with the set of general transformation equations in  $R_4$  from coordinates  $x^r$  to  $x'^r$  and vice versa

$$\begin{aligned} x'^r &= \phi^r(x^0, x^1, x^2, x^3), \\ x^r &= \phi^{-1r}(x'^0, x'^1, x'^2, x'^3), \quad (r = 0, 1, 2, 3) \end{aligned} \quad \dots \quad (1.1)$$

\*An abstract of this paper was read at the 52-nd session of Indian Science Congress, 1965.

with 16 covariant transformation coefficients  $\partial x^r/\partial x'^p$  we first impose the following 8 restrictive conditions on the function  $\phi'$  given by

$$\begin{aligned} \begin{pmatrix} 0 \\ 0 \end{pmatrix} &= \lambda \begin{pmatrix} 3 \\ 3 \end{pmatrix}, & \begin{pmatrix} 0 \\ 3 \end{pmatrix} &= -\lambda \begin{pmatrix} 3 \\ 0 \end{pmatrix}, \\ \begin{pmatrix} 0 \\ 1 \end{pmatrix} &= \lambda \begin{pmatrix} 3 \\ 2 \end{pmatrix}, & \begin{pmatrix} 0 \\ 2 \end{pmatrix} &= \lambda \begin{pmatrix} 3 \\ 1 \end{pmatrix}, \\ \begin{pmatrix} 1 \\ 0 \end{pmatrix} &= \lambda \begin{pmatrix} 2 \\ 3 \end{pmatrix}, & \begin{pmatrix} 2 \\ 0 \end{pmatrix} &= \lambda \begin{pmatrix} 1 \\ 3 \end{pmatrix}, \\ \begin{pmatrix} 1 \\ 1 \end{pmatrix} &= \lambda \begin{pmatrix} 2 \\ 2 \end{pmatrix}, & \begin{pmatrix} 2 \\ 1 \end{pmatrix} &= -\lambda \begin{pmatrix} 1 \\ 2 \end{pmatrix}, \end{aligned} \quad \dots \quad (1.2)$$

where  $\lambda$  is either  $+1$  or  $-1$ , the symbol  $(r_p)$  denoting  $\partial x^r/\partial x'^p$ . If  $\lambda = +1$ , the system of transformations will possess group property and we call it a proper general transformation. With  $\lambda = -1$ , the system does not possess group property and we call it an improper general transformation.

The conditions (1.2) admit of being expressed in terms of contravariant transformation coefficients. These are of the same type as (1.2) provided the symbol  $(r_p)$  is replaced by  $\partial x'^r/\partial x^p$ .

2. Let us now define a special transformation in the above scheme by introducing an antisymmetric covariant tensor  $C'_{pq}$  with non-vanishing components  $C'_{01} = -C'_{10} = 1$ ,  $C'_{23} = -C'_{32} = 1$ , and postulating that it remains invariant. Referring to (1.1) the transformation equation of  $C'_{pq}$  is given by

$$C''_{rs} = C'_{pq} \frac{\partial x^p}{\partial x'^r} \frac{\partial x^q}{\partial x'^s} \quad (r, s = 0, 1, 2, 3) \quad \dots \quad (2.1)$$

For invariance of  $C'_{pq}$  the full set of conditions are given in my last paper (Ghosh, 1964). Here, in addition to conditions (1.2) two more conditions independent of  $\lambda$  have to be satisfied. These are

$$\begin{aligned} \begin{pmatrix} 01 \\ 01 \end{pmatrix} + \begin{pmatrix} 01 \\ 23 \end{pmatrix} &= 1, \\ \begin{pmatrix} 02 \\ 01 \end{pmatrix} + \begin{pmatrix} 02 \\ 23 \end{pmatrix} &= 0, \end{aligned} \quad \dots \quad (2.2)$$

where the symbol  $\begin{pmatrix} pq \\ rs \end{pmatrix}$  denotes  $\begin{pmatrix} p \\ r \end{pmatrix} \begin{pmatrix} q \\ s \end{pmatrix} - \begin{pmatrix} p \\ s \end{pmatrix} \begin{pmatrix} q \\ r \end{pmatrix}$ .

Alternatively we can write (2.2) as

$$\begin{aligned} \begin{pmatrix} 01 \\ 01 \end{pmatrix} + \begin{pmatrix} 23 \\ 01 \end{pmatrix} &= 1, \\ \begin{pmatrix} 01 \\ 02 \end{pmatrix} + \begin{pmatrix} 23 \\ 02 \end{pmatrix} &= 0, \end{aligned} \quad \dots \quad (2.3)$$

This special transformation will be called unimodular tensor transformation, proper if  $\lambda = 1$  and improper if  $\lambda = -1$ . The contravariant tensor associated to  $C_{pq}$  will be denoted by  $C^{pq}$  having non-vanishing components  $C^{01} = -C^{10} = 1$ ,  $C^{23} = C^{32} = 1$ . It may be noted that the contravariant and covariant coefficients of a unimodular tensor transformation are connected by the equation

$$\frac{\partial x'^q}{\partial x^p} = C_{rs} C^{pq} \frac{\partial x^r}{\partial x'^s}. \quad \dots (2.4)$$

This gives

$$\begin{aligned} \left\{ \begin{smallmatrix} 0 \\ 0 \end{smallmatrix} \right\} &= \left( \begin{smallmatrix} 1 \\ 1 \end{smallmatrix} \right) \cdot \left\{ \begin{smallmatrix} 1 \\ 0 \end{smallmatrix} \right\} = - \left( \begin{smallmatrix} 1 \\ 0 \end{smallmatrix} \right) \cdot \left\{ \begin{smallmatrix} 2 \\ 0 \end{smallmatrix} \right\} = \left( \begin{smallmatrix} 1 \\ 3 \end{smallmatrix} \right) \cdot \left\{ \begin{smallmatrix} 3 \\ 0 \end{smallmatrix} \right\} = - \left( \begin{smallmatrix} 1 \\ 2 \end{smallmatrix} \right) \cdot \left\{ \begin{smallmatrix} 3 \\ 1 \end{smallmatrix} \right\}, \\ \left\{ \begin{smallmatrix} 0 \\ 1 \end{smallmatrix} \right\} &= \left( \begin{smallmatrix} 0 \\ 1 \end{smallmatrix} \right) \cdot \left\{ \begin{smallmatrix} 1 \\ 1 \end{smallmatrix} \right\} = \left( \begin{smallmatrix} 0 \\ 0 \end{smallmatrix} \right) \cdot \left\{ \begin{smallmatrix} 2 \\ 1 \end{smallmatrix} \right\} = \left( \begin{smallmatrix} 0 \\ 3 \end{smallmatrix} \right) \cdot \left\{ \begin{smallmatrix} 3 \\ 1 \end{smallmatrix} \right\} = \left( \begin{smallmatrix} 0 \\ 2 \end{smallmatrix} \right) \cdot \left\{ \begin{smallmatrix} 3 \\ 2 \end{smallmatrix} \right\}, \\ \left\{ \begin{smallmatrix} 0 \\ 2 \end{smallmatrix} \right\} &= \left( \begin{smallmatrix} 3 \\ 1 \end{smallmatrix} \right) \cdot \left\{ \begin{smallmatrix} 1 \\ 2 \end{smallmatrix} \right\} = \left( \begin{smallmatrix} 3 \\ 0 \end{smallmatrix} \right) \cdot \left\{ \begin{smallmatrix} 2 \\ 2 \end{smallmatrix} \right\} = \left( \begin{smallmatrix} 3 \\ 3 \end{smallmatrix} \right) \cdot \left\{ \begin{smallmatrix} 3 \\ 2 \end{smallmatrix} \right\} = \left( \begin{smallmatrix} 3 \\ 2 \end{smallmatrix} \right) \cdot \left\{ \begin{smallmatrix} 3 \\ 3 \end{smallmatrix} \right\}, \\ \left\{ \begin{smallmatrix} 0 \\ 3 \end{smallmatrix} \right\} &= - \left( \begin{smallmatrix} 2 \\ 1 \end{smallmatrix} \right) \cdot \left\{ \begin{smallmatrix} 1 \\ 3 \end{smallmatrix} \right\} = \left( \begin{smallmatrix} 2 \\ 0 \end{smallmatrix} \right) \cdot \left\{ \begin{smallmatrix} 2 \\ 3 \end{smallmatrix} \right\} = \left( \begin{smallmatrix} 2 \\ 3 \end{smallmatrix} \right) \cdot \left\{ \begin{smallmatrix} 3 \\ 3 \end{smallmatrix} \right\} = \left( \begin{smallmatrix} 2 \\ 2 \end{smallmatrix} \right) \cdot \left\{ \begin{smallmatrix} 3 \\ 3 \end{smallmatrix} \right\}, \end{aligned} \quad \dots (2.5)$$

where we have used the notation  $\left\{ \begin{smallmatrix} p \\ q \end{smallmatrix} \right\}$  to denote  $\partial x'^p / \partial x^q$ .

The tensors  $C^{pq}, C_{pq}$  may be regarded as metric tensors in  $R_4$ . Raising and lowering of indices may be performed according to the rule

$$A_q C^{pq} = A^p, \quad A^p C_{pq} = A_q, \quad \dots (2.6)$$

so that

$$C^{pq} C_{pr} = C^{qp} C_{rp} = \delta_r^q.$$

Thus

$$A = A_1, \quad A' = A_0, \quad A^2 = A_3, \quad A^3 = -A_2.$$

We note here the relations

$$A_p A^p = 0, \quad A_p B^p + B_p A^p = 0. \quad \dots (3.7)$$

Consider now a mixed tensor  $M_r^p$  defined in terms of 4 quantities  $h_k$ , forming a vector, by means of an equation

$$M_r^p = T^{kp}_r h_k \quad (k = 0, 1, 2, 3), \quad \dots (3.8)$$

where  $T$ 's are connecting tensors having the following structure :

$$\begin{aligned} T^0_r{}^p &= \begin{pmatrix} 0 & 0 & 1 & 0 \\ 0 & 0 & 0 & 1 \\ 1 & 0 & 0 & 0 \\ 0 & 1 & 0 & 0 \end{pmatrix}, & T^1_r{}^p &= \begin{pmatrix} 0 & 0 & 0 & 1 \\ 0 & 0 & -1 & 0 \\ 0 & -1 & 0 & 0 \\ 1 & -1 & 0 & 0 \end{pmatrix}, \\ T^2_r{}^p &= \begin{pmatrix} -1 & 0 & 0 & 0 \\ 0 & -1 & 0 & 0 \\ 0 & 0 & 1 & 0 \\ 0 & 0 & 0 & 1 \end{pmatrix}, & T^3_r{}^p &= \begin{pmatrix} 0 & 0 & 1 & 0 \\ 0 & 0 & 0 & 1 \\ 1 & 0 & 0 & 0 \\ 0 & 1 & 0 & 0 \end{pmatrix} \end{aligned} \quad (3.9)$$



Thus

$$\begin{aligned} M_0^0 &= M_1^1 = -h_2, & M_2^2 &= M_3^3 = h_2, & M_2^1 &= -M_0^3 = -h_1, \\ M_3^0 &= -M_1^2 = h_1, & M_2^0 &= M_1^3 = h_0 + h_3, & M_0^2 &= M_3^1 = -h_0 + h_3, \\ M_1^0 &= M_0^1 = M_3^2 = M_2^3 = 0. \quad \dots \quad (3.10) \end{aligned}$$

Applying the rule (2.6) one can see that  $M^p_r$  will have the above structure if it is taken in a bilinear form  $A^p B_r - B^p A_r$ ,  $A^p$ ,  $B_r$  being arbitrary tensors of rank 1.

Inverting (3.8) we write

$$h_k = \frac{1}{4} T_{kp}^r M^p_r, \quad \dots \quad (3.11)$$

where

$$T_{kp}^r = g_{kl} T^{lr}_p, \quad \dots \quad (3.12)$$

$g_{kl}$  denoting the tensor with non-vanishing components

$$g_{00} = -1, \quad g_{11} = g_{22} = g_{33} = 1.$$

Let  $M^p_r$  undergo a unimodular tensor transformation

$$M'^p_r = M^q_s \left\{ \begin{smallmatrix} p \\ q \end{smallmatrix} \right\} \left( \begin{smallmatrix} s \\ r \end{smallmatrix} \right), \quad \dots \quad (3.13)$$

where the transformation coefficients satisfy relations (1.2), (2.2,4). It is found that after the transformation  $M'^p_r$  will have the same structure as that of  $M^p_r$ , so that we can express  $M'^p_r$  in the same way as (3.8)

that is, 
$$M'^p_r = T^{kp}_r h'_k, \quad \dots \quad (3.14)$$

where  $h'_k$  denotes the transformed vector  $h_k$  induced by the unimodular tensor transformation with regard to  $M^p_r$

Inverting (3.14) we write

$$h'_k = \frac{1}{4} T^p_{kr} M'^p_r. \quad \dots \quad (3.15)$$

Using (3.13), the above becomes

$$h'_k = \frac{1}{4} T^p_{kr} M^q_s \left\{ \begin{smallmatrix} p \\ q \end{smallmatrix} \right\} \left( \begin{smallmatrix} s \\ r \end{smallmatrix} \right). \quad \dots \quad (3.16)$$

Writing  $h'_k = a^l_k h_l$  and  $M^q_s = T^{lq}_s h_l$ , we obtain

$$a^l_k = \frac{1}{4} T^r_{kr} T^{lq}_s \left\{ \begin{smallmatrix} p \\ q \end{smallmatrix} \right\} \left( \begin{smallmatrix} s \\ r \end{smallmatrix} \right). \quad \dots \quad (3.17)$$

Observing that the invariant  $M_r^p M_p^r = 4(h_1^2 + h_2^2 + h_3^2 - h_0^2)$  we remark that when  $M_r^p$  undergoes a unimodular tensor transformation the vector  $h_k$  undergoes a Lorentz transformation leaving  $h_1^2 + h_2^2 + h_3^2 - h_0^2$  invariant.

4. In matrix form (3.17) is expressible as

$$\begin{bmatrix} a_0^0 & a_1^0 & a_2^0 & a_3^0 \\ a_0^1 & a_1^1 & a_2^1 & a_3^1 \\ a_0^2 & a_1^2 & a_2^2 & a_3^2 \\ a_0^3 & a_1^3 & a_2^3 & a_3^3 \end{bmatrix} = \frac{1}{2} \begin{bmatrix} \begin{pmatrix} 03, 12 \end{pmatrix} & \begin{pmatrix} 03, 12 \end{pmatrix} & \begin{pmatrix} 03, 12 \end{pmatrix} & \begin{pmatrix} 03, 12 \end{pmatrix} \\ \begin{pmatrix} 03, 12 \end{pmatrix} & \begin{pmatrix} 13, 02 \end{pmatrix} & \begin{pmatrix} 01, 32 \end{pmatrix} & \begin{pmatrix} 12, 30 \end{pmatrix} \\ \begin{pmatrix} 13, 02 \end{pmatrix} & \begin{pmatrix} 13, 02 \end{pmatrix} & \begin{pmatrix} 13, 02 \end{pmatrix} & \begin{pmatrix} 13, 02 \end{pmatrix} \\ \begin{pmatrix} 03, 12 \end{pmatrix} & \begin{pmatrix} 13, 02 \end{pmatrix} & \begin{pmatrix} 01, 32 \end{pmatrix} & \begin{pmatrix} 12, 30 \end{pmatrix} \\ \begin{pmatrix} 01, 32 \end{pmatrix} & \begin{pmatrix} 01, 32 \end{pmatrix} & \begin{pmatrix} 01, 32 \end{pmatrix} & \begin{pmatrix} 01, 32 \end{pmatrix} \\ \begin{pmatrix} 03, 12 \end{pmatrix} & \begin{pmatrix} 13, 02 \end{pmatrix} & \begin{pmatrix} 01, 32 \end{pmatrix} & \begin{pmatrix} 12, 30 \end{pmatrix} \\ \begin{pmatrix} 12, 30 \end{pmatrix} & \begin{pmatrix} 12, 30 \end{pmatrix} & \begin{pmatrix} 12, 30 \end{pmatrix} & \begin{pmatrix} 12, 30 \end{pmatrix} \\ \begin{pmatrix} 03, 12 \end{pmatrix} & \begin{pmatrix} 13, 02 \end{pmatrix} & \begin{pmatrix} 01, 32 \end{pmatrix} & \begin{pmatrix} 12, 30 \end{pmatrix} \end{bmatrix} \quad \dots \quad (4.1)$$

where the symbol  $\begin{pmatrix} pq, rs \\ tu, vw \end{pmatrix}$  denotes  $\begin{pmatrix} pq \\ tu \end{pmatrix} + \begin{pmatrix} pq \\ vw \end{pmatrix} + \begin{pmatrix} rs \\ tu \end{pmatrix} + \begin{pmatrix} rs \\ vw \end{pmatrix}$ .

By elementary operations utilising the relations (1.2) the determinant of the right-hand matrix in (4.1) may be reduced to

$$4 \times \begin{vmatrix} \frac{1}{2} \begin{pmatrix} 12 \\ 12 \end{pmatrix} & \begin{pmatrix} 12 \\ 02 \end{pmatrix} & \begin{pmatrix} 12 \\ 01 \end{pmatrix} & \frac{1}{2} \begin{pmatrix} 12 \\ 03 \end{pmatrix} \\ \begin{pmatrix} 02 \\ 12 \end{pmatrix} & \begin{pmatrix} 02 \\ 02 \end{pmatrix} + \begin{pmatrix} 02 \\ 13 \end{pmatrix} & \begin{pmatrix} 02 \\ 01 \end{pmatrix} + \begin{pmatrix} 02 \\ 32 \end{pmatrix} & \begin{pmatrix} 02 \\ 03 \end{pmatrix} \\ \begin{pmatrix} 01 \\ 12 \end{pmatrix} & \begin{pmatrix} 01 \\ 02 \end{pmatrix} + \begin{pmatrix} 01 \\ 02 \end{pmatrix} & \begin{pmatrix} 01 \\ 01 \end{pmatrix} + \begin{pmatrix} 01 \\ 32 \end{pmatrix} & \begin{pmatrix} 01 \\ 03 \end{pmatrix} \\ \frac{1}{2} \begin{pmatrix} 03 \\ 12 \end{pmatrix} & \begin{pmatrix} 03 \\ 02 \end{pmatrix} & \begin{pmatrix} 03 \\ 01 \end{pmatrix} & \frac{1}{2} \begin{pmatrix} 03 \\ 03 \end{pmatrix} \end{vmatrix} \quad \dots \quad (4.2)$$

Introducing the quantities

$$a_1 = \begin{pmatrix} 0 \\ 0 \end{pmatrix} \begin{pmatrix} 1 \\ 1 \end{pmatrix} + \begin{pmatrix} 0 \\ 3 \end{pmatrix} \begin{pmatrix} 1 \\ 2 \end{pmatrix} \quad b_1 = \begin{pmatrix} 0 \\ 0 \end{pmatrix} \begin{pmatrix} 1 \\ 2 \end{pmatrix} - \begin{pmatrix} 0 \\ 3 \end{pmatrix} \begin{pmatrix} 1 \\ 1 \end{pmatrix}.$$

$$a_2 = \begin{pmatrix} 0 \\ 0 \end{pmatrix} \begin{pmatrix} 0 \\ 1 \end{pmatrix} + \begin{pmatrix} 0 \\ 3 \end{pmatrix} \begin{pmatrix} 1 \\ 2 \end{pmatrix} \quad b_2 = \begin{pmatrix} 0 \\ 0 \end{pmatrix} \begin{pmatrix} 0 \\ 2 \end{pmatrix} - \begin{pmatrix} 0 \\ 3 \end{pmatrix} \begin{pmatrix} 1 \\ 1 \end{pmatrix}.$$

$$a_3 = \begin{pmatrix} 0 \\ 0 \end{pmatrix} \begin{pmatrix} 1 \\ 0 \end{pmatrix} + \begin{pmatrix} 0 \\ 3 \end{pmatrix} \begin{pmatrix} 1 \\ 3 \end{pmatrix} \quad b_3 = \begin{pmatrix} 0 \\ 0 \end{pmatrix} \begin{pmatrix} 1 \\ 3 \end{pmatrix} - \begin{pmatrix} 0 \\ 3 \end{pmatrix} \begin{pmatrix} 1 \\ 0 \end{pmatrix}.$$

$$a_4 = \begin{pmatrix} 0 \\ 1 \end{pmatrix} \begin{pmatrix} 1 \\ 0 \end{pmatrix} + \begin{pmatrix} 0 \\ 2 \end{pmatrix} \begin{pmatrix} 1 \\ 3 \end{pmatrix}, \quad b_4 = \begin{pmatrix} 0 \\ 1 \end{pmatrix} \begin{pmatrix} 1 \\ 3 \end{pmatrix} - \begin{pmatrix} 0 \\ 2 \end{pmatrix} \begin{pmatrix} 1 \\ 0 \end{pmatrix},$$

$$a_5 = \begin{pmatrix} 0 \\ 1 \end{pmatrix} \begin{pmatrix} 1 \\ 1 \end{pmatrix} + \begin{pmatrix} 0 \\ 2 \end{pmatrix} \begin{pmatrix} 1 \\ 2 \end{pmatrix}, \quad b_5 = \begin{pmatrix} 0 \\ 1 \end{pmatrix} \begin{pmatrix} 1 \\ 2 \end{pmatrix} - \begin{pmatrix} 0 \\ 2 \end{pmatrix} \begin{pmatrix} 1 \\ 1 \end{pmatrix},$$

$$a_6 = \begin{pmatrix} 1 \\ 0 \end{pmatrix} \begin{pmatrix} 1 \\ 1 \end{pmatrix} + \begin{pmatrix} 1 \\ 3 \end{pmatrix} \begin{pmatrix} 1 \\ 2 \end{pmatrix}, \quad b_6 = \begin{pmatrix} 1 \\ 0 \end{pmatrix} \begin{pmatrix} 1 \\ 2 \end{pmatrix} - \begin{pmatrix} 1 \\ 3 \end{pmatrix} \begin{pmatrix} 1 \\ 1 \end{pmatrix}.$$

$$c_1 = \frac{1}{2} \begin{pmatrix} 0 \\ 0 \end{pmatrix}^2 + \frac{1}{2} \begin{pmatrix} 0 \\ 3 \end{pmatrix}^2, \quad c_2 = \frac{1}{2} \begin{pmatrix} 0 \\ 1 \end{pmatrix}^2 + \frac{1}{2} \begin{pmatrix} 0 \\ 2 \end{pmatrix}^2,$$

$$c_3 = \frac{1}{2} \begin{pmatrix} 1 \\ 0 \end{pmatrix}^2 + \frac{1}{2} \begin{pmatrix} 1 \\ 3 \end{pmatrix}^2, \quad c_4 = \frac{1}{2} \begin{pmatrix} 1 \\ 1 \end{pmatrix}^2 + \frac{1}{2} \begin{pmatrix} 1 \\ 2 \end{pmatrix}^2 \quad (4.3)$$

(4.2) may be expressed as

$$4 \times \begin{array}{cccc} \lambda c_4 & \lambda a_6 & -\lambda b_6 & \lambda c_3 \\ \lambda a_5 & \lambda(a_1 + a_4) & \lambda(b_4 - b_1) & \lambda a_3 \\ b_5 & b_1 + b_4 & a_1 - a_4 & b_3 \\ \lambda c_2 & \lambda a_2 & -\lambda b_2 & \lambda c \end{array} \quad (4.4)$$

Omitting the multiplier 4, the Laplace expansion of (4.4) gives

$$\begin{aligned} & \lambda^2(c_1 a_3 - c_3 a_5)(b_4 b_2 + b_1 b_2 + a_1 a_2 - a_2 a_4)(-\lambda) \\ & - \lambda(c_4 b_3 - c_3 b_5)(b_2 a_1 + b_2 a_4 + a_2 b_4 - a_2 b_1)(-\lambda^2) \\ & + \lambda^2(c_1 c_4 - c_2 c_3)(a_1^2 - a_4^2 - b_4^2 - b_1^2)\lambda \\ & + \lambda(a_5 b_3 - b_5 a_1)(a_6 b_2 - b_6 a_2)(-\lambda^2) \\ & - \lambda^2(c_1 a_5 - c_2 a_3)(a_6 a_1 - a_6 a_4 + b_6 b_4 + b_1 b_6)\lambda \\ & + \lambda(c_1 b_5 - c_2 b_3)(a_6 b_4 - a_6 b_1 + b_6 a_1 - b_6 a_4)\lambda^2. \end{aligned} \quad (4.5)$$

Let us now take note of the following identities :

$$\begin{aligned} a_1 a_2 + b_1 b_2 &= 2c_1 a_5, & a_1 b_2 - b_1 a_2 &= -2c_1 b_6, \\ a_2 a_4 - b_2 b_4 &= 2c_2 a_3, & a_2 b_4 + b_2 a_4 &= 2c_2 b_3, \\ a_4 a_6 - b_4 b_6 &= 2c_3 a_5, & a_4 b_6 + b_4 a_6 &= 2c_3 b_5, \\ a_1 a_6 + b_1 b_6 &= 2c_4 a_3, & a_1 b_6 - b_1 a_6 &= -2c_4 b_3, \\ a_5 b_3 - b_5 a_3 &= a_6 b_2 - a_6 b_6. \end{aligned} \quad (4.6)$$

Substituting from the above (4.5) becomes

$$\lambda^3[4c_2c_4a_3^2 + 4c_1c_3a_5^2 + 4c_2c_4b_3^2 + 4c_1c_3b_5^2 - 4(c_1c_4 + c_2c_3)(a_3a_5 + b_3b_5) - (a_5b_3 - b_5a_3)^2 + (c_1c_4 - c_2c_3)(a_1^2 - a_4^2 - b_4^2 + b_1^2)]. \quad (4.7)$$

Using further the typical relations

$$\begin{aligned} 4c_1c_4 &= a_1^2 + b_1^2, \quad 4c_1c_2 = a_2^2 + b_2^2, \quad 4c_1c_3 = a_3^2 + b_3^2, \\ 4c_2c_3 &= a_4^2 + b_4^2, \quad 4c_2c_4 = a_5^2 + b_5^2, \quad 4c_3c_4 = a_6^2 + b_6^2. \end{aligned} \quad \dots \quad (4.8)$$

(4.7) can be expressed as

$$\lambda^3[2(c_1c_4 + c_2c_3) - (a_3a_5 + b_3b_5)]^2. \quad \dots \quad (4.9)$$

By a straight-forward calculation the above can be shown to be

$$\lambda^3 \left[ \frac{1}{2} \left\{ \binom{0}{0} \binom{1}{1} - \binom{0}{1} \binom{1}{0} + \binom{0}{2} \binom{1}{3} - \binom{0}{3} \binom{1}{2} \right\}^2 \right]. \quad (4.10)$$

Referring to (2.2), the value of the determinant (4.2) is therefore  $\lambda^3$ , which is 1 if  $\lambda = 1$  and -1 if  $\lambda = -1$ . Thus the representation (4.1) corresponds to 4-dimensional Lorentz transformation both proper and improper. The relevant conditions to be satisfied by the transformation coefficients ( $\frac{p}{q}$ ), being given by (1.2), (2.2). The linearity with regard to the Lorentz transformation will follow if we start with the set of transformation equations (1.1) all linear, so that the coefficients of transformation are constants.

5. We shall now show that under this new transformation scheme one can set up a system of 'Dirac equations'. Let us first construct the differential operator  $\Delta_q^p$

given by 
$$\Delta_q^p = T^{kp} \partial_k. \quad \dots \quad (5.1)$$

where  $\partial_k$  denotes  $\partial/\partial x^k$ . The four components of the operator  $\Delta_q^p$  are given by

$$\Delta_0^0 = \Delta_1^1 = -\Delta_2^2 = -\Delta_3^3 = -\partial_2, \quad \Delta_2^1 = -\Delta_0^3 = \Delta_1^2 = -\Delta_3^0 = -\partial_1. \quad \dots \quad (5.2)$$

$$\Delta_2^0 = \Delta_1^3 = \partial_0 + \partial_3, \quad \Delta_0^2 = \Delta_3^1 = -\partial_0 + \partial_3, \quad \Delta_1^0 = \Delta_0^1 = \Delta_3^2 = \Delta_2^3 = 0.$$

Consider now the invariant divergence equation

$$\Delta_q^p M_p^q = 0, \quad \dots \quad (5.3)$$

where

$$M_p^q = A^q B_p - B^q A_p.$$

Expanding (5.3) we get

$$(\Delta_q^p A^q) B_p + A^q (\Delta_q^p B_p) - (\Delta_q^p B^q) A_p - B^q (\Delta_q^p A_p) = 0. \quad \dots \quad (5.4)$$

It is easy to show that

$$A^q(\Delta_q^p B_p) = -(\Delta_q^p B^q)A_p,$$

where  $A$  and  $B$  can be interchanged.

Hence (5.4) becomes

$$(\Delta_q^p A^q)B_p - (\Delta_q^p B^q)A_p = 0, \quad \dots \quad (5.5)$$

Introducing the subsidiary equations

$$\begin{aligned} \Delta_q^p A^q &= mB^p, \\ \Delta_q^p B^q &= nA^p, \quad (m, n \text{ arbitrary constants}) \end{aligned} \quad \dots \quad (5.6)$$

into (5.5), it is automatically satisfied by virtue of the first of the relations (3.7). The symmetry in (5.4) shows that  $m$  and  $n$  are equal.

The equation (5.5) is also satisfied if we introduce the subsidiary equations

$$\begin{aligned} \Delta_q^p A^q &= mA^p, \\ \Delta_q^p B^q &= -mB^p, \end{aligned} \quad \dots \quad (5.7)$$

and take into account the 2nd of the relations (3.7). Combining the two sets of equations in (5.6) with  $m = n$ , we obtain the wave equation

$$\Delta_p^r \Delta_q^p A^q = m^2 A^r. \quad \dots \quad (5.8)$$

6. Let us now consider the infinitesimal unimodular tensor transformation. Starting with the infinitesimal transformation equations

$$x'^r = x^r + \epsilon f^r(x^0, x^1, x^2, x^3), \quad \dots \quad (6.1)$$

where  $\epsilon$  is an infinitely small quantity we impose the conditions (1.2) with  $\lambda = 1$  to (6.1) and obtain

$$\begin{aligned} f_0^0 &= f_3^3, & f_3^0 &= -f_0^3, \\ f_1^0 &= f_2^3, & f_2^0 &= -f_1^3, \\ f_0^1 &= f_3^2, & f_0^2 &= -f_3^1, \\ f_1^1 &= f_2^2, & f_1^2 &= -f_2^1, \end{aligned} \quad \dots \quad (6.2)$$

where  $f_p^r$  denotes  $\partial f^r / \partial x^p$ . Further, the imposition of conditions (2.2) yields

$$f_0^0 + f_1^1 = 0, \quad f_2^1 - f_0^3 = 0. \quad \dots \quad (6.3)$$

An infinitesimal unimodular tensor transformation will be defined by (6.1) where  $f$ 's are restricted by (3.2, 3). Its connection with infinitesimal Lorentz transformation can be exhibited by means of the formula

$$\omega_k^l = \frac{\epsilon}{4} [T_{kp}^l f_m^p - T_m^l f_p^k], \quad \dots \quad (6.4)$$

where  $\omega_k^l$  denotes the coefficient of infinitesimal Lorentz transformation. Evaluating the above we get

$$\begin{aligned}\omega_0^0 &= \omega_1^1 = \omega_2^2 = \omega_3^3 = 0 \\ \omega_1^0 &= \omega_0^1 = -c(f_0^1 + f_1^0), & \omega_2^0 &= \omega_0^2 = c(f_0^2 + f_2^0), \\ \omega_3^0 &= \omega_0^3 = 2cf_0^0, & \omega_2^1 &= -\omega_1^2 = 2cf_2^1, & \dots \quad (6.5) \\ \omega_3^1 &= -\omega_1^3 = c(f_0^1 - f_1^0), & \omega_3^2 &= -\omega_2^3 = -c(f_0^2 - f_2^0).\end{aligned}$$

The author wishes to thank Prof. S. N. Bose, F.R.S., for helpful comments.

#### REFERENCES

Ghosh, N. N., 1964, *Proc. nat. Inst. Sci., India*, **30**, 396

# Letters to the Editor

*The Board of Editors does not hold itself responsible for opinions expressed in the letters published in this section. The notes containing short reports of original investigations communicated to this section should not contain many figures and should not exceed 500 words in length. The contributions reaching the Secretary by the 15th of any month may be expected to appear in the issue for the next month. No proof will be sent to the author.*

19

## INVESTIGATION ON RAMAN AND INFRARED SPECTRA OF TWO ISOMERIC AROMATIC NITRILES IN DIFFERENT STATES.

D. K. MUKHERJEE AND K. K. DEB

OPTICS DEPARTMENT, INDIAN ASSOCIATION FOR THE CULTIVATION OF SCIENCE, CALCUTTA-32.

(Received, May 24, 1965)

The Raman spectra of a few organic nitriles in the solid state at  $-180^{\circ}\text{C}$  were studied earlier (Bishui 1948; Deb, 1961; Deb and Mukherjee, 1963). It has been observed from the results that the lines due to  $C \equiv N$  vibrations in each case undergo changes and in some cases a few low frequency Raman lines appear in the spectra with the solidification of the liquids at low temperatures. Later, Deb (1963) concluded from the results of investigation of the Raman spectra of a large number of organic compounds that certain vibrational modes perpendicular to the benzene ring shift to low frequency region due to the intermolecular association in the crystal lattices of the compounds at low temperatures. In the present work similar investigation has been made in the case of two aromatic nitriles viz, ortho and paratoluenitriles in order to find out how the local field surrounding the  $C \equiv N$  bond is affected in the solid state in the case of the two molecules due to the presence of  $\text{CH}_3$  group in the benzene ring. The infrared spectra of the two compounds in the pure state and in solutions in some suitable solvents have also been studied in order to find out how the results support the above view.

### RESULTS AND DISCUSSIONS

The observed Raman shifts of the compounds in the liquid and solid states at  $-180^{\circ}\text{C}$  are tabulated in Tables I and II. The states of polarisation of the Raman lines of the liquids are indicated by the usual letters 'P' and 'D' which mean partially polarised and totally depolarised respectively.

TABLE I  
Raman and infrared spectra of ortho-tolunitrile

Raman shifts in $\text{cm}^{-1}$			Infrared bands in $\text{cm}^{-1}$ (Present authors)
Liquid Lundolt- Bornstein Table (1951)	Liquid at 30°C Present authors	Solid at -180°C Present authors	
		80 (1)	
150 (10b)	150 (6) D	155 (4b)	
169 (8)	163 (8) D		
217 (4)	223 (1b)	242 (0b)	
342 (1)			
385 (1)			
457 (8)	460 (6) D		
	541 (3) D		
587 (3)	583 (0)		
	638 (1) P		
715 (9)	718 (8) P	720 (2)	708 (ms)
761 (2)			760 (vs)
819 (3)			942 (vw)
991 (1)			
1045 (8)	1048 (8) P	1048 (2)	1038 (w)
1108 (2)			1108 (w)
1159 (5)	1158 (2) D		1160 (w)
1208 (10)	1210 (8) P		1210 (w)
		1219 (6)	
1287 (1)			1290 (w)
1378 (4)	1381 (0b)		1385 (w)
			1440 (ms)
			1450 (ms)
1486 (3)			1488 (ms)
	1509 (0)		
1571 (3)			
1599 (9)	1600 (8) P	1602 (6)	1600 (ms)
2225 (10b)	2226 (15) D	2226 (0)	2238 (s)
2922 (1)	2925 (4b) P		2922 (w)
3050 (3)	3057 (6) D		3040 (w)
3070 (2)	3067 (4) D	3060 (0)	3070 (w)



TABLE II  
Raman and Infrared spectra of para tolunitrile

Raman shifts in $\text{cm}^{-1}$			Infrared bands in $\text{cm}^{-1}$ (Present authors)
Liquid Landolt- Börnstein Table (1951)	Liquid at 30°C Present authors	Solid at -180°C Present authors	
		88 (4)	
161 (7)	160 (6) D	155 (0)	
252 (3)	255 (1) P		
345 (1)			
410 (4)	407 (4) D	407 (0)	
437 (1)			
516 (0)			
549 (3)	556 (1)		
648 (4)	652 (6) D	652 (0b)	
705 (1)	705 (0)		704 (w)
797 (2)			
819 (3)	824 (6) P	824 (6)	818 (vs)
			946 (vw)
1020 (0)			1022 (w)
			1040 (w)
			1100 (vw)
			1120 (w)
1172 (10)	1180 (8) P	1180 (8)	1180 (ms)
1194 (4)	1194 (2) P		1200 (vw)
			1280 (w)
1309 (0)			
1378 (2)	1383 (2) P		1385 (w)
			1412 (w)
1445 (0)	1453 (0)		1450 (ms)
			1508 (ms)
	1517 (0)		
1604 (10)	1609 (10) D	1609 (8)	1610 (s)
2228 (10)	2230 (15) P	2227 (6)	
			2242 (s)
2875 (2)	2880 (1)		2875 (w)
2926 (1)	2929 (2)		2930 (ms)
3048 (4)			3050 (w)
	3063 (2b) D	3063 (0b)	

(a) *Changes in the Raman spectra with solidification of the liquids :*

It can be seen from the Tables I and II that in the solid state at  $-180^{\circ}\text{C}$  the line  $163\text{ cm}^{-1}$  of ortho tolunitrile and  $160\text{ cm}^{-1}$  of para tolunitrile representing probably the out-of-plane bending vibration of C—N bond appear to split up into two component in each case. The line  $163\text{ cm}^{-1}$  splits up into two lines with components at  $155$  and  $80\text{ cm}^{-1}$  and the line  $160\text{ cm}^{-1}$  splits up into two lines  $155$  and  $88\text{ cm}^{-1}$  respectively. The splitting up of the lines  $163$  and  $160\text{ cm}^{-1}$  due respectively to ortho and paratolunitriles is owing to weak molecular association of different strengths in the crystal lattices at low temperatures. The lines  $460$  and  $2226\text{ cm}^{-1}$  due to orthotolunitrile assigned respectively to  $\text{C}\equiv\text{N}$  deformation and  $\text{C}\equiv\text{N}$  stretching oscillation of the molecule become weak with the solidification of the liquid. Similar changes in the intensity of the frequency  $407\text{ cm}^{-1}$  due to  $\text{C}\equiv\text{N}$  deformation oscillation and that of the line  $2230\text{ cm}^{-1}$  due to  $\text{C}\equiv\text{N}$  stretching oscillation were also observed in the case of the para isomer. The change in intensity of the frequencies of  $\text{C}\equiv\text{N}$  bond is more pronounced in the case of ortho isomer than in the case of para isomer. The fact indicates stronger molecular association through  $\text{C}\equiv\text{N}$  group in the case of ortho isomer than in the case of para isomer. Also the line  $1210\text{ cm}^{-1}$  due to ortho tolunitrile representing probably the  $\text{CH}$  bending oscillation in  $\text{CH}_3$  group shifts to  $1219\text{ cm}^{-1}$  under similar condition. In addition to the above changes some other frequencies due to different modes of the two molecules undergo changes at low temperatures which further support the above view.

(b) *Changes in infrared spectra in solutions*

It is observed from the infrared spectra of ortho and para-tolunitriles in the pure state and in their solutions in the solvents (polar and non-polar) that the intensity and position of the  $\text{C}\equiv\text{N}$  band are slightly affected in different polar solvents while in non-polar solvents no such changes are observed. The results fairly agree with those reported earlier in the case of other nitriles (Brown, 1958, Bayliss *et al.* (1959)). However, the shift of the frequency due to  $\text{C}\equiv\text{N}$  vibration is more pronounced in the case of ortho isomer than in the case of para isomer, which may be due to weak perturbation of the local field of the  $\text{C}\equiv\text{N}$  group in the case of ortho isomer in polar solvents.

## ACKNOWLEDGEMENT

The authors express their thanks to Professor G. S. Kastha, D.Sc., for his keen interest in the work.

## REFERENCES

- Bishui, B. M., 1948, *Ind. J. Phys.*, **22**, 167.  
 Brown, T. L., 1958, *J. Am. Chem. Soc.*, **80**, 794.  
 Deb, K. K., 1961, *Ind. J. Phys.*, **35**, 16.  
 Deb, K. K., 1963, Thesis submitted for D.Phil. (C.U.).  
 Deb, K. K. and Mukherjee, D. K., 1963, *Ind. J. Phys.*, **36**, 339.  
 Landolt-Bornstein Table (1951), Zahlenwerte und Funktionen, 1. Band, Atom und Molekulan Physik, 318, 306.  
 Bayliss, N. S., *et al.*, 1959, *Spectrochimica Acta.*, **15**, 12.

# EFFECT OF ELECTRIC FIELD ON THE NATURAL CONVECTIVE HEAT-TRANSFER TO INSULATING LIQUIDS

S. P. BASU AND D. B. SINHA

DEPARTMENT OF APPLIED PHYSICS, CALCUTTA UNIVERSITY

(Received August 29, 1965)

Many investigators (Allen, 1959, Watson, 1961, Caro and Swan, 1963), in recent years have worked on the problem of change in the rate of heat transfer due to the application of electric fields. They investigated the effects of both d.c. and a.c. fields. In almost all cases the max. field applied at the surface of the heater was quite high, of the order of 300 kv/cm. Watson explained the increment in heat transfer observed by him as the result of forced flow from the heater surface down the gradient of permittivity caused by the temp gradient. Ostronmov in 1956, observed motion of insulation liquids under the action of electric fields in a non-convective thermal field. Ostronmov in his experiments applied quite modest fields of the order of 1 kv/cm. In the present investigation, we have studied the effect of electric fields from 0-15 kv/cm. on different liquids, both a.c. and d.c. fields being used.

The apparatus consists of a heater tube surrounded by a sector shaped cylindrical electrode which runs almost over the entire length of the heater. This particular shape of the electrode was adopted so as to allow the convection currents to flow unhindered. The heater tube and also the electrodes were kept horizontal.

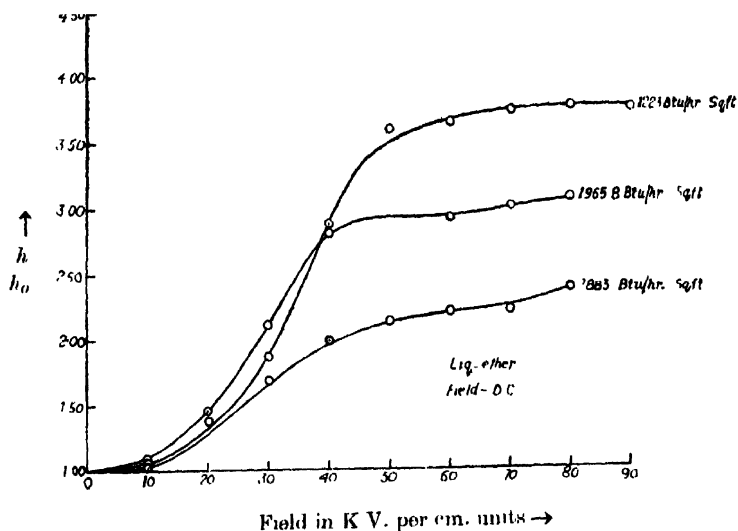


Fig. 1.

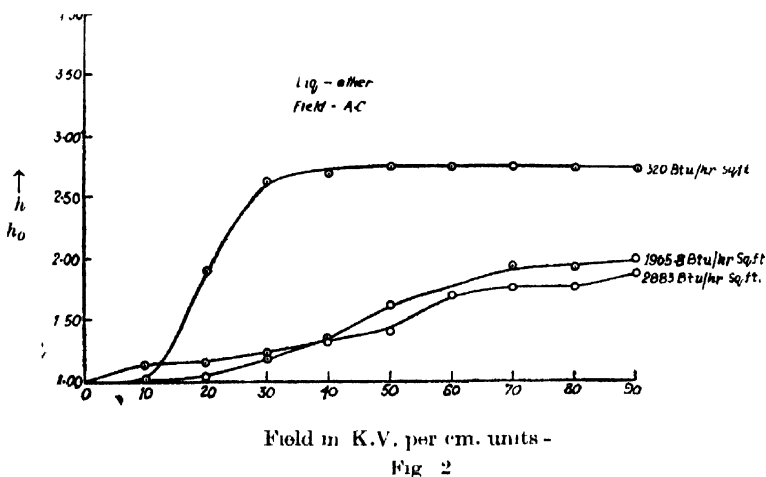


Fig. 2

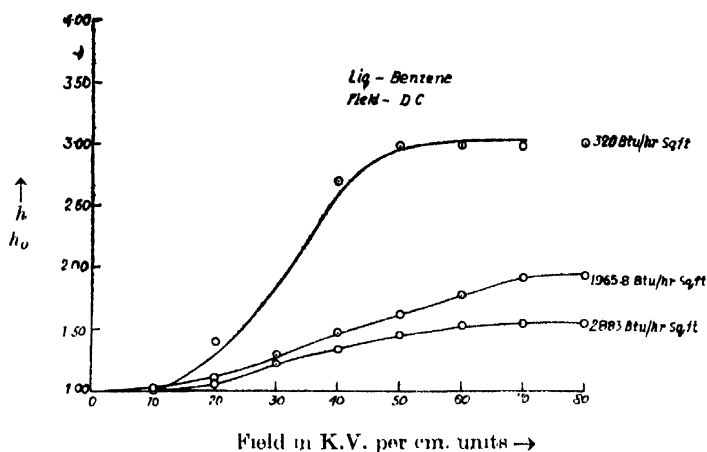


Fig. 3

The heater tube was itself used as a resistance thermometer (Basu 1964) and was maintained at ground potential. The bulk temperature of the liquid was measured by copper-constants thermocouples using a Disselhorst thermo-electric-free potentiometer which was also used to evaluate the surface temperature of the heater tube.

The a.c. voltages (50 c/s) used were obtained from a small transformer. The d.c. voltages were obtained from a rectifier provided with necessary filters. The ripple content was less than 0.3%. The voltages (both d.c. and a.c.) applied could be varied smoothly over the entire range. Fig. 1, 2, 3, 4, depict the results for di-ethyl ether and benzene. The liquids were supplied by Messrs. B.D.H. (Pvt.) Ltd. and were labelled pure. The heater tube was of 0.476 cm. external diameter and the outer electrode of 2 cm internal diameter.

The curves were plotted with  $h/h_0$  as the ordinate (where  $h_0$  stands for heat transfer coefficient without the electric field and  $h$ , the heat transfer coefficient with the field,  $h$  is here expressed in Btu/hr Sq.ft., °F.) and field in kv/cm units as the abscissae. The actual maximum field applied was 15-17 kv/cm.

For diethyl ether [Fig. 1, Fig. 4(a)] the application of d.c. field increases the rate of heat transfer but the effect gradually decreases with increasing values

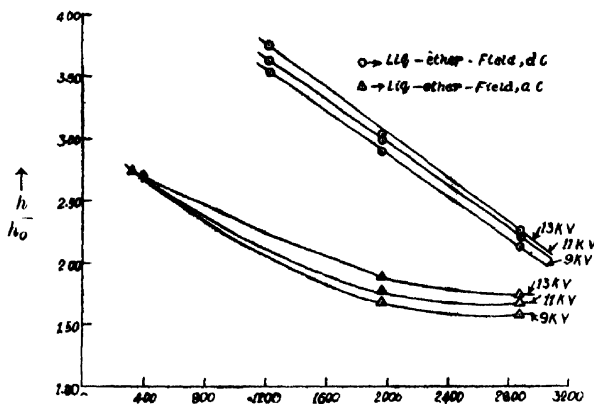


Fig 4(a)  $q \rightarrow$  heat flux ( $q \rightarrow$  Btu/hr sq. ft)

of heat flux. For a.c. fields [Fig. 2, Fig. 4(a)] also the rate of increase of heat transfer gradually decreases with heat flux.

For benzene [Fig. 3 Fig. 4(b)] with d.c. field also a similar pattern as above follow.

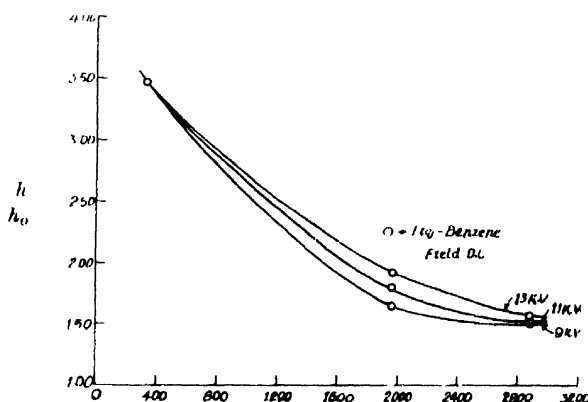


Fig 4(b)  $q \rightarrow$  heat flux, Btu/hr. sq. ft.

From the present set of experiments it is clear that with the increase in the values of the heat flux the rate of heat transfer decreases. This is due to the fact that as the heat flux increases, circulation in the liquid improves and thereby

the permittivity gradient resulting from the diminished temperature gradient also falls. So the heat transfer also should fall. The saturation stage for each curve is reached when the increased heat transfer due to increased circulation is inhibited by the fall of heat transfer resulting from the fall of the permittivity gradient.

## REFERENCES

- Allen, P. H. G., 1959, *Brit. J. of App. Phys.*, **10**, 347.  
Basu, S. P., 1964, *Ind. J. Phys.*, **38**, 87.  
Care, J. M. and Swan, D. W., 1963, *Brit. J. of App. Phys.*, **14**, 263.  
Ostronmov, G. A., 1956, *Soviet Phys., J.E.T.P.*, **3**, No. 2.  
Watson, P. K., 1961, *Nature, Lond.*, **189**, 563.

# COUPLING CONSTANT SUM RULES FOR THE DECAY OF THE $J^P = 2^+$ NONET IN BROKEN SU(3)

V. P. GAUTAM AND P. GHOSE

INDIAN ASSOCIATION FOR THE CULTIVATION OF SCIENCE, JADAVPUR, CALCUTTA-32.

(Received September 15, 1965)

Currently the assignment of the  $J^P = 2^+$  mesons  $K^{**}$  (1430),  $A_2$  (1320),  $f'$  (1500) and  $f$ (1250) to the reducible  $1 \oplus 8$  representation of SU(3) with considerable  $f'-f$  mixing is being discussed by many authors (Hwa *et al.*, Glashow *et al.*, Barnes *et al.*, Chung *et al.*, 1965). Since unitary symmetry is found, in fact, to be broken in nature, it is more realistic to compare observed decay widths with broken SU(3) predictions. We give in this note coupling constant sum rules for the decay of these mesons into (a) a pair of pseudoscalar mesons and (b) a vector and a pseudoscalar meson. The violation of unitary symmetry is assumed to transform like the eighth component of a unitary octet and the mixing angles are kept arbitrary.

In case (a) there are five sum rules for the ten coupling constants

$$\sqrt{\frac{2}{3}} \{G(f, \pi\pi) - 2\sqrt{2}G(f, K\bar{K}) + 3\sqrt{2}G(f, \eta\eta)\} \\ = \{2\sqrt{6}G(A_2, K\bar{K}) - 6G(A_2, \pi\eta)\} \sin \theta \quad (1)$$

$$\sqrt{\frac{2}{3}} \{G(A_2, K\bar{K}) - G(A_2, \pi\eta) - G(K^{**}, K\eta) + \frac{1}{3}G(K^{**}, K\pi)\} \quad (2)$$

$$\sqrt{3}G(f', \eta\eta) - \sqrt{\frac{4}{3}} \{G(f', K\bar{K}) + \frac{1}{3}G(f', \pi\pi)\} \\ = \{2G(A_2, K\bar{K}) - \sqrt{6}G(A_2, \pi\eta)\} \cos \theta \quad (3)$$

$$3G(f, \eta\eta) + \frac{1}{\sqrt{3}} \{G(f, \pi\pi) - 2G(f, K\bar{K})\} \\ = \{3G(f', \eta\eta) - 2G(f', K\bar{K}) + \frac{1}{\sqrt{3}}G(f', \pi\pi)\} \tan \theta \quad (4)$$

$$\sqrt{\frac{1}{2}} \{G(f, K\bar{K}) - \sqrt{\frac{3}{2}} \{G(f, \pi\pi) \left( \frac{2}{3} - \cos^2 \theta \right) - \sqrt{\frac{3}{2}} \sin \theta \cos \theta G(f', \pi\pi)\} \\ = \sqrt{\frac{1}{2}} G(A_2, K\bar{K}) \left( x \frac{\cos \theta}{4} - \sqrt{\frac{10}{3}} - \frac{\sin \theta}{\sqrt{3}} \right) \\ - \sqrt{\frac{1}{2}} G(K^{**}, K\pi) \left( \frac{4\sqrt{2}}{3} \sin \theta + \frac{\sqrt{5}}{3} x \cos \theta \right) \quad (5)$$

In case (b) also there are five sum rules for the nine coupling constants :

$$G(K^{**}, K^*\pi) = G(K^{**}, \rho K) \quad \dots \quad (6)$$

$$G(K^{**}, \phi K) = G(K^{**}, K^*\eta) \cos \varphi \quad \dots \quad (7)$$

$$G(K^{**}, \omega K) = G(K^{**}, K^*\eta) \sin \varphi \quad \dots \quad (8)$$

$$\frac{5}{3\sqrt{2}} [G(K^{**}, K^*\pi) + G(f', K^*\bar{K}) \cos \theta + G(f, K^*K) \sin \theta] \\ - \frac{1}{\sqrt{2} \sin \varphi} [G(K^{**}, \omega K) + \frac{1}{2\sqrt{3}} G(A_2, \rho \pi)] \quad (9)$$

$$G(f', K^*K) \cos \theta + G(f, K^*K) \sin \theta$$

$$\frac{1}{\sqrt{3}} [G(A_2, K^*K) + \frac{1}{\sqrt{3}} G(A_2, \rho \pi) - \frac{4\sqrt{2}}{3} G(K^{**}, K^*\pi)] \quad (10)$$

$\theta \simeq 20^\circ - 30^\circ$  (Glashow *et al.*, Barnes *et al.*) and  $\varphi \simeq 40^\circ$  (Sakurai 1962) are the  $f' - f$  and  $\omega - \phi$  mixing angles respectively.  $x$  is related to the parameters  $F$  and

$$G$$
 of Glashow and Socolow by  $x = \sqrt{\frac{2}{5}} \cdot \frac{G}{F} = \frac{4}{\sqrt{5}}$ .

The sum rules listed above can be properly tested only when more extensive and accurate experimental data become available. Detailed considerations will be published elsewhere.

We are grateful to Prof. S. N. Bose and Prof. D. Basu for their encouragement and kind interest in this work. We wish to thank Dr. B. Dutta Roy for helpful discussions and Mr. K. R. Chatterjee for checking the results.

#### REFERENCES

- Barnes, V. E. *et al.*, 1965, *Phys. Rev. Letters*, **15**, 322.  
 Chung, S. U., *et al.*, 1965, *Phys. Rev. Letters*, **15**, 325. The references to other experimental data are given here.  
 Glashow, S. L. and Socolow, R. H., 1965, *Phys. Rev. Letters*, **15**, 329. The references to other theoretical works regarding this Nonet are given here.  
 Hwa, R. C. and Patil, S. H., 1965, *Phys. Rev.*, **139**, B969.  
 Sakurai, J. J., 1962, *Phys. Rev. Letters*, **9**, 472.



# CHANGE IN THE SHAPE OF THE $\text{NO}_3$ ION DURING THE FORMATION OF A HYDRATE IN AQUEOUS SOLUTIONS

N. RAJESWARA RAO, K. V. RAMANIAH AND S. MOHANA RAO.

PHYSICS DEPARTMENT, OSMANIA UNIVERSITY, HYDERABAD

(Received August 3, 1965)

It was reported by Rajeswara Rao and Ramaniah (1964) that in a solution of sodium nitrate, the nitrate ion becomes pyramidal in shape at about  $16^\circ\text{C}$  and on heating to about  $90^\circ\text{C}$  it becomes planar. This conclusion was drawn to explain (1) a slight increase in the frequency of the total symmetric line  $\nu = 1050\text{ cm}^{-1}$  at lower temperature where the ions can be expected to be hydrated better than at higher temperature and (2) appearance of a faint line at  $\nu = 594\text{ cm}^{-1}$  which disappears at higher temperatures. The formation of the hydrogen bonding is evidenced by the low intensity of this line ( $\nu = 1050\text{ cm}^{-1}$ ) at lower temperature.

During the formation of hydrogen bond, one normally expects the bond strength of NO to decrease. Increased frequency of the total symmetric line, however, throws doubt on this point. A normal coordinate treatment of pyramidal  $\text{NO}_3$  ion is made and the force constants determined to settle this point.

The F and G matrices of pyramidal molecules are given by Venkateswarlu (1956). The bond length  $d$  of NO is taken to be 1.299 A.U. (Venkateswarlu) and the bond angle  $\alpha$  between the NO bonds is  $111^\circ 32'$  and the frequencies are taken to be 594, 720, 1050 and  $1420\text{ cm}^{-1}$ . This data are taken from a paper by some of the present authors referred to earlier. If one neglects  $f_{da}$  (calculation justifies such an assumption), the secular equation reduces to two quadratic equations that can be readily solved. The force constants thus obtained are  $f_d = 7.127$ ,  $f_{dd} = 0.230$ ,  $d^2f_\alpha = 1.818$ ,  $d^2f_{\alpha\alpha} = 0.233$  in units of  $10^5$  dynes/cm. Comparing with  $f_d = 7.848$ ,  $f_{dd} = 1.281$  and  $d^2(f_\alpha - f_{\alpha\alpha}) = 0.2335$ , reported by Venkateswarlu for planar  $\text{NO}_3$  ion,  $f_d$  is found to be smaller as one expects during the formation of hydrogen bond. Therefore, though the total symmetric stretch line slightly shifts to higher frequency, on hydration, the bond strength really decreases.

## REFERENCES

- Rajeswara Rao, N. and Ramaniah, K. V., 1964, *Ind. J. Phys.*, **38**, 144.  
Venkateswarlu, K., 1956, *Proc. Phys. Soc. Lond.* **69**, 180

## BOOK REVIEW

ONE TWO THREE...INFINITY—by G. Gamow; MacMillan and Co. Ltd., London 1962. Price 16s. net.

Going for the second time through this excellent book in its revised form I found my interest in it not a bit flagged from the pitch to which it was raised (when I first came across it). Though in this edition no considerable fresh material has been added, I enjoyed each wit and humour with the same zest as in 1949. In those early days I had succumbed to my the bad habit of skipping over the tougher portions and enjoying the story of this popular science exposition. But in this second reading I faced bravely and scrupulously each bit of logic, till I reached the last page all out of breath. No, not because of the exertion; Gamow really takes one breath away by the amazingly clear and pointed summary of all the important outstanding problems of modern science, vividly picturized by apt analogies creating the proper perspective for the understanding through the witty comments

By the time I finished, I also had agreed with Gamow that the book did not have too serious difficulties for the layman but it was surely not for children. What was my surprise when I found that the children of the present generation are so well up in the known facts of science, that they are able not only to follow but enjoy with gusto not less than 80% of the book. This refers to a boy of 14 reading in class X of a local good standard English medium school. The 10% he did not follow consisted mainly of the section on "Riddle of Life" to which he is totally apathetic, being keen to become an inorganic chemist. Another girl a little older and interested mostly in Biology and Chemistry enjoyed the book thoroughly fortifying herself with a small lecture from me on qualitative relativity and quantum mechanics. About the section on theory of numbers and topology both of them were sufficiently imaginative to enjoy the expositions

So the book is becoming more and more a success belying the misgivings of the author that it is not suitable for children and we congratulate him and thank his publishers for bringing out this paperback edition to make it available to a large section of scientifically inclined layman and children of the modern age.

A. Bose

# VARIATIONAL METHOD AND THE ELASTIC SCATTERING OF SLOW ELECTRONS BY HYDROGEN ATOM

SATYANARAYAN BANERJEE, RAMESHWAR JHA AND N. C. SIL

DEPARTMENT OF THEORETICAL PHYSICS, INDIAN ASSOCIATION FOR THE CULTIVATION OF SCIENCE, JADAVPUR, CALCUTTA-32.

(Received September 25, 1965)

**ABSTRACT.** The collision of electron and hydrogen atom has been investigated by the variational method of Hulten in the energy range below the threshold for the excitation of second quantum level (10.2 eV) of atomic hydrogen. The influence of the polarisation has been taken in the wave function which includes a term indicating virtual excitation to  $2s$  and  $2p_0$  levels, here this choice leads to the occurrence of pronounced resonance at 9.74 eV energy which agrees with the theoretical results of Burke and Schey (1962) in their  $1s$ - $2s$ - $2p$  close coupling approximation. Recently Schulz (1964) has experimentally found a resonance peak at 9.7 eV energy.

## INTRODUCTION

The scattering of electrons by hydrogen atom is theoretically the simplest of all electron-atom collision problems, hence it has been the subject of detailed theoretical investigation. This has many important applications in astrophysics, controlled thermonuclear devices and other processes.

A number of experiments have been carried out on slow electron scattering by atomic hydrogen by Neynaber (1961), Brackmann, Fite *et al.*, (1958). Recently Schulz (1964) has reported an experimental evidence for a resonance in the elastic scattering of electrons by atomic hydrogen, below the onset of excitation of the electronic states of hydrogen atom.

The scattering at low energy involves the effect of exchange because of the indistinguishability of the incident electron from atomic electron. There is a great probability of the incident electron being captured and the atomic electron being ejected in the process of slow collision. Moreover, due to the influence of the incoming electron, there is a polarisation effect arising out of the distortion of the spherically symmetrical charge distribution of  $1s$ -electron cloud in the neutral atomic hydrogen.

Massey and Moiseiwitsch (1951) have used variational method to calculate the  $S$ -wave phase shift due to scattering of electrons by atomic hydrogen, taking the exchange effect and the partial distortion of the atomic cloud. They have treated this distortion by introducing explicitly in the trial wave function a term which depends on the electron-electron correlation distance  $r_{12}$ . In some of the

more recent works (cf. Burke and Schey (1962) with the use of modern computing machines, sets of coupled equations resulting from the retention of only a few selected excited states of the hydrogen atom in the wave function, have been solved numerically. Burke and Schey (1962) have utilised a close-coupling approximation in which the total wave-function has been expanded in hydrogen eigen states and only terms corresponding to the 1s, 2s and 2p states are retained. In their investigations, they have found that except for the very low energy region below .68 ev the short-range distortion effect dominates over the long-range one and the 2s-state gives a larger contribution to the phase-shift than 2p state. Moreover, once all states corresponding to second quantum level have been incorporated in the formulation of the problem, all other remaining states have negligible effects. Recently, Temkin and Pohle (1963) have calculated the singlet S-wave phase shift in electron hydrogen atom collisions below the inelastic threshold, they have obtained two resonances, the first one centred at 9.4 ev is broader than the second one occurring at 10.1 ev.

In the present paper, we have investigated the the S-wave phase-shift values in electron-hydrogen atom collisions. Since the proton is very massive compared to the electron the wavefunction for the electron-hydrogen system will depend only upon the coordinates of the bound and free electrons. Here we assume that the distortion of the initial 1s-state is in the form of a superposition of higher excited states induced temporarily when the incident electron is close to the target; but when the colliding electron is far away, the original 1s-state of the bound electron is restored. Our formulation is in conformity with the remark of Burke and Schey (1962). For simplicity of calculations, we have considered the virtual excitation to 2s and  $2p_0$  states only, the polar axis being taken along the target nucleus. We have used Hulthén's variational method to calculate the S-wave phase-shift as a function of energy and we have neglected the effect of exchange. By making use of Breit-Wigner formula we obtain a resonance at an energy 9.74 ev which agrees favourably with the most recent experimental findings by Schulz (1964).

It is worth mentioning that previous calculations with the variational method by Massey and Moiseiwitsch (1951) and Geltman (1960) have failed to show the occurrence of resonance, whereas our suitable choice of the wavefunction brings out the resonance with the same variational method.

## THEORY

The wave function  $\psi(\mathbf{r}_1, \mathbf{r}_2)$  of the system of two electrons moving in the field of a proton satisfies the wave equation

$$(H-E)\psi(\mathbf{r}_1, \mathbf{r}_2) = 0 \quad \dots (1)$$

with 
$$H = \left[ -\frac{\nabla_1^2}{2} - \frac{\nabla_2^2}{2} - \frac{1}{r_1} - \frac{1}{r_2} + \frac{1}{r_{12}} \right]$$

in atomic units (i.e.  $e = m = \hbar = 1 = a_0$ ); here  $\mathbf{r}_1$  and  $\mathbf{r}_2$  are the co-ordinate of the atomic electron and impinging electron, respectively, relative to the proton and  $r_{12}$  is the distance between the electrons.

Expanding the total wave function  $\psi$  in terms of the eigen states of the target Hamiltonian, we have

$$\psi(\mathbf{r}_1, \mathbf{r}_2) = (\sum_n + \int) \psi_n(\mathbf{r}_1) F_n(\mathbf{r}_2) \quad \dots (2)$$

where the summation and integration signs have their usual meanings. Here  $\psi_n(\mathbf{r}_1)$  represents the wave function for the  $n$ -th state of the hydrogen atom and satisfies the eigen-value equation  $\left( \nabla_1^2 - \frac{2}{r_1} - 2E_n \right) \psi_n(\mathbf{r}_1) = 0$  where  $E_n$  represents the eigen-energy of the  $n$ -th state of the atom. If the kinetic energy of the incident electron is  $\frac{K_0^2}{2}$ , the functions  $F_n$  must have the asymptotic forms

$$F_0 \sim e^{i\mathbf{K}_0 \cdot \mathbf{r}_2} + \frac{e^{iK_0 r_2}}{r_2} f(\theta_2, \phi_2)$$

and

$$F_n \sim \frac{e^{iK_n r_2}}{r_2} f_n(\theta_2, \phi_2) \quad \dots (3)$$

where

$$E = \frac{K_0^2}{2} + E_0 = \frac{K_n^2}{2} + E_n$$

Here  $E_0$  and  $E_n$  represent the energies of the ground state and the  $n$ -th state of the atom respectively and  $\mathbf{K}_0$  and  $\mathbf{K}_n$  represent respectively the momenta of the incident electron and scattered electron after excitation of the  $n$ -th state of the atom.

To solve equation (1) under the prescribed boundary conditions in (2), we shall apply the variational method of Hulthén (1944). We make a choice of the following trial wave function

$$\psi(\mathbf{r}_1, \mathbf{r}_2) = \chi(\mathbf{r}_1, \mathbf{r}_2) F(\mathbf{r}_2)$$

$$\text{where } \chi(\mathbf{r}_1, \mathbf{r}_2) = \psi_{1s}(r_1) \left( 1 - \frac{\alpha^2 + \beta^2}{2} e^{-2r_2} \right) + \alpha \psi_{2s}(r_1) e^{-r_2} + \beta \psi_{2p_0}(r_1, r_2) e^{-r_2}$$

$$F(\mathbf{r}_2) = \left\{ e^{i\mathbf{K}_0 \cdot \mathbf{r}_2} + (a + b e^{-r_2})(1 - e^{-r_2}) \frac{\cos K_0 r_2}{K_0 r_2} \right\},$$

here we have taken only the S-wave part of the scattered wave and  $\chi(\mathbf{r}_1, \mathbf{r}_2)$  satisfies the normalisation condition  $\int \chi^* \chi d\mathbf{r}_1 = 1$ , correct to terms of the order of  $\alpha^2$  and  $\beta^2$ . The wave function  $F(\mathbf{r}_2)$  having adjustable parameters  $a$  and  $b$  has the asymptotic form  $\{e^{i\mathbf{K}_0 \cdot \mathbf{r}_2} + a \cos K_0 r_2 / K_0 r_2\}$  and is finite at the origin. The S-wave phase-shift  $\eta_0$  is given by  $\eta_0 = \tan^{-1} a$ .

We substitute the trial wave function  $\psi(\mathbf{r}_1, \mathbf{r}_2)$  in the variational integral

$$L = \int \psi^* (H - E) \psi d\mathbf{r}_1 d\mathbf{r}_2 \quad \dots (4)$$

and evaluate it. The value of the phase-parameter ' $\alpha$ ' is obtained from the following set of simultaneous equations

$$L(\alpha, \beta, b; a) = 0$$

$$\frac{\partial L}{\partial \alpha} = 0$$

$$\frac{\partial L}{\partial \beta} = 0$$

$$\frac{\partial L}{\partial b} = 0$$

It is to be noted that cubes and higher powers of  $\alpha$  and  $\beta$  in  $L$  have been neglected.

The elastic S-wave cross-section  $Q_0$  is  $\frac{4\pi}{K_0^2} \sin^2 \eta_0$

In discussing the resonance effect, we decompose the total phase shift into two parts as  $\eta_{total} = \eta_{potential} + \eta_{resonance}$  where  $\eta_{potential}$  is the slowly varying potential part of the phase-shift and  $\eta_{resonance}$  is the phase shift due to the resonance effect. Following Burke and Schey, we write

$$Q_{total} = \frac{\pi}{K_0^2} |A_{res} + A_{pot}|^2$$

where

$$A_{res} = e^{2i\eta_{pot}} [e^{2i\eta_{res}} - 1]$$

and

$$A_{pot} = [e^{2i\eta_{pot}} - 1]$$

The S-wave resonant part of the cross section is written as

$$Q_{res} = \frac{\pi}{K_0^2} |A_{res}|^2 = \frac{4\pi}{K_0^2} \sin^2 \eta_{res}$$

Hence we get  $Q_{res}$  as a function of  $K_0^2$ .

### Calculation of $L$

The variation integral  $L$  in (4) can be written in the form :

$$L = L_1 + L_2$$

where

$$L_1 = \int A^* P d\mathbf{r}_2 + \int B^* Q d\mathbf{r}_2 + \iint C^* R \psi_{2p_0}^*(\mathbf{r}_1, \mathbf{r}_2) \psi_{2p_0}(\mathbf{r}_1, \mathbf{r}_2) d\mathbf{r}_1 d\mathbf{r}_2$$

$$\text{and} \quad L_2 = \int \int \left( \frac{2}{r_2} - \frac{2}{r_{12}} \right) [A^* \psi_{1s}^*(r_1) + B^* \psi_{2s}^*(r_1) + C^* \psi_{2p_0}^*(\mathbf{r}_1, \mathbf{r}_2)]$$

$$\times [A \psi_{1s}(r_1) + B \psi_{2s}(r_1) + C \psi_{2p_0}(\mathbf{r}_1, \mathbf{r}_2)] d\mathbf{r}_1 d\mathbf{r}_2$$

in which

$$A = \left( 1 - \frac{\alpha^2 + \beta^2}{2} e^{-2r_2} \right) F(\mathbf{r}_2)$$

$$B = \alpha e^{-r_2} F(\mathbf{r}_2)$$

$$C = \beta e^{-r_2} F(\mathbf{r}_2)$$

$$P = \nabla_2^2 \{ F(\mathbf{r}_2) \left[ - \left( \frac{\alpha^2 + \beta^2}{2} \right) \nabla_2^2 \{ e^{-2r_2} F(\mathbf{r}_2) \} + K_0^2 F(\mathbf{r}_2) - K_0^2 \left( \frac{\alpha^2 + \beta^2}{2} \right) e^{-2r_2} F(\mathbf{r}_2) \right]$$

$$Q = \nabla_2^2 \{ e^{-r_2} F(\mathbf{r}_2) \} + K_0^2 e^{-r_2} F(\mathbf{r}_2) + 2(\epsilon_1 - \epsilon_2) e^{-r_2} F(\mathbf{r}_2)$$

$$R = \frac{1}{\cos \theta_{12}} \nabla_2^2 \{ e^{-r_2} F(\mathbf{r}_2) \cos \theta_{12} \} + K_0^2 e^{-r_2} F(\mathbf{r}_2) + 2(\epsilon_1 - \epsilon_2) e^{-r_2} F(\mathbf{r}_2)$$

$A^*$ ,  $B^*$  and  $C^*$  are the complex conjugates of  $A$ ,  $B$  and  $C$  respectively, and  $\epsilon_1$  and  $\epsilon_2$  are the binding energies of the ground state (1s) and 2s (also 2p) states of the atom respectively.

On carrying out the integrations over  $d\mathbf{r}_1$  and over the angular co-ordinates  $\theta_2$ ,  $\phi_2$  of  $d\mathbf{r}_2$ -space, we get

$$\begin{aligned} L_1 &= \frac{2\pi}{K_0^2} \int_0^\infty [ps(1 + \cos 2K_0 r_2) + s \sin 2K_0 r_2] dr_2 \\ &- \frac{4\pi}{K_0^2} \int_0^\infty [q(1 - \cos 2K_0 r_2) + pq \sin 2K_0 r_2] dr_2 \\ &- \frac{\pi\alpha^2}{2K_0^2} \int_0^\infty [7p^2(1 + \cos 2K_0 r_2) + 14p \sin 2K_0 r_2] e^{-2r_2} dr_2 \\ &- \pi\alpha^2 \int_0^\infty [7r_2^2] e^{-2r_2} dr_2 \\ &- \frac{\pi\beta^2}{2K_0^2} \int_0^\infty [7p^2(1 + \cos 2K_0 r_2) + 14p \sin 2K_0 r_2] e^{-2r_2} dr_2 \\ &- \frac{\pi\beta^2}{K_0^2} \int_0^\infty [4p^2(1 + \cos 2K_0 r_2) + 8p \sin 2K_0 r_2] \frac{e^{-2r_2}}{r_2^2} dr_2 \\ &- \pi\beta^2 \int_0^\infty [7r_2^2 + 8] e^{-2r_2} dr_2 \end{aligned}$$

where

$$p = (a + be - r_2)(1 - e - r_2)$$

$$q = ae - r_2 + b(2e - 2r_2 - e - r_2)$$

$$s = -ae - r_2 + b(e - r_2 - 4e - 2r_2)$$

Similarly, we get

$$\begin{aligned} L_2 = & \frac{4\pi}{K_0^2} \int_0^\infty \left[ \left( 1 + \frac{1}{r_2} \right) e^{-2r_2} \right] t \, dr_2 \\ & + 8\pi \int_0^\infty [(r_2^2 + r_2)e^{-2r_2}] dr_2 \\ & + \frac{\pi\alpha^2}{2K_0^2} \int_0^\infty \left[ \left( r_2^2 + 2r_2 + 6 + \frac{8}{r_2} \right) e^{-3r_2} - 8 \left( 1 + \frac{1}{r_2} \right) e^{-4r_2} \right] t \, dr_2 \\ & + \pi\alpha^2 \int_0^\infty [(r_2^4 + 2r_2^3 + 6r_2^2 + 8r_2)e^{-3r_2} - 8(r_2^2 + r_2)e^{-4r_2}] dr_2 \\ & + \frac{\pi\beta^2}{2K_0^2} \int_0^\infty \left[ \left( -\frac{96}{r_2^3} \right) e^{-2r_2} + \left( r_2^2 + 6r_2 + 22 + \frac{56}{r_2} + \frac{96}{r_2^3} + \frac{96}{r_2^2} \right) e^{-3r_2} \right. \\ & \quad \left. - 8 \left( 1 + \frac{1}{r_2} \right) e^{-4r_2} \right] t \, dr_2 \\ & + \pi\beta^2 \int_0^\infty \left[ \left( -\frac{96}{r_2} \right) e^{-2r_2} + (r_2^4 + 6r_2^3 + 22r_2^2 + 56r_2 + 96 + \frac{96}{r_2}) e^{-3r_2} \right. \\ & \quad \left. - 8(r_2^2 + r_2) e^{-4r_2} \right] dr_2 \\ & + \frac{\pi\alpha\beta}{2K_0^2} \int_0^\infty \left[ \left( \frac{48}{r_2^3} \right) e^{-2r_2} - \left( 2r_2^2 + 8r_2 + 24 + \frac{48}{r_2} + \frac{48}{r_2^2} \right) e^{-3r_2} \right] t \, dr_2 \\ & + \pi\alpha\beta \int_0^\infty [(48)e^{-2r_2} - (2r_2^4 + 8r_2^3 + 24r_2^2 + 48r_2 + 48)e^{-3r_2}] dr_2 \end{aligned}$$



$$\begin{aligned}
 & -\frac{32 \times 2^{\frac{1}{2}}}{27} \times \frac{\pi \alpha}{2K_0^2} \int_0^{\infty} \left[ (3r_2 + 2) e^{-5/2r_2} \right] t dr_2 \\
 & -\frac{32 \times 2^{\frac{1}{2}}}{27} \times \pi \alpha \int_0^{\infty} \left[ (3r_2^3 + 2r_2^2) e^{-5/2r_2} \right] dr_2 \\
 & + \frac{32 \times 2^{\frac{1}{2}}}{243} \cdot \frac{\pi \beta}{2K_0^2} \int_0^{\infty} \left[ \left( 27r_2 + 72 + \frac{96}{r_2} + \frac{64}{r_2^2} \right) e^{-5/2r_2} - \frac{64}{r_2^2} e^{-r_2} \right] t dr_2 \\
 & + \frac{32 \times 2^{\frac{1}{2}}}{243} \times \pi \beta \int_0^{\infty} \left[ (27r_2^3 + 72r_2^2 + 96r_2 + 64) e^{-5/2r_2} - 64e^{-r_2} \right] dr_2
 \end{aligned}$$

where  $t = p^2(1 + \cos 2K_0 r_2) + 2p \sin 2K_0 r_2$

There is no further difficulty in carrying out the integrations appearing in  $L_1$  and  $L_2$ , although the calculations become very tedious due to the occurrence of a large number of terms. For simplicity in calculations, we have taken  $b = 0$ .

In the low energy region we first find the solutions of the quadratic equation  $L = 0$  obtained by putting  $\alpha = \beta = 0$ . One of the solutions agrees with the results of Massey and Moiseiwitsch (1951). Now to find the required solution of the sixth degree equation at low energy we search the root in the neighbourhood of the particular solution mentioned above; a root is obtained differing only slightly

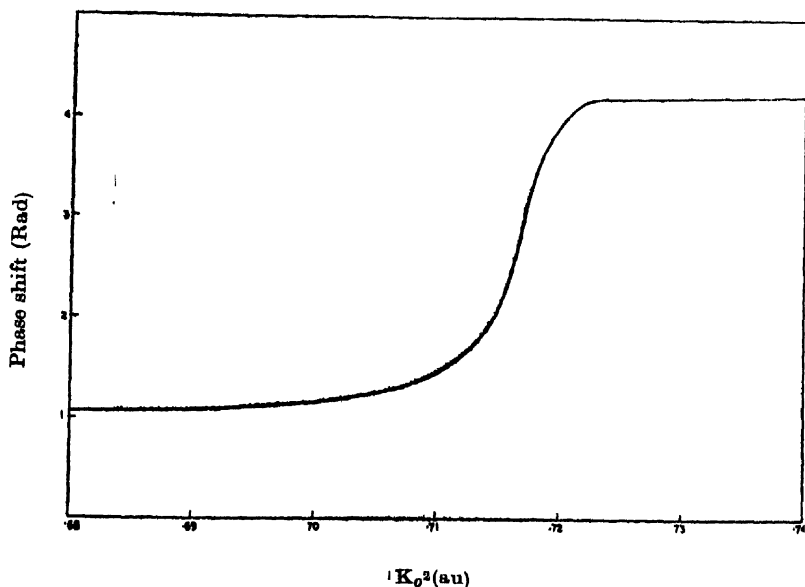


Fig. 1. The S-wave phase shift is plotted as a function of  $K_0^2$  in the neighbourhood of resonance.

from the particular solution chosen of the quadratic equation. Once the root has been fixed for a particular low energy, the phase-shifts for higher energies have been obtained by solving the sixth degree equation and using the continuity property of the phase-shift.

### RESULTS AND DISCUSSIONS

We have evaluated the S-wave phase-shift values for the case  $b = 0$  in the trial function  $F(\mathbf{r}_2)$ , for energies ranging from 3.4 ev to 9.85 ev by using only the coupling of 1s, and the virtually excited 2s and 2p<sub>0</sub> states.

We give a plot of S-wave phase shift values  $\eta_0$  versus  $K_0^2$  in Fig. 1. In the present calculation the 2s state gives a large correction to the S-wave phase shift than the 2p<sub>0</sub> state at the energy range under consideration. This fact has been corroborated by the results obtained by Bruke and Schey (1962).

The most notable characteristic part of our result is the sharp increase in phase shift values above  $K_0^2 = .70$ . The curve has a pronounced resonating behaviour, with a definite flattening out before the threshold is reached.

In the Fig. (2), we have plotted  $Q_{res}$  as a function of  $K_0^2$  Using Breit-Wigner cross section formula

$$Q_{res} = \frac{4\pi}{K_0^2} \frac{\Gamma^2/4}{(E - E_{res})^2 + \frac{\Gamma^2}{4}}$$

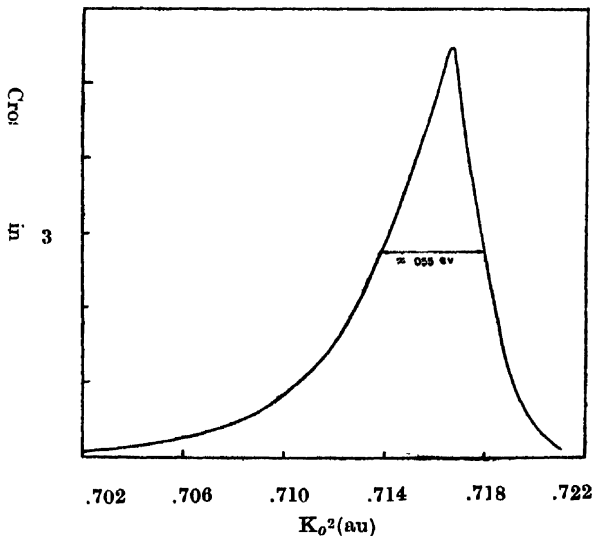


Fig. 2. The resonant part of S-wave cross-section is plotted as a function of  $K_0^2$ .

we obtain  $E_{res} = (.7158 \text{ a.u.}) 9.735 \text{ ev}$ , which agrees very favourably with experimental findings by Schulz (1964). The value of our resonance cross section comes out to be  $5.203\pi a_0^2$  and the calculated value of the width  $\Gamma$  of the resonance state is found to be about .055 ev.

In experiments by Schulz (1964) it has been observed that the width of resonance in atomic hydrogen is approximately double that of helium, which could not be resolved due to limited energy resolution ( $\sim .3$  ev) and the drop in the elastic scattering cross-section, indicative of resonance is centred in the vicinity of  $9.7 \pm .15$  ev. Hence the position of hydrogen resonance in our case is in very good agreement with the experimental findings by Schulz (1964). Also our total S-wave cross section  $Q_0$ , for the energy 3.4 ev comes out to be equal to 12.32 in units of  $\pi a_0^2$  whereas the experimental value of the total cross section from the curve of Neynaber (1961) is about  $11.18 \pi a_0^2$ . Hence our result for total S-wave cross section without exchange in the low energy region agrees reasonable well with experiment.

Recently, several theoretical papers have appeared showing the existence of off resonance level below the threshold for excitation of the second quantum level. Thus, Burke and Schey (1962) have obtained a resonance at 9.61 ev, with a width of .109 ev in  $1S$  state and the corresponding resonance cross section being  $5.66 \pi a_0^2$ . Numerical calculations taking the effect of exchange into account are in progress and will be published soon.

#### ACKNOWLEDGEMENT

The authors are thankful to Prof. D. Basu for his kind interest and valuable discussions throughout the progress of the work.

#### REFERENCES

- Brackmann, R. T., Fite, W. L. and Neynaber, R. H., 1958, *Phys. Rev.*, **112**, 1157.  
 Burke, P. G. and Schey, H. M., 1962, *Phys. Rev.*, **126**, 147.  
 Geltman, S., 1960, *Phys. Rev.*, **119**, 1283.  
 Hulthen, L., 1944, *K. fysogr. Sallsk. Lund. Forh.*, **14**, No. 21.  
 Massey, H. S. W. and Mosierwitsch, B. L., 1951, *Proc. Roy. Soc.*, **205**, 483.  
 Neynaber, R. H., Marmo, L. L., Rothe, E. W. and Trujillo, S. M., 1961, *Phys. Rev.*, **124**, 135.  
 Schulz, G. J., 1964, *Phys. Rev., Letters*, **13**, No. 20.  
 Temkin, A. and Pohl, R., 1963, *Phys. Rev. Lett.* **10**, 22, **10**, 268 (E).

# $\pi^* \leftarrow \pi$ SYSTEM IN THE ELECTRONIC SPECTRA OF PARA-BROMOPHENOL

KAILASH CHANDRA

DEPARTMENT OF PHYSICS, UNIVERSITY OF GORAKHPUR, GORAKHPUR

(Received June 9, 1964)

## Plate IV

**ABSTRACT.** The near ultraviolet absorption spectrum of *p*-bromophenol vapour in the region 3003-2630 Å has been recorded for the first time and vibrational assignments have been proposed. The intense band at 2872.8 Å (34799  $\text{cm}^{-1}$ ) has been identified as the 0,0 band while other bands have been explained in terms of thirteen ground state (195, 251, 293, 323, 490, 574, 636, 825, 858, 1022, 1068, 1189 and 1256  $\text{cm}^{-1}$ ) and thirteen excited state (188, 249, 277, 472, 581, 768, 795, 923, 1016, 1057, 1180, 1272 and 1554  $\text{cm}^{-1}$ ) fundamental vibrations. The band system has been attributed to the  $\pi^* \leftarrow \pi$  transition of the phenyl group.

## INTRODUCTION

It is known that the electronic transition which occurs in benzene in the region 2700-2200 Å appears at longer wavelengths upon substitution. It was pointed out by the author on theoretical grounds (Chandra and Tripathi 1963) that, for weak interacting groups, if both substituents of a di-derivative of benzene are either ortho-para directing or meta directing groups, the order of red shift of 0, 0 band of ortho, meta and para compounds is  $o < m < p$ . It is in harmony with the observed red shifts of 0, 0 bands of halogenated di-derivatives of benzene, fluoro toluenes and bromotoluenes. Since -OH is a para directing strong interacting group, it was worthwhile to study the effect of substitution of halogens upon the longest wavelength  $\pi^* \leftarrow \pi$  system in the electronic spectrum of phenol. Fluoro phenols (Tewari, 1949-63; Sharma and Tripathi, 1963), chlorophenols (Ramasastry, 1951; Misra and Banerjee, 1961; Joshi, 1949-63; and Upadhyaya, 1949-63) and ortho-bromophenol (Banerjee, 1956) have drawn the attention of several workers. It was, therefore, considered useful to study the absorption spectra of brominated phenol vapours in the region 2600 Å, as they have not been studied before in this part of the spectrum. This paper deals with the results on the *p*-brom. phenol. Some ground state frequencies of this isomer are known since Raman (Kohlrausch and Ypsilanti, 1935; Landolt-Bornstein Tables, 1951) and infra-red (Parodi and Cotton, 1941; Lecomte, 1938) spectra of it have been taken in the liquid state. No polarization data are however, given.

## EXPERIMENTAL

The procedure followed in obtaining the present spectrum is the same as in the previous similar studies from this laboratory (Chandra and Sharma, 1963). Spectrogram was photographed on Hilger medium and large quartz spectrographs, using path lengths of the absorption cells varying from 25 to 100 cm., and temperatures ranging between 30°C and 150°C at reduced as well as atmospheric pressure. The spectrum was recorded on Ilford N-30 and N-40 plates. Slit widths of about 20 microns were used. A hydrogen arc lamp served as the source of continuous radiation. The exposure of 10 minutes to 3 hours were required to record the spectra in the vapour phase. Iron arc was photographed on each spectrogram as comparison. Measurements were made on three different plates, four times on each, with the help of Hilger comparator having a least count of 0.0001 cm. Calculations were made with Hartmann dispersion formula and weighted mean values of wavelengths were taken. It is believed that the positions of sharp bands were obtained with an accuracy of about  $\pm 3 \text{ cm}^{-1}$ . The chemical was B.D.H.'s highest grade. The bands were carefully checked for the presence of the bands of phenol and the other derivatives of benzene and none were detected.

## RESULTS

Fig. 1 shows the enlarged reproduction of the near ultraviolet absorption spectrum of *p*-bromophenol using a pathlength of 75 cm at atmospheric pressure and different temperatures. The lower and upper strips are at  $\sim 70^\circ \text{C}$  with exposure times of one hour and half hour respectively, while the central strip was photographed at  $\sim 110^\circ \text{C}$  with exposure time of one and a half hour. The values of wave-numbers together with visually estimated intensities, separations from 0, 0 band and the proposed assignments are given in Table I.

The bands lying in the region 3003-2630 Å represent the longest wavelength  $\pi^* \leftarrow \pi$  system of this isomer (Chandra, 1964). As can be seen from the reproductions, the bands are degraded to the red. Most of the bands show fairly sharp edges towards the violet, and fall into several groups. The groups become gradually less pronounced towards the shorter wavelength side of the spectrum.

## ANALYSIS AND DISCUSSIONS

By replacing the two parahydrogen atoms of benzene by  $-\text{Br}$  and  $-\text{OH}$  group *p*-bromophenol  $\text{C}_6\text{H}_4(\text{OH})\text{Br}$ , is obtained. To a first approximation ( $-\text{OH}$  group is taken to be one mass-point), this molecule reduces to  $\text{C}_{2v}$  symmetry from  $\text{D}_{6h}$  of benzene, the symmetry elements being  $\sigma_h$  the molecular plane containing all the atoms,  $\text{C}_2$  the two fold axis passing through para  $-\text{Br}$  and  $-\text{OH}$  substituent groups and the  $\sigma_v$  plane, perpendicular to the molecular plane and passing through the two fold axis of the molecule. Under the reduced symmetry the transition  $\text{B}_2 \leftarrow \text{A}_1$ , with the transition moment in the plane (YZ) of the mole-

cule and corresponding to the forbidden transition  $B_{2u} \leftarrow A_{1g}$  of benzene, becomes allowed. It is thus expected that the spectrum of this isomer should show the features (Sponer and Teller, 1941) of an allowed transition, namely, a strong 0, 0 band and excitation of totally symmetrical vibrations, with nontotally symmetrical vibrations appearing as 0, 0, 1, 1... $\nu - \nu$  transitions, and more weakly as  $\Delta\nu = 2, 4$  etc., and one should not expect the features of a forbidden transition to appear with any prominence. It is also to be expected that the 0, 0 band (the pure electronic transition) should be present in the first group of bands towards longer wavelengths and the band at  $34799 \text{ cm}^{-1}$  ( $2872.8\text{\AA}$ ) is consequently assigned as the 0, 0 band. Towards longer wavelengths from the 0, 0 transition, a number of bands were found which appeared under different conditions according to their different Boltzmann factors. The separations 195, 251, 293, 323, 490, 574, 636-825, 858, 1022, 1068, 1189 and  $1256 \text{ cm}^{-1}$  of these bands from the 0, 0 band give obviously the fundamental frequencies of vibrations in the ground state, and they should agree with the Raman and infra-red frequencies (Table II).

Towards the violet side of the 0, 0 band one observes a number of strong bands, which belong to different groups. The separations of these from the 0, 0 band give the frequencies of vibration in the upper electronic state of the molecule. Prominent bands on the short wavelength side of the 0, 0 band were found to involve the excited state fundamental frequencies 188, 249, 277, 472, 581, 768, 795, 923-1016, 1057, 1180, 1272 and  $1554 \text{ cm}^{-1}$ . The excited state vibrations 277, 472 and  $795 \text{ cm}^{-1}$  are found in several progressions and combinations. These frequencies are definitely associated with totally symmetric vibrations ( $a_1$ ) in the excited state of the molecule.

In discussing the nature of these various vibrations we shall begin with the identification of carbon ring vibration of the type  $e_{2g}$  (in benzene) which splits in the case of  $C_{2v}$  symmetry into the two components, one totally symmetric ( $a_1$ ) and the other nontotally symmetric ( $b_2$ ). In mono-bromobenzene (Satya Prakash, 1949-63) the corresponding values are  $316a_1$  and  $615b_2$  respectively. This benzene  $606 \text{ cm}^{-1}$  splits into two vibrations  $527a_1$  and  $623b_2$  in the case of mono-hydroxybenzene. Known shifts in the spectra of other derivatives of benzenes are, for example, bromobenzene  $615 \rightarrow 518$  (16%) (Satya Prakash, 1949-63) *p*-fluorophenol  $643 \rightarrow 564$  (12%) and  $465 \rightarrow 418$  (11%) (Sharma and Tripathi, 1963) and *p*-chlorophenol  $642 \rightarrow 538$  (16%) and  $377 \rightarrow 350$  (7%) (Upadhyaya, 1949-63). One would expect the percentage decrease of the same order in this case also. With this in mind, we have tried a greater number of combinations. It is found that the pairs  $636 \rightarrow 581$ ,  $323 \rightarrow 277$  show reasonable shifts and their  $\Delta\nu$ 's fit observations. It seems reasonable to take them as  $a_1$  and  $b_2$  components of benzene  $606 \text{ cm}^{-1}$  —C—C in plane bending vibration.

In phenol the infrared frequency 810 is ascribed (Lecomte, 1937) to the totally symmetrical —C—OH vibration. The corresponding frequencies in the case of hydroquinone, resorcinol and catechol are given as 829, 748 and  $768 \text{ cm}^{-1}$

respectively (Beck, 1950).<sup>1</sup> One should expect the same order of totally symmetric  $\text{C}-\text{OH}$  vibration in this case also. In Raman spectrum of *p*-bromophenol 810 and  $825\text{ cm}^{-1}$  are two frequencies with intensities 10 and 5 respectively. In searching on the red side of the 0,0 band for frequencies found in the Raman spectrum two nearly equally intense bands displaced by  $825$  and  $858\text{ cm}^{-1}$  respectively are obtained. According to the analysis given in Landolt-Bornstein (1951) and considering the  $\text{C}-\text{OH}$  stretching fundamentals of other derivatives of phenol, the lower of the two is taken as  $\text{C}-\text{OH}$  stretching vibration (Table III). The corresponding excited state fundamental is taken as  $768\text{ cm}^{-1}$ . This frequency separation towards shorter wavelength side of 0,0 band could also be explained as  $0 + 795 - 28$ . But the intensity and broadness of this band together with similarity in separation between any component in the structure of this band and a corresponding component in the structure of 0,0 band suggested to take it as fundamental. Werner (1962) has suggested  $8.2\mu$  as the wavelength corresponding to the band connecting the  $\text{OH}$  group to aromatic ring. Kletz and Price (1947) have also taken the region of strong absorption around 1200 wave-number (in infra-red spectra of alkyl phenol) corresponding to the valency vibration of the strongly polar  $\text{C}-\text{O}$  band. There are a number of weaker bands in the wave-length region in question all of which have other reasonable explanations. It does not seem desirable to correlate any of them with totally symmetric  $\text{C}-\text{OH}$  stretching mode of vibration without depolarization data of the Raman spectrum.

As has already been mentioned, the excited state vibrations  $795$  and  $472\text{ cm}^{-1}$  are prominent and progression forming in the spectrum of *p*-bromophenol. The respective frequencies in the ground state are taken as  $858$  and  $574\text{ cm}^{-1}$  (Raman values  $825$  and  $602\text{ cm}^{-1}$ ) respectively. In Landolt and Bornstem Table (1951)  $825\text{ cm}^{-1}$  band with intensity 5 has been assigned as  $\text{C}-\text{H}$  out of plane bending vibration. Because depolarisation data for Raman spectrum of this molecule are not available it seems probable that the medium intensity of the band has been taken into consideration for this assignment. Narasimham Sabban and Nielson (1956) have suggested  $810\text{ cm}^{-1}$  to be the symmetric carbon breathing mode in case of *p*-fluorobromobenzene. The unit  $\text{O}-\text{H}$  has molecular weight of about 17 which is very nearly the atomic weight of fluorine. It can be expected that *p*-bromophenol and *p*-bromo-fluoro-benzene may have the ring breathing fundamental of the same order. Taking this into account and considering the shape and percentage absorption of  $830\text{ cm}^{-1}$  band in infra-red region  $825\text{ cm}^{-1}$  in *p*-bromophenol has been considered to be the counter-part of the totally symmetric carbon ring benzene vibration  $992\text{ cm}^{-1}$  instead of  $\text{C}-\text{H}$  out of plane bending vibration.

The excited state fundamental  $472\text{ cm}^{-1}$  forms the progression upto  $\Delta v = 5$ . These progression forming bands decrease in intensity as expected in view of

Boltzmann factor. The corresponding ground state fundamental is  $574\text{ cm}^{-1}$ . These frequencies in view of their appearance and combining power seem to be totally symmetric. In infra-red spectrum of *p*-bromo-fluoro-benzene  $596\text{ cm}^{-1}$  (Narasimham, Sabban and Nielsen, 1956) is assigned as  $\text{—C—Br}$  stretching mode of vibration. In view of this fact, these fundamentals  $574$  and  $472\text{ cm}^{-1}$  are taken as totally symmetric  $\text{C—Br}$  stretching mode of vibrations in the ground and excited states respectively.

Assignments for a few more fundamentals involving very likely totally symmetric vibrations may be suggested. The excited state fundamentals  $923$ ,  $1272$  and  $1554\text{ cm}^{-1}$  by forming combinations with other ground and excited state fundamentals, account for the majority of the bands in this system. Their frequent occurrence is suggestive of the ring vibrations and this would correlate them with  $1010$   $\text{C—C}$  in plane bending,  $1485$ — $\text{C—C}$  stretching and  $1596$ — $\text{C—C}$  stretching groundstate benzene vibrations respectively.

Three frequencies at  $1016$ ,  $1057$  and  $1180\text{ cm}^{-1}$  are represented by strong and medium strong bands respectively in the ultraviolet spectrum. Corresponding to these the ground state frequencies are  $1068$ ,  $1189$  and  $1256\text{ cm}^{-1}$  respectively. There are three Raman lines at  $1064$ ,  $1186$  and  $1276\text{ cm}^{-1}$  which correspond to above stated fundamentals. The two pairs  $1068$ ,  $1016$  and  $1189$ ,  $1057\text{ cm}^{-1}$  may represent the lower and upper state fundamental frequencies respectively of two totally symmetric  $\text{C—H}$  in plane bending vibrations.

The upper state frequency  $1180\text{ cm}^{-1}$  forms progression upto  $\Delta r = 2$ . On applying the selection rules, it appears to be a totally symmetric vibration. It is assigned as  $\text{C—H}$  in plane bending vibration corresponding to  $1236\text{ a}_{2g}$  benzene vibration.  $\text{A}_{2g}$  state reduces to nontotally symmetric  $\text{B}_2$  state in  $\text{C}_{2v}$  point group and totally symmetric  $\text{A}'$  state in  $\text{C}_s$  point group. If we take  $\text{—OH}$  group as one unit, para-bromophenol molecule at best belongs to the point group  $\text{C}_{2v}$ . If we take  $\text{—OH}$  bond bending to  $\text{C}_{arom}$ ,  $\text{O}$  bond in the molecular plane, this molecule belongs to the point group  $\text{C}_s$  with only the molecular plane as the element of the symmetry. The behaviour of the upper state fundamental  $1180\text{ cm}^{-1}$  as a totally symmetric vibration indicates that the molecule para-bromophenol belongs to  $\text{C}_s$  point group in the excited state.

Kohlrausch and Ypsilanti (1935) have reported  $290\text{ cm}^{-1}$  as ground state fundamental in Raman spectrum of this molecule. Corresponding to it the ground state fundamental in the ultra-violet absorption spectrum of *p*-bromophenol is  $293\text{ cm}^{-1}$ . On comparing the data for other substituted phenols (Landolt-Bornstein, 1951), it is found that  $371$ ,  $331$ ,  $290$ ,  $378$  and  $296\text{ cm}^{-1}$  are given as  $\text{—C—OH}$  in plane bending ground state fundamentals of *p*-fluorophenol, *p*-chlorophenol, *p*-bromophenol, *o*-chlorophenol and *o*-bromophenol respectively. It can be seen that there is a systematic variation between the ground state fundamentals of these molecules and hence assignment seems to be correct. In searching on the



TABLE I  
Ultraviolet Absorption bands of para-bromophenol

Wave number ( $\nu$ ) $\text{cm}^{-1}$	Relative intensity Pathlength 75 cm Temperatures 110°C      70°C	Shift from 0.0 band ( $\Delta\nu$ ) $\text{cm}^{-1}$	Assignments
1	2	3	4
33300	1	-1499	0 858 636
33445	1	-1354	0- 1022- 323
33543	2	-1256	0 1256
33577	2	-1222	0-1022-195
33610	0.5	-1189	0-1189
33666	2	-1133	0-636-490
33694	0.5	-1105	0 1022-2(43)
33731	4	1068	0 1068, 0 1022 43
33777	3	-1022	0 1022
33909	2	-890	0-858 28
33941	4	-858	0 858
33974	4	-825	0 825
34076	1	-723	0 636-2(43)
34147	0.5	652	0 636 18, 0 2(323)
34163	2	-636	0 636
34183	0.5	-616	0 574-43, 0 323 293
34208	0.5	-591	0 574-18; 0-2(293)
34255	4	574	0 -574
34232	0	567	0 490-74
34269	0	-530	0-490 43
34309	0.5	-490	0-490
34334	0.5	-465	0-1189 + 720
34361	0.5	-438	0-1022 + 581
34394	1	-405	0-323-86
34422	5	2	0-323 56
34447	6	2	0-323 28, 0-293-56
34476	8	3	0 323, 0-293 28
34506	8	4	0-323 + 33, 0-293
34519	0.5b	280	0 251-28, 0-858 + 581
34548	0.5b	-251	0-251
34578	0.5b	-221	0 3(74)
34604	0b	-195	0-195
34624	0b	-175	0-4(43); 0-1189 + 1016
34653	3	-146	0-2(74); 0-1068 + 923
34669	4	-130	0-3(43); 0-1189 + 1057
34686	5	113	0-4(28); 0-2(636) + 2(581)
34699	6	100	0 574 + 472, 0-1022 + 923
34713	6	-86	0-3(28); 0-2(43)
34725	7b	-74	0-323 + 249
34743	8	-56	0-2(28), 0-636 + 581; 0-825 + 768
34756	5	-43	0-293 + 249
34771	9	-28	0-825 + 795
34781	2	-18	0-490 + 472
34799	10	0,0	0,0
34895	1d	+6	0 + 581-574

TABLE I (contd.)

Wave number ( $\nu$ ) $\text{cm}^{-1}$	Relative intensity Pathlength 75 cm. Temperatures 110° C      70° C	Shift from 0.0 band ( $\Delta\nu$ ) $\text{cm}^{-1}$	Assignments
1	2	3	4
34832	1bd	+ 33	0 + 1057 - 1022
34866	1b	+ 67	0 + 923 - 858
34905	0.5	+ 106	0 + 188 - 86
34932	0.5	+ 133	0 + 188 - 56
34960	2	+ 161	0 + 188 - 28,    0 + 249 - 2(43)
34987	1	+ 188	0 + 188
35002	3	+ 203	0 + 277 - 74;    0 + 249 - 43
35018	5	+ 219	0 + 277 - 56;    0 + 249 - 28
35031	0.5	+ 232	0 + 277 - 43,    0 + 249 - 18
35048	7b	+ 249	0 + 277 - 28,    0 + 249
35060	2	+ 261	0 + 277 - 18
35076	8	+ 277	0 + 277
35106	0.5d	+ 307	0 + 277 + 33
35117	0.5d	+ 318	0 + 249 + 67
35143	0.5d	+ 344	0 + 277 + 67
35180	1d	+ 381	0 + 2(188);    0 + 249 + 188 - 56
35212	2b	+ 413	0 + 472 - 56,    0 + 249 + 188 - 28
35239	2b	+ 440	0 + 472 - 28;    0 + 249 + 188
35258	3bd	+ 459	0 + 472 - 18
35271	5	+ 472	0 + 472
35288	3bd	+ 489	0 + 795 - 293 - 18
35304	5	+ 505	0 + 795 - 293
35327	3	+ 528	0 + 581 - 56
35339	2	+ 540	0 + 581 - 43
35352	3	+ 553	0 + 581 - 28;    0 + 2(277)
35363	1	+ 564	0 + 581 - 18
35380	4	+ 581	0 + 581
35417	2d	+ 618	0 + 581 + 33
35448	2d	+ 649	0 + 581 + 67
35473	3	+ 674	
35482	3	+ 683	0 + 768 - 86
35492	4b	+ 693	0 + 795 - 100;    0 + 768 - 74
35519	6b	+ 720	0 + 795 - 74;    0 + 768 - 43
35541	4	+ 742	0 + 795 - 56;    0 + 768 - 28
35567	8b	+ 768	0 + 795 - 28;    0 + 768
35594	9	+ 795	0 + 795
35602	4	+ 803	0 + 1057 - 251;    0 + 768 + 33
35627	2bd	+ 828	0 + 795 + 33;    0 + 3(277)
35659	2bd	+ 860	0 + 795 + 67
35682	2	+ 883	0 + 923 - 43
35697	1	+ 898	0 + 923 - 28
35722	3	+ 923	0 + 923
35742	4	+ 943	0 + 1016 - 74;    0 + 2(472)
35759	4	+ 960	0 + 1016 - 56
35771	5	+ 972	0 + 1016 - 43

TABLE I (contd.)

Wave number ( $\nu$ ) $\text{cm}^{-1}$	Relative intensity Pathlength 75 cm Temperatures 110°C      70°C	Shift from 0,0 band ( $\Delta\nu$ ) $\text{cm}^{-1}$	Assignments
1	2	3	4
35787	8	+988	0+1016-28
35799	3	+1000	0+1016-18
35815	9	+1016	0+1016; 0+768+249
35848	4bd	+1049	0+1016+33
35856	3	+1057	0+1057
35869	5bd	+1070	0+795+277
35908	1	+1109	0+1180-74; 0+4(277)
35922	1	+1123	0+1180-56; 0+2(581)-43
35936	1	+1137	0+1180-43; 0+2(581)-28
35957	2	+1158	0+1180-28; 0+2(581)
35979	4	+1180	0+1180
35998	3bd	+1199	0+1272-74; 0+2(581)+33
36018	4	+1219	0+1272-56
36031	5	+1232	0+1272-43
36045	7	+1246	0+1272-28
36055	2	+1256	0+1272-18
36071	8	+1272	0+1272
36092	4	+1293	0+1016+277
36118	2b	+1319	0+795+2(277)-28
36130	2b	+1331	0+1057+277
36147	2b	+1348	0+795+2(277); 0+768+581
36161	2	+1362	0+1554-195; 0+5(277)-28
36181	2b	+1382	0+3(472)-28; 0+5(277)
36123	2	+1414	0+3(472); 0+1016+472-74
36249	1	+1450	0+1554-100; 0+1016+472-43
36275	2b	+1476	0+1554-74; 0+1016+472-18
36291	4	+1492	0+2(795)-100; 0+1016+472
36316	4b	+1517	0+2(795)-74
36353	5	+1554	0+1554
36393	6	+1594	0+2(795); 0+1016+581
36412	0.5d	+1613	0+1057+2(277)
36470	0.5d	+1671	0+1180+795-293-18
36488	0.5d	+1689	0+1180+795-293; 0+768+923
36510	2b	+1711	0+1016+795-100
36531	2	+1732	0+1180+2(277)
36551	2	+1752	0+1016+795-56
36560	3	+1761	0+1180+581
36579	4b	+1780	0+1016+795-28
36608	5b	+1809	0+1016+795
36641	1b	+1842	0+2(923)
36650	1b	+1851	0+1272+581; 0+1057+795
36665	1b	+1866	0+4(472)-28; 0+2(795)+277
36691	1b	+1892	0+4(472)
36715	1	+1916	0+1180+795-56
36747	1	+1948	0+1180+795-28; 0+1554+472-74

TABLE I (contd).

Wave number ( $\nu$ ) $\text{cm}^{-1}$	Relative intensity Pathlength 75 cm. Temperatures 110° C      70° C	Shift from 0,0 band ( $\Delta\nu$ ) $\text{cm}^{-1}$	Assignments
1	2	3	4
36758	1	+1959	0+1180+795-18
36773	3bd	+1974	0+1180+795
36793	2	+1994	0+1554+472-28
36808	3b	+2009	0+1180+795+33; 0+1554+472-18
36823	4	+2024	0+1272+795-43; 0+1554+472
36862	3	+2063	0+1272+795
36885	3	+2086	0+1016+795+277
36910	0 5d	+2111	0+2(1057)
36936	0 5d	+2137	0+2(795)+2(277)
36966	0 5d	+2167	0+1016+795+472-113
36978	1bd	+2179	0+1016+795+472-100
37003	0.5b	+2204	0+1016+795+472-74
37032	0.5	+2233	0+1016+795+472-56
37054	2	+2255	0+1016+795+472-28
37067	1	+2268	0+1016+795+472-18
37081	3	+2282	0+1016+795+472
37110	0.5	+2311	0+1016+795+472+33
37133	1	+2334	0+3(795)-56; 0+2(1180)-28
37158	1	+2359	0+3(795)-28; 0+2(1180)
37183	2	+2384	0+3(795)
37219	0.5	+2420	0+3(795)+33
37247	0.5	+2448	0+3(795)+67
37262	0.5	+2463	0+1272+795+472-74
37287	0.5	+2488	0+1272+795+472-56
37305	0.5	+2506	0+1272+795+472-28
37327	1	+2528	0+1554+1016-43
37332	1	+2533	0+1272+795+472
37367	1	+2568	0+1554+1016
37399	2	+2600	0+1554+795+277-28; 0+1016+2(795)
37425	1	+2626	0+1554+795+277
37453	0.5	+2654	0+1554+795+277+33; 0+1554+1180-74
37481	0 5b	+2682	0+1554+1180-56
37508	0.5b	+2709	0+1554+1180-28
37532	1	+2733	0+1554+1180
37553	0 5b	+2754	0+1016+795+2(472)
37564	0 5b	+2765	0+1272+472+795+277-56; 0+3(923)
37581	0 5b	+2782	0+1272+472+795+277-28
37613	1b	+2814	0+1272+472+795+277
37641	0.5b	+2842	0+1554+1016+277
37695	0 5b	+2896	0+1554+1016+472-2(74)
37762	0.5b	+2963	0+1554+1016+472-74
37809	0 5b	+3010	0+1554+1016+472-28
37836	0.5b	+3037	0+1554+1016+472
37866	0.5b	+3067	0+1554+472+795+277-28
37993	1	+3094	0+1554+472+795+277

b = broad; d = diffuse; bd = broad and diffuse.

TABLE II  
Assignments of Modes of Vibrations for *p*-bromophenol

Raman Shifts* cm <sup>-1</sup>		Infra-red fundamentals cm <sup>-1</sup>			Ultraviolet absorption		Nature of vibra- tion
Kohlrausch and Ypsilanti	Landolt- Bornstein	M- Parodi	Locomte	Author	Ground State vibra- tions† cm <sup>-1</sup>	Excited State† vibra- tions cm <sup>-1</sup>	
—	—	236	—	—	251(0.5)	188(4)	$\beta$ C—Br
290(9)	290(9)	267	—	—	293(8)	249(7)	$\beta$ C—OH
319(5)	319(5)	310	—	—	323(8)	277(8)	$\beta$ C—C
497(1)	—	510	—	—	490(0.5)	—	$\gamma$ C—C
602( $\frac{1}{2}$ )	—	—	610	—	574(4)	472(5)	$\nu$ C—Br
632(3)	632(3)	—	—	—	636(2)	581(4)	$\beta$ C—C
687(0)	687(0b)	—	—	—	—	—	$\gamma$ C—H
810(10)	810(10)	—	820	814	825(4)	768(8)	$\nu$ C—OH
825(5)	825(5)	—	860	830	858(4)	795(9)	$\nu$ C—C breathing
1007(2)	1005(2)	—	960	1010	1022(3)	923(3)	$\beta$ C—C
1064(8)	1064(8)	—	1060	1070	1068(4)	1016(9)	$\beta$ C—H
1186(3)	1163(3)	—	1180	1176	1189(0.5)	1057(3)	$\beta$ C—H
1276(3b)	1252(3b)	—	—	1238	1256(2)	1180(4)	$\beta$ C—H
1415(0)	—	—	—	1431	—	1272(8)	$\nu$ C—C
1585(5b)	1585(5b)	—	—	1592	—	1554(5)	$\nu$ C—C
3055(3b)	3055(3b)	—	—	—	—	—	$\nu$ C—H

 $\nu$  - Stretching vibration. $\beta$  - in plane bending vibration. $\gamma$  - out of plane bending vibration.

\*Figures within parentheses indicate intensities as given by authors.

†Visually estimated intensities are given in parentheses.

TABLE III  
Correlation of C—OH stretching ground state fundamentals of  
monoderivatives of phenol with that of phenol (810 cm<sup>-1</sup>)

Molecule	Isomer	Ortho cm <sup>-1</sup>	Meta cm <sup>-1</sup>	Para cm <sup>-1</sup>
Fluoro Phenol		840	839	835
Chloro Phenol		833	—	818
Bromo Phenol		830	774	810
Hydroxy Phenol		768	748	829

TABLE IV

Shift of 0, 0 band towards longer wavelength side of mono-derivatives of phenol with respect to 0, 0 band of benzene

Molecule	Isomer	Ortho cm <sup>-1</sup>	Meta cm <sup>-1</sup>	Para cm <sup>-1</sup>
Fluoro Phenol		1287	1469	2958
Chloro Phenol		2197	2328	3268
Bromo Phenol		2271	2372	3290

violet side of 0, 0 band for a frequency corresponding to 293 cm<sup>-1</sup> ground state fundamental, a medium strong broad band at 35048 cm<sup>-1</sup> is obtained. It is separated at a frequency separation of 249 cm<sup>-1</sup> from the 0, 0 band and is assigned as 0 | 277 28. If it is alternatively taken to be an excited state fundamental corresponding to 293 cm<sup>-1</sup> ground state frequency it explains the bands towards the longer wavelength side of itself in the same way as the bands towards longer wavelength side of 0,0 band has been explained. Further it helps in explaining the band at 34756 separated at 43 cm<sup>-1</sup> towards longer wavelength side of 0, 0 band, and other companion bands which appear at 43, 2 × 43, 3 × 43, and 4 × 43 cm<sup>-1</sup> on the red side of the main bands (Table I). Thus 249 cm<sup>-1</sup> has been assigned as - C—OH in plane bending vibration in the excited state of this molecule.

Lastly we take up the lower state fundamental 251 cm<sup>-1</sup>. Padhiye and Viladkar (1959) have suggested 254 cm<sup>-1</sup> as —C—Br in plane bending vibration in the case of bromobenzene. It could, therefore, be suggested that 251 cm<sup>-1</sup> represent the —C—Br in plane bending vibration in the lower electronic state of *p*-bromo- phenol molecule. The corresponding excited state fundamental is 188 cm<sup>-1</sup>.

The ground state fundamentals obtained in these investigations have been compared (Table II) with the Raman (Kohlrausch and Ypsilanti, 1935; Landolt-Bornstein, 1951) and infra-red (Parodi and Cotton, 1941; Lecomte, 1938) frequencies of this molecule. The agreement can be seen to be quite satisfactory. The corresponding excited state frequencies and their correlations with modes of vibrations are also included in Table II. Since the depolarization data for the Raman lines are not available, the assignments can not be considered altogether unambiguous.

In the end some remarks should be made about the shift of the 0, 0 bands of *o*-, *m*- and *p*-isomers of halogenated phenols with respect to the 0, 0 band of benzene. The general formulae for di-derivatives of benzene, which have been obtained by us (Chandra and Tripathi, 1963) after taking both inductive effect and migration effect of the substituent into consideration, are in position to explain the order of the red shift of 0,0 bands of *o*-, *m*- and *p*-di-derivatives of

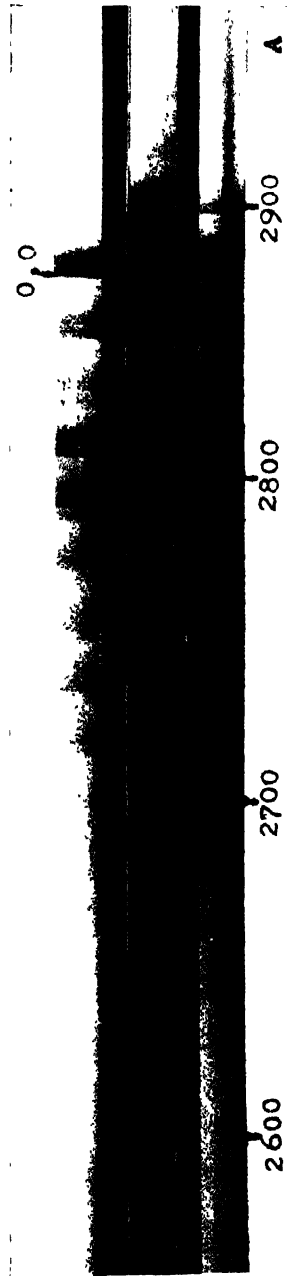


Fig. 1.—Longest wave length  $\Pi^* \leftarrow \Pi$  system in the electronic spectra of p-bromophenol.  
All the three spectra have been obtained under similar conditions (at path-length 75 cm. and atmospheric pressure) except the temperature which was higher in the case of central strip.





benzene compounds. These formulae show that for weak interacting groups, if both substituents are either ortho-para directing or meta directing groups, the order of red shift is  $0 < m < p$ . Since  $-\text{OH}$ ,  $-\text{F}$ ,  $-\text{Cl}$  and  $-\text{Br}$  are all ortho-para directing groups the order of red shift of 0, 0 bands of *o*-, *m*- and *p*-halogenated mono-derivatives of phenol must be as  $0 < m < p$ . Table IV shows that the shift from ortho to para in the case of halogenated phenols is in keeping with the results expected.

## ACKNOWLEDGMENTS

The author is indebted to Professor D. Sharma for his keen interest and valuable guidance throughout this investigation.

## REFERENCES

- Banerjee, S. B., 1956, *Ind. J. Phys.*, **30**, 353.  
Banerjee, S. B. and Misra, T. N., 1961, *Ind. J. Phys.*, **35**, 203  
Bock, C. A., 1950, *J. Chem. Phys.*, **18**, 1135  
Chandra, K. and Sharma, D., 1963, *Ind. J. Phys.*, **37**, 405.  
Chandra, K. and Tripathi, G. N. R., 1963, C.S.I.R. Symposium on Spectroscopy and Allied Problems, B.H.U., Varanasi, 122.  
Chandra, K., 1964, *Ind. J. Pure & Appl. Phys.*, **2**, 134  
Joshi, B. D., 1949-63, Research Report, Dept. Phys., B.H.U., Varanasi.  
Klotz, T. A. and Price, W. C., 1947, *J. Chem. Soc.*, **644**.  
Kohrausch, K. W. F. and Ypsilanti, G. P., 1935, *S.B. Bayer. Akad. Wiss.*, **144**, 417.  
Landolt Bornstein Tables, 1951, Auflage, 6, Teil **2**, 310  
Locomte, J., 1937, *J. de Phys. et. Rad.*, **8**, 489.  
——— 1938, *J. de Phys. et. Rad.*, **9**, 13.  
Padhye, M. R. and Viladkar, B. G., 1959, *J. Sci. Industr. Res.*, **18B**, 506.  
Parodi, M. and Cotton, M. A., 1941, *Acad. Des. Sci.*, **30**, 1138.  
Prakash, S., 1949-63, Research Report, Dept. Phys. B.H.U., Varanasi.  
Ramasastry, C., 1951, *Proc. Nat. Inst. Sci. (India)*, **17**, 349  
——— 1951, *Current Science*, **20**, 15.  
Rao, K. N. and Sponer, H., 1957, *Canad. J. Phys.*, **35**, 332  
Rao, V. R. and Suranarayana, 1956, *Ind. J. Phys.*, **30**, 117  
Roy, S. B., 1958, *Ind. J. Phys.*, **32**, 525.  
Sharma, D. and Tripathi, L. N., 1963, *Ind. J. Pure & Appl. Phys.*, **1**, 229.  
Sponer, H. and Teller, E. 1941, *Rev. Mod. Phys.*, **13**, 75.  
Tewari, S. K., 1949-63, Research Report, Dept. Phys. B.H.U., Varanasi.  
Upadhyay, K. N., 1949-63, Research Report, Dept. Phys. B.H.U., Varanasi  
Werner, B., 1962, An Introduction to Infra-red Spectroscopy, 337.

# VIBRATION OF A CLAMPED—CLAMPED BAR UNDER TENSION

SUNIL KUMAR BANERJEE

DEPARTMENT OF MATHEMATICS, RISHI BANKIM COLLEGE, NAIHATI 24-PARGANAS

(Received August 11, 1965)

**ABSTRACT.** Dynamics of vibration of a bar clamped at both ends and excited by transverse impact by an inelastic load has been worked out following operational method. We consider in this paper the dynamics of such a bar struck at the mid-point only. Two distinct cases have been worked out: (1) The tension is large compared to stiffness, (2) Stiffness is large compared to the tension. In case (1) series solution is obtained from which the solution for any epoch may be calculated easily. In case (2) a periodic solution is obtained.

## INTRODUCTION

The problem of Vibration of a bar Clamped at both ends and held under tension is in effect the same as that of a Stiff—String.

When a string is under tension and also has stiffness, its equation of motion can be obtained by combining the derivatives in connection with the vibration of the string and transverse vibration of a bar. Velocity of the wave remains strictly constant if the wire has no stiffness, but the velocity changes and becomes more and more frequency-dependent if stiffness is considered. The same is true for a bar clamped at both ends, held under tension and vibrating transversely. So we prefer to use the word Stiff-String in place of Clamped—Clamped bar in our subsequent discussions. The present problem discusses two distinct cases: (1) when the tension is the chief agent in the vibration (2) when the stiffness is the chief agent in the vibration.

In this paper we solve the general problem of vibration of a stiff string excited by the transverse impact by an inelastic load using the powerful operational method in a similar way as adopted by Ghosh (1938) in solving the general problem of pianoforte string. The only assumption in the present formulation is that the string behaves like a loaded one so long as the load is in contact with it.

## EXPLANATION OF THE SYMBOLS USED

- $l$  = Length of the string =  $a + b$
- $a$  = Shorter segment of the string
- $b$  = longer segment of the string
- $t$  = Variable time

## Vibration of a Clamped—Clamped Bar under Tension 477

$x$  = Variable, measured along the string, the string being clamped at  $x = 0$  and at  $x = l$

$y$  = Displacement of any point of the string at any time

$y_1$  = Displacement of any point,  $x < a$

$y_2$  = Displacement of any point,  $x > a$

$y_a$  = Displacement of the struck point  $x = a$

$A$  = Area of cross-section of the string

$\rho$  = Density of the material of the string

$T$  = Permanent tension along the string

$c$  = Velocity of transverse waves along the string  $= (T/\rho A)^{1/2}$

$E$  = Young's Modulus of the material of the string

$I$  = Moment of Inertia of the cross-section of the string about the neutral axis.

$P$  = Pressure exerted by the load

$m$  = Mass of the striking body

$\theta = 2a/c$ .

$t_n = t - n\theta$ , where  $n = 1, 2, 3$  etc.

$v_0$  = Velocity of Impact

$J = mv_0$

$D$  = Operator  $\frac{d}{dt}$ .

The equation of motion of the stiff string or, a bar clamped at both ends and held under tension,

$$\rho A \frac{d^2 y}{dt^2} = T \frac{d^2 y}{dx^2} - EI \frac{d^4 y}{dx^4} \quad (1)$$

Equation (1) in the operational notations becomes,

$$EI \frac{d^4 y}{dx^4} - T \frac{d^2 y}{dx^2} - \rho A D^2 y = 0 \quad (2.0)$$

The general solution (2.0) is,

$$y = A_1 \exp(K_1 x) + A_2 \exp(-K_1 x) + A_3 \exp(K_2 x) + A_4 \exp(-K_2 x) \dots \quad (2.1)$$

$$\text{where } K_1^2 = [T + (T^2 - 4EI\rho AD^2)^{1/2}]/2EI \quad \dots \quad (2.2)$$

$$K_2^2 = [T - (T^2 - 4EI\rho AD^2)^{1/2}]/2EI \quad \dots \quad (2.3)$$

and  $A_1, A_2, A_3, A_4$  are constant to be determined with the help of end-conditions.

Case I :  $T^2 > 4EI\rho AD^2$

In this case the root of (2.0) are all real and  $K_1$  and  $K_2$  can be written simply by,

$$K_1 = \pm (T/EI)^{1/2} \quad \dots \quad (2.4)$$

$$K_2 = \pm D/c \quad \dots \quad (2.5)$$

The general solution (2.1) now takes up the form

$$y = A_1 \exp \{T/EI)^{1/2}x\} + A_2 \exp \{- (T/EI)^{1/2}x\} + A_3 \exp \{(D/c)x\} + A_4 \exp \{-D/c)x\} \quad \dots \quad (3)$$

Since the string is clamped at both ends, the terminal conditions are,

$$\text{at } x = 0, \quad y_1 = 0, \quad \frac{dy_1}{dx} = 0 \quad \dots \quad (3.1)$$

$$x = l, \quad y_2 = 0, \quad \frac{dy_2}{dx} = 0 \quad \dots \quad (3.2)$$

$$x = a \quad y_1 = y_2 = y_a \quad \dots \quad (3.3)$$

The hammer strikes at  $x = a$ ; if  $y_a$  be the displacement of the struck-point we get from (3), (3.1), (3.2) and (3.3)

$$y_1 = y_a \frac{\cosh (T/EI)^{1/2}x - \cosh (D/c)x}{\cosh (T/EI)^{1/2}a - \cosh (D/c)a}, \quad (0 \leq x \leq a) \quad \dots \quad (4.0)$$

$$y_2 = y_a \frac{\cosh (T/EI)^{1/2}(l-x) - \cosh (D/c)(l-x)}{\cosh (T/EI)^{1/2}b - \cosh (D/c)b}, \quad (a \leq x \leq l) \quad \dots \quad (4.1)$$

The string is excited by a transverse impact of impulse  $J$  by an inelastic load. The corresponding pressure  $P$  exerted by the load is given by,

$$P = m \frac{d^2 y_a}{dt^2} \quad \dots \quad (5.0)$$

and the subsequent motion of the load during contact is,

$$m \frac{d^2 y_a}{dt^2} = T \Delta \left( \frac{dy}{dx} \right)_{x=a} - EI \Delta \left( \frac{d^3 y}{dx^3} \right)_{x=a} \quad \dots \quad (5.1)$$

where  $\Delta(dy/dx)_{x=a}$  and  $\Delta(d^3y/dx^3)_{x=a}$  denote the changes in the values of  $(dy/dx)$  and  $(d^3y/dx^3)$  incurred in crossing the point  $x = a$ .

Now substituting the values of  $\Delta(dy/dx)_{x=a}$  and  $\Delta(d^3y/dx^3)_{x=a}$  as obtained from (4.0) and (4.1) in equation (5.1) and imposing the boundary conditions we get,

$$mD^2 y_a = -[(TD/c) - (EID^3/c^3)] \times \left\{ \frac{\sinh (D/c)a}{\cosh (D/c)a - k} + \frac{\sinh (D/c)b}{\cosh (D/c)b - k'} \right\} + DJ \quad \dots \quad (5.2)$$

Whence we get,

$$y_a = \frac{1}{F(D)} v_0 \quad \dots \quad (6.0)$$

Where,

$$F(D) = D + \frac{1}{2} \{q - (2EI/mc^3)D^2\} \left[ \frac{\sinh(D/c)a}{\cosh(D/c)a - k} + \frac{\sinh(D/c)b}{\cosh(D/c)b - k'} \right] \dots (6.1)$$

$$\text{and,} \quad q = \frac{2T}{EI} \dots (6.2)$$

$$k = \cosh(T/EI)^{1/2}a \dots (6.3)$$

$$k' = \cosh(T/EI)^{1/2}b \dots (6.4)$$

The equation (6.1) is to be used for finding the displacement at any point along the string.

In the absence of stiffness, equation (1) reduces to that of a flexible string but if stiffness is made zero in equation (6.1) we can not expect the behaviour of a flexible string because of difference in end conditions. But it represents the case of a clamped-clamped bar held under high tension [Kar (1956)]

*String is finite :*

The Hammer strikes at the middle point of the string. Here  $a = b$  and we get from (6.1)

$$F(D) = D + \{q - (2EI/mc^3)D^2\} \left[ \frac{\sinh(D/c)a}{\cosh(D/c)a - k} \right] \dots (7.0)$$

On substituting the exponential values for hyperbolic Sines and Cosines in equation (7.0) and writing  $D_1 = D + \alpha$ ,  $D_2 = D + \beta$  we get finally,

$$F(D) = \frac{D_1 D_2}{(\alpha + \beta) \{1 - 2k \exp\{-(D/c)a\} + \exp\{-2(D/c)a\}\}} \\ \times \left[ 1 - \frac{(D - \alpha)(D - \beta)}{D_1 D_2} \left\{ 1 + \frac{2k(\alpha + \beta)}{(D - \alpha)(D - \beta)} \exp(D/c)a \right\} \right] \dots (8.0)$$

$$\text{where, } D_1 D_2 = (D + \alpha)(D + \beta) = D^2 - \frac{mc^3}{2EI} D - \frac{mqc^3}{2EI} \dots (9.0)$$

$$\text{and } -\alpha, -\beta \text{ are the roots of, } D^2 - \frac{mc^3}{2EI} D - \frac{mqc^3}{2EI} = 0 \dots (10)$$

given by,

$$[\alpha, \beta] = \frac{1}{2} \left[ \frac{mc^3}{2EI} \pm \left( \frac{m^2 c^6}{4E^2 I^2} + \frac{2mqc^3}{EI} \right)^{1/2} \right] \dots (11)$$

Expanding the term under the radical sign, binomially and retaining up to terms containing  $(1/mc^3)$ , and remembering that,  $c = (T/\rho A)^{1/2}$ ,  $g = 2T/mc$ , equation (11) reduces to,

$$|\alpha, \beta| = - \left( \frac{T}{\rho A} \right)^{1/2} \left[ \frac{2\rho A}{m} + \frac{mT}{2EI\rho A} - \left( \frac{2\rho A}{m} \right)^3 \frac{EI}{T} \right],$$

$$\left( \frac{T}{\rho A} \right)^{1/2} \left[ \frac{2\rho A}{m} - \left( \frac{2\rho A}{m} \right)^3 \frac{EI}{T} \right] \dots \quad (12)$$

#### *Displacement of the struck-point during contact*

With the help of equation (8.0) we get from (6.0) the displacement of the string at the struck-point during contact of the load.

$$y_a = \frac{v_0(\alpha + \beta) \left[ 1 - 2k \exp \left\{ -\frac{Da}{c} \right\} + \exp \left\{ -\frac{2D\alpha}{c} \right\} \right]}{D_1 D_2} \times \left[ 1 - \frac{(D-\alpha)(D-\beta)}{D_1 D_2} \left\{ 1 + \frac{2k(\alpha + \beta)}{(D-\alpha)(D-\beta)} \exp \left( \frac{Da}{c} \right) \right\} \right]^{-1} \dots \quad (13)$$

Expanding the above multinomial expression in power series we get after simplification,

$$y_a = \left[ \frac{(\alpha + \beta)}{D_1 D_2} - \left\{ \frac{2(\alpha + \beta)^2 D}{D_1^2 D_2^2} - \frac{2(\alpha + \beta)}{D_1 D_2} \right\} \exp(-D\theta) + \left\{ \frac{4(\alpha + \beta)^3 D^2}{D_1^3 D_2^3} - \frac{6(\alpha + \beta)^2 D}{D_1^2 D_2^2} \right. \right. \\ \left. \left. + \frac{2(\alpha + \beta)}{D_1 D_2} \right\} \exp(-2D\theta) - \dots \right] v_0 + 2k \left[ \left\{ \frac{(\alpha + \beta)^2 D}{D_1^2 D_2^2} - \frac{(\alpha + \beta)}{D_1 D_2} \right\} \exp \left( -\frac{1}{2} D\theta \right) \right. \\ \left. - \left\{ \frac{4(\alpha + \beta)^3 D^2}{D_1^3 D_2^3} - \frac{5(\alpha + \beta)^2 D}{D_1^2 D_2^2} + \frac{(\alpha + \beta)}{D_1 D_2} \right\} \exp \left( -\frac{3}{2} D\theta \right) \right. \\ \left. + \left\{ \frac{12(\alpha + \beta)^4 D^3}{D_1^4 D_2^4} - \frac{20(\alpha + \beta)^3 D^2}{D_1^3 D_2^3} + \frac{9(\alpha + \beta)^2 D}{D_1^2 D_2^2} - \frac{(\alpha + \beta)}{D_1 D_2} \right\} \exp \left( -\frac{5}{2} D\theta \right) - \dots \right] v_0 \\ + 4k^2 \left[ \left\{ \frac{(\alpha + \beta)^3 D^2}{D_1^3 D_2^3} - \frac{(\alpha + \beta)^2 D}{D_1^2 D_2^2} \right\} \exp(-D\theta) - \left\{ \frac{6(\alpha + \beta)^4 D^3}{D_1^4 D_2^4} - \frac{8(\alpha + \beta)^3 D^2}{D_1^3 D_2^3} \right. \right. \\ \left. \left. + \frac{2(\alpha + \beta)^2 D}{D_1^2 D_2^2} \right\} \exp(-2D\theta) + \dots \right] v_0 + 8k^3 \left[ \left\{ \frac{(\alpha + \beta)^4 D^3}{D_1^4 D_2^4} - \frac{(\alpha + \beta)^3 D^2}{D_1^3 D_2^3} \right\} \right]$$

$$\exp \left( -\frac{\alpha}{2} D\theta \right) \cdot \left\{ \frac{8(\alpha + \beta)^5 D^4}{D_1^5 D_2^5} - \frac{11(\alpha + \beta)^4 D^3}{D_1^4 D_2^4} + \frac{3(\alpha + \beta)^3 D^2}{D_1^3 D_2^3} \right\} \\ \exp \left( -\frac{\alpha}{2} D\theta \right) + \left] v_0 + 16k^4 \left[ \left\{ \frac{(\alpha + \beta)^4 D^4}{D_1^5 D_2^5} - \frac{(\alpha + \beta)^4 D^3}{D_1^4 D_2^4} \right\} \exp \left( -2D\theta \right) \dots \right] v_0 \dots \right] \quad (14)$$

Writing,

$$\frac{(\alpha + \beta)}{D_1 D_2} v_0 = f_1(t)$$

$$\frac{(\alpha + \beta)^2 D}{D_1^2 D_2^2} v_0 = f_2(t)$$

etc.,

$$\frac{(\alpha + \beta)^n D^n}{D_1^n D_2^n} v_0 = f_n(t)$$

and remembering that,  $f(t) \exp \left( -nD\theta \right) = f(t - n\theta) = f(t_n)$ ,

equation (14) reduces to,

$$y_a = [f_1(t) - \{2f_2(t_1) - 2f_1(t_1)\} + \{4f_3(t_2) - 6f_2(t_2) + 2f_1(t_2)\} - \dots] \\ + 2k \left[ \left\{ f_2 \left( t - \frac{\theta}{2} \right) - f_1 \left( t - \frac{\theta}{2} \right) \right\} - \left\{ 4f_3 \left( t - \frac{3\theta}{2} \right) - 5f_2 \left( t - \frac{3\theta}{2} \right) + f_1 \left( t - \frac{3\theta}{2} \right) \right\} \right. \\ \left. + \left\{ 12f_4 \left( t - \frac{5\theta}{2} \right) - 20f_3 \left( t - \frac{5\theta}{2} \right) + 9f_2 \left( t - \frac{5\theta}{2} \right) - f_1 \left( t - \frac{5\theta}{2} \right) \right\} - \dots \right] \\ + 4k^2 [\{f_3(t_1) - f_2(t_1)\} - \{6f_4(t_2) - 8f_3(t_2) + 2f_2(t_2)\} + \dots] \\ + 8k^3 \left[ \left\{ f_4 \left( t - \frac{3\theta}{2} \right) - f_3 \left( t - \frac{3\theta}{2} \right) \right\} - \left\{ 8f_5 \left( t - \frac{5\theta}{2} \right) - 11f_4 \left( t - \frac{5\theta}{2} \right) \right. \right. \\ \left. \left. + 3f_3 \left( t - \frac{5\theta}{2} \right) \right\} + \dots \right] + 16k^4 [\{f_5(t_2) - f_4(t_2)\} - \dots]$$

Equation (15) is the general expression for displacement of the struck point during impact. Any function in the above expression will appear only from the time obtained by equating the corresponding argument to zero.

It is clear from the above equation that at intervals of a period (i.e.  $2a/c$ ) two types of reflected wave generate in succession—two waves similar to those in case of a flexible string, and two more, 'now stiffness controlled' proceeding towards the struck point, where new waves (represented by  $f_2$ ,  $f_3$  etc) are continuously being generated. It is obvious that the functions representing the waves generated during impact only will exist in the value of  $y_a$ .

The value of the functions occurring in equation (15) is the same as those obtained by Ghosh (1953).

If the tension be infinitely large or if the stiffness of the string be zero, we get,

$$f_1(t) = \frac{v_0}{\beta} (1 - e^{-\beta t}) = \frac{v}{q} (1 - e^{-qt}) \quad \dots \quad (16.1)$$

$$f_2(t) = \frac{v_0}{\beta} \cdot \beta t e^{-\beta t} = \frac{v_0}{q} \cdot q t e^{-qt} \quad \dots \quad (17.2)$$

$$f_3(t) = \frac{v_0}{\beta} \left( \beta t - \frac{\beta^2 t^2}{2} \right) e^{-\beta t} = \frac{v_0}{q} \left( q t - \frac{q^2 t^2}{2} \right) e^{-qt} \quad \dots \quad (18.3)$$

and so on.

Those values of  $f_1(t)$ ,  $f_2(t)$ ,  $f_3(t)$  etc. as obtained in (16.1), (17.2) and (18.3) etc. are similar to those obtained by Ghosh, (loc. cit).

The first term of equation (15) is zero for negative values of time for positive values, i.e.,

$$0 < t < \theta,$$

$$y_a = f_1(t) + 2k \left[ f_2 \left( t - \frac{\theta}{2} \right) - f_1 \left( t - \frac{\theta}{2} \right) \right] \quad (18.1)$$

During,

$$\theta < t < 2\theta,$$

$$\begin{aligned} y_a = & y_a(0 < t < \theta) - \{2f_2(t_1) - 2f_1(t_1)\} \\ & - 2k \left\{ 4f_3 \left( t - \frac{3\theta}{2} \right) - 5f_2 \left( t - \frac{3\theta}{2} \right) + f_1 \left( t - \frac{3\theta}{2} \right) \right\} \\ & + 4k^2 \{f_3(t_1) - f_2(t_1)\} + 8k^3 \left\{ f_4 \left( t - \frac{3\theta}{2} \right) - f_3 \left( t - \frac{3\theta}{2} \right) \right\} \end{aligned} \quad (18.2)$$

Similarly during,

$$2\theta < t < 3\theta$$

$$\begin{aligned} y_a = & y_a(\theta < t < 2\theta) + \{4f_3(t_2) - 6f_2(t_2) + 2f_1(t_2)\} \\ & + 2k \left\{ 12f_4 \left( t - \frac{5\theta}{2} \right) - 20f_3 \left( t - \frac{5\theta}{2} \right) + 9f_2 \left( t - \frac{5\theta}{2} \right) - f_1 \left( t - \frac{5\theta}{2} \right) \right\} \\ & - 4k^2 \{6f_4(t_2) - 8f_3(t_2) + 2f_2(t_2)\} \\ & - 8k^3 \left\{ 8f_5 \left( t - \frac{5\theta}{2} \right) - 11f_4 \left( t - \frac{5\theta}{2} \right) + 3f_3 \left( t - \frac{5\theta}{2} \right) \right\} \\ & + 16k^4 \{f_5(t_2) - f_4(t_2)\} \quad \dots \quad (18.3) \end{aligned}$$

and so on.



The pressure exerted by the load during impact may now be easily obtained by using equations (5.0) and (18.1)–(18.3) successively for each epoch. By studying the pressure equations thus obtained and equating each to zero it will be shown in a subsequent publication how to calculate the duration of impact at different intervals of time.

We now study the case when stiffness is the chief agent in the vibration.

Case II

$$4EI\rho AD^2 \ll T^2$$

Here all the four roots of equation (2.1) are imaginary and the general solution of the equation can be written as,

$$y = A_1 \cosh \mu_1 x + A_2 \sinh \mu_1 x + A_3 \cos \mu_2 x + A_4 \sin \mu_2 x \quad \dots (20)$$

where,

$$\mu_1 = \{i(4EI\rho AD^2 - T^2)^{1/2} + T^{1/2}/2EI\}^{1/2} \quad \dots (20.1)$$

$$\mu_2 = \{i(4EI\rho AD^2 - T^2)^{1/2} - T^{1/2}/2EI\}^{1/2} \quad \dots (20.2)$$

and  $A_1, A_2, A_3, A_4$  are constant to be determined from boundary conditions.

Equation (20) with the help of the boundary conditions (3.1), (3.2) and (3.3), becomes

$$y_1 = y_a \frac{\cosh \mu_1 x - \cosh \mu_2 x}{\cosh \mu_1 a - \cosh \mu_2 a}, \quad (0 \leq x \leq a) \quad \dots (21.0)$$

$$y_2 = y_a \frac{\cosh \mu_1(l-x) - \cosh \mu_2(l-x)}{\cosh \mu_1 b - \cosh \mu_2 b}, \quad (a \leq x \leq l) \quad \dots (21.1)$$

The hammer strikes at  $x = a$  and the corresponding displacements are given by (21.0), (21.1). The pressure exerted by the load is given by

$$P = m \frac{d^2 y_a}{dt^2} \quad \dots (22.0)$$

and the subsequent equation of motion of the load is,

$$m \frac{d^2 y_a}{dt^2} = T \Delta \left( \frac{dy}{dx} \right)_{x=a} - EI \Delta \left( \frac{d^3 y}{dx^3} \right)_{x=a} \quad \dots (22.1)$$

Not substituting the values of  $\Delta(dy/dx)_{x=a}$  and  $\Delta(d^3 y/dx^3)_{x=a}$  as obtained from (21.0) and (21.1) in equation (22.1) and imposing the boundary conditions we get,

$$m D^2 y_a = -T y_a \left[ \frac{\mu_1 \sinh \mu_1 b + \mu_2 \sinh \mu_2 b}{\cosh \mu_1 b - \cosh \mu_2 b} + \frac{\mu_1 \sinh \mu_1 a + \mu_2 \sinh \mu_2 a}{\cosh \mu_1 a - \cosh \mu_2 a} \right] \\ + EI y_a \left[ \frac{\mu_1^3 \sinh \mu_1 b - \mu_2^3 \sinh \mu_2 b}{\cosh \mu_1 b - \cosh \mu_2 b} + \frac{\mu_1^3 \sinh \mu_1 a - \mu_2^3 \sinh \mu_2 a}{\cosh \mu_1 a - \cosh \mu_2 a} \right] + DJ \quad (22.2)$$

# HAMMER STRIKES AT THE MIDDLE POINT OF THE STRING

In this case  $a = b$ , equation (22.2) now takes up the form,

$$mD^2y_a = -2Ty_a \left[ \frac{\mu_1 \sinh \mu_1 a}{\cosh \mu_1 a} + \frac{\mu_2 \sin \mu_2 a}{\cos \mu_2 a} \right] + 2EIy_a \left[ \frac{\mu_1^3 \sinh \mu_1 a}{\cosh \mu_1 a} + \frac{\mu_2^3 \sin \mu_2 a}{\cos \mu_2 a} \right] + DJ \quad (22.3)$$

Replacing  $J$  by  $mv_0$  we have from equation (22.3)

$$y_a = \frac{D}{F(D)} v_0 \quad (23.0)$$

Where,

$$F(D) = D^2 + \frac{2}{m} \left[ \frac{(T\mu_1 - EI\mu_1^3) \sinh \mu_1 a}{\cosh \mu_1 a} + \frac{(T\mu_2 + EI\mu_2^3) \sin \mu_2 a}{\cos \mu_2 a} \right] \quad (23.1)$$

$$\text{Now writing,} \quad EI\mu_1^2 - T = -EI\mu_2^2 \quad (23.2)$$

we have,

$$F(D) = D^2 + \frac{2EI}{m} \mu_1 \mu_2 \frac{\mu_1 \sinh \mu_2 a}{\cosh \mu_1 a} - \frac{\mu_2 \sinh \mu_1 a}{\cos \mu_2 a} \quad (23.3)$$

From equation (20.1) and (20.2), we have by expansion and retaining only upto linear power of  $EI$  the final of  $F(D)$  to be,

$$F(D) = D^2 \left[ 1 + \frac{M}{3m} - \frac{Ma^2T}{90mEI} \right] + \frac{Ma^4\rho A}{1890mEI} D^4 \quad \dots \quad (23.4)$$

where,

$$M = 2a\rho A$$

Thus equation (23.0) can be written in the form with the help (23.4),

$$y_a = \frac{v}{\beta} \cdot \frac{1}{D(D^2 + \alpha^2)} = \frac{v_0}{\beta\alpha^2} \left[ t - \frac{1}{\alpha} \sin \alpha t \right] \quad \dots \quad (24.0)$$

where,

$$\alpha = \left[ \frac{1}{\beta} \left( 1 + \frac{M}{3m} - \frac{Ma^2T}{90mEI} \right) \right]^{1/2} \quad \dots \quad (24.1)$$

$$\beta = \frac{Ma^4\rho A}{1890mEI} \quad \dots \quad (24.2)$$

Substituting the values of  $\alpha$  and  $\beta$  in (24.0) we get,

$$y_a = \frac{v_0}{\left(1 + \frac{M}{3m} - \frac{Ma^2T}{90mEI}\right)} \left[ t - \frac{\sin \left\{ \frac{1890mEI}{Ma^4\rho A} \left(1 + \frac{M}{3m} - \frac{Ma^2T}{90mEI}\right)\right\}^{\frac{1}{2}} \cdot t}{\left\{ \frac{1890mEI}{Ma^4\rho A} \left(1 + \frac{M}{3m} - \frac{Ma^2T}{90mEI}\right)\right\}^{\frac{1}{2}}} \right] \quad \dots (24.3)$$

If now the stiffness of the string is very large compared to tension (24.3) becomes,

$$y_a = \frac{v_0}{\left(1 + \frac{M}{3m}\right)} \cdot t \quad \dots (24.4)$$

Equation (24.4) shows that when stiffness is very large the string behaves as a rigid rod, a conclusion similar to that derived by Ghosh (1938) in the case of pianoforte string of very short length.

Pressure exerted by the load during impact as obtained by equation (22.0) and (24.0), is given by,

$$P = mD^2y_a \\ = - \frac{mv_0}{\beta\alpha} \sin \alpha t. \quad \dots (25.0)$$

Thus the pressure exerted by the load on the string at the beginning is zero and attains a maximum value  $mv_0/\beta\alpha$  after a time  $\pi/2\alpha$  and the pressure falls to zero at the end of time  $t = \phi$  the duration of impact, given by

$$\phi = \frac{\pi}{\alpha} = \frac{\pi}{\left[ \frac{1890mEI}{Ma^4\rho A} \left(1 + \frac{M}{3m} - \frac{21c^2}{a^2}\right) \right]^{\frac{1}{2}}} \quad \dots (26)$$

#### ACKNOWLEDGMENT

The author expresses his thanks to Dr. S. K. Ghosh Reader of Physics, Jadavpur University, for guidance in preparing the paper.

#### REFERENCES

- Kar, K. C., 1956, *Int. to Th. Phys.*, **11**, 162.  
 Ghosh, M., 1938, *Ind. J. Phys.*, **12**, 437.  
 Ghosh, S. K., 1953, *Indian J. Theo. Phys.*, **1**, No. 1.

# RESPONSES IN A PIEZO-ELECTRICAL PLATE-TRANSDUCER

S. K. GHOSH AND SUNIL KUMAR BANERJI

DEPARTMENT OF PHYSICS, JADAVPUR UNIVERSITY, CALCUTTA-32

(Received August 11, 1965)

**ABSTRACT.** The responses of a Piezo Electrical Plate Transducer, vibrating in a thickness mode excited by transient stress input has been worked out following the powerful operational method due to Heaviside. The problem is discussed in two different cases, (a) the transducer is open at both ends, (b) to one end of the transducer there is a resistance loading. As a particular case the results corresponding to periodic stress input to the Plate Transducer has also been discussed in the present paper.

## INTRODUCTION

Rigorous theory for a Piezo-Electric Crystal Vibrator of any form and orientation, vibrating in any desired mode would have to take account of all boundary conditions, size and position of electrodes, losses due to dielectric and mounting non-linear effects, coupling due to different modes of vibration, non-uniformity of electric field, and when the electrodes separated by a gap, including possible resonance effect in the air itself. While no such general theory has been attempted, special problem involving most of these considerations have been attacked by many writers. We consider a few simple cases here. In practice, the commonest type of Piezo-Transducers are the bar, vibrating compressionally lengthwise and the Plate vibrating in the thickness mode. For this purpose one employs an X-cut quartz plate. With this cut the vibrations are compressional, the Plate becoming alternately thicker and thinner. The experimental evidence of this mode of vibration is that acoustics waves in the air are emitted from the surface. A number of practical problems involve the application of a transient electrical or mechanical signal to Piezo Electrical Transducer and also continuous wave generation for ultrasonic use and detection. Redwood (1961) has studied the characteristics of transient pulses, responses etc. for a Piezo Electric Transducer (both Plate and Bar) in the case when the input exciting function is a step function. In this paper the input is taken as a mathematical function of time. Special cases have been worked out using sinusoidal exciting function both Mechanical and Electrical acting as continuous wave-guide which, as Redwood has remarked elsewhere, is nearer the type of source obtained in practice than those represented by simple mathematical functions. The results worked out here after reasonable approximations agree with the results arrived at by Redwood.

EXPLANATIONS OF THE SYMBOLS USED

$X$  = Length of the Plate

$t$  = Variable time.

$x$  = Variable length, measured along the length of the Plate.

$\xi$  = Mechanical displacement of any particle in the  $x$ -direction

$\xi_0$  = Mechanical displacement of any particle at  $x = 0$ .

$v$  = Velocity of propagation of wave along the Plate

$F$  = Mechanical stress applied to the surface normal to  $x$ -direction at  $x = 0$

$h$  = Piezo-electric constant.

$Q$  = Total charge at the surface of the Plate

$V$  = Potential across the Plate from  $x = 0$  to  $x = X$ .

$E$  = Young's Modulus of the material of the Plate

$C_0$  = Static Capacitance of the Plate-transducer.

$R$  = Resistance due to Plate Transducer.

$D = \frac{d}{dt}$  (Operator).

SOLUTION OF THE PROBLEM

In the present problem we propose to find out electrical response when a Piezo-electric Plate transducer is excited by transient mechanical stress input and vice-versa. The equation of vibration of a Piezo-electric Plate-transducer is,

$$\frac{\partial^2 \xi}{\partial t^2} = v^2 \frac{\partial^2 \xi}{\partial x^2} \quad \dots (1.0)$$

solution of which is,

$$\xi = A \cosh \frac{D}{v} x + B \sinh \frac{D}{v} x \quad \dots (1.1)$$

$A, B$  being constants.

We consider that the Plate is vibrating mechanically in a thickness-mode and the  $x$ -axis coincides with this particular direction. The potential difference across the Plate transducer is related with the corresponding displacements of the two ends of the Plate by,

$$V = - [(\xi)_{x=X} - (\xi)_{x=0}] + \frac{Q}{C_0} \quad \dots (2.0)$$

The equation for the plane compressional wave propagation along  $x$ -direction at  $x = 0$  of the Plate can be written as,

$$F + hQ = E \left( \frac{\partial \xi}{\partial x} \right)_{x=0} \quad \dots (3.0)$$

The problem has been discussed in two distinct cases. In case I, the transducer is open at both ends i.e., the Plate is cemented between two semi-infinite mechanical systems and in case II, to one end of the transducer there is a resistance loading analogous to the case of a fixed-free system.

The two cases are explained following the powerful operational method due to Heaviside which is very straight forward, shortcut and gives results of higher accuracy.

#### *Case I*

Here the circuit may be taken to be open, the condition for which is at

$$x = 0, \quad \xi = \xi_0 \quad \dots \quad (4.0)$$

$$x = X, \quad \frac{\partial \xi}{\partial x} = 0 \quad \dots \quad (4.1)$$

$$Q = 0$$

Relation (4.1) together with these end-conditions give

$$\xi = \xi_0 \frac{\cosh(Dr)(c - X)}{\cosh(Dr)X} \quad \dots \quad (5.0)$$

and the equation for compressional wave propagation is,

$$F = E \left( \frac{\partial \xi}{\partial r} \right)_{r=0} \quad \dots \quad (5.1)$$

From (5.0) and (5.1)

$$\xi_0 = - \frac{Fr}{E} \cdot \frac{1}{D} \coth \frac{D}{r} X \quad \dots \quad (5.2)$$

Thus the potential difference as obtained by the help of (5.2) and (2.0) is

$$V = - \frac{hFr}{E} \left[ \tanh \left( \frac{1}{2} \frac{D}{r} X \right) \right] H(t) \quad \dots \quad (6.0)$$

$$\text{where,} \quad H(t) = \int \phi(t) dt, \quad F(t) = F_0 \phi(t) \quad \dots \quad (6.1)$$

The equation (6.0) representing the series can also be summed up like a geometrical progression when

$$V = - \frac{hFr}{E} (1 - 1) \left[ \frac{t - \frac{X}{r}}{r} \right] (t = 0) \quad \dots \quad (6.2)$$

The average value of  $t/(X/r)$  for  $t$  between  $nX/r$  and  $(n+1)X/r$  is,

$$n + \frac{1}{2} = \left[ \frac{t - \frac{X}{r}}{r} \right] = \frac{1}{2}$$

where  $\left[ t/\frac{X}{c} \right]$  is the greatest integer but not greater than  $t/\frac{X}{c}$ . Then the quantity

$$t/\frac{X}{c} - \left[ t/\frac{X}{c} \right] = \frac{1}{2} \quad \text{at } t = 0$$

increases uniformly to  $1 - \frac{1}{2}$  as  $t \rightarrow \infty$ , drops discontinuously at  $t = \frac{X}{c}$  to  $-\frac{1}{2}$  and then repeats itself periodically. This elementary theory does not take into account the attenuation due to losses within the material (Jefferys 1956).

If the mechanical stress applied be periodic step input i.e. if

$$F(t) = F_0 \cos \omega t = H(t) \frac{\sin \omega t}{\omega} \quad \dots (7.0)$$

From (6.0) and (7.0) it follows that there corresponds a periodic step voltage response in agreement with that derived by Sinha (1962).

#### *Case II*

Here the transducer is connected to a finite electrical impedance or resistance  $R$  ohms. The boundary conditions are at

$$\left. \begin{aligned} t = 0 \quad \xi = \xi_0 \\ t = X \quad \xi = \xi_1 = 0 \end{aligned} \right\} \quad \dots (8.0)$$

The relation (1.1) with the above boundary conditions give

$$\begin{aligned} \xi - \xi_0 &= \sinh \frac{D}{c} (X - c) \\ &= \sinh \frac{D}{c} X \end{aligned} \quad \dots (9.0)$$

and the electro-mechanical stress relation at the input end of the Plate is given by,

$$F = hQ = E \left( \frac{\partial \xi}{\partial r} \right)_{r=0} \quad \dots (10.0)$$

From (9.0) and (10.0)

$$\xi_0 = \frac{(F - hQ)c}{E} = \frac{1}{D} \tanh \frac{D}{c} X \quad \dots (10.1)$$

The expression for the electrical response can now be obtained by the help of the equations (10.1), (2.0) and the relation  $V = DQR$  to be

$$V = \frac{hFc}{E} = \frac{1}{\psi(D)} \quad \dots (11.0)$$

where,

$$\psi(D) = \left[ 1 + \frac{1}{D C_0 R} - \frac{h^2 v}{ER} \cdot \frac{1}{D^2} \tanh \frac{D}{a} X \right] \left[ \frac{1}{D} \tanh \frac{D}{v} X \right] \dots \quad (11.1)$$

Now substituting the exponential values for hyperbolic tangents in equation (11.1) and writing  $D+\alpha \equiv D_1$ ,  $D+\beta \equiv D_2$  respectively, we get

$$\psi(D) = \frac{D_1 D_2}{D \left\{ 1 - \exp \left( -\frac{2DX}{v} \right) \right\}} \left[ 1 + \left\{ 1 - \frac{2\alpha\beta}{D_1 D_2} \right\} \exp \left( -\frac{2DX}{v} \right) \right] \dots \quad (11.2)$$

$$\text{where, } D_1 D_2 = (D+\alpha)(D+\beta) = D^2 + \frac{1}{C_0 R} D - \frac{h^2 v}{ER} \dots \quad (12.0)$$

and  $-\alpha$ ,  $-\beta$  are the roots of the equation,  $D_1 D_2 = 0$  given by,

$$[\alpha, \beta] = \frac{1}{2} \left[ \frac{1}{C_0 R} + \left( \frac{1}{C_0^2 R^2} + \frac{4h^2 v}{ER} \right)^{\frac{1}{2}} \right] \dots \quad (12.1)$$

With the help of (11.0) and (11.2) the difference of potential across the ends of the Piezo-electric Plate transducer can be obtained as,

$$V = -\frac{h\nu F}{E} \cdot \frac{D}{D_1 D_2} \left\{ 1 - \exp \left( -\frac{2DX}{v} \right) \right\} \left[ 1 + \left\{ 1 - \frac{2\alpha\beta}{D_1 D_2} \right\} \exp \left( -\frac{2DX}{v} \right) \right]^{-1} \dots \quad (13.0)$$

Neglecting terms containing higher powers of  $\alpha\beta$  other than unity in the multinomial expansion of relation (13.0) we obtain,

$$V = -\frac{h\nu F}{E} \left[ \frac{D}{D_1 D_2} - \left( \frac{2D}{D_1 D_2} - \frac{2\alpha\beta D}{D_1^2 D_2^2} \right) \exp \left( -\frac{2DX}{v} \right) + \left( \frac{2D}{D_1 D_2} - \frac{6\alpha\beta D}{D_1^2 D_2^2} \right) \right. \\ \left. \exp \left( -\frac{4DX}{v} \right) - \left( \frac{2D}{D_1 D_2} - \frac{10\alpha\beta D}{D_1^2 D_2^2} \right) \exp \left( -\frac{6DX}{v} \right) + \dots \right] \dots \quad (13.1)$$

Thus,

$$V = \left[ f'_1(t) - \{2f'_1(t) - 2f_2(t)\} \exp \left( -\frac{2DX}{v} \right) + \{2f'_1(t) - 6f_2(t)\} \exp \left\{ -\frac{4DX}{v} \right\} \right. \\ \left. - \{2f'_1(t) - 10f_2(t)\} \exp \left( -\frac{6DX}{v} \right) + \dots \right] \dots \quad (13.2)$$



$$\begin{aligned} \text{where, } f_1(t) &= -\frac{h\nu F}{E} \cdot \frac{1}{D_1 D_2} \\ &= -\frac{h\nu F}{E} \cdot \left(\frac{1}{\alpha} - \frac{1}{\beta}\right) \left[ \frac{1}{\beta} (1 - e^{-\beta t}) - \frac{1}{\alpha} (1 - e^{-\alpha t}) \right] \quad \dots \quad (14.0) \end{aligned}$$

$$\begin{aligned} \text{and } f_2(t) &= -\frac{h\nu F}{E} \cdot \frac{\alpha\beta D}{D_1^2 D_2^2} \\ &= -\frac{h\nu F}{E} \frac{\alpha\beta}{(\alpha-\beta)^2} \left[ \frac{1}{\beta} \left( 1 - \frac{\alpha+\beta}{\alpha-\beta} + \beta t \right) e^{-\beta t} + \frac{1}{\alpha} \left( 1 + \frac{\alpha+\beta}{\alpha-\beta} + \alpha t \right) e^{-\alpha t} \right] \\ &\quad \dots \quad (14.1) \end{aligned}$$

Therefore,

$$\begin{aligned} V &= \left[ f'_1(t) - \left\{ 2f'_1 \left( t - \frac{2X}{v} \right) - 2f_2 \left( t - \frac{2X}{v} \right) \right\} \right. \\ &\quad + \left\{ 2f'_1 \left( t - \frac{4X}{v} \right) - 6f_2 \left( t - \frac{4X}{v} \right) \right\} \\ &\quad \left. - \left\{ 2f'_1 \left( 1 - \frac{6X}{v} \right) - 10f_2 \left( t - \frac{6X}{v} \right) \right\} + \dots \right] \quad \dots \quad (15.0) \end{aligned}$$

Relation (15.0) is the electrical voltage response corresponding to the given mechanical stress input to the Plate transducer, a result quite in agreement with that derived by Redwood (1961).

## DISCUSSIONS

*Discussion I:* If further approximation be made in the right hand side expression for the value  $V$  in (15.0) by neglecting terms containing higher powers of  $h$  other than one, the expression for  $V$  is,

$$V = \left[ f'_1(t) - 2f'_1 \left( t - \frac{2X}{v} \right) + 2f'_1 \left( t - \frac{4X}{v} \right) - \dots \right] \quad \dots \quad (16.0)$$

The first term of which is,

$$f'_1(t) = -\frac{h\nu F}{E} \cdot \frac{D}{D_1 D_2} \quad \dots \quad (17.0)$$

$$= -\frac{h\nu F}{E} \cdot \frac{e^{-\beta t} - e^{-\alpha t}}{\alpha - \beta} \quad \dots \quad (17.1)$$

$$\frac{h\nu_0 RF}{E} \left( 1 - e^{-\frac{1}{c_0 R} t} \right) \quad (17.2)$$

Now  $R$  is very large

$$f'_1(t) = \frac{h\nu F}{E} e^{-t} \quad (18.0)$$

Thus to the first order of approximation

$$V = \frac{h\nu F}{E} e^{-t} \quad (19.0)$$

Equation (19.0) shows  $V$  is linearly dependent on time  $t$

*Discussion II* If periodic stress is applied i.e. if

$$F = F_1 e^{i\omega t} = F_1 \frac{D}{D - i\omega} \quad (20.0)$$

The first term of the expression of  $V$  in equation (16.0) is

$$f'_1(t) = \frac{h\nu F_1}{E} \frac{D}{(D - i\omega)D_1 D_2} \quad (21.0)$$

Since  $\alpha = \beta - i\omega$  are the simple zeros of the denominator by Heavisides expansion theorem we get

$$f'_1(t) = \frac{h\nu F_1}{E} \left[ \frac{\alpha e^{-\alpha t}}{(\alpha - i\omega)(\alpha - \beta)} + \frac{\beta e^{-\beta t}}{(\beta - i\omega)(\beta - \alpha)} + \frac{i\omega e^{i\omega t}}{(\alpha - i\omega)(\beta - i\omega)} \right] \quad (21.1)$$

The real part of the right hand side of (21.1) is given by,

$$\frac{h\nu F_1}{E} \left[ \frac{\beta^2 e^{-\beta t}}{(x^2 - \omega^2)(\beta - \alpha)} + \frac{\beta^2 e^{-\beta t}}{(\beta^2 - \omega^2)(\beta - \alpha)} + \frac{\omega^2(x + \beta)}{(x^2 - \omega^2)(\beta^2 - \omega^2)} \cos \omega t \right. \\ \left. + \frac{\omega(x\beta - \omega^2)}{(x^2 - \omega^2)(\beta^2 - \omega^2)} \sin \omega t \right] \quad \dots \quad (22.0)$$

Since the higher powers of  $h$  is neglected we have,  $\beta \rightarrow 0$ ,  $\alpha \approx 1/c_0 R$ . If now  $R$  is very large  $\alpha \rightarrow 0$  and the first term of  $V$  becomes

$$V = \frac{h\nu F_1}{E} \frac{1}{\omega} \sin \omega t \quad \dots \quad (23.0)$$

quite similar to that obtained by Sinha in the case of an open circuit.

If further  $\omega$  is very small (23.0) becomes

$$\frac{hrF_1}{E} \quad \dots \quad (24.0)$$

Thus the electrical voltage response under different cases and approximations can be obtained by results in relations (6.3) (7.0) (15.0) (23.0) and (24.0).

The converse problem i.e. the Mechanical stress response corresponding to voltage input is under consideration of the authors and will be published soon.

#### REFERENCE §

- Jefferys, H., 1956, *Methods of Mathematical Physics*, pp. 406.  
 Redwood, M., 1961, *Jour. of Acoust. Soc. of Amer.*, **33**, No. 4, 527.  
 Sinha, D. K., 1962, *Ind. Jour. of Theor. Phys.* **10**, No. 1 pp. 21-28.

# Letters to the Editor

*The Board of Editors does not hold itself responsible for opinions expressed in the letters published in this section. The notes containing short reports of original investigations communicated to this section should not contain many figures and should not exceed 500 words in length. The contributions reaching the Secretary by the 15th of any month may be expected to appear in the issue for the next month. No proof will be sent to the author.*

23

## THE CRYSTAL STRUCTURE OF $\alpha$ -LEAD AZIDE, $\alpha$ -Pb(N<sub>3</sub>)<sub>2</sub>

PRASENJIT SAHA,

CENTRAL GLASS & CERAMIC RESEARCH INSTITUTE, JADAVPUR, CALCUTTA-32.

(Received August 6, 1965)

$\alpha$ -Lead Azide crystallizes in the Orthorhombic system, Space Group Pna2<sub>1</sub>;  $Z = 12$ ; calculated density = 4.705;  $a = 6.65 \text{ \AA}$ ,  $b = 11.37 \text{ \AA}$ ,  $c = 16.32 \text{ \AA}$ . Earlier studies of this crystal were made by Miles (1931), Pfefferkorn (1948) and Azároff (1956). Azároff came to the conclusion that the Space Group is either Pcmn or Pc2<sub>1</sub>n, and that no distinction can be made between these two Space Groups on the basis of the lead positions. Asymmetric nature of the azide group led Azároff to believe that the Space Group is Pc2<sub>1</sub>n. Subsequent three-dimensional refinement carried out by the author of the lead positions given by Azároff showed that the  $R$ -factor comes down considerably if the noncentrosymmetric Space Group is assumed. Pna2<sub>1</sub> was adopted instead of Pc2<sub>1</sub>n in order to conform to the IBM 704 programming.

Three dimensional X-ray data using Cu $\text{K}\alpha$  radiation were collected by the author at the Crystal Research Laboratory, The Pennsylvania State University. This compound has the properties of a detonator, and considerable experimental difficulties were encountered while taking the three-dimensional X-ray data. Mo $\text{K}\alpha$  radiation could not be used since it was found that the crystals, when irradiated, started to disintegrate after three or four days. Linear absorption coefficient for Cu $\text{K}\alpha$  radiation was found to be extremely high ( $\mu = 819 \text{ cm.}^{-1}$ ), and hence it was necessary to correct for absorption. The crystals could not be made into cylinders because of the danger of explosion. A uniform cylindrical absorption correction for the crystals was assumed, though the crystals were prismatic and somewhat rhombic in cross-section. After 3 to 4 days' irradiation, the crystals started to disintegrate, and hence separate crystals had to be used to obtain data for each layer. Data on six layers (971 observable reflections) were collected in

this fashion. Since "a" was the zone axis for the prisms and the crystals could not be cut across the prism faces without the danger of explosion, it was not possible to obtain  $hk0$  or  $h0l$  data. The three-dimensional data were scaled and rescaled after each phase of IBM computation by calculating scale factors ( $\Sigma F_o/\Sigma F_e$ ) for each layer from structure factor calculations. Owing to these experimental difficulties it was assumed that the X-ray data would not be too accurate, though they were subsequently found to be accurate enough for distorted nitrogen peaks to appear in the three-dimensional Fourier sections calculated with lead positions only. More reliance was placed on the  $0kl$  neutron data for absolute confirmation of the structure determination, collected by Danner and Kay at the Brookhaven National Laboratory.

### Structure Determination

Consideration of two sets of strong reflections (006 and 203 for Space Group Pnma) led Azároff (1956) to propose the following approximate coordinates of the lead atoms :

$$8 \text{ Pb atoms in } (d) \quad x = \sim 3/8 \quad y = 0.130 \quad z = 0.083$$

$$4 \text{ Pb atoms in } (c) \quad x = \sim 1/8 \quad y = 0.870 \quad z = 1/4$$

Structure factors calculated with these coordinates were used by the author to scale different layers. These coordinates were then used for three-dimensional refinement of the lead positions using Space Group Pna2<sub>1</sub>. The *R*-factor dropped from 0.62 to 0.45. The observed data for different layers were then rescaled and further refinement of the lead positions resulted in the following coordinates :

$$4 \text{ Pb atoms in } (a) \quad x = 0.331 \quad y = 0.136 \quad z = 0.084$$

$$4 \text{ Pb atoms in } (a) \quad x = 0.344 \quad y = 0.122 \quad z = 0.407$$

$$4 \text{ Pb atoms in } (a) \quad x = 0.069 \quad y = 0.872 \quad z = 0.237$$

The *R*-factor dropped from 0.42 to 0.36.

At this stage the three-dimensional Fourier sections began to show distorted peaks in the non-lead positions, and approximate coordinates for nine nitrogen atoms could be found out. The coordinates of these nine atoms were then used in conjunction with the refined lead positions for the next cycle of refinement. The *R*-factor dropped from 0.32 to 0.21. Positions of the rest of the nitrogen atoms could be discerned in the new three-dimensional Fourier sections, though considerable difficulties were encountered because of the presence of ripples around the lead peaks, which sometimes rather obscured the nitrogen peaks.

Approximate coordinates of the lead and nitrogen atoms in the structure of  $\alpha$ -lead azide has thus been ascertained with the help of three-dimensional X-ray data, and they are listed in Table I :

TABLE I

Type of atom

Pb	0.064	0.867	0.240	3.532
Pb	0.344	0.119	0.406	3.252
Pb	0.333	0.131	0.084	3.835
N	0.163	0.281	0.184	2.50 approx.
N	0.154	0.276	0.251	2.50 „
N	0.146	0.271	0.326	2.50 „
N	0.098	0.228	0.488	2.50 „
N	0.108	0.267	0.560	2.50 „
N	0.116	0.300	0.624	2.50 „
N	0.122	0.284	0.860	2.50 „
N	0.110	0.262	0.924	2.50 „
N	0.100	0.239	0.996	2.50 „
N	0.500	0.490	0.365	2.50 „
N	0.362	0.498	0.407	2.50 „
N	0.213	0.506	0.443	2.50 „
N	0.875	0.468	0.243	2.50 „
N	0.025	0.528	0.240	2.50 „
N	0.163	0.592	0.237	2.50 „
N	0.475	0.495	0.117	2.50 „
N	0.337	0.489	0.084	2.50 „
N	0.188	0.481	0.048	2.50 „

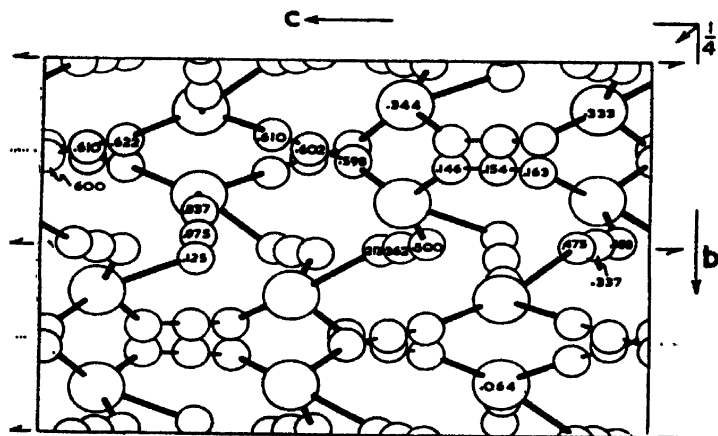


Fig. 1. Approximate Structure of  $\alpha$ -Pb (N<sub>3</sub>)<sub>2</sub>  
 O—lead      O—nitrogen

A diagrammatic representation of the structure in the  $0kl$  plane has been shown in Fig. 1.

The observed data require about two or more cycles of refinement and data for each layer require rescaling after each cycle of refinement.

$0kl$  structure factor calculations were made with the S-FAC giving equal weight to the lead and nitrogen atoms (neutron scattering length for lead is  $0.96 \times 10^{-12}$  cm. and that for nitrogen is  $0.94 \times 10^{-12}$  cm.) and using the coordinates listed above. The calculated data has been compared to the observed  $0kl$  neutron data for  $\alpha$ -Pb(N<sub>3</sub>)<sub>2</sub>, and the correspondence between the observed and calculated structure factors for low and moderately high order reflections was found to be quite good. It may be difficult to refine the neutron data owing to the overlap of several nitrogen and lead atoms in the  $0kl$  projection, as shown in Fig. 1.

#### DISCUSSION OF THE STRUCTURE

A 4-fold configuration of nitrogen atoms around lead (Fig. 1), somewhat intermediate between a distorted pyramid and a square, can be postulated in the case of  $\alpha$ -lead azido.

From bond energy considerations Pauling and Brockway (1937) have shown that the linear azido group will be asymmetric if the bonding is homopolar, as in the case of  $\alpha$ -lead azido. Indications of this are already evident in the case of  $\alpha$ -lead azide, and further refinement of the structure will most probably confirm this. In most organic and metal azides it has been found that the angle between the nitrogen atoms at the ends of the azide group and the heavy atom or molecular group attached to them is apparently  $120^\circ$  (Wells, 1945) and this has also been found to be true in the case of  $\alpha$ -lead azide.

Further refinement of the structure is required to calculate accurate bond distances and bond lengths.

#### REFERENCES

- Azaroff, Leonid V., 1956, *Zeit. Krist.*, **107**, 362-369.  
Miles, F. D., 1931, *J. Chem. Soc. (London)*, 2532.  
Pauling, L. and Brockway, L. O., 1937, *J. Amer. Chem. Soc.*, **59**, 13.  
Pfefferkorn, Gerhard, 1948, *Z. Naturforsch.*, **3**, 364.  
Wells, A. F., 1945, *Structural Inorganic Chemistry*, 2nd Ed., Clarendon Press Oxford, pp. 164-166.

# INTEGRATED FIELD INTENSITY OF ATMOSPHERICS IN RELATION TO MONSOON THUNDERCLOUDS

M. K. DAS GUPTA AND A. K. SEN

INSTITUTE OF RADIO PHYSICS AND ELECTRONICS, CALCUTTA UNIVERSITY

(Received September 7, 1965)

Close association of atmospherics with thunderstorms is now well established. During the International Geophysical Year, observational programme directed solely towards the location and tracking of thunderstorms by recording atmospherics at a distance were undertaken in several countries (Pierce, 1956; Aipert and Borodina, 1956; Skieb, 1956; Maikowski, 1957; Kimpapa, 1959, Samson and Linefield, 1962). In fact, even a single thunderstorm of nearby origin may give rise to quite large increase of atmospheric radio noise (Yabsley, 1960; Aiya, 1962). Large enhancements of atmospherics associated with severe pre-monsoon thunderstorms, popularly known as Nor'wester, were observed in Calcutta (Das Gupta and Sen, 1963; Sen, 1965a). Thundersqualls occurring in the monsoon season (June to October) also give rise to somewhat similar enhancements with, however, certain characteristic features. We were thus prompted to examine the daily records of the integrated field intensity of atmospherics particularly in relation to monsoon thunderstorms to study in details the nature of this association.

For the last four years we have been recording the integrated field intensity of atmospherics (abbreviated henceforth as i.f.i.a.) at Calcutta (lat.  $22^{\circ}34'N$ , long.  $88^{\circ}24'E$ ) on 30 kc/s. The receiver employed for the present observations was based on the design adopted during the International Geophysical Year (Ellison, 1955) primarily for the purpose of solar flare patrol by the s.e.a. technique (sudden enhancement of atmospherics subsequent to solar flares) with some modifications. In Fig. 1 three typical records as obtained at Calcutta are shown. The upper one shows the i.f.i.a. recorded on a normal premonsoon day (26 March, 1962) while the lower two show i.f.i.a. when severe thundersqualls were experienced in and around Calcutta on two different dates. The record on a normal day shows the usual diurnal variations in the integrated field intensity of atmospherics (WMO, 1957) viz., sunrise drop (A), morning minimum (D), afternoon maximum (E), late minimum (F) and night maximum (G). The record (lower-left) on a disturbed day shows the sunrise effect (A) and morning minimum (D), after which unusually large enhancement of i.f.i.a. occurs, starting at 13-20 hrs. I.S.T. and obscuring E, F and G as observed on a normal day. Simi-



larly on another occasion as shown in the lower-right record the gradual increase in i.f.i.a. is also quite marked. However the predominant feature of these records seems to be the sudden decrease of i.f.i.a. about the time of onset of heavy raining associated with the thundersquall as obtained from meteorological data. Figure in the left shows that i.f.i.a. starts decreasing at 18-00 hrs. I.S.T. while the local raining started at 17-20 hrs. I.S.T. and for the other one these occurred at 15-05 hrs. and 15-20 hrs. I.S.T. respectively.

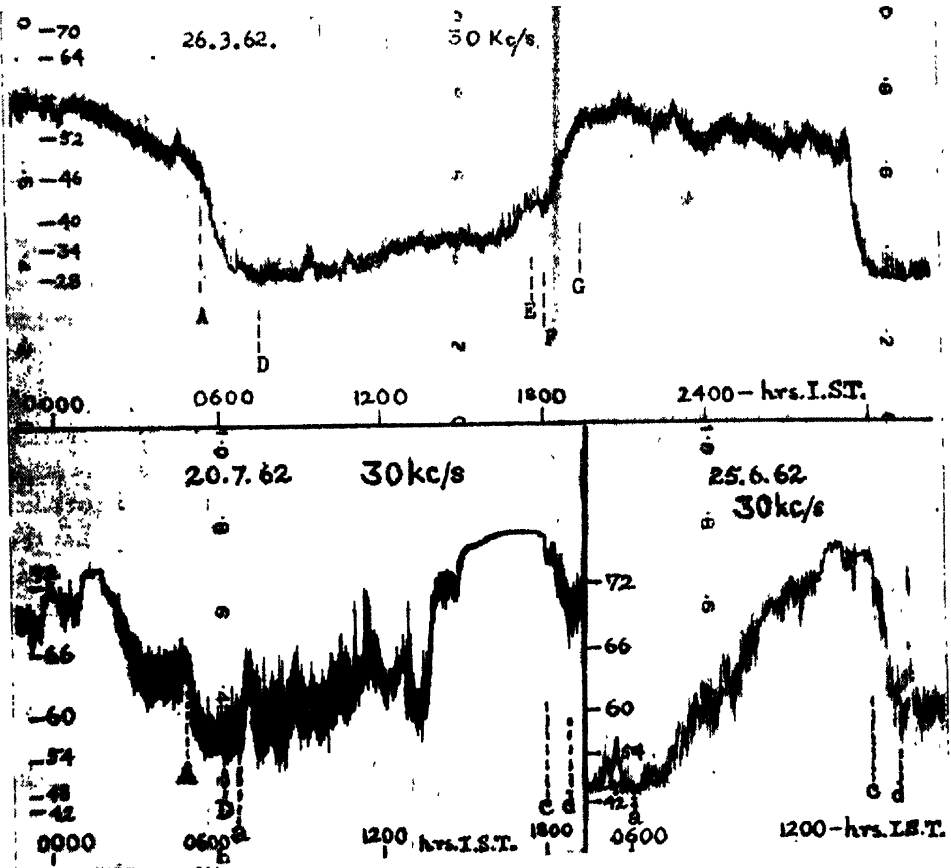


Fig. 1. Upper record shows the usual diurnal variations in the integrated field intensity of atmospherics on a normal premonsoon day (A : sunrise effect; D : morning minimum; E : afternoon maximum; F : late minimum; G : night maximum). The record on the lower left shows i.f.i.a. on a day when a severe thundersquall was experienced in Calcutta (a : i.f.i.a. starts rising gradually; c : decrease of i.f.i.a. starts; d : i.f.i.a. regains normal value). The lower right record shows i.f.i.a. on another day when a severe thundersquall was experienced in Calcutta. The ordinate shows the r.m.s. field strength for a 1 kc/s bandwidth in decibels above 1 $\mu$ V/m.

The results obtained in this analysis can be summarised as follows :

1. During the monsoon period under observation (June-September) there were altogether eleven thundersqualls reported by the Meteorological Department. In all these cases gradual increase in i.f.i.a. as shown in the above illustrations was detected.

2. The increase started in general 4 to 11 hours before the reported time of respective thundersqualls.

3. In all the cases sudden decrease of i.f.i.a. as depicted in the illustrations above occurred within  $\pm 20$  mins. of the reported time of onset of raining associated with the thundersquall. However, in majority of the cases the starting time of sudden decrease in i.f.i.a. seemed to cluster around the time of onset of the raining.

4. I.f.i.a. came down to the normal value within 12 to 180 minutes after the observed starting time of the decrease mentioned above.

The close association of the sudden decrease of i.f.i.a. with the onset of the heavy raining appears to be something peculiar to the monsoon thunderclouds. The sudden decrease of i.f.i.a. might be attributed to the falling out of charged rain from the cloud layer leading to a vanishing of the bipolar structure of the cloud. As a result probably all electrical discharges within the layer ceased.

It is now generally accepted that in a thundercloud, there are two processes of charge separation, one in the region above the freezing point level and the other below. Chaimers (1956) suggested that the two processes of charge separation are opposite to each other. In the present observations it appears likely that the process occurring below the freezing point level is significant, at least in the final stage of the cloud development. It might be that the Dinger and Gunn process of melting ice is at work at such times. According to them (Dinger and Gunn, 1946), ice particles contain entrapped air. On melting the entrapped air becomes charged negatively while the water drops receive positive charge. It thus appears that when the drops begin to fall as rain the bipolar structure of the cloud layer vanishes leading to the observed sudden decrease of i.f.i.a. That the i.f.i.a. decreases with raining also lends support to a view that the process of charge separation above the freezing point level characterized by its association of a marked increase of i.f.i.a. (Sen, 1965a) is significant in the final stage of the cloud development.

In support of the above discussions reference may be made to a recent evidence obtained from the measurement of the time lag between electric field change at ground and the onset of rain which also supports the view that the raining occurs from a height below the freezing level in cases of thunderstorms occurring in the monsoon season (Sivaramakrishnan, 1960). Comparative studies on i.f.i.a. associated with nor'westers and monsoon thundersqualls over an extended period

are in progress and will be reported in due course. It appears that simultaneous observations of i.f.i.a. supplemented by directional studies and of radar reflections from the thunderclouds might prove to be useful in locating the seat of the different types of enhancements as well as the decrease associated with the monsoon thunderclouds and might provide new insight into the process of formation of such thunderclouds.

We are grateful to Prof. J. N. Bhar. Head of the Department of Radio Physics and Electronics, Calcutta University, for his kind interest. Thanks are due to Dr. S. N. Sen, Regional Director, Alipore Meteorological Observatory, India Meteorological Department, Government of India, for kindly providing us with the relevant meteorological data. One of us (A.K.S.) is also thankful to the University Grants Commission, Government of India for financial assistance.

#### REFERENCE S

- Aiya, S. V. C., 1962, *J. Sci. Industr. Res.*, **21D**, 203.  
 Aipert, Y. L. and Borodina, S. V., 1956, *Radiotek. Electron.*, **3**, 293.  
 Chaimers, J. A., 1956, *J. Atmosph. Terr. Phys.*, **9**, 311.  
 Das Gupta, M. K. and Sen, A. K., 1963, *J. Atmosph. Terr. Phys.*, **25**, 306.  
 Dinger, J. E. and Guin, R., 1946, *Terr. Mag. Atmosph. Elect.*, **51**, 477.  
 Ellison, M. A., 1955, U.R.S.I. Information Bulletin No. 92, 12.  
 Kimpara, A., 1959, *Recent Advances in Atmospheric Electricity*, Pergamon, 565.  
 Malkowski, G., 1957, *Arch. Met. Wien.*, **10A**, 101.  
 Pierce, E. T., 1956, *Vistas in Astronomy*, Pergamon, 2850.  
 Samson, C. A. and Linefield, R. F., 1962, *J. Geophys. Res.*, **67**, 627.  
 Sen, A. K., 1965a, *J. Atmosph. Terr. Phys.*, to be published.  
 Sivaramakrishnan, M. V., 1960, *Indian J. Met. Geophys.*, **11**, 258.  
 Skieb, G., 1956, *Deutscher Wett. Berichte*, **4**, 146.  
 W. M. O., 1957, Final report of the working group of atmospherics, World Meteorological Organization.  
 Yabsley, D. E., 1960, C.S.I.R.O. (Australia), Division of Radiophysics, RPR 136.

# SPACE GROUP AND UNIT CELL DIMENSIONS OF COPPER PROPIONATE MONOHYDRATE

(Mrs.) ALOKA PODDER AND S. N. GIRI

INDIAN ASSOCIATION FOR THE CULTIVATION OF SCIENCE, CALCUTTA-32.

(Received September 16, 1965)

Copper propionate monohydrate crystals are obtained by slow evaporation from an aqueous solution of the substance.

The crystals belong to the monoclinic system.

The unit cell dimensions are obtained from rotation and Weissenberg photographs along  $[01(\sigma)]$ . That the unit cell is a reduced one is tested by Buerger's method (1957). The dimensions of the unit cell are given below :

$$a = 15.2 \text{ \AA}$$

$$b = 17.4 \text{ \AA}$$

$$c = 15.4 \text{ \AA}$$

$$\text{and } \beta = 94^\circ 18'$$

They correspond well with Groth's values of  $a : b : c = 0.874 : 1 : 0.886$  and  $\beta = 94^\circ 22'$ .

Zero and first layer Weissenberg photographs along  $[010]$  and  $[001]$  were taken and the following systematic extinctions were observed.

$hkl$ — all present

$hol$ — $h = 2n+1$  absent

$oko$ — $k = 2n+1$  absent

From the above conditions the space group is assigned as  $P2_1/a$ .

The density was determined by flotation method by using a mixture of bromoform and benzene. This gives a value of  $d = 1.42 \text{ g cm}^{-3}$ . The density calculated by considering 16 molecules in the unit cell is  $1.48 \text{ g cm}^{-3}$ .

Further work on the determination of the complete structure of the substance is in progress.

The authors express their sincerest gratitude to Dr. R. K. Sen D.Sc. for constant guidance, and to Prof. K. Banerjee, D.Sc., F.N.I. for his kind encouragement throughout the course of the work. One of the authors (S.N.G.) is grateful to C.S.I.R. for financial help.

REFERENCES

- Buerger, M. J., 1957, *Zeit. Krist.*, **109**, 42-60.  
Groth, P., *Chemische Kristallographie*, III, 205.

## BOOK REVIEW

**ELECTROMAGNETIC SCATTERING**—Edited by Milton Kerker. Publisher —Pergamon Press. Price £7 net.

The present book edited by Milton Kerker contains the papers presented at the interdisciplinary Conference on scattering of electromagnetic wave. The papers are divided into the following six sections :

- 1) Particle scattering
- 2) Light scattering in the atmosphere and space
- 3) Microwave and Radio wave scattering in atmosphere
- 4) Light scattering in solutions
- 5) Interactions in solids and liquids
- and 6) Multiple scattering.

The first section mainly presents new calculations of electromagnetic scattering from various types of non-spherical particles and inhomogeneous media. A few papers are concerned with the numerical calculations of the scattering intensities by the conventional theories for particles of various sizes having different values of the refractive index. A few very interesting papers in the next section analyse the observation on solar *F*-corona, zodiacal light and the cometary head on the basis of the theory of light scattering by oriented interstellar particles. Theories of back scattering of microwaves by dielectric spheroids are the subject matter of a few papers under the third section. A very useful paper in this section gives the theory of radio wave scattering by a medium possessing irregular dielectric structure and its application to explore the refractive index structure of the atmosphere which is dependant on humidity and temperature gradient. Papers in the fourth session mainly consider the scattering of light and small angle X-rays scattering by solutions of macromolecules and micellar films of soaps. The next section concerns itself with papers on the scattering of light and X-rays from dense systems—such as polymers with heterogeneous structure, metal precipitates in semi conductors etc. The application of the light scattering studies for the evaluation of the crystalline-amorphous structure of a polymeric solid is nicely discussed in a paper by Stein. The last section deals with a few theoretical papers on multiple scattering. From the above short review it is clear that the papers cover a wide field of interest and indicate the possible applications of the studies of electromagnetic scattering for characterising the structure of macromolecules as well as the atmosphere and the interstell particles. The book is very useful for future workers in various disciplines ranging from the biology to the matereology. The book is not meant, however, for the beginners. The figures and photographs are well represented. The book will be an useful addition to a Science library

*R. K. Sen*

# STUDY OF SOME ALPHA GROUPS FROM AMERICIUM—241

M. RAMA RAO

SAHA INSTITUTE OF NUCLEAR PHYSICS, CALCUTTA-9.

(Received November 3, 1965)

**ABSTRACT.** Alpha decay of Americium-241 has been investigated with a low pressure expansion cloud chamber. It has been possible to measure the energies and relative abundances of at least 5 alpha ray groups. Based on these experimental data a partial level scheme for Neptunium-237 is presented and discussed.

## INTRODUCTION

Alpha radioactivity has been observed to be a property common to all the elements beyond lead in the periodic classification of elements. The alpha particles from a given radioactive nuclide are emitted in groups with discrete energies. Investigation on the  $\alpha$ -decay characteristics of several  $\alpha$ -emitters has revealed certain interesting features common to them. Thus in the case of all even-even  $\alpha$ -emitters it has been found that transitions to the ground state of the product nucleus is most abundant, whereas transitions by a lower energy group is in lower abundance. These observations are in good agreement with the demands of the simple  $\alpha$ -decay theory presented by Gamow. There is, however, a good deal of departure from this regularity in the case of odd nucleon type. It is noticed that for the odd nucleon type, the ground state transition is most highly hindered, whereas one or more of the lower energy groups are in relatively higher abundance than would be expected on the basis of their respective energies. For example, in the case of  $\text{Am}^{241}$  which is of the odd-even type, analysis of the fine structure  $\alpha$ -ray groups in transitions to different excited levels of  $\text{Np}^{237}$  shows that the highest energy  $\alpha$ -group leading to the ground state is in very poor abundance compared to 85% abundance of a lower energy group leading to a level 59 keV above the ground state. A detailed knowledge of the energy of the several  $\alpha$ -ray groups and their abundances can possibly lead to a better understanding of the complex behaviour of such odd-even species in particular and eventually advance our ideas in the realisation of a rigid  $\alpha$ -decay theory. We choose  $\text{Am}^{241}$  as a good representative of the odd-even species for making our investigations. Besides the intrinsic interest in the  $\alpha$ -decay characteristics of  $\text{Am}^{241}$ , the energy differences of the various  $\alpha$ -groups involved allow us to picture a level scheme of the excited states of  $\text{Np}^{237}$ . Neptunium is one of the most widely studied nuclei. Information on the excited states of  $\text{Np}^{237}$  has been

obtained mostly through experiments based on (i)  $\beta$ -decay of  $\text{U}^{237}$ , Baranov (1956), Rasmussen (1957), Bunker (1957) (ii) electron capture in  $\text{Pu}^{237}$ , Haffmen (1958), (iii) coulomb excitation of  $\text{Np}^{237}$ , Newton (1958). Such information has also been obtained by Wolfson (1964) through studies on the low energy  $\gamma$ -ray transitions in  $\text{Np}^{237}$  following the  $\alpha$ -decay of  $\text{Am}^{241}$  by an examination of the internal conversion spectrum. However, relatively much less is known about the excitation levels of  $\text{Np}^{237}$  from direct measurements on  $\alpha$ -transitions in the decay of  $\text{Am}^{241}$ . Asaro *et al.* (1952) and Rosenblum (1957) have reported  $\alpha$ -transitions measured directly to seven  $\text{Np}^{237}$  levels. The recent investigations of Baranov (1964), using a magnetic spectrograph of high resolution, has considerably enhanced our knowledge by revealing the existence of a strikingly large number of  $\alpha$ -ray groups hitherto unknown.

In view of the recent findings,  $\text{Am}^{241}$  offers a worthwhile study from the view point of the intrinsic characteristics of  $\alpha$ -decay as well as the excitation levels of  $\text{Np}^{237}$  appearing through the  $\alpha$ -decay of Americium. A low pressure expansion cloud chamber has been used for resolving several of the  $\alpha$ -groups emitted by  $\text{Am}^{241}$ . Their relative intensities have also been estimated. Based on these experimental data a partial level scheme of  $\text{Np}^{237}$  is presented.

#### APPARATUS AND EXPERIMENTAL ARRANGEMENT

A low pressure expansion type cloud chamber reported by the author in an earlier publication (1961) has been used in determining the energies of the various  $\alpha$ -ray groups from measurements of their respective ranges. The dimensions of the chamber are 25 cm in diameter and 5 cm in depth. Argon and iso-amyl alcohol is the gas-vapour mixture used for the chamber filling. The working pressure of the chamber has been maintained at  $\approx 15$  cm Hg. By such a choice of the gas-vapour composition and the working pressure inside the chamber it is possible to magnify the track lengths of the  $\alpha$ -particles so as to extend almost across the entire diameter of the chamber. In so doing, the range differences of the various  $\alpha$ -ray groups are accentuated, thus facilitating more precise measurements on the ranges and consequently better energy estimates.

The source for investigation is isotopically pure  $\text{Am}^{241}$  obtained from Oak Ridge Technical Enterprises Corporation (ORTEC), Tennessee. Deposited on a platinum backing, the active source diameter is 3 mm and has a strength of  $0.154 \mu$  Cur. This source has been mounted on the wall of the perspex chamber internally. An electrochemically deposited source of polonium of low activity has also been installed inside the chamber so as to photograph suitable reference tracks along with  $\alpha$ -ray tracks of  $\text{Am}^{241}$ . In order to avoid jamming every picture with Po- $\alpha$  tracks, thereby making measurements on  $\text{Am}^{241}$  alphas less cumbersome, the Po-alphas were interrupted by a shutter arrangement operated electromagnetically so that the reference tracks were only introduced into the picture at



chosen intervals. Such an arrangement would help to checkup the constancy of pressure over the entire operating period of the chamber.

The  $\alpha$ -tracks are photographed under a stereo set-up. For a spatial reconstruction of the tracks, the developed negatives are reintroduced into the same camera assembly and strongly illuminated so as to project the images on a translucent viewing screen arranged to be conveniently adjusted to any desired plane. The screen is so oriented that the image of a given track as projected from the two lens system of the camera is observed to coincide throughout, thus re-establishing the original position of a track relative to the camera assembly. Measurement of the true length of a track under investigation is made from the life-size image thus produced.

#### EXPERIMENTAL RESULTS

With the above setup 4000 stereo photographs were obtained, each picture having on an average about 15 tracks, thus accounting for a total of nearly 60,000 tracks during the whole run. Fresh chamber filling was made every day so as to keep the gas-vapour composition identical, and it was ensured that all the other working conditions were maintained steady all through. After applying the standard criteria for selection of tracks, the number of acceptable tracks reduced to about 35,000 and length measurements were confined only to this number. Accuracy no better than 0.5 mm in length measurements has been attempted. The data are presented in Fig. 1 in the form of length distribution curve

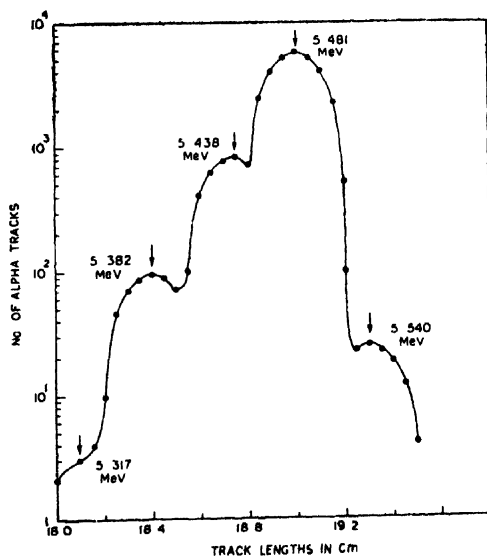


Fig. 1. Track length distribution for Am<sup>241</sup>  $\alpha$ -particles.

The mean values of the ranges in cm corresponding to the different energy groups as obtained from the track length distribution curve are presented in column 1 of Table I.

TABLE I  
Data on alpha decay of americium-241

Measured ranges of $\alpha$ -particles (cm)	Reduced air equivalent ranges (cm)	$\alpha$ -particle energy (MeV)	Obs. rel. Intensity %	Calc. rel. Intensity %	Energy level (keV)
19.30	4.110	5.540	—	—	0
19.00	4.047	5.481	85.0	85.6	59.6
18.75	3.993	5.438	12.8	12.2	103.0
18.40	3.919	5.382	1.45	2.2	158.6
18.10	3.855	5.317	—	—	226.0

These mean ranges of the track lengths have been converted to cm of air equivalent range by using the stopping power of the gas. If the stopping power of the gas is defined as the ratio of the mean range of  $\alpha$ -particles in air to the range in the gas under the working conditions, then the reduced air ranges are obtained by multiplying the measured lengths by this factor. The stopping power has been experimentally determined in a preliminary investigation by obtaining the mean range of Po- $\alpha$  particles and comparing it with the known mean range of Po- $\alpha$  particles in air under standard conditions (3.84 cm at 760 mm Hg and 15°C). The stopping power has been determined to be 0.213. The choice of Po<sup>210</sup> alphas is appropriate for this purpose firstly for the reason that the tracks rendered by the source are homogeneous and secondly the energy of Po- $\alpha$  (5.303 MeV) is comparable to that of Am<sup>241</sup> alphas so that the value of the stopping power deduced can directly be employed in reducing the Am<sup>241</sup> data without involving serious error.

The reduced air equivalent ranges are shown in column 2 of Table 1. The energies corresponding to the different range groups are obtained by utilising Bethe's range-energy curves, Bethe (1950), and these are given in column 3.

#### DISCUSSION OF THE RESULTS

The energy level scheme of Np<sup>237</sup> based on our experimental results is shown in Fig. 2.

We have been able to measure the energies of five groups of  $\alpha$ -particles. The different groups are associated with transitions to levels belonging to two rotational bands. The 59.6, 103, 158.6 and 226 KeV levels constitute members of the most highly developed band based on 5/2—[523] orbital in terms of Nilsson's theoretical single particle states. The spin of the lowest member of this band is 5/2. The other rotational band 5/2+[642] comprises of the ground state and the 33KeV level. The 33 KeV level with a reported intensity of 0.24% occurs at a distance of only 26 KeV from a line whose intensity is 85% (roughly 350 times stronger).

The inadequate resolution of the apparatus has made it difficult to resolve this level at 33 KeV. The ground state spin of  $\text{Np}^{237}$  has been measured by Tomkins (1948), as  $5/2$ . Hollander *et al.* (1956) have assigned parity to the ground state band and the 59 KeV band to be respectively even and odd.

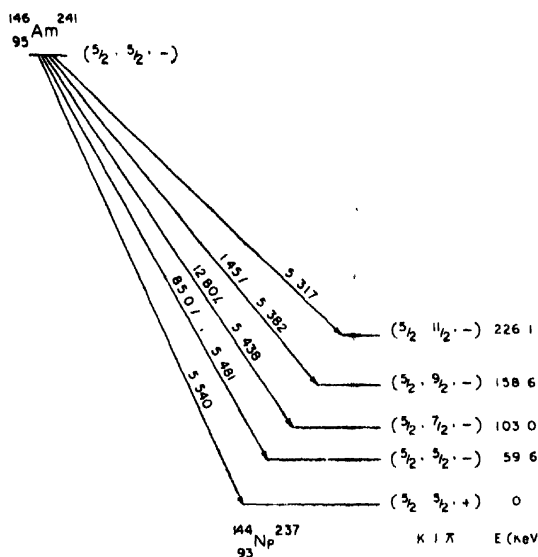


Fig. 2. Energy level scheme of  $\text{Np}^{237}$

According to the theory of Bohr and Mottelson (1953), the rotational states of an odd nucleus can have the following energy and spin sequence :

$$E_I = \frac{\hbar^2}{2g} [I(I+1) - I_0(I_0+1)]$$

$$I = I_0, I_0+1, I_0+2, \dots$$

where  $I_0$  is the spin of the lowest state in the band  
 $I$  is the spin of the considered excited state and  
 $g$  is the effective nuclear moment of inertia.

Making use of the energy difference of 43 KeV between the  $5/2$  and  $7/2$  states, the quantum of rotation  $\frac{\hbar^2}{2g}$  has been calculated to be 6.14 KeV. Again, utilising the energy difference of 56 KeV between the  $7/2$  and  $9/2$  states, the calculated value of  $\frac{\hbar^2}{2g}$  comes out to be 6.22 KeV. We thus notice the good agreement of the energy level spacings between levels of this band in conformity with Bohr-Mottelson theory for rotational excitation energies.

Further, denoting by  $I_i, K_i (I_f, K_f)$  the spin and its projection on the symmetry

axis of the initial (final) nucleus. the probability of a favoured  $\alpha$ -transition for an odd mass nucleus is given by the formula Bohr. (1955)

$$P = P_0(Z, E) \sum_i C_i < I_i l K_i 0 | I_i l_f K_f >^2 \quad \dots (1)$$

where  $P_0(Z, E)$  is given by Geiger-Nuttall law :

$$\log_{10} P_0 = C - DE^{-1/2} \quad \dots (2)$$

The constants  $C$ ,  $D$  and  $C_i$  are determined from the the  $\alpha$ -transition probabilities of the neighbouring even-even nuclei.  $E$  is the energy of the fine structure component in question. The bracketted term in the formula (1) is the vector addition of the angular momenta  $I_i$  and  $l$  to form the resultant  $I_f$ . Utilising  $C_0 = 1$ ,  $C_2 = 0.7$  and  $C_4 = 0.01$  and appropriate values for spins of initial and final states of the nucleus, the relative intensities of the  $\alpha$ -transitions to different excited states have been calculated and these are presented in column 5. Five energy peaks are evident from Fig. 1, thereby revealing 5 fine structure  $\alpha$ -ray groups from  $\text{Am}^{241}$ . The relative intensities of 3 levels of the favoured band as estimated from the full-energy peaks of the spectrum are presented in column 4.

In column 6, the best and undisputed values of the excitation energies are included. It can be seen that there is a fairly good agreement between the observed transition intensities and those calculated with the help of the expression for  $\alpha$ -transition probabilities for odd mass nuclei. Thus for transitions involving  $l = 0, 2, 4$ , our data lends support to the validity of formula (1) for  $\alpha$ -transition probabilities of odd mass nuclei.

#### ACKNOWLEDGMENT

The author is thankful to Prof. B. D. Nag Chaudhury, Director, Saha Institute of Nuclear Physics, for his many valuable suggestions. Thanks are due to Prof. D. N. Kundu for his keen interest and helpful discussions.

#### REFERENCES

- Asaro, F., Reynolds, F. L. and Perlman I., 1952, *Phys. Rev.*, **87**, 277.  
 Baranov, S. A., Kulakov, V. M. and Shatinskii, V. M., 1964, *JETP.*, **18**, 1241.  
 Baranov, S. A. and Shliagin, K. N., 1956, *JETP.*, **3**, 200.  
 Bethe, H. A., 1950, *Rev. Mod. Phys.*, **22**, 213.  
 Bohr, A., Froman, P. O. and Mottelson, B. R., 1955, *Kgl. Danske Videnskab, Selskab. Mat. Fys. Medd.*, **29**, No. 10.  
 Bohr, A. and Mottelson, B. R., 1953, *Phys. Rev.*, **89**, 316.  
 Bunker, M. E., Mize, J. P. and Starnner, J. W., 1957, *Bull. Am. Phy. Soc.*, **2**, 104.  
 Haffmen, D. C. and Dropesky, B. J., 1958, *Phys. Rev.*, **109**, 1282.  
 Hollander, J. M., Smith, W. G. and Rasmussen, J. O., 1956, *Phys. Rev.*, **102**, 1372.  
 Newton, J. O., 1958, *Nuclear Physics*, **5**, 218.  
 Rama Rao, M., 1961, *Ind. J. Phys.*, **35**, 92, 361.  
 Rasmussen, J. O., Canavan, F. L. and Hollander, J. M., 1957, *Phys. Rev.*, **107**, 141.  
 Rosenblum, S., Valadares, M., and Milsted, J., 1957, *J. Phys. Radium.*, **18**, 609.  
 Tomkins, F. S., 1948, *Phys. Rev.*, **73**, 1214.  
 Wolfson, J. L. and Park, J. J. H., 1964, *Can. J. Phys.*, **42**, 1387,

# DISPERSION RELATIONS FOR ELECTRON PLASMA IN AN EXTERNAL MAGNETIC FIELD

SAROJ K MAJUMDAR

SAHA INSTITUTE OF NUCLEAR PHYSICS, CALCUTTA, INDIA

(Received September 25, 1965)

**ABSTRACT.** The Boltzmann-Vlasov equation is solved by integrating it over the characteristic trajectory of the electrons. The dispersion laws for parallel and perpendicular wave propagation are obtained in terms of a function which belongs to the family of Bessel's function. Explicit expressions for this function has been obtained for low temperature plasma.

## INTRODUCTION

The theory of wave propagation in a plasma placed in an external magnetic field has been developed by many authors e.g., by Gross (1951), Sitenks and Stepanov (1957) Bernstein (1958) Allis *et al.* (1962) and others. Most of these investigations are concerned with solving the Boltzmann-Vlasov kinetic equation coupled with Maxwell's e.m. field equations. From the condition of the existence of the solution of these equations, one obtains the dispersion relation of the plasma. The dielectric coefficient for a magnetic plasma turns out to be a tensor whose nine elements have extremely complicated form. Only in the case of low temperature plasma, these elements can be simplified to a certain extent. However, it is possible to express all the elements in terms of a single function which makes the mathematical tasks less involved. This will be done in the present paper and in the paper that will be published subsequently.

In this paper we start by solving the Boltzmann-Vlasov kinetic equation, by integrating it over the characteristic trajectory of the electron. The plasma will be assumed "collisionless" and ion motions will be neglected. We shall calculate the dispersion law for waves propagating (a) parallel, and (b) perpendicular, to the magnetic field. In the next paper, we extend the calculation for an arbitrary direction of wave propagation.

## CHARACTERISTIC INTEGRATION OF BOLTZMANN - VLASOV EQUATION

The linearised Boltzmann-Vlasov equation for the plasma electrons is

$$\frac{\partial f_1}{\partial t} + \mathbf{v} \cdot \frac{\partial f_1}{\partial \mathbf{r}} - \frac{e}{mc} (\mathbf{v} \times \mathbf{H}_0) \cdot \frac{\partial f_1}{\partial \mathbf{v}} = \frac{e}{m} \mathbf{E} \cdot \frac{\partial f_0}{\partial \mathbf{v}}, \quad \dots (1)$$

where  $f_1$  is a small perturbation in the distribution function of the electrons over

the steady state distribution  $f_0$ .  $\mathbf{E}$  is the electric field in the plasma created due to  $f_1$ , and  $\mathbf{H}_0$  is the externally applied steady magnetic field. Other quantities have their usual meaning.

The characteristic trajectory of the electrons is given by

$$\frac{1}{d\tau} = \frac{\mathbf{v}}{d\mathbf{r}} = - \frac{e}{mc} (\mathbf{v} \times \mathbf{H}_0) \cdot \frac{d}{d\mathbf{v}}. \quad \dots (2)$$

Let  $\mathbf{v}_e(\tau)$ ,  $\mathbf{r}_e(\tau)$  denote the characteristic velocity and position of the electrons as a function of the characteristic time  $\tau$ , and these obey eqns. (2). Replacing  $\mathbf{r}$  by  $\mathbf{r} + \mathbf{r}_e(\tau)$ ,  $\mathbf{v}$  by  $\mathbf{v}_e(\tau)$  and  $t$  by  $t + \tau$  in eqn. (1), it reduces to the following form :

$$\frac{d}{d\tau} f_1(\mathbf{r} + \mathbf{r}_e(\tau), \mathbf{v}_e(\tau), t + \tau) = \frac{e}{m} \mathbf{E}(\mathbf{r} + \mathbf{r}_e(\tau), t + \tau) \cdot \frac{\partial f_0}{\partial \mathbf{v}_e(\tau)}. \quad \dots (3)$$

We choose the initial conditions such that at time  $t$  (i.e.,  $\tau = 0$ ),  $\mathbf{r}_e(0) = 0$  and  $\mathbf{v}_e(0) = \mathbf{v}$ , and at  $t = 0$ ,  $f_1 = 0$ . With these conditions, we integrate (3) over  $\tau$  from  $\tau = -t$  to  $\tau = 0$  and obtain .

$$f_1(\mathbf{r}, \mathbf{v}, t) = \frac{e}{m} \int_0^t \mathbf{E}(\mathbf{r} + \mathbf{r}_e(-\tau), t - \tau) \cdot \frac{\partial f_0}{\partial \mathbf{v}_e(-\tau)} d\tau.$$

From this equation, by taking Fourier space-transform and Laplace time-transform of the form

$$f_1(\mathbf{k}, \mathbf{v}, \omega) = \int_0^\infty dt \int d\mathbf{k} f_1(\mathbf{r}, \mathbf{v}, t) e^{i(\omega t - \mathbf{k} \cdot \mathbf{r})},$$

we obtain

$$f_1(\mathbf{k}, \mathbf{v}, \omega) = \frac{e}{m} \mathbf{E}(\mathbf{k}, \omega) \cdot \Omega(\mathbf{k}, \mathbf{v}, \omega), \quad \dots (4)$$

where

$$\Omega(\mathbf{k}, \mathbf{v}, \omega) = \int_0^\infty e^{i\mathbf{k} \cdot \mathbf{r}_e(-\tau) + i\omega\tau} \frac{\partial f_0}{\partial \mathbf{v}_e(-\tau)} d\tau. \quad \dots (5)$$

#### DISPERSION RELATION

Let us assume that a test particle of charge  $q$ , mass  $M$ , and moving with a velocity  $\vec{V}_0(t)$ , disturbs the plasma from the steady state. The two Maxwell's equations in that case, are given by :

$$\nabla \times \mathbf{E}(\mathbf{r}, t) = - \frac{1}{c} \frac{\partial \mathbf{H}}{\partial t}, \quad \dots (6a)$$

$$\nabla \times \mathbf{H}(\mathbf{r}, t) = \frac{1}{c} \frac{\partial \mathbf{E}}{\partial t} - \frac{4\pi e}{c} \int f_1(\mathbf{r}, \mathbf{v}, t) \mathbf{v} d\mathbf{v} + \frac{4\pi q}{c} \delta(\mathbf{r} - \mathbf{r}_1) \vec{V}_0(t). \quad \dots (6b)$$

In (6b), the position  $\mathbf{r}_1$  of the test particle is exactly given by the Dirac's  $\delta$ -function.

We take Fourier-Laplace transform of eqns. (6) as before. Then eliminating the two quantities  $\mathbf{H}$  and  $f_1$ , from the resulting equations and eqn. (4), we obtain an equation for the electric field in the plasma :

$$\left( k^2 - \frac{\omega^2}{c^2} \right) \mathbf{E}(\mathbf{k}, \omega) - (\mathbf{k} \cdot \mathbf{E}) \mathbf{k} + i \frac{4\pi e^2 \omega}{mc^2} \int d\mathbf{v} \mathbf{v} \mathbf{E}(\mathbf{k}, \omega) \Omega(\mathbf{k}, \mathbf{v}, \omega) = i \frac{\omega}{c^2} 4\pi q \vec{\Gamma}, \quad (7)$$

where

$$\vec{\Gamma} = \int_0^\infty \vec{V}_0(t) e^{i\mathbf{k} \cdot \mathbf{r}_1 + i\omega t} dt. \quad (8)$$

It we define a matrix

$$A_{ij} = \left( k^2 - \frac{\omega^2}{c^2} \right) \delta_{ij} - k_i k_j + i \frac{4\pi e^2 \omega}{mc^2} \int d\mathbf{v} v_i \Omega_i(\mathbf{k}, \mathbf{v}, \omega),$$

where the subscripts  $i, j = x, y, z$  and

$$\delta_{ij} = 0, \text{ for } i \neq j$$

$$= 1, \text{ for } i = j.$$

then eqn. (7) becomes

$$A_{ij} E_j = i \frac{\omega}{c^2} 4\pi q \Gamma_i. \quad (10)$$

The condition for vanishing of the determinant of the matrix  $A_{ij}$  gives the dispersion relation

$$\det |A_{ij}| = 0. \quad \dots (11)$$

We take the magnetic field  $\mathbf{H}_0$  along the positive  $z$ -direction of cylindrical coordinates, and write

$$\mathbf{k} = \mathbf{k}_z + \mathbf{k}_\rho,$$

$$\mathbf{v} = \mathbf{v}_z + \mathbf{v}_\rho, \quad \dots (12)$$

where the subscripts  $z$  and  $\rho$  denote components along and at right angles to the magnetic field. Then solving eqns. (2) we get an expression for the characteristic path of the electrons in plasma;

$$\mathbf{r}_e(\tau) = \mathbf{e}_x a [\sin(\theta_0 + \omega_e \tau) - \sin \theta_0] - \mathbf{e}_\rho a [\cos(\theta_0 + \omega_e \tau) - \cos \theta_0] + \mathbf{e}_z v_z \tau. \quad \dots (13)$$

Here, the  $\mathbf{e}$ 's are three unit vectors along the coordinate axes,  $\theta_0$  is the azimuthal angle of  $\mathbf{v}_\rho$  and

$$a = \frac{v_\rho}{\omega_e}$$

$$\omega_e = \frac{eH_0}{mc} \quad \dots (14)$$

are respectively the Larmor radius and cyclotron frequency of electrons.

#### DISPERSION LAW FOR PARALLEL PROPAGATION

For propagation parallel to  $\mathbf{H}_0$ , we set  $\mathbf{k}_\rho = 0$ . Using (13), we get

$$\mathbf{k} \cdot \mathbf{r}_c(-\tau) = -k_z v_z \tau. \quad \dots (15)$$

The steady state distribution function  $f_0$  is taken to be Maxwellian :

$$f_0 = n_0 (m/2\pi T)^{3/2} \exp \left( -\frac{m}{2T} [v_z^2 + v_\rho^2] \right), \quad \dots (16)$$

where  $n_0$  is the number of electrons per c.c., and the plasma temperature  $T$  is in e.v.

Writing 
$$I_{ij} = i \frac{4\pi e^2 \omega}{mc^2} \int d\mathbf{v} v_i \Omega_j \quad \dots (17)$$

and noticing that the characteristic velocity is given by

$$\mathbf{v}_c(\tau) = \mathbf{e}_x v_\rho \cos(\theta_0 + \omega_c \tau) + \mathbf{e}_y v_\rho \sin(\theta_0 + \omega_c \tau) + \mathbf{e}_z v_z, \quad \dots (18a)$$

while the random thermal velocity is

$$\mathbf{v} = \mathbf{e}_x v_\rho \cos \theta_0 + \mathbf{e}_y v_\rho \sin \theta_0 + \mathbf{e}_z v_z, \quad \dots (18b)$$

we can evaluate the various integrals  $I_{ij}$  given by (17) in a quite straight forward manner, using eqns. (5), (15), (16) and (18). The result is

$$I_{xz} = I_{zx} = I_{yz} = I_{zy} = 0. \quad \dots (19)$$

$$I_{xx} = I_{yy} = I_1 = -\frac{\omega_p^2 \omega}{2c^2} \int_{-\infty}^{+\infty} dv_z F_0(v_z) \left[ \frac{1}{k_z v_z - (\omega - \omega_c)} + \frac{1}{k_z v_z - (\omega + \omega_c)} \right], \quad \dots (20)$$

$$I_{xy} = -I_{yx} = I_2 = i \frac{\omega_p^2 \omega}{2c^2} \int_{-\infty}^{+\infty} dv_z F_0(v_z) \left[ \frac{1}{k_z v_z - (\omega - \omega_c)} - \frac{1}{k_z v_z - (\omega + \omega_c)} \right] \quad \dots (21)$$

and

$$I_{zz} = I_3 = -\frac{\omega_p^2 \omega}{c^2} \frac{m}{T} \int_{-\infty}^{+\infty} \frac{dv_z v_z^2 F_0(v_z)}{k_z v_z - \omega}. \quad \dots (22)$$

In these equations the quantity  $F_0(v_z)$  is given by

$$F_0(v_z) = (m/2\pi T)^{1/2} \exp(-mv_z^2/2T), \quad \dots (23)$$



and  $\omega_p$  is the plasma frequency

$$\omega_p = (4\pi e^2 n_0 / m)^{1/2}. \quad \dots \quad (24)$$

Using eqn. (9) and eqns. (19) to (22) the dispersion law (11) gives rise to the following relations for the three uncoupled waves.

$$\frac{\omega^2}{c^2} - I_3 = 0 \quad \dots \quad (25)$$

for longitudinal plasma waves, and

$$k_z^2 - \frac{\omega^2}{c^2} + I_1 + iI_2 = 0 \quad \dots \quad (26a)$$

$$k^2 - \frac{\omega^2}{c^2} + I_1 - iI_2 = 0, \quad \dots \quad (26b)$$

for transverse circularly polarised e.m. waves.

The path of integration in the  $v_z$ -plane of the integrals in (20) to (22) can be prescribed by giving a small imaginary part to  $\omega$  and then deforming the contour around the pole (See for ex., Stix 1962). It is then possible to write the following expression for  $I_1 + iI_2$  valid for all  $\omega$ :

$$I_1 + iI_2 = \frac{1}{k_z} P \int_{-\infty}^{+\infty} \frac{F_0(v_z) dv_z}{v_z - \frac{\omega - \omega_c}{k_z}} - i \frac{\pi}{k_z} F_0 \left( \frac{\omega - \omega_c}{k_z} \right). \quad \dots \quad (27)$$

The principal value part, denoted by  $P$  can be easily evaluated and one obtains from eqn. (26a),

$$k_z^2 c^2 - \omega^2 + \frac{c^2(\omega - \omega_c)}{\lambda_D^2 \eta^2 \omega} \phi \left( 1, 3/2; -\frac{c^2(\omega - \omega_c)^2}{2\omega^2 \eta^2 \omega_p^2 \lambda_D^2} \right) + \frac{i\pi}{k_z} \omega \omega_p^2 F_0 \left( \frac{\omega - \omega_c}{k_z} \right) = 0. \quad \dots \quad (28)$$

In (28),  $\eta = ck_z/\omega$  is the plasma refractive index,  $\lambda_D = (T/m)^{1/2} \omega_p$  is the Debye length, and  $\phi$  is confluent hypergeometric function, Erdelyi (1953). Writing  $\omega = \omega_r + i\omega_i$  with  $\omega_i \ll \omega_r$  in eqn. (28), and separating the real and imaginary parts we obtain

$$2 - 1 = -\frac{c^2(\omega - \omega_c)}{\lambda_D^2 \eta^2 \omega^3} \phi \left( 1, 3/2; -\frac{c^2(\omega - \omega_c)^2}{2\omega^2 \eta^2 \omega_p^2 \lambda_D^2} \right), \quad \dots \quad (29)$$

and

$$\omega_i \approx -\frac{\pi}{2k_z} \omega_p^2 F_0 \left( -\frac{\omega - \omega_c}{k_z} \right). \quad \dots (30)$$

Eqs. (29) and (30) give the dispersion law and damping decrement for the circularly polarised mode (26a). These relations were earlier obtained by Pradhan (1957) by a different method. For low temperature plasma,  $\lambda_D$  is small, so that one can use the asymptotic expansion of  $\phi$  in (29). If we keep terms only up to first order in  $\lambda_D^2$  (i.e. first order in  $T$ ), we obtain the following expression for the refractive index of the mode (26a).

$$\eta^2 = \left[ 1 - \frac{\omega_p^2}{\omega(\omega - \omega_c)} \right] / \left[ 1 + \frac{\omega_p^4 \lambda_D^2 \omega}{c^2(\omega - \omega_c)^2} \right]. \quad \dots (31)$$

The two other modes, (25) and (26b) can be similarly treated.

#### DISPERSION LAW FOR PERPENDICULAR PROPAGATION

In this case we set  $k_z = 0$ , and without any loss of generality we can assume that  $k_y = 0$ , so that  $k = k_\rho = k_x$ . Using eqn. (13) the quantity  $\mathbf{k} \cdot \mathbf{r}_c(-\tau)$  is then given by,

$$\mathbf{k} \cdot \mathbf{r}_c(-\tau) = -2ak_\rho \sin \frac{\omega_c \tau}{2} \cos \left( \theta_0 - \frac{\omega_c \tau}{2} \right). \quad \dots (32)$$

Using (32) and (18), the three components of  $\Omega$  of eqn. (5) can be written down in the following form :

$$\Omega_x = 2v_\rho f'_0(v^2) \int_0^\infty e^{i\omega t - iA \cos \left( \theta_0 - \frac{\omega_c t}{2} \right)} \cos(\theta_0 - \omega_c t) dt, \quad \dots (33a)$$

$$\Omega_y = 2v_\rho f'_0(v^2) \int_0^\infty e^{i\omega t - iA \cos \left( \theta_0 - \frac{\omega_c t}{2} \right)} \sin(\theta_0 - \omega_c t) dt, \quad \dots (33b)$$

$$\Omega_z = 2v_z f'_0(v^2) \int_0^\infty e^{i\omega t - iA \cos \left( \theta_0 - \frac{\omega_c t}{2} \right)} dt, \quad \dots (33c)$$

where prime denotes differentiation w.r.t. argument, and

$$A = 2 \frac{k_\rho v_\rho}{\omega_c} \sin \frac{\omega_c t}{2},$$

Eqs. (33) together with eqn. (17) will give us the various integrals  $I_{ij}$  needed to evaluate the elements  $A_{ij}$ . We shall briefly indicate how this can be done for the case of  $I_{xx}$ . The remaining integrals can be evaluated in the same manner.

From equns. (17) and (33a), the integral  $I_{xx}$  can be written down as follows :

$$I_{xx} = -n_0 \left( \frac{m}{2\pi T} \right) \frac{m}{T} \int_{-\infty}^{+\infty} dv_z e^{-\frac{m}{2T} v_z^2} \int_0^{\infty} dv_{\rho} v_{\rho}^3 e^{-\frac{m}{2T} v_{\rho}^2} \\ \int_0^{2\pi} d\theta_0 \cos \theta_0 \int_0^{\infty} dt e^{i\omega t - iA \cos \left( \theta_0 - \frac{\omega_c t}{2} \right)} \cos (\theta_0 - \omega_c t).$$

The integral over  $v_z$  is straightforward. We integrate over  $\theta_0$  first and then over  $v_{\rho}$ . These are standard integrals and by quite straight forward manner one obtains :

$$I_{xx} = -i \frac{\omega_p^2 v}{c^2} e^{-z} \left[ -z + z \frac{\partial}{\partial z} + z \frac{\partial^2}{\partial z^2} \right] S_{\nu}(z), \quad \dots (34)$$

where

$$S_{\nu}(z) = \int_0^{\infty} e^{i\nu t + z \cos t} dt, \quad \dots (35)$$

$$\nu = \frac{\omega}{\omega_c}, \quad z = \frac{k_{\rho}^2 T}{m \omega_c^2}. \quad \dots (36)$$

The expression (34) for  $I_{xx}$  can be further simplified in the following way : Writing

$$\int_0^{\infty} = \int_0^{2\pi} + \int_{2\pi}^{4\pi} + \dots + \int_{\infty}^{\infty},$$

the function  $S_{\nu}(z)$  transforms into the form

$$S_{\nu}(z) = (1 + e^{2\pi\nu i} + e^{4\pi\nu i} + \dots) \int_0^{2\pi} e^{i\nu t + z \cos t} dt.$$

At all points in the complex  $\nu$ -plane, except where  $\nu =$  integers the infinite series on the r.h.s. can be replaced by  $1/(1 - e^{2\pi\nu i})$ , so that  $S_{\nu}(z)$  becomes

$$S_{\nu}(z) = \frac{i\pi}{\sin \nu\pi} M_{\nu}(z), \quad \dots (37)$$

where

$$M_{\nu}(z) = \frac{1}{\pi} \int_0^{\pi} e^{-z \cos t} \cos \nu t dt \quad \dots (38)$$

The function  $M_{\nu}(z)$  reduces to  $I_{\nu}(-z)$ , i.e. modified Bessel's function of the first kind, whenever  $\nu =$  integers. Otherwise, it is a distinct function and bears the

same relation to  $I_\nu(z)$ , as Anger functions do to ordinary Bessel functions (Watson 1952). The function  $M_\nu(z)$  has the following recurrence relations :

$$\begin{aligned} M_{-\nu}(z) &= M_\nu(z), \\ M_{\nu+1}(z) + M_{\nu-1}(z) &= -2M'_\nu(z), \\ M_{\nu-1}(z) - M_{\nu+1}(z) &= \frac{2}{\pi z} e^z \sin \pi \nu - \frac{2\nu}{z} M_\nu(z). \end{aligned} \quad \dots (39)$$

Expressing the functions  $S_\nu(z)$  in terms of  $M_\nu(z)$ , and using eqn. (39), one can reduce  $I_{xx}$  to the following simple form .

$$I_{xx} = \frac{\omega_p^2}{c^2} \frac{\nu^2}{z} [1 + i\nu e^{-z} S_\nu(z)]. \quad \dots (40)$$

In a similar manner we deduce

$$I_{yy} = I_{xx} + i \frac{\omega_p^2}{c^2} (2\nu z) \frac{\partial}{\partial z} e^{-z} S_\nu(z), \quad \dots (41)$$

$$I_{zz} = -i \frac{\omega_p^2}{c^2} \nu (e^{-z} S_\nu(z)), \quad \dots (42)$$

$$I_{xy} = -I_{yx} = -\frac{\omega_p^2}{c^2} \nu^2 \frac{\partial}{\partial z} (e^{-z} S_\nu(z)), \quad \dots (43)$$

and

$$I_{xz} = I_{zx} = I_{yz} = I_{zy} = 0. \quad \dots (44)$$

We thus notice that if expressed in terms of the function  $e^{-z} S_\nu(z)$ , the formidable looking integrals  $I_{ij}$  reduce to particularly simple expression. The dispersion relation (11) in this case has the following form :

$$\begin{pmatrix} -\frac{\omega^2}{c^2} + I_{xx} & I_{xy} & 0 \\ I_{yx} & k_\rho^2 - \frac{\omega^2}{c^2} + I_{yy} & 0 \\ 0 & 0 & k_\rho^2 - \frac{\omega^2}{c^2} + I_{zz} \end{pmatrix} = 0.$$

We shall conclude the calculation in this paper by giving the explicit expression of  $I_{xx}$  etc. for low temperature plasma. When  $T$  is small, the quantity  $z$

given by eqn. (36) can be taken as less than unity. Hence, to a first approximation we can expand the quantity  $e^{-z \cos t}$  which occurs in the expression for  $M_\nu(z)$  in powers of  $z$  and integrate term by term to obtain an expression for  $M_\nu(z)$  and hence that of  $S_\nu(z)$ . We also expand,  $e^{-z} = 1 - z$ . Using these result is eqn. (40) [or in (34) along with eqn. (39)], and keeping only terms upto the first power of  $z$  (i.e. first order in  $T$ ), we obtain

$$I_{xx} = \frac{\omega_p^2}{c^2} \left[ \frac{1}{1-\beta^2} + \frac{3z\beta^2}{(1-4\beta^2)(1-\beta^2)} \right]$$

where

$$\beta = \frac{1}{v} = \frac{\omega_c}{\omega}.$$

In a similar manner we deduce

$$I_{yy} = \frac{\omega_p^2}{c^2} \left[ \frac{1}{1-\beta^2} + z\beta^2 \frac{1+8\beta^2}{(1-4\beta^2)(1-\beta^2)} \right]$$

$$I_{zz} = \frac{\omega_p^2}{c^2} \left[ 1 + \frac{z\beta^2}{1-\beta^2} \right]$$

$$I_{xy} = -I_{yx} = -\frac{\omega_p^2}{c^2} \beta \left[ \frac{1}{1-\beta^2} + \frac{6z\beta^2}{(1-\beta^2)(1-4\beta^2)} \right].$$

It may be noted that these relations for  $I_{ij}$ 's reduce to the usual expression for zero magnetic field for  $\beta = 0$ . If higher temperature correction is desired one must keep terms upto second order in  $z$  in the expansion of  $M_\nu(z)$ .

## CONCLUSIONS

From the calculation given in the last section we may notice one interesting point. In case of perpendicular propagation, the problem of finding the dispersive behaviour of magnetic plasma, reduces to discussions of the properties of the function  $M_\nu(z)$ , or  $S_\nu(z)$ . This function, as given in (35) or (37) includes the plasma temperature ( $z$ ) and the ratio of wave frequency to cyclotron frequency ( $v$ ) as parameters. In comparison to ordinary Bessel functions, we may refer to  $v$  and  $z$  as the order and argument respectively of the function  $S_\nu(z)$ . If we can find suitable expression for  $S_\nu(z)$  for different combinations of small and large  $v$  and  $z$ , we shall be able to solve the problem completely.

## ACKNOWLEDGEMENTS

The author expresses his sincere gratitude to the Director Prof B. D. Nag

for providing him with the facilities to carry out the research. He also thanks Dr. S. Mukherjee for many valuable discussions.

## REFERENCES

- Allis, W. P., Buchsbaum, S. J. and Bers, A. 1962, Special Tech. Report No. 8, Research Lab. of Electronics, M.I.T., Cambridge, MASS.
- Bernstein, I. B., 1958, *Phys. Rev.*, **109**, 10.
- Erdelyi, A., 1953, *Higher Transcendental Functions*, (McGraw-Hill Book Co., Inc., Ch. VI.
- Gross, E. P., 1951, *Phys. Rev.*, **82**, 232.
- Pradhan, T., 1957, *Phys. Rev.*, **107**, 1222.
- Sitenko, A. G. and Stepanov, K. M., 1957, *Sov. Phys. JETP.*, **4**, 512.
- Stix, T. H., "*The Theory of Plasma Waves*", McGraw-Hill Book Co., Inc., 1962, Ch. 7, p. 146.
- Watson, G. N., "*Theory of Bessel Functions*, 2nd Ed. (Cambridge), 1962.

# DIRECTIONAL CORRELATION STUDY OF GAMMA CASCADES IN THE DECAY OF $\text{Sb}^{124}$ .

R. V. RAMA MOHAN, K. VENKATA REDDY, B. B. VENKATAPATHI  
RAJU AND SWAMI JNANANANDA

THE LABORATORIES FOR NUCLEAR RESEARCH, ANDHRA UNIVERSITY,  
WALTAIR, India.

(Received March 4, 1965)

**ABSTRACT.** The decay scheme of  $\text{Sb}^{124}$  is studied and the gamma-gamma directional correlation measurements are carried out for few cascades. On the basis of the experimental data on directional correlations, the spin assignments are made for the 603, 1326, 1964, 2313, 2688 keV excited levels of  $\text{Te}^{124}$ . Multipole assignments are made for 989, 1362 keV transitions.

## INTRODUCTION

The disintegration of 60 day  $\text{Sb}^{124}$  leads to a complex spectrum. Beta emission of  $\text{Sb}^{124}$  results in the formation of  $\text{Te}^{124}$  in different excited states. The beta spectrum has been thoroughly analysed by various investigators using absorption methods and magnetic analysers. The spin assignments for the levels have been investigated by directional correlation studies by several workers. There are however, other levels in addition to the levels mentioned above which have not been studied by angular correlation method. In the present investigation angular correlation study has been undertaken for all the possible gamma cascades.

## EXPERIMENTAL TECHNIQUE

A fast slow triple coincidence scintillation spectrometer having a time resolution of 30 nano seconds is designed and constructed. The head assembly consists of  $\text{NaI(Tl)}$  scintillator coupled to Dumont 6292 photomultipliers, a fast amplifier and an emitter follower. The power to the photomultipliers is supplied from a well regulated negative high tension unit. This arrangement permits direct coupling of the photomultiplier anode to the input of the fast amplifier, which has a band width of over 60 megacycles per second. The output pulse from the cathode follower has a fast rise (better than 0.01 microsecond) a flat top and long trailing edge suitable for clipping by the shorted delay technique. The standard Bell Graham and Petch coincidence circuit is used with reversal of diode connections since the pulses encountered are negative. The triple coincidence circuit is an additive type cathode follower having a resolving time of two microseconds. Compton graded inverted cone type of shields are used around the

scintillators in order to eliminate crystal to crystal scattering effects and other interfering effects. The energy resolution of each spectrometer is found to be 8.5% for the 662 KeV gamma rays of  $\text{Cs}^{137}$ .

A cylindrical perspex container having a cavity of 4mm diameter and 10mm depth with a wall thickness of 0.25mm is used as source holder. This source container is mounted vertically at the intersection of the axes of the two detectors and about 5 cm from the crystals. The spectrometer is initially tested for angular correlation measurements using the standard cascade of  $\text{Ni}^{60}$  and found to be quite satisfactory for correlation measurements.

### RESULTS

The gamma spectrum is recorded employing a weak source of  $\text{Sb}^{124}$  in  $2\pi$  geometry. The intensity versus the pulse height is plotted for the singles spectrum as shown in Figs. 1 and 2, for the regions of low and high energies. An analysis

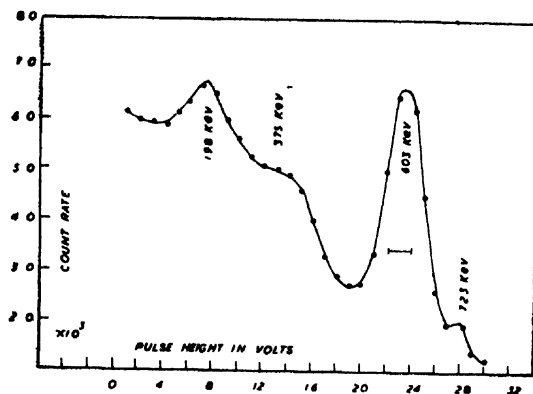


Fig. 1. Singles spectrum of  $\text{Sb}^{124}$  (low energy region)

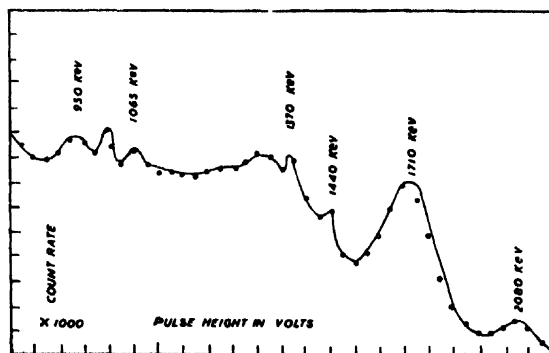


Fig. 2. Singles spectrum of  $\text{Sb}^{124}$  (high energy region)

of these spectra show the presence of gamma transitions with energies 198, 375, 603, 723, 950, 989, 1065, 1370, 1440, 1710, and 2085 KeV. The strong peak observed



at 198 KeV is due to the gamma photons scattered backwards. At the high energy side there are indications of faint peaks with energies of 950 and 1440 KeV and the remaining peaks are well resolved and prominent. The 603 KeV gamma component is found to be the most intense of all the radiations indicating that this radiation is emitted as result of the transition from the first excited state to the ground state of  $\text{Te}^{124}$ .

In the present investigation coincidences are observed by focussing one of the channels to a prominent peak and scanning the other channel through the entire energy spectrum. The two counters are so fixed as to subtend an angle of  $90^\circ$  between them in order to minimise the crystal to crystal scattering. Similarly coincidences are observed by focussing the fixed channel to all the prominent peaks and the experiment is repeated. The coincidence curves are shown in Figs. 3. to 6.

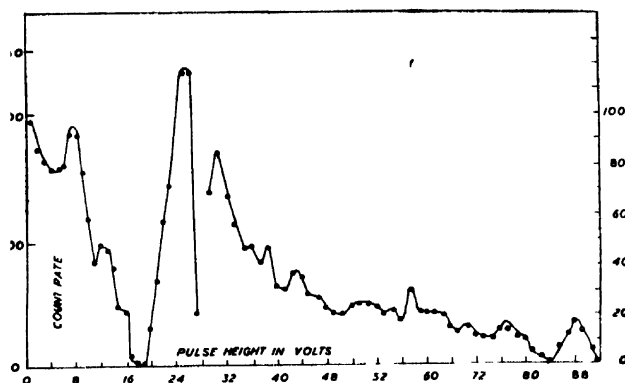


Fig. 3. Coincidence spectrum with 603 KeV gamma component.

The component with an energy 603 KeV is in coincidence with the gamma rays of energies 2085, 1710, 1362, 989, 723, 603 and 200 KeV. The 989 KeV component is in coincidence with components of energies 603 and 1362 KeV. The well resolved component with an energy of 1710 KeV prominently coincides with the 603 KeV component and less prominently with 723 KeV component. The 2085 KeV gamma component is only in coincidence with 603 KeV component. While observing all these coincidences the gates of the two channel are so adjusted as to eliminate the possibility of the interference of any strong peak on the adjacent weak component. On the basis of the coincidence data obtained in the present investigation a level scheme is drawn as shown in Fig. 11.

The gamma-gamma directional correlation study for the 2085-603 KeV, 1710-603 KeV, 1362-603 KeV and 989-723 KeV cascades are studied in order to assign spins for some levels and multiplicities for some of the transitions in the decay of  $\text{Sb}^{124}$ . In the present case only those cascades in which the radiations are well resolved with a considerable number of coincidences are taken into

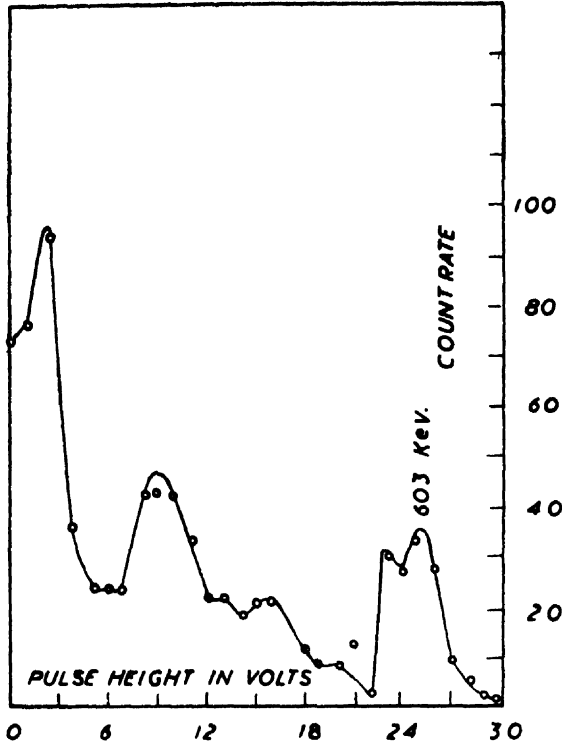


Fig. 4. Coincidence spectrum with 1362 KeV gamma component

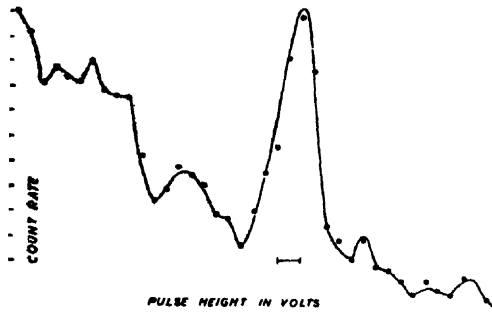


Fig. 5. Coincidence spectrum with 1710 KeV gamma component.

consideration. In these observations care is taken to see that the source is intense and is vertically mounted. It is centered within 0.5% variation of the count rate. A reasonable number of coincidences are collected in each observation until the statistics are found to be satisfactory. These coincidences are corrected for accidental coincidences and the resulting data are used to evaluate the correlation coefficients  $A_2$  and  $A_4$  employing White's analytical method of analysis (White,

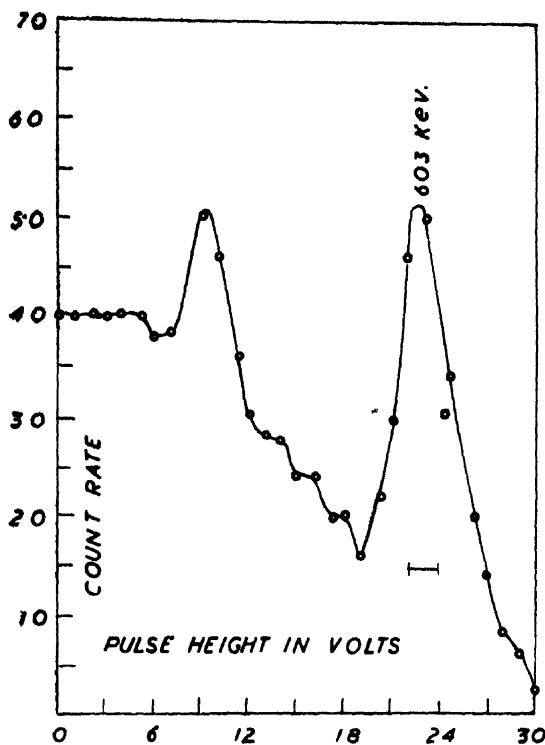


Fig. 6 Coincidence spectrum with 2085 KeV gamma component.

1963). Then the correction for finite angular resolution of the detectors is applied for the experimentally obtained correlation coefficients.

The angular correlation functions for the cascades that are studied in the present investigation are as follows :

$$W(\theta)_{2085-603 \text{ KeV}} = 1 - (0.042 \pm 0.006)P_2 \cos \theta + (0.006 \pm 0.004)P_4 \cos \theta$$

$$W(\theta)_{1710-603 \text{ KeV}} = 1 - (0.0698 \pm 0.0072)P_2 \cos \theta + (0.0082 \pm 0.0048)P_4 \cos \theta$$

$$W(\theta)_{1362-603 \text{ KeV}} = 1 + (0.288 \pm 0.0064)P_2 \cos \theta - (0.695 \pm 0.0375)P_4 \cos \theta$$

$$W(\theta)_{989-723 \text{ KeV}} = 1 + (0.207 \pm 0.006)P_2 \cos \theta - (0.0015 \pm 0.0022)P_4 \cos \theta$$

These values of correlation functions given are plotted against the angle subtended between the movable and the fixed detectors. The respective plots for all the functions are shown in Figs. 7 and 8.

#### DISCUSSION

The study of angular correlation of the cascades with energies 603–1710 KeV and 603–2085 KeV is under taken in order to assign the spins for the levels 603, 2313 and 2688 KeV of  $\text{Te}^{124}$ . The correlation coefficients for 603–1710 KeV cascade are  $-0.06981 \pm 0.0072$  and  $+0.0082 \pm 0.0048$ . The probable spin sequen-

ces for this cascade are 4-2-0, 3-2-0, 2-2-0. The possibility of the spin value greater than 4 for the level 2313 KeV is excluded on the basis of the results obtained

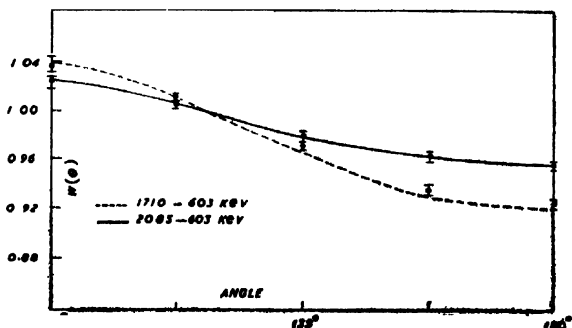


Fig. 7 Plots of  $W(\theta)$  vs  $\theta$  for the cascades 1085- 603 KeV & 1710- 603 KeV.

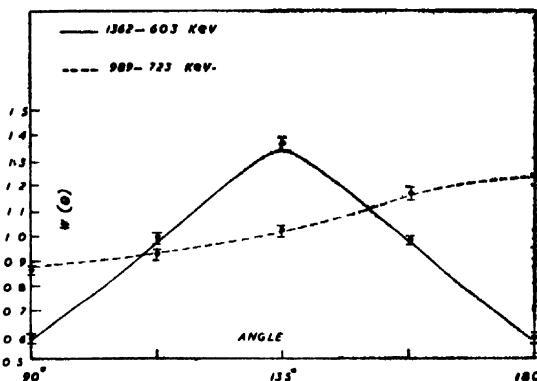


Fig. 8. Plots of  $W(\theta)$  vs  $\theta$  for the cascades 1362- 603 KeV & 989- 723 KeV.

from the conversion measurements (Hutchinson *et al.*, 1952). A comparison of theoretically computed coefficients  $A_2$  and  $A_4$  with experimentally obtained ones eliminates all spin combinations with the exception of 3(D) 2(Q)0. The small difference in the values of theoretical and experimental coefficients can be ascribed to the presence of 1% quadrupole admixture in the 1710 KeV transition. But this small amount of admixture can be neglected and 1710 KeV transition can be considered as pure dipole. From this data a spin of 3 units is assigned to the level at 2313 KeV.

The life time (Temmer *et al.*, 1956) of the 603 KeV level ( $1.3 \times 10^{-11}$  sec) being small, the correlation coefficients obtained in the present experimental analysis are not perturbed by external fields; with this consideration it can reasonably be concluded that the 603 KeV excited level has a spin of 2 units which agrees well with the conversion measurements of this level (Metzer, 1952; Schraff-Goldhaber *et al.*, 1955). The spin value and the sequence are consistent with the general characteristics of even-even nuclei in which the first excited

states have a spin of 2 units and the transition from the first excited state to ground state is a pure quadrupole transition.

The spin of the first excited state has further been confirmed by studying the cascade 2085-603 KeV. the same analysis is also used for the spin assignment of the 2688 KeV level. The correlation coefficients obtained can be best fitted into the spin sequence 3(D) 2(Q)0. Theoretical values with any other sequence are not concurrent with the experimentally obtained values. The little divergence in the value of the experimentally obtained coefficients with those computed from theory for 3(D) 2(Q)0 sequence may be attributed to the presence of a small amount of quadrupole admixture (less than 1%) in the 2085 KeV transition. The spin value has not been reported by the internal conversion measurements, this may be due to the small intensity of the 2085 KeV transition. The 2085 KeV-603 KeV cascade shows a correlation form similar to that of 1710-603 KeV cascade. The spin assignments and the small admixtures of quadrupole content in the 2085 KeV transition are in agreement with the results of previous investigators (Lindquist *et al*, 1957 ; Weitkamp, 1963 ; Metzger, 1952).

In the present investigation the 1362-603 KeV cascade is studied for the spin assignment of the 1964 KeV level. The values of  $A_2$  and  $A_4$  obtained are consistent with the theoretically computed values of the sequence 3(DQ)2(Q)0. The slight divergence between the coefficients when analysed showed an admixture

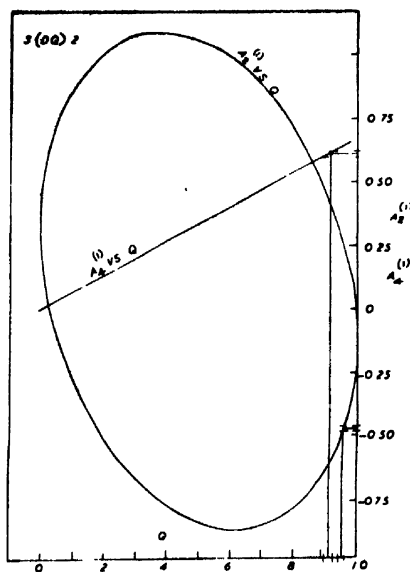


Fig. 9. Multipole admixture plot for the 1362 KeV transition.

of 5% dipole in the 1362 KeV transition which is shown in the Fig. 9. From this analysis a spin value of 3 units is assigned to the 1964 KeV level.



transition it is found that this transition is a mixture of 98% dipole and 2% quadrupole, which is shown in Fig. 10. From this the multipole admixture of the 989 KeV transition is established and the spin of the 1964 KeV level has been fixed as 3 units.

From the coincidence curves it is inferred that the 603 KeV radiation is in coincidence with 723 KeV and 645 KeV radiations. But these cascades are highly interfering with one another. Hence a correlation study of the type employed in the present investigation is not suitable for a clear cut analysis, on the other hand only the method employed by Glaubman *et al* (1964) is suitable for such a complex analysis. Due to this difficulty the spin assignment of the 1248 KeV excited state is not established in the present work.

Employing the values of the energies of the excited levels and those of transitions along with their respective characteristics, a detailed level scheme of  $\text{Te}^{124}$  is drawn as shown in Fig. 11. The 0, (2), 4) spin assignment to the 0, 603, and 1348 KeV rotations as given by Bohr-Mottelson model. The ratio of the energy of the second excited state to the first excited state is 2.06, which is in accordance with the theoretical predictions of Schraff-Goldhaber and Weneser (1955) for even-even nuclei in the slightly deformed region  $44 \leq A \leq 154$ .

#### REFERENCES

- Cook, C. S. and Langer, L. M., 1948, *Phys. Rev.*, **73**, 1149.  
 Glaubman, M. J. and Oberholtzer, J. D., 1964 *Phys. Rev.*, **135**, B1313.  
 Hales, E. B. and Jordon, E. B., 1943, *Phys. Rev.*, **64**, 202.  
 Hutchinson, D. R. and Wiedenbeck, M. L., 1952, *Phys. Rev.*, **88**, 699.  
 Journey, E. T. and Mitchell, A. C. G., 1948, *Phys. Rev.*, **73**, 1153.  
 Kern, B. D., Zuffarano, D. J. and Mitchell, A. C. G., 1948, *Phys. Rev.*, **73**, 1142.  
 Langer, L. M., Moffat, R. A. and Price, H. C., 1950, *Phys. Rev.*, **79**, 808.  
 Lindquist, T. and Marklund, J., 1957, *Nucl. Phys.*, **4**, 189.  
 Livingood J. J. and Seaborg, G. T., 1936, *Phys. Rev.*, **50**, 435.  
 Metzger, F. R., 1952, *Phys. Rev.*, **86**, 435., 1953, *Phys. Rev.*, **90**, 328.  
 Mitchell, A. C. G., Langer, L. M. and McDaniel, P. W., 1940, *Phys. Rev.*, **57**, 1107.  
 Mitter, L. C. and Curtiss, L. F., 1946, *Phys. Rev.*, **70**, 983.  
 Schraff-Goldhaber, G. and Weneser, J., 1955, *Phys. Rev.*, **98**, 212.  
 Swami Jnanananda, 1947, *Phys. Rev.*, **72**, 1124.  
 Temmer, G. M. and Heydenberg, N. P., 1956, *Phys. Rev.*, **104**, 967.  
 Weitkamp, C., 1963, *Nucl. Phys.*, **43**, 57.  
 White, D. H., 1963, *Nucl. Inst.*, **21**, 209.

# CRYSTAL FIELD THEORY OF $\text{Cu}^{++}$ ION IN THE MAGNETICALLY DILUTED CRYSTAL OF $2\text{K}_2 (\text{Zn,Cu}) (\text{SO}_4)_2 \cdot 6\text{H}_2\text{O}$

S. BANERJI AND A. MOOKHERJI

PHYSICS LABORATORY, THE UNIVERSITY OF BURDWAN

(Received September 25, 1965)

**ABSTRACT.** Following the treatment of Polder and Stevens the theory of the crystalline electric field acting on  $\text{Cu}^{++}$  ion in  $\text{K}_2\text{Cu}(\text{SO}_4)_2 \cdot 6\text{H}_2\text{O}$  crystal was developed. From the temperature variation of the magnetic anisotropy ( $\Delta K$ ) of the salt the field parameters were evaluated. Changing the sign of the tetragonal field coefficients and using the same tetragonal field parameters as those of the undiluted salts a good agreement was obtained with the observed values of  $\Delta K$  for the crystal having .81%  $\text{Cu}^{++}$  ion.

## INTRODUCTION

X-ray studies, magnetic birefringence and optical absorption data on the Tutton salts of iron group of elements point to the existence of an axially distorted octahedral cluster of water dipoles surrounding the paramagnetic ion. The crystal field acting on the paramagnetic ion arises out of this distorted octahedral cluster and the direct and indirect influence of the charges outside this primary cluster. The intensity and asymmetry of this field which depend upon the distribution of electric charges will determine the magnetic anisotropy of the ion. When paramagnetic Tutton Salts are diluted with the corresponding zinc or magnesium Tutton Salt the charge distribution is likely to remain constant except for the distant charges.

Bagguley and Griffiths (1952), however, from paramagnetic resonance experiment came to the conclusion that for diluted copper salt  $2\text{K}_2(\text{Cu-Zn})(\text{SO}_4)_2 \cdot 6\text{H}_2\text{O}$ , having less than 1% of  $\text{Cu}^{++}$  ion, the susceptibility at 300°K along the axis of symmetry of the cluster ( $K_{||}$ ) is smaller than that for directions normal to the symmetry axis ( $K_{\perp}$ ), while at 90°K,  $K_{||}$  is greater than  $K_{\perp}$ , whereas for the undiluted salts  $K_{||} > K_{\perp}$  at all temperatures.

Mookherji and Lal (1965) from their studies on a magnetically diluted salt of copper ( $\text{Cu}^{++}$  ion being 0.81%) at different temperatures attempted a qualitative verification of the findings of Bagguley and Griffiths (1952).

In this communication we have tried to explain the temperature variation of the magnetic anisotropy of the diluted salt  $2\text{K}_2(\text{Zn,Cu})(\text{SO}_4)_2 \cdot 6\text{H}_2\text{O}$  having



0.81% of  $\text{Cu}^{++}$  ion, following the crystal field treatment of Polder (1942) and Stevens (1952).

#### SYMMETRY OF THE CRYSTAL FIELD

Copper potassium sulphate is monoclinic in the space group  $C_{2h}^5$ . The unit has the dimension  $a, b, c = 9.1 \text{ \AA}, 12.2 \text{ \AA}$  and  $6.1 \text{ \AA}$  (Hoffman, 1931). There are two magnetically inequivalent paramagnetic clusters in the unit cell. Each cluster consists of a  $\text{Cu}^{++}$  ion located at the centre of an approximate square formed by four water dipoles. The other two are located centrally above and below this square. The  $\text{Cu}-\text{H}_2\text{O}$  distance normal to the square is greater than those in the plane of the square. Thus  $\text{Cu}^{++}$  ion is at the centre of an ionic cluster which is an approximate octahedron as derived from a regular one by elongating one of its diagonals symmetrically. Hence this octahedron will have very nearly a tetragonal symmetry. Recent PMR measurements by Bose *et al* (1964) show that the departure from tetragonal symmetry is small in this case particularly at low temperatures. As a result the crystal field acting on  $\text{Cu}^{++}$  ion is predominantly cubic with a small nearly tetragonal component superimposed on it. Now taking the  $\text{Cu}^{++}$  ion at the origin of a suitably oriented rectangular coordinate system the electric potential of an electron placed at the point  $(X, Y, Z)$  in the neighbourhood of the  $\text{Cu}^{++}$  ion may be represented by (Abragam and Pryce 1951)

$$V(X, Y, Z) = K'(X^4 + Y^4 + Z^4 - \frac{3}{5}r^4) + A'(3Z^2 - r^2) \\ - \frac{1}{2}Q'[5(X^4 + Y^4 + Z^4 - \frac{3}{5}r^4) - 3(X^4 + Y^4 - 6X^2Y^2)] \quad \dots (1)$$

where  $K'$  is the cubic field coefficient and  $A'$  and  $Q'$  are those for the tetragonal field.

#### STARK SPLITTING OF THE GROUND STATE OF THE FREE ION

The ground state of the free  $\text{Cu}^{++}$  ion is  $3d^9 2D_{5/2}$ . From group theoretical considerations of Bethe (1929) it is known that the ground state breaks up into two levels in a field of cubic symmetry, while a tetragonal field breaks these levels into four, each of which will have Kramers degeneracy. This degeneracy is lifted only by a magnetic field.

The complete Hamiltonian for the system is

$$H = H^0 + V + H_{LS} + H(L+2S),$$

where  $H^0$  is the free ion Hamiltonian,  $H_{LS}$  is the spin-orbit interaction  $\lambda L.S$ . ( $\lambda$  = spin-orbit coupling coefficient) and  $H(L+2S)$  is the effect of the magnetic field on the ion.

The matrix elements in the manifold of states spanning  $L = 2$  are determined by changing the potential operator as given by equation (1) into its equivalent

angular momentum operator following Stevens (1952). Thus the secular matrix for the ground state is

	2	-2	1	-1	0
2	$A_2$	$B$	0	0	0
-2	$B$	$A_2$	0	0	0
1	0	0	$A_1$	0	0
-1	0	0	0	$A_1$	0
0	0	0	0	0	$A_0$

where  $A_2 = \langle \pm 2 | V | \pm 2 \rangle = -K'r^{\bar{2}} \frac{2}{105} + \frac{4}{7} A'r^2 - \frac{10}{105} Q'r^4$

$$A_1 = \langle \pm 1 | V | \pm 1 \rangle = K'r^4 \frac{8}{105} - \frac{2}{7} A'r^2 + \frac{40}{105} Q'r^4$$

$$A_0 = \langle 0 | V | 0 \rangle = -K'r^4 \frac{12}{105} - \frac{4}{7} A'r^2 - \frac{60}{105} Q'r^4$$

$$B = \langle \pm 2 | V | 2 \rangle = -K'r^4 \frac{10}{105} + \frac{70}{105} Q'r^4$$

Solving this  $5 \times 5$  matrix we get the energy levels as,

$$\left. \begin{aligned} F_3 &= -6K + 4A + 3Q = A_2 + B \\ F_4 &= +4K + 4A - 4Q = A_2 - B \\ F_5 &= +4K - 2A + 2Q = A_1 \\ F_1 &= -6K - 4A - 3Q = A_0 \end{aligned} \right\} \dots (2)$$

where  $K = \frac{2}{105} K'r^4$ ,  $A = \frac{1}{7} A'r^2$ ,  $Q = \frac{20}{105} Q'r^4$  and  $\bar{r}^n$  is the average  $r^n$  ( $n=2,4$ )

of the 3d electrons.

The corresponding wave functions are.

$$\begin{aligned} F_3 &\rightarrow \frac{1}{2} [ |2\rangle + |-2\rangle ]; \quad F_4 \rightarrow \frac{1}{2} [ |2\rangle - |-2\rangle ] \\ F_5 &\rightarrow |1\rangle \quad \text{and} \quad |-1\rangle ; \quad F_1 \rightarrow |0\rangle \end{aligned} \dots (3)$$

Optical absorption findings (Mookherji and Chhonkar 1959) show two peaks and hence to evaluate the three constants  $K$ ,  $A$  and  $Q$  we have utilized the mean centres of the energy levels as given by equation 2.

Bose *et al* (1957) have studied the temperature variation of  $\Delta K = (K_{\parallel} - K_{\perp})$

for  $\text{K}_2\text{Cu}(\text{SO}_4)_2 \cdot 6\text{H}_2\text{O}$  crystals. After many trials the set of parameters which gave the best fit with the observed values of Bose *et al* (1957) are.

$$K = +1460 \text{ cm}^{-1}, Q = -11 \text{ cm}^{-1}, \text{ and } A = -90 \text{ cm}^{-1}.$$

It must be mentioned here that for a correct set of field parameters one should consider the temperature variation of  $\Delta K$  and not that of the mean moment (Mookherji and Mookherji, 1965 ; Neogy and Mookherji 1965). With the above field parameters the energy levels are

$$F_3 = -9153 \text{ cm}^{-1}, F_1 = -8367 \text{ cm}^{-1}, F_4 = +5524 \text{ cm}^{-1}, F_5 = +5998 \text{ cm}^{-1}$$

The corresponding wave functions (eq. 3) and the order of energy levels show that  $F_3$  lies lowest as obtained by Polder (1942) but the splittings are widely different. Taking  $F_3$  as zero we have the energy levels as 0, (786), 14677 and 15151  $\text{cm}^{-1}$ . The tetragonal separation ( $F_5 - F_4$ ) is 474  $\text{cm}^{-1}$ . This agrees well with the optical absorption finding (470  $\text{cm}^{-1}$ ) of Mookherji and Chhonkar (1959). The other tetragonal separation i.e.  $F_3 - F_1 = 786 \text{ cm}^{-1}$  is significant.

Now introducing proper spin functions and calculating the spin-orbit and magnetic perturbations we get (Polder)

$$K_{\parallel} = \frac{N\beta^2}{KT} \left( 1 - \frac{4\lambda}{F_4 - F_3} \right)^2 + \frac{8N\beta^2}{F_4 - F_3}$$

$$K_{\perp} = \frac{N\beta^2}{KT} \left( 1 - \frac{\lambda}{F_5 - F_3} \right)^2 + \frac{2N\beta^2}{F_5 - F_3}$$

$$\text{From which } K_{\parallel} - K_{\perp} = \frac{N\beta^2}{KT} \left[ \left( 1 - \frac{4\lambda}{F_4 - F_3} \right) - \left( 1 - \frac{\lambda}{F_5 - F_3} \right) \right]^2 \\ + N\beta^2 \left( \frac{8}{F_4 - F_3} - \frac{2}{F_5 - F_3} \right)$$

Substituting the values of  $\lambda = -829 \text{ cm}^{-1}$ ,  $F_4 - F_3$  and  $F_5 - F_3$  the values of  $\Delta K$  are calculated. These are given in table I along with those observed by Bose *et al* (1957) for comparison.

TABLE I  
Anisotropy Compared

	T°K	300	200	100	90
$\Delta K \times 10^6$	Observed	572	829	1573	1734
	Calculated	595	840	1574	1738

The fit may be considered as satisfactory in view of the fact that the tetragonal part of the field has been taken to be the same at all the temperatures. Thermal expansion of the crystal will probably change this part of the field and hence no single suitable set of tetragonal field parameters will be able to provide

an exact fit both at room and at low temperatures. Moreover the findings of Bagguley and Griffith show that above  $150^\circ\text{K}$  the field has an appreciable rhombic component. The variation of the setting angle with temperature indicates the variation of tetragonal field parameters, it does not indicate the magnitude of the tetragonal part (Bose *et al.*, 1961); Mookherji and Mathur, 1965).

#### EFFECT OF MAGNETIC DILUTION

Paramagnetic resonance data (Bagguley and Griffiths, 1952) show that for  $\text{K}_2\text{Cu}(\text{SO}_4)_2 \cdot 6\text{H}_2\text{O}$  diluted with the corresponding zinc Tutton salt ( $\text{Cu}^{++}$  less than 1%)  $K_{\parallel}$  becomes smaller than  $K_{\perp}$  at  $300^\circ\text{K}$  and reverse is the case at  $90^\circ\text{K}$ ; consequently the tetragonal field coefficients will change sign in this diluted salt. According to Van Vleck (1958) this change of sign will effect an inversion of the tetragonal stark levels.

Introducing this change of sign of  $Q'$  and  $A'$  in equation (1) and treating the crystal field perturbation as before we find that the form of the secular matrix is the same as before but the values of  $A_1$ ,  $A_2$ ,  $A_0$  and  $B$  are different. Taking  $K = 1680 \text{ cm}^{-1}$  and using the same tetragonal field parameters of  $\text{CuK}_2(\text{SO}_4)_2 \cdot 6\text{H}_2\text{O}$  crystal (undiluted) the energy levels are given by

$$F_3 = -6K - 4A - 3Q = -9687 \text{ cm}^{-1}$$

$$F_4 = +4K - 4A + 4Q = +7036 \text{ cm}^{-1}$$

$$F_5 = +4K + 2A - 2Q = +6562 \text{ cm}^{-1}$$

$$F_1 = -6K + 4A + 3Q = -10473 \text{ cm}^{-1}$$

The corresponding wave functions remain the same as given by equation (3). Thus  $F_1$  now lies lowest and  $F_4$  is higher than  $F_5$  showing an inversion of tetragonal stark levels with change of sign of the tetragonal field coefficients  $Q'$  and  $A'$ .

Taking the lowest as zero the energy levels are 0, (786), (17035), (17509)  $\text{cm}^{-1}$ . The tetragonal separation  $474 \text{ cm}^{-1}$  in this case also  $\text{cm}^{-1}$ , is expected as the percentage anisotropy of both the undiluted and diluted salt is ( $\approx 34\%$ ) the same.

When spin functions  $\alpha$  and  $\beta$  corresponding to the components  $s_z = \pm \frac{1}{2}$  with respect to z-axis are introduced the ground state  $|0\rangle$  is still doubly degenerate. These two states  $|0, \frac{1}{2}\rangle$  and  $|0, -\frac{1}{2}\rangle$  are modified by the spin orbit coupling the first order as follows :

$$f^+ = \left| 0, \frac{1}{2} \right\rangle - \frac{\lambda}{F_5 - F_0} \cdot \frac{\sqrt{6}}{2} \left| +1, -\frac{1}{2} \right\rangle$$

$$f^- = \left| 0, -\frac{1}{2} \right\rangle - \frac{\lambda}{F_5 - F_0} \cdot \frac{\sqrt{6}}{2} \left| -1, \frac{1}{2} \right\rangle$$

The degeneracy of these two states are lifted by the external magnetic field. On carrying out magnetic field perturbation calculations we get using the well-known formula of Van Vleck,

$$K_{\parallel} = \frac{N\beta^2}{KT} \quad \text{and} \quad K_{\perp} = \frac{N\beta^2}{KT} \left[ 1 - \frac{3\lambda}{F_5 - F_1} \right]^2 + \frac{6N\beta^2}{F_5 - F_1}$$

Hence 
$$K_{\parallel} - K_{\perp} = \frac{N\beta^2}{KT} \left[ 1 - \left( 1 - \frac{3\lambda}{F_5 - F_1} \right)^2 \right] - \frac{6N\beta^2}{F_5 - F_1}$$

Thus in this case  $K_{\perp}$  becomes greater than  $K_{\parallel}$  since  $\lambda$  is negative. The values of  $(K_{\perp} - K_{\parallel})$  are calculated and are included in Table II along with the observed values of Mookherji and Lal (1965) for a crystal  $2\text{K}_2(\text{Cu.Zn})(\text{SO}_4)_2 \cdot 6\text{H}_2\text{O}$  in which the amount of  $\text{Cu}^{++}$  ion is 0.81%.

TABLE II  
Magnetic anisotropy of diluted salt compared

	T°K	300	200	140	100	90
$(K_{\perp} - K_{\parallel})10^6$	Observed	470	661	1008	1545	-1734
	Calculated	482	678	930	1267	-1740

The fit is satisfactory except at 100°K considering the neglect of variation of the field parameters  $A$ ,  $Q$  with temperature. Thus the set of tetragonal field parameters which explain the magnetic behavior of the undiluted salt can explain also that of the diluted salt containing 0.81% of  $\text{Cu}^{++}$  ion with their signs changed in the potential function

#### SPECTROSCOPIC SPLITTING FACTOR

Abragam and Pryce (1951) have calculated the spectroscopic splitting factor  $g$  for  $\text{Cu}^{++}$  ion in the undiluted salt under the influence of a crystal field which is predominantly cubic in symmetry and over which is superimposed a small tetragonal component. For directions parallel and perpendicular to the tetragonal axis neglecting the square and product terms we have

$$g_{\parallel} = 2 - \frac{8\lambda}{F_4 - F_3} \quad \text{and} \quad g_{\perp} = 2 - \frac{2\lambda}{F_5 - F_3}$$

Using the values of  $(F_4 - F_3)$  and  $(F_5 - F_3)$  as deduced from magnetic anisotropy data we get

$$g_{\parallel} = 2.45 \quad \text{and} \quad g_{\perp} = 2.11$$

These compare well with observed values  $g_{\parallel} = 2.45$  and  $g_{\perp} = 2.05$  (Bleaney *et al*, 1949).

Now coming to the case of diluted crystal of  $2K_2(Cu\ Zn)(SO_4)_2 \cdot 6H_2O$  having less than 1% of  $Cu^{++}$  ion,  $g_{||}$  and  $g_{\perp}$  as calculated by Bagguley and Griffiths (1952) are given by.

$$g_{||} = 2.0 \text{ and } g_{\perp} = 2 - \frac{6\lambda}{F_5 - F_1}$$

Substituting for  $F_5 - F_1$  as deduced from magnetic anisotropy data gives  $g_{||} = 2.0$  and  $g_{\perp} = 2.29$ . These compare favourably with paramagnetic resonance data (2.05 and 2.26).

Further improvement on the theory including covalency factors is in progress in this laboratory.

We are thankful to Dr. D. Neogy, Pool Officer, to Messrs T. Mookherji and S. P. Chachra, Research Scholars of this Laboratory for their helpful discussions. Thanks are also due to Professor A. Bose, D.Sc., F.N.I. for helpful suggestions.

One of us (S.B) is grateful to the U.G.C. for the grant of a research scholarship.

#### REFERENCES

- Abragam, A. and Pryce, M. H. L., 1951, *Proc. Roy. Soc.*, **A205**, 135; **A206**, 164, 171.  
 Bagguley, D. M. S. and Griffiths, H. E., 1952, *Proc. Phys. Soc.*, **65**, 594.  
 Bethe, H., 1929, *Ann. der Phys.*, **3**, 133.  
 Bleaney, B., Penrose, R. P. and Plumptre, B. I., 1949, *Proc. Roy. Soc.*, **A198**, 406.  
 Bose, A., Mitra, S. C. and Dutta, S. K., 1957, *Proc. Roy. Soc.*, **A239**, 165.  
 Bose, A., Ghosh, U. S., Bagchi, R. N. and Pal, A. K., 1964, *Ind. J. Phys.*, **38**, 361.  
 Bose, A., Chakraborty, A. S. and Chatterjee, R., 1961, *Proc. Roy. Soc.*, **A261**, 43.  
 Hoffman, W., 1931, *Z. Krist.*, **78**, 279.  
 Mookherji, A. and Lal, R. B., 1965, *Ind. J. Pure & Appl. Phys.*, **3**, 288.  
 Mookherji, T. and Mookherji, A., 1965, *Ind. J. Pure & Appl. Phys.* (In press).  
 Mookherji, A. and Chhonkar, N. S., 1959, *Ind. J. Phys.*, **33**, 74.  
 Mookherji, A. and Mathur, S. C., 1965, *Physica* (In press).  
 Neogy, D. and Mookherji, A., 1965, *Physica* (In press).  
 Polder, D., 1942, *Physica*, **9**, 713.  
 Stevens, K. W. H., 1952, *Proc. Phys. Soc.*, **65**, 209.,  
 Van Vleck, J. H., 1958, *Ions of the Transition element-99, Disc. Faraday Soc.*, No. 26.

# ON THE INFRARED SPECTRA OF p-FLUORO- AND o-, m-, AND p-CHLORO TOLUENE IN THE VAPOUR STATE

D. K. MUKHERJEE, P. K. BISHTUI AND S. C. SIRKAR

INDIAN ASSOCIATION FOR THE CULTIVATION OF SCIENCE, CALCUTTA-32, INDIA

(Received September 30, 1965)

**ABSTRACT.** The infrared spectra of each of parafluoro-, and ortho-, meta- and para-chlorotoluene in the vapour and liquid states and in solution have been recorded on the same chart in order to find any changes which may take place in the spectra with the change of phase. It has been observed that some of the bands given by the compounds in the vapour state excepting orthochlorotoluene are absent in the spectra due to the compounds in the liquid state. It has been concluded that formation of dimers in some percentages of the molecules takes place even in the vapour phase of these three compounds. Orthochlorotoluene does not show such changes.

From a comparison of the infrared frequencies with the Raman frequencies of the compounds in the liquid state assignments of the frequencies have been made. It has been pointed out that some of the assignments made by previous workers need revision in view of the fact that the observed infrared bands cannot be explained satisfactorily by the earlier assignments.

## INTRODUCTION

The infrared spectra of a very large number of mono- and disubstituted benzenes were investigated previously by many workers who used mostly solutions of the compounds in suitable solvents. Recently, the present authors pointed out (Sirkar *et al.*, 1964) that the spectra of fluoro-, chloro-, bromo- and iodobenzene in the vapour state show additional bands which are absent in the spectra of the compounds in the liquid state. It was concluded from a comparison of the spectra of each of these compounds in the two states that partial intermolecular association takes place in all these compounds even in the vapour state and the percentage of the associated molecules increases when the vapours are liquefied. A comparison of these spectra with the Raman spectra of the substances in the liquid state was found to be helpful in assigning the frequencies to different modes of vibration of the molecules.

Disubstituted benzenes in which one of the substituents is a halogen atom are expected to exhibit such association in the liquid state. The spectra of chlorotoluenes in the vapour state were not studied by any previous worker and although those of fluorotoluenes were studied both in liquid and vapour states by Thompson and Temple (1948) the significance of the changes in the spectra produced by the

change of the state was not discussed by those authors. Hence, the present investigation on the infrared spectra of parafluorotoluene, parachlorotoluene, orthochlorotoluene and metachlorotoluene in the vapour and liquid states and in solution in carbon tetrachloride and cyclohexane was undertaken with a view to finding out whether the spectra reveal the evidence of intermolecular association and also assigning the frequencies to different modes of vibration from a comparison of the spectra with the Raman spectra of the substances in the liquid state.

#### EXPERIMENTAL

The liquids supplied by British Drug House and Light and Company of England were of chemically pure quality and they were redistilled under reduced pressure. The purity of the liquids was tested by studying the Raman spectra.

The infrared spectra were recorded with a Perkin-Elmer model 21 double beam infrared spectrophotometer provided with NaCl prism. In the case of the pure liquid a thin film enclosed between two NaCl plates was used. A multiple reflection 100-cm gas cell supplied by Perkin-Elmer Corporation was used to record the infrared absorption spectra of the vapours at the room temperature. In the case of the solution, a compensation cell was placed in the reference beam, but the bands appearing in the positions of the strong bands of the solvents were suppressed. The spectrophotometer was calibrated with the help of the spectrum due to a thin sheet of polystyrene and the corrections required in observed frequencies in the different regions were found out and applied to get the correct values of the frequencies. In order to find out the changes in the spectrum with the change from the vapour to the liquid phase, the spectra due to the two phases of each of the compounds were recorded on the same chart.

#### RESULTS AND DISCUSSIONS

The spectra are reproduced in Figs. 1, 2, 3 and 4 respectively. The corrected values of the observed frequencies are given in Tables I, II, III and IV in which, besides the bands due to the solutions, the Raman frequencies of the liquids reported by previous workers have also been included for comparison. The assignments of the frequencies in terms of the corresponding modes of benzene have been given in the last column of the Tables. The results are discussed separately in the following sections.

#### PARAFLUOROTOLUENE

The Raman frequencies of this liquid are taken from Mecke-Kerkhof (1951), but the three frequencies 311, 501 and 728  $\text{cm}^{-1}$  are taken from Magat (1936).

It can be seen from Fig. 1 as well as Table I that the structure of some of the bands in the spectrum of the vapour changes when the vapour is liquefied. In the spectrum due to the vapour there are doublets at 720, 730  $\text{cm}^{-1}$ ;



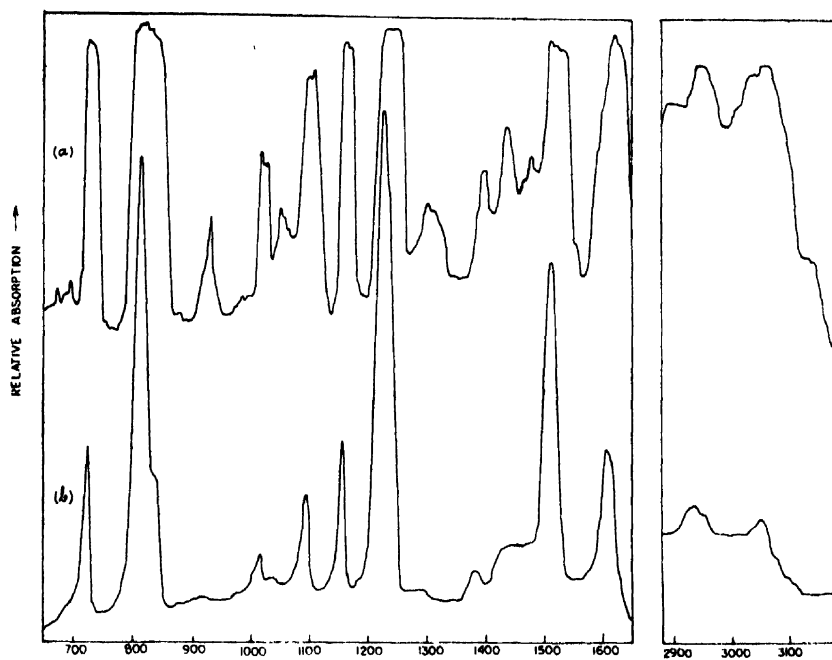


Fig. 1. Spectra of parafluorotoluene  
(a) Vapour

(b) Liquid

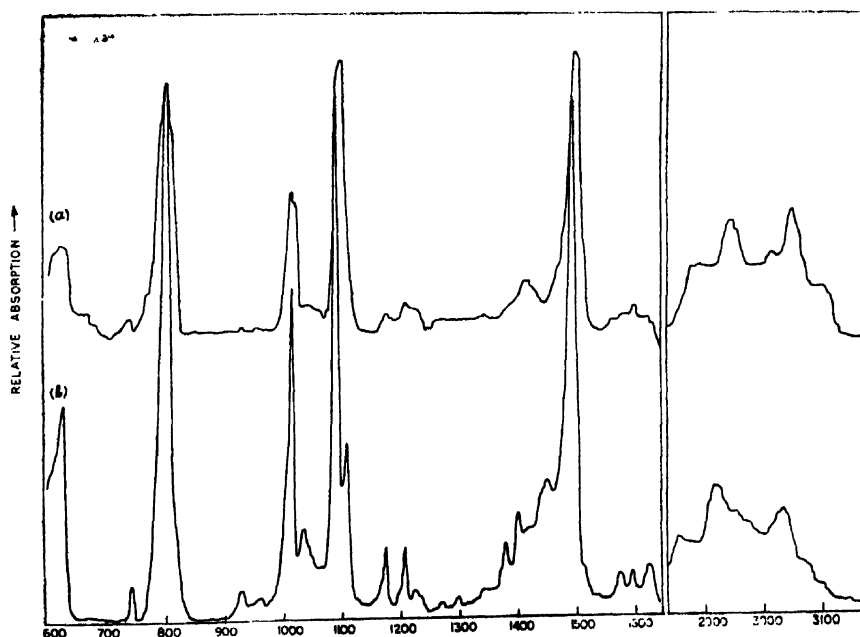
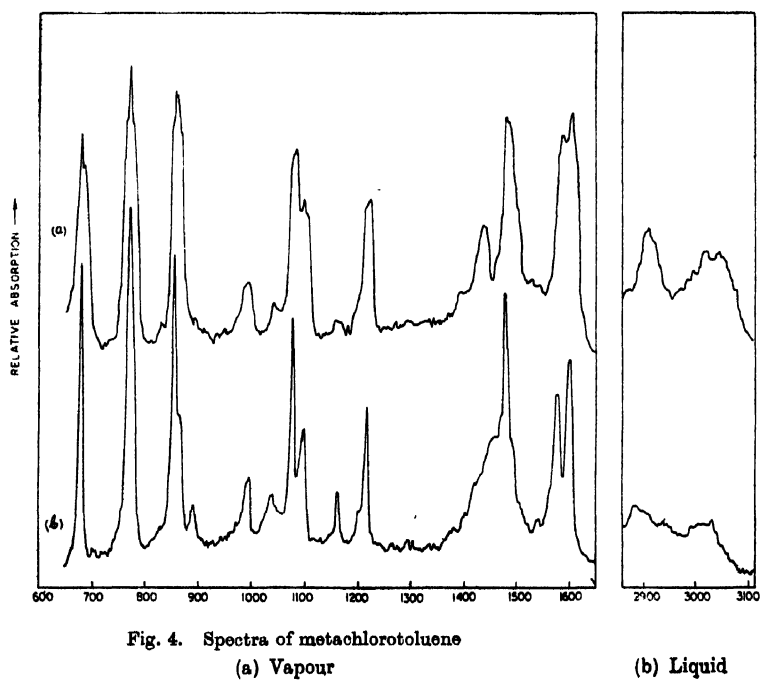
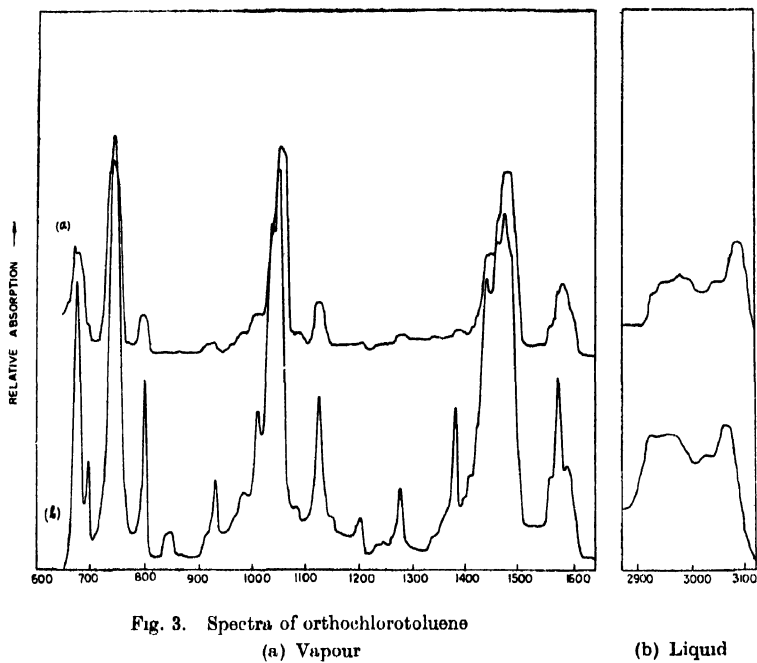


Fig. 2. Spectra of parachlorotoluene  
(a) Vapour

(b) Liquid



810, 820  $\text{cm}^{-1}$ ; 830, 840  $\text{cm}^{-1}$ ; 1095, 1104  $\text{cm}^{-1}$ ; 1158, 1166  $\text{cm}^{-1}$  and 1232, 1248  $\text{cm}^{-1}$  respectively, but in the corresponding positions the spectrum due to the liquid shows only single bands at 720, 810, 833, 1095, 1158 and 1222  $\text{cm}^{-1}$  respectively. Evidently, the vapour consists of two types of molecules. These are probably the single molecules and dimers formed by intermolecular hydrogen-bonding and the higher of the two frequencies in each doublet is the frequency of the single molecule. The frequencies reported by Thompson and Temple (1948) for the liquid differ slightly from those given in Table I. A comparison of the spectra due to the vapour and the liquid reproduced in Fig. 1, however, shows that the band of higher frequency in each of the doublets mentioned above is absent in the spectrum due to the liquid and this conclusion is not affected by any small error in calibration of the spectrophotometer which is less than 2  $\text{cm}^{-1}$  in the region 610–1200  $\text{cm}^{-1}$ .

TABLE I  
Parafluorotoluene

Raman frequencies (liquid) $\Delta\nu$ in $\text{cm}^{-1}$	Infrared frequencies in $\text{cm}^{-1}$				Assignment (correspond- ing modes of $\text{C}_6\text{H}_5$ )
	Vapour	Liquid	Soln. in $\text{CCl}_4$	Soln. in cyclohexane	
311 (0)*					11
338 (3), <i>dp</i>					10 B
453 (3), <i>p</i>					6 A
501 (0.5)*					18 B
636 (2), <i>dp</i>					6 B
693 (0), <i>p</i>				715 (10)	3 (?)
	720 (s)	720 (s)			
728 (1)*	730 (s)			730 (m)	9 B
	810 (s)	810 (vs)	805 (m)		
			815 (vs)	817 (vs)	12
	820 (s)				
824 (6n), <i>p</i>	830 (s)				
		833 (m)			10 A
			838 (m)	838 (m)	
	840 (w)				
841 (3), <i>p</i>	847 (w)				1
	928 (m)				18 A
					17 A
1001 (0), <i>p</i>	1015 (m)	1015 (vw)		1015 (w)	
	1025 (m)			1030 (w)	
	1032 (w)				
			1090 (vw)		
	1095 (s)	1095 (m)	1098 (w)		19 A
	1104 (s)				
1157 (1), <i>p</i>	1158 (s)	1158 (m)	1160 (m)		9 A
	1166 (s)				

TABLE I (*contd.*)

Raman frequencies (liquid) $\Delta\nu$ in $\text{cm}^{-1}$	Infrared frequencies in $\text{cm}^{-1}$				Assignment (correspond- ing modes $\text{C}_6\text{H}_6$ )
	Vapour	Liquid	Soln. in $\text{CCl}_4$	Soln. in cyclohexane	
1211 (3b), <i>p</i>			1210 (vw)	1216 (vw)	2
	1222 (vw)	1222 (vs)			
	1232 (vs)		1230 (vs)	1232 (vs)	
	1248 (vs)				20 A
1297 (0), <i>p</i>	1292 (w)	1290 (vw)			13
1383 (1), <i>p</i>	1378 (vw)	1378 (w)			$\text{CH}_3$ bending
	1390 (m)				
	1415 (vvw)	1415 (w)			
1453 (0), <i>dp</i>	1429 (m)				
	1468 (vw)				$\text{CH}_3$ bending
	1505 (vs)	1505 (vs)	1505 (vs)		
	1516 (s)			1516 (s)	19 B
	1528 (s)				
	1584 (w)	1586 (w)			
1599 (1)	1598 (m)	1600 (m)	1602 (m)	1595 (vvw)	8 A
	1612 (vs)	1608 (m)	1610 (w)	1610 (w,b)	8 B
1615 (1)					
	1622 (s)				
	1632 (m)				
	1735 (w)				
	1742 (w)				
	1752 (m)				
	1870 (m)	1865 (m)	1865 (vw)		
	1880 (m)	1875 (m)	1875 (vw)		
	1978 (w)				
	2085 (vw)				
	2400 (vw)				
	2465 (vw)				
2739 (0)					
	2750 (vw)				
	2850 (vw)	2850 (m)			
2872 (3)		2885 (m)			
	2890 (m)				
	2900 (s)	2900 (m)			
2926 (3)	2930 (vw)	2930 (s)			$\text{CH}_3$ valence
	2940 (vs)				
	2960 (vs)	2950 (w)			
	3020 (s)				
	3030 (s)	3030 (s)	3030 (m)	3030 (m)	
	3040 (s)	3040 (vw)			
3048 (7)					7 B
3073 (8)	3075 (m)	3075 (w)	3070 (vw)	3070 (vw)	20 B & 2'
	3115 (m)				
3207 (0)					

The frequency  $841\text{ cm}^{-1}$  has been assigned to a mode corresponding to the breathing vibration of benzene. This frequency has been assigned by Mecke-Kerkhof (1951) to C-F valence oscillations, but the fact that the corresponding infrared band is extremely weak shows that such an assignment is not correct. The frequency of the mode in the single molecule is  $847\text{ cm}^{-1}$  as shown by the weak infrared band. The assignment of the frequency  $1095\text{ cm}^{-1}$  of the liquid to mode No. 19A (Pitzer and Scott, 1943) is in accordance with such an assignment made in the case of similar molecules by Mecke-Kerkhof (1951). The Raman line  $1211\text{ cm}^{-1}$  of the liquid is highly polarized, but this frequency is absent in the infrared spectrum of the liquid. So the mode of this frequency is of symmetric type and cannot be assigned to  $\nu_{12}$  as has been done by Mecke-Kerkhof (1951). Hence this frequency has been assigned to a mode similar to mode No. 2 of benzene in which the C-F, C-CH<sub>3</sub> and C-H valence oscillations take part simultaneously in phase with each other. Similarly, the frequency  $1248\text{ cm}^{-1}$  has been assigned to a mode of the single molecule arising from  $\nu_{20A}$  of benzene and the corresponding frequency in the dimer is  $1222\text{ cm}^{-1}$ . Again, the frequency  $1297\text{ cm}^{-1}$  has been assigned to a mode similar to  $\nu_{13}$  of benzene and not to  $\nu_{19A}$ . The frequency  $1608\text{ cm}^{-1}$  of the liquid which is assigned to mode  $\nu_{8B}$  of benzene ring has two more companions at  $1622$  and  $1632\text{ cm}^{-1}$  respectively in the case of the vapour. The frequency  $1622\text{ cm}^{-1}$  may be that of the single molecule and  $1632\text{ cm}^{-1}$  may be due to an alternative configuration of the mode as suggested previously (Sirkar *et al.*, 1964) in the case of mono substituted benzenes. The frequency  $1600\text{ cm}^{-1}$  is assigned to  $\nu_{8A}$  of the ring, as done by the above authors.

As regards the frequencies of C-H valence oscillations it appears that the strong  $3030\text{ cm}^{-1}$  band of the liquid is due to a mode different from that producing the strong Raman line  $3048\text{ cm}^{-1}$ . This line is evidently due to a mode similar to  $\nu_{7B}$  of benzene which is forbidden in the infrared spectrum. The band  $3030\text{ cm}^{-1}$  may then be due to  $\nu_{20B}$  of benzene in the dimer formed by association, the band  $3075\text{ cm}^{-1}$  due to the vapour being the corresponding band of the single molecule. The strong Raman line  $3073\text{ cm}^{-1}$  is also produced by a mode different from  $\nu_{20}$  which is forbidden in the Raman effect and it appears that when hydrogen-bonding takes place between the hydrogen atoms of the CH<sub>3</sub> group and the fluorine atom, as indicated by the change in the relative intensities of the bands  $2940$  and  $2930\text{ cm}^{-1}$  with the change of state, the C-H vibrations in the four C-H groups of the ring take place in accordance with the symmetry of  $\nu_2$  of benzene and such a mode produces the Raman line  $3073\text{ cm}^{-1}$ .

It is therefore concluded that the vapour of parafluorotoluene is a mixture of single molecules and dimers while the liquid consists almost wholly of dimers.

#### PARACHLOROTOLUENE

In the case of parachlorotoluene also there is a strong polarised Raman line at  $796\text{ cm}^{-1}$ , but the corresponding infrared band is weak. This frequency has

**TABLE II**  
**Parachlorotoluene**

Raman frequencies (liquid) $\Delta\nu$ in $\text{cm}^{-1}$	Infra red frequencies in $\text{cm}^{-1}$				Assignment (correspond- ing modes of $\text{C}_6\text{H}_5$ )
	Vapour	Liquid	Soln. in $\text{CCl}_4$	Soln. in cyclohexane	
304 (3), <i>dp</i>					10 B
377 (12), <i>p</i>					6 A
	612 (vw)	610 (w)			
	624 (m)	626 (s)			18 A
635 (3), <i>dp</i>	634 (w)		630 (s)		6 B
	638 (w)				
				672 (vw)	9 B
692 (0), <i>dp</i>	720 (vvw)				
	742 (w)	742 (w)			
796 (5), <i>p</i>	795 (m)				1
	805 (s)	802 (vs)		802 (s)	12
	810 (m)				10 <sup>a</sup> A
819 (1), <i>p</i>	1012 (s)	1013 (vs)			
	1020 (m)				17 A
1036 (1)	1030 (vw)	1030 (w)			
	1045 (w)	1045 (vw)			
1090 (5), <i>p</i>	1088 (m)	1088 (vs)			
	1096 (vs)				19 A
	1106 (vw)	1106 (w)	1106 (s)		
1175 (1)	1172 (vw)	1172 (w)	1172 (m)	1172 (w)	9 A
1208 (3), <i>p</i>	1208 (w)	1208 (w)	1206 (w)	1208 (w)	2
	1225 (vw)		1225 (vvw)		
			1296 (vw)		7 A (?)
1303 (0)					13 (?)
1377 (2), <i>p</i>		1375 (w)	1380 (m)		$\text{CH}_3$ bending
	1392 (vvw)				
		1396 (w)			
	1408 (w)		1402 (s)		
			1418 (vw)		
	1442 (vw)	1445 (vw)			
1452 (0), <i>dp</i>	1455 (w)		1450 (s)		$\text{CH}_3$ bending
			1475 (vs)		
	1490 (s)	1490 (vs)			19 B
	1498 (s)				
	1570 (vvw)	1572 (w)		1575 (w)	
1596 (8), <i>p</i>	1590 (w)	1592 (w)		1598 (w)	8 A
	1618 (vvw)	1620 (w)		1624 (s)	8 B
	1628 (vw)		1630 (s)		

TABLE II (contd.)

Raman frequencies (liquid) $\Delta\nu$ in $\text{cm}^{-1}$	Infra red frequencies in $\text{cm}^{-1}$				Assignment (corresponding modes of $\text{C}_6\text{H}_6$ )
	Vapour	Liquid	Soln. in $\text{CCl}_4$	Soln. in cyclohexane	
			1720 (w)	1720 (w)	
			1772 (m)	1770 (vw)	
	1880 (w)	1880 (m)	1890 (s)	1885 (s)	
	1890 (w)				
		2855 (m)			
	2885 (m)		2880 (s)		
	2920 (vw)	2920 (vs)			
2922 (3), <i>p</i>	2940 (vs)		2930 (vs)		( $\text{CH}_3$ valence)
		2950 (vw)			
			2970 (w)		
	2985 (w)		2990 (w)		
	3010 (vw)	3010 (vw)			
	3035 (vs)	3020 (s)	3026 (vs)		
3047 (2)					
3062 (4)		3060 (m)			7 B
3070 (1)	3080 (m)		3070 (m)		2'
					20 B

been assigned to the total symmetric vibration similar to  $\nu_1$  of benzene and not to C-Cl valence oscillation alone. The bands 805, 1012, 1030, 1088, 1208, 1490 and  $2920 \text{ cm}^{-1}$  have close companions at 810, 1020, 1045, 1096, 1225, 1498 and  $2940 \text{ cm}^{-1}$  respectively in the spectrum due to the vapour, but these latter bands are absent in the spectrum due to the liquid. Hence in this case also the vapour consists of monomeric and dimeric molecules, the percentage of the latter being smaller than that in the case of parafluorotoluene in the vapour state. The liquid seems to consist wholly of associated molecules. As in the case of parafluorotoluene the mode  $\nu_{12}$  has the frequency  $810 \text{ cm}^{-1}$  in the single molecule and  $802 \text{ cm}^{-1}$  in the associated molecules in the liquid, this frequency being much lower than  $1208 \text{ cm}^{-1}$  assigned by Mecke-Kerkhof (1951) to this mode. There is no reason why the frequency of this mode in this substituted molecule should be higher than that in benzene. The fact that this frequency does not appear in the Raman spectrum of the liquid clearly indicates the correctness of its assignment to a mode of the ring which is of symmetry  $b_{1u}$ . In this case also the mode giving the strong and polarized Raman line  $1208 \text{ cm}^{-1}$  produces only a weak band in the infrared, and therefore, this frequency has been assigned to a mode similar to  $\nu_2$  of benzene. The assignment of the frequency  $1096 \text{ cm}^{-1}$  to  $\nu_{12A}$  of the ring of the monomeric molecule agrees with that of the frequency  $1090 \text{ cm}^{-1}$  made by Mecke-Kerkhof (1951) to this mode in the liquid. In this case also the change in the  $\text{CH}_3$  frequencies with the change of phase indicates the formation of

hydrogen bonds in the liquid. The Raman lines 3047 and 3062  $\text{cm}^{-1}$  are to be assigned respectively to  $\nu_{7B}$  and  $\nu_2$  of the dimers as in the case of parafluorotoluene, while  $\nu_{20B}$  has the value 3080  $\text{cm}^{-1}$  in the case of the single molecule and 3020  $\text{cm}^{-1}$  in the associated molecule in the liquid.

# ORTHOCHLOROTOLUENE

The Raman frequencies of this liquid have been taken both from Magat (1936) and Mecke-Kerkhof (1951). A comparison of the infrared bands for the vapour and the liquid shows that except the bands at 1060  $\text{cm}^{-1}$  and 1580  $\text{cm}^{-1}$  all the other bands of high and medium strengths given by the vapour appear also in the spectrum of the liquid. The two bands 668 and 676  $\text{cm}^{-1}$  of the vapour are replaced by a single band of intermediate frequency 672  $\text{cm}^{-1}$ . The band 743  $\text{cm}^{-1}$  is also produced in the same way in place of the two sharp bands 740 and 745  $\text{cm}^{-1}$ . Probably the intermolecular forces in the liquid make the components

TABLE III  
Orthochlorotoluene

Raman frequencies (liquid) $\Delta\nu$ in $\text{cm}^{-1}$	Infra red frequencies in $\text{cm}^{-1}$				Assignment (correspond- ing modes of $\text{C}_6\text{H}_6$ )
	Vapour	Liquid	Soln. in $\text{CCl}_4$	Soln. in cyclohexane	
166 (8), <i>dp</i>					10 B
247 (5), <i>dp</i>					10 A
361 (3), <i>dp</i>					6 A
447 (4)					18 B
552 (7)					6 B
	668 (m)	672 (s)			
678 (6), <i>p</i>	676 (m)		674 (vs)	676 (s)	9 B
	695 (vw)	695 (w)	694 (vw)	696 (m)	
745 (1)	740 (s)	743 (s)		740 (vs)	12
	745 (m)				
	795 (vw)				
803 (4)	800 (vw)	800 (m)		802 (m)	1
		847 (vw)			
852 (00)				910 (vvw)	
	918 (vvw)	918 (vvw)			
	930 (vvw)	930 (m)	933 (m)	932 (w)	
989 (1)	985 (vvw)	986 (m)	986 (w)	986 (w)	17 A
1016 (0)	1012 (vw,b)	1012 (m)	1012 (w)	1010 (s)	
	1038 (m)	1036 (s)	1038 (vs)	1025 (m)	
1045 (8), <i>p</i>				1040 (m)	
	1050 (vs)	1050 (vs)	1050 (s)	1050 (s)	19 A
	1060 (s)				



TABLE III—(contd.).

Raman frequencies (liquid) $\Delta\nu$ in $\text{cm}^{-1}$	Infra red frequencies in $\text{cm}^{-1}$				Assignment (correspond- ing modes of $\text{C}_6\text{H}_6$ )
	Vapour	Liquid	Soln. in $\text{CCl}_4$	Soln. in cyclohexane	
	1124 (vw)	1124 (m)	1086 (vw) 1126 (s)	1086 (vw) 1127 (m)	
1132 (2)					
1156 (2)			1152 (vw)		9 A
1204 (5)	1204 (vvw)	1206 (w)	1203 (vvw)	1206 (vw)	2
1279 (0.5)	1278 (w,b)	1273 (w)	1278 (m)		7 A
	1380 (vw)	1380 (m)	1382 (s)	1342 (vvw) 1374 (vw)	$\text{CH}_3$ bending
1426 (0)	1422 (vvw)		1408 (vw) 1425 (w)		$\text{CH}_3$ bending
	1442 (m)	1440 (m)	1442 (vs)		
	1460 (w)	1460 (m)	1460 (m)		
	1472 (vs)	1472 (vs)	1470 (s)		
	1482 (vs)	1482 (w)			
	1560 (vw)	1560 (vw)			19 B
1574 (3)	1570 (vw)	1570 (m)		1573 (m)	8 A
	1580 (m)				
1592 (3)	1590 (vw)	1590 (w)		1594 (m)	8 B
	1600 (vw)				
			1670 (w)	1670 (vvw)	
	1780 (vw,b)		1785 (m)	1780 (w)	
	1820 (vvw)		1830 (w)	1820 (vw)	
			1870 (vw)	1865 (vvw)	
	1905 (vw)		1908 (m)	1904 (w)	
	1950 (vw)		1950 (m)	1950 (w)	
2859 (0)	2850 (vw)	2855 (vw)			
			2870 (m)		
	2880 (w)	2880 (w)			
2926 (5)	2930 (m)	2930 (s)		2930 (m)	$\text{CH}_3$ valence symmetric
			2940 (s)		
	2950 (s)	2950 (s)			
			2960 (s)	2960 (m)	
	2970 (s)	2970 (s)			
			2980 (m)	2980 (m)	$\text{CH}_3$ valence asymmetric
3013 (0)					7 B
		3025 (w)	3020 (w)	3020 (vw)	
	3040 (w)				
		3055 (s)	3055 (vs)	3055 (vs)	20 B
3062 (7)					2'
	3080 (s)				

of the bands too broad to be resolved. The disappearance of the bands  $1060\text{ cm}^{-1}$  and  $1580\text{ cm}^{-1}$  is, however, of different nature. It seems that each of these modes

has two alternative configurations in the vapour but one of these cannot take place in the liquid. So, it is concluded that the vapour consists of single molecules and in the liquid also the intermolecular forces are too weak to change the frequencies appreciably. The frequencies of  $\text{CH}_3$  valence oscillations also remain unchanged with the change of state, which shows that no hydrogen bond is formed in this case through the  $\text{CH}_3$  group.

In assigning the Raman frequencies in the region  $100\text{ cm}^{-1}$  to  $600\text{ cm}^{-1}$  the expected change of frequency of vibration with substitution has been chosen as the guiding factor. The two lines  $247\text{ cm}^{-1}$  and  $166\text{ cm}^{-1}$  are depolarised and very intense. So, they have been assigned to modes similar to  $\nu_{10A}$  and  $\nu_{10B}$  of benzene in which the displacements are perpendicular to the plane of symmetry. Similarly, the lines  $552\text{ cm}^{-1}$  and  $361\text{ cm}^{-1}$  have been assigned respectively to modes similar to  $\nu_{6B}$  and  $\nu_{6A}$  of benzene, because the frequency of the former mode should be larger than that of the latter mode. The line  $447\text{ cm}^{-1}$  is evidently due to an in-plane vibration and has been assigned to  $\nu_{18B}$ . In place of the strong and polarised Raman line  $678\text{ cm}^{-1}$  there is a strong infra-red band. So the corresponding mode is derived from a centro-symmetric mode of benzene and  $\nu_{9B}$  has been chosen for this frequency. In  $\nu_{9A}$  either the chlorine atom or the  $\text{CH}_3$  group may remain at rest and this may give rise to two different frequencies. The Raman lines  $1156\text{ cm}^{-1}$  and  $1132\text{ cm}^{-1}$  have been assigned to those two alternative configurations. In the spectrum of the liquid there is a strong Raman line  $1045\text{ cm}^{-1}$  and a strong infrared band at  $1050\text{ cm}^{-1}$ . This is assigned to a mode similar to  $\nu_{19A}$  of benzene. As in the previous two cases, the strong Raman line  $1204\text{ cm}^{-1}$  is due to a mode derived from a symmetric mode of benzene and therefore it has been assigned to  $\nu_2$ .

It is found that the frequencies of the bands due to  $\text{CH}_3$  valence oscillation remain unchanged with the change from vapour to the liquid phase, but the bands  $3080\text{ cm}^{-1}$  and  $3040\text{ cm}^{-1}$  due to C-H valence oscillation of the benzene ring shift respectively to  $3055\text{ cm}^{-1}$  and  $3025\text{ cm}^{-1}$  with liquefaction of the vapour. These two bands can be assigned to modes similar to  $\nu_{20B}$  and  $\nu_{7B}$  of benzene respectively and it seems that such oscillations can take place even when one of the four C-H groups is substituted by a CX group. The shift may be due to influence of dielectric constant of the liquid, because even in the solutions such a shift takes place. The Raman line  $3062\text{ cm}^{-1}$  is also due to a vibration in which symmetric C-H valence oscillation takes place in two diametrically opposite C-H groups.

#### METACHLOROTOLUENE

The Raman frequencies of the liquid included in Table IV are taken from the data reported by Biswas (1955). A comparison of the infrared bands due to the vapour with those due to the liquid shows that the bands at  $774$ ,  $854$ ,  $859$ ,  $1082$ ,  $1100$ ,  $1482$  and  $3080\text{ cm}^{-1}$  produced by the vapour are absent in the spectrum

TABLE IV  
Metachlorotoluene

Raman frequencies (liquid) $\Delta\nu$ in $\text{cm}^{-1}$	Infrared frequencies in $\text{cm}^{-1}$				Assignment (correspond- ing modes of $\text{C}_6\text{H}_6$ )
	Vapour	Liquid	Soln. in $\text{CCl}_4$	Soln. in cyclohexane	
187 (5), <i>dp</i>					10 B
222 (5), <i>dp</i>					10 A'
247 (5), <i>dp</i>					10 A
394 (1), <i>p</i>					18 B
419 (7), <i>p</i>					6 A
522 (6), <i>p</i>					6 B
	670 (w)				
	676 (s)	676 (vs)	676 (vs)		
683 (7), <i>p</i>	682 (m)			680 (vs)	
	687 (w)			745 (vw)	9 B
	758 (w)				
	763 (w)				
	768 (vs)	768 (vs)	770 (vs)	766 (vs)	
775 (2)	774 (m)			772 (w)	12
				776 (m)	
	850 (m)	851 (vs)	850 (s)		
	854 (s)				
	859 (s)		859 (vw)		
861 (3), <i>p</i>					18 A
		863 (m)			
	864 (m)				
884 (0)					
		890 (vw)	890 (s)		
948 (0)					
			983 (m)	988 (s)	
	990 (w)	992 (w)			
998 (10), <i>p</i>					1
1042 (1)	1036 (vw)	1036 (vw)	1036 (s)		
	1075 (s)	1074 (s)	1072 (vs)	1074 (vs)	
1077 (4), <i>p</i>					
	1082 (m)			1080 (m)	19 A
1102 (2)	1095 (m)	1095 (m)	1094 (vs)	1095 (w)	9 A'
	1100 (w)				
1160 (2)	1160 (vw)	1160 (w)	1162 (s)	1162 (s)	9 A
			1200 (m)		
				1206 (m)	
1209 (1)	1210 (m)		1210 (m)		7 A
1219 (4), <i>p</i>	1215 (w)	1215 (m)		1215 (vs)	2
			1292 (vw)		
			1330 (vvw)		
			1378 (vw)		

TABLE IV—(*contd.*)

Raman frequencies (liquid) $\Delta\nu$ in $\text{cm}^{-1}$	Infrared frequencies in $\text{cm}^{-1}$				Assignment (corresponding modes of $\text{C}_6\text{H}_6$ )
	Vapour	Liquid	Soln. in $\text{CCl}_4$	Soln. in cyclohexane	
1383 (2), $p$	1385 (vvw)		1385 (vw)		$\text{CH}_3$ bending
			1400 (m)		
	1430 (m)		1420 (m)		
	1450 (vw)	1450 (w)	1450 (vs)		
	1465 (w)	1462 (vw)	1462 (w)		19 B
	1475 (s)	1473 (vs)	1475 (s)		
	1482 (m)				
	1490 (vw)	1490 (vw)	1492 (vw)		
1574 (3), $dp$	1570 (w)	1570 (m)	1570 (m)		
	1575 (w)				
	1582 (m)			1580 (s)	8 A
		1592 (s)	1592 (vs)		
1601 (4), $dp$	1598 (vs)			1598 (m)	
	1607 (w)			1606 (s)	8 B
			1940 (m)	1940 (m)	
2862 (2)		2840 (vw)			
	2860 (w)		2865 (m)		
2962 (6b), $p$	2905 (vw)	2902 (m)			
	2925 (s)	2925 (vw)	2930 (vs)		$\text{CH}_3$ valence
	2955 (vvw)	2950 (vw)	2955 (w)		
	3000 (vw)	3000 (w)	2980 (w)		
	3020 (m)	3020 (m)	3025 (s)		
3062 (10b), $p$	3050 (m)	3050 (vvw)	3050 (s)		
					2' & 7 A'
	3080 (w)		3080 (w)		20 B

of the liquid. These are weaker companions of the adjacent strong bands. The disappearance of these weaker bands shows that probably they are due to the small percentage of the single molecules present in the vapour and that in the liquid almost all the molecules are dimers formed by intermolecular association.

The Raman lines 998, 1219 and  $1209\text{ cm}^{-1}$  have been assigned respectively to modes similar to  $\nu_1$ ,  $\nu_2$  and  $\nu_{7A}$  of benzene. The line  $1077\text{ cm}^{-1}$  is represented by a strong band in the infrared spectrum and therefore it has been assigned to  $\nu_{19A}$ . The assignment of this frequency agrees with that made by Mecke-Kerkhof (1951), but it disagrees with the assignment made by Katritzky and Simmons (1959) who assume the frequency of  $\nu_{19A}$  in this case to be  $1476\text{ cm}^{-1}$ . In the case of parachlorotoluene also they have made similar assumption. The Raman line  $1102\text{ cm}^{-1}$  may be due to an alternative configuration of  $\nu_{9A}$  in which the  $\text{CH}_3$  group remains at rest.

The frequencies of  $\text{CH}_3$  valence oscillations seem to remain unaltered with the change of phase in this case, but the relative intensities of some of the bands due

to  $\text{CH}_3$  and C-H oscillations undergo remarkable changes. Thus, the bands  $2925\text{ cm}^{-1}$  and  $3050\text{ cm}^{-1}$  become very weak and the bands  $2902\text{ cm}^{-1}$  and  $3020\text{ cm}^{-1}$  become stronger when the vapour is liquefied. The frequency  $3020\text{ cm}^{-1}$  may be that of the dimeric molecule in the liquid. The Raman line  $3062\text{ cm}^{-1}$  is evidently due to a mode different from that producing the infrared band  $3020\text{ cm}^{-1}$  and it may be due to symmetric valence oscillation in two dimetrically opposite C-H groups. Such an oscillation is possible both in  $\nu_2$  and  $\nu_{7B}$  with the same frequency and therefore this Raman line has been assigned to two such modes designated as  $\nu_2$  and  $\nu_{7B}$ .

As regards the Raman lines in the region  $180\text{--}300\text{ cm}^{-1}$  it is significant that in place of the two depolarised lines  $247$  and  $166\text{ cm}^{-1}$  due to orthochlorotoluene, three depolarised lines at  $247$ ,  $222$  and  $187\text{ cm}^{-1}$  are given by metachlorotoluene. The frequency  $247\text{ cm}^{-1}$  is assigned to a mode corresponding to  $\nu_{10A}$  in which the chlorine atom remains at rest. When the  $\text{CH}_3$  group remains at rest in a similar mode (marked  $10A'$  in Table IV) the frequency is lowered and the line  $227\text{ cm}^{-1}$  may be due to such a mode. In the case of orthochlorotoluene also such an alternative mode would be expected, but probably the two components produce a broad band and are not resolved from each other.

#### ACKNOWLEDGMENT

The work was done in a scheme sanctioned by the Council of Scientific and Industrial Research. Two of the authors (S.C.S. and P.K.B.) are indebted to the Council for the financial help. The authors' thanks are also due to the authorities of the Indian Association for the Cultivation of Science for providing all the facilities for carrying out the investigation.

#### REFERENCES

- Biswas, D. C., 1955, *Ind. J. Phys.*, **29**, 257.  
 Katritzky, A. R. and Simmons, P., 1959, *J. Chem. Soc. (London)*, p. 2051; 2058.  
 Magat, M., 1936, *Annual Table of Constants*, p. 26-77.  
 Mecke-Kerkhof, 1951, *Landolt-Bornstein Tables*, Auf. 6, Band, I, Teil 2.  
 Pitzer, K. S. and Scott, D. W., 1943, *J. Amer. Chem. Soc.*, **65**, 803.  
 Sirkar, S. C., Mukherjee, D. K. and Bishui, P. K., 1964, *Ind. J. Phys.*, **38**, 610.  
 Thompson, H. W. and Temple, R. B., 1948, *J. Chem. Soc. (London)*, p. 1432.

# Letters to the Editor

The Board of Editors does not hold itself responsible for opinions expressed in the letters published in this section. The notes containing short reports of original investigations communicated to this section should not contain many figures and should not exceed 500 words in length. The contributions reaching the Secretary by the 15th of any month may be expected to appear in the issue for the next month. No proof will be sent to the author.

26

## LOW ENERGY SCATTERING OF ELECTRON BY HELIUM ATOM BY THE VARIATIONAL METHOD

SATYA NARAYAN BANERJEE, RAMESHWAR JHA AND N. C. SIL

DEPARTMENT OF THEORETICAL PHYSICS,

INDIAN ASSOCIATION FOR THE CULTIVATION OF SCIENCE, JADAVPUR, CALCUTTA-32.

(Received September 14, 1965).

The elastic scattering cross section of electrons by helium is being investigated for such low energy of the incident electron when only *S*-wave phase shift needs to be considered. We apply the variation method of Hulthen with an open shell wave function and with a polarization term in the potential to take into account the distortion of the helium charge cloud due to the presence of the incident electron. Further the exchange effect due to the indistinguishability of the electrons has been included.

The system of helium atom and the incident electron satisfies the wave equation

$$(H-E)\psi(r_1, r_2, r_3) = 0 \quad \dots (1)$$

where *H* is the total Hamiltonian and *E* the energy of the system, *r*<sub>1</sub>, *r*<sub>2</sub> and *r*<sub>3</sub> are the distances of the electrons from the nucleus. To include exchange effect we choose  $\psi$  in the following way

$$\begin{aligned} \psi(r_1, r_2, r_3) = & \psi_0(r_1, r_2) \frac{F(r_3)}{\sqrt{2}} (\alpha_1 \beta_2 - \alpha_2 \beta_1) \alpha_3 \\ & + \psi_0(r_2, r_3) \frac{F(r_1)}{\sqrt{2}} (\alpha_2 \beta_3 - \alpha_3 \beta_2) \alpha_1 \\ & + \psi_0(r_3, r_1) \frac{F(r_2)}{\sqrt{2}} (\alpha_3 \beta_1 - \alpha_1 \beta_3) \alpha_2 \quad \dots (2) \end{aligned}$$

---

\* On leave from C. M. College, Darbhanga, Bihar University.

where  $\alpha$ 's and  $\beta$ 's are the spin functions in the usual notation  $F(r)$  is the wave function of the free electron and  $\psi_0$  is the ground state wave function of the helium atom which is taken as (cf. Shull and Löwdin, 1956).

$$\psi_0(r_1, r_2) = .708991a_0^{-3/2} \left[ e^{-2.1832 \frac{r_1}{a_0}} - 1.1886 \frac{r_1^2}{a_0^2} + e^{-1.1886 \frac{r_1}{a_0}} - 2.1832 \frac{r_2^2}{a_0^2} \right].$$

$a_0$ , being the Bohr-radius.

Substituting expression (2) for  $\psi$  in (1), multiplying by  $\frac{1}{\sqrt{2}} (\alpha_1\beta_2 - \alpha_2\beta_1)\alpha_3$

$\psi_0(r_1, r_2)$ , summing over the spin co-ordinates and integrating with respect to  $r_1$  and  $r_2$  (Mukherjee and Sil, 1962) we get an integro-differential equation for  $F(r_3)$ .

We have obtained from the above equation the S-wave phase-shift by the variational method of Hulthen (1944) adopted by Moiseiwitsch (1953) for a similar calculation with a different wave function and without the polarisation term. To include the long range polarisation effect the direct interaction term has been modified as in the work of Williamson and McDowell (1965) by the addition of a polarisation potential  $-\frac{\alpha(r)}{r^4}$  where  $\alpha(r)$  as given by Bethe (1943) has the following

properties :

$$\alpha(r) \rightarrow \alpha = 1.32a_0^8 ; \alpha(r) \rightarrow \beta r^6 + O(r^7) \\ r \rightarrow \infty \qquad \qquad \qquad r \rightarrow 0$$

The calculated value of the S-wave phase shift at 13.6 ev incident electron energy is 2.108 radians whereas the corresponding theoretical value of Williamson and McDowell who solved the coupled integro-differential equation numerically is 1.963 radians. Further work is in progress.

#### ACKNOWLEDGMENTS

The authors are thankful to Prof. D. Basu for his kind interest and valuable discussions during the progress of the work.

#### REFERENCES

- Bethe, H. A., 1943, *Handb. d. Phys. (Ann. Arbor.)*, **24**, 339-349.  
 Hulthen, L., 1944, *K. Fysiogr Sallsk Forth.*, **14**, No. 21.  
 Moiseiwitsch, B. L., 1953, *Proc. Roy. Soc., A.*, **219**, 102.  
 Mukherjee, S. C., and Sil, N. C., 1962, *Ind. J. Phys.*, **36**, 283.  
 Shull, H., and Löwdin, P., 1956, *J. Chem. Phys.*, **25**, 1035-1040.  
 Williamson, J. H. and McDowell, M. R. C., 1965, *Proc. Phys. Soc.*, **85**, 719.

## BOOK REVIEW

**INTRODUCTION TO PHYSICS**--A. Kitaigorodsky; Foreign Languages Publishing House, Moscow; 720 pages. Translated from Russian by O. Smith.

The book is meant for those who after leaving the secondary school have taken up engineering as their subject of study. It covers the entire field of Physics except those which are taught in high schools. The book is divided into three main parts. Part one deals with mechanical and thermal motion and includes in it the fundamental laws of mechanics, mechanical energy, momentum, rotation of a rigid body, vibrations, travelling and standing waves, acoustics, temperature and heat, thermodynamic processes and entropy, kinetic theory of gases and processes of transition to equilibrium. Part two deals with electromagnetic fields which includes electric and magnetic fields, electromagnetic fields, energy transformation in electromagnetic fields, electromagnetic radiation, phenomena of interference and scattering, diffraction of X-rays by crystals, double refraction, theory of relativity and the quantum nature of a field. The third part deals with structure and properties of matter and includes in it motion of charged particles, wave properties of microparticles, atomic structure, molecules, atomic nuclei, nuclear transformations, atomic structure of bodies, phase transformations, deformation of bodies, dielectrics, magnetic substances and effect of electronic structure on properties of bodies. The book thus covers practically the whole of Physics and the different basic aspects of it have been developed in a fairly logical sequence. But attempt has nowhere been made to make the treatments of different subjects exhaustive obviously because it is not meant for students of Physics degree course. Experimental physics and the historical development of different physical ideas have also not been considered in this book. The omission was intentional because firstly the author feels that in understanding of the modern techniques employed for an experiment in any branch of physics, knowledge of practically all the branches of physics is required and in consequence, 'experimental physics can not be subdivided' but should be treated as a separate subject; secondly since the book is not meant for those who want to be physicists inclusion of historical development was thought to be unnecessary. In spite of the omissions the basic physical ideas of the different branches have been explained in sufficiently clear and concise language. The book is undoubtedly a useful text book for students of the engineering degree courses and a helpful book for subsidiary reading by the students of physics honours courses.

*A.K.D.*



# EFFECT OF ANHARMONICITY ON THE THERMODYNAMIC BEHAVIOUR OF A SOLID

D. N. SINGH

DEPARTMENT OF PHYSICS, SCIENCE COLLEGE, PATNA-5.

(Received June 22, 1964).

**ABSTRACT.** A method is suggested, to take into account the effect of anharmonicity on the thermodynamic functions, in a temperature range where quantum effects are important. Expressions for the Gibb's function  $G$  and the specific heat at constant pressure  $C_p$  are deduced for a simple model of a solid. These results reduce to the well known classical expressions in the limit of high temperatures.

## INTRODUCTION

Much work has been done (Born, 1939, 1943; Bradburn, 1943; Dugdale and MacDonald, 1954) about the role of the anharmonic terms in the potential energy on the thermodynamic properties of solids at high temperatures. A term linear in temperature, occurs in the specific heat of a solid at high temperatures (Poiris, 1955; Leibfried, 1955) due to this.

The influence of anharmonicity in the temperature range where quantum effects are significant, has not been considered in a logical way. Stern (1957) after developing the whole theory classically, replaces  $3R$  by  $3R.F(\theta/T)$  in the end, where  $F$  is the Debye function, as a first factor in the specific heat  $C_p$  of an anharmonic solid. It tells only a part of the story and is incomplete in its development from the quantum point of view.

In the following, first a general formulation of the quantum mechanical thermodynamic perturbation theory (Landau and Lifshitz, S. M., 1958) is given. It is then applied to a model of a solid, to arrive at the expressions for the Gibb's function  $G$  and the specific heat at constant pressure  $C_p$ . In the end it is shown that this gives the correct expression for the specific heat at high temperatures.

## GENERAL FORMULATION

The partition function at constant pressure,  $Q$  when  $E_n$  are the energy eigen values of the system, is given by,

$$Q = \sum_n e^{-E_n/kT} \quad \dots (1)$$

The energy eigen levels  $E_n$  of the perturbed system, using quantum perturbation theory up to second-order corrections are,

$$E_n = E_n^0 + V_{nn} + \sum_m' \frac{V_{nm} V_{mn}}{(E_n^0 - E_m^0)} \\ = E_n^0 + E_n^1 + E_n^2 \quad \dots (2)$$

where  $E_n^0$  are the unperturbed energy levels and  $E_n^1$  and  $E_n^2$  are the 1st- and 2nd- order corrections due to the perturbing potential  $V$ .

The condition for the validity of the quantum perturbation theory i.e.  $|V_{mn}| \ll |E_n^0 - E_m^0|$  is assumed.

Substituting (2) in (1),

$$Q = \sum_n e^{-E_n/kT} \\ = \sum_n e^{-E_n^0/kT} \cdot e^{-(E_n^1 + E_n^2)/kT} \\ = \sum_n e^{-E_n^0/kT} \cdot \left[ 1 - \frac{(E_n^1 + E_n^2)}{kT} + \frac{(E_n^1 + E_n^2)^2}{2k^2T^2} \right]$$

(neglecting higher order terms of the expansion).

The condition for the applicability of this expansion being that  $(E_n^1 + E_n^2) \ll kT$  where the perturbation energy is per particle. Hence the partition function,

$$Q = \sum_n e^{-E_n^0/kT} \left[ 1 + \frac{\sum_n e^{-E_n^0/kT} \cdot \frac{1}{kT} \left\{ -(E_n^1 + E_n^2) + \frac{(E_n^1 + E_n^2)^2}{2kT} \right\}}{\sum_n e^{-E_n^0/kT}} \right] \\ = Q_0 \left[ 1 + \frac{1}{Q_0} \sum_n e^{-E_n^0/kT} \cdot \frac{1}{kT} \left\{ -(E_n^1 + E_n^2) + \frac{(E_n^1 + E_n^2)^2}{2kT} \right\} \right] \dots (3)$$

$Q_0$  being the partition function for the unperturbed system.

The equilibrium condition of the system which determines the coefficients of the potential energy is defined at constant pressure and not at constant volume as is usually done (Stern, 1958). This accounts for calling  $Q$ , the partition function at constant pressure, which gives the Gibb's function  $G$  through the relation  $e^{-G/kT} = Q$ .

Taking the logarithms of both sides of (3), multiplying by  $-kT$  and using the expansion  $\ln(1+y) = y - y^2/2$  (neglecting higher order terms),

$$\begin{aligned}
 G &= -kT \ln Q \\
 &= -kT \ln Q_0 - kT \cdot \frac{1}{Q_0} \sum_n e^{-E_n^0/kT} \cdot \frac{1}{kT} \left\{ -(E_n^1 + E_n^2) + \frac{(E_n^1 + E_n^2)^2}{2kT} \right\} \\
 &\quad + \frac{1}{2} kT \cdot \left[ \frac{1}{Q_0} \sum_n e^{-E_n^0/kT} \cdot \frac{1}{kT} \left\{ -(E_n^1 + E_n^2) + \frac{(E_n^1 + E_n^2)^2}{2kT} \right\}^2 \right] \\
 &= G_0 + \sum_n e^{(G_0 - E_n^0)/kT} \cdot \left\{ (E_n^1 + E_n^2) - \frac{(E_n^1 + E_n^2)^2}{2kT} \right\} \\
 &\quad + \frac{1}{2kT} \left[ \sum_n e^{(G_0 - E_n^0)/kT} \cdot \left\{ (E_n^1 + E_n^2) - \frac{(E_n^1 + E_n^2)^2}{2kT} \right\}^2 \right]
 \end{aligned}$$

where  $G_0$  is the Gibb's function for the unperturbed system.

As we are interested only in the 1st- and 2nd- order changes in the energy and the thermodynamic functions, (because we have only 1st- and 2nd- order corrections in the energy levels),  $G$  in that approximation becomes,

$$\begin{aligned}
 G &= G_0 + \sum_n e^{(G_0 - E_n^0)/kT} \cdot \left[ (E_n^1 + E_n^2) - \frac{(E_n^1)^2}{2kT} \right] \\
 &\quad + \frac{1}{2kT} \left[ \sum_n e^{(G_0 - E_n^0)/kT} \cdot E_n^1 \right]^2 \\
 &= G_0 + \sum_n e^{(G_0 - E_n^0)/kT} \cdot (E_n^1 + E_n^2) - \frac{1}{2kT} \sum_n e^{(G_0 - E_n^0)/kT} \cdot (E_n^1)^2 \\
 &\quad + \frac{1}{2kT} \left[ \sum_n e^{(G_0 - E_n^0)/kT} \cdot E_n^1 \right]^2 \quad \dots \quad (4)
 \end{aligned}$$

#### THERMODYNAMIC FUNCTIONS FOR A SIMPLE MODEL

For the model of a solid, it is considered as a collection of  $3N$  linear anharmonic oscillators having the same frequency.  $N$  is the total number of atoms in the solid. The characteristic frequency  $\omega$  is the Einstein frequency related to the characteristic temperature  $\theta$  by the relation  $\hbar\omega = k\theta$ ,

The Hamiltonian of a linear anharmonic oscillator, including cubic and quartic terms in displacement  $X$  can be written as,

$$H = \left( \frac{p^2}{2m} + \frac{1}{2} aX^2 \right) + (bX^3 + cX^4) \\ = H_0 + V \quad \dots (5)$$

where  $H_0 = (p^2/2m + 1/2 aX^2)$  is the unperturbed (Harmonic) Hamiltonian and  $V = (bX^3 + cX^4)$  is the perturbing potential.

The perturbed energy levels  $E_n$  of such a perturbed system, using quantum mechanical perturbation theory, is the well known (Landau and Lifshitz, Q. M., 1958) result,

$$E_n = \left( n + \frac{1}{2} \right) \hbar \omega + C \cdot \frac{3}{4} \left( \frac{\hbar}{m\omega} \right)^2 (2n^2 + 2n + 1) \\ - b^2 \cdot \frac{15}{4\hbar\omega} \left( \frac{\hbar}{m\omega} \right)^3 \cdot \left( n^3 + n + \frac{11}{30} \right) \quad \dots (6)$$

The contribution to the 2nd-order correction has been considered only from the cubic term but not from the quartic term.

Having known the energy levels of the perturbed oscillator one can calculate the thermodynamic functions making use of the general formula (4). In the general notation,

$$\left. \begin{aligned} E_n^0 &= \left( n + \frac{1}{2} \right) \hbar \omega \\ E_n^1 &= C \cdot \frac{3}{2} \left( \frac{\hbar}{m\omega} \right)^2 \cdot \left( n^2 + n + \frac{1}{2} \right) \\ \text{and} \quad E_n^2 &= -b^2 \cdot \frac{15}{4\hbar\omega} \left( \frac{\hbar}{m\omega} \right)^3 \cdot \left( n^3 + n + \frac{11}{30} \right) \end{aligned} \right\} \quad \dots (7)$$

As in the perturbed energy levels  $E_n$ , the contribution of  $cX^4$  in the second order perturbation is not considered (which would have given otherwise, a term multiplied by  $c^2$ ) for a consistent approximation the last two terms of (4) are dropped.

The expression for  $G$  (per oscillator) becomes then from (4),

$$G = G_0 + \sum e^{(G_0 - E_n^0)/kT} \cdot (E_n^1 + E_n^2)$$

which on putting  $E_n^1$  and  $E_n^2$  from (7) and collecting terms in powers of  $n$  reduces to,

$$G = G_0 + A e^{(G_0 - \frac{1}{2} \hbar \omega)/kT} \left[ \sum_n n^2 e^{-n \cdot \frac{\hbar \omega}{kT}} + \sum_n n e^{-n \cdot \frac{\hbar \omega}{kT}} \right] \\ + B e^{(G_0 - \frac{1}{2} \hbar \omega)/kT} \cdot \sum_n e^{-n \cdot \frac{\hbar \omega}{kT}}$$

putting

$$\frac{\hbar \omega}{T} = x$$

$$= G_0 + A e^{(G_0 - \frac{1}{2} \hbar \omega)/kT} \cdot \left[ \sum_n n^2 e^{-nx} + \sum_n n e^{-nx} \right] + B$$

$$\sum_n [n + B] e^{-nx}$$

$$= G_0 + A \cdot \frac{1}{f(x)} [f''(x) - f'(x)] + B \quad \dots (8)$$

The primes on  $f$  denote differentiation with respect to  $x$ . The coefficients  $A$  and  $B$ , and the function  $f(x)$  are,

$$\left. \begin{aligned} A &= C \cdot \frac{3}{2} \left( \frac{\hbar}{m\omega} \right)^2 - b^2 \cdot \frac{15}{4\hbar\omega} \left( \frac{\hbar}{m\omega} \right)^3 \\ B &= C \cdot \frac{3}{4} \left( \frac{\hbar}{m\omega} \right)^2 - b^2 \cdot \frac{11}{8\hbar\omega} \left( \frac{\hbar}{m\omega} \right)^3 \end{aligned} \right\} \quad \dots (9)$$

$$\text{and} \quad f(x) = \sum_n e^{-nx} = \frac{e^x}{(e^x - 1)}$$

With the substitution of  $f''(x)$  and  $f'(x)$  of the function  $f(x)$ , defined in (9), the expression for  $G$  in (8) takes the form,

$$G = G_0 + 2A \cdot \frac{e^x}{(e^x - 1)^2} + B \quad \dots (10)$$

Having obtained the expression for the Gibb's function  $G$ , the specific heat at constant pressure  $C_p$  (per oscillator) can be calculated using the formula,

$$C_p = -T \left( \frac{\partial^2 G}{\partial T^2} \right)_p$$

$$= -T \left( \frac{\partial^2 G_0}{\partial T^2} \right)_p + \frac{4A}{T} \cdot \frac{x(e^x + e^{2x})}{(e^x - 1)^3} - \frac{2A}{T} \cdot \frac{x^2(e^x + 4e^{2x} + e^{3x})}{(e^x - 1)^4}$$

$$= k \cdot \frac{x^2 \cdot e^x}{(e^x - 1)^2} + \frac{4A}{T} \cdot \frac{x(e^x + e^{2x})}{(e^x - 1)^3} - \frac{2A}{T} \cdot \frac{x^2(e^x + 4e^{2x} + e^{3x})}{(e^x - 1)^4} \dots \quad (11)$$

This is the expression for the specific heat at constant pressure  $C_p$  (per oscillator).

Equations (10) and (11) give the Gibb's function  $G$  and the specific heat  $C_p$  for each oscillator or mode of vibration of the solid. For the model of the solid that is used here, to know  $G$  and  $C_p$  for the whole solid one has to multiply the expressions (10) and (11) by  $3N$ . It has already been mentioned earlier that the angular frequency  $\omega$  is the characteristic (Einstein) frequency, related to the characteristic temperature  $\theta$  by the relation  $\hbar\omega = k\theta$ .

To see whether the above development is on the right lines, one can take the limiting form of  $C_p$  at high temperatures i.e. when  $kT \gg \hbar\omega$  and compare the result with the classical expression. In this limit ( $x \ll 1$ ),

$$C_p^{cl} = k - \frac{4A}{T} \cdot \frac{1}{x^2}$$

putting  $x = \frac{\hbar\omega}{kT}$

and the value of  $A$  from (9)

$$= k - \frac{4k^2T}{(\hbar\omega)^2} \left[ c \cdot \frac{3}{2} \left( \frac{\hbar}{m\omega} \right)^2 - b^2 \cdot \frac{15}{4\hbar\omega} \left( \frac{\hbar}{m\omega} \right)^3 \right]$$

$$\omega = \sqrt{\frac{a}{m}}$$

$$= k \left[ 1 + \left( \frac{15b^2}{a^3} - \frac{6c}{a^2} \right) kT \right].$$

which agrees with the classical result (Peierls, 1955).

The validity of the above expressions (10) and (11) over a temperature range, is limited by the range of convergence of the quantum mechanical perturbation energy (2) and the range of convergence of the thermodynamic perturbation expansion (3). The results are not expected to be true at very low temperatures and that is the reason for believing that the Einstein model is good enough for the range of validity of the above expressions.

ACKNOWLEDGMENT

The author would like to express his thanks to Prof. B. N. Singh for his constant encouragement and to Dr. H. N. Yadav for some helpful suggestions.

REFERENCES

- Born, M., 1939, *J. Chem. Phys.*, **7**, 591.  
Born, M. and Bradburn, M., 1943, *Proc. Cambridge Phil. Soc.*, **39**, 104.  
Bradburn, M., 1943, *Proc. Cambridge Phil. Soc.*, **37**, 113  
Dugdale, J. S. and MacDonald, D. K. C., 1954, *Phys. Rev.*, **96**, 57.  
Landau, L. D. and Lifshitz, E. M., 1958, *Quantum Mechanics*, Pergamon Press, 136.  
\_\_\_\_\_, 1958, *Statistical Physics*, Addison-Wesley Publishing  
Company, 93.  
Leibfried, G., 1955, *Handbuch der Physik*, Springer-Verlag, **VII/1**, 274.  
Peierls, R. E., 1955, *Quantum Theory of Solids*, Clarendon Press, Oxford, 34.  
Stern, E. A., 1958, *Phys. Rev.*, **111**, 786.

# DENSITY-WAKE OF A CHARGED PARTICLE MOVING THROUGH A PLASMA

SAROJ K. MAJUMDAR

SAHA INSTITUTE OF NUCLEAR PHYSICS, CALCUTTA, INDIA.

(Received September 25, 1965)

**ABSTRACT.** The method developed by the author in a previous paper has been applied to investigate the density wake created by a moving test particle in the plasma. Those wakes are analysed separately for different harmonics of the cyclotron frequency, and for small velocity perpendicular to the applied magnetic field. It is shown that only the first few harmonics are important to develop the wake in the plasma.

## INTRODUCTION

In a previous paper by the author, (Majumdar, 1963), the shape of the wake of a test particle moving through plasma placed in a steady magnetic field has been investigated. In the present paper, we extend the calculation for a general motion of the test particle in the plasma.

It is known that when we neglect the motion of plasma ions, there are three different wave motions in the plasma: one is a plasma-electron wave the two others are transverse e.m. waves as shown by Oster (1960). One of the e.m. waves is strongly coupled with the plasma wave, which is a slow wave, while the other e.m. wave propagates freely and is a fast wave. (Allis, *et al.* 1962). In this paper we shall investigate only qualitatively, the nature of the wake of the test particle on the above assumptions of two coupled slow waves and a fast wave. We shall employ the same set of hydrodynamic equations as has been done in (Majumdar, 1962). It has been shown there that the wake of the moving charged particle is determined solely by the nature of the wave-surface surrounding it. This wave surface is obtained by plotting the parallel versus perpendicular (to the external magnetic field) component of the wave-vector  $\mathbf{k}$ . The actual wake of the moving particle, i.e. the disturbance in the plasma created by it in the form of density wave, is obtained by taking the polar reciprocal of the wave surface. If the wave surface is real, the charge density takes the form of a radiated wave emanating from the particle. If it is imaginary, this radiated wave is to be replaced by a damped density distribution around the particle.



### BASIC EQUATIONS

The motion of the plasma electrons is represented by the linearised transport equation (Spitzer, 1956).

$$\frac{\partial \mathbf{v}}{\partial t} + \frac{e}{m} \mathbf{E} + \frac{V^2}{n_0} \nabla n + \omega_c \mathbf{v} \times \mathbf{e}_z = 0, \quad \dots (1)$$

together with the equation of continuity

$$\frac{\partial n}{\partial t} + \nabla \cdot (n_0 \mathbf{v}) = 0, \quad \dots (2)$$

and the set of Maxwell's equations :

$$\nabla \times \mathbf{E} = -\frac{1}{c} \frac{\partial \mathbf{H}}{\partial t}, \quad \dots (3)$$

$$\nabla \times \mathbf{H} = \frac{1}{c} \frac{\partial \mathbf{E}}{\partial t} - \frac{4\pi}{c} n_0 e \mathbf{v} + \frac{4\pi q}{c} \mathbf{V}_0(t) \delta(\mathbf{r} - \mathbf{r}_T). \quad \dots (4)$$

In these four equations,  $\mathbf{v}$  and  $n$  are perturbations in velocity and density of plasma electrons,  $n_0$  and  $V$  are the average density and average velocity, and

$$\omega_c = \frac{eH_0}{mc}$$

is the cyclotron frequency,  $H_0$  being the external magnetic field applied in the  $Z$ -direction, represented by the unit vector  $\mathbf{e}_z$ .  $q$  is the test particle's charge moving with a velocity  $\mathbf{V}_0(t)$ ,  $\mathbf{r}_T$  is its position denoted by the Dirac delta-function  $\delta$ .

We take Fourier transform w.r.t. space and time of the form

$$f(\mathbf{k}, \omega) = \int_{-\infty}^{+\infty} \int d\mathbf{r} \, dt \, f(\mathbf{r}, t) e^{i(\mathbf{k} \cdot \mathbf{r} - \omega t)},$$

of all the variables in eqn.(1) to (4), and then eliminate the quantities  $\mathbf{v}$ ,  $\mathbf{H}$  and  $n$ . This gives us the following equation for the electric field in the plasma :

$$a\mathbf{E} + \mathbf{k} \left( i \frac{V^2}{\omega} 4\pi q \mathbf{k} \cdot \Gamma - [c^2 - V^2] \mathbf{k} \cdot \mathbf{E} \right) - ib(\mathbf{E} \times \mathbf{e}_z) - i \frac{\omega_c}{\omega} c^2 (\mathbf{k} \cdot \mathbf{E})(\mathbf{k} \times \mathbf{e}_z) + 4\pi q \omega_c \Gamma \times \mathbf{e}_z - i4\pi q \omega \Gamma = 0, \quad \dots (5)$$

where

$$\left. \begin{aligned} a &= k^2 c^2 + \omega_p^2 - \omega^2 \\ b &= \omega_c \left( \omega - \frac{c^2 k^2}{\omega} \right) \end{aligned} \right\} \quad \dots (6)$$

and

$$\omega_p = \left( \frac{4\pi n_0 e^2}{m} \right)^{\frac{1}{2}}$$

is the plasma frequency. The quantity  $\Gamma$  is the source function generated by the moving test particle

$$\Gamma = \int_{-\infty}^{+\infty} V_0(t) e^{-i\mathbf{k} \cdot \mathbf{r}_T + i\omega t} dt. \quad \dots (7)$$

In eqn. (5)  $\mathbf{E}$  is actually the Fourier transform  $\mathbf{E}(\mathbf{k}, \omega)$  of the electric field. Now, our aim is to obtain an expression for the charge density in the plasma, caused by the moving test particle. For this, we take Fourier transform of Poisson's equation

$$\vec{\nabla} \cdot \mathbf{E} = -4\pi ne + 4\pi q\delta(\mathbf{r} - \mathbf{r}_T), \quad \dots (8)$$

and combine the transform equation with eqn. (5). We thus obtain finally the following expression for the Fourier transform of the charge density :

$$\begin{aligned} \rho(\mathbf{k}, \omega) &= en(\mathbf{k}, \omega) = \\ &= qI_0 \left( 1 + k_z V_{0z} \frac{P}{D} \right) \\ &\quad + qI_+ e^{i(\phi - \theta)} k_\rho V_{0\rho} \frac{Q + a\omega_c \omega p^2}{2D} \\ &\quad + qI_- e^{-i(\phi - \theta)} k_\rho V_{0\rho} \frac{Q - a\omega_c \omega p^2}{2D}, \end{aligned} \quad \dots (9)$$

where

$$I_0 = \int_{-\infty}^{+\infty} e^{-i\mathbf{k} \cdot \mathbf{r}_T + i\omega t} dt, \quad \dots (10a)$$

$$I_{\pm\Omega} = \int_{-\infty}^{+\infty} e^{-i\mathbf{k} \cdot \mathbf{r}_T + i(\omega \pm \Omega)t} dt, \quad \dots (10b)$$

and

$$D = a(a^2 - b^2) - (a^2 k^2 - b^2 k_z^2)(c^2 - V^2) - ab \frac{\omega_c}{\omega} c^2 k_\rho^2, \quad \dots (11a)$$

$$P = \omega(a^2 - b^2) - \frac{V^2}{\omega} (a^2 k^2 - b^2 k_z^2), \quad \dots (11b)$$

$$Q = P + \omega_c \omega p^2 b. \quad \dots (11c)$$

In eqn. (9), the subscripts  $\rho$  and  $z$  denote the component perpendicular and parallel to  $z$ -axis,

$$\left. \begin{aligned} k^2 &= k_\rho^2 + k_z^2; \quad k_\rho^2 = k_x^2 + k_y^2 \\ V_0^2 &= V_{0\rho}^2 + V_{0z}^2; \quad V_{0\rho}^2 = V_{0x}^2 + V_{0y}^2 \end{aligned} \right\} \quad \dots (12)$$

$$\left. \begin{aligned} k_x &= k_\rho \cos \theta; \quad k_y = k_\rho \sin \theta \\ V_{0z} &= V_{0\rho} \cos(\Omega t + \phi); \quad V_{0y} = V_{0\rho} \sin(\Omega t + \phi) \end{aligned} \right\} \quad \dots \quad (13)$$

and finally

$$\Omega = \frac{qH_0}{Mc} \quad \dots \quad (14)$$

is the cyclotron frequency of the test particle.

#### APPROXIMATIONS FOR LOWER HARMONICS OF CYCLOTRON FREQUENCY

Without any loss of generality we assume that  $k_y = 0$  and  $\phi = 0$ . Let us also identify the moving test particle with the plasma electrons, so that  $\Omega = \omega_e$ . In that case, we can write

$$\begin{aligned} \text{where} \quad e^{-i\vec{k} \cdot \vec{r}_T} &= e^{-iz \sin \theta \omega_e t - ik_z V_{0z} t}, \\ z &= \frac{k_x V_{0\rho}}{\omega_e} \end{aligned} \quad \dots \quad (15)$$

Using the well known expansion

$$e^{iz \sin \theta} = \sum_{n=-\infty}^{+\infty} J_n(z) e^{in\theta}$$

we then obtain from eqns. (10),

$$I_0 = \sum_{n=-\infty}^{+\infty} J_n(z) \delta(\omega - n\omega_e - k_z V_{0z})$$

$$I_{\pm\Omega} = \sum_{n=-\infty}^{+\infty} J_n(z) \delta(\omega - n\omega_e \pm \omega_e - k_z V_{0z}).$$

Using these results in eqn. (9) and taking the inverse transform w.r.t. time, we get the following expression for  $\rho$ :

$$\begin{aligned} \rho(\mathbf{k}) &= e \sum_{n=-\infty}^{+\infty} e^{i(n\omega_e + k_z V_{0z})t} J_n(z) \left( 1 + k_z V_{0z} \frac{P}{D} \right)_{\omega = n\omega_e + k_z V_{0z}} \\ &+ ce^{-i\theta} \sum_{n=-\infty}^{+\infty} e^{i[(n-1)\omega_e + k_z V_{0z}]t} J_n(z) k_\rho V_{0\rho} \left( \frac{Q - a\omega_e \omega_p^2}{2D} \right)_{\omega = (n-1)\omega_e + k_z V_{0z}} \\ &+ ce^{+i\theta} \sum_{n=-\infty}^{+\infty} e^{i[(n+1)\omega_e + k_z V_{0z}]t} J_n(z) k_\rho V_{0\rho} \left( \frac{Q - a\omega_e \omega_p^2}{2D} \right)_{\omega = (n+1)\omega_e + k_z V_{0z}} \dots \quad (16) \end{aligned}$$

Now, for small values of  $V_0$  and large magnetic field, the quantity  $z$  given by (15) is much less than unity. In that case we need to consider only lower harmonic terms (small  $n$ ) in the above summations over  $n$ , and for all practical purposes, it is sufficient to keep only  $n = 0$  and  $n = \pm 1$  terms. After obtaining the expressions for  $\rho(\mathbf{k})$  for  $n = 0$  and  $n = \pm 1$ , we can apply the method developed in (Majumdar, 1963) to integrate them over the variable  $\mathbf{k}$  and obtain expressions for  $\rho(\mathbf{r}, t)$  for  $n = 0$  and  $n = \pm 1$  terms. In the process of doing that integration it is observed that the wave-surfaces are given by plotting  $k_z$  vs.  $k_\rho$  from the dispersion relation

$$D = 0$$

This plot, as is shown in (Majumdar, 1963), will determine the wake of the moving test particle in plasma.

#### NATURE OF THE WAVE SURFACE

The dispersion relation (17) is a six degree equation and is quite complicated. We therefore make two simplifying assumption : (i) there are one fast wave and two coupled slow waves, and (ii)  $k^2 c^2 \gg \omega_p^2$  and  $V^2, V_z^2 \ll c^2$ . The implications regarding these assumptions has been fully explained in (Majumdar, 1963). With these assumptions, eqn. (7) degenerates into two separate equations : For fast waves :

$$(k^2 c^2 - \omega^2)[2\omega_p^2 \omega^2 + \omega_e^2 \omega^2 - \omega_e^2 c^2 k_z^2] + \omega^2 \omega_p^2 (k^2 V^2 + \omega_p^2 - \omega^2) = 0, \quad \dots \quad (18)$$

and for slow waves :

$$k^2 \omega^2 (k^2 V^2 + \omega_p^2 - \omega^2) - (k^2 V^2 + \omega_p^2) c^2 k_z^2 + \omega_e^2 k^2 \omega^2 = 0 \quad \dots \quad (19)$$

As has already been shown in connection with eqn. (16),  $\omega$  in eqns. (18) and (19) are given by

$$\omega = k_z V_{0z} \pm n \omega_e, \quad \dots \quad (20)$$

where  $n = 0, 1, 2$ . For  $n = 0$ , eqns. (18) and (19) reduce to eqns. (33) and (37) of (Majumdar, 1963), which is true only when the test particle is moving parallel to the magnetic field. Hence we come to the conclusion that for the fundamental frequency  $\omega = k_z V_{0z}$ , the effect of the test particle on its wake is the same as if the particle is moving parallel to the magnetic field.

To see the effects of the harmonics of cyclotron frequency, we put  $V_{0z} = 0$  in (20) and set  $\omega = \pm n \omega_e$ , ( $n = 1, 2$ ) in eqns. (18) and (19). Thus in the case of slow waves, eqn. (19) for  $n = 1$  reduces to the following simple form :

$$k_\rho^2 \left( k_\rho^2 + k_z^2 + \frac{\omega_p^2}{V^2} \right) = 0. \quad \dots \quad (21)$$

Now, it has been shown in (Majumdar, 1963) that a real wave surface means a radiation from the test particle, whereas an imaginary surface denotes an attenua-

ted charge distribution around the test particle. The surface represented by (21) is an imaginary one, so that for  $\omega = \omega_0$ , there is no real radiation from the moving test particle.

Setting now  $n = 2$ , in eqn. (19) we obtain the following equation :

$$k_p^4 + \frac{7}{4} k_p^2 k_z^2 + \frac{3}{4} k_z^4 + \frac{\omega_p^2 - 3\omega_c^2}{V^2} k_p^2 + \frac{3(\omega_p^2 - \omega_c^2)}{V^2} k_z^2 = 0. \quad \dots \quad (22)$$

For  $3\omega_p^2 \neq \omega_c^2$ , eqn. (22) is a non-factorizable bi-quadratic equation. To get an idea of the wave surface we follow the procedure developed in (Majumdar, 1963). We first plot  $k_p^2$  vs.  $k_z^2$  from eqn. (22). This plot is always a hyperbola. From this plot, we take only that portion which lies in the first quadrant ( $k_z^2 > 0, k_p^2 < 0$ ). Then taking square-root of each point of the curve which lies on this portion, we may separately plot  $k_p$  vs.  $k_z$ , and thus obtain the real wave surface. Thus, if

$$\alpha = -\frac{4}{V^2} (15\omega_p^2 - 3\omega_c^2)$$

$$\beta = +\frac{4}{V^2} (17\omega_p^2 - 3\omega_c^2), \quad (23)$$

then a plot of  $k_z^2$  vs.  $k_p^2$  of eqn. (22), will be as shown in Fig. 1. It can be easily verified from Fig. 1, that

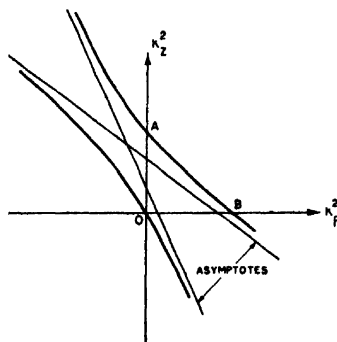


Fig. 1.  $k_p^2$  vs.  $k_z^2$  plot of eqn. (22).

$$OA = \frac{4}{V^2} (-\omega_p^2); OB = \frac{1}{V^2} (3\omega_c^2 - \omega_p^2). \quad (24)$$

Therefore, for real surface in  $k_p$  vs.  $k_z$ , plot,  $OA$  and  $OB$  should both be positive i.e., for radiative waves, we should have  $\omega_c^2 > \omega_p^2$ . Otherwise the wave surface is imaginary, and we have only attenuated charge distribution around the test particle. If we approximate the  $AB$  part of the curve (which lies in the first quadrant) of Fig. 1, by straight line  $AB$ , then its equation is given by

$$\frac{k_p^2}{OB} + \frac{k_z^2}{OA} \quad (25)$$

This equation, in  $k_\rho$  vs.  $k_z$  plot, represent an ellipse if  $OA \neq OB$ , and a circle, if  $OA = OB$ , i.e. if  $3\omega_p^2 = \omega_c^2$ . In either case we have a radiated wave, either elliptical or, circular, radiating from the test particle. As explained before, when  $OA$  or  $OB$  has negative value, (i.e.  $\omega_c^2 < \omega_p^2$ ), then this radiative wave is replaced by and attenuated (damped) charge distribution around the moving test particle. Once the wave surface around the test particle is obtained it is now a matter of geometrical construction to get the constant charge-density surface. Without going into the mathematical details (as has been done in (Majumdar, 1963), this latter surface can be obtained from the  $k$ -surface (wave-surface) by constructing to polar reciprocals. When the wave surface is real, its polar reciprocal is also real, meaning thereby a radiated wave from the test particle. For imaginary polar reciprocal of the  $k$ -surface, the radiated wave is replaced by a damped density distribution around the particle.

### CONCLUSIONS

We have discussed the wave surface only for  $n = 0, 1$  and  $2$ . The calculation can be easily extended for higher values of  $n$ . For  $n = 1, 2$ , we had to assume that  $V_{0z} = 0$ . This has been necessary to simplify the mathematical complications. For non-zero  $V_{0z}$ , the wave surface is represented by a full-sixth degree equation which is very difficult to handle.

The method developed here can be applied to any kind of wave propagation in plasma (e.g., ion-cyclotron waves, Alfvén waves etc.) for which it is only necessary to obtain the dispersion relation in a suitable form. The type of investigation developed here will give us the physical picture of how the charge density is associated with various kind of wave phenomena in magnetic plasma.

### ACKNOWLEDGMENT

The author expresses his sincere thanks to Prof. B. D. Nag, Director of the Institute for his kind interest in the work.

### REFERENCES

- Allis, W. P., Buchsbaum, S. J. and Bers, A., 1962, *Special Tech. Report No. 8*, Research Lab. of Electronics, M.I.T., Cambridge, MASS.
- Majumdar, S. K., 1963, *Proc. Phys. Soc.*, **82**, 669.
- Oster, L., 1960, *Rev. Mod. Phys.*, **32**, 141.
- Spitzer, L., 1956, *Physics of Fully Ionised Gases*, Interscience Publishers, Inc., New York.

# LIGHT ABSORPTION IN $\text{NO}_3$ ION IN STATE OF SOLUTION

## PART IV.—EFFECT OF DILUTION

A. MOOKHERJI AND S. P. TANDON\*

PHYSICAL LABORATORIES, BURDWAN UNIVERSITY, BURDWAN, WEST BENGAL, INDIA.

(Received August 26, 1965)

**ABSTRACT.** 200  $m\mu$  band which has been assigned to an allowed  $\pi \rightarrow \pi^*$  transition of nitrate ion, exhibits blue shift with progressive dilution in state of aqueous solution. This shift has been attributed to hydrogen bonding which occurs at the oxygen atoms decreasing the electron density around oxygen atoms in the nitrate ion.

### INTRODUCTION

In part II of the present series of the papers (Mookherji and Tandon, 1965), a systematic study of the energy, band-width, intensity and structure of the 200 $m\mu$  band at concentrations  $\sim 10^{-2}M$  of nitrate ion has been reported. Evidences have been cited for its assignment to an allowed  $\pi \rightarrow \pi^*$  transition.

Solvents are known to influence (McConnell, 1952; Strickler, 1961; Strickler and Kasha, 1961) the position of the bands of the solute. Study of the  $n \rightarrow \pi^*$  transitions of the organic (Borawoy, 1939; Kasha, 1950; Coggeshall and Pozefsky, 1951) and inorganic molecules (McConnell, 1952; Strickler, 1951; Strickler and Kasha, 1961; Meyerstein and Troinin, 1961) reveals a blue shift of the bands in increasing polarity solvents. Water is a strongly polar solvent abounding in hydrogen bonding. In state of aqueous solution the hydrogen bonding increases with dilution. Consequently, the spectral shift of the solute is expected to increase with progressive dilution. Since  $\pi$ -orbitals in nitrate ion are similarly situated (Mookherji and Tandon, 1965) as  $n$ -orbitals,  $\pi \rightarrow \pi^*$  transitions in this ion are expected to exhibit band shifts similar to that of  $n \rightarrow \pi^*$  transitions.

The present communication reports the study of the 200 $m\mu$  band of nitrate ion, which has been assigned to  $\pi \rightarrow \pi^*$  transition (Mookherji and Tandon, 1962, 1965), at different concentrations ( $\sim 10^{-1}M$  to  $10^{-4}M$ ) in state of aqueous solution with UVISPEK spectrophotometer. The results have been discussed in the light of Griffiths and Symons (1960) and Strickler (1961).

### EXPERIMENTAL AND RESULTS

Chemicals used were of Merk's analytical reagent quality. Triple distilled water was used for making solutions.

---

\* Present address : Physical Laboratories, University of Jodhpur, Jodhpur, Rajasthan, India.

The measurements were carried out with Hilger's UVISPEK spectrophotometer by the method described earlier (1961), scanning the spectrum at an interval of  $2.5 \text{ \AA}$  on five nitrates- $\text{LiNO}_3$ ,  $\text{NaNO}_3$ ,  $\text{KNO}_3$ ,  $\text{NH}_4\text{NO}_3$  and  $\text{AgNO}_3$ , at different concentrations ( $10^{-1}$  to  $10^{-4} M$ ) in state of aqueous solution. Since the nature of absorption in all these salts was same, to avoid repetition, the absorption curves of lithium nitrate are given in Fig. 1.

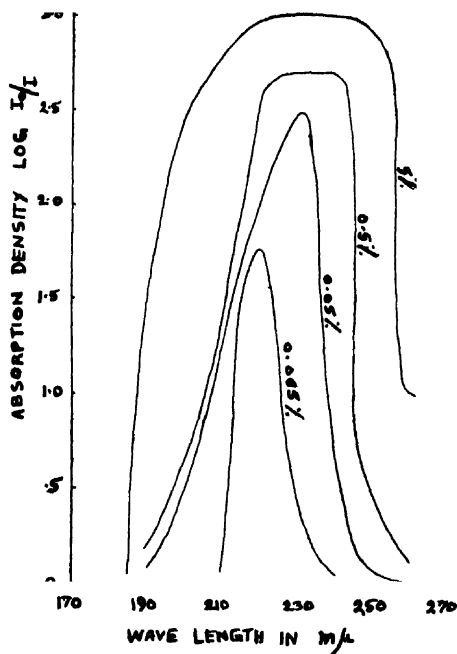


Fig. 1. Absorption curves showing blue shift of 200  $m\mu$  band of lithium nitrate with progressive dilution in state of aqueous solution.

The measurements centred round about  $25^\circ\text{C}$ . No observable change in the position of the absorption maxima was noticed for small room temperature variations.

#### DISCUSSION

Close study of Fig. 1. reveals a blue shift  $\sim 10^3 \text{ cm}^{-1}$  in going from  $10^{-1} M$  to  $10^{-4} M$  concentration of aqueous solution of nitrates. At high concentrations the absorption maxima are flat and become sharp with dilution.

To explain similar influence of environment several models (Griffiths and Symons, 1960) have been used (Cleaver *et al*, 1961; Shimoji, 1961). In "expanded model" (Platzman and Franck, 1964) the orbital of the excited electron is regarded as invading surrounding medium quite deeply whereas in "confined model" (Smith and Symons, 1958), the orbitals of the excited electron are confined within the



nearest neighbour shell. Simple calculations of the retaining force on the excited electron, representing it by an infinite square well potential having spherical and symmetry and radius  $R_0$ , show that  $R_0$  comes out to be much larger than the sum of the radii of the cation and anion in complete disagreement with the case of iodide ion (Smith and Symons, 1958), which is known to give electron transfer spectra. This coupled with the study of the effects (Strickler, 1961) of temperature and solvent, suggest that the observed spectrum of the nitrate ion is not due to electron transfer but is due to the electron transitions localized on the ion itself. Consequently, the above described modes of influence of environment, which are meant for the electron transfer spectra, cannot be used in the case of nitrate ion.

Nitrate ion is known to have planar structure with oxygen atoms at the corners of an equilateral triangle and the nitrogen at the centre, having  $D_3$  symmetry and positive charge on nitrogen atom in close proximity to the negative charge on the nitrate ion (Janz and Mikawa, 1960). LCAO-MO treatment of the ion shows that  $\pi$ -orbitals like  $n$ -orbitals are localized on the oxygen atoms whereas  $\pi^*$ -orbitals on the nitrogen atom in the nitrate ion. Hence  $\pi \rightarrow \pi^*$  transitions also remove an electron from an antibonding  $\pi$ -orbital and places it in a strongly antibonding  $\pi^*$ -orbital. This results in a decrease in electron density in the region where  $\pi$ -orbital was located. A hydrogen bond formed with the oxygen atom having  $\pi$ -orbital, places a positive charge near that orbital, making it more difficult to remove the electron. This causes the increase in the energy of  $\pi \rightarrow u^*$  transition, shifting the band to higher frequencies. As hydrogen bonding increases with dilution, the blue shift of the band should also increase with progressive dilution. This is what has been observed

#### REFERENCES

- Borawoy, A., 1939, *J. Chem. Soc.*, 1177.  
 Cleaver, B., Rhodes, E. and Ubbelohde, A. R., 1961, *Disc. Faraday Soc., London*, **32**, 22.  
 Coggeshall, N. D., and Pozefsky, A., 1951, *J. Chem. Phys.*, **19**, 980.  
 Griffiths, T. R. and Symons, M. C. R., 1960, *Trans. Faraday Soc., London*, **56**, 1125.  
 Janz, G. J. and Mikawa, Y., 1960, *J. Molecular Spectrosc.*, **5**, 92.  
 Kasha, M., 1950, *Disc. Faraday Soc., London*, **9**, 14.  
 McConnell, H., 1952, *J. Chem. Phys.*, **20**, 700.  
 Meyerstein, D. and Tremin, A., 1961, *Trans. Faraday Soc., London*, **57**, 2104.  
 Mookherji, A. and Tandon, S. P., 1962, *Ind. J. Phys.*, **36**, 211, 344.  
 ————, ————, ————, 1965, *Ind. J. Phys.*, **39**, 137.  
 Platzman, R. and Franck, J., 1954, *Z. Physik.*, **138**, 411.  
 Shimoji, M., 1961, *Disc. Faraday Soc., London*, **32**, 66.  
 Smith, M. and Symons, M. C. R., 1958, *Trans. Faraday Soc., London*, **54**, 346.  
 Strickler, S. J., 1961, *Ph.D. Dissertations*, Florida State University.  
 Strickler, S. J. and Kasha, M., 1961, *J. Chem. Phys.*, **34**, 1077.  
 Tandon, S. P., 1961, *Raj. Univ. Studies*, **7**, 69.

# THE VISIBLE EMISSION SPECTRUM OF BiF

K. MADHUSUDHANA RAO AND P. TIRUVENGANNA RAO

SPECTROSCOPIC LABORATORIES, ANDHRA UNIVERSITY, WALTAIR.

(Received July 16, 1964; resubmitted August 9, 1965)

## Plate V

**ABSTRACT.** The visible band system of BiF has been reinvestigated both under low and high dispersion. The vibrational analysis of the system has been considerably extended to include about 65 bands in the region ( $\lambda$  5000–5700 Å). From a rotational analysis of four bands (2,0), (1,4), (2,5), and (3,3) the constants of the upper  $v' = 2$  and 3 and lower  $v'' = 4$  and 5 levels have been newly determined.

## INTRODUCTION

Recently T. A. P. Rao and P. T. Rao (1962) studied the emission spectrum of BiF excited in high frequency discharge in the visible and ultraviolet regions. The well known visible system in the region ( $\lambda$  3600– $\lambda$  5200 Å) was designated as  $A-X_1$ . In the ultraviolet region ( $\lambda$  2250– $\lambda$  3200 Å), system  $C'$  reported by Rochester (1937) was observed and analysed into three systems designated as  $C_1-X_2$ ,  $C_2-X_3$  and  $C_3-X_1$ . The levels  $X_1$ ,  $X_2$  and  $X_3$  were identified with  $^3\Sigma^-$ ,  $^1\Delta$ ,  $^1\Sigma^+$  of the ground state electron configuration

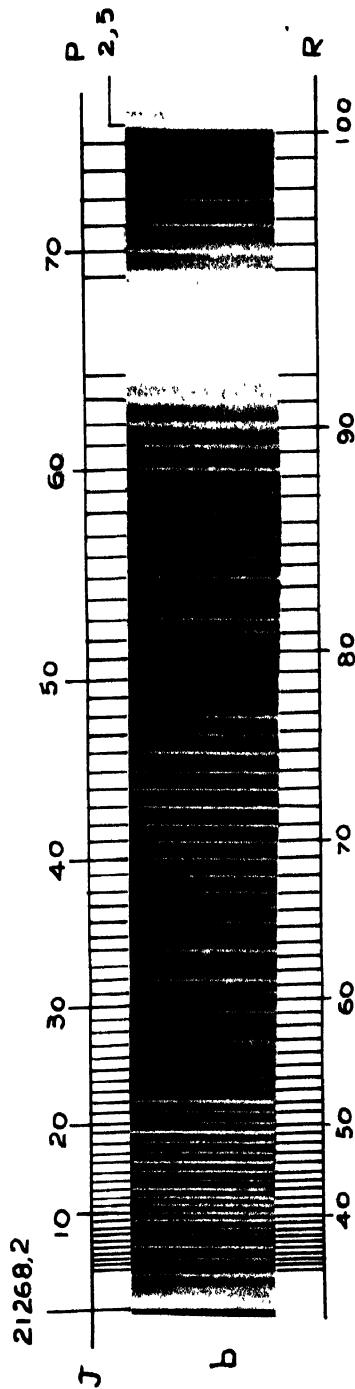
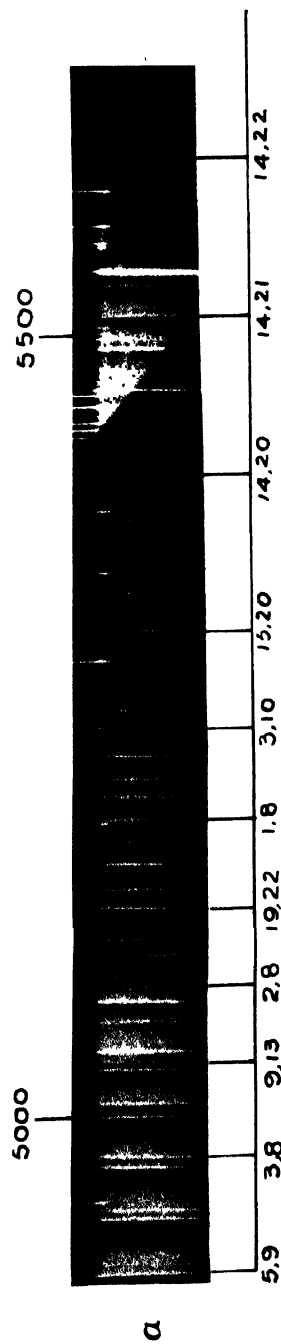
$$(z\sigma)^2 (y\sigma)^2 (x\sigma)^2 (w\pi)^4 (v\pi)^2 \dots ^3\Sigma^-, ^1\Delta, ^1\Sigma^+$$

The first excited state  $A$  was attributed to  $^3\Sigma^-$  of the first excited electron configuration

$$(z\sigma)^2 (y\sigma)^2 (x\sigma)^2 (w\pi)^3 (v\pi)^3 \dots ^3\Sigma^-$$

From the results of a rotational analysis of five bands (1, 0), (0, 0), (0, 1), (0, 2) and (0, 3), it was shown by Rao and Rao (1962), that this system arises from a  $0^+ - 0^+$  transition which is a case (c) equivalent of  $^3\Sigma^- - ^3\Sigma^-$ . The rotational constants of the upper state  $A$  have been carried out only for the vibrational levels  $v' = 0$  and 1. The rotational structure of four bands (2,0), (1,4), (2, 5) and (3, 3) has now been examined in the second order of a 21ft. grating spectrograph (dispersion 1.25 Å/mm). From a detailed rotational analysis of these bands reported below the rotational constants of  $v' = 2$  and 3 of the upper state and  $v'' = 4$  and 5 of the lower state have been newly determined.

The vibrational analysis of the  $A-X_1$  system in the region ( $\lambda$  3600–5900 Å) has been considerably extended to include about 65 bands newly obtained in the present investigation.



(a) New additional bands in the visible A—X<sub>1</sub> system of BiF  
(b) Fine structure of the (1. 4) Band of the A—X<sub>1</sub> system of BiF



## EXPERIMENTAL

The  $A-X_1$  system of BiF was easily excited in a high frequency discharge from a 500 Watt oscillator working at a frequency of 30-40 Mc/sec using speepure sample of BiF<sub>3</sub> taken in a conventional type of quartz discharge tube. When a characteristic bluish discharge was maintained by continuous external heating of the substance, in the visible system, new bands in the region ( $\lambda$  5000-5700 Å) were observed and photographed on a Hilger three prism glass Littrow Spectrograph. About 65 bands have been measured on a Hilger comparator using iron arc standards.

Some of the bands of the  $A-X_1$  system were also photographed in the 2nd order of a 21 ft. concave grating spectrograph using Agfa Isopan super special plates. The rotational structure of the four bands (2, 0), (1, 4), (2, 5) and (3, 3) was found to be free from overlapping of the neighbouring bands. The rotational lines of these bands were measured using iron arc wavelength standards. The relative accuracy in the measurement of rotational lines is about 0.07 cm<sup>-1</sup>.

(a) *Vibrational analysis*

The  $A-X_1$  system of BiF was reported by previous workers (Howell and Rochester, 1939 and Morgan, 1936) to consist of only about 40 bands in the region ( $\lambda$  4150- $\lambda$  5100 Å). In the present experiments about 65 new bands have been obtained in the region ( $\lambda$  5000- $\lambda$  5700 Å) and reproduced in plate 1(a). According to Howell the band heads of the  $A-X_1$  system could be represented by the Quantum formula

$$\nu = 22959.7 + 381.0(v' + 1/2) - 3.00(v' + 1/2)^2 + 010(v' + 1/2)^3 \\ - 510.7(v'' + 1/2) + 2.05(v'' + 1/2)^2$$

A vibrational analysis of the new bands has shown that they constitute an extension of the  $A-X_1$  system. The wavenumbers, classification and other data of the bands are given in Table I. About 60 bands could be classified and represented by the above quantum formula. The agreement between the observed and calculated values for most of the bands is within 4 cm<sup>-1</sup> as can be seen from Table I.

(b) *Rotational analysis*

From considerations of electron configurations and electronic states in BiF, the  $A-X_1$  visible system was assigned as  $^3\Sigma^- - ^3\Sigma^-$ . Since the rotational structure of each of the bands (1, 0), (0, 0), (0, 1), (0, 2) and (0, 3) reveals only the existence of only two branches  $P$  and  $R$ , the bands were assumed to arise from a  $0^+ - 0^+$  transition which is a case (c) equivalent of  $^3\Sigma^- - ^3\Sigma^-$ . The rotational structure of each of the four bands examined in the present work also reveals the presence of the two branches  $P$  and  $R$  thus confirming the above transition. The  $J$  numbering is fixed for the (2, 0) and (2, 5) bands by a comparison of the upper state combination differences. The  $J$  numbering in the (1, 4) band is fixed by

TABLE I

Assignment		Intensity	$\nu$ Obs	$\nu$ Cal	$\nu$ Obs— $\nu$ Cal
$\nu'$	$\nu''$				
0	4	7	20894.7	20893.0	+1.7
5	8	6	20787.4	20788.2	—0.8
1	5	6	20781.5	20780.3	+1.2
6	9	6	20670.5	20670.3	+0.2
2	6	6	20665.4	20664.6	+0.8
7	10	4	20555.4	20554.3	+1.1
3	7	6	20548.0	20545.8	+2.2
8	11	4	20435.3	20440.9	—5.6
5	9	6	20315.3	20313.1	+2.2
1	6	4	20295.5	20292.2	+3.3
6	10	6	20203.9	20200.6	+3.3
2	7	5	20185.0	20179.7	+5.3
7	11	5	20095.6	20088.7	+6.9
3	8	5	20071.8	20067.9	+3.9
8	12	5	19982.9	19979.4	+3.5
4	9	5	19960.3	19955.9	+4.4
9	13	3	19874.4	19873.3	+1.1
5	10	5	19850.5	19844.7	+4.8
10	14	3	19774.6	19771.0	+3.6
6	11	5	19739.4	19734.9	+4.5
2	8	2	19707.7	19702.2	+5.5
17	20	5	19638.9	19636.4	+2.5
19	22	5	19534.1	19536.9	—2.8
20	23	4	19497.9	19501.5	—3.6
0	7	3	19430.3	19434.5	—4.2
5	11	3	19376.0	19379.1	—3.1
1	8	4	19335.8	19331.9	+3.9
6	12	4	19278.5	19273.4	+5.1
17	21	4	19216.8	19211.8	+5.0
3	10	2	19124.5	19124.4	+0.1
20	24	4	19088.3	19089.2	—0.9
13	18	3	19059.6	19056.1	+3.5
4	11	2	19025.5	19020.6	+4.9
14	19	3	18982.2	18979.1	+3.1
9	15	2	18968.5	18970.8	—2.3
0	8	2	18959.5	18956.6	+2.9
5	12	2	18918.6	18917.6	+1.0
15	20	4	18909.2	18908.9	+0.3
6	13	2	18817.1	18816.0	+1.1
11	17	2	18790.4	18787.0	+3.4

TABLE I (contd.)

Assignment $v' \quad v''$		Intensity	$\nu$ Obs	$\nu$ Cal	$\nu$ Obs— $\nu$ Cal
7 14		3	18720.0	18716.4	+3.6
21 26		2	18664.9	18664.2	+0.7
4 12		3	18558.1	18559.1	-1.0
14 20		2	18546.2	18550.4	-4.2
5 13		3	18465.4	18460.2	+5.2
6 14		2	18366.9	18362.7	+4.2
11 18		2	18348.8	18350.1	-1.3
18 24		1	18330.7	18332.9	-2.2
2 11		3	18295.0	18293.1	+1.9
14 21		2	18125.9	18125.8	+0.1
5 14		2	18009.7	18006.9	+2.8
17 24		2	17965.1	17962.7	+2.4
1 11		1	17920.0	17922.8	-2.8
6 15		1	17910.6	17913.5	-2.9
20 27		1	17881.4	17876.9	+4.5
21 28		1	17867.9	17868.3	-0.4
2 12		0	17832.3	17831.5	+0.8
13 21		1	17772.1	17770.0	+2.1
14 22		1	17709.1	17705.3	+3.8
5 15		0	17556.2	17557.7	-0.5
20 28		0	17481.8	17481.0	+0.8

TABLE II

Vacuum wave numbers and rotational assignments for 2-0, 1-4, 2-5 and 3-3 bands

$J$	2—0		1—4		2—5		3—3	
	$R(J)$	$P(J)$	$R(J)$	$P(J)$	$R(J)$	$P(J)$	$R(J)$	$P(J)$
1								
2				21263.97				22490.18
3		23637.09		63.49				89.62
4		36.52		62.92				88.97
5		35.88		62.33				88.31
6		35.16		61.74				87.49
7		34.47		61.08				86.86
8		33.71		60.44				86.06
9		32.86		59.78				85.25
10		32.00		59.00				84.35

TABLE II (contd.)

<i>J</i>	2—0		1—4		2—5		3—3	
	<i>R(J)</i>	<i>P(J)</i>	<i>R(J)</i>	<i>P(J)</i>	<i>R(J)</i>	<i>P(J)</i>	<i>R(J)</i>	<i>P(J)</i>
11		31.17		58.31				83.64
12		30.22		57.54		21137.91		82.76
13		29.28		56.75		37.10		81.80
14		28.16		55.91		36.21		80.81
15		27.16		55.02		35.48		79.82
16		26.02		54.08		34.57		78.70
17		23624.89		21253.10		21133.73		22477.61
18		23.90		52.17		32.80		76.65
19		22.90		51.13		31.82		75.44
20		21.63		50.15		30.83		74.15
21		20.37		49.30		29.84		73.00
22		19.01		47.94		28.77		71.78
23	23637.09	17.63		47.03		27.75	22490.79	70.57
24	36.52	16.12		46.04		26.55	90.18	69.14
25	35.88	14.67		44.87		25.45	89.62	67.79
26	35.16	13.19		43.74		24.59	88.97	66.40
27	34.47	11.59		42.57		23.43	88.31	64.99
28	33.71	10.00		41.24		22.26	87.49	63.47
29	32.86	08.35		39.96		21.08	86.86	61.91
30	32.00	06.57	21263.97	38.67		19.69	86.06	60.71
31	31.17	04.90	63.49	37.29		18.53	85.25	59.24
32	30.22	03.13	62.92	35.95		17.25	84.35	57.63
33	23629.28	23601.39	21262.33	21234.62		21115.88	22483.64	22455.90
34	28.16	23599.54	61.74	33.18		14.63	82.76	54.28
35	27.16	97.60	61.08	31.61		13.21	81.80	52.66
36	26.02	95.72	60.44	30.23		11.83	80.81	50.89
37	24.89	93.62	59.78	28.73		10.47	79.82	49.14
38	23.60	91.65	59.00	27.17		08.86	78.70	47.28
39	22.39	89.59	58.31	25.69		07.43	77.61	45.39
40	21.03	87.52	57.54	24.00		05.88	76.65	
41	19.77	85.33	56.75	22.35		04.30	75.44	
42	18.35	83.17	55.91	20.69	21137.91	02.66	74.15	
43	16.91	80.96	55.02	18.92	37.10	01.05	73.00	
44	15.42	78.70	54.08	17.16	36.21	21099.50	71.78	
45	13.91	76.39	53.10	15.42	35.48	97.82	70.57	
46	12.36	73.96	52.17	13.58	34.57	96.11	69.14	
47	10.72	71.47	51.13	11.66	33.73	94.37	67.79	
48	09.14	68.91	50.15	10.01	32.80	92.65	66.40	
49	23607.47	23566.43	21249.30	21208.06	21131.82	21090.83	22464.99	
50	05.63	63.85	47.94	06.17	30.83	89.02	63.47	



TABLE II—(contd).

<i>J</i>	2—0		1—4		2—5		3—3	
	<i>R(J)</i>	<i>P(J)</i>	<i>R(J)</i>	<i>P(J)</i>	<i>R(J)</i>	<i>P(J)</i>	<i>R(J)</i>	<i>P(J)</i>
51	03.79	61.20	46.90	04.24	29.84	87.15		
52	02.10	58.49	45.64	02.22	28.77	85.23		
53	00.20	55.84	44.49	00.20	27.75	83.37		
54	23598.28	53.21	43.19	21198.11	26.55	81.54		
55	96.29	50.44	41.91	96.04	25.45	79.55		
56	94.28	47.66	40.65	93.84	24.24	77.55		
57	92.24	44.73	39.30	91.83	22.96	75.59		
58	90.09	41.80	37.93	89.62	21.66	73.45		
59	88.00	38.82	36.57	87.40	20.48	71.31		
60	85.69	35.88	35.12	85.21	19.08	69.18		
61	83.52	32.90	33.71	82.86	17.92	67.11		
62	80.96	29.75	32.17	80.58	16.36	64.94		
63	78.70	26.60	30.66	78.30	14.92	62.76		
64	76.38	23.35	29.11	75.96	13.55	60.45		
65	73.96	20.08	27.52	73.50	11.83	58.18		
66	23571.47	23516.83	21225.69	*—	21110.47	21055.95		
67	68.91	13.52	24.00	*—	08.86	53.56		
68	66.43	10.13	22.35	*—	07.43	51.19		
69	63.85	06.76	20.69	21163.47	05.88	48.73		
70	61.20	03.24	18.92	60.93	04.30	46.34		
71	58.49		17.16	58.35	02.66	43.92		
72	55.84		15.42	55.65	01.05	41.41		
73	52.85		13.58	52.96	21099.21	38.95		
74	49.95		11.66	50.27	97.48	36.33		
75	47.08		09.68		95.51	33.65		
76	44.08		07.67		93.81	30.97		
77	41.08		05.61		91.93	28.52		
78	37.95		03.62		89.99			
79	34.94		01.48		88.08			
80	31.75		21199.32		86.08			
81	28.54		97.21		84.07			
82	25.30		94.99		82.03			
83	21.96		92.80		80.00			
84	23518.65		21190.41		21077.96			
85	15.16		88.18		75.59			
86	11.68		85.84		73.44			
87	08.18		83.50		71.31			
88	04.58		81.04		69.18			
89			78.66		66.92			
90			75.96		64.39			
91			73.50		62.06			
92			*—		59.76			
93			*—		57.29			
94			*—		54.74			
95			63.09		52.27			
96			60.31		49.67			
97			57.55		47.14			
98			54.81		44.56			
99					41.81			

\* Masked by an atomic line.

TABLE III

$v' \ v''$	Band Origin	$B'_v$ cm <sup>-1</sup>	$B''_v$ cm <sup>-1</sup>	$D'_v \ 10^{-6}$ cm <sup>-1</sup>	$D''_v \ 10^{-6}$ cm <sup>-1</sup>
2,0	23639.20	0 2082	0.2307	0.35	0.43
1,0	23269.44	0 2090	0 2307	0.35	0.43
0,0	22892.65	0.2097	0 2307	0.35	0.43
0,1	22384.67	0.2097	0.2289	0.35	0.34
0,2	21880 75	0.2097	0 2273	0.35	0.31
0,3	21382.12	0.2097	0 2262	0 35	0.23
1,4	21265 25	0 2090	0 2244	0.35	0.23
2,5	21145 28	0 2082	0 2227	0 35	0.23
3,3	22491 43	0 2073	0 2262	0.35	0.23

comparison of the upper state combination differences of (1, 0) band while in the (3, 3) band the numbering is fixed by a comparison of the lower state combination differences of (0, 3) band analysed by Rao and Rao (1962). The rotational constants of the four bands (2, 0), (1, 4), (2, 5) and (3, 3) were determined from the equation (Herzberg page 182)

$$\frac{\Delta_2 F(J)}{J+1/2} = 4B_v - 8D_v(J+1/2)^2$$

in which the combination differences of the upper and lower states are obtained from

$$\Delta_2 F'(J) = R(J) - P(J)$$

$$\Delta_2 F''(J) = R(J-1) - P(J+1)$$

by following the usual graphical procedure. The vacuum wavenumbers and the rotational assignments for the four bands are given in Table II. The  $J$  numbering of the  $P$  and  $R$  branches of 1, 4 band is shown in Plate 1(b). In determining the rotational constant of the upper state  $v' = 2$ , the average values of the upper state combination differences  $\Delta_2 F'(J)$  for the (2, 0) and (2, 5) bands were used. The band origins,  $B_v$  and  $D_v$  values of the various upper and lower levels are collected in Table III. The values of  $B_e$  and  $\alpha_e$  on the basis of the present work agree very well with the values reported earlier by Rao and Rao. The variation of  $D_v$  with  $v$  is too small and hence the same value of  $D_v$  is given for the levels  $v'' = 4$  and 5.

ACKNOWLEDGMENTS

The authors wish to express their thanks to Prof. K. R. Rao for his interest in the work. One of the authors (K. M. Rao) is thankful, to Dr. T. A. Prasada Rao for his help in bringing out this paper, and to the C.S.I.R. (New Delhi) for the financial assistance.

REFERENCES

- Herzberg, G., 1950, *Spectra of Diatomic Molecules*, D. Van Nostrand Co., Inc., New York.
- Howell, H. G., 1936, *Proc. Roy. Soc. (Lond.)*, **155**, 141.
- Howell, H. G. and Rochester, G. D., 1939, *Proc. Phys. Soc. (London)*, **51**, 329.
- Morgan, F., 1936, *Phys. Rev.*, **49**, 41.
- Prasada Rao, T. A. and Tiruvenganna Rao, P., 1962, *Ind. J. Phys.*, **36**, 85.
- 
- 1962, *Can. J. Phys.*, **40**, 1077.
- Rochester, G. D., 1937, *Phys. Rev.*, **51**, 486.

# DYNAMICS OF THE VIBRATION OF AN ELASTIC-PLASTIC STRING UNDER TRANSVERSE IMPACT

S. K. GHOSH AND SUNIL KUMAR BANERJEE

DEPARTMENT OF PHYSICS, JADAVPUR UNIVERSITY, CALCUTTA-32

(Received August 11, 1965)

**ABSTRACT.** Dynamics of an elastic-plastic string struck by an inelastic transverse load, has been worked out in this paper following the well known operational method due to Heaviside. The importance of this paper is that unlike the case of an ordinary flexible string the velocities of the transverse wave motion at different points on both sides of the struck-point of the elastic-plastic string, depend mainly on the strains at the corresponding points in the two portions of the string. The study of the displacements and pressure at the struck point due to elastic-plastic wave generation in the string is the main feature of the problem, published in two distinct cases I and II.

In case I, the displacement and pressure have been obtained when the string is struck at the middle point and in case II the general expression for displacement of the string is found when it is struck near one end.

## INTRODUCTION

The Dynamics of vibration of string excited by transverse impact have been worked out by a number of workers. The new idea included in the theory of the present topic is that, unlike the case of an ordinary flexible string, the velocities due to transverse wave propagation at different points on both sides of the struck point of the string depend on unknown functions of strains at the corresponding points. A second important assumption, in this paper, is that the tension of the string is known non-linear function of strain but does not depend upon the strain rate. The useful contributions of these assumptions are mainly, the strains, the velocities of transverse waves and their gradients are different from point to point on both sides of the struck point of the string. In fact, the changes in the velocity-gradients at points being assumed to be different unknown functions of strains, being in the idea of elastic-plastic wave generation in the string vibrating under transverse impact.

The plane motion of the struck-string (Ghosh, 1938) is studied by means of the equation of motion,

$$\rho \frac{d^2 y}{dt^2} = \frac{d}{ds} \left( \frac{T}{1 + \epsilon} \frac{dy}{ds} \right) \quad \dots (1.0)$$

The complete dynamics of the present problem have been studied using the powerful operational method due to Heaviside, and the results obtained after suit-

able approximation, agree well with those derived in the case of an ordinary flexible string.

# EXPLANATION OF THE SYMBOLS USED

- $l$  = Length of the string =  $a + b$   
 $a$  = Shorter segment of the string.  
 $b$  = Longer segment of the string.  
 $s$  = Variable measured along length of the string fixed at  $s = 0$  and  $s = l$   
 $t$  = Variable time.  
 $y$  = Displacement of any point at any time  $t$ .  
 $y_1$  = Displacement of any point, in  $0 < s < a$ .  
 $y_2$  = Displacement of any point, in  $a < s < l$ .  
 $y_a$  = Displacement of the struck point,  $s = a$ .  
 $\rho$  = Linear density of the string.  
 $m$  = Mass of the hammer.  
 $T$  = Tension of the string, a known function of strain.  
 $\epsilon$  = Variable Strain at any point of the string.  
 $c_1(\epsilon)$  = Velocity of transverse wave motion of the string in the portion  $0 < s < a$ .  
 $c_2(\epsilon)$  = Velocity of transverse wave motion of the string in the portion,  $a < s < l$ .  
 $c_a(\epsilon)$  = Velocity of transverse wave motion at  $s = a$   
 $\theta_a = 2a/c_a$   
 $v_0$  = Velocity of impact.  
 $t_n = t - n\theta_a$ . Where  $n = 1, 2, 3, 4$  etc.  
 $J = mv_0$   
 $P$  = Pressure exerted by the hammer.  
 $D$  = Operator  $d/dt$ .

# SOLUTION OF THE PROBLEM

The equation of motion of the Elastic-Plastic string can be approximately written as,

$$\rho \frac{d^2 y}{dt^2} = \frac{d^2}{ds^2} \left( \frac{T}{1+\epsilon} y \right) \quad \dots \quad (1.1)$$

Equation (1.1) in the operational notation is,

$$\frac{d^2}{ds^2} (\rho c^2 y) = \frac{D^2}{c^2} (\rho c^2 y) \quad \dots \quad (1.2)$$

where,

$$c^2 = \frac{T}{\rho(1+\epsilon)} \quad \dots \quad (1.3)$$

The solution of (1.2) is,

$$\rho c^2 y = A \cosh \frac{D}{c} s + B \sinh \frac{D}{c} s. \quad \dots (1.4)$$

$A, B$  being constants.

Here the string is clamped and the terminal conditions are, at,

$$\left. \begin{aligned} s = 0 \quad y = 0 \\ s = a_1 \quad y = y_a, \quad c = c_a \end{aligned} \right\} \quad \dots (2.0)$$

The hammer strikes the string at  $s = a$  if  $y$  be the displacement of the struck point we get from (1.4) and (2.0),

$$y_1 = y_a \left( \frac{c_a}{c_1} \right)^2 \frac{\sinh \frac{D}{c_1} s}{\sinh \frac{D}{c_1} a} \quad (0 < s < a) \quad \dots (3.0)$$

$$y_2 = y_a \left( \frac{c_a}{c_2} \right)^2 \frac{\sinh \frac{D}{c_2} (l-s)}{\sinh \frac{D}{c_2} b} \quad (a < s < l) \quad \dots (3.1)$$

The string which is straight initially, is supposed to behave like a loaded string attached to  $s = a$ , excited by an impulse  $J$ . The subsequent equation for the load is given by,

$$m \frac{d^2 y_a}{dt^2} = \left( \rho c_2^2 \frac{dy_2}{ds} \right)_{s=a} - \left( \rho c_1^2 \frac{dy_1}{ds} \right)_{s=a} \quad \dots (4.0)$$

where the right hand side of (4.0) is the change in the value of  $(\rho c^2 dy/ds)$  in crossing the point  $(s = a)$  in the positive direction.

The corresponding pressure exerted by the hammer is given by the equation,

$$P = m \frac{d^2 y_a}{dt^2} \quad \dots (4.1)$$

Now equations (4.0), (3.0) and (3.1), together with boundary conditions give,

$$\begin{aligned} m D^2 y_a = -2 y_a \rho c_a \left[ \left( \frac{dc_2}{ds} \right)_{s=a} - \left( \frac{dc_1}{ds} \right)_{s=a} \right] \\ - y_a \rho c_a D \left[ \coth \frac{D a}{c_a} + \coth \frac{D b}{c_a} \right] + D J \quad \dots (5.0) \end{aligned}$$

Since the string is elastic-plastic in nature,  $(dc_2/ds)_{s=a} - (dc_1/ds)_{s=a}$  can be taken as any function of strain say,  $\psi(\epsilon)$ .

Equation (5.0) then becomes,

$$mD^2y_a = -2y_a \rho c_a \psi(\epsilon) - y_a \rho c_a D \left[ \coth \frac{Da}{c_a} + \coth \frac{Db}{c_a} \right] + DJ \quad (5.1)$$

whence we have,  $y_a = \frac{D}{F(D)} v_0 \quad \dots \quad (6.0)$

where,  $F(D) = D^2 + \frac{\rho c_a}{m} D \left\{ \coth \frac{Da}{c_a} + \coth \frac{Db}{c_a} + \frac{2\rho c_a}{m} \psi(\epsilon) \right\} \quad \dots \quad (6.1)$

# STRING SEMI-INFINITE : HAMMER STRIKES AT MIDDLE POINT

In this case we put  $b = a$ , and equation (6.1) becomes,

$$F(D) = D^2 + qD \coth \frac{Da}{c} + r \quad \dots \quad (7.0)$$

where  $q = \frac{2\rho c_a}{m}$  and  $r = q\psi(\epsilon) \quad \dots \quad (7.1)$

On substituting the exponential values of hyperbolic cotangent in equation (7.0) and writing  $D_1 = D + \alpha$  and  $D_2 = D + \beta$  the final form of  $F(D)$  is,

$$F(D) = \frac{D_1 D_2}{\left[ 1 - \exp \left( -\frac{2Da}{c_a} \right) \right]} \left\{ 1 - \frac{(D-\alpha)(D-\beta)}{D_1 D_2} \exp \left( -\frac{2Da}{c_a} \right) \right\} \quad (8.0)$$

where,  $D_1 D_2 = (D + \alpha)(D + \beta) = D^2 + qD + r \quad \dots \quad (8.1)$

and  $-\alpha = -\beta$  are the roots of  $D^2 + qD + r = 0 \quad \dots \quad (8.2)$

given by,  $|\alpha, \beta| = \frac{1}{2}\{q \pm (q^2 - 4r)^{\frac{1}{2}}\} \quad \dots \quad (8.3)$

The displacement  $y_a$  of the struck point can now be obtained by the equations (6.0) and (8.0),

$$y_a = \frac{D}{D_1 D_2} \left\{ 1 - \exp \left( -\frac{2Da}{c_a} \right) \right\} \left[ 1 - \frac{(D-\alpha)(D-\beta)}{D_1 D_2} \exp \left( -\frac{2Da}{c_a} \right) \right] v_0 \quad \dots \quad (9.0)$$

Expanding multinomially, the right hand side, eqn. (9.0) becomes,

$$\begin{aligned}
 y_a = & \left[ \frac{D}{D_1 D_2} - \frac{2(\alpha + \beta) D^2}{D_1^2 D_2^2} \exp(-D\theta_a) \right. \\
 & + \left\{ \frac{4(\alpha + \beta)^2 D^3}{D_1^3 D_2^3} - \frac{2(\alpha + \beta) D^2}{D_1^2 D_2^2} \right\} \exp(-2D\theta_a) \\
 & - \frac{8(\alpha + \beta)^3 D^4}{D_1^4 D_2^4} - \frac{8(\alpha + \beta)^2 D^3}{D_1^3 D_2^3} + \frac{2(\alpha + \beta) D^2}{D_1^2 D_2^2} \left. \right\} \\
 & \exp(-3D\theta) + \dots \Big] v_0 \dots \quad (9.1)
 \end{aligned}$$

now writing,

$$f_1(t) = \frac{1}{D_1 D_2} v_0 \quad \dots \quad (10.1)$$

$$f_2(t) = \frac{(\alpha + \beta) D}{D_1^2 D_2^2} v_0 \quad \dots \quad (10.2)$$

etc.,

$$f_n(t) = \frac{(\alpha + \beta)^{n-1} D^{n-1}}{D_1^n D_2^n} v_0 \quad \dots \quad (10.3)$$

and remembering that,  $t_n = t - n\theta_a$  we get,

$$y_a = f_1'(t), -2f_2'(t_1), +4f_3'(t_2) - 2f_2'(t_2), -8f_4'(t_3) + 8f_3'(t_3) - 2f_2'(t_3) + \dots \quad \dots \quad (11.0)$$

Now  $f_1'(t)$ ,  $f_2'(t)$  etc., can be obtained as follows :

$$f_1'(t) = \frac{v_0 A}{(\alpha + \beta)} [e^{-\alpha t} - e^{-\beta t}] \quad \dots \quad (12.0)$$

$$f_2'(t) = \frac{v_0 A^2}{(\alpha + \beta)} [(A - \alpha t)e^{-\alpha t} - (A + \beta t)e^{-\beta t}] \quad \dots \quad (12.1)$$

$$\begin{aligned}
 f_3'(t) = & \frac{v_0 A^3}{(\alpha + \beta)} \left[ \left\{ -\frac{1}{2} + \frac{3A^2}{2} - \frac{1}{2} (3A + 1)\alpha t + \frac{\alpha^2 t^2}{2!} \right\} e^{-\alpha t} \right. \\
 & \left. + \left\{ \frac{1}{2} - \frac{3A^2}{2} - \frac{1}{2} (3A - 1)\beta t - \frac{\beta^2 t^2}{2!} \right\} e^{-\beta t} \right] \quad \dots \quad (12.2)
 \end{aligned}$$

and so on, where  $A = \frac{\beta + \alpha}{\beta - \alpha}$ ,  $\alpha$  and  $\beta$  being given by (8.3).



Thus the displacements of the struck point at different intervals of time are, as follows :

during,  $0 < t < \theta_a$ ,

$$y_a = f'_1(t) = \frac{v_0 A}{\beta + \alpha} [e^{-\alpha t} - e^{-\beta t}] \quad \dots \quad (13.0)$$

during,  $\theta_a < t < 2\theta_a$ ,

$$y_a = y_a(0 < t < \theta_a) - \frac{2v_0 A^2}{(\alpha + \beta)} [(A - \alpha t_1)e^{-\alpha t_1} - (A + \beta t_1)e^{-\beta t_1}] \quad \dots \quad (13.1)$$

similarly during,  $2\theta_a < t < 3\theta_a$ ,

$$\begin{aligned} y_a = & y_a(\theta_a < t < 2\theta_a) \\ & + \frac{4v_0 A^3}{(\alpha + \beta)} \left[ \left\{ -\frac{1}{2} + \frac{3A^2}{2} - \frac{1}{2} (3A + 1)\alpha t_2 + \frac{\alpha^2 t_2^2}{2!} \right\} e^{-\alpha t_2} \right. \\ & \left. + \left\{ \frac{1}{2} - \frac{3A^2}{2} - \frac{1}{2} (3A - 1)\beta t_2 - \frac{\beta^2 t_2^2}{2!} \right\} e^{-\beta t_2} \right] \\ & - \frac{2v_0 A^2}{(\alpha + \beta)} [(A - \alpha t_2)e^{-\alpha t_2} - (A + \beta t_2)e^{-\beta t_2}] \quad \dots \quad (13.2) \end{aligned}$$

and so on.

Equations (13.0), (13.1), (13.2) etc. are the expressions of the displacements of the struck point at different intervals of time. These equations together with equations (3.0) and (3.1) will enable us to determine the general displacement of any point of the elastic-plastic string.

It is interesting to note in this connection that if  $\psi(\epsilon) = 0$  we have from (8.3),  $\beta = 0$  and the expressions for the displacements of the struck-point at different intervals of time takes up the following forms :

During,  $0 < t < \theta_a$ ,

$$y_a = \frac{v_0}{q} (1 - e^{-qt}) \quad \dots \quad (14.0)$$

During,  $\theta_a < t < 2\theta_a$ ,

$$y_a = y_a(0 < t < \theta_a) - \frac{2v_0}{q} [1 - (1 + qt_1)e^{-qt_1}] \quad \dots \quad (14.1)$$

During,  $2\theta_a < t < 3\theta_a$ ,

$$y_a = y_a(\theta_a < t < 2\theta_a) + \frac{2v_0}{q} [1 - (1 + qt_2 + q^2 t_2^2)e^{-qt_2}] \quad \dots \quad (14.2)$$

Equations (14.0), (14.1) and (14.2) are the expressions for the displacements of

the struck point at different epoch with the above approximations. These are exactly the same as those derived by Ghose (1938) in the case of an ordinary flexible string.

The pressure at different epochs exerted by the hammer on the string can be obtained by means of equations (4.1) and (11.0) as follows :

During,  $0 < t < \theta_a$ ,

$$P_1 = \frac{mv_0}{(q^2 - 4r)^{1/2}} [\alpha^2 e^{-\alpha t} - \beta^2 e^{-\beta t}] \quad \dots \quad (15.0)$$

During,  $\theta_a < t < 2\theta_a$ ,

$$P_2 = P_1 + \frac{2mv_0 q}{q^2 - 4r} [\alpha^2(2 + A - \alpha t_1) e^{-\alpha t_1} + \beta^2(2 - A - \beta t_1) e^{-\beta t_1}] \quad \dots \quad (15.1)$$

During,  $2\theta_a < t < 3\theta_a$ ,

$$\begin{aligned} P_3 = P_2 + \frac{4mv_0 q^2}{(q^2 - 4r)^{3/2}} & \left[ \alpha^2 \left\{ -\frac{1}{2} + \frac{3A^2}{2} - \frac{1}{2}(3A+1)\alpha t_2 + \frac{\alpha^2 t_2^2}{2} \right\} e^{-\alpha t_2} \right. \\ & + 2\alpha \left\{ \frac{1}{2}(3A+1)\alpha - \alpha^2 t_2 \right\} e^{-\alpha t_2} + \alpha^2 e^{-\alpha t_2} \\ & + \beta^2 \left\{ \frac{1}{2} - \frac{3A^2}{2} - \frac{1}{2}(3A-1)\beta t_2 - \frac{\beta^2 t_2^2}{2!} \right\} e^{-\beta t_2} \\ & + 2\beta \left\{ \frac{1}{2}(3A-1)\beta + \beta^2 t_2 \right\} e^{-\beta t_2} - \beta^2 e^{-\beta t_2} \left. \right] \\ & + \frac{2mv_0 q}{(q^2 - 4r)^{1/2}} [\alpha^2(2 + A - \alpha t_2) e^{-\alpha t_2} + \beta^2(2 - A - \beta t_2) e^{-\beta t_2}] \quad \dots \quad (15.2) \end{aligned}$$

Here also if we take  $\psi(\epsilon) = 0$  the plastic behaviour disappears from the string and the different expressions for pressure as stated in (15.0), (15.1) and (15.2) become quite similar to those obtained by Ghose (1938) for a flexible string.

#### STRING SEMI-INFINITE : HAMMER STRIKES NEAR ONE END

If hammer strikes the elastic-plastic string at  $s = \alpha$  which is too small compared to  $b$ , and as  $\lim_{b \rightarrow \infty} \text{Coth}(Db/c_a) = 1$  (6.0) becomes,

$$F(D) = D^2 + \frac{1}{2} \frac{\rho c_a}{m} D \left( \coth \frac{D\alpha}{c_a} + 1 \right) + r \quad \dots \quad (16.0)$$

Expanding  $\coth(D\alpha/c_a)$  in a power series of  $D\alpha/c_a$  and retaining terms containing  $\alpha/c_a$  only, it is found,

$$F(D) = D^2 \left( 1 + \frac{\rho\alpha}{3m} \right) + \frac{\rho c_a}{m} D + \left( \frac{\rho c_a^2}{am} + r \right) \quad \dots \quad (16.1)$$

From (6.0) and (16.1) we have,

$$y_a = \frac{m}{m_0} \frac{D}{(D-q)(D-p)} \cdot v_0 = \frac{m}{m_0} \frac{v_0}{q-p} (e^{qt} - e^{pt}) \quad \dots (17.0)$$

where  $\frac{m_0}{m} = 1 + \frac{\rho a}{3m}$  and  $q, p$  are the roots of,

$$D^2 + \frac{\rho c_a}{m_0} D + \frac{m}{m_0} \left( \frac{\rho c_a^2}{\alpha m} + r \right) = 0 \quad \dots (17.1)$$

given by,

$$p = -\mu - i\nu \quad \dots (18.0)$$

$$q = -\mu + i\nu \quad \dots (18.1)$$

whence,

$$\mu = \frac{\rho c_a}{2m_0} \quad \dots (19)$$

and,

$$\nu = \left[ \left( \frac{\rho c_a^2}{m_0} + \frac{m}{m_0} r \right) - \frac{\rho^2 c_a^2}{4m_0^2} \right]^{\frac{1}{2}} \quad \dots (19.1)$$

Thus from (17.0) and (18.0), (18.1) we have,

$$y_a = \frac{m}{m_0} \cdot \frac{v_0}{\nu} e^{-\mu t} \sin \nu t \quad \dots (20.0)$$

Equation (20.0) shows that the displacement curve is of the damped oscillatory nature. Clearly the damping is introduced due to the plastic nature of the string. Also the frequency is affected by the strain at the corresponding struck-point. Thus unlike the case of an ordinary flexible string, the frequency of vibration of

the elastic-plastic string is found to increase by an amount  $\frac{m}{m_0} r = \frac{2\rho c}{m_0} \psi(\epsilon)$  as

in the frequency equation (19.1) when the string is struck near one end.

In the case of flexible string  $\psi(\epsilon) = 0$  and the corresponding frequency equation reduces to that derived by Ghosh (loc. cit).

#### REFERENCES

- Ghose, M., 1938, *Ind. J. Phys.*, **12**, 317.  
 Lee, E. H. and Symonds, P. H., 1960, *Proceedings of the 2nd Symposium on naval structural Mechanics* (Pergamon Press) pp. 414.

# PERFORMANCE OF UNSTABLE PENDANT DROPS IN SURFACE TENSION MEASUREMENTS

K. G. PARVATIKAR,

DEPARTMENT OF PHYSICS, GOVERNMENT FIRST GRADE COLLEGE, KOLAR

(Received September 13, 1965)

**ABSTRACT.** Tawde and Parvatikar have evolved an experimental technique to subject the unstable pendant drops for surface tension measurements. In this paper modifying this technique and using a table drawn from fundamental considerations utilising Fordham's tables, surface tension measurements have been made from the observed data on four liquids which compare favourably with the accepted values.

## INTRODUCTION

The use of pendant drops for surface tension measurements has been suggested by several workers such as Worthington (1885) and Ferguson (1912). The method remained in disrepute for a considerable time because of difficult measurements involved in it. Recently, it has been made useful for exact work as a result of critical study of it by Andreas, *et al.* (1938). This method has been placed on better foundations by Fordham (1948) by supplying a table for the calculation of surface tension from measurements on pendant drops. Brown and McCormick (1948), while working out a new drop-weight method have shown by dimensional analysis that the shapes of all drops forming on a conical tip are similar at the unstable stage.

As shown by Adam (1941), the equation to the outline of any pendant drop referred to axes of  $x$  and  $z$  can be written in the dimensionless form

$$\frac{1}{\rho/b} + \frac{\sin \phi}{x/b} = 2 + \beta \frac{z}{b} \quad \dots (1)$$

where  $b$  is the radius of curvature at the origin, which is the vertex of the drop,  $\rho$  is the radius of curvature in the plane of the paper at the point  $(x, z)$ , and  $\beta = \frac{2b^2}{a^2}$ , where  $a^2$  is the capillary constant which connects the surface tension  $\gamma$  by the relation  $a^2 = \frac{2\gamma}{g\sigma}$ ,  $\sigma$  being the effective density of the liquid. The angle  $\phi$  is the inclination at the point  $(x, z)$  to the horizontal.

Bashforth and Adams (1883), giving numerical solution of this equation have drawn up a table of  $x/b$  and  $z/b$  for many values of  $\phi$  and  $\beta$ . These tables were

extended by Fordham while supplying a tabular set of values necessary in the pendant drop method suggested by Andreas, Hauser and Tucker.

It is shown possible here that for a given value of  $\beta$ , the ratio  $d/r$ ,  $d(=z_e)$ , being the depth of a pendant drop from the equatorial plane and  $r(=x_e)$  the radius of it in that plane, may be related to  $a^2/r^2$ . Obviously  $\phi = 90^\circ$ , when the point lies on the equatorial plane.

$$\text{Now,} \quad \frac{d}{r} = \frac{z_e}{x_e} = \frac{z_e/b}{x_e/b} \quad \dots (2)$$

$$\text{and} \quad a^2 = \frac{2b^2}{\beta} \left( \text{since } \beta = \frac{2b^2}{a^2} \right)$$

$$\text{therefore,} \quad \frac{a^2}{r^2} = \frac{a^2}{x_e^2} = \frac{2}{\beta(x_e/b)^2} \quad \dots (3)$$

Knowing the values of  $z_e/b$  and  $x_e/b$  by interpolation from the tables of Bashforth and Adams, and Fordham, it is possible to calculate  $d/r$  from Eq. (2) and  $a^2/r^2$  from Eq.(3). The computed values necessary for the present problem are given in Table I. This table allows for direct interpolation of the intermediate values of  $d/r$ .

TABLE I

$\beta$	$Z_e/b$	$X_e/b$	$d/r$	$a^2/r^2$	Interpolated values	
					$d/r$	$a^2/r^2$
0.4500	1.309,01	1.103,67	1.186,05	3.648,71	1.186	3.648,71
0.4625	1.327,12	1.108,00	1.197,76	3.522,40	1.197	3.529,95

If it is possible to measure  $d/r$  of a pendant drop formed on a conical tip at the stage of instability,  $a^2/r^2$  can be known for the corresponding measured value of  $d/r$ , and hence  $\gamma$ , the surface tension can be calculated. It may be noted here, as mentioned above, that since the shapes of all drops forming on a conical tip are similar at the unstable stage, only one value of  $a^2/r^2$  is required to be known precisely for an accurately measured value of  $d/r$ .

The experimental problem was, therefore, of measuring the equatorial radius  $r$ , and the depth  $d$  of a pendant drop formed on a conical tip at the critical stage of instability. If sufficient time is allowed for proper development of a drop formed on a conical tip, it is possible to follow the changing shape and size of the drop until it just collapses from it,

## EXPERIMENTAL AND RESULTS

The experimental set up devised and the operations involved were exactly the same as adopted by Tawde and the author (1956), with the following modifications. The source  $S$  was a monochromatic radiation of sodium lamp and the microscope was replaced by a camera, its lens being fitted in a tube which was fixed to the front window of the thermostat chamber. The camera was set on an optical bench at a suitable distance in order to get an enlarged sharp image of the drop. There was a channel connecting the tube in which lens was inserted and the camera. In the place of the photographic plate in the camera, an oiled paper was enclosed in between two thin plane glass plates. A weighted silk thread was hung as a plumb line very near to the glass plate and its image defined the vertical. A sharp blade was fixed to a fine screw arrangement which was fitted to the frame of the camera. By turning the screw, it was possible to move the edge of the blade up and down even to a very small extent. The image of the edge of the blade was perfectly horizontal.

As the method involved measurements on the images of drops and the actual radius of the drop in the equatorial plane, it was necessary to know the magnification ratio ( $M$ ). This was achieved by measuring the base of the actual conical tip and its enlarged image. The base of the conical tip was  $12.60 \pm 0.02$  mm. By loosening the pinch-cock screw, a drop was allowed to grow slowly under gravity at the conical tip. The time taken for a drop to develop fully to the point of detachment was atleast seven minutes. The image of the plumb line was first adjusted so that the edge of the conical tip coincided with it. At the unstable stage of the pendant drop, the point lying on the equatorial plane was observed by a microscope capable of reading 0.001 cm. and at the same time by turning the screw the image of the edge of the blade was set tangential to the bottom of the drop. From these two settings on the image of the drop,  $D/R (= d/r)$  was obtained. Readings were repeated a number of times on fresh drops to obtain

TABLE II

Liquid at 30°C	Effective density in gm./cc.	$M$	$D$ in mm.	$R$ in mm.	$D/R$	$r$ in mm.	$\frac{a^2}{r^2}$ (From Table I)	$a^2$ in sq. mm.	$\gamma$ in dynes/cm.	
									Present author	I.C.T.
Water	0.9946	5.054	12.29	10.27	1.196	2.032	3.540,75	14.620	71.14	71.18 $\pm 0.05$
Toluene	0.8525	7.684	12.49	10.44	1.196	1.358	3.540,75	6.529	27.23	27.30 $\pm 0.10$
Benzene	0.8622	7.685	12.50	10.45	1.196	1.360	3.540,75	6.548	27.62	27.60 $\pm 0.05$
m-xylene	0.8530	7.698	12.62	10.55	1.196	1.370	3.540,75	6.646	27.74	27.80 $\pm 0.10$

confirmation of the ratio  $D/R$ . The actual radius  $r$  of the drop was computed knowing  $R$  and  $M$ . The liquids chosen for surface tension measurements were water, toluene, benzene and *m*-xylene. A sample set of observations which are the mean of at least ten independent drops of each liquid which did not vary appreciably from each other are given in Table II. No attempt has been made at this stage to obtain the estimate of accuracy of results.

On comparing the results in the last two columns of Table II, it is apparent that there is a fair agreement of measured values of surface tension with those of I.C.T. Furthermore, since the shape factor  $d/r$  is the same for drops of different liquids formed on a conical tip, the investigation shows that the shapes of *all* drops forming on a conical tip are similar at the unstable stage—a conclusion reached by Brown and McCormick by dimensional analysis. It would be interesting to examine how far the unstable pendant drops can be used to measure the surface tension of liquids on this basis. This point is under investigation in this laboratory.

#### ACKNOWLEDGMENT

The author wishes to thank Professor L. Sibaiya, D.Sc., of the National Institute of Engineering, Mysore, for the helpful interest which he has displayed in this work. He is also thankful to the authorities of the Collegiate Education and also to Professor K. R. Udupa, Principal of this College, for providing the necessary facilities for this research and to his colleague Mr. M. Z. Hakh for helpful discussions.

#### REFERENCES

- Adam, N. K., 1941, *The Physics and Chemistry of surfaces*, Oxford University Press, p. 366.
- Andreas, J. M., Hauser, E. A and Tucker, W. B., 1938, *J. Phy. Chem*, **42**, 1001.
- Bashforth, F. and Adams, J. C., 1883, *An attempt to test the theories of capillary action*. Cambridge University Press
- Brown, R. C. and McCormick, H., 1948, *Phil. Mag.*, **39**, 420.
- Ferguson, A., 1912, *Phil. Mag.*, **23**, 417.
- Fordham, S., 1948, *Proc. Roy. Soc.*, **194**, 1.
- Tawde, N. R. and Parvatikar, K. G., 1956, *Ind. J. Phys.*, **30**, 348.
- Worthington, A. M., 1885, *Phil. Mag.*, **19**, 46.

## ELASTIC MISFITTING SHELLS

R. D. BHARGAVA AND D. PANDE\*

INDIAN INSTITUTE OF TECHNOLOGY, KANPUR

*(Received August 19, 1964; resubmitted August 23, 1965).*

**ABSTRACT.** In this paper the problem of  $n$  elastic spherical and tubular shells misfitting in each other is considered. Linear simultaneous equations determining the equilibrium boundaries have been formulated, the solution of which gives the values of the parameters determining not only the equilibrium configuration but also the stress-strain field and the related problems in the structure. Results for a particular problem, when the shells are 3 in number, are given for the case of spherical shells.

## INTRODUCTION

Consider a spherical shell of outer radius  $a_0$  and inner radius  $a_1$ , in which a concentric shell of outer radius  $a_1(1+\delta_1)$  and inner radius  $a_2$  is embedded. In this latter shell another one of outer radius  $a_2(1+\delta_2)$  and inner radius  $a_3$  is embedded. In this way let a shell of outer radius  $a_r(1+\delta_r)$  and inner radius  $a_{r+1}$  be embedded into the shell of outer radius  $a_{r-1}(1+\delta_{r-1})$  and inner radius  $a_r$ . This is schematically shown in the adjoining figure. Each of the  $\delta$ 's are supposed to be within the elastic limits. Further we suppose that no relative slipping takes place and continuity of the material is maintained throughout.

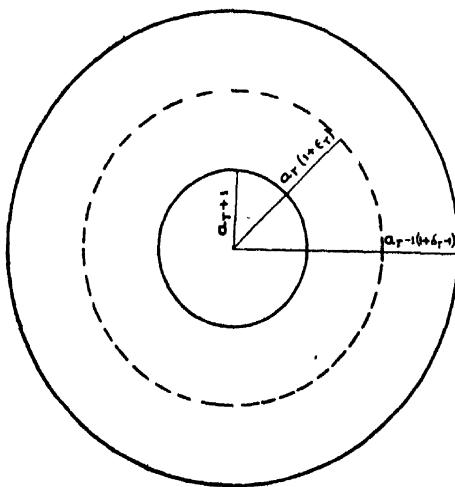


Fig. 1

Due to the misfits in the sizes of the shells stresses develop within the structure. Determination of the elastic field and the equilibrium position form the subject matter of the paper.

\* Christ Church College, Kanpur, India.



Such problems have been studied by Mott and Nabarro (1940), Frankel (1946), Jaswon and Bhargava (1961), Bhargava and Radhakrishna (communicated) but in each case there was one single solid material inside. In a recent paper Bhargava and Pande (1963), have considered hollow inclusions. This paper generalises the above case in as much as the inner materials are hollow and are more in number. This problem is technically important as it is useful when the boundaries are reinforced. The problem has been solved by Energy Method suggested by one of the authors Bhargava (1963). This consists in taking an arbitrary, physically consistent equilibrium position and finding the energy in the material. That position will give the true equilibrium boundary which minimises the energy.

For ease of exposition we name the shells as follows: The shell whose outer and inner radii are  $a_{r-1}(1 + \delta_{r-1})$  and  $a_r$  respectively be named  $A_r$ . It may be noted that for the outermost shell the outer radius is  $a_r$  i.e.  $\delta_0 = 0$ .

On physical grounds the interface both in the case of spherical as well as tubular shells will be concentric spherical or tubular. We thus take the common boundary of  $A_r$  and  $A_{r+1}$  to be  $a_r(1 + \epsilon_r)$ . We find the energy in the medium consisting of all the shells. We first give briefly the case for spherical shells.

*Spherical shells:* Each shell will be under uniform normal pressure due to the shells above and below it. It is known that for such a case, the normal, hoop and shear stresses  $p_{rr}$ ,  $p_{\theta\theta}$  and  $p_{r\theta}$  are respectively of the form

$$p_{rr} = \frac{\zeta}{r^3} + D; \quad p_{\theta\theta} = -\frac{\zeta}{2r^3} + D, \quad p_{r\theta} = 0. \quad \dots (1)$$

The radial and transverse displacements are

$$u_r = -\frac{c}{4\mu r^2} + \frac{D}{3K} r; \quad u_\theta = 0 \quad \text{respectively.} \quad \dots (2)$$

The radial, hoop and shear strains will respectively be

$$e_{rr} = \frac{c}{2\mu r^3} + \frac{D}{3k}; \quad e_{\theta\theta} = -\frac{\zeta}{4\mu r^3} + \frac{D}{3k} \quad \text{and} \quad e_{r\theta} = 0 \quad \dots (3)$$

$\mu$  and  $K$  being the shear and bulk moduli of the material. Let  $\mu_{r-1}$  and  $K_{r-1}$  be the shear and bulk moduli for  $A_r$ .

As the transverse displacements are zero throughout we write  $u_r$  for the radial displacement. Let the radial displacements for the outer and inner boundaries of  $A_r$  respectively be

$$u_0 = -a_{r-1}(\delta_{r-1} - \epsilon_{r-1}) \quad \text{and} \quad u_s = a_r \epsilon_r.$$

On substituting these values in (2) and solving for  $C$  and  $D$  we get

$$\zeta_r = -\frac{4\mu_{r-1}a^3_{r-1}a_r^3\{\delta_{r-1}-\epsilon_{r-1}+\epsilon_r\}}{a^3_{r-1}-a_r^3}; D_r = -\frac{3k_{r-1}\{a_r^3c_r+a^3_{r-1}(\delta_{r-1}-\epsilon_{r-1})\}}{a^3_{r-1}-a_r^3} \quad (3a)$$

for the shell  $A_r$ .

The total mechanical energy of the shell  $A_r$  is given by

$$W_r = \frac{1}{2} \int_{a_r}^{a_{r-1}} \{p_{rr}e_{rr} + 2p_{..}e_{..}\} 4\pi r^2 dr - \iiint_V F_r dv - \iint_{\Omega} f d\sigma$$

where the three terms of the right member of this equation give energy due to elastic forces, body forces and the forces on the boundary. But there being no body or surface forces, the last two terms will contribute nothing. Hence on substituting for  $p_{rr}$ ,  $p_{..}$ ,  $e_{rr}$  and  $e_{..}$  and integrating we get the energy for  $A_r$  as

$$W_r = 2\pi\{a^3_{r-1}-a^3_r\} \left[ \frac{c_r^2}{4\mu_{r-1}a^3_{r-1}a_r^3} + \frac{D_r^2}{3k_{r-1}} \right].$$

It may be noted that for  $A_1$  and  $A_n$  the expressions for energy would not be symmetrical to  $A_r$ . They would actually be

$$W_1 = -\frac{24\pi\mu_0k_0a_1^3(a_0^3-a_1^3)}{4\mu_0a_1^3+3k_0a_0^3} \epsilon_1^2 \quad W_n = -\frac{24\pi\mu_{n-1}k_{n-1}a_{n-1}^3(a_{n-1}^3-a_n^3)}{4\mu_{n-1}a_{n-1}^3+3k_{n-1}a_n^3} (\delta_{n-1}-c_{n-1})^2.$$

The energy for the whole system would be  $W = \sum_{r=1}^n W_r$ .

The true values of  $\epsilon_r$  are those which minimise the value of  $W$ . By the known theorem the extreme values of  $W$  are obtained by solving  $\partial W/\partial \epsilon_r = 0$  ( $r = 1, 2, \dots, n-1$ ). On simplifying we obtain the following set of equations for determining  $\epsilon_r$ .

$$\begin{aligned} (B'_0 + B_1 + a_1^6 B_2) \epsilon_1 - (B_1 + a_1^3 a_2^3 B_2) \epsilon_2 &= (B_1 + a_1^6 B_2) \delta_1 \\ (B_1 + a_1^3 a_2^3) \epsilon_1 - (B_1 + a_2^6 B_2 + B_3 + a_2^6 B_4) \epsilon_2 + (B_3 + a_2^3 a_3^3 B_4) \epsilon_3 \\ &= (B_1 + a_2^3 a_3^3 B_2) \delta_1 - (B_3 + a_2^6 B_4) \delta_2 \\ (B_3 + a_2^3 a_3^3 B_4) \epsilon_2 - (B_3 + a_3^6 B_4 + B_5 + a_3^6 B_6) \epsilon_3 + (B_5 + a_3^3 a_4^3 B_6) \epsilon_4 \\ &= (B_3 + a_3^3 a_4^3 B_4) \delta_2 - (B_5 + a_3^6 B_6) \delta_3 \\ \dots & \dots \dots \dots \dots \dots \\ \dots & \dots \dots \dots \dots \dots \\ (B_{2r-3} + a_{r-1}^3 a_r^3 B_{2r-2}) \epsilon_{r-1} - (B_{2r-3} + a_r^6 B_{2r-2} + B_{2r-1} + a_r^6 B_{2r}) \epsilon_r \\ &+ (B_{2r-1} + a_r^3 a_{r+1}^3 B_{2r}) \epsilon_{r+1} = (B_{2r-3} + a_{r-1}^3 a_r^3 B_{2r-2}) \delta_{r-1} - (B_{2r-1} + a_{r+1}^6 B_{2r}) \delta_r \\ \dots & \dots \dots \dots \dots \\ \dots & \dots \dots \dots \dots \dots \end{aligned} \quad (3b)$$

$$(B_{2n-5} + a_{n-2}^3 a_{n-2}^3 B_{2n-4}) \epsilon_{n-2} - (B_{2n-5} + a_{n-1}^6 B_{2n-4} + B_n') \epsilon_{n-1} \\ = (B_{2n-5} + a_{n-2}^3 a_{n-1}^3 B_{2n-4}) \delta_{n-2} - B_n' \delta_{n-1}$$

where  $B'_0 = \frac{12\mu_0 k_0 a_1^3 (a_0^3 - a_1^3)}{4\mu_0 a_1^3 + 3k_0 a_0^3}$  ;  $B_{2r-1} = \frac{4\mu_r a_r^3 a_{r+1}^3}{a_r^3 - a_{r+1}^3}$  ;

$$B_{2r} = \frac{3k_r}{a_r^3 - a_{r+1}^3} ; \quad B'_n = \frac{12\mu_{n-1} k_{n-1} a_{n-1}^3 (a_{n-1}^3 - a_n^3)}{4\mu_{n-1} a_{n-1}^3 + 3k_{n-1} a_n^3}.$$

Note that all  $B_k$  are constants.

These equations can be more systematically put in the matrix form

$$L\epsilon = M\delta$$

where  $\epsilon$  is a column vector  $\{\epsilon_1, \epsilon_2, \dots, \epsilon_{n-1}\}$ ,  $L$  is a symmetric matrix of order  $(n-1) \times (n-1)$ .

$$\begin{bmatrix} -(B'_0 + B_1 + a_1^6 B_2) & (B_1 + a_1^3 a_2^3 B_2) & & & 0 & 0 & \dots & 0 & 0 \\ (B_1 + a_1^3 a_2^3 B_2) & -(B_1 + a_2^6 B_2 + B_3 + a_2^6 B_4) & (B_3 + a_3^3 a_3^3 B_4) & & 0 & 0 & \dots & 0 & 0 \\ 0 & (B_3 + a_2^3 a_3^3 B_4) & -(B_3 + a_3^6 B_4 + B_5 + a_3^6 B_6) & (B_5 + a_3^3 a_4^3 B_6) & \dots & 0 & 0 \\ - & - & - & - & \dots & - & - & - \\ - & - & - & - & \dots & - & - & - \\ 0 & 0 & 0 & 0 & -(B_{2n-7} + a_{n-2}^6 B_{2n-6} + B_{2n-5} + a_{n-2}^6 B_{2n-4}) & & & \\ & & & & (B_{2n-5} + a_{n-2}^3 a_{n-1}^3 B_{2n-4}) & & & \\ 0 & 0 & 0 & 0 & \dots & (B_{2n-5} + a_{n-2}^3 a_{n-1}^3 B_{2n-4}) - (B_{2n-5} + a_{n-1}^6 B_{2n-4} + B_n') \end{bmatrix}$$

The determinant of the above matrix is called the continuant matrix. It is comparatively easy to find a recurring inversion formula for such a matrix.

$M$  is the matrix of order  $(n-1)(n-1)$

$$\begin{bmatrix} -(B_1 + a_1^6 B_2) & 0 & 0 & \dots & \dots & 0 \\ (B_1 + a_1^3 a_2^3 B_2) & -(B_3 + a_2^6 B_4) & 0 & \dots & 0 & 0 \\ 0 & (B_3 + a_2^3 a_3^3 B_4) & -(B_5 + a_3^6 B_6) & \dots & 0 & 0 \\ - & - & - & \dots & - & - \\ - & - & - & \dots & - & - \\ 0 & 0 & 0 & (B_{2n-5} + a_{n-2}^3 a_{n-1}^3 B_{2n-4}) & -B_n' \end{bmatrix}$$

$\delta$  is the column vector  $\{\delta_1, \delta_2 \dots \delta_{n-1}\}$ .

The value of  $\epsilon$  will be

$$\epsilon = L^{-1}M\delta$$

where  $L^{-1}$  is the inverse matrix of  $L$ .

This gives the values of  $\epsilon_r$  in terms of known quantities.

Having known  $\epsilon_r$ ,  $p_{rr}$ ,  $p_{\theta\theta}$ ,  $p_{r\theta}$  can be found from equation (1), after finding the values of  $C_r$ ,  $D_r$  from equations (3a). It is difficult, in the general case to prove the continuity of the normal stress  $p_{rr}$  at the equilibrium interface. This can, however, be seen indirectly from the following argument. At the interface of  $A_r$  and  $A_{r+1}$  if  $p_{rr}$  is to be continuous, we must have

$$\frac{C_r}{a_r^3(1+\epsilon_r)^3} + D_r = \frac{C_{r+1}}{a_{r+1}^3(1+\epsilon_r)^3} + D_{r+1}, \quad \text{i.e. } C_r - C_{r+1} = a_r^3(D_{r+1} - D_r),$$

to the first order of approximation.

This equation is identical with the simultaneous equations obtained above when approximate values of  $C_r$ ,  $C_{r+1}$ ,  $D_r$ ,  $D_{r+1}$  are substituted. In fact, the equation is the equation (3b).

*Tubular Shells* : For the tubular shells we use the same notation as for the spherical shells. In this case also each shell would be under uniform normal pressure due to similar shells above and below it. The normal, hoop and shear stresses in this case will be

$$p_{rr} = \frac{C}{r^2} + D; \quad p_{\theta\theta} = -\frac{C}{r^2} + D; \quad p_{r\theta} = 0 \quad \dots (1)$$

radial and transverse displacements will be

$$u_r = -\frac{C}{2\mu r} + \frac{D}{2(\lambda + \mu)} \quad r; \quad u_\theta = 0 \quad \dots (2)$$

and, radial, hoop and shear strains will be

$$e_{rr} = \frac{C}{2\mu r} + \frac{D}{2(\lambda + \mu)}; \quad e_{\theta\theta} = -\frac{C}{2\mu r} + \frac{D}{2(\lambda + \mu)}; \quad e_{r\theta} = 0$$

where  $\lambda$  and  $\mu$  are the Lamé's constants. For  $A_r$  let these constants be  $\lambda_{r-1}$ ,  $\mu_{r-1}$ .

As throughout the transverse displacements are zero we write for the radial displacement  $u_0$  for  $A_r$ . Let  $u_0 = -a_{r-1}(\delta_{r-1} - \epsilon_{r-1})$  be the displacement at the outer boundary and  $u_i = a_r \epsilon_r$  the corresponding displacement at the inner boundary.

Substituting these values of  $u_0$ ,  $u_i$  in (2) and solving for  $C_r$  and  $D_r$  we get

$$C_r = -\frac{2\mu_{r-1}a_{r-1}^2a_r^2(\delta_{r-1} - \epsilon_{r-1} + \epsilon_r)}{a_{r-1}^2 - a_r^2} \quad \text{and} \quad D_r = -\frac{2(\lambda_{r-1} + \mu_{r-1})\{a_r^2\epsilon_r + a_{r-1}^2(\delta_{r-1} - \epsilon_{r-1})\}}{a_{r-1}^2 - a_r^2}$$

For the outermost and the innermost shells these constants are evaluated from the equations obtained by equating to zero the normal pressure at the outer boundary in the first case and inner boundary in the second case and equating the displacements to  $a_1\epsilon_1$ , at the inner and  $-a_{n-1}(\delta_{n-1}-\epsilon_{n-1})$  at the outer boundary.

Thus the elastic strain energy for  $A_r$  will be

$$V_r = \frac{1}{2} \int_{a_r}^{a_{r-1}} (p_{rr}e_{rr} + p_{\theta\theta}e_{\theta\theta}) 2\pi r dr = \pi(a_{r-1}^3 - a_r^3) \left[ \frac{\xi_r^2}{2\mu_{r-1}a_{r-1}^2a_r^2} + \frac{D_r^2}{2(\lambda_{r-1} + \mu_{r-1})} \right].$$

Also elastic strain energy for  $A_1$  and  $A_n$  will be

$$V_1 = \frac{2\pi\mu_0(\lambda_0 + \mu_0)a_1^2(a_0^2 - a_1^2)}{\mu_0a_1^2 + (\lambda_0 + \mu_0)a_0^2} \epsilon_1^2$$

and

$$V_n = \frac{2\pi\mu_{n-1}(\lambda_{n-1} + \mu_{n-1})a_{n-1}^2(a_n^2 - a_{n-1}^2)}{\mu_{n-1}a_{n-1}^2 + (\lambda_{n-1} + \mu_{n-1})a_n^2} (\delta_{n-1} - \epsilon_{n-1})^2.$$

The total elastic strain energy of the system, therefore, will be

$$V = \sum_{r=1}^n V_r$$

We know that the total mechanical energy for the system

$$W = V - \int \int \int_V F_r dv - \int \int_\Omega f_r d\sigma$$

where the second and third integrals signify the energy due to body forces  $F_r$  and the boundary forces  $f_r$  of the system. In this case since both  $F_r$  and  $f_r$  are zero we have, therefore,

$$W = V$$

The true values of  $\epsilon_r$  as in the spherical shell case will minimise  $W$ .

Thus equating  $\partial W / \partial \epsilon_r = 0$  and simplifying we get the following set of equations.

$$\begin{aligned} (B'_0 + B'_1 + a_1^4 B'_2) \epsilon_1 - (B'_1 + a_1^2 a_2^2 B'_2) \epsilon_2 &= (B'_1 + a_1^4 B'_2) \delta_1 \\ (B'_1 + a_1^2 a_2^2 B'_2) \epsilon_1 - (B'_1 + a_2^4 B'_2 + B'_2 + a_2^2 B'_4) \epsilon_2 + (B'_2 + a_2^2 a_3^2 B'_4) \epsilon_3 \\ &= (B'_1 + a_1^2 a_2^2 B'_2) \delta_1 - (B'_2 + a_2^4 B'_2) \delta_2 \\ (B'_2 + a_2^2 a_3^2 B'_4) \epsilon_2 - (B'_2 + a_2^4 B'_4 + B'_3 + a_3^4 B'_4) \epsilon_3 + (B'_3 + a_3^2 a_4^2 B'_4) \epsilon_4 \\ &= (B'_2 + a_2^2 a_3^2 B'_4) \delta_2 - (B'_4 + a_3^4 B'_4) \delta_3 \\ \text{---} & \quad \text{---} & \quad \text{---} & \quad \text{---} & \quad \text{---} \\ \text{---} & \quad \text{---} & \quad \text{---} & \quad \text{---} & \quad \text{---} \end{aligned}$$



$$\begin{aligned}
& \left[ \frac{4\mu_2 k_2 a_2^3 (a_2^3 - a_3^3)}{4\mu_2 a_2^3 + 3k_2 a_3^3} \left\{ \frac{4\mu_0 k_0 a_1^3 (a_0^3 - a_1^3)}{4\mu_0 a_1^3 + 3k_0 a_0^3} + \frac{a_1^3 (4\mu_1 a_2^3 + 3k_1 a_1^3)}{a_1^3 - a_2^3} \right\} \delta_2 - \right. \\
& \quad \left. - \frac{4\mu_0 k_0 a_1^3 (a_0^3 - a_1^3)}{4\mu_0 a_1^3 + 3k_0 a_0^3} \left\{ \frac{a_1^3 a_2^3 (4\mu_1 + 3k_1)}{a_1^3 - a_2^3} \right\} \delta_1 \right] \\
\epsilon_2 = & \left[ \left\{ \frac{4\mu_0 k_0 a_1^3 (a_0^3 - a_1^3)}{4\mu_0 a_1^3 + 3k_0 a_0^3} + \frac{a_1^3 (4\mu_1 a_2^3 + 3k_1 a_1^3)}{a_1^3 - a_2^3} \right\} \left\{ \frac{a_1^3 (4\mu_1 a_2^3 + 3k_1 a_1^3)}{a_1^3 - a_2^3} + \right. \right. \\
& \quad \left. \left. + \frac{4\mu_2 k_2 a_2^3 (a_2^3 - a_3^3)}{4\mu_2 a_2^3 + 3k_2 a_3^3} \right\} - \frac{a_1^6 a_2^6 (4\mu_1 + 3k_1)^2}{(a_1^3 a_2^3)^2} \right].
\end{aligned}$$

## REFERENCES

- Bhargava, R. D. and Pande, D., 1963, *Jour. Sci. and Engg. Res. Kharagpur*, **7**, Part II  
 Bhargava, R. D. and Radhakrishna, H. C., *Communicated to Mathematics Student*.  
 Frankel, J., 1946, *Kinetic Theory of Liquids*, Oxford.  
 Jaswon, N. A. and Bhargava, R. D., 1961, *Proc. Camb. Phil. Soc.*, **57**, 669.  
 Mott, N. F. and Nabarro, R. N., 1940, *Proc. Phys. Soc.*, **52**, 86.  
 Timoshenko and J. N. Goodier, 1951, *Theory of Elasticity*, McGraw Hill.

# Letters to the Editor

The Board of Editors does not hold itself responsible for opinions expressed in the letters published in this section. The notes containing short reports of original investigations communicated to this section should not contain many figures and should not exceed 500 words in length. The contributions reaching the Secretary by the 15th of any month may be expected to appear in the issue for the next month. No proof will be sent to the author.

26

## A POSSIBLE EXAMPLE OF A ${}_{\Lambda}B^{12}$ HYPERFRAGMENT.

K. M. PATHAK

DEPARTMENT OF PHYSICS, COTTON COLLEGE, GAUHATI.

(Received August 10, 1964).

### Plate VI

The present communication describes an event observed in a systematic study of hyperfragments produced as a result of the interactions of 3 GeV  $\Pi^-$ -mesons with the G5 emulsion nuclei. The event which has been interpreted as being due to a  ${}_{\Lambda}B^{12}$  hypernucleus is emitted from a parent star of the type  $(9+2) \Pi^-$ . A microphotograph of the event is given in Plate VI.

The hypernucleus after travelling a distance of  $20.94 \mu\text{m}$  comes to rest as manifested by its tapering as well as end scattering. It decays into a 4-prong star. All the four visible prongs of the second star stop in the same pellicle. The relevant data for this event have been shown in the following Table I :

TABLE I

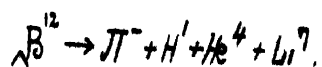
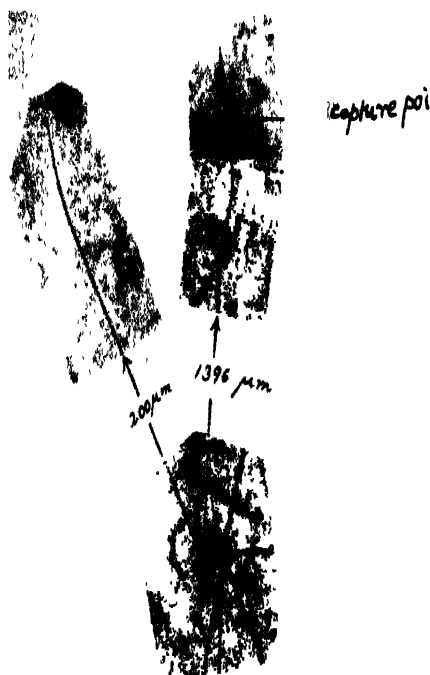
Track	Range in micron.	Dip angle	Angle ' $\theta$ ' between the tracks in the plane of the emulsion.	Probable identity	Energy in MeV
HF	20.94	$47.4^\circ \pm 2^\circ$	$\theta_{1-2} = 108^\circ$	${}_{\Lambda}B^{12}$	
1	12.3	$38.8^\circ \pm 2^\circ$		$\text{He}^4$	3.51
2	5.066	$50^\circ \pm 5^\circ$	$\theta_{2-3} = 125^\circ$	$\text{Li}^7$	2.37
3	200	0	$\theta_{3-4} = 34^\circ$	$\text{H}^1$	5.4
4	1396	$-14.8^\circ \pm 1^\circ$	$\theta_{4-1} = 93^\circ$	$\pi^-$	7.6

The track (4) can be definitely identified as due to a  $\Pi^-$ -meson from the nature of Coulomb scatterings and its end characteristics. At the end, this track gives



K. M. Pathak

PLATE—VI



PLATE—V

A microphotograph of the event observed in a systematic study of hyperfragments produced as a result of the interactions of 3 Gev  $\pi^-$ -mesons with the G5 emulsion nuclei



rise to a single prong capture star. Track (3) which is flat one seems to be due to a singly charged particle. The track (1) may be due to a particle of charge either  $Z = 1$ , or 2. Main difficulty arises in identifying track (2) which is a short and steep recoil. Various identities for the tracks (1) and (3) have been assumed to interpret the recoil (2). At first, the direction and magnitude of the resultant unbalanced momentum of the track (4) and for different identities of the track (1) and (3) has been calculated out in space. It is found that only in few cases the the direction of the unbalanced momentum is found to be approximately in opposite sense to the direction of emission of the recoil; the slight variation in the resultant direction for these cases is not appreciably large and lies within experimental error of measurements. Thus for these schemes we can very well neglect the emission of energetic neutral particle. Knowing thus the unbalance of momentum, the expected range of the recoil for its different identity has been determined with the help of the Wilkins curves. By trial, it is observed that the best identities for the tracks (1) and (3) would be  $\text{He}^4$  and  $\text{H}^1$  respectively. With this assumption for the particles, the unbalance of momentum (176.1 Mev/c) if attributed to a  $\text{Li}^7$ -nucleus, the expected range of the recoil ( $5\mu\text{m}$ ) fits well with its observed range.

Thus we can write the most plausible decay scheme for the event as follows :



and the corresponding  $B_{\Lambda} = 10.03 \pm 0.74$  Mev. The ' $Q$ '-value of the  $\Lambda^0$ -decay was taken to be  $37.58 \pm 0.15$  MeV (Ammar *et al.*, 1960). Further, in calculating the  $B_{\Lambda}$ -values, it has been assumed that the nuclear fragments i.e.  ${}_{\Lambda}\text{B}^{12}$  and  $\text{Li}^7$  are produced in their ground states.

If the emission of one (or more) neutron is assumed, it becomes difficult to fit any such scheme.

#### REFERENCES

- Baumann, G., Braun, H. et Cüer, P., 1963, *Physics Letters*, **5**, 85.  
 Beniston, M. J. and Davies, D. H., 1962, *Phil. Mag.*, **7**, 2119.  
 Pathak, K. M., 1963, *D. Phil. Thesis*, Gauhati University.  
 Schlein, P. E. and Slater, W. E., 1961, *Nuo. Cim.*, **21**, 13.

## BOOK REVIEW

**MATHEMATICAL APPARATUS OF THE THEORY OF ANGULAR MOMENTUM**—by A. P. Yutsis, I. B. Levinson and V. V. Vanagas. Published by the Israel Program for Scientific translation. Price...

The book under review, an English translation from the original Russian, is an important and fruitful contribution to the current literature on the highly useful and specialized branch of quantum mechanics—the theory of angular momentum. It starts with a brief discussion of the relation between angular momentum operators and spatial rotations. The subsequent chapters mainly deal to begin with the problem of vector addition of two angular momenta, then with the problem of addition of an arbitrary number of angular momenta, and finally discuss the various properties of vector coupling co-efficients. A major part has been devoted to the highly useful graphical methods for operations with  $Jm$ - and  $3nJ$ -coefficients, and properties of irreducible tensor operators and their matrix elements. The book thus, may be considered as a review of the properties of vector coupling co-efficients — the so-called Clebs-Gordon and Wigner coefficients, an important mathematical apparatus in the quantum mechanical calculations involving the coupling of a number of angular momentum operators. In vector coupling problem, one usually finds various terminologies, used by different workers such as Clebs-Gordon coefficients, Wigner coefficients, Racah's  $W$ -coefficients,  $3J$ -coefficients,  $Jm$ -coefficients,  $3nJ$ -coefficients etc., between which confusion in definitions is often met with in literature. The authors have, carefully and preserved their distinction to their as well as readers' convenience with specific definition for each of them.

The authors appear to have assumed the reader's preliminary acquaintance with the methods of group theory and the properties of quantum mechanical angular momentum operator and one encounters the frequent reference to Condon and Shortby's book "The Theory of Atomic Spectra", Wigner's book "Group theory" and Racah's work (1942, Phys. Rev). Moreover, many of the results and mathematical inferences have been simply quoted without giving their proofs, perhaps to avoid cumbersome and tedious algebraic computation. Stress has been laid on the methods of calculation rather than on the derivation of these methods. Of course, the authors did not fail to give the complete references of the original works where an inquisitive reader may find the necessary proofs to his satisfaction. On the whole, the book will be highly useful to the scientific workers engaged in advanced research in many branches of Theoretical Physics, and interested more in having the ready formulae and methods of calculation rather than in their complicated derivations.

As stated earlier, the present contribution is a translation from the original Russian and the reviewer is unable to assure the faithfulness to the translations. However, the translator in his note admits that "translation, unlike rotation, cannot be always represented in a 'unitary' form". Even assuming unavoidable deviations from the original Russian, the translation lacks no clarity, continuity and lucidity of exposition.

*U. S. Ghosh*